

Seismic behaviour of masonry buildings with timber diaphragms

Mirra, M.

DOI

[10.4233/uuid:e2fdb0c4-a80d-49c7-889c-7e492fb20ca3](https://doi.org/10.4233/uuid:e2fdb0c4-a80d-49c7-889c-7e492fb20ca3)

Publication date

2022

Document Version

Final published version

Citation (APA)

Mirra, M. (2022). *Seismic behaviour of masonry buildings with timber diaphragms*. [Dissertation (TU Delft), Delft University of Technology]. <https://doi.org/10.4233/uuid:e2fdb0c4-a80d-49c7-889c-7e492fb20ca3>

Important note

To cite this publication, please use the final published version (if applicable).
Please check the document version above.

Copyright

Other than for strictly personal use, it is not permitted to download, forward or distribute the text or part of it, without the consent of the author(s) and/or copyright holder(s), unless the work is under an open content license such as Creative Commons.

Takedown policy

Please contact us and provide details if you believe this document breaches copyrights.
We will remove access to the work immediately and investigate your claim.

Seismic behaviour of masonry buildings with timber diaphragms

Dissertation

for the purpose of obtaining the degree of doctor

at Delft University of Technology

by the authority of the Rector Magnificus, Prof. dr. ir. T.H.J.J. van der Hagen,

Chair of the Board for Doctorates,

to be defended publicly on

Wednesday 4 May 2022 at 10:00 o'clock

by

Michele MIRRA

Master of Science in Civil Engineering

University of Padua, Italy

born in Abano Terme, Italy

This dissertation has been approved by the promotor.

Composition of the doctoral committee:

Rector Magnificus	chairperson
Univ.-Prof. dr. ir. J.W.G. van de Kuilen	TU Delft & TU München, promotor
Prof. dr. A.V. Metrikine	TU Delft, promotor

Independent members:

Prof. dr. ir. J.G. Rots	TU Delft
Prof. ir. S.N.M. Wijte	TU Eindhoven
Prof. ing. A. Ceccotti	IUAV, Italy
Dr. ing. R. Scotta	University of Padua, Italy
Prof. dr. ir. M.A.N. Hendriks	TU Delft, reserve member

Other member:

Dr. ir. G.J.P. Ravenshorst	TU Delft
----------------------------	----------



This research was funded by *Nederlandse Aardolie Maatschappij B.V. (NAM)*.

Keywords:	Timber diaphragms, Masonry buildings, Seismic retrofitting, Energy dissipation, Seismic optimization, Plywood panels, Time-history analyses
-----------	--

Printed by:	Ipskamp printing, Enschede
Cover design:	Michele Mirra

Copyright © 2021 by M. Mirra. All rights reserved.

ISBN 978-94-6421-710-0

An electronic version of this dissertation is available at
<http://repository.tudelft.nl/>

*And the rain fell, and the floods came, and the winds blew and beat on that house, but
it did not fall, because it had been founded on the rock.*

Matthew 7:25

Summary

Existing masonry buildings are very frequently part of the architectural context for several countries all over the world. These constructions often feature masonry walls as vertical structural elements, and timber floors and roofs as horizontal components. The often poor characteristics of masonry, along with the in-plane flexibility of the floors and their frequently weak connections to the walls, make such buildings very vulnerable against seismic actions, as proved by the destructive consequences of several earthquakes in the last decades.

The improvement of seismic capacity of existing masonry buildings is still an open research topic, with several retrofitting techniques for masonry walls and timber floors being proposed and tested. An acknowledged way of increasing the structural performance of a masonry building under an earthquake consists of the development of the so-called box behaviour, enabling the construction to react as a whole to the ground motion. To pursue the box behaviour, the main adopted retrofitting methods are linked to in-plane stiffening of the timber floors, and seismic strengthening of the connections. In this context, several (nonlinear) analysis method for masonry buildings (e.g. the *pushover* analysis) assume that rigid floors are present, and out-of-plane failure mechanisms of masonry are prevented. Therefore, also in the context of numerical modelling, the in-plane response of the diaphragms is generally not taken into account in detail, since they are only considered as linear elastic orthotropic membranes or stiff elements.

However, past seismic events demonstrated that an excessive stiffening of the diaphragms can also be detrimental. This triggered the study of several lighter, moderately stiff strengthening methods for timber floors, referred to various architectural frameworks. Since existing floors proved to be excessively flexible, but also too stiff diaphragms could not be recommendable, the overarching research question of this dissertation arises:

“How is it possible to predict the global seismic behaviour of existing and retrofitted masonry buildings, and to optimize it by quantifying the influence of strengthening interventions on timber floors and timber-masonry connections?”

The research question is answered starting from the specific situation of the Groningen area, in the northern part of the Netherlands, where human-induced earthquakes caused by gas extraction take place. The local building stock is composed for more than 50% of low-rise masonry constructions with timber floors and roofs, none of which was designed or realized with seismic events in mind, since earthquakes were absent until recently.

Up to now, these events have not caused extensive structural damage, because their intensity was from low to moderate, but according to probabilistic studies, more intense earthquakes might also occur. For this reason, a seismic characterization of local timber and masonry structural components was firstly necessary: this dissertation focused in particular on the testing and modelling of as-built and retrofitted timber diaphragms and timber-masonry connections.

As a first step, because it was not possible to test a large number of whole structural components on site, a replication method based on material properties was defined. This ensured that the specimens constructed in laboratory could be representative for the actual structural components in practice. With regard to timber diaphragms, in-plane quasi-static reversed-cyclic tests were performed on five as-built samples, which showed an approximately linear, and very flexible response. For these diaphragms, a retrofitting technique enhancing not only strength and stiffness, but also energy dissipation of the diaphragms, was designed. This dissipative contribution of the floors can be relevant, because it can potentially (greatly) dampen the seismic shear forces on masonry walls, and this characteristic can be even more important for the Groningen area, where low-quality masonry and very slender piers are often present. The strengthening technique for the floors consisted of an overlay of plywood panels screwed along their perimeter to the existing sheathing: the retrofitted diaphragms exhibited a great enhancement in seismic properties, with relevant increase in strength, stiffness, and energy dissipation.

The great potential of the developed retrofitting technique could not be limited to an experimental characterization: an analytical model was also necessary to enable the design of the strengthening for other contexts or floor configurations. Hence, starting from the analytical formulation of the load-slip behaviour of the single screws connecting planks and plywood panels, the global in-plane response of the floors was derived, including their characteristic pinching behaviour. This analytical model had also another important function, because it was the basis for an advanced numerical implementation of the seismic response of timber diaphragms in finite element software. This enabled to account in detail for the (dissipative) in-plane behaviour of the diaphragms, so that the seismic response of existing masonry buildings could be optimized with a well-designed retrofitting of the floors.

Yet, this energy dissipation can only be activated by means of the in-plane deflection of the diaphragms: to avoid out-of-plane collapses of masonry walls, this deflection has not to be excessive, but at the same time also effectively strengthened timber-masonry connections are needed. Therefore, an experimental characterization of two as-built and five strengthened timber-masonry connections was conducted. The joints were tested under monotonic, cyclic, and also high-frequency dynamic loading, by subjecting them to an induced Groningen seismic signal. Seven replicates per joint type were built and tested, and analytical models for evaluating strength and stiffness of the joints were derived, useful for design purposes or as input for numerical models.

Finally, in order to study the possible optimization of seismic capacity of existing masonry buildings, it is also necessary to define proper criteria for an optimal retrofitting. The current seismic design framework is extensively based on peak ground acceleration, which cannot, however, take into account factors such as load duration and quantification of structural damage. These parameters can play a crucial role for the Groningen region, because of the transient nature of the local earthquakes, featuring short, high-frequency and sudden signals, if compared to the longer and more damaging tectonic earthquakes.

Therefore, an energy-based approach was adopted, which allows to predict and quantify the hysteretic energy provided by a building as a function of its period and the load duration of the earthquake.

This approach opened up the opportunity to quantify structural damage in terms of number of cycles on the system: the role of timber diaphragms becomes, then, even more relevant, because with an optimized retrofitting the floors are only moderately stiff, thus the period of a building would be higher than that of the same structure featuring stiff diaphragms. Furthermore, the possibility to include load duration enables a characterization of the seismic capacity independent of the context or the earthquake type.

Thus, to prove the beneficial, dissipative effect of the optimized retrofitting of floors, as well as the effectiveness of the adopted modelling strategies, numerical time-history analyses were performed on three case-study buildings. The first two were typical Dutch constructions, subjected to induced earthquakes, while the third was a country house from the Italian context, to which tectonic earthquakes were imparted. This additional building was included because it enabled to demonstrate that the developed retrofitting and modelling principles, along with the energy-based characterization of seismic capacity, can be generalized to other context besides the reference Dutch one.

The results from the analyses show that excessively flexible floors cause, as expected, out-of-plane collapses in masonry walls, while excessively stiff floors limit the energy dissipation to masonry piers only, thus reducing the seismic capacity of the building. On the contrary, an optimized retrofitting is able to retrieve the global base shear of the building, and at the same time its maximum displacement capacity within masonry drift limits. The optimal strengthening also corresponds to the maximum hysteretic energy that can be provided by the structure. Furthermore, the period of the building is also increased compared to stiff floor configurations, meaning that the structure is subjected to a lower number of cycles, besides benefitting from the additional damping effect activated by dissipative diaphragms. This dissipative contribution can be brought into play provided that an effective strengthening of timber-masonry joints is realized. The beneficial, dissipative effect of well-retrofitted, optimized timber floors was quantified in terms of an equivalent hysteretic damping ratio of 15% (additional to the dissipation already provided by masonry walls), and of an increased behaviour factor (q) range for masonry structures: from the usual values of $q = 1.5 \div 2.5$ to $q = 2.5 \div 3.5$ in presence of dissipative diaphragms.

This research study can contribute to a more efficient seismic retrofitting of existing buildings, enabling preservation of the architectural heritage and more dissipative, earthquake-safe masonry structures.

Samenvatting

Bestaande gebouwen opgebouwd uit metselwerk zijn vaak onderdeel van de historische architecturale context in landen over de hele wereld. Een gebruikelijke bouwtechniek voor deze gebouwen zijn metselwerk wanden als constructieve verticale elementen en houten vloeren en daken als constructieve horizontale elementen. Een slechte staat van het metselwerk, in combinatie met zeer slappe horizontale vloerschijven en een slechte verbinding tussen vloeren en metselwerk, maken deze gebouwen zeer kwetsbaar voor seismische belastingen. Dit is ondervonden in aardbevingen in recente decennia, waarbij er zeer grote schade aan dit type gebouwen heeft plaatsgevonden.

Het verbeteren van de seismische capaciteit van bestaande gebouwen is een actueel onderzoekveld, waarbij diverse retrofittingstechnieken worden onderzocht, zowel voor het metselwerk als de houten vloeren. Een algemeen aanvaard principe voor het vergroten van de seismische capaciteit van gemetselde gebouwen is het vergroten van het box-gedrag van het gebouw, waarmee de samenhang van de constructieve onderdelen wordt verbeterd. Om dit te bereiken, is versterking van de houten vloeren en van de verbindingen hiervan met het metselwerk, onderdeel van de retrofit maatregelen. Verschillende (niet-lineaire) analysemethoden voor gemetselde gebouwen (zoals bijvoorbeeld de push-over analyse) ervan uit dat er volledig starre vloeren aanwezig zijn (na retrofitting), en dat zo bezwijken van metselwerk uit het vlak kan worden voorkomen. Daarom wordt, ook in numerieke modelering, de niet-lineaire respons van de houten vloerschijven over het algemeen niet meegenomen; ze worden als lineair-elastische orthotopie membranen of stijve elementen aangenomen.

Aardbevingen in het verleden hebben echter aangetoond dat het toepassen van te stijve vloeren ook negatief kan uitpakken, met aanzienlijke schade. Dat was de aanleiding voor onderzoek naar lichtere versterkingsmethoden die een meer flexibel gedrag vertonen. Aangezien bestaande houten vloeren extreem slap zijn, is in dit proefschrift de volgende onderzoeksvraag geformuleerd:

“Op welke manier is het mogelijk om het globale seismische gedrag van bestaande en versterkte metselwerk gebouwen te beschrijven en de invloed van de versterkingen van houten vloeren en hout-metselwerk verbindingen hierop te kwantificeren?”

De onderzoeksvraag wordt beantwoord vanuit de specifieke situatie in de regio Groningen in het noorden van Nederland, waar door gaswinning veroorzaakte aardbevingen plaatsvinden. De lokale gebouwenvoorraad bestaat voor meer dan 50% uit laagbouw metselwerkgebouwen met houten vloeren en daken, die niet zijn ontworpen en uitgevoerd op seismische belastingen, aangezien deze tot voor kort niet voorkwamen. Tot dusver

hebben de opgetreden aardbevingen geen grote instortingen veroorzaakt, omdat deze qua intensiteit nog beperkt waren, maar vanuit probabilistisch oogpunt zijn zwaardere aardbevingen mogelijk. Als eerste stap was daarom een seismische karakterisering van bestaande constructieve componenten van metselwerk en hout noodzakelijk: dit proefschrift richt zich in het bijzonder op het testen en modeleren van zowel bestaande als versterkte houten vloerschijven en hout-metselwerk verbindingen.

Omdat het testen in bestaande huizen niet mogelijk was, zijn in het laboratorium replica's van constructieve onderdelen gemaakt, gebaseerd op materiaaleigenschappen die bepaald zijn op proefstukken verkregen uit gesloopte huizen. Hiermee kon de representativiteit van de replica's ten opzichte van het materiaal in de gesloopte huizen worden vastgesteld. Er zijn quasi-statische cyclische testen in het vlak uitgevoerd op vijf onversterkte vloerschijven, die een lineair en zeer flexibel gedrag vertoonden. Voor deze vloerschijven is een retrofittechniek ontworpen die niet tot doel had om niet alleen de sterkte en stijfheid te vergroten, maar ook de energiedissipatie. Deze energiedissipatie kan relevant zijn, doordat het de grootte van de optredende krachten op de metselwerk muren kan verlagen. Met name in de regio Groningen, waar vaak slanke penanten van slechte kwaliteit metselwerk aanwezig zijn. De versterkingstechniek bestond uit een laag van triplexpanelen bevestigd met schroeven langs hun omtrek op de onderliggende vloerplanken. Deze achteraf aangebrachte triplex panelen hadden een sterke seismische verbetering van de vloerschijven tot gevolg, met een significante toename in zowel sterkte als stijfheid, maar ook energiedissipatie. Om de invloed van de versterkingen te kwantificeren voor andere afmetingen en andere configuraties is een analytisch model opgesteld om de sterkte-, stijfheid-, en dissipatie-eigenschappen te voorspellen. Uitgaande van het kracht-vernappingsgedrag van een enkele schroef die triplexplaten en planken met elkaar verbindt, kan het globale gedrag van een met triplexpanelen versterkte vloer worden afgeleid, inclusief het karakteristieke "pinching" gedrag van de schroeven. Het analytische model vormde tevens de basis voor een geavanceerde numerieke implementatie van de seismische respons van houten vloerschijven in eindige elementen software. Dit maakt het mogelijk om nauwkeurig rekening te houden met het (dissipatieve) gedrag in het vlak van de vloerschijven in de beoordeling van het globale gedrag onder seismische belasting van gemetselde gebouwen, en om verschillende optimaliseringsconfiguraties te onderzoeken.

De energiedissipatie kan alleen worden geactiveerd door doorbuiging in het vlak van de vloerschijven. Om bezwijken uit het vlak van de metselwerkwallen te voorkomen, mag deze doorbuiging niet te groot worden, en zijn ook goede (indien nodig versterkte) verbindingen van de houten vloerschijf met de metselwerk wanden noodzakelijk. Om dat laatste te onderzoeken zijn twee bestaande in de praktijk toegepaste verbindingen getest, als mede vijf op verschillende manieren uitgevoerde versterkte verbindingen. De verbindingen zijn getest onder monotone, cyclische en hoogfrequente dynamische belastingen, door ze te onderwerpen aan een signaal, gebaseerd op metingen tijdens een aardbeving in Groningen. Per verbindingstype zijn zeven replica's vervaardigd en getest. Daarna zijn analytische modellen opgesteld om het gedrag van de verbindingen te beschrijven, die gebruikt kunnen worden voor ontwerpdoeleinden en als input voor numerieke modellen.

Om de mogelijke optimalisatie van de seismische capaciteit van bestaande metselwerk gebouwen te bestuderen, is het noodzakelijk de criteria te definiëren waaraan deze optimalisatie moet voldoen. De huidige praktijk is dat het seismische ontwerp grotendeels

is gebaseerd op de grondpiekversnelling, waarbij echter geen rekening kan worden gehouden met factoren als belastingduur en kwantificering van de constructieve schade. Deze parameters kunnen een belangrijke rol spelen voor de regio Groningen, vanwege het karakter van de lokale aardbevingen, met korte, hoogfrequente en plotselinge bewegingen in vergelijking met de langere en meer schadelijke tektonische aardbevingen. Daarom is gekozen voor een op energie gebaseerde benadering, die het mogelijk maakt om de hysteretische energie die door een gebouw wordt geleverd te voorspellen en te kwantificeren als functie van de periode en de belastingsduur van de aardbeving.

Deze benadering opent de mogelijkheid om de constructieve schade te kwantificeren in termen van het aantal cycli waarmee het systeem belast wordt. De rol van de houten vloerschijven wordt dan nog relevanter, omdat bij een geoptimaliseerde versterking de vloeren een flexibele stijfheid bezitten, waardoor de periode van het gebouw hoger wordt dan bij volledig stijve vloerschijven. Bovendien maakt het meenemen van de duur van de belasting een karakterisering van de seismische capaciteit mogelijk, onafhankelijk van het type gebouw of aardbeving.

Om het gunstige, dissipatieve effect van de geoptimaliseerde versterkingen te onderzoeken, in combinatie met de ontwikkelde modeleringstrategieën, zijn numerieke time-history analyses uitgevoerd op drie case-study gebouwen. De eerste twee onderzochte gebouwen waren typisch Nederlandse gebouwen, die werden onderworpen aan seismische belastingen representatief voor door mensen geïnduceerde aardbevingen, het derde gebouw was een Italiaans landhuis onderworpen aan tektonische seismische belastingen. Dit laatste gebouw is in de analyse opgenomen om aan te tonen dat de ontwikkelde principes voor retrofitten en modeleren, algemeen toegepast kunnen worden op verschillen typologieën van metselwerkgebouwen en aardbevingen.

De resultaten van de analyses tonen aan dat extreem slappe vloeren, zoals deze in de huidige Groningse gebouwen aanwezig zijn, zoals verwacht, uit het vlak bezwijken van metselwerk wanden niet kunnen voorkomen. Tevens tonen de analyses aan dat volledig stijve vloeren de energiedissipatie beperken tot de metselwerk wanden, waardoor de seismische capaciteit van de gebouwen wordt begrensd. Wanneer de vloerschijven worden geoptimaliseerd door een specifieke versterking, is een vergroting van de globale capaciteit van het gebouw mogelijk, waarbij de maximale verplaatsingen binnen de grenzen blijven om lokaal bezwijken van het metselwerk te voorkomen.

De optimale uitvoering van de versterking is die waarbij de constructie de maximale hysteretische energie kan leveren. Tevens wordt dan de natuurlijke periode van het gebouw vergroot in vergelijking met volledig stijve vloerconfiguraties, wat betekent dat de constructie wordt onderworpen aan een lager aantal cycli, naast het effect van de extra damping die wordt geactiveerd. Dit dissipatief gedrag kan worden geactiveerd mits een effectieve versteviging van de hout-metselwerk verbindingen wordt gerealiseerd. Het gunstige, dissipatieve effect van geoptimaliseerd versterkte houten vloerschijven kan worden gekwantificeerd in termen van een equivalente hysteretische dempingsratio van 15% (bovenop de dissipatie die al geleverd wordt door gemetselde muren), en van een grote gedragsfactor (q) voor metselwerkconstructies: van de gebruikelijke waarden van $q = 1.5$ tot 2.5 kan deze vergroot worden naar $q = 2.5$ tot 3.5 bij de aanwezigheid van geoptimaliseerde dissipatieve vloerschijven.

Dit resultaten van dit onderzoek kunnen bijdragen aan een efficiëntere aanpassing van bestaande metselwerk gebouwen, waardoor dit architectonisch erfgoed met een hogere en dissipatievere seismische capaciteit kan worden behouden.

Symbols and abbreviations

The dissertation uses the following general notations and abbreviations as much as possible for consistency. In general the notations are also introduced, along with explanations, in the main body for additional clarity.

Roman Symbols

a	Spacing between primary joists (mm)
a'	Spacing between secondary joints (mm)
A_b	Area of a brick (mm ²)
A_i	Area of an incision in a timber-masonry connection (mm ²)
A_n	First constant of the harmonic function q_n (m)
A_s	Area of the sliding part in a timber-masonry connection (mm ²)
b	Width of a primary joist cross section (mm)
b'	Width of a secondary joist cross section (mm)
B	Width of a timber floor (dimension parallel to the in-plane load, mm)
B_n	Second constant of the harmonic function q_n (m)
b_p	Width of a plywood panel (mm)
c	Viscous damping coefficient (kg/s)
\mathbf{C}	Damping matrix
d	Nominal diameter of a fastener (mm)
D	Factor accounting for pinching cycles degradation, based on a strain ratio
d_1	Inner diameter of a fastener (mm)
d_{ip}	In-plane drift of masonry
d_{max}	Displacement corresponding to peak strength of a fastener (mm)
D_n	Displacement of the equivalent single-degree-of-freedom system (mm)

\dot{D}_n	Velocity of the equivalent single-degree-of-freedom system (mm/s)
\ddot{D}_n	Acceleration of the equivalent single-degree-of-freedom system (mm/s ²)
d_{oop}	Out-of-plane drift of masonry
D_p	Factor accounting for pinching cycles degradation, based on a slip ratio
d_s	Displacement of a fastener (mm)
e	Distance of a screw from the plywood panel edge (mm)
E	Young modulus (MPa)
E_d	(Viscous) energy dissipated in one full cycle (kNmm)
E_{dyn}	Dynamic modulus of elasticity of timber (MPa)
E_e	Elastic energy (kNmm)
E_{eq}	Equivalent Young modulus (MPa)
E_{hys}	Hysteretic energy (kNmm)
E_k	Kinetic energy (kNmm)
E_i	Seismic input energy (kNmm)
F	Force (kN)
F	External forces vector
F_0	Yielding force on a fastener (kN)
f_1	First frequency of a timber structural element (Hz)
f_{ax}	Withdrawal resistance parameter (MPa)
F_{ax}	Additional force activated in a timber joint due to rope effect (kN)
F_b	Adherence force in a hook anchor timber-masonry connection (kN)
$f_{c,k}$	Compressive strength of concrete (MPa)
F_e	Force needed to cause brick extraction in a timber-masonry connection (kN)
F_g	Strength of an epoxy incision in a timber-masonry connection (MPa)
f_h	Embedment strength of timber (MPa)
F_{leaf}	Strength of a portion of a masonry leaf in a timber-masonry connection (kN)
f_m	Compressive strength of mortar (MPa)
F_{max}	Maximum force reached in the load-slip curve during a fastener test (kN)

F_p	Peak load in a mortar pocket timber-masonry connection (kN)
F_{res}	Residual load in a mortar pocket timber-masonry connection (kN)
F_s	Force on a fastener (kN)
f_u	Tensile strength of screws (MPa)
f_v	Shear strength of masonry (MPa)
F_v	Vertical load acting on a timber-masonry connection (kN)
$f_{v,0}$	Shear strength of masonry at no pre-compression (MPa)
f_w	Bond strength of masonry (MPa)
F_w	Strength of a wallet surrounding a timber-masonry connection (kN)
G	Shear modulus (MPa)
G_d	Equivalent shear stiffness (N/mm)
h	Height of a primary joist cross section (mm)
h'	Height of a secondary joist cross section (mm)
H_w	Height of a masonry wall (m)
I	Moment of inertia (mm ⁴)
k	Structural stiffness (N/m)
k^*	Stiffness of the equivalent single-degree-of-freedom system (kN/mm)
K	Stiffness matrix
K_{ax}	Axial stiffness of a screw (kN)
K_0	Initial stiffness of a fastener (kN/mm)
$K_{0,rot}$	Initial rotational stiffness of a nail couple (kNmm/rad)
$K_{1,rot}$	Post-yielding rotational stiffness of a nail couple (kNmm/rad)
K_a	Stiffness of a mechanical anchor (kN/mm)
K_{eq}	Equivalent stiffness (kN/mm)
K_i	Initial stiffness of a timber-masonry connection (kN/mm)
K_s	Stiffness in shear sliding (kN/mm)
l	Length of a (timber) structural element (mm)
L	Span of a timber floor (dimension orthogonal to the in-plane load, mm)
l_b	Embedded length of a hook anchor (mm)

l_c	Length of a plywood panel column (mm)
l_{ef}	Effective threaded length of a screw (mm)
l_p	Length of a plywood panel (mm)
L_w	Length of a masonry walls (m)
m	Seismic mass (kg)
m^*	Seismic mass of the equivalent single-degree-of-freedom system (kg)
M	Plastic bending moment of a fastener (kNmm)
M	Mass matrix
M_0	Yielding bending moment provided by a nail couple (kNmm)
M_i	Resisting moment of the i-th nail couple (kNmm)
M_L	Richter magnitude
M_p	Plastic bending moment of a fastener (kNmm)
m_r	Macro-elements rows parallel to the applied load
M_w	Moment magnitude
$m.c.$	Moisture content (%)
n	Number of tested samples
n_a	Number of mechanical anchors in a timber-masonry connection
n_b	Number of bricks
n_c	Number of panel columns in a floor
$n_{couples}$	Number of nail couples in a floor joist
n_{cyc}	Number of cycles underwent by a structural system during an earthquake
n_v	(Average) number of screws in a line orthogonal to the in-plane load
n_v	(Average) number of screws in a line orthogonal to the in-plane load
p	Distributed load (kN/m)
q	Behaviour factor
q_n	Harmonic function describing the time variation of the seismic displacements
R	Stiffness ratio between floors and walls (%)
R	Vector of internal resisting forces
R^2	Coefficient of determination

r_b	Radius of a hook anchor (mm)
s	Number of trusses (or springs) in macro-elements simulating the floors
S_a	Spectral acceleration (mm/s ²)
S_d	Spectral displacement (mm/s)
S_v	Spectral velocity (mm/s)
t	Thickness of the floor planking (mm)
t_p	Thickness of the plywood panels overlay (mm)
t_w	Thickness of a masonry wall (m)
T	Tensile strength of a fastener (MPa)
T_n	Natural vibration period of a system (s)
$T_{n,eff}$	Effective vibration period at collapse of a system (s)
u	Axial displacement of a truss in a macro-element (mm)
V	Shear force (kN)
w	Width of a floor plank (mm)
W	Pre-compression acting on the sliding part of a timber-masonry connection (kN)
w_c	Width of a column of panels in a floor (mm)
x	Displacement of a single-degree-of-freedom system relative to the ground (m)
\mathbf{X}	Displacements matrix
\dot{x}	Velocity of a single-degree-of-freedom system relative to the ground (m/s)
$\dot{\mathbf{X}}$	Velocity matrix
\ddot{x}	Acceleration of a single-degree-of-freedom system relative to the ground (m/s ²)
$\ddot{\mathbf{X}}$	Acceleration matrix
\ddot{x}_g	Ground acceleration (m/s ²)
X_i	Coordinate of the i-th nail couple along the in-plane floor span (mm)

Greek Symbols

α	Bending angle of a fastener (rad)
α_s	Angle between a truss in a macro-element and the loading direction (rad)

β	Ratio between embedment strengths of two timber members in a joint
γ	Drift of a structural element (%)
γ_f	Factor increasing the global in-plane flexural stiffness of a floor
Γ_n	Coefficient relating an equivalent single-degree-of-freedom system to the original multi-degree-of-freedom one
δ	(Mid-span) in-plane displacement of a floor (mm)
δ_c	Displacement of a timber-masonry connection (mm)
δ_{max}	(Mid-span) in-plane displacement of a floor at peak strength (mm)
δ_{sp}	Axial displacement of a macro-element spring in <i>OpenSees</i> (mm)
Δt_e	Strong motion duration (s)
Δt_e^r	Effective strong motion duration (s)
ε	Strain value in user-supplied subroutine
ε_0	Initial strain at the beginning of the current load step
$\varepsilon_{c,max}$	Maximum compressive strain ever reached
$\varepsilon_{c,y}$	Yielding compressive strain
ε_{max}	Input strain at peak stress for the user-supplied subroutine
$\varepsilon_{t,max}$	Maximum tensile strain ever reached
$\varepsilon_{t,y}$	Yielding tensile strain
η	Factor modifying the response spectrum as a function of damping
ϑ	Rotation of a panel column (rad)
K_0	Input initial stiffness in user-supplied subroutine (MPa)
μ	Ductility
μ_p	Static (peak) friction coefficient
μ_{res}	Residual friction coefficient
μ_s	Shear friction coefficient
ν	Poisson coefficient
ξ	Damping ratio
ρ	Density (kg/m ³)
ϱ	Harmonic displacement amplitude (m)

σ	Stress value in user-supplied subroutine (MPa)
σ_{max}	Input maximum stress for the user-supplied subroutine (MPa)
σ_y	Yielding stress in user-supplied subroutine (MPa)
τ	Time (s)
τ_b	Adherence shear stress (MPa)
τ_g	Detachment tangential stress for epoxy glue (MPa)
v	Versor describing the direction of the ground motion
φ	Rotation to which a nail couple is subjected (mm)
ϕ_n	Deflected mode shape vector
$\bar{\omega}$	Excitation frequency (Hz)
ω_n	Natural frequency of a system (Hz)

Abbreviations

Av.	Average
BBM	Block-based models for masonry
CLT	Cross-laminated timber
CM	Continuum models for masonry
CoV	Coefficient of variation
EFM	Equivalent frame models for masonry
EMM	Engineering masonry model
FE	Finite element
FRP	Fiber-reinforced polymer
GBM	Geometry-based models for masonry
LVDT	Linear variable displacement transducer
LVL	Laminated veneer lumber
MDOF	Multi degree of freedom
MM	Macro-element models for masonry
OSB	Oriented strand board
PGA	Peak ground acceleration
RC	Reinforced concrete
SDOF	Single degree of freedom
URM	Unreinforced masonry
US	United States

Contents

Summary	V
Samenvatting	IX
Symbols and abbreviations	XIII
1 Introduction	1
1.1 Background	1
1.2 Problem statement	2
1.3 Aim of the dissertation	5
1.4 Research question	6
1.5 Outline of the dissertation	7
2 State of the art	9
2.1 Introduction	9
2.2 Description of masonry buildings in the analyzed architectural context .	10
2.3 Evaluation of seismic capacity of structural systems	10
2.3.1 Brief recall of structural dynamics	10
2.3.2 Assessment of seismic capacity of URM buildings	12
2.3.3 The case of the induced earthquakes in the Province of Groningen	17
2.4 Seismic behaviour of timber diaphragms	19
2.4.1 General	19
2.4.2 Relevant research studies on the in-plane response of as-built and retrofitted timber diaphragms	21
2.4.3 Methods for the calculation of the in-plane stiffness of timber diaphragms	30
2.5 Seismic behaviour of connections between timber floors and masonry walls	32
2.6 Seismic behaviour of masonry walls	35
2.6.1 General	35
2.6.2 Research studies on the in-plane behaviour of masonry piers . . .	37
2.6.3 Research studies on the out-of-plane behaviour of masonry walls	38
2.7 Interaction among structural components	39
2.7.1 General	39
2.7.2 Experimental studies	40
2.7.3 Numerical analyses	43
2.8 Elements of novelty of the dissertation	44

2.8.1	Introduction	44
2.8.2	Experimental	44
2.8.3	Analytical	45
2.8.4	Numerical	47
2.8.5	Physical	47
3	Methodology for replicating and testing of structural components	49
3.1	Introduction	49
3.2	A multi-scale approach	49
3.3	Replication process	50
3.3.1	General	50
3.3.2	Selection and extraction of timber diaphragms samples from site	52
3.3.3	Determination of material properties of timber and fasteners . .	55
3.3.4	Determination of cyclic behaviour of plank-joist connections . .	56
3.3.5	Extraction, characterization and replication of masonry samples	56
3.4	Definition of the full-scale specimens to be tested	57
3.4.1	Timber diaphragms	57
3.4.2	Timber-masonry connections	63
3.4.3	Masonry walls	69
3.5	Adopted test setups and testing methods for structural components . .	72
3.5.1	Timber diaphragms	72
3.5.2	Timber-masonry connections	73
3.5.3	Masonry walls	79
4	Experimental results	85
4.1	Introduction	85
4.2	Results from material characterization	85
4.2.1	Material properties of extracted and replicated timber samples and fasteners	85
4.2.2	Cyclic behaviour of extracted and replicated plank-joist connections	86
4.2.3	Material properties of replicated timber-masonry connections . .	87
4.3	Analysis of test results for timber diaphragms	89
4.3.1	General	89
4.3.2	Specimens loaded parallel to the joists	90
4.3.3	Specimens loaded perpendicular to the joists	90
4.3.4	Roof pitch specimen	91
4.3.5	Discussion	93
4.3.6	Dissipative properties of the retrofitted diaphragms	93
4.3.7	Comparison of the results with similar research studies from literature	96
4.4	Analysis of test results for timber-masonry connections	107
4.4.1	Results from pilot study	107
4.4.2	Quasi-static monotonic and cyclic tests	108
4.4.3	Dynamic tests	112
4.4.4	Comparison between quasi-static and dynamic tests	115
4.4.5	Failure modes of the connections	118
4.4.6	Dissipative properties of the connections	118

4.5	Summary of test results for masonry walls	121
4.5.1	General	121
4.5.2	In-plane tests on masonry walls	122
4.5.3	Out-of-plane tests on masonry walls	122
4.5.4	Interaction between masonry structural components	128
5	Modelling the seismic response of structural components	133
5.1	Introduction	133
5.2	Analytical and numerical models for as-built timber diaphragms	134
5.2.1	Analytical modelling of as-built diaphragms	134
5.2.2	Numerical modelling of as-built diaphragms	139
5.3	Analytical models for retrofitted timber diaphragms	141
5.3.1	Introduction	141
5.3.2	Definition of the load-slip behaviour of fasteners	142
5.3.3	Prediction of the global behaviour of diaphragms	148
5.3.4	Application of the analytical model for the tested floors	156
5.4	Numerical modelling approach for retrofitted diaphragms	161
5.4.1	Introduction	161
5.4.2	Implementation of the floors response in <i>OpenSees</i> based on the analytical model	162
5.4.3	Implementation of a user-supplied subroutine simulating the seis- mic response of floors in DIANA FEA	165
5.5	Analytical and numerical models for timber-masonry connections	173
5.5.1	Introduction	173
5.5.2	Analytical modelling of timber-masonry connections	173
5.5.3	Numerical modelling approaches for timber-masonry connections	183
5.6	Drift limits and numerical modelling strategies for masonry walls	189
5.6.1	General	189
5.6.2	Drift limits for in-plane loaded masonry walls	190
5.6.3	Drift limits for out-of-plane loaded masonry walls	190
5.6.4	Numerical modelling approaches for masonry structures	190
6	Seismic capacity of URM buildings and its optimization	197
6.1	Introduction	197
6.2	Estimating energy dissipation and damage	198
6.2.1	General	198
6.2.2	Energy components in linear elastic SDOF systems	198
6.2.3	Energy components in nonlinear SDOF systems	199
6.2.4	The role of spectral velocity	201
6.2.5	Predicting seismic energy dissipation of SDOF systems with spec- tral velocity	205
6.3	Analyses on SDOF URM buildings	209
6.3.1	General	209
6.3.2	Characteristics of the analyzed SDOF URM buildings	209
6.3.3	Results of the numerical analyses	210
6.4	Summary	223

7	Numerical modelling of the seismic response of existing URM buildings	227
7.1	Introduction	227
7.2	Evaluation of the modelling approach against an experimental shake-table test	228
7.2.1	Properties of tested prototype and numerical model	228
7.2.2	Evaluation of seismic response	231
7.2.3	Evaluation of damage	232
7.3	Overview of the analyzed case-study buildings and configurations	234
7.4	First case-study building (B1)	236
7.4.1	Model properties	236
7.4.2	Results from eigenvalue analyses	241
7.4.3	Results from time-history analyses	241
7.4.4	Assessment of building B1 at damage limit state	246
7.5	Second case-study building (B2)	248
7.5.1	Model properties	248
7.5.2	Results from eigenvalue analyses	253
7.5.3	Results from time-history analyses	256
7.6	Third case-study building (B3)	261
7.6.1	Model properties	261
7.6.2	Results from eigenvalue analysis	268
7.6.3	Results from time-history analyses	270
7.7	Additional considerations on the role of timber diaphragms	271
7.8	Role of timber-masonry connections	277
7.9	Final summary and concluding remarks	277
8	Design recommendations for assessing and optimizing seismic capacity of URM buildings	283
8.1	Introduction	283
8.2	Step 1: Inspection of existing building of interest	283
8.3	Step 2: Design of retrofitting methods for diaphragms and joints	284
8.4	Step 3: Creation of the numerical model	284
8.5	Step 4: Performing seismic analyses	286
8.5.1	Lateral force method	286
8.5.2	Modal analysis	287
8.5.3	Pushover analysis	287
8.5.4	Time-history analysis	288
9	Conclusions and outlook	291
9.1	Main outcomes of the dissertation and concluding remarks	291
9.2	Recommendations for further research	293
	Bibliography	295
A	Pictures of the as-built and retrofitted tested diaphragms	311

B Drawings of the tested timber-masonry connections	317
B.1 Samples tested within the pilot study	317
B.2 Samples tested within the second experimental campaign	320
C Main properties of timber diaphragms compared from literature	325
D Example of calculation of input parameters for numerical model of retrofitted timber floors	337
E Listing of the implemented user-supplied subroutine	339
F Optimal dissipative retrofitting of case-study diaphragms	345
G Example of hysteretic energy estimation	349
H Complete results from time-history analyses	351
List of publications	379
Curriculum vitae et studiorum	383
Acknowledgements	385

List of Figures

1.1	(a) Total out-of-plane wall collapse of a building after the Emilia earthquake (2012); (b) local out-of-plane collapse of a gable after Central Italy earthquake (2016); (c) total collapse of a house in which timber diaphragms were substituted with concrete slabs after L'Aquila earthquake (2009).	3
1.2	(a) The region of Groningen in the Netherlands; (b) building with structural damage after the numerous induced earthquakes taking place in the region.	5
1.3	Outline of the dissertation.	8
2.1	Examples of masonry buildings from the Dutch and the Italian context.	11
2.2	Representation of a building by means of an SDOF oscillator.	12
2.3	Procedure for deriving response spectra: ground acceleration (a); displacement response of SDOF systems (b); displacement response spectrum (c); pseudo-velocity response spectrum (d); pseudo-acceleration response spectrum (e). Adapted from [32].	13
2.4	Principle and main steps of pushover analysis.	16
2.5	Comparison between pushover capacity curve and (overdamped) demand response spectrum in the acceleration-displacement diagram (from [35]).	17
2.6	Probabilistic seismic hazard map for the Groningen area, referred to a return period of 475 years. The black solid line indicates the boundary of the Groningen gas field. From [39].	18
2.7	Comparison between the 1971 Ancona earthquake signal (a) and the 1994 Northridge accelerogram (b). Although the PGA was similar, way different damage was observed after the two earthquakes. Adapted from [28],[40]-[42].	20
2.8	Timber diaphragm sample tested by [15, 16]; dimensions in mm.	22
2.9	Timber diaphragm sample tested by [18]; dimensions in mm.	23
2.10	Timber diaphragm sample tested by [19, 20]; dimensions in mm.	24
2.11	Timber diaphragm sample tested by [21]; dimensions in mm.	24
2.12	Timber diaphragm sample tested by [22]; dimensions in mm.	25
2.13	Timber diaphragm sample tested by [23]; dimensions in mm.	26
2.14	Timber diaphragm sample tested by [24]; dimensions in mm.	27

2.15	Timber diaphragm samples tested by [24]: (a) specimen loaded parallel to the joists, (b) specimen loaded perpendicular to the joists; dimensions in mm.	28
2.16	Timber diaphragm samples tested by [25]; dimensions in mm.	29
2.17	(a) Definition of yield values for a load-slip curve with two well-defined linear parts; (b) definition of yield values for a load-slip curve without two well-defined linear parts. From [45].	31
2.18	Bilinear methods for schematizing the experimentally obtained backbone curves: (a) procedure according to FEMA guidelines [49, 50], (b) elastic-plastic bilinearization according to ASTM E 2126 [51]; both methods are based on the principle of the energy equivalence between the two curves.	33
2.19	Side and front view of samples representing timber-masonry connections. From [54].	34
2.20	Test setup and picture of a timber-masonry joint sample. From [55].	34
2.21	In-situ test setup for timber-masonry connections. From [57]	35
2.22	Main in-plane failure mechanisms of a masonry pier: (a) flexural failure; (b) shear-diagonal failure; (c) shear-sliding failure. From [58].	36
2.23	Overview of possible collapse mechanisms of masonry walls in an existing building. From [59].	36
2.24	Out-of-plane collapse of masonry walls in one-way or two-way bending. From [60].	37
2.25	Force-displacement hysteretic response and crack pattern of a slender wall subjected to in-plane rocking failure. From [75].	38
2.26	Force-displacement hysteretic response and crack pattern of a squat wall subjected to in-plane shear-diagonal failure. From [75].	39
2.27	Out-of-plane response of a URM wall loaded in one-way (left) and two-way bending (right). Adapted from [104].	40
2.28	Full-scale building tested by MAGENES et al. [116]. Dimensions in cm.	42
2.29	Elements of novelty addressed by the doctoral thesis.	46
3.1	Multi-scale approach followed for the definition of the conducted large-scale testing campaign.	51
3.2	Process followed for the determination of material properties of timber and plank-joist connections for original and replicated samples: (a) in-situ investigation and selection of samples; (b) extraction of floor and roof samples; (c) construction of replicated specimens on the basis of the characteristics of original ones; (d) characterization of material properties and cyclic behaviour of plank-joist connections, with comparison between extracted (e) and replicated samples (f). From [132].	53
3.3	Extracted timber diaphragms samples: G1 (a), G2 (b), G3 before cutting (c), G4 (d); geometrical parameters of interest for replication (e). From [132].	54
3.4	(a) Schematic representation of the diaphragms tested parallel to the joists (specimens DFpar-1 and 1s, DFpar-2 and 2s, view from decking side); dimensions in mm; (b) sample DFpar-1 positioned in the test setup.	60

3.5	Schematic representation of the diaphragms tested perpendicular to the joists (specimens DFper-3 and 3s, DFper-4 and 4s, view from decking side); (b) sample DFper-3 positioned in the test setup.	61
3.6	Schematic representation of the tested roof pitch (specimens DFpar-5 and 5s, view from the inner side); dimensions in mm; (b) sample DRpar-5 positioned in the test setup.	62
3.7	Replicated roof specimen from a terraced house tested at LNEC laboratories. From [147].	63
3.8	As-built timber-masonry connections typical of the Groningen area: masonry pocket in a single-leaf wall (a); masonry pocket in a double wythe wall (b); example of hook anchor (c); hook anchor in a single-leaf wall (d); hook anchor masoned in a double-wythe wall (e).	65
3.9	Configurations of timber-masonry connections tested within the pilot study: as-built with masonry pocket (CLAY-A and CS-A), as-built with hook anchor (CLAY-B and CS-B), strengthened with steel angle (CLAY-C and CS-C).	66
3.10	Principle of the tested sample representing a timber-masonry connection.	67
3.11	Overview of the seven configurations tested in the second phase: as-built with mortar pocket (A); as-built with hook anchor (B); strengthened with steel angle (C); strengthened with additional joist and steel brackets (D); strengthened with hook anchor glued into the wall (E); strengthened with two screws glued into the wall (F); strengthened with timber blocks (G).	68
3.12	Example of specimen prepared for testing pull-out and shear strength of mechanical anchors in masonry: sample before (a) and after testing (b); specimen after removal from test setup (c). From [151].	70
3.13	Wall TUD_COMP23 (sample with asymmetric opening). From [157].	70
3.14	Principle for the adopted test configuration of floors and roofs. From [132].	72
3.15	Test setup and measurement plan for the experimental campaign on timber diaphragms. From [132].	74
3.16	Test setup (a) and measurement plan (b) for the experimental campaign on timber-masonry connections. From [151].	75
3.17	Pattern applied to a sample to detect out-of-plane displacements of the masonry wall with DIC technique. From [150].	76
3.18	Adopted signal for HFD tests and performed runs; for as-built configurations A and B the maximum reached amplitude was 150% of the reference signal, linked to a 2475 years return period.	79
3.19	Test setup and measurement plan adopted for the in-plane tests on slender (a) and squat walls (b). From [156].	81
3.20	Test setup adopted for the out-of-plane tests on slender (a) and squat walls (b). From [104].	82
3.21	Measurement plan adopted for for the out-of-plane tests on slender (a) and squat walls (b); both load cells (FN or FV) and sensors (S) are highlighted. From [158].	83
4.1	Comparison between the cyclic response of original and replicated plank-joist connections. From [132].	87

4.2	Experimental cyclic in-plane response of the as-built and retrofitted timber diaphragms tested parallel to the joists.	91
4.3	Experimental cyclic in-plane response of the as-built and retrofitted timber diaphragms tested perpendicular to the joists.	92
4.4	Experimental cyclic in-plane response of the as-built and retrofitted sample representing a roof pitch.	92
4.5	Examples of in-plane deformed shape: as-built (a) and strengthened (b) floors loaded parallel to the joists (reported for two adjacent rows of panels); as-built (c) and strengthened (d) floors loaded perpendicular to the joists. From [132].	94
4.6	In-plane deformed shape of as-built (a) and strengthened roof sample (b). From [132].	95
4.7	Determination of the equivalent damping ratio from the energy dissipated in one full cycle and the corresponding elastic energy. From [168].	96
4.8	Evaluation of the equivalent damping ratio for the retrofitted timber diaphragms as a function of drift: sample DFpar-1s (a), DFpar-2s (b), DFper-3s (c), DFper-4s (d), DRpar-5s (e). From [168].	97
4.9	Estimation of a reference average value of equivalent damping ratio up to 0.5% (a) and 1% drift (b), in comparison to the present value proposed in NPR 9998 for general timber structural members; the dots correspond to analytically calculated values. From [168].	98
4.10	Overview of the timber diaphragms examined in the comparison. For visual comparison, the static schemes are reported at the same scale, along with in-plane deformed shapes and drifts γ . The first given dimension is always the one orthogonal to the load; sample names are reported according to the authors' nomenclature. From [169].	100
4.10	Continued. From [169].	101
4.11	Derivation of the stiffness K at different drift levels: 0.1%, 1.0% and at a conventional yielding point, defined as the intersection between an initial stiffness determined according to EN 12512 [45], and the tangent to the experimental curve at 1.0% drift. From [169].	102
4.12	Comparison of the equivalent shear stiffness of strengthened diaphragms at 0.1% (a) and 1.0 % (b) drift, and at yielding (c); in the latter case the corresponding drift is also indicated. The retrofitting techniques are divided by groups, and colors identify specific strengthening characteristics. From [169].	106
4.13	Cyclic response of the timber-masonry connections tested within the pilot study: samples CLAY-A (a), CLAY-B (b), CLAY-C (c), CS-A (d), CS-B (e), CS-C (f).	109
4.14	Damage and cracks on walls occurred after testing to samples CLAY-A (a), CLAY-B (b), CLAY-C (c), CS-A (d), CS-B (e), CS-C (f). From [148].	110
4.15	Summary of monotonic (a) and cyclic test results for configurations A (b), B (c), C (d), D (e), E (f), F (g), and G (h). A representative picture of a sample after testing is also shown. From [151].	113
4.16	Example of acceleration response measured at 100% signal amplitude on sample G-HFD-1 (a); dynamic test results for configurations A (b), B (c), C (d), D (e), E (f), F (g), G (h). From [151].	114

4.17	Visual comparison of damage and cracks occurred to the walls under quasi-static cyclic and dynamic loading after the tests. From [151]. . . .	116
4.18	Comparison of crack pattern under the same displacement amplitude at peak strength detected by DIC for configurations E and F in quasi-static cyclic and dynamic tests. From [151].	117
4.19	Comparison between the hysteretic response of configuration C under an induced (a) or tectonic (b) signal; damage on the masonry wall and the joint after the tests with induced (c) and tectonic signal (d). From [151].	119
4.20	Summary of the possible failure modes (in italic those not observed in the tests, but possible in practice) and main outcomes from the tests for each connection type. From [151].	120
4.21	Cyclic response of sample TUD_COMP-0a. From [156].	122
4.22	Cyclic response of sample TUD_COMP-1. From [156].	122
4.23	Cyclic response of sample TUD_COMP-2. From [156].	123
4.24	Cyclic response of sample TUD_COMP-3. From [156].	123
4.25	Cyclic response of sample TUD_COMP-4. From [156].	123
4.26	Cyclic response of sample TUD_COMP-5. From [156].	124
4.27	Cyclic response of sample TUD_COMP-6. From [156].	124
4.28	Cyclic response of sample TUD_COMP-20. From [157].	124
4.29	Cyclic response of sample TUD_COMP-21. From [157].	125
4.30	Cyclic response of sample TUD_COMP-22. From [157].	125
4.31	Cyclic response of sample TUD_COMP-22. From [157].	125
4.32	Cyclic response of sample TUD_COMP-23. From [157].	126
4.33	Cyclic response of sample TUD_COMP-24. From [157].	126
4.34	Cyclic response of sample TUD_COMP-25. From [157].	126
4.35	Cyclic response of sample TUD_COMP-7. From [104].	128
4.36	Cyclic response of sample TUD_COMP-10. From [104].	128
4.37	Cyclic response of sample TUD_COMP-11. From [104].	129
4.38	Cyclic response of sample TUD_COMP-12. From [104].	129
4.39	Cyclic response of sample TUD_COMP-26. From [158].	129
4.40	Cyclic response of sample TUD_COMP-27. From [158].	130
4.41	Cyclic response of sample TUD_COMP-28. From [158].	130
4.42	Cyclic pushover test on a full-scale clay brick masonry assemblage representing a terraced house unit: 3D view of the building (a); test setup and measurement plan (b); capacity curve (c). From [171].	131
5.1	Summary of the adopted procedure for the analytical and numerical modelling of as-built and retrofitted timber-diaphragms and timber-masonry connections.	135
5.2	Scheme for the analytical calculation of the floor deflection in the direction orthogonal to the joists: for the moments given by nail couples, the shown average backbone curve calibrated from the conducted experimental tests in torsion on plank-joist connections was used. From [132].	137
5.3	Value of the factor γ_f increasing the global flexural stiffness of the diaphragms as a function of the moment of inertia I of a single structural element of the floor.	139

5.4	Static schemes for calculating the in-plane deflections of whole diaphragms loaded parallel (a) or perpendicular (b) to the joists, and of roof pitches (c). From [27].	140
5.5	Example of timber diaphragms retrofitted with a plywood panels overlay, and basic principles for the conducted tests and the formulation of the analytical model. From [174].	142
5.6	Samples prepared for the tests on screws fastening the plywood panels to the existing sheathing: schematic description (a) and example of specimen (b). From [174].	143
5.7	Determination from experimental tests of the branches representing the initial stiffness (linear branch of Eq. 5.6) and the global response (parabolic branch of Eq. 5.6) of the screws when loading the plywood panel parallel to the plank (a) and perpendicular to it (b). Experimental data points correspond to the amplitudes of each cycle on the various backbones. From [174].	145
5.8	Proposed load-slip curve (dashed) in comparison to the experimental data points and backbones for the direction parallel to planks (a) and perpendicular to them (b). The main parameters of the curve equation are also reported. From [174].	146
5.9	Comparison between the analytically derived curve and the two obtained from the experimental data. From [174].	148
5.10	Principle of the analytical model formulated for the seismic design of the proposed strengthening technique, when the panels are arranged vertically (a); individuation of the horizontal and vertical screws columns when the panels are arranged horizontally (b). From [174].	151
5.11	Principle for the calculation of the global deflection of the floor from each column of panels. From [174].	152
5.12	Procedure for the determination of the pinching cycles from the analytical backbone curve. From [174].	155
5.13	Comparison between analytical backbone (red) and estimated pinching cycle (dark blue) with the experimental hysteretic response (light blue) for the floors tested parallel to the joists: global (left) and initial (right) response of samples DFpar-1s (a) and DFpar-2s (b). From [174].	158
5.14	Comparison between analytical backbone (red) and estimated pinching cycle (dark blue) with the experimental hysteretic response (light blue) for the floors tested perpendicular to the joists: global (left) and initial (right) response of samples DFper-3s (a, with in grey the overall recorded cycle and light blue the sheathing's one) and DFper-4s (b); crack opening in a plank during softening phase of sample DFper-4s (c). From [174].	159
5.15	Comparison between analytical backbone (red) and estimated pinching cycle (dark blue) with the experimental hysteretic response (light blue) for the roof pitch [14]: global (left) and initial (right) response of sample DFpar-5s. From [174].	160
5.16	Example of comparison, for (a) a floor (DFpar-2s) and (b) a roof sample (DRpar-5s), between the analytically predicted equivalent damping ratio (adopting both the linearized and the refined pinching cycle) and the one calculated in Section 4.3.6. From [174].	161

5.17	Schematic representation of the OpenSees Pinching4 material [180]: the input backbone curve and pinching cycle are highlighted.	162
5.18	Implementation procedure of the analytical model based on OpenSees Pinching4 material [180] when the aim is to model the global response of the floors (a) or their nonlinear behaviour in an entire building (b). From [174].	164
5.19	Numerical model for the diaphragm representation (a); results of the numerical analysis when implementing the analytical model to assess the global (b) and initial (c) response of the diaphragms. The experimental cycle (grey) refers to sample DFpar-1s, the numerical cycle is depicted in black. From [174].	166
5.20	Adopted strategy for modelling in-plane and out-of-plane behaviour of timber diaphragms in DIANA FEA, with a mesh of macro-elements overlapped to linear elastic orthotropic shell elements. From [183]. . . .	167
5.21	Representation of the input parameters for the user-supplied subroutine. From [183].	168
5.22	Loading, unloading and reloading branches implemented in the user-supplied subroutine.	168
5.23	Model of the retrofitted diaphragm for the validation of the user-supplied subroutine. From [183].	170
5.24	Results from the analyses conducted for the validation of the user-supplied subroutine and the overall modelling strategy for timber floors: out-of-plane static analysis under vertical loads (a); complete displacement-based in-plane cyclic analysis (b); displacement-based in-plane cyclic analysis with local loops (c); in-plane time-history analysis under an induced Groningen earthquake accelerogram (d). From [183].	172
5.25	Seismic signal used for the time-history analysis of the trial retrofitted diaphragm model. From [183].	173
5.26	Validation of the user-supplied subroutine against the tested diaphragms: experimental (a) and numerical (b) response of sample DFpar-1s; experimental (c) and numerical (d) response of sample DFper-4s; experimental (e) and numerical (f) response of sample DRpar-5s.	174
5.27	Comparison between the experimental cyclic response of configuration A and the proposed frictional model (a); sliding of bricks in the masonry leaf behind the timber joist (b); prediction of the strength increase because of the additional masonry leaf behind the joist according to Eq. 5.36 (c). . .	176
5.28	Analytical response of the hook anchor connection type: determination of the effective length of the resisting wall portion (a); comparison between the analytical expression of Eq. 5.39 and the backbone curves of the tested samples.	179
5.29	Comparison between the analytically predicted and experimental behaviour of strengthened configuration C.	180
5.30	Comparison between the analytically predicted and experimental behaviour of strengthened configuration D.	181
5.31	Comparison between the analytically predicted and experimental behaviour of strengthened configuration E.	182

5.32	Comparison between the analytically predicted and experimental behaviour of strengthened configuration F.	182
5.33	Main contribution to connection slip from the various fasteners (a); comparison between the analytically predicted and experimental behaviour of strengthened configuration G (b).	184
5.34	Main parameters of the <i>Steel01</i> material (a) in OpenSees; stress, strain, damage (b) and pinching (c) parameters of the <i>Hysteretic</i> material. From [180].	186
5.35	Comparison between the numerically implemented connection in OpenSees and representative experimental results: configurations A (a), B (b), C (c), D (d), E (e), F (f), and G (g).	188
5.36	Force-elongation diagram for spring elements in DIANA FEA. From [182].	189
5.37	Representation of the in-plane and out-of-plane drift limits in a basic masonry building with a timber diaphragm.	189
5.38	Numerical modelling strategies for masonry structures. From [189]. . . .	191
5.39	Comparison between the experimental and numerical crack pattern (a) and cyclic load-displacement response (b) of the squat wall tested in [75]. From [190].	194
5.40	Comparison between the experimental and numerical capacity curve of the prototype simulating a terraced house tested at TU Delft [171]. Adapted from [191].	195
5.41	Example of a masonry macro-model implemented in OpenSees (a): sub modules, elements connecting wall sub-modules and equivalent external compression forces because of steel ties (F); numerical validation of the macro-model against the test results of [77] (b). From [11].	196
6.1	Dynamic response of an linear elastic, undamped SDOF system subjected to the 2018 Zeerijp induced earthquake: seismic input acceleration \ddot{x}_g (a); displacement time-history of the system x (b); overview of the single energy components (c).	200
6.2	Dynamic response of a linear elastic, damped elastic SDOF system ($\xi = 0.05$) subjected to the 2018 Zeerijp induced earthquake signal of Fig. 6.1a: displacement time-history of the system x (a); overview of the single energy components (b).	201
6.3	Dynamic response of a damped nonlinear SDOF system ($\xi = 0.05$) subjected to the 2018 Zeerijp earthquake of Fig. 6.1a amplified up to plasticization of the system: load-displacement response (a); displacement time-history of the system x (b); overview of the single energy components (c).	202
6.4	Comparison between the 2018 Zeerijp earthquake and the 1980 Irpinia earthquake in terms of pseudo-acceleration (a) and lower-bound input energy S_v^2 (b) response spectra.	204
6.5	Example of pushover analyses on basic URM buildings with a flexible (a), retrofitted stiff (b), and retrofitted dissipative (c) timber floor. The control node correspond to the centre of mass of the floor.	205

6.6	Relevant geometrical parameters (a) of the basic case-study buildings with Dutch (b) and Italian (c) features. The main properties of the models, as well as the macro-element calibration, are reported.	211
6.7	Induced seismic signals (a-g) and their average response spectrum (h) [203] adopted for the analyses on building A.	212
6.8	Tectonic seismic signals (a-g) and their average response spectrum (h) [204] adopted for the analyses on building B.	213
6.9	Spectral velocity (a), PGA at collapse (b) and estimated behaviour factor (c) as a function of the stiffness ratio R for building A.	215
6.10	Recorded and predicted hysteretic energy dissipated by the building and its components (a) under signal 4; evolution of the number of cycles sustained by the walls with the increase in floor stiffness (b).	217
6.11	Correlations between normalized PGA (a) and normalized S_v^2 with normalized hysteretic energy for building A.	218
6.12	Spectral velocity (a), PGA at collapse (b) and estimated behaviour factor (c) as a function of the stiffness ratio R for building B.	220
6.13	Recorded and predicted hysteretic energy dissipated by the building and its components (a) under signal 1; evolution of the number of cycles sustained by the walls with the increase in floor stiffness (b).	221
6.14	Correlations between normalized PGA (a) and normalized S_v^2 with normalized hysteretic energy for building B.	222
6.15	(a) in-plane response of a masonry wall of building B under signal 1 at the same amplitude for the optimal configuration with dissipative floor and that with stiff diaphragm: the damping contribution of the well-retrofitted floor is evident; (b) average capacity response spectra of the dissipative and stiff floor configurations; (c) rheological model schematizing the contributions in mass, stiffness and damping of masonry walls and timber floors.	224
7.1	Prototype EUC-BUILD2 tested at EUCENTRE. Adapted from [206].	229
7.2	Real EUC-BUILD2 prototype (a) and realized numerical model in DIANA FEA (b).	230
7.3	Seismic signal with increasing amplitude adopted for the time-history analyses on the EUCENTRE prototype model.	231
7.4	Results from eigenvalue analysis in terms of first fundamental frequency and associated mode shape.	232
7.5	Experimental and numerical seismic response of the building prototype under the first applied signal in undamaged conditions (a) and at collapse (b). Adapted from [206].	233
7.6	Comparison between the experimentally observed damage and the numerically obtained crack pattern (in terms of principal cracks Ecw1) at collapse for the north (a), west (b), south (c), and east (d) side.	235
7.7	Overview of the analyzed case-study buildings and nomenclature adopted for their configurations.	237
7.8	Main properties and geometry of the first case-study building B1; dimensions in mm. From [183].	238

7.9	Results from eigenvalue analysis in terms of fundamental periods and associated mode shapes for the three configurations of case-study building B1.	242
7.10	PGA at collapse for the three configurations in the x (left) and y direction (right).	243
7.11	Base shear vs. roof displacement response, including trilinear backbone, and damage level in terms of principal crack opening (Ecw1) for the three configurations: B1-AB (a), B1-RC (b), B1-PP (c).	244
7.12	Schematic representation of the in-plane and out-of-plane drifts underwent by the masonry walls for the three configurations of building B1 under signal 1 (plan view).	245
7.13	Recorded and predicted hysteretic energy of retrofitted configurations B1-RC and B1-PP as a function of the proposed behaviour factor ranges.	247
7.14	Results in terms of crack pattern and maximum recorded displacement during the analysis at damage limit state, under half-scaled signal 1 in the x direction.	249
7.15	Main properties and geometry of the first case-study building; dimensions in mm.	250
7.16	Constitutive laws assigned to the nodal springs without cross terms representing the timber-masonry connections: mortar pocket (a) used in configurations B2-AB-MP and B2-AB-MP-NI; hook anchor joint (b) used in configuration B2-AB-HA; timber blocks connection (c) used in configurations B2-PP and B2-PP-NI.	254
7.17	Results from eigenvalue analysis in terms of fundamental periods and associated mode shapes for the three as-built configurations of case-study building B2.	255
7.18	Results from eigenvalue analysis in terms of fundamental periods and associated mode shapes for the four retrofitted configurations of case-study building B2.	257
7.19	PGA at collapse referred to both directions x (left) and y (right) for all analyzed configurations, with well (a) and poorly interlocked (b) walls.	258
7.20	Base shear vs. top floor displacement response, including trilinear backbone, and damage level in terms of principal crack opening (Ecw1) for the three as-built configurations: B2-AB-MP (a), B2-AB-HA (b), B2-AB-MP-NI (c).	259
7.21	Out-of-phase oscillation of the out-of-plane walls at first and top floor level. The displacements time-history refer to the centre of mass of both diaphragms.	260
7.22	Comparison between the relative displacement between top floor and out-of-plane wall of the mortar pocket and hook anchor configuration.	260
7.23	Base shear vs. top floor displacement response, including trilinear backbone, and damage level in terms of principal crack opening (Ecw1) for the two retrofitted configurations with well-interlocked walls: B2-RC (a), B2-PP (b).	262

7.24	Base shear vs. top floor displacement response, including trilinear backbone, and damage level in terms of principal crack opening (Ecw1) for the two retrofitted configurations with poorly connected internal walls: B2-RC-NI (a), B2-PP-NI (b).	263
7.25	Recorded and predicted hysteretic energy of retrofitted configurations B2-RC and B2-PP as a function of the proposed behaviour factor ranges.	264
7.26	Effective periods at collapse for the retrofitted configurations B2-RC and B2-PP as a function of their behaviour factor ranges.	264
7.27	Main properties and geometry of the first case-study building; dimensions in mm.	266
7.28	Results from eigenvalue analysis in terms of fundamental periods and associated mode shapes for the three configurations of case-study building B3.	269
7.29	PGA at collapse for the three configurations in the x (left) and y direction (right).	270
7.30	Base shear vs. roof displacement response, including trilinear backbone, and damage level in terms of principal crack opening (Ecw1) for the three configurations: B3-AB (a), B3-RC (b), B3-PP (c).	272
7.31	Recorded and predicted hysteretic energy of retrofitted configurations B3-RC and B3-PP as a function of the proposed behaviour factor ranges.	273
7.32	Out-of-plane displacement time-histories of the front gable for configurations B1-AB (a), B1-RC (b), B1-PP (c) at collapse. From [212].	275
7.33	Examples of top floor and in-plane walls displacement time-histories for configurations B2-AB-MP (a), B2-RC (b), B2-PP (c). From [212].	276
7.34	Out-of-plane displacement time-histories of the front wall for configurations B3-AB (a), B3-RC (b), B3-PP (c) at collapse. From [212].	278
7.35	Hysteretic energy vs. time for the retrofitted configurations at near-collapse state. The dissipative role of the diaphragms retrofitted with plywood panels, in comparison to the rigid concrete slabs, is evident. From [212].	279
7.36	Effect of the diaphragms stiffness and dissipation on the in-plane response of the most solicited wall in building B1. From [212].	280
8.1	Example for a reference 4 by 4.6 m floor (a) of the influence of screw diameter d (b), number of screws orthogonal to the in-plane loading $n_v(c)$, and width of a row of panels $w_c(c)$ on the obtained load-slip response and pinching cycles.	285
8.2	Typically Dutch terraced house tested at EUCENTRE [218] and its model in Abaqus [217].	287
8.3	Recommendations proposed in this dissertation for seismic analyses on existing URM buildings with (retrofitted) timber diaphragms.	289
A.1	Diaphragms DFpar-1 (a) and DFpar-1s (b).	312
A.2	Diaphragms DFpar-2 (a) and DFpar-2s (b).	313
A.3	Diaphragms DFper-3 (a) and DFper-3s (b).	314
A.4	Diaphragms DFper-4 (a) and DFper-4s (b).	315
A.5	Diaphragms DRpar-5 (a) and DRpar-5s (b).	316

B.1	Configuration CLAY-A.	317
B.2	Configuration CLAY-B.	318
B.3	Configuration CLAY-C.	318
B.4	Configuration CS-A.	319
B.5	Configuration CS-B.	319
B.6	Configuration CS-C.	320
B.7	Configuration A.	320
B.8	Configuration B.	321
B.9	Configuration C.	321
B.10	Configuration D.	322
B.11	Configuration E.	322
B.12	Configuration F.	323
B.13	Configuration G.	323
F.1	Characteristics of the diaphragms retrofitted with plywood panels in building B1.	346
F.2	Characteristics of the diaphragms retrofitted with plywood panels in building B2.	347
F.3	Characteristics of the diaphragms retrofitted with plywood panels in building B3.	348
G.1	Pseudo-velocity response spectrum of signal 2 at collapse.	350
H.1	Complete base shear-top floor displacement curves for the seven applied accelerograms; analyzed configuration, control node, and earthquake direction are highlighted.	352
H.2	Complete base shear-top floor displacement curves for the seven applied accelerograms; analyzed configuration, control node, and earthquake direction are highlighted.	353
H.3	Complete base shear-top floor displacement curves for the seven applied accelerograms; analyzed configuration, control node, and earthquake direction are highlighted.	354
H.4	Complete base shear-top floor displacement curves for the seven applied accelerograms; analyzed configuration, control node, and earthquake direction are highlighted.	355
H.5	Complete base shear-top floor displacement curves for the seven applied accelerograms; analyzed configuration, control node, and earthquake direction are highlighted.	356
H.6	Complete base shear-top floor displacement curves for the seven applied accelerograms; analyzed configuration, control node, and earthquake direction are highlighted.	357
H.7	Complete base shear-top floor displacement curves for the seven applied accelerograms; analyzed configuration, control node, and earthquake direction are highlighted.	358
H.8	Complete base shear-top floor displacement curves for the seven applied accelerograms; analyzed configuration, control node, and earthquake direction are highlighted.	359

H.9 Complete base shear-top floor displacement curves for the seven applied accelerograms; analyzed configuration, control node, and earthquake direction are highlighted.	360
H.10 Complete base shear-top floor displacement curves for the seven applied accelerograms; analyzed configuration, control node, and earthquake direction are highlighted.	361
H.11 Complete base shear-top floor displacement curves for the seven applied accelerograms; analyzed configuration, control node, and earthquake direction are highlighted.	362
H.12 Complete base shear-top floor displacement curves for the seven applied accelerograms; analyzed configuration, control node, and earthquake direction are highlighted.	363
H.13 Complete base shear-top floor displacement curves for the seven applied accelerograms; analyzed configuration, control node, and earthquake direction are highlighted.	364
H.14 Complete base shear-top floor displacement curves for the seven applied accelerograms; analyzed configuration, control node, and earthquake direction are highlighted.	365
H.15 Complete base shear-top floor displacement curves for the seven applied accelerograms; analyzed configuration, control node, and earthquake direction are highlighted.	366
H.16 Complete base shear-top floor displacement curves for the seven applied accelerograms; analyzed configuration, control node, and earthquake direction are highlighted.	367
H.17 Complete base shear-top floor displacement curves for the seven applied accelerograms; analyzed configuration, control node, and earthquake direction are highlighted.	368
H.18 Complete base shear-top floor displacement curves for the seven applied accelerograms; analyzed configuration, control node, and earthquake direction are highlighted.	369
H.19 Complete base shear-top floor displacement curves for the seven applied accelerograms; analyzed configuration, control node, and earthquake direction are highlighted.	370
H.20 Complete base shear-top floor displacement curves for the seven applied accelerograms; analyzed configuration, control node, and earthquake direction are highlighted.	371
H.21 Complete base shear-top floor displacement curves for the seven applied accelerograms; analyzed configuration, control node, and earthquake direction are highlighted.	372
H.22 Complete base shear-top floor displacement curves for the seven applied accelerograms; analyzed configuration, control node, and earthquake direction are highlighted.	373
H.23 Complete base shear-top floor displacement curves for the seven applied accelerograms; analyzed configuration, control node, and earthquake direction are highlighted.	374

H.24 Complete base shear-top floor displacement curves for the seven applied accelerograms; analyzed configuration, control node, and earthquake direction are highlighted.	375
H.25 Complete base shear-top floor displacement curves for the seven applied accelerograms; analyzed configuration, control node, and earthquake direction are highlighted.	376
H.26 Complete base shear-top floor displacement curves for the seven applied accelerograms; analyzed configuration, control node, and earthquake direction are highlighted.	377

List of Tables

3.1	Characteristics of the extracted samples.	54
3.2	Geometrical characteristics of the five tested diaphragms, reported for their as-built configurations.	58
3.3	Characteristics of the strengthened versions of the five tested diaphragms.	59
3.4	Characteristics of the masonry walls tested in plane.	71
3.5	Characteristics of the masonry walls tested out of plane.	71
3.6	Overview of the tests performed in the preliminary pilot study and adopted nomenclature.	77
3.7	Overview of the tests performed in the second large-scale campaign and adopted nomenclature.	78
4.1	Comparison of the material properties of timber joists and planks from extracted and replicated samples.	86
4.2	Comparison of the characteristics of fasteners (3 × 65 mm nails) from extracted and replicated samples.	86
4.3	Material properties of the plywood panels used for strengthening the diaphragms.	87
4.4	Material properties of the timber joists used for the construction of timber-masonry connection samples.	88
4.5	Material properties of clay brick masonry used for the construction of timber-masonry connection samples, determined according to Section 3.4.2.	88
4.6	Material properties of calcium silicate brick masonry used for the construction of timber-masonry connection samples, determined according to Section 3.4.2	89
4.7	Pull-out, shear strength and stiffness of mechanical anchors; the obtained values for clay brick masonry are also compared to the characteristic values reported by the producer with reference to C20/25 concrete [153].	89
4.8	Overview of in-plane stiffness values for the as-built (O) and strengthened (S) timber diaphragms selected for comparison. Values of equivalent shear stiffness that are size-dependent because of the flexural properties of as-built floors are reported in italic, while the symbol (*) denotes values obtained from an extrapolation of the experimental curve and not directly from it, because the test was stopped slightly before reaching this drift value.	105

4.9	Peak strength in pulling and pushing, and stiffness evaluated at 2 mm for the joints tested within the pilot study.	108
4.10	Comparison between quasi-static and dynamic tests in terms of peak force in pulling and pushing, and stiffness evaluated at 2 mm displacement. Both average values and, in brackets, their standard deviations are reported.	117
4.11	Values of equivalent damping ratio evaluated for each tested connection configuration. Both average values and, in brackets, their standard deviations are reported.	121
4.12	Summary of the failure modes of the tested in-plane walls.	127
5.1	Comparison between the experimental and analytical values of displacement for as-built specimens loaded parallel and perpendicular to the joists. The symbol (*) refers to a load value obtained after subtracting the contribution of friction between planks, equal to ≈ 0.9 kN for sample DFper-3 and to ≈ 0.5 kN for specimen DFper-4.	138
5.2	Variations in the characteristics of the full-scale tested diaphragms with respect to the small-size tests on screws fastening plywood panel and plank.	143
5.3	Comparison among the values of initial stiffness K_0 for a single screw obtained experimentally and calculated according to equations from standards or literature.	147
5.4	Material properties of the tested plank-plywood panel joints used for the derivation of the analytical curve.	149
5.5	Calculated parameters based on diaphragms configurations of Table 5.2. The variation in results compared to samples DFpar-1s and DRpar-5s, having the same properties as the reference tests on plank-plywood panel joints, is noticeable.	149
5.6	Values of the parameters used to predict the global in-plane response of the diaphragms according to the properties of tested samples.	154
5.7	Comparison between initial stiffness K_0 , peak force F_{max} and corresponding displacement d_{max} obtained from test results and calculated with the analytical model. The cause of failure observed during the tests is also reported for each sample.	160
5.8	Properties adopted in the trial retrofitted floor model.	171
5.9	Values of the parameters <i>\$pinchx</i> and <i>\$pinchy</i> adopted for the implementation of the timber-masonry connections in OpenSees.	187
6.1	Values of initial period, effective period at collapse, and behaviour factor as a function of R of building A for each signal.	216
6.2	Values of initial period, effective period at collapse, and behaviour factor as a function of R of building B for each signal.	219
7.1	Material properties adopted for masonry shell elements (210 mm thickness) based on [166] and [206].	230
7.2	Equivalent properties adopted for timber diaphragms shell elements (24 mm thickness), according to the modelling strategy presented in Section 5.2.2 and the example provided in Appendix D.	230

7.3	Material properties adopted for masonry shell elements (thickness = 210 mm) based on [166] and [207].	236
7.4	Equivalent properties adopted for the shell elements (thickness = 18 mm) representing the flexible diaphragms in configuration B1-AB, in agreement with the modelling strategy presented in Section 5.2.2 and the example provided in Appendix D.	239
7.5	Material properties adopted for the shell elements (thickness = 58 mm) representing the concrete slabs in configuration B1-RC.	240
7.6	Equivalent properties adopted for the macro-elements and shell elements (thickness = 36 mm) representing the diaphragms retrofitted with plywood panels in configuration B1-PP, in agreement with the modelling strategy presented in Section 5.4.3 and the example provided in Appendix D.	241
7.7	Effective periods at collapse for the retrofitted configurations B1-RC and B1-PP as a function of their behaviour factor ranges.	246
7.8	Equivalent properties adopted for the shell elements (18 mm thickness) representing the flexible diaphragms in configurations B2-AB-MP, B2-AB-HA and B2-AB-MP-NI, in agreement with the modelling strategy presented in Section 5.2.2 and the example provided in Appendix D.	252
7.9	Material properties adopted for the shell elements (thickness = 68 mm) representing the concrete slabs in configurations B2-RC and B2-RC-NI.	252
7.10	Equivalent properties adopted for the macro-elements and shell elements (thickness = 36 mm) representing the diaphragms retrofitted with plywood panels in configurations B2-PP and B2-PP-NI, in agreement with the modelling strategy presented in Section 5.4.3 and the example provided in Appendix D.	253
7.11	Material properties adopted for masonry shell elements (380 mm thickness) based on [75, 77, 78].	265
7.12	Equivalent properties adopted for the shell elements (20 mm thickness) representing the flexible diaphragms in configuration B3-AB, in agreement with the modelling strategy presented in Section 5.2.2 and the example provided in Appendix D.	267
7.13	Material properties adopted for the shell elements (thickness = 70 mm) representing the concrete slabs in configuration B3-RC.	267
7.14	Equivalent properties adopted for the macro-elements and shell elements (thickness = 38 mm) representing the diaphragms retrofitted with plywood panels in configuration B3-PP, in agreement with the modelling strategy presented in Section 5.4.3 and the example provided in Appendix D.	268
7.15	Effective periods at collapse for the retrofitted configurations B3-RC and B3-PP as a function of their behaviour factor ranges.	271
7.16	Summary of the main results from the numerical analyses on the three case-study buildings.	281
C.1	Characteristics of the as-built and strengthened floors tested by VALLUZZI et al. [19, 20] and values of their in-plane stiffness.	326

C.2	Characteristics of the as-built and strengthened floors tested by CORRADI et al. [18] and values of their in-plane stiffness.	327
C.3	Characteristics of the as-built and strengthened floors tested by BRANCO et al. [21] and values of their in-plane stiffness.	328
C.4	Characteristics of the as-built and strengthened floors tested by GUBANA and MELOTTO [22] and values of their in-plane stiffness.	329
C.5	Characteristics of the as-built and strengthened floors tested by PERALTA et al. [23] and different values of their in-plane stiffness.	330
C.6	Characteristics of the as-built and strengthened floors tested by BRIGNOLA et al. [24] and different values of their in-plane stiffness.	331
C.7	Characteristics of the as-built and strengthened floors tested by GIONGO et al. [26] and values of their in-plane stiffness.	332
C.8	Characteristics of the as-built and strengthened floors tested by Wilson et al. [25] and values of their in-plane stiffness.	333
C.9	Characteristics of the as-built and strengthened floors tested at TU Delft [132] in the direction parallel to the joists, and values of their in-plane stiffness.	334
C.10	Characteristics of the as-built and strengthened floors tested at TU Delft [132] in the direction perpendicular to the joists, and different values of their in-plane stiffness.	335
C.11	Characteristics of the as-built and strengthened roof sample tested at TU Delft [132] and different values of its in-plane stiffness.	336

Chapter 1

Introduction

1.1 Background

Earthquakes are daunting and widespread hazards. Independently of countries, cultures or traditions, seismic events are unfortunately still leading to damage to buildings and cities, and causing many victims. This phenomenon represents a crucial issue for seismic territories: on the one hand, a socio-economical problem arises, with scared people who are often willing to leave those areas without rebuilding their houses, thus impoverishing whole regions; on the other hand, a cultural problem also has to be considered. Existing buildings are often part of the history of a country, and their destruction might cause a loss of identity for the nation itself.

However, if it was possible to prevent existing buildings from collapsing or undergoing excessive damage during an earthquake, both the cultural heritage of countries and of people's lives and environments could be protected. This is precisely the toughest challenge of seismic engineering, which strives to minimize the risks derived from earthquakes and their consequences for a certain territory. Yet, while for the design of new buildings this goal can be achieved by following the rules imposed by standards or guidelines, for existing buildings many more uncertainties and issues are present, such as the quality of the materials and the effectiveness of the interaction between *structural components*, in particular floors, walls and the connections among them.

Another aspect of complexity is represented by the earthquake type: several regions in the world are well known for being high-risk seismic areas (e.g. California, Japan, Italy, Greece, Turkey, Indonesia, among others), due to the presence of extended faults causing tectonic earthquakes; yet, the issue of human-induced earthquakes has also recently arisen, with seismic events caused, for instance, by gas extraction or fracking. These induced earthquakes are normally not as intense as tectonic events, but their occurrence is very frequent and they involve buildings not designed for seismic actions, since these were absent in the past.

1.2 Problem statement

Standards and guidelines for seismic design focus on the use of a single material, as is often appropriate to new buildings [1]-[3]. Yet, larger uncertainties are present in the material properties compared to the present standardized building materials used for constructing new structures. Besides, a large amount of historical or existing buildings tend to be aggregated constructions: walls are made of *stone* or *brick masonry*, while floors and roofs, which are generally regarded as *diaphragms*, are composed of timber structural elements. The possibility of a building surviving an earthquake is then related to an effective interaction among its structural components, and this has to be considered as the goal for a proper seismic design.

The main sources of seismic vulnerability in existing buildings consist of the presence of (often low-quality and/or brittle) masonry walls, and flexible timber diaphragms inadequately connected to them. During an earthquake, the very low in-plane stiffness of the floors frequently causes out-of-plane collapses of masonry walls (Fig. 1.1a-b). These local failures occur because the masonry walls cannot withstand the excessive displacements induced by flexible diaphragms. Besides, existing timber floors may not be able to fully transfer and redistribute seismic loads, increasing once more the chance of local collapses.

In this framework, the main strategy to reduce seismic vulnerability is to develop the so-called *box-like behaviour* [4]. This consists of several methods enabling structural components to work together to increase in *seismic capacity*, the global strength of the building against an earthquake. The concept of box-like behaviour is acknowledged as an improvement in the overall seismic capacity of buildings. Since earthquakes cause vibrations and displacements in a construction, the principles that have to be followed to enhance its performance are related to the strengthening and stiffening of existing structural components, and to the creation of effective connections systems among them. In this way, a building can withstand earthquakes as a whole construction, preventing single structural elements from collapsing and causing severe damage to the global edifice. By applying the aforementioned principles, which are generally called *retrofitting methods*, the seismic capacity of buildings can be increased.

Unfortunately, retrofitting interventions especially involving the existing timber diaphragms have often proved to be unsatisfactory, or even to worsen the structural performance, as it has been observed in many collapses of strengthened buildings after intense earthquakes (Fig. 1.1c) [5]-[7]. A number of studies have demonstrated that some retrofitting methods that were widely applied in the past could even decrease the seismic capacity with respect to the state of the building before the intervention [8]-[14]. This means that the effectiveness of local strengthening methods in improving the global seismic behaviour of a building has to be well evaluated and quantified: in this way, it is possible to design a retrofitting intervention truly optimizing the seismic response.

Therefore, to be sure to improve the resistance of existing buildings against earthquakes, the concept of box-like behaviour has to be pursued by reliably assessing seismic capacity, starting from the properties of structural components. Moreover, an optimal balance among these properties has to be reached and clearly quantified when designing the retrofitting interventions, focusing on the timber diaphragms and their connections to masonry walls. Otherwise, the response of buildings could even be worsened, as it



Figure 1.1: (a) Total out-of-plane wall collapse of a building after the Emilia earthquake (2012); (b) local out-of-plane collapse of a gable after Central Italy earthquake (2016); (c) total collapse of a house in which timber diaphragms were substituted with concrete slabs after L'Aquila earthquake (2009).

happened in the past. Thus, in order to achieve these goals, three main open issues have to be overcome.

First, in recent years, several strengthening methods for timber diaphragms have been proposed and tested [15]-[26]. However, the research studies focused mainly on an experimental characterization, not necessarily followed by specific design rules or calculation models. Furthermore, these tests were conducted on newly-built samples, highlighting that their properties could not always match those of ancient structural components [24]. Besides, many techniques focus only on strengthening and stiffening the components [15]-[18], without taking into account an improvement of their potential dissipative properties: earthquakes provide energy to the buildings, and if they have to withstand seismic events, this amount of energy needs to be dissipated by each and every structural component.

Second, many available retrofitting techniques could be applied to single structural components, but this can be dangerous if their impact on the whole building is not properly considered [8]-[14]; instead, it is necessary to be more aware of this influence and to be able to quantify it. In other words, retrofitting is in itself not enough, because it changes the properties of the building: therefore, even the structural response to the seismic input is altered and can become unpredictable, from component to building level. The goal has to become *effective-retrofitting*, enabling a tangible and quantifiable improvement in the structural performance, which can subsequently be optimized. Only in this way it could be possible to transform the possibly inadequate timber floors from an acknowledged cause of seismic vulnerability to structural components maximizing the response to earthquakes of existing buildings.

Third, earthquakes are normally identified with their ground motion parameters: acceleration, velocity and displacement. Since, within the design phase, one is interested in the maximum force that the building has to bear, an intuitive way to calculate this load could be by simply taking the *peak ground acceleration* (PGA), amplifying it according to the vibration period of the building, and combining this acceleration with the mass of the construction. This is in the end Newton's equation, according to which the force equals the product of the mass and the acceleration. Such an intuitive principle has led to the use of PGA in standards and guidelines for the design of earthquake-resistant

buildings [3, 4, 27]. However, PGA alone is only a ground parameter determined from seismic signals, and is not directly related to the structural behaviour of the building, which is instead taken into account in the *response spectrum*. The response spectrum is a plot of the peak value of a response quantity (acceleration, velocity or displacement) as a function of the natural vibration period of the structure. Yet, response spectra cannot completely describe the actual energy dissipation and structural damage to a building, because characteristics such as the type of earthquake and its duration cannot be taken into account [28].

Therefore, strengthening existing buildings is by itself a very complex process, given the many uncertainties that are intrinsically and that can propagate in an uncontrolled way with the wrong retrofitting interventions, sometimes even decreasing seismic capacity with respect to the original state. Nevertheless, historical buildings can also have an advantage, because they may already contain the memory of past earthquakes, which emerges in specific building techniques or ancient technical expedients to defend the structure from seismic motions. However, the situation can be very different if human-induced earthquakes suddenly start to take place in areas that have never experienced them.

An example for this situation in the Groningen area, a region in the northern part of the Netherlands, where shallow earthquakes are causing structural damage (Fig. 1.2). These seismic events are not natural, because faults and tectonic movements are not present; instead, they have been induced by gas extraction in that territory [29]. The intensity of these earthquakes is lower than natural ones, and their duration is limited: up to now, the most intense seismic event was recorded in 2012 in Huizinge, and had a magnitude of 3.6 on the Richter scale [30]. Yet, according to probabilistic studies, more intense earthquakes might occur [31]. In the meantime, the impact on society of these human-induced seismic events proved to be considerable. People living in that territory do not feel comfortable anymore and are scared by these very frequent phenomena: even low-intensity earthquakes can be frightening when the population does not have any memory of or experience with them. Moreover, the existing building stock is composed of low-rise constructions with slender masonry walls and very flexible timber diaphragms, and the most ancient structures were realized only according to good-practice building techniques of that time. Therefore, also structural components are not able to withstand seismic forces, because earthquakes were not present until recently.

Consequently, the three aforementioned issues – seismic characterization of timber floors, effectiveness of retrofitting, and earthquakes description – are even more relevant to the current situation in the province of Groningen. More specifically, given the absence of past earthquakes, there is little knowledge on seismically relevant material properties of structural components in Dutch buildings, and before even proposing a strengthening technique, it is necessary to carefully characterize the as-built constructions. Furthermore, the impact of retrofitting interventions on the timber diaphragms and their connections to the walls has to be clearly determined, because the region in which earthquakes occur has a limited surface, and the intensity of these events can vary within a few kilometers. The interventions, thus, have to be quite adaptable and at the same time have to prevent buildings in the higher-risk areas from being damaged. Finally, such human-induced shallow earthquakes are different from tectonic ones, and characterizing the performance of the buildings by means of PGA might not provide the complete



Figure 1.2: (a) The region of Groningen in the Netherlands; (b) building with structural damage after the numerous induced earthquakes taking place in the region.

picture on their seismic response: further correlations between other parameters, such as energy dissipation and structural damage, have to be investigated.

1.3 Aim of the dissertation

This lack of knowledge about the Dutch context has given the opportunity to conduct specific research for improving the general understanding of the impact of strengthening interventions for timber diaphragms on the seismic response of existing buildings.

In particular, having as a final goal the improvement of seismic capacity, this dissertation aims to define and quantify an optimal balance among the properties of (retrofitted) structural components, enabling the buildings to perform at their best when subjected to earthquakes. To this end, the concept of seismic capacity will also be extended, in order to better take into account duration of the seismic motion and earthquake type, which are both linked to structural damage and energy dissipation.

The following methodology is adopted for achieving the main goals:

- First, it is necessary to characterize the material properties of structural components for the under-studied Dutch context by means of experimental tests. Since it is not possible to extract and test whole components from existing buildings, an accurate replication has to be made in laboratory. In this way, it is possible to match the properties of the tested samples with those of ancient buildings, and also to perform tests on a larger number of specimens. Within this phase, retrofitting techniques for timber diaphragms and timber-masonry connections are defined and tested as well, preferring those boosting the energy dissipation of these components.
- Second, analytical models describing the seismic response of single as-built and retrofitted structural components have to be formulated starting from the experimental results. The development of reliable analytical models for predicting the

seismic behaviour of the retrofitted components enables to design these strengthening measures, and provide input for numerical models.

- Third, before putting together the structural components (timber diaphragms, masonry walls, and timber-masonry connections) and studying the global response of buildings, the concept of seismic capacity has to be extended. In other words, it is necessary to investigate seismic indicators that can give a more precise picture on structural damage and energy dissipation. On the one hand, this type of characterization is useful for the specific Groningen case, because low-duration and high-frequency induced earthquakes can be less detrimental compared to tectonic ones; on the other, it enables a generalization of the results, which can be independent of the earthquake type.
- Finally, with the previous models it is possible to predict and quantify the effect of single components, and therefore also the impact of a retrofitting intervention, on the global behaviour of buildings. This step reveals how to properly strengthen existing timber diaphragms and timber-masonry connections in order to optimize the seismic capacity of the building, reflected in an optimal balance among the characteristics of the structural components.

Therefore, the originality of this dissertation lies primarily in the investigation of how a proper, dissipative retrofitting of timber diaphragms, combined with timber-masonry connections strengthening, could dampen the seismic actions on the masonry walls, preserving them from collapse and increasing the overall seismic capacity. With this aim in mind, other elements of novelty arise from the described methodology. Innovative and more accurate testing methods are investigated to assess the seismic behaviour of structural components. Novel and refined analytical and numerical models are developed to seismically assess and design (retrofitted) structural components. Finally, an extended and more complete approach for evaluating seismic capacity is investigated, along with the application of this concept for predicting and optimizing the global resistance of existing masonry buildings against earthquakes.

1.4 Research question

Considering the current situation in assessing the impact of retrofitting interventions on existing buildings, and having described the possible ways to improve our knowledge in this field, as well as the methodology to achieve these proposed solutions, the following overarching research question can now be formulated:

“How is it possible to predict the global seismic behaviour of existing and retrofitted masonry buildings, and to optimize it by quantifying the influence of strengthening interventions on timber floors and timber-masonry connections?”

This research question will be answered throughout the dissertation, according to the outline presented in Section 1.5 and schematized in Fig. 1.3.

1.5 Outline of the dissertation

The literature review in *Chapter 2* provides an overview of the state of the art on the current testing methods and retrofitting techniques for structural components, as well as the seismic analysis of existing unreinforced masonry (URM) buildings. In particular, it firstly discusses research on the seismic behaviour of timber diaphragms, masonry walls and timber-masonry connections. Secondly, it addresses the current methods for analyzing the structural response to earthquakes of URM buildings, also with reference to the specific case of the Groningen area. Starting from this literature review, the elements of novelty in this dissertation are presented more thoroughly from the experimental, analytical, numerical, and physical point of view.

Chapter 3 illustrates the adopted replication process that, starting from the extraction of samples from existing buildings, allows to rebuild specimens in the laboratory with similar properties. Therefore, such samples can provide reliable results, representative for the actual structural components, after testing. Furthermore, the various samples to be tested are defined, together with the testing methods used to assess the seismic properties of timber diaphragms, timber-masonry connections, and URM walls.

In *Chapter 4*, the test results of the whole experimental campaign conducted at Delft University of Technology are reported and analyzed. The discussion particularly focuses on timber diaphragms and timber-masonry connections, in both as-built and strengthened configurations. As for masonry walls, a separate experimental campaign was conducted by a different research group: the main outcomes of this study are reported as well, in order to provide a complete overview of the tests results for structural components.

On the basis of the experimental outcomes, *Chapter 5* describes the formulation of analytical models describing the seismic response of timber diaphragms and timber-masonry connections; drift limits for URM walls are defined as well. These calculation methods allow to predict the capacity of the existing components and to define and quantify the improvement in their properties given by the proposed and tested strengthening techniques. Besides, starting from these analytical calculations, the numerical modelling of the structural components is discussed: this represents an important step towards predicting the performance of existing buildings. However, first it is necessary to well identify how to characterize their seismic capacity, and which parameters are the most suitable to describe it.

This latter analysis takes place in *Chapter 6*, in which seismic indicators correlated to structural damage and energy dissipation of buildings are investigated. This correlation reveals broader truths about seismic capacity, because it allows to take into account the type of earthquake and its duration. In this way, an extended approach for evaluating seismic capacity for both tectonic and induced earthquakes is possible, and completes the partial information provided by PGA only.

Once a more complete and refined concept of seismic capacity evaluation has been proposed, this is applied in *Chapter 7*, together with the developed analytical and numerical models for structural components. Based on these inputs, the global seismic behaviour of a number of case-study buildings is numerically investigated. The optimal balance among the characteristics of the components is evaluated, focusing especially on the role of (retrofitted) timber diaphragms and timber-masonry connections. In this way, an optimization of seismic capacity of URM buildings can be achieved and

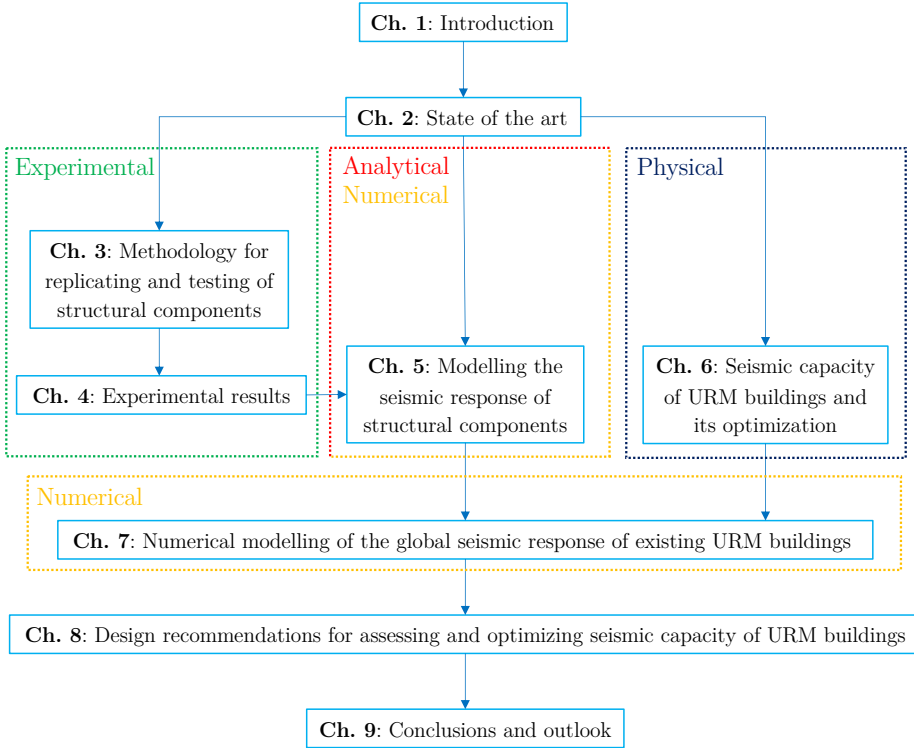


Figure 1.3: Outline of the dissertation.

quantified. These analyses cover not only the Dutch context, but also the Italian one, thus extending the results for a country in which tectonic earthquakes are present, and other configurations of masonry buildings exist.

The results obtained from the investigations on case-study buildings are at the basis of the recommendations for seismic analysis and retrofitting of URM buildings with timber diaphragms, provided in *Chapter 8*. The proposed approaches are summarized and discussed, and can provide new information for professional civil engineers willing to apply these outcomes.

In *Chapter 9*, the conclusions of this study are drawn, and indications for further research are given. In addition, the process of achieving the goals of this dissertation is summarized, recalling the main steps and finally answering the global research question.

Chapter 2

State of the art

2.1 Introduction

As discussed in the Introduction, this dissertation aims to optimize the seismic capacity of existing masonry buildings through a dissipative retrofitting of their timber floors.

Thus, this chapter presents a systematic literature review on the seismic behaviour of existing buildings and their structural components. The focus of this literature review will be, in particular, on past research studies on timber diaphragms and their interaction with masonry walls through the connections among them. Since many studies investigated the seismic behaviour of timber floors, large amount of data is available, but often not comprehensive or comparable. These issues are caused by the different analyzed contexts, the various testing methods, and the assumptions in interpreting the obtained test results.

Firstly, a description of the characteristics of masonry structures in the analyzed building frameworks is provided (Section 2.2). Secondly, the concept of seismic capacity and the current methods for its evaluation are discussed with reference to existing buildings in Section 2.3, where the need of detailed knowledge of the properties of structural components will be highlighted.

Subsequently, the state of the art is presented with regard to seismic assessment and retrofitting of timber diaphragms (Section 2.4) and floor-to-wall timber-masonry connections (Section 2.5). Besides, the structural response to earthquakes of masonry walls (Section 2.6), as well as the interaction between these and the timber diaphragms are recalled (Section 2.7).

Finally, the extensive literature review enables the definition of the knowledge gaps and elements of novelty that the dissertation will cover (Section 2.8), thus highlighting the originality of the doctoral thesis.

2.2 Description of masonry buildings in the analyzed architectural context

Before presenting the state of the art on the seismic analysis of masonry buildings and the possible retrofitting strategies to improve their seismic capacity, this section briefly describes the main characteristics of the constructions studied within this dissertation. Section 1.5 highlighted that the main focus will be on the Dutch context, but in order to extend and generalize the results, also a case-study building from the Italian framework will be analyzed. Fig. 2.1 shows a comparison of a Dutch and an Italian masonry building with timber diaphragms; the main features typical of the two building contexts can be summarized as follows:

- For the Dutch context, a frequent presence of slender structural elements can be noticed. This corresponds to light, small-size and flexible structural elements composing the timber diaphragms, and to generally thin (single-leaf or double wythe) masonry walls. The in-plane and out-of-plane slenderness of the piers, along with the presence of poorly connected diaphragms, make the local constructions very vulnerable to seismic loads.
- For the Italian framework, the structural elements are often more massive, even if they depend on the context of specific regions. However, a thick masonry wall could not always be linked to a higher seismic strength, because the interior of the pier might be composed of poor-quality material, as is often found, for instance, in several building of Central Italy, one of the areas with the highest seismic risk. Also the timber diaphragms feature structural elements with larger dimensions compared to those belonging to the Dutch context. Besides, in well-known Italian seismic areas, historical or existing buildings might already incorporate a number of measures against earthquakes, such as improved connections between floors and walls, or presence of ties enhancing the box behaviour of masonry.

Starting from the knowledge of the main characteristics of the analyzed masonry buildings, the following sections will focus on the evaluation of their seismic capacity, along with the role of the single structural components and their interaction.

2.3 Evaluation of seismic capacity of structural systems

2.3.1 Brief recall of structural dynamics

Before addressing the current methodologies for evaluating seismic capacity of existing buildings, and the main issues with reference to the Groningen framework, a brief summary of basic concepts from structural dynamics is presented, to better contextualize the subject.

By schematizing a building by means of a generic SDOF system (Fig. 2.2) having mass m , stiffness k , viscous damping coefficient c , and subjected to an earthquake excitation, its equation of motion reads [32]:



Figure 2.1: Examples of masonry buildings from the Dutch and the Italian context.

$$m\ddot{x}(\tau) + c\dot{x}(\tau) + kx(\tau) = -m\ddot{x}_g(\tau) \quad (2.1)$$

In the former equation, $\ddot{x}(\tau)$, $\dot{x}(\tau)$, and $x(\tau)$ are the acceleration, velocity, and displacement time-history responses of the system relative to the ground, respectively; $\ddot{x}_g(\tau)$ is the ground acceleration. Dividing Eq. 2.1 by m , and considering that the natural frequency of the system $\omega_n = \sqrt{k/m}$, and its damping ratio $\xi = c/(2m\omega_n)$, one obtains:

$$\ddot{x}(\tau) + 2\omega_n\xi\dot{x}(\tau) + \omega_n^2x(\tau) = -\ddot{x}_g(\tau) \quad (2.2)$$

This equation describes the complete response of the system in the time domain. However, for engineering purposes and to simplify the structural analysis, the following approximation has been considered: it can be sufficient to know only the maximum displacement $|x_{max}|$ (and thus, the maximum internal force) occurring during the response. This consideration led to the definition of the *response spectra*.

A response spectrum is a plot of the peak value of a response quantity (acceleration, velocity or displacement) as a function of the natural vibration period $T_n = 2\pi/\omega_n$ of the system, at a fixed damping ratio ξ . Fig. 2.3 shows the procedure to determine the response spectra: starting from a given ground motion (Fig. 2.3a), the displacement time-history induced by this seismic excitation is calculated for several SDOF systems having the same damping ratio (in Fig. 2.3b, three SDOF oscillators are considered, with $T_n = 0.5, 1$ and 2 s, at 2% damping ratio). For each system, the peak displacement value $|x_{max}|$ (or *spectral displacement* S_d) is recorded and reported in a graph as a function of

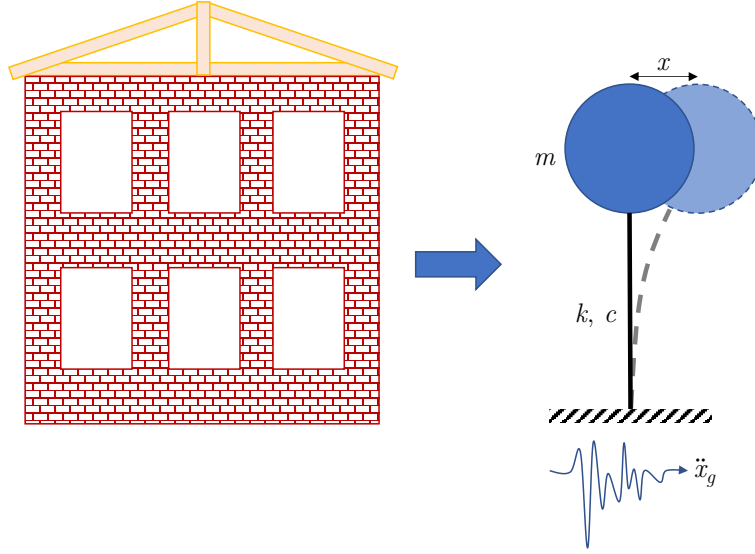


Figure 2.2: Representation of a building by means of an SDOF oscillator.

the period (Fig. 2.3c), obtaining the *displacement response spectrum*. In a similar way, having defined the quantities $\omega_n S_d$ (*pseudo-velocity* S_v), and $\omega_n^2 S_d$ (*pseudo-acceleration* S_a), the corresponding response spectra can be determined as well (Fig. 2.3d and e, respectively).

The pseudo-acceleration response spectrum is usually the reference plot adopted in seismic standards [3, 4], because it provides the peak pseudo-acceleration of a certain structure, according to its period: therefore, by knowing the excited mass, it is also possible to determine the maximum equivalent elastic force to which the system is subjected. The characteristic of this response spectrum is that for $T_n = 0$, S_a corresponds to the maximum acceleration of the seismic signal (*peak ground acceleration*, PGA), because an infinitely stiff structure vibrates by identically following the ground motion.

Consequently, design response spectra are always anchored to a specific value of PGA, provided by standards according to the location of the structure. Yet, the use of PGA only as potential indicator for structural damage implicitly accepts that no information on the potential earthquake duration is provided: this specific aspect can, instead, be of great importance for the Groningen case (Section 2.3.3). Before discussing more in depth the specific situation of the induced seismicity in the Northern part of the Netherlands, next section briefly recalls the available methods for seismic analysis of existing URM buildings, linked to the aforementioned concepts from structural dynamics.

2.3.2 Assessment of seismic capacity of URM buildings

According to current European seismic standards and guidelines for existing URM buildings [4], four types of analyses can be performed for assessing their seismic capacity, and herein briefly recalled:

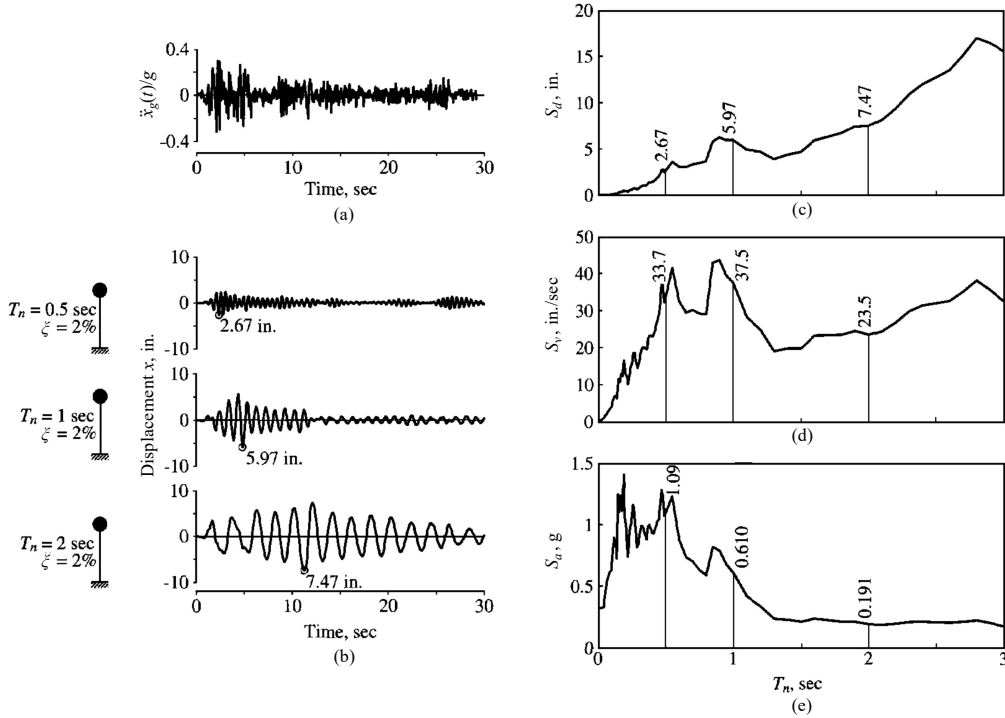


Figure 2.3: Procedure for deriving response spectra: ground acceleration (a); displacement response of SDOF systems (b); displacement response spectrum (c); pseudo-velocity response spectrum (d); pseudo-acceleration response spectrum (e). Adapted from [32].

- Equivalent linear static analysis (or lateral force method);
- Linear dynamic analysis (or modal analysis);
- Nonlinear static analysis (or pushover analysis);
- Nonlinear dynamic analysis (or time-history analysis).

The **equivalent linear static analysis** defines a series of forces acting at floor levels on a building to represent the effect of earthquake ground motion. The equivalent forces are calculated from a design response spectrum, and it is assumed that the building responds in its fundamental vibration mode. This strong hypothesis is only acceptable for low-rise and very regular (in plan and height) buildings. Therefore, the regularity of the structure allows for its schematization as SDOF system: after having determined the first (and dominant) natural period of the structure, the design response spectrum directly provides the pseudo-acceleration to which the building is subjected. The seismic capacity of the structure is then calculated in terms of a seismic base shear. This analysis is fully linear, therefore nonlinearities are schematized in a simplified way: a halved

stiffness of masonry elements accounts for cracks and damage [4], while ductility and energy dissipation of the structure are considered in a global parameter, defined as *behaviour factor* q , and reducing the seismic action because of these beneficial damping effects. For URM buildings, values of $q = 1.5 \div 2.5$ are recommended [3], therefore the seismic forces can be reduced up to 2.5 times for good-quality masonry buildings.

When the structures are less regular (in plan or height), the influence of higher vibration modes, besides the first one, becomes relevant. In this case, a **modal analysis** is necessary, because a building cannot be approximately considered as an SDOF system. For linear MDOF structures, Eq. 2.1 is then written in matrix form:

$$\mathbf{M}\ddot{\mathbf{X}}(\tau) + \mathbf{C}\dot{\mathbf{X}}(\tau) + \mathbf{K}\mathbf{X}(\tau) = -\mathbf{M}\mathbf{v}\ddot{x}_g(\tau) \quad (2.3)$$

In the former equation, \mathbf{M} , \mathbf{C} and \mathbf{K} are the mass, damping and stiffness matrixes, respectively; $\ddot{\mathbf{X}}(\tau)$, $\dot{\mathbf{X}}(\tau)$, and $\mathbf{X}(\tau)$ are the acceleration, velocity, and displacement vectors, respectively; \mathbf{v} is a versor describing the direction of the ground motion \ddot{x}_g . The MDOF structure is, thus, described as a system of equations, one per degree of freedom, which can be associated with each floor of the building. The single equation describes the response of a DOF having a certain frequency ω_n , and the overall seismic response of the MDOF system will be a combination of the responses of each DOF. The modal analysis is conducted considering the case of an undamped MDOF system in free vibration, thus $\mathbf{C} = \mathbf{0}$ and $\ddot{x}_g = 0$:

$$\mathbf{M}\ddot{\mathbf{X}}(\tau) + \mathbf{K}\mathbf{X}(\tau) = \mathbf{0} \quad (2.4)$$

The free vibration of an undamped system in one of its natural vibration modes, can be described mathematically by:

$$\mathbf{X}(\tau) = q_n(\tau)\phi_n \quad (2.5)$$

This is a combination of a deflected shape ϕ_n , which does not vary with time, and a harmonic function $q_n(\tau)$ describing the time variation of the displacements:

$$q_n(\tau) = A_n \cos \omega_n t + B_n \sin \omega_n t \quad (2.6)$$

Substituting this form of $\mathbf{X}(\tau)$ in Eq. 2.4 gives:

$$[-\omega_n^2 \mathbf{M}\phi_n + \mathbf{K}\phi_n] q_n(\tau) = \mathbf{0} \quad (2.7)$$

This equation can be satisfied in two ways. If $q_n(\tau) = 0$, then there is no motion of the system (trivial solution). On the contrary, if the system vibrates, then the natural frequencies ω_n and modes ϕ_n have to satisfy the *eigenvalue problem*:

$$[\mathbf{K} - \omega_n^2 \mathbf{M}] \phi_n = \mathbf{0} \quad (2.8)$$

Again, a trivial solution implying no motion is $\phi_n = 0$; the nontrivial solution is obtained when $\det [\mathbf{K} - \omega_n^2 \mathbf{M}] = 0$. The number of roots of this equation coincides with the number of DOFs, for which the corresponding *eigenfrequencies* are determined. Once a natural vibration frequency is known, Eq. 2.8 can be solved for the corresponding eigenvector ϕ_n (*natural modes of vibration*) to within a multiplicative constant: the eigenvalue problem does not fix the absolute amplitude of the vectors ϕ_n , but only

their shape. Therefore, the modal analysis provides the natural frequencies of each DOF: in this way, it is possible to associate these periods with a corresponding pseudo-acceleration from a design response spectrum. The pseudo-accelerations of each vibration mode are multiplied by the corresponding participating mass, and by combining all the resulting forces, an estimation of the global base shear can be obtained. In other words, this method essentially consists of a combination of single equivalent linear static analyses, but considers also the dynamic influence of all relevant mode shapes. For URM buildings, this analysis is useful to determine the eigenfrequencies, and to visualize the main natural modes of vibration, which can be of help in identifying specifically vulnerable portions of large or irregular structures.

The two aforementioned methods are fully linear, and therefore very simplified. A further step is introducing nonlinearities in materials and structural elements, while keeping an equivalent static procedure: these are the premises for the **pushover analysis**, a method widely adopted in the seismic assessment of URM buildings [33, 34]. The structure is subjected to a distribution of shear forces acting at floor levels (Fig. 2.4), similarly to the equivalent linear static analysis; alternatively, a distribution of displacements can be applied, if the analysis is displacement-based. These forces (or displacements) are progressively increased until the collapse of the structure is reached: with this procedure, the *capacity curve* is obtained, i.e. the plot showing the evolution of the base shear with the displacement of a reference node of the building (often at roof level, Fig. 2.4). In the pushover analysis, the MDOF system is schematized as an equivalent SDOF system. This is a strong assumption, similar to the hypothesis at the basis of the equivalent linear static analysis: the structure has to be regular, and a vibration mode ϕ_n (generally, the first one) should be dominant in the seismic response. The theoretical background of pushover analysis starts from rewriting Eq. 2.3 for nonlinear MDOF structures:

$$\mathbf{M}\ddot{\mathbf{X}}(\tau) + \mathbf{C}\dot{\mathbf{X}}(\tau) + \mathbf{R}(\mathbf{X}(\tau), \dot{\mathbf{X}}(\tau)) = -\mathbf{M}\mathbf{v}\ddot{x}_g(\tau) \quad (2.9)$$

In the former equation, \mathbf{R} is the vector of the internal resisting forces of the structure. The nonlinearities in the materials imply that \mathbf{R} depends on both the displacements and their time-history. Premultiplying Eq. 2.9 by ϕ_n , and substituting the deformed shape of the n-th mode of the MDOF system described through Eq. 2.5, one obtains:

$$\phi_n^T \mathbf{M} \phi_n \ddot{q}_n + \phi_n^T \mathbf{C} \phi_n \dot{q}_n + \phi_n^T \mathbf{R}(\phi_n q_n, \phi_n \dot{q}_n) = -\phi_n^T \mathbf{M} \mathbf{v} \ddot{x}_g \quad (2.10)$$

It is assumed that a distribution of forces \mathbf{F} proportional to the n-th mode acts on the structure, and keeps this load profile also in the nonlinear field. In this case:

$$\mathbf{R} \equiv \mathbf{F} = \mathbf{K}\mathbf{X} = \mathbf{M}\phi_n\omega_n^2 q_n \quad (2.11)$$

Substituting Eq. 2.11 in Eq. 2.10, the equation of a nonlinear SDOF system having dynamic characteristics equivalent to those of the n-th mode of the MDOF system is obtained:

$$\ddot{D}_n^* + 2\xi\omega_n\dot{D}_n^* + \omega_n^2 D_n^* = -\ddot{x}_g \quad (2.12)$$

with:

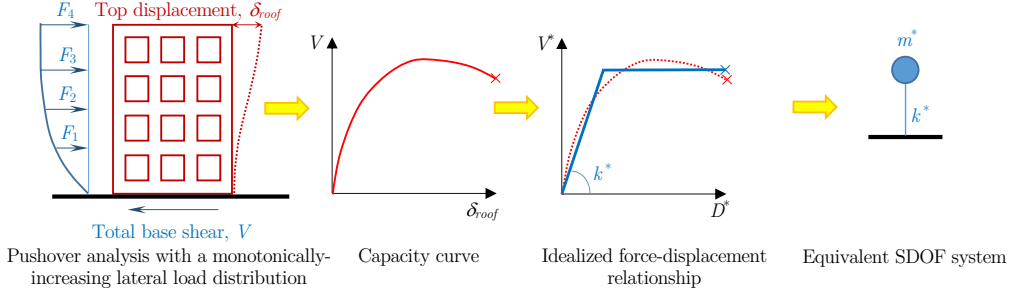


Figure 2.4: Principle and main steps of pushover analysis.

$$D_n^* = \frac{q_n}{I_n} \quad (2.13)$$

and

$$I_n = \frac{\phi_n^T \mathbf{M} \mathbf{v}}{\phi_n^T \mathbf{M} \phi_n} \quad (2.14)$$

The equivalent SDOF system has a mass $m^* = \phi_n^T \mathbf{M}$, and a stiffness k^* evaluated through an energy-equivalent bi-linearization of the capacity curve (Fig. 2.4). The MDOF and the SDOF system are then related to each other through the coefficient I_n . For assessing the seismic performance of the building, the capacity curve is compared to the demand, represented by a design response spectrum. For a visual estimation of the capacity, the two graphs are plotted in an acceleration-displacement diagram (Fig. 2.5), according to the procedure proposed by FAJFAR [35], and its refinement, specifically for URM buildings, introduced by GUERRINI et al. [36]. Since in the pushover analysis the cyclic hysteretic behaviour of materials is not taken into account from the capacity curve, the demand response spectrum may be over-damped (thus reducing the seismic demand), by means of a global system ductility value [35] or an equivalent viscous damping ratio [36] that have to be estimated based on the knowledge of the potential dissipative characteristics of the structural components. This analysis appears to be suitable for sufficiently regular buildings, but for specific configurations it might be difficult to represent a whole structure through a single reference node, especially when irregularities or flexible diaphragms are present [37]. A sufficient floor stiffness is thus necessary for the pushover analysis to be conducted, and this specific aspect might also have contributed to the usual past retrofitting interventions that excessively stiffened the timber floors.

The last method for seismic assessment is the **time-history analysis**, in which the full nonlinear and cyclic response of the building is considered. Once a correct and accurate numerical model of a building can be realized, this analysis is the most complete and realistic, because it consists of subjecting the structure to an actual earthquake signal and fully calculating the seismic response in the time domain, by solving Eq. 2.9; the main drawbacks of this method are the high computational cost and the required knowledge of the hysteretic behaviour of structural components. Given the different nature of dynamic signals, the standards [3, 4] prescribe that the structure has

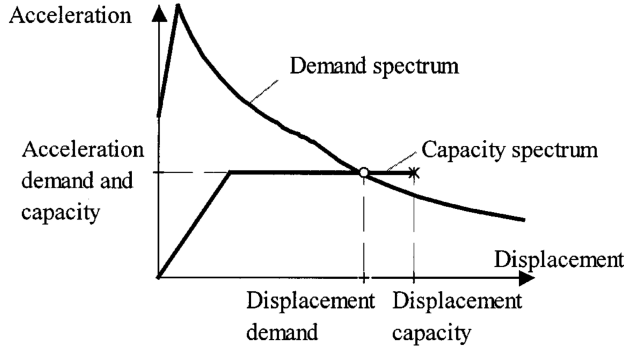


Figure 2.5: Comparison between pushover capacity curve and (overdamped) demand response spectrum in the acceleration-displacement diagram (from [35]).

to be subjected by several seismic accelerograms, which should be compatible to the design response spectrum of a specific location. If at least seven signals are used, then the mean structural response can be considered; if only three accelerograms are adopted, then the worst case has to be taken into account. The analyses are usually conducted by starting from a small-amplitude seismic signal, and progressively increasing the intensity until the collapse of the structure is reached. For this reason, they are also known as *nonlinear incremental dynamic analyses*. The seismic capacity of the building is identified in terms of both force-displacement response, and also PGA (or spectral acceleration linked to first-mode period) at collapse. Although the use of PGA and the link to response spectra is still present because of provisions from standards, load duration and structural damage are fully taken into account with this method.

Hence, nonlinear time-history analyses will be the main tool adopted in this dissertation for evaluating the seismic performance of URM buildings with (retrofitted) timber diaphragms. However, because a deep knowledge of the material, damping and cyclic properties of structural components is needed, both experimental and analytical studies will be performed, to provide accurate input to the numerical analyses. Therefore, after briefly addressing the specific case of the induced Groningen earthquakes, an extensive literature review will be presented in Sections 2.4 to 2.7, in order to describe the state of the art on seismic assessment and retrofitting of timber diaphragms, timber-masonry connections, masonry walls, and their mutual interaction in existing buildings.

2.3.3 The case of the induced earthquakes in the Province of Groningen

In the previous section, the main methods for seismic assessment of URM buildings were summarized. It can be noticed that ground-related parameters such as PGA play an essential role in these analyses, but may not be sufficient to describe the specific situation of the induced earthquakes in the Groningen area.

In this region of the Netherlands, large on-land gas reservoirs are present with considerable national economic importance, and which have been exploited since 1960. Yet, during the last decades, this gas extraction has initiated small-magnitude (up to now maximum $M_L = 3.6$ on the Richter scale), shallow seismic events [29].

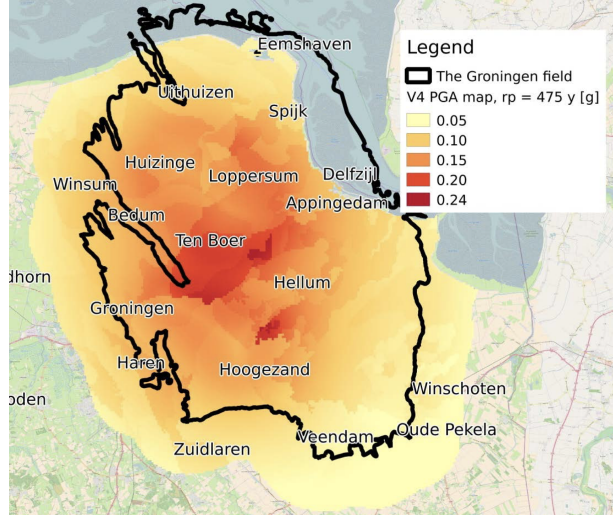


Figure 2.6: Probabilistic seismic hazard map for the Groningen area, referred to a return period of 475 years. The black solid line indicates the boundary of the Groningen gas field. From [39].

The rising seismicity has also caused light structural damage to local buildings, and growing concern to the population. Consequently, a method has been established, in order to assess the future likelihood of ground motion events, known as *Probabilistic Seismic Hazard Assessment* (PSHA) [31]. PSHA consists of two essential elements: the *seismological model* and the *ground motion model*. The combination of these two elements results in an estimate for the probability distribution of future ground motion events at a site of interest.

The aim of the seismological model is to predict how induced earthquakes are generated, in terms of location, magnitude and recurrence. This prediction starts from specific geotechnical models, which for the Groningen case have been based on an empirical stochastic relationship between strain partitioning and reservoir compaction [31].

The ground motion model refers to a distribution of values of a strong motion parameter (often PGA) at a certain distance from an earthquake with given magnitude. These values are usually determined through empirical equations [38], and also for the Groningen case seismic hazard curves in terms of PGA have been derived (Fig. 2.6) for every location near to the seismically active zones, as a function of reference return periods. Subsequently, a set of *earthquake scenarios* for local structures has been defined in terms of bands of PGA: this indicates a reasonable correlation between PGA and the probability of failure. Therefore, this parameter plays a key role in the probabilistic seismic hazard and risk assessment of Groningen induced earthquakes, and this is reflected in the current Dutch seismic guidelines (NPR 9998) as well [27].

However, the link between PGA and structural damage has been derived based on tectonic earthquakes, for which the load duration and damaging potential are different from the induced Groningen seismic events. PANZA et al. [28] recognize that PGA is the most commonly used measure of amplitude of a particular ground motion. Since inertial forces depend directly on acceleration, PGA is one of the parameters widely

used to describe the intensity and damage potential of an earthquake at a given site. However, the authors also point out that PGA is a poor indicator of damage, since it has been observed that time histories with the same PGA could be very different in frequency content, strong motion duration, and energy level, thus causing varying amounts of damage. In fact, PGA may be associated with high frequency pulses which do not produce significant damage to the buildings, as most of the impulse is absorbed by the inertia of the structures with little deformation. On the other hand, a more moderate acceleration may be associated with a long-duration pulse of low-frequency leading to significant deformations of the structure.

For instance, after the 1971 Ancona earthquake (Richter magnitude $M_L = 4.7$) a large PGA value (716 cm/s^2) was recorded at Rocca station, located at a distance of about 7 km from the surface projection of the fault rupture. However, this high PGA value was associated to a short duration pulse of high frequency, as indicated in Fig. 2.7a, and generated limited damage. A PGA close (827 cm/s^2) to the aforementioned one, was recorded at the Sylmar station (Fig. 2.7b), sited at about 2 km from the surface projection of the fault rupture, after the destructive 1994 Northridge earthquake (moment magnitude $M_w = 6.7$). In this case, PGA is associated to a long-duration pulse of low frequency. The moderate difference between these two PGA values seems to disagree with both the large difference in magnitude of the two seismic events, and the notably different damage to existing structures (Fig. 2.7). In other words, even small earthquakes can produce high accelerations that are not necessarily damaging.

It should be noticed that this conclusion can be applied to induced Groningen earthquakes as well, given their specific high-frequency, low-duration nature. This also means once more that, in general, response spectra only are not sufficient for the estimation of the damage potential of the earthquake ground motion, because they cannot describe precisely the quantity of energy (imparted by the earthquake) that will be dissipated through hysteretic behaviour, and they cannot account for load duration [28]. Consequently, having as a goal the optimization of URM buildings through a dissipative retrofitting of timber diaphragms, PGA cannot be the single parameter describing the seismic capacity (or performance) of these buildings. An extended approach has to be formulated, so that the optimal behaviour of a URM building can be identified in a more general way, also accounting for specific characteristics of the context or of the earthquake type (tectonic or induced).

2.4 Seismic behaviour of timber diaphragms

2.4.1 General

The mechanical behaviour of existing timber diaphragms is largely dependent on the conditions and the properties of their structural elements, usually consisting of beams (or joists), on which boards (or planks) are fastened. The state of timber members plays an essential role, because possible phenomena of decay and degradation can cause a significant decrease in structural performance. Equivalently, properties such as density, dimensions, and moisture content of the diaphragms, as well as the arrangement of joists and planks, strongly influence the behaviour of the floors.

When performing a structural assessment of existing diaphragms, these factors have to be taken into account, independently of the loading direction: with static loads, a floor

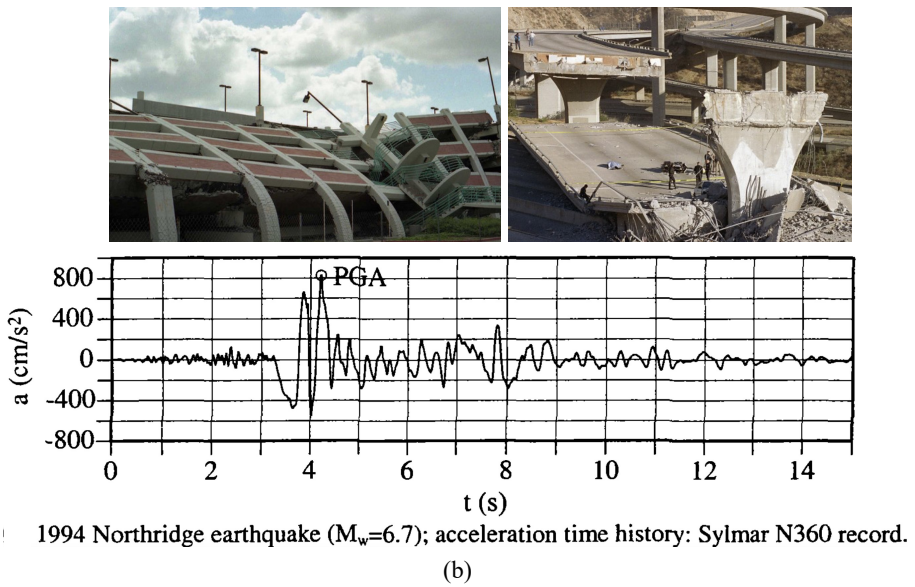
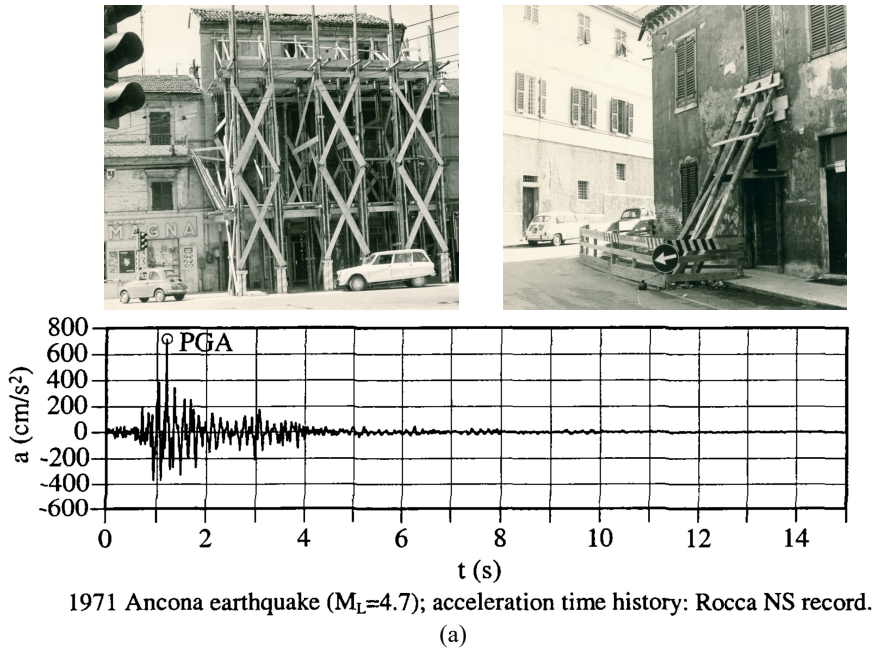


Figure 2.7: Comparison between the 1971 Ancona earthquake signal (a) and the 1994 Northridge accelerogram (b). Although the PGA was similar, way different damage was observed after the two earthquakes. Adapted from [28],[40]-[42].

is solicited out of its plane; with seismic loads in its plane, but in both cases conditions and properties of timber members are key aspects to investigate. Therefore, such aspects will also be highlighted when examining previous research studies, discussed in the next section, focusing on the earthquake-related in-plane response of timber diaphragms.

2.4.2 Relevant research studies on the in-plane response of as-built and retrofitted timber diaphragms

Timber diaphragms are often present in many old, historical or existing buildings and houses, and are therefore part of the architectural heritage of several countries. Due to the fact that the (historical) construction techniques are context-dependent, it is still difficult to get comprehensive data on the structural behaviour of the floors under seismic loading. In general, given the very simple structure of timber diaphragms, with a thin sheathing of planks nailed to the main joists, their in-plane performance is often poor, and not sufficient to transfer the expected seismic loads on the walls. If, then, the floors are not even well connected to the walls, an existing building can become very vulnerable to earthquakes due to the risk of (local) collapses of masonry walls.

Therefore, several experimental campaigns have been conducted on the in-plane behaviour of timber diaphragms in the recent years, especially to perform a seismic assessment of the as-built floors, and to develop and test many strengthening techniques for improving their in-plane behaviour. A number of relevant research studies will be summarized, covering different contexts in Europe, the United States and New Zealand, and investigating the structural response to earthquakes of the floors. In the following, the dimensions and static schemes of the tested diaphragms will all be reported at the same scale, in order to show the variety of configurations and testing methods adopted.

A relevant study on the in-plane behaviour of timber diaphragms in monumental buildings was performed by PIAZZA et al. [15] and BALDESSARI [16]: an extensive experimental campaign on as-built and differently refurbished timber floors was conducted. The full-scale diaphragms (Fig. 2.8) measured 5200×4000 mm and were composed by 180×180 mm GL24C [43] beams arranged in the direction parallel to load, and 200×30 mm C22 [44] planks. The beams were 4200 mm long, and arranged at 500 mm spacing, while the straight-sheathed planks had different longitudinal dimensions, varying from 600 to 1600 mm. When the planks intersected each beam, the connection was realized by means of four 2.8×80 mm nails. The test set-up was designed in such a way that it was possible to test the whole floor with a good approximation of a distributed horizontal load, due to the four points of application of force. Besides the as-built configuration, a number of retrofitting techniques were applied and tested:

- Overlay of planks arranged at 45° with respect to the existing sheathing;
- Diagonal bracing of the existing wood planks by means of light-gauge steel plates;
- Diagonal bracing of the existing wood planks by means of fiber-reinforced polymer (FRP) laminae;
- Superposition of three layers of plywood panels glued on the existing wood planks;
- Cast of a reinforced-concrete (RC) slab connected by means of steel studs (a very common intervention applied in practice for stiffening timber diaphragms, also known as the TURRINI-PIAZZA method [17]).

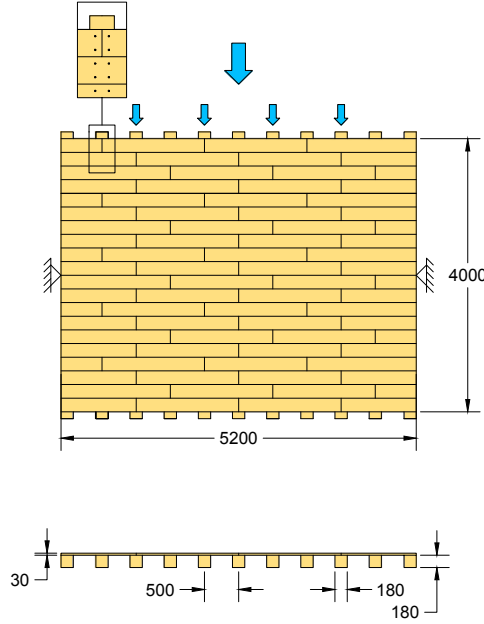


Figure 2.8: Timber diaphragm sample tested by [15, 16]; dimensions in mm.

Quasi-static reversed-cyclic tests were performed under displacement control, following the procedure of EN 12512 [45]. All retrofitting techniques provided a moderate to considerable increase in in-plane stiffness: by 10 times with the overlay of planks; by 20 to 50 times with the diagonal bracing systems (where the FRP strips appeared to be more effective than the light-gauge nailed plates); by 100 times with the concrete slab and the glued plywood panels.

CORRADI et al. [18] focused on floor typologies widespread in the Italian and European context. The specimens represented a half of the floor, and the setup allowed for a single point of application of load (Fig. 2.9); monotonic tests were conducted. The diaphragms measured 3000×3000 mm, and their structure was composed of the following elements:

- Main $180 \times 180 \times 3100$ mm chestnut beams, parallel to load, at 1100 mm spacing;
- Secondary rafters ($80 \times 80 \times 1100$ mm), orthogonal to load, positioned on the beams at 300 mm spacing;
- Planking realized with $125 \times 18 \times 600$ mm elements connected to the rafters only at their ends with one or three nails, depending on the specimen.

Three strengthening techniques were tested: an overlay of planks arranged at 90° with respect to the existing sheathing; the cast of an RC slab; a diagonal bracing with FRP laminae, similarly to [15]. The overlay of planks slightly increased the strength of the samples, but was not so effective in improving the in-plane stiffness, which was, instead, significantly enhanced with the other two strengthening techniques.

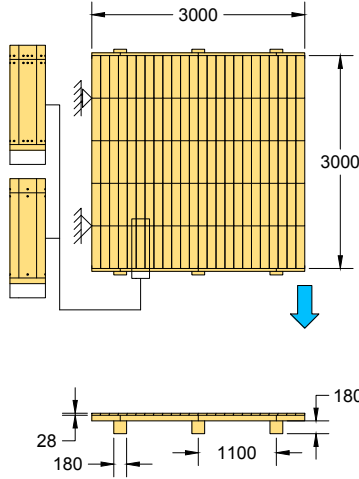


Figure 2.9: Timber diaphragm sample tested by [18]; dimensions in mm.

VALLUZZI et al. [19, 20] analysed the in-plane behaviour of traditional timber diaphragms and a number of strengthening techniques. The diaphragms measured 2120×2120 mm and were composed of $120 \times 140 \times 2420$ mm spruce beams at 500 mm spacing, and 135×20 mm spruce planks, connected to them by means of two 2.75×60 mm nails placed at every intersection among the elements. The in-plane load was applied in a single point (Fig. 2.10), and monotonic tests were conducted. Besides the non-strengthened diaphragm, five main types of retrofitted configurations were tested:

- Fastening of a diagonal punched metal strip;
- Overlay of planks placed at 45° with respect to the existing sheathing, either using common or tongue-and-groove boards;
- Double overlay of planks placed at 45° with respect to the existing sheathing, using tongue-and-groove boards;
- Fastening of a single diagonal board, equivalent to the punched metal strip;
- Fastening of two diagonal thick timber boards.

The tests showed, in general, a better performances of tongue-and-groove connections among boards for all configurations. The retrofitting intervention consisting of the double overlay of planks was the most efficient, followed by the single boards overlay and the diagonal strengthening.

The innovative use of engineered wood products, such as cross-laminated timber (CLT), oriented strand board (OSB), or plywood panels was also studied with the purpose of seismic retrofitting of existing diaphragms. BRANCO et al. [21] conducted an experimental campaign aimed at quantifying the improvement in in-plane stiffness gained with a traditional strengthening technique (overlay of planks placed at 90° with respect to the existing sheathing), and by means of differently arranged CLT timber panels fastened on the as-built floors. The timber diaphragms consisted of $100 \times 160 \times 2420$

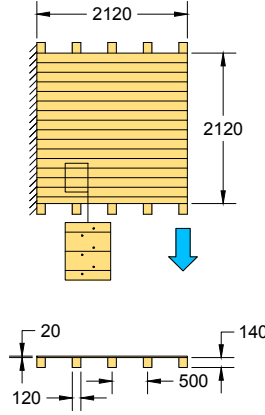


Figure 2.10: Timber diaphragm sample tested by [19, 20]; dimensions in mm.

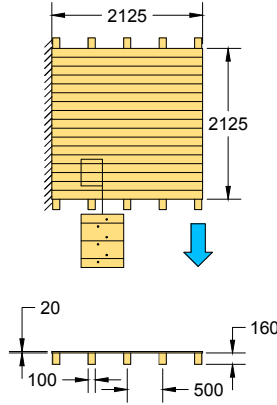


Figure 2.11: Timber diaphragm sample tested by [21]; dimensions in mm.

mm C24 [44] beams at a heart-to-heart distance of 500 mm, and of $125 \times 20 \times 2125$ mm straight-sheathed planks connected to them with two 2.5×60 mm nails at every intersection. The analysed floors represented a portion of $1/4$ of a real diaphragm and measured 2125×2125 mm in total (Fig. 2.11). The floors were monotonically tested, and the load was applied in a single point. The results showed that strengthening using a second layer of boards could double the stiffness of the as-built floors, while the specimens retrofitted with CLT panels were approximately five to ten times stiffer than the non-strengthened diaphragms.

Use of CLT and OSB panels as retrofitting technique was also investigated by GUBANA and MELOTTO [22]. The diaphragms were composed of $160 \times 160 \times 3000$ mm beams at 500 mm spacing, and $23 \times 145 \times 3160$ mm planks, fastened to the joists with two 2.5×65 mm nails. The floor were monotonically and cyclically tested, and the load was applied in a single point (Fig. 2.12). An improvement in stiffness of 6 to 7 times compared to the as-built samples was achieved, along with a strongly nonlinear behaviour of the diaphragms, with cyclic energy dissipation. Besides, the proposed

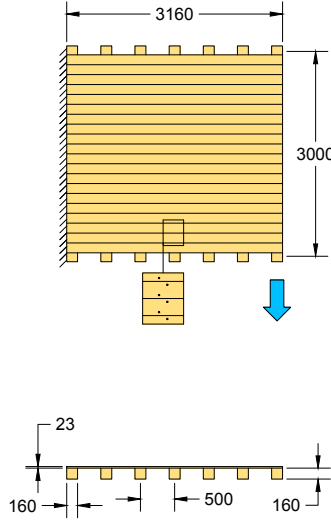


Figure 2.12: Timber diaphragm sample tested by [22]; dimensions in mm.

interventions appeared to be reversible and minimally invasive, and were identified as efficient solutions for the seismic retrofit of existing buildings in seismic-prone areas.

PERALTA et al. [23] investigated the use of a plywood panels overlay for retrofitting timber diaphragms with typical characteristics of the US context. The test setup was designed to study a whole floor subjected to an in-plane load applied in two points (Fig. 2.13). The diaphragms measured 7320×3660 mm, and were composed of $38 \times 235 \times 3660$ mm joists at 406 mm spacing, and 140×19 mm planks with various lengths. The connection of the sheathing to the beams was realized by means of two common 8d nails at every intersection, except for the ends of each plank, in which three nails were positioned. All structural elements were made of local South-American pine wood. Cross-bridging members for laterally supporting the joists were also present, to reproduce the construction techniques of US pre-1950 diaphragms. Bridging was typically made of short wood boards that were set nailed diagonally between joists to form an “X” pattern perpendicular to them. In this case, the specimens featured two rows of bridging elements, placed at 1220 mm from the floor edges, and with a cross section of 38×89 mm. The retrofitting with plywood panels was realized in two ways:

- An unblocked configuration, in which the panels were simply fastened to the existing floor;
- A blocked configuration, in which additional timber elements were placed in between the joists, in correspondence to the panels edges, and the panels were nailed through the sheathing to these timber blocks; additional fasteners were also used, compared to the unblocked configuration.

Both strengthening techniques greatly improved the in-plane response of the diaphragms compared to the as-built configuration, but the blocked configuration exhibited an approximately doubled stiffness with respect to the unblocked one.

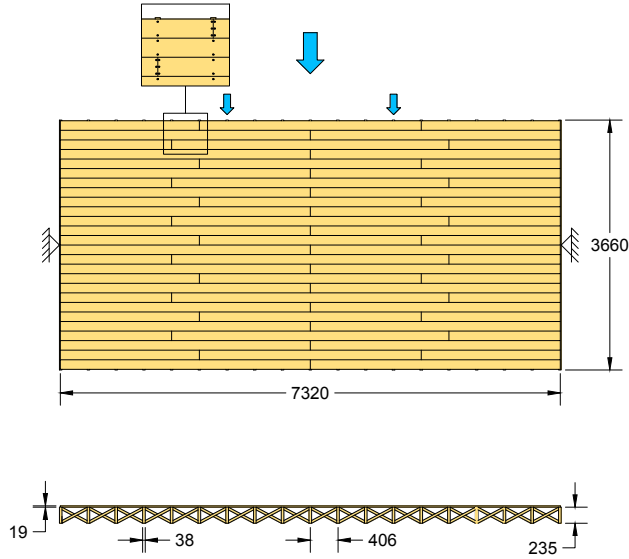


Figure 2.13: Timber diaphragm sample tested by [23]; dimensions in mm.

A plywood panels retrofitting solution was also examined by BRIGNOLA et al. [24], with reference to the New Zealand building context. The setup was designed to test whole floors subjected to a horizontal load applied in two points. The diaphragms measured 4000×3000 mm and were composed by $20 \times 250 \times 4000$ mm *Radiata* pine joists at 500 mm spacing, and 150×25 mm pine planks with a length of 1000 or 2000 mm. The connection of the sheathing to the beams was realized by means of two 3.15×75 mm nails at every intersection, and also at the ends of each plank two nails were positioned. The tests were performed according to EN 12512 [45], and a great enhancement of the in-plane properties of the retrofitted diaphragms, compared to the as-built ones, was noticed: strength, stiffness, and energy dissipation were strongly improved.

WILSON et al. [25] conducted an experimental campaign on a series of as-built and retrofitted timber floors, focusing on their orthotropic behaviour: the full-scale floors were tested in the two in-plane loading directions, parallel and perpendicular to the main joists. In order to simulate a distributed seismic load, the diaphragms were subjected to cyclic in-plane forces applied in four points (samples tested parallel to the joists, Fig. 2.15a) or two points (samples tested orthogonal to the joists, Fig. 2.15b). The diaphragms measured 10400×5500 mm and were composed by $45 \times 290 \times 5500$ mm joists at 400 mm spacing, and 135×18 mm planks with various lengths. The connection of the sheathing to the beams was realized by means of two 3.15×75 mm nails at every intersection, and also at the ends of each plank two nails were positioned. In order to ensure the stability of the floor, at 1845 mm spacing a 45×75 mm cross bracing system was positioned in the samples tested parallel to the joists, while for the specimens tested perpendicular to the joists the bracing system was substituted with blocks having the same cross-section as the main joists. The adopted retrofitting technique consisted of an overlay of structural plywood panels, which enabled a great improvement of in-plane strength, stiffness and energy dissipation of the diaphragms. Interestingly, both

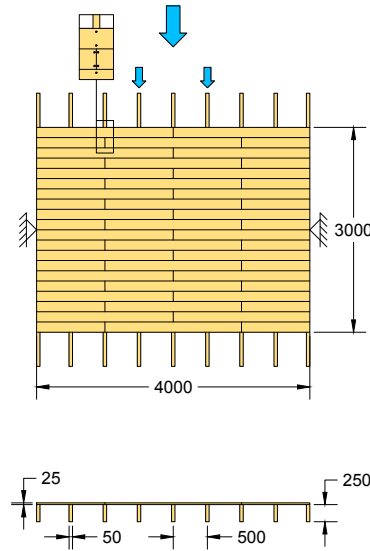


Figure 2.14: Timber diaphragm sample tested by [24]; dimensions in mm.

the as-built and strengthened samples showed an orthotropic behaviour, which could, however, be potentially mitigated with specific detailing.

The previous research studies provided useful information on the in-plane response of as-built and differently retrofitted timber floors; however, all samples were built with new material prior to testing them in laboratory: this could lead to an overestimation of the relevant in-plane properties of especially the as-built floors, as explicitly stated in [15, 16, 24]. Therefore, GIONGO et al. [26] conducted an in-situ testing campaign in a masonry buildings with timber floors typical of New Zealand. Two portions of diaphragm were tested, which presented structural elements made of native wood species (*Rimu* and *Matai*). The floors had $50 \times 300 \times 4700$ mm joists at 450 mm spacing, and 122×22 mm planks with various lengths. To ensure an appropriate lateral support to the joists, the floor presented also cross-bracing elements between the joists, at 1500 mm spacing. Additionally, 50-mm-thick timber blocking elements were placed on the floors supported edges, to improve the otherwise poor connection to masonry. Cyclic tests were carried out on different configurations: an as-built one, a re-nailed one, and a retrofitted one. The strengthening method consisted, also in this case, of a plywood panels overlay. The panels were arranged aiming at creating an interlocking effect, to reduce a possible orthotropic response, noticed in [25]. The static scheme and the floors characteristics are reported in Fig. 2.16: as can be noticed, a distributed load was applied to the diaphragms. A relevant stiffening effect was noticed after retrofitting the floors, but also the simple re-nailing of planks proved to be beneficial to increase the in-plane performance of the diaphragms.

From the reported relevant research studies on the in-plane response of timber diaphragms, a large variety of retrofitting techniques, configurations, static schemes, and testing methods is noticeable. Although the results of these studies provided new

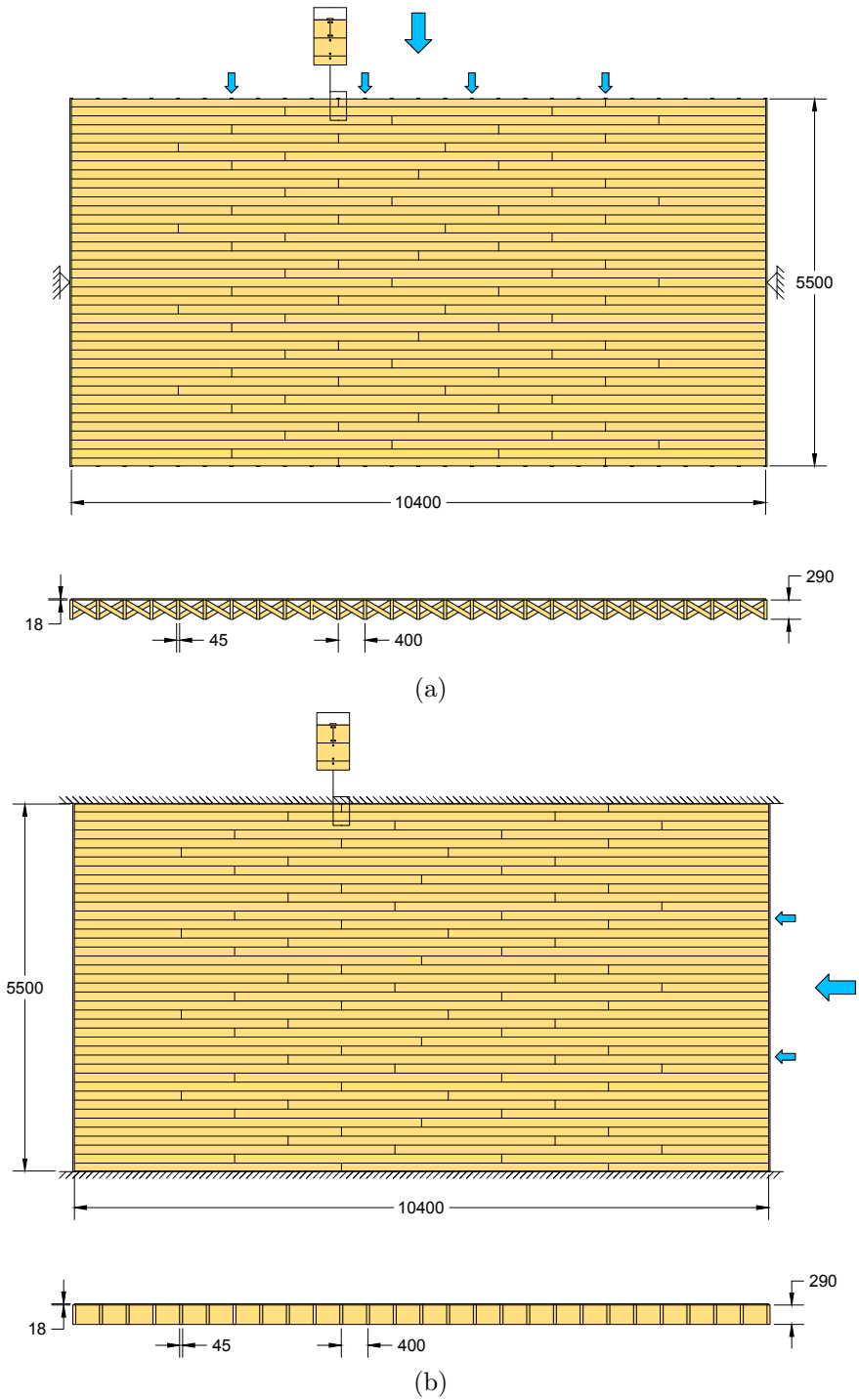


Figure 2.15: Timber diaphragm samples tested by [24]: (a) specimen loaded parallel to the joists, (b) specimen loaded perpendicular to the joists; dimensions in mm.

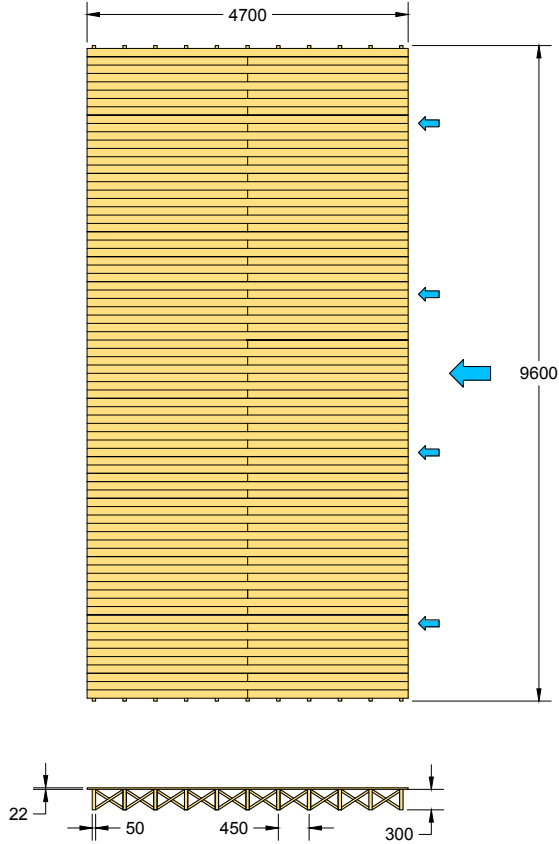


Figure 2.16: Timber diaphragm samples tested by [25]; dimensions in mm.

and useful information on the subject, the outcomes are still context-dependent, and especially not comparable among each other as they are reported, mainly because of the different assumptions and standards adopted for evaluating the in-plane stiffness, as discussed in the next section.

2.4.3 Methods for the calculation of the in-plane stiffness of timber diaphragms

A common way to homogenize the in-plane stiffness values of timber diaphragms is to adopt a size-independent parameter, the so-called *equivalent shear stiffness* G_d :

$$G_d = G \cdot t \quad (2.15)$$

In the former equation, G is the global shear modulus of the floor, and t the thickness of the floor planking. It is important to underline that this parameter can be considered reliable for diaphragms for which the in-plane behaviour can be assumed as shear-related, such as the strengthened ones; for as-built floors with continuous planks and joists, the flexural response is dominant, and hence G_d is size-dependent and loading-direction-dependent [25, 46, 47]. Furthermore, because of the highly nonlinear response of timber diaphragms, the use of a single standardized stiffness value could lead to a poor estimation of their in-plane properties. Yet, as will be discussed in Section 2.7, the stiffness of timber floors plays a crucial role in the seismic response of existing buildings, thus a better characterization of the diaphragms would be necessary.

In the previously presented research studies, the authors adopted different standards to determine the in-plane stiffness and strength of timber diaphragms from experimental tests. The inhomogeneity in available data does not only depend on the different contexts or standards (from testing protocols to stiffness calculations), but is also related to authors' assumptions, leading to not uniform results.

A widely applied standard for stiffness calculation is EN 12512 [45]. Although this standard is intended for timber joints, especially in the European context it is often adopted also for determining the in-plane stiffness of timber floors. According to the formulation in the standard, the stiffness is calculated after determining a conventional yielding point on the experimental load-displacement backbone curve; two different methods are prescribed:

- If the load-displacement curve is clearly defined by two linear parts, then the yielding point is found as the intersection of the lines tangent to these two branches (Fig. 2.17a);
- When the load-displacement curve is not composed of two linear parts, after defining the maximum (peak) load F_{max} , the yielding point is found as the intersection of two lines defined as follows: the first one intersects the two points on the load-displacement curve corresponding to $0.1F_{max}$ and $0.4F_{max}$, while the second one is the line tangent to the load-displacement curve, having a slope of $1/6$ with respect to the first one (Fig. 2.17b). This procedure almost always applies to describe the seismic response of timber diaphragms, due to their usual strong nonlinearity.

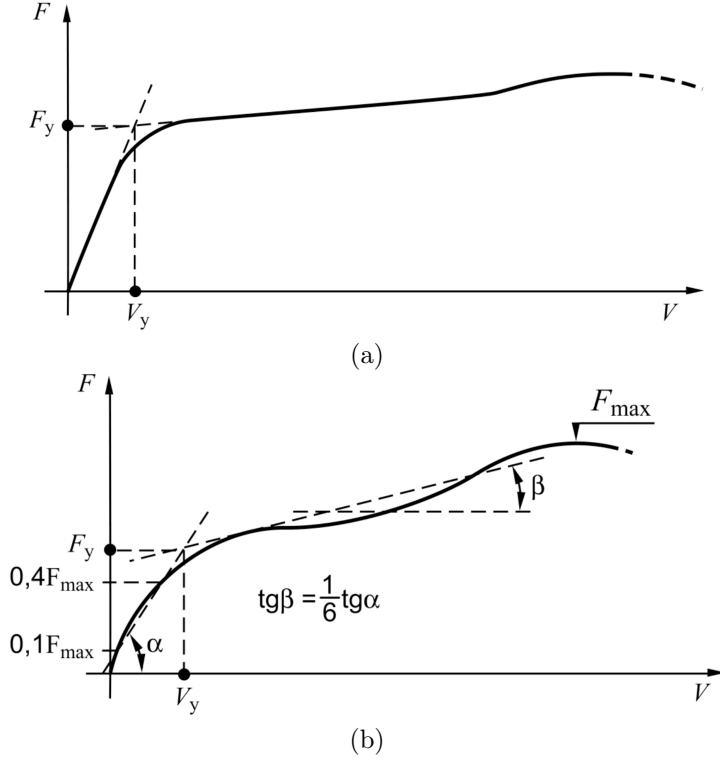


Figure 2.17: (a) Definition of yield values for a load-slip curve with two well-defined linear parts; (b) definition of yield values for a load-slip curve without two well-defined linear parts. From [45].

The main issue of this formulation is related to the choice of the value of F_{max} for flexible diaphragms: in fact, while for instance PIAZZA et al. [15] and GUBANA and MELOTTO [22] refer to the entire load-displacement curve, VALLUZZI et al. [19, 20] and BRANCO et al. [21] consider also the fact that the maximum force should not correspond to a too large value of displacement, which would imply an out-of-plane collapse of the masonry walls supporting the floor in an existing building. Therefore, the value of F_{max} to be chosen in this second case should not be the absolute maximum one, but the highest level of load in an acceptable displacement range.

Another standard adopted for the calculation of the stiffness of the diaphragms is ASTM E 519-81 [48]. This standard was developed as a guideline for experimental set-up and interpretation of the diagonal compression test on masonry, in order to evaluate its shear strength. The shear stiffness is evaluated at the secant stiffness at 1/3 of the maximum load. This same procedure was applied for timber diaphragms by CORRADI et al. [18].

The American guidelines FEMA 273 [49], FEMA 356 [50], and ASTM E 2126 standard [51] are also relevant to this subject. Both FEMA guidelines were adopted by PERALTA et al. [23]; ASTM E 2126 was instead referred to in WILSON et al. [25]. For all three cases, the formulation consists of the definition of a simplified bilinear backbone

curve that approximates the experimental one: this equivalent bilinear system is found in such a way that it presents the same energy absorption as the real system, and this determines the initial stiffness as well. While for FEMA guidelines the bilinear curve has a hardening phase, for ASTM E 2126 it is elastic-perfectly plastic (Fig. 2.18).

The aforementioned standards were all adopted for calculating the stiffness of the diaphragms from the experiments. Yet, when performing in practice a seismic assessment and retrofitting of existing buildings, only indicative values of G_d could be used. Some suggested values are provided again in the FEMA guidelines, as well as in ASCE/SEI 41 [52] for the American context, and in the NZSEE standards [53] for the New Zealand one. These values also account for the conditions of the diaphragms (good, fair, or decayed), but the estimation of their in-plane stiffness appears to be quite poor, as underlined by several studies [23, 24, 25, 47]. The reasons for this poor estimate are mainly related to the direction-dependent and size-dependent response of the as-built floors, to the nonlinear behaviour of the diaphragms, and to the influence of e.g. different amount of nails/screws, or sizes and structure of panels or planks. Thus, for a thorough seismic assessment and an aware design of retrofitting methods for timber floors, the present way of schematizing the in-plane response appears to be not sufficient, because a single value of shear stiffness cannot account for orthotropy, nonlinearity, and potential energy dissipation of the diaphragms.

2.5 Seismic behaviour of connections between timber floors and masonry walls

Although the connections among timber diaphragms and masonry walls play an essential role in the global seismic response of existing buildings, few research studies were conducted, having this topic as specific focus. Furthermore, similarly to what observed for timber diaphragms (Section 2.4), the available results are again context-dependent.

For the US framework, LIN and LAFAVE [54] conducted an extensive campaign on compact samples representing as-built timber-masonry connections. The specimens consisted of either a joist embedded in a masonry pocket with mortar, or the same configuration with the additional presence of a nailed anchor. Quasi-static monotonic or cyclic, and dynamic cyclic tests were performed. In the latter loading protocol, ten high-frequency cycles at the same amplitude were repeated, and the signal was progressively scaled to describe the full nonlinear behaviour of the connections. The samples were very compact (Fig. 2.19), so that the response of the whole wall portion around the joint could not be captured, while the frictional response and the failure modes of nails and anchors were thoroughly characterized. Due to the specific configuration of the connections, the detected response was asymmetric: when pulling the joist, only the nails and the anchor could resist the load, while in the opposite direction also the masonry bricks played a role.

As-built and retrofitted wall-to-floor connections with Portuguese features were studied by MOREIRA et al. [55, 56], by performing pull-out and cyclic tests on full-scale samples. The proposed strengthening solution consisted of a tie rod anchoring the wall to the joist through a steel angle. Several elements of the connection were tested (nails, rings, steel brackets, ties), and their various failure modes were identified and discussed. Besides, the large dimensions of the tested samples (Fig. 2.20) enabled to account for

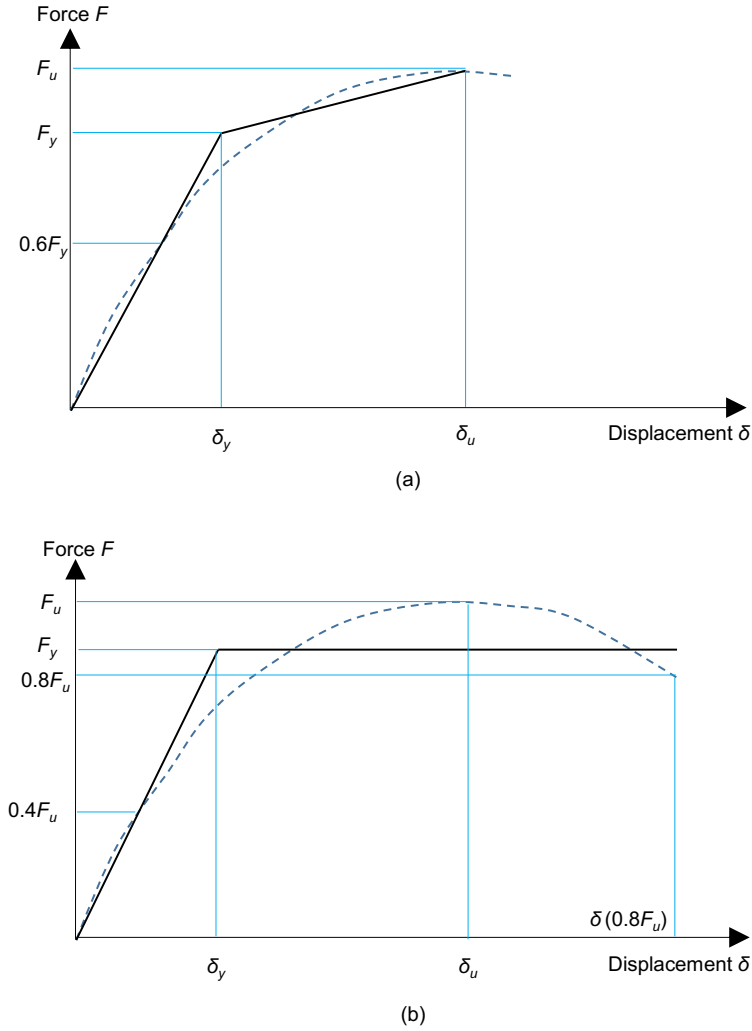


Figure 2.18: Bilinear methods for schematizing the experimentally obtained backbone curves: (a) procedure according to FEMA guidelines [49, 50], (b) elastic-plastic bilinearization according to ASTM E 2126 [51]; both methods are based on the principle of the energy equivalence between the two curves.



Figure 2.19: Side and front view of samples representing timber-masonry connections. From [54].

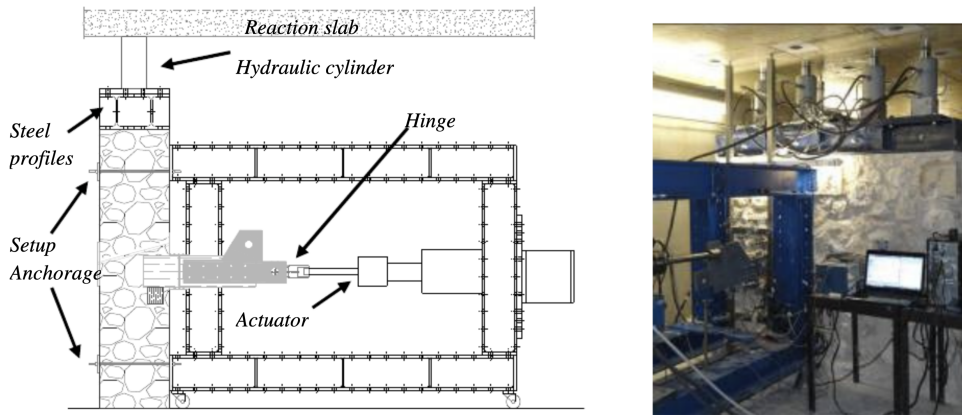


Figure 2.20: Test setup and picture of a timber-masonry joint sample. From [55].

the effect of the masonry portion around the floor joist, as well as the influence of the wall thickness. It should be noticed that the specimens featured massive masonry components, which are not to be expected for the Dutch context.

Finally, DIZHUR et al. [57] conducted in-situ monotonic tests on two unreinforced masonry buildings in New Zealand (Fig. 2.21): plate anchor and timber blocking connection types were studied, and failure modes were thoroughly discussed. Timber joist splitting was the most commonly observed failure mode for the plate anchor connections, showing that its capacity was mainly governed by the conditions of the timber joist or the characteristics of the wall. Instead, the existing connections realized with timber blocks anchored to the masonry showed great ductility, but in general less capacity compared to plate anchors.

Although limited research has been conducted on the topic of timber-masonry connections, the available results highlighted the seismic inadequacy of as-built joints, when no anchoring element is present between the timber floor joists and the masonry walls. Furthermore, only one retrofitting method was investigated, with reference to the Portuguese context [55, 56]. Yet, the role of the connections between walls and

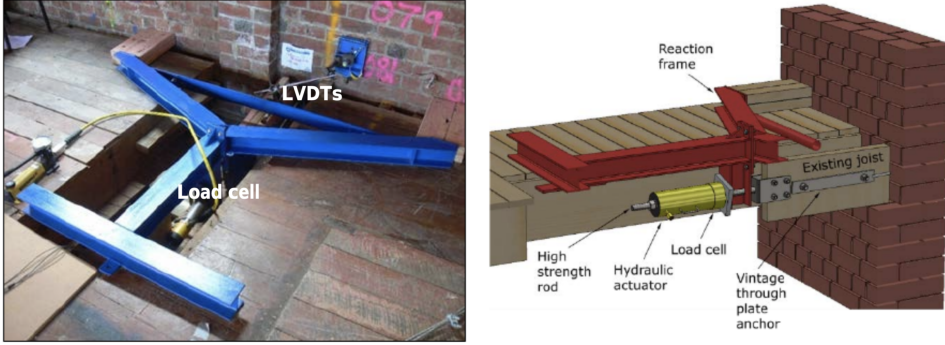


Figure 2.21: In-situ test setup for timber-masonry connections. From [57]

diaphragms is essential, because these joints are responsible for the shear transfer on structural components, as well as for the overall box behaviour of a building.

2.6 Seismic behaviour of masonry walls

2.6.1 General

When a masonry structure is subjected to seismic loading, the walls are loaded in their plane or out of their plane, depending on their position in the building. In-plane failure mechanisms are of three types:

- Rocking (flexural failure, Fig. 2.22a), usually in presence of slender and lowly pre-compressed walls; this failure mode could be associated to toe crushing after reaching the compressive strength of masonry;
- Diagonal cracking (shear-diagonal failure, Fig. 2.22b), usually in presence of squat and highly pre-compressed walls;
- Sliding (shear-sliding failure, Fig. 2.22c), usually in presence of very squat and highly pre-compressed walls.

Out-of-plane failure mechanisms are even more dependent on the local boundary conditions of the wall. With poor connections among masonry components, or low-quality masonry, a monolithic behaviour of the wall can be expected, with collapse of a whole façade of a building (Fig. 2.23, failure modes A, B1, B2). Apart from other local failure mechanisms (corner failure, partial collapse or gable overturning), a frequently observed out-of-plane collapse is linked to walls subjected to one-way bending. In this case, the diaphragms are sufficiently stiff to retain the top and bottom edge of a wall, which will tend to develop a flexural crack at approximately half of its height, when subjected to a seismic action (Fig. 2.23, failure mode F; Fig. 2.24). In buildings with sufficiently stiff floors and masonry walls well connected among each other, a two-way bending failure mechanism could occur (Fig. 2.24).

After having shortly summarized the collapse mechanisms of masonry structural components, a brief overview of relevant research studies will be provided, focusing on the in-plane and out-of-plane seismic response of brick masonry walls.

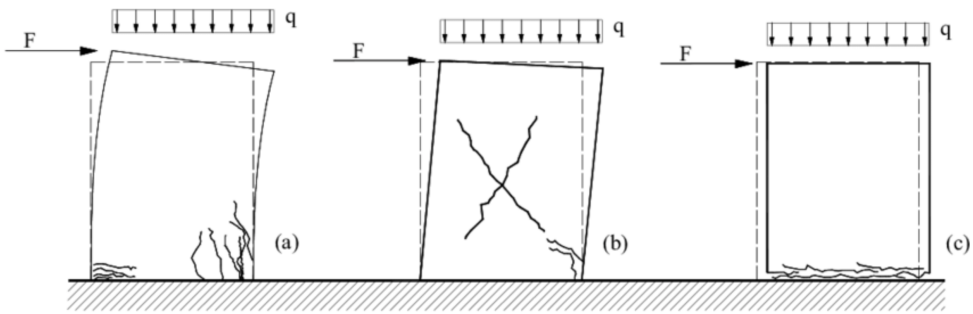
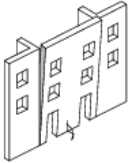
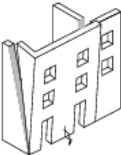
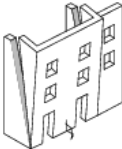
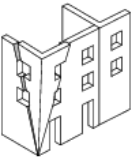
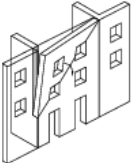
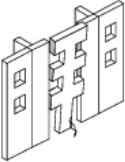
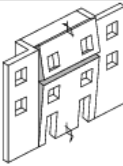
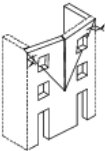
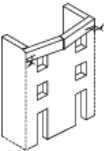
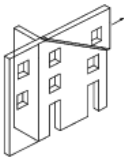


Figure 2.22: Main in-plane failure mechanisms of a masonry pier: (a) flexural failure; (b) shear-diagonal failure; (c) shear-sliding failure. From [58].

A	B1	B2	C	D
VERTICAL OVERTURNING	OVERTURNING WITH 1 SIDE WING	OVERTURNING WITH 2 SIDE WINGS	CORNER FAILURE	PARTIAL OVERTURNING
				

E	F	G		H
VERTICAL STRIP OVERTURNING	VERTICAL ARCH	HORIZONTAL ARCH		IN PLANE FAILURE
		G	TOP STOREY	
				



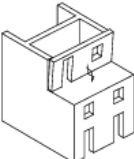

FURTHER PARTIAL FAILURES		ASSOCIATED FAILURES	
I	L	ROOF/FLOORS COLLAPSE	MASONRY FAILURE
VERTICAL ADDITION	GABLE OVERTURNING		 Insufficient cohesion in the fabric
			

Figure 2.23: Overview of possible collapse mechanisms of masonry walls in an existing building. From [59].

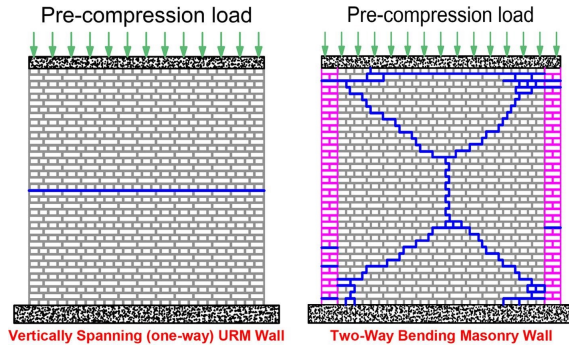


Figure 2.24: Out-of-plane collapse of masonry walls in one-way or two-way bending. From [60].

2.6.2 Research studies on the in-plane behaviour of masonry piers

The first relevant investigations on the lateral in-plane capacity of brick masonry walls aimed at characterizing experimentally and analytically the aforementioned failure mechanisms, as well as the main material properties of masonry, with a view to seismic assessment [61]–[72]. While for the rocking behaviour an estimation of the pier strength can be obtained from equilibrium calculations, the shear failures are more complex to describe, because they could involve only the mortar joints, or also the masonry units (bricks). Besides the application of the usual MOHR-COULOMB criterion, for shear-diagonal failure accurate strength estimation can be obtained through the TURNŠEK-ČAČOVIČ formulation [68] and its further refinements [69]–[71], or the MANN-MÜLLER model [72]. These criteria well predicts the lateral capacity of the wall, but do not provide information on drift limits.

A growing interest in the seismic behaviour of masonry, with a view to the displacement capacity of the piers, led to several full-scale experimental campaigns. Key studies in the understanding of the in-plane response of piers have been conducted since the early '90s: among others, the detailed characterizations of ABRAMS [73], SHAH and ABRAMS [74], ANTHOINE et al. [75], MAHMOUD et al. [76], MAGENES and CALVI [77, 78], and ALLEN et al. [81] are worth mentioning. These campaigns revealed the different nonlinear behaviour when the piers are subjected to rocking or shear failure mechanisms. In the former case (Fig. 2.25) very narrow hysteretic cycles are obtained, while in the latter (Fig. 2.26) a great energy dissipation can be achieved. The obtained relevant results in terms of strength and displacement capacity of the walls became a standard reference for the seismic assessment of masonry structures [2, 4], as well as their nonlinear characterization [79, 80]. Finally, an overview and critical review of the most widespread strength criteria present in literature, and of the standards for interpreting the in-plane failure modes of piers, is given in CALDERINI et al. [82].

Besides the piers, when masonry structures are loaded in their plane, an important role is also played by *spandrels*. The failure mechanisms of spandrels are similar to those of piers, and were characterized and investigated with a view to their seismic behaviour by, among others, BEYER [83, 84], GATTESCO et al. [85], RINALDIN et al. [86]. These structural elements can be particularly relevant in the response of a whole building,

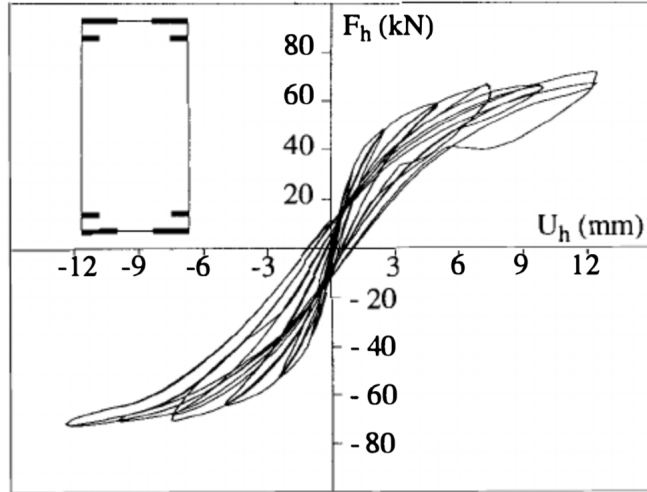


Figure 2.25: Force-displacement hysteretic response and crack pattern of a slender wall subjected to in-plane rocking failure. From [75].

because they can couple the action of each single pier [87, 88]. This beneficial effect is maximized when horizontal ties are present, inducing a pre-compression load on the spandrels [89].

2.6.3 Research studies on the out-of-plane behaviour of masonry walls

The out-of-plane collapse of (portion of) masonry walls is one of the most widespread failure mechanisms and damage sources observed in URM buildings after an earthquake has occurred. These collapses are not only caused by the weakness of the walls out of their plane, but mainly by the absence of appropriate connections among vertical and horizontal structural elements [90]. A thorough, extensive overview on the analysis of out-of-plane failures of masonry walls has been presented by FERREIRA et al. [91]. One of the main methodologies adopted to evaluate out-of-plane failure mechanisms of masonry structural elements is a kinematic limit analysis linked to the application of equilibrium relations, after having schematized the walls as rocking single-degree-of-freedom (SDOF) [92] or multi-degree-of-freedom (MDOF) rigid bodies [93].

These assumptions show, in general, good agreement with experimental tests on walls subjected to one-way bending, and led to widely adopted analytical formulations for estimating the load-displacement response, such as the methods proposed by DOHERTY et al. [94, 95], GRIFFITH et al. [96], and DERAKHSHAN et al. [97, 98]. Yet, collapses related to one-way bending out-of-plane behaviour of walls can be analytically represented in an easier way compared to the two-way bending failure mechanisms, already mentioned in Section 2.6.1.

For walls subjected to out-of-plane two-way bending seismic loads, an extensive research has been conducted in Australia by DERAKHSHAN et al. [99], GRIFFITH et al. [100], and VACULIK and GRIFFITH [101, 102]. These studies have shown that the

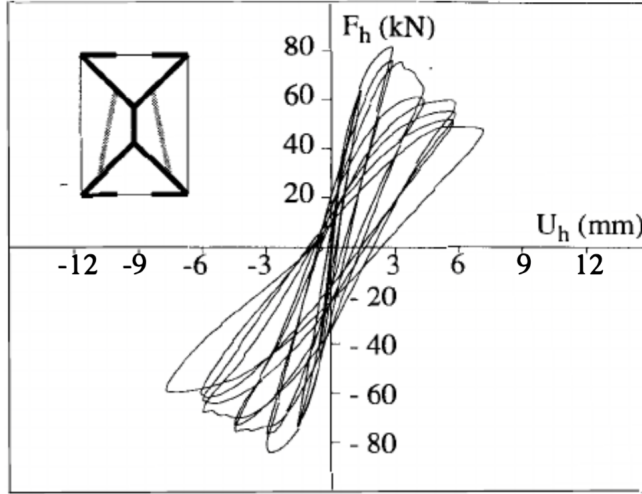


Figure 2.26: Force-displacement hysteretic response and crack pattern of a squat wall subjected to in-plane shear-diagonal failure. From [75].

displacement capacity and strength of such masonry walls can be much larger compared to a one-way bending loading configuration. The hysteretic behaviour is also quite different (Fig. 2.27), with a rapid softening phase (mainly due to loss of equilibrium) and a much lower cyclic energy dissipation for the walls subjected to one-way bending.

The analytical formulations to describe the two-way bending out-of-plane response of URM walls are more complex and still excessively conservative, therefore further research is ongoing for a more complete characterization of such failure mechanism [103].

2.7 Interaction among structural components

2.7.1 General

After having reported a number of research studies and fundamental concepts on the seismic behaviour of timber diaphragms, floor-to-wall timber-masonry connections, and masonry walls, this section puts together the structural components, presenting their interaction during an earthquake. This topic remains still open and relevant, and besides the valuable lessons learnt from seismic collapses during the last decades, several experimental and numerical studies have been conducted on the subject [105]. The outcomes of these analyses show how the in-plane stiffness of the timber diaphragms and the effectiveness of their connections to the walls can play a crucial role in the seismic response of existing buildings [105, 106]. Since a too flexible floor may cause the out-of-plane collapse of (portions of) masonry walls, several stiffening interventions have been developed (Section 2.4), among which the cast of a concrete slab has been dominantly applied in past seismic retrofitting interventions [17, 105]. In fact, although such strengthening technique increases the mass subjected to seismic excitation, it contemporarily induces a higher pre-compression on the walls, thus improving their

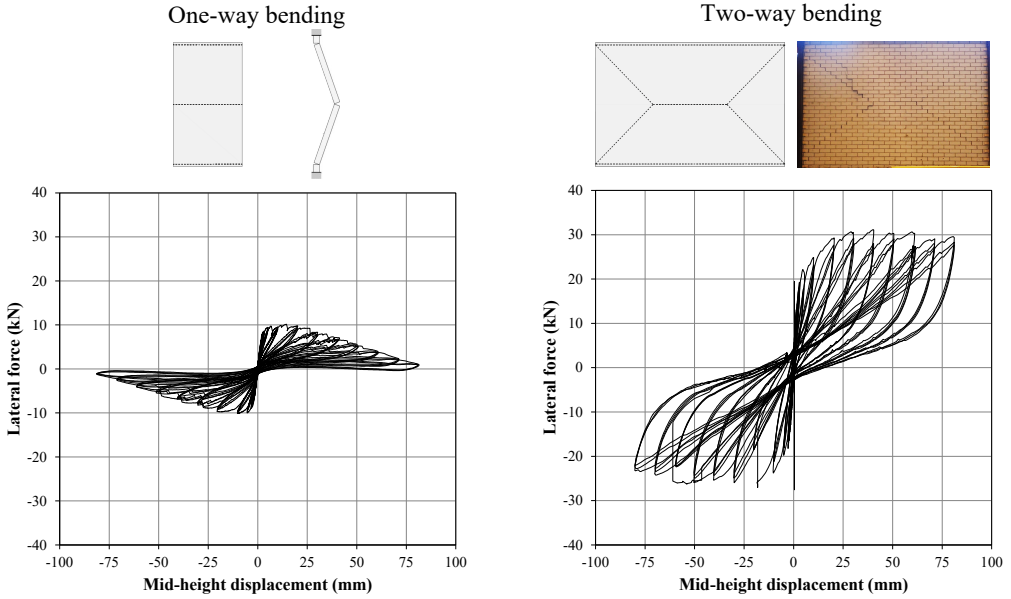


Figure 2.27: Out-of-plane response of a URM wall loaded in one-way (left) and two-way bending (right). Adapted from [104].

strength. Besides, a stiff floor provides a better redistribution of seismic shear forces among the walls, compared to a flexible diaphragm.

However, evidence from several earthquake collapses (see, for instance, Fig. 1.1) showed that too stiff floors can be inadequate for URM buildings, or even worsen their seismic response [105], because they immediately bring into play the in-plane strength masonry walls. Yet, the application of techniques excessively stiffening the diaphragms has been widespread, and the hypothesis of infinitely (or sufficiently) stiff diaphragms in some of the seismic calculation methods for masonry structures [4, 33, 107] has not been helpful in achieving a more aware and conscious design of floor retrofitting interventions. With reference to these aspects, Sections 2.7.2 and 2.7.3 report a number of experimental and numerical investigations, respectively.

2.7.2 Experimental studies

Starting from the early '90s, a number of experimental campaigns on whole URM buildings have been conducted, in order to investigate their global seismic behaviour. Several structures have been analysed, by means of shaking-table tests. An extensive overview of these analyses is provided in [105], while this section will focus on the research studies considering the influence of timber diaphragms and/or wall-to-floor timber-masonry connections on the seismic response of masonry buildings.

A first, relevant contribution was provided by TOMAŽEVIČ et al. [108]–[110]. The authors performed two series of shaking table tests on reduced-scale (1:4) two-storey stone masonry building models (1.0×1.1 m in plan, 1.5 m high). The research study aimed at investigating the effect of the rigidity of floors: thus, four configurations were

tested. A first building was provided with timber floors poorly connected to the masonry walls; the second configuration was provided with RC slabs in place of the floors; the third building featured prestressed steel ties located underneath the timber beams, improving the connections among structural elements; in the fourth configuration, a brick vault and a timber floor were present. For constructing all structures, poor quality materials, typical for old buildings, were used. This study revealed that poorly connected, as-built timber diaphragms can be detrimental for masonry structures, due to their excessive flexibility; at the same time, even if the highest seismic performance was obtained with RC slabs, the presence of steel ties already enabled a satisfactory response of the building.

These tests started to highlight that an excessive stiffening of floors is not always recommendable, or necessary, but an improvement in connections can already be hugely beneficial in preventing out-of-plane collapses of the walls. This was also confirmed by other shake-table experimental investigations on buildings with flexible diaphragms [111]-[114], confirming the essential role of the timber-masonry joints and the in-plane stiffness of floors.

Another extensive experimental campaign focusing on the influence of timber diaphragms and floor-to-wall connections was conducted by MAGENES et al. [115]-[117]: shaking table tests were performed on three full-scale two-storey stone masonry buildings with timber floors and roofs (Fig. 2.28). The buildings were subjected to a series of scaled accelerograms representing the 1979 Montenegro earthquake [118]. The first structure was tested in its as-built configuration, the other two after applying retrofitting techniques, such as the enhancement of the diaphragms stiffness by means of a plywood panels overlay, the improvement of the connections of horizontal and vertical members, the substitution of the floors with reinforced concrete slabs. It was noticed that stiffening the diaphragms may generate an increase in the local stresses exchanged between floors and walls, i.e. through their connections, which have therefore to be of sufficient quality. Although having observed a good performance of the building configuration retrofitted with RC slabs, the authors warn against the potential detrimental effect due to the significant increase of the inertial mass of the diaphragms. Furthermore, in comparison with the as-built configuration, the building with improved wall-to-floor connections, but with still moderately flexible diaphragms retrofitted with plywood panels, already showed a great improvement in seismic performance, almost comparable to the third configuration with RC slabs. This similarity can be explained by considering that in both cases the in-plane strength of the walls was activated, although the stiffness of the diaphragms was very different. As explicitly stated by the authors [117]:

“It appears that the major part of the enhancement on the seismic performance is related more to the improvement of the floor-to-wall and roof-to-wall connections, and to the consequent prevention of local out-of-plane collapse mechanisms, rather than to a strong in-plane stiffening of the diaphragms.”

This strong statement is also in line with the evidence from recent earthquakes, which showed the inadequacy and ineffectiveness of improper interventions on the diaphragms in URM buildings [5]-[7]. Therefore, starting from these experimental results, the role of timber diaphragms has been further investigated, by means of a number of numerical studies, discussed in the next section.



Figure 2.28: Full-scale building tested by MAGENES et al. [116]. Dimensions in cm.

2.7.3 Numerical analyses

Several numerical studies have been conducted having as main subject the behaviour of URM buildings with timber diaphragms. GALLONELLI [119] and GIONGO et al. [120] demonstrated that timber floor stiffening is beneficial for existing buildings, mainly because of the improved box behaviour and seismic shear forces redistribution on the masonry walls. ALEMAN et al. [121] performed an advanced modelling of floor-to-wall connections and flexible as-built timber diaphragms to seismically characterize multi-storey URM buildings typical of the area around New York (USA). The presence of flexible, often rotted, timber diaphragms was recognized as an aspect of vulnerability of such structures.

MENDES and LOURENÇO [122] conducted nonlinear parametric analyses on typically Portuguese building typologies, noticing that an already moderate stiffening of floors can be beneficial in improving the global response of these constructions. Similar conclusions were also obtained by MASROOR et al. [123], as well as GUBANA and MELOTTO [124], who analyzed a simple building with as-built flexible diaphragms and with floors retrofitted with a plywood or CLT panels overlay. These results from numerical analyses are in line with some of the aforementioned experimental outcomes [108]-[110], [115]-[117].

The influence of the floor stiffness in simple masonry buildings was also studied by NAKAMURA et al. [125]. A wide range of diaphragm stiffnesses were considered, ranging from practically rigid to almost completely flexible. The analyses identified that the diaphragm flexibility can increase or reduce the displacement demands on the in-plane walls, depending on the level of diaphragm flexibility and the presence of stiffness and strength eccentricities in the walls. Interestingly, the reduction of the wall displacement demand was found to be induced by diaphragms that were relatively flexible compared to the masonry piers. On the contrary, an increased wall displacement demand was noticed in plan-asymmetric systems, with stiff diaphragms that deformed in a shear-dominant shape, causing large displacement amplification of the weaker side of the structure. Thus, retrofitting interventions have to be designed by carefully accounting for the local boundary conditions of a specific building, but also of adjacent ones, in presence of aggregated structures, as pointed out by STAVROULAKI [126].

In all previous cases, the diaphragms were modelled in a simplified way, mainly as linear elastic orthotropic elements. Yet, the key role of timber diaphragms in the seismic capacity of URM buildings triggered additional investigations aiming at understanding a potential dissipative effect of the floors. In fact, while for as-built diaphragms the behaviour may often be approximately elastic [113], with specific light strengthening techniques their energy dissipation can be increased [15]-[26]. A number of studies has started to focus more on this dissipative potential of the diaphragms in the recent years; the analyses conducted by PRETI et al. [127], SCOTTA et al. [8]-[12], and TRUTALLI et al. [13, 14] are worth mentioning. These investigations involved relatively simple or basic structures, and the role of timber-masonry connections was not evaluated in detail. Yet, these research studies revealed that an excessive stiffening of the floors could even worsen the capacity of the buildings, and suggested further analyses on the beneficial role that the energy dissipation of the diaphragms could play in the seismic response of URM structures.

From these outcomes, the natural consequence that arises is the possibility of optimizing this response by means of a properly designed dissipative retrofitting of

timber diaphragms, connected to URM walls with effective systems: this will precisely be the focus of this dissertation.

2.8 Elements of novelty of the dissertation

2.8.1 Introduction

The former sections presented the state of the art on the seismic analysis of URM buildings with timber diaphragms. One of the complexities of the subject lies in the fact that several different fields are involved, in terms of materials or components characterization, but also seismic analysis strategies. Within the current framework, a number of knowledge gaps arise: these elements of novelty, at the basis of the present dissertation, are addressed in the following with reference to the experimental, analytical, numerical and physical point of view, having as final goal the seismic optimization of URM buildings and the characterization of the interaction between timber diaphragms and masonry walls. Fig. 2.29 shows an overview of the identified knowledge gaps and how they are related to the structure and flow of the doctoral thesis.

2.8.2 Experimental

With regard to the characterization of the in-plane behaviour of timber diaphragms (Section 2.4), only in one case an in-situ test was conducted [26], while all other experimental campaign involved newly-built samples. This has often been indicated as a limitation [15, 16, 24, 26], with the recommendation of a careful use of the obtained results. Since it is practically not possible to perform a large number of in-situ tests in the Province of Groningen, the diaphragms have to be tested in laboratory, but only after replicating both material properties and fasteners response from the existing floors. In this way, a larger number of tests can be conducted, and at the same time the floor specimens can be representative for the timber diaphragms in practice. Moreover, although numerous, all research studies have focused on a specific framework, meaning that very little knowledge is available on the seismic performance of timber diaphragms belonging to the Dutch context. Finally, besides the seismic assessment of as-built diaphragms, a retrofitting measure has to be developed, which should be able to improve the dissipative behaviour of the diaphragms. Since this technique has to be applied in the Groningen region, where within few kilometers the earthquake intensity can be very different, the strengthening method should also be versatile, affordable, easy to install in practice. Thus, in line with the most recent trends in seismic strengthening of timber diaphragms in URM buildings [128], a light, sustainable, and reversible retrofitting measure has to be designed.

The subject of floor-to-wall timber-masonry connections has not been widely explored, and no information on the Dutch context is available, similarly to the seismic assessment of timber diaphragms. A detailed evaluation and replication of existing joints has to be performed, along with the design of suitable strengthening techniques. Besides, given the crucial role of the connections among structural components in the seismic response of existing URM buildings, the joints have to be tested dynamically, in order to evaluate the influence of sudden, induced earthquakes on their response. To put into practice this innovative testing method, a versatile setup has to be designed as well.

The characterization of in-plane and out-of-plane behaviour of masonry walls with Dutch features is also novel. The buildings in the Groningen area usually feature large openings and single-leaf or double-wythe walls. The high slenderness of such components, as well as the frequent presence of poor-quality masonry, are the main sources of seismic vulnerability. The experimental campaign on masonry walls has been conducted by a different research group (Section of *Applied Mechanics*), and is not part of the research project presented in this dissertation, which focuses more on the wood-based structural components. Yet, since the main results of the tests on masonry components are relevant for the analysis and modelling of whole URM structures, they will be summarized anyhow, to provide a complete picture of the seismic characterization of existing buildings with Dutch features.

All these knowledge gaps from the experimental point of view constitute the basis for the conducted testing campaigns. For all structural components, Chapter 3 provides an overview of the materials and methods adopted or developed, while Chapter 4 presents the test results (Fig. 2.29).

2.8.3 Analytical

The retrofitting techniques for timber floors described in Section 2.4 had as main purpose the in-plane stiffening of the diaphragms. Therefore, the role of the strengthened diaphragms has been limited to the transfer of seismic shear forces to the URM walls, without undergoing excessive deflections. Instead, in order to also account for the potential dissipative effect of the retrofitted timber diaphragms, a specific analytical model has to be formulated for the retrofitting technique that will be developed, so that the in-plane response of the floors can be fully described. This also allows us to overcome the current definition of an equivalent in-plane shear stiffness of the diaphragms: Section 2.4 showed that this parameter is not well predicted by seismic guidelines, and is not fully suitable to account for orthotropic and nonlinear behaviour of the diaphragms. Besides, the different authors derived reference values of G_d for specific strengthening techniques from their test results following different methods, depending on adopted standards or specific assumptions. This means that it is not possible to compare the single values of equivalent shear stiffness among each other. Therefore, since it is useful to compare the performance of the developed retrofitting method with similar techniques from literature, a uniform criterion for comparison has to be identified as well.

Given the lack of information on timber-masonry connections, analytical models enabling the seismic assessment of existing joints and the design of retrofitting solutions need to be formulated. Along with the analytical characterization of timber diaphragms, these models will serve as input for numerical analyses.

With regard to masonry walls, in-plane and out-of-plane drift limits will be defined, based on past research studies and the specific outcomes from the experimental campaign on Dutch masonry piers. All elements of novelty from the analytical point of view (Fig. 2.29) are the basis for Chapter 5. Besides, since the performed analytical study involves novel contributions related to strengthening methods on timber diaphragms and timber-masonry connections, recommendations for optimized retrofitting approaches will be provided as well (Chapter 8).

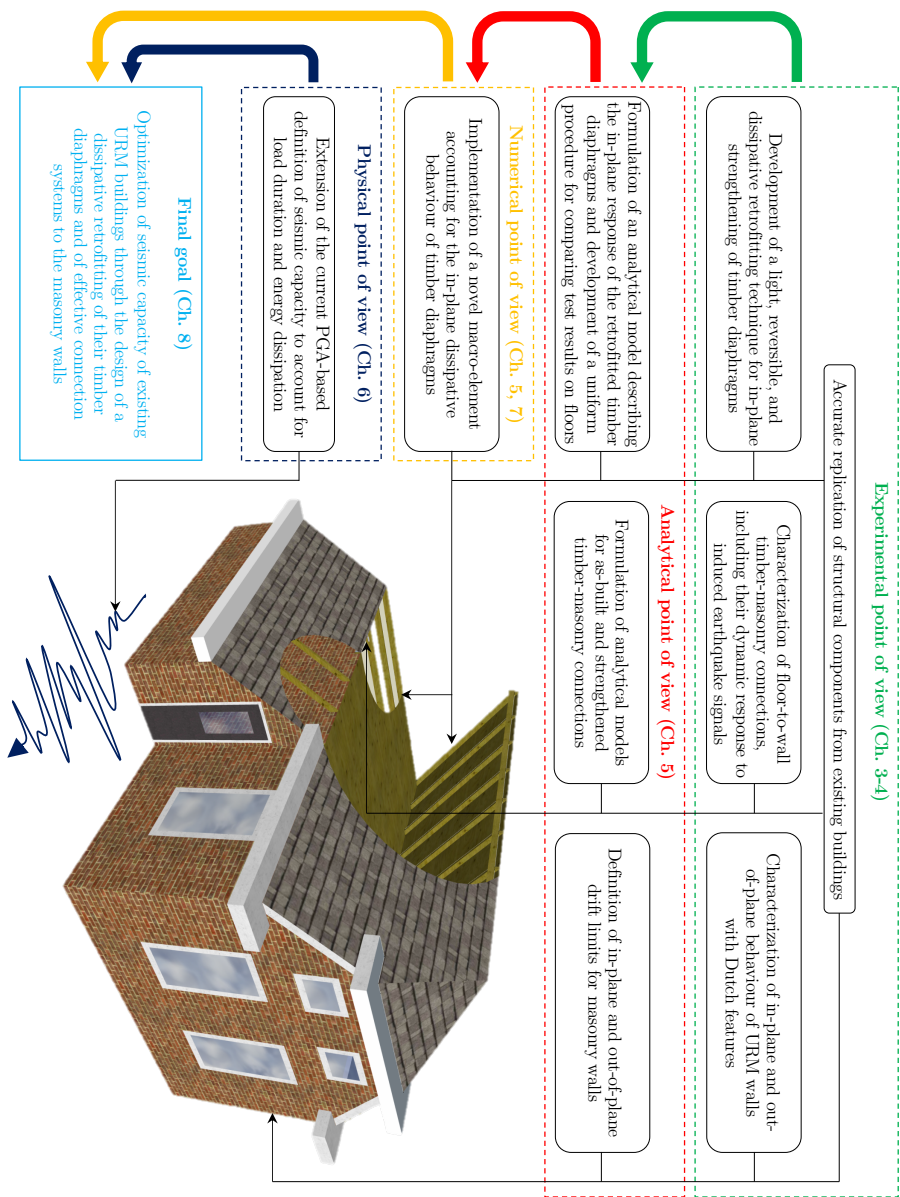


Figure 2.29: Elements of novelty addressed by the doctoral thesis.

2.8.4 Numerical

The characterization of the floors by means of the equivalent shear stiffness, as well as the use of analyses methods having as hypothesis the infinite stiffness of diaphragms, led not surprisingly also to a very simplified numerical modelling of these structural components. Timber floors are generally modelled as linear elastic elements, and often schematized as orthotropic slabs [129]. However, in this way the dissipative contribution of the diaphragms cannot be represented, whereas at the same time modelling each and every structural elements (beams, joists, nails) could become computationally too onerous. Taking into account these aspects, a modelling strategy based on macro-elements appears to be suitable, and has already been successfully adopted in some past studies for describing the in-plane response of diaphragms [8]-[14]. The formulated analytical model will thus be implemented in a novel macro-element (Chapter 5) to be used for the finite element (FE) analysis of whole URM buildings (Chapter 7). The use of this macro-element, combined with the advanced nonlinear modelling of masonry and timber-masonry connections, will finally enable the quantification and prediction of the beneficial effect of timber diaphragms in URM buildings. The whole novel seismic characterization approach will be summarized in Chapter 8 (Fig. 2.29).

2.8.5 Physical

The physical point of view is linked to the specific situation of Groningen, and the occurrence of induced earthquakes (Section 2.3.3). Similarly to Eurocode 8, the current Dutch seismic guidelines rely on PGA only for seismic assessment of URM buildings. However, it has been shown that this indicator cannot account for important aspects such as energy dissipation and load duration [28]. Therefore, to quantify seismic capacity and structural damage of the buildings also for the case of induced earthquakes, with their characteristic short-duration and high-frequency signals, an extension of the current framework is needed. This opens up the opportunity for a more complete and generalized seismic assessment of URM buildings with (retrofitted) timber diaphragms, described in Chapter 6 (Fig. 2.29). In fact, the developed procedure will be verified against not only induced earthquakes, but also tectonic events.

Chapter 3

Methodology for replicating and testing of structural components

3.1 Introduction

The literature review of Chapter 2 allowed to identify a number of knowledge gaps: this chapter examines the experimental point of view, and presents the adopted methodology for the seismic characterization of structural components, with a specific focus on timber diaphragms and timber-masonry connections typical of the Groningen area.

Firstly, the whole multi-scale approach followed throughout the experimental campaign and the subsequent studies is discussed (Section 3.2). Secondly, since the response of newly-built samples has to be representative for the one expected in a very ancient building (see Chapter 2), a replication process was conducted, whose principles are presented in Section 3.3. Finally, after defining the full-scale structural components to be tested (Section 3.4), the testing methods adopted for the experimental campaigns on the seismic characterization of timber diaphragms, timber-masonry connections, and masonry walls are described (Section 3.5).

3.2 A multi-scale approach

The conducted testing campaign aimed to investigate the seismic performance of the building stock in the Province of Groningen, for which little information was available. To this end, a large number of tests was necessary, and it would have been practically neither feasible nor convenient to perform all these experiments on site, in several existing buildings. Therefore, after characterizing the local building stock, representative structural components were replicated and tested in laboratory.

Firstly, a survey on the most common building typologies of the Groningen area was conducted by ARUP [130]. URM constructions with timber diaphragms constitute more than 50% of the building stock; almost all buildings are residential, and two main typologies can be distinguished:

- Detached houses, constructed with either single-leaf or double-wythe clay-brick masonry, and having timber floors and roofs;
- Terraced houses, realized with a cavity wall system, and having timber or RC diaphragms. The cavity wall system consists of an external single-leaf clay-brick masonry wall, and an internal single-leaf calcium-silicate-brick one; the two leaves are connected with slender ties.

Secondly, after determining these main targets of the large-scale experimental campaigns, a multi-scale approach was adopted (Fig. 3.1). Firstly, representative buildings were selected, in order to perform in-situ tests and/or to extract timber or masonry samples. This first step was essential to determine the main properties of the two structural materials: by knowing these characteristics, a detailed replication was conducted (Section 3.3), in such a way that newly-built samples could be representative for the extracted ones. Starting from this characterization at material level, the seismic assessment of several replicated timber and masonry components, as well as connections, was conducted with laboratory tests (Section 3.4). Besides, retrofitting methods for timber diaphragms and timber-masonry connections were also designed and tested. Finally, the large amount of information at material, connection, and component level constitutes both the basis for analytical models, and useful input for numerical analyses, thus enabling also the full-scale seismic characterization of URM buildings typical of the Groningen area.

3.3 Replication process

3.3.1 General

The following sections present the extraction, characterization and replication process of timber and masonry samples from existing buildings. Since it was not possible to extract complete structural components and directly test them in laboratory, small-scale samples were taken, and replicas were accurately manufactured after the characterization of the extracted specimens. The replication process is described focusing specifically on timber structural elements (Sections 3.3.2 to 3.3.4), because masonry was characterized by a different research group at TU Delft; for completeness, a brief overview of masonry replication is reported in Section 3.3.5.

With regard to timber diaphragms, the relevant parameters governing their in-plane behaviour are the material properties of wood, as well as strength, stiffness and energy dissipation of the fasteners connecting all structural elements [131]. Fig. 3.2 shows the followed process for the determination of these characteristics: after extracting original samples from local detached houses (Section 3.3.2), all elements were subdivided into smaller specimens to be tested. Subsequently, the relevant properties of timber and fasteners from original samples were determined (Section 3.3.3): with regard to timber, the investigated properties were the wood species, the density ρ , the elastic modulus E , and the moisture content $m.c.$; the fasteners were characterized in terms of tensile strength and plastic bending moment. According to these outcomes, materials with similar properties were ordered and tested for checking that an accurate replication was achieved. Additionally, cyclic tests on both extracted and replicated plank-joint connections were performed (Section 3.3.4), to further confirm the representativeness of

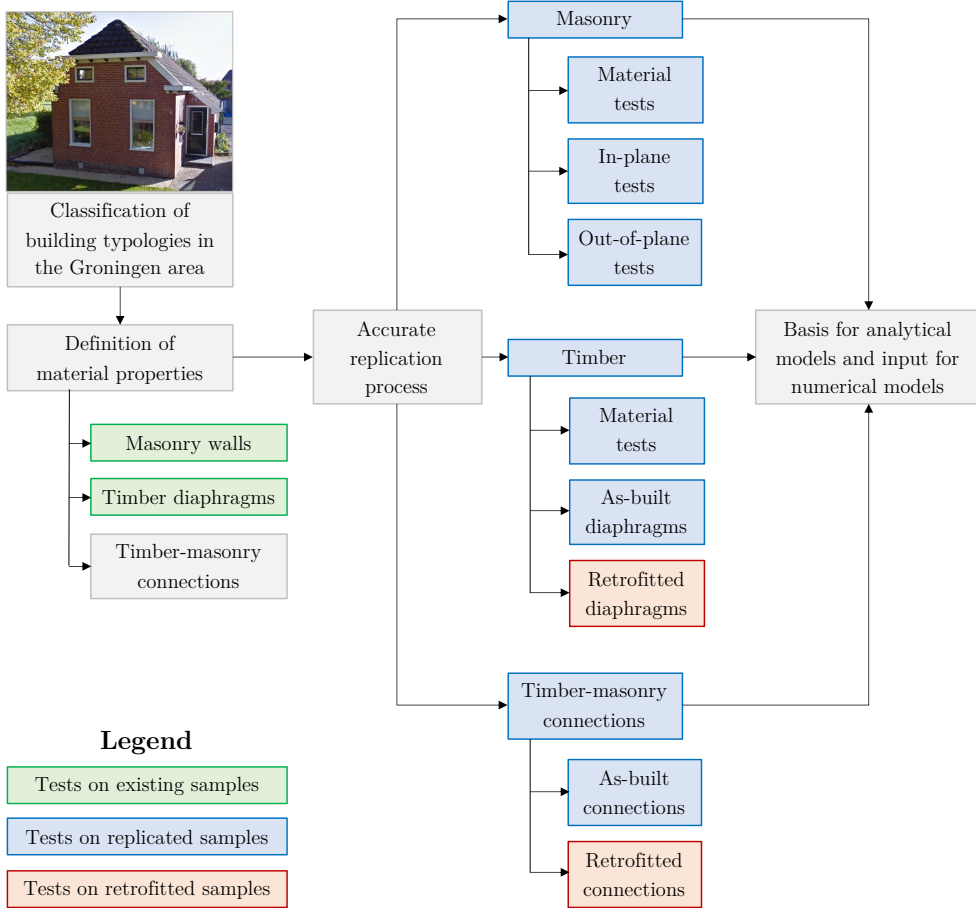


Figure 3.1: Multi-scale approach followed for the definition of the conducted large-scale testing campaign.

the replication. These tests were conducted perpendicular to the joists (configuration A), parallel to the joists (configuration B) and in rotation (configuration C), according to Fig. 3.2e-f. Following these preliminary tests, the full-scale samples representing timber diaphragms with Dutch features were built (Section 3.4.1). Besides, by combining the characteristics of replicated wooden structural elements and masonry, the specimens representing timber-masonry connections were realized (Section 3.4.2).

3.3.2 Selection and extraction of timber diaphragms samples from site

After a survey in the most common typologies of traditional timber diaphragms in the Groningen area, four representative samples (Fig. 3.3) were extracted from existing detached houses (built 1890-1930) to be demolished. Three of them were wooden floors, while the fourth was part of a pitched roof; the extracted portions measured approximately 2×2 m and were labelled with letter *G* (*Groningen*), followed by the progressive number. In most samples, joists and boards were made of spruce (*Picea abies*), but in sample G4 pine (*Pinus sylvestris*) planks were found. The joists and the planks had dimensions, geometry and fasteners (common round or square nails) as given in Table 3.1. With reference to Fig. 3.3, the relevant geometrical dimensions measured were:

- Width w and thickness t of planks;
- Height h , width b , and spacing a of main joists (or rafters);
- Height h' , width b' , and spacing a' of secondary beams (only applicable to roof purlins from sample G2).

These properties were taken as the basis for the construction of the replicas and the strengthened samples described in section 3.4.1. From an observation of the extracted specimens, some typical characteristics of traditional Dutch timber floors appeared to be relevant:

- The structural elements are normally smaller than the ones belonging to other contexts [15]-[26]: for instance, a main joist of a floor can have a cross section of 60×130 mm (or even 50×105 mm for a roof), with large spacings ranging from 600 to 900 mm;
- The floor sheathing is realized with continuous planks: since these elements are not interrupted, the global behaviour depends above all on the flexural stiffness of the planks (or of the joists, according to the loading direction) and on the rotational stiffness of the nail couples fastening the planks to the main joists [46]. Given this mainly flexural behaviour, the equivalent shear stiffness cannot be fully suitable to characterize the in-plane response of these as-built diaphragms [132];
- Roofs of detached houses are usually composed of main and secondary beams, the former supported by a wall plate, i.e. a timber element positioned on top of the external walls of the building. Because of the very simple connection between main rafters and wall plate, this kind of roof structure appears to be extremely flexible when subjected to horizontal loads, because the rafters can be considered as practically hinged on the wall plate.

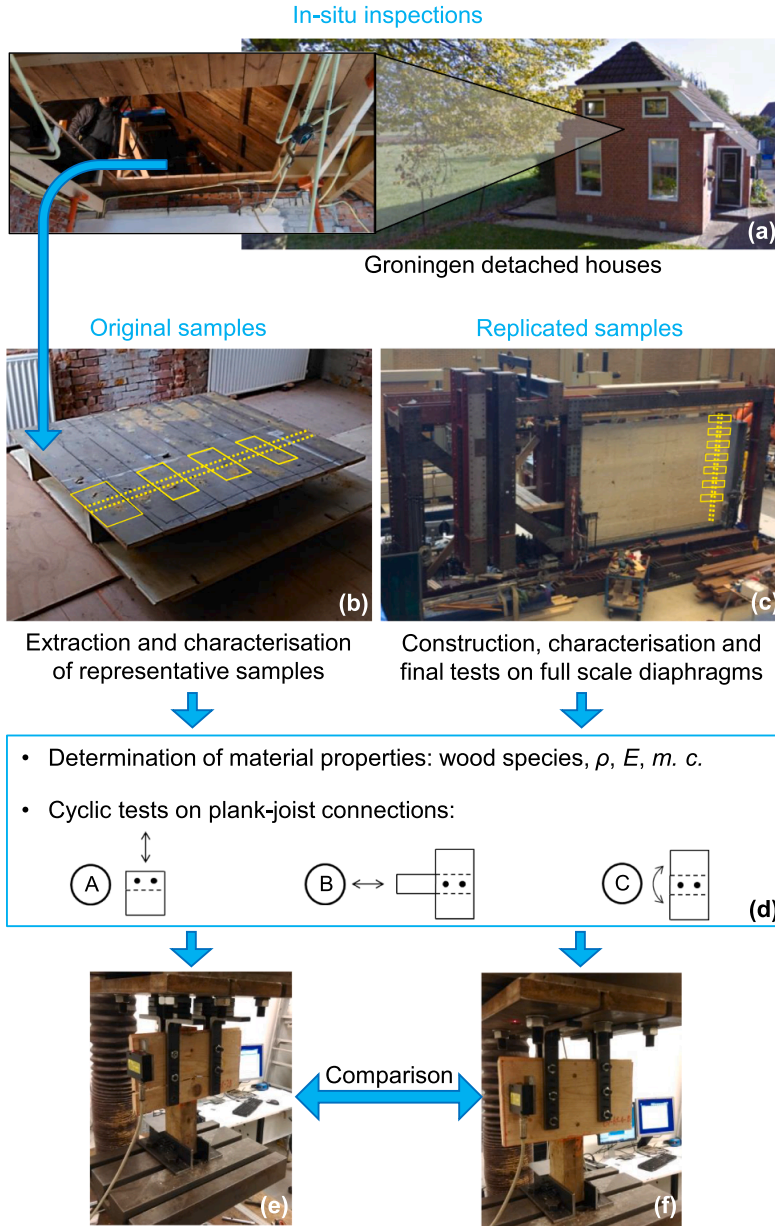


Figure 3.2: Process followed for the determination of material properties of timber and plank-joint connections for original and replicated samples: (a) in-situ investigation and selection of samples; (b) extraction of floor and roof samples; (c) construction of replicated specimens on the basis of the characteristics of original ones; (d) characterization of material properties and cyclic behaviour of plank-joint connections, with comparison between extracted (e) and replicated samples (f). From [132].

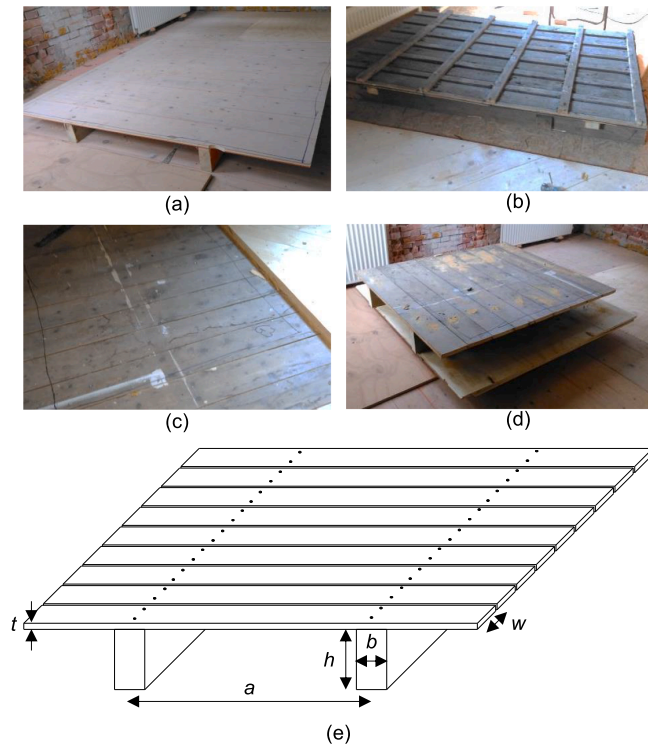


Figure 3.3: Extracted timber diaphragms samples: G1 (a), G2 (b), G3 before cutting (c), G4 (d); geometrical parameters of interest for replication (e). From [132].

Table 3.1: Characteristics of the extracted samples.

Specimen	G1 (floor)	G2 (roof)	G3 (floor)	G4 (floor)
w (mm)	162	164	163	166
t (mm)	18	15	23	23
h (mm)	112	105	118	165
b (mm)	51	52	62	61
a (mm)	788	912	736	650
h' (mm)	N. A.	35	N. A.	N. A.
b' (mm)	N. A.	62	N. A.	N. A.
a' (mm)	N. A.	820	N. A.	N. A.
- Two 3×55 mm nails at				
Fasteners	Two 3×65 mm nails at	every intersection	Two 3×65 mm nails at	Two 3×65 mm nails
	every intersection	plank/purlin;	every intersection	at every intersection
	plank/joist	- One 5×110 mm nail at	plank/joist	plank/joist
		every intersection		
		purlin/rafter.		

The extraction of samples was conducted according to the following process:

- A visual survey was performed prior to the selection of timber samples;
- Existing finishes, such as carpeting, were removed, in such a way that each specimen was void of anything but the structural floor: joists, planks and nails; for roof samples the tiles were removed;
- The locations of the samples in the buildings were marked and identified, and a sketch or photograph of each proposed sampling location was prepared;
- Any imperfections (cracks, damage, etc.) on the samples were marked;
- The extraction of the specimens was performed carefully and accurately;
- The samples were removed from the construction site, set on a dry and stable horizontal surface, and kept out of the sun to prevent deformations or cracks;
- All specimens were moved to the site of preparation for transport and their condition on all exposed sides was documented;
- The samples were protected on all sides to prevent damage during transportation.

After the extraction and transportation, all samples were delivered at TU Delft Stevin II Laboratory, and their relevant material properties were determined, according to the methodology described in the next section.

3.3.3 Determination of material properties of timber and fasteners

This section presents the adopted methodology for determining material properties of timber structural elements and fasteners. The procedure was firstly followed for the extracted samples, and then repeated for the replicated specimens, after they were built.

With regard to timber members, including plywood panels, the determined material properties were wood species, density, modulus of elasticity, and moisture content.

The density was measured by weighing each sample, and dividing the weight by its volume.

The modulus of elasticity was dynamically determined by longitudinal vibration measurements with a *Brookhuis MTG 960* [133]. With this apparatus, the first natural frequency f_1 of the timber pieces was determined: by also knowing the length l of the structural elements and their density, the dynamic modulus of elasticity E_{dyn} was calculated as:

$$E_{dyn} = 4\rho f_1^2 l^2 \quad (3.1)$$

E_{dyn} is on average 8% higher than the static modulus of elasticity [134], determined in accordance with EN 408 [135].

The moisture content of timber was determined with the oven-dry method as specified in EN 13183-1 [136].

With regard to fasteners, and namely the nails connecting the main structural elements, two material properties were determined: tensile strength (T) and plastic bending moment (M_p), in agreement with EN 409 [137].

Based on these determined properties, the materials for constructing the full-scale diaphragms (Section 3.4.1) were selected and ordered. The results of the aforementioned measurements and tests are reported in Section 4.2.1, along with a comparison between extracted and replicated samples.

3.3.4 Determination of cyclic behaviour of plank-joint connections

A well-performed replication of the cyclic response of plank-joint connections is of importance, because the in-plane behaviour of timber diaphragms largely depends on them. With newly-built samples, the connections might display much higher strength and stiffness compared to existing ones [26, 131]. Therefore, it was chosen to test and replicate their cyclic behaviour, to investigate whether adjustment factors for the properties of replicated samples were needed.

The specimens representing plank-joint connections were loaded quasi-static reversed-cyclically in accordance with ISO 16670 [138], in order to determine their hysteretic behaviour. Ten tests were conducted for each loading direction, thus perpendicular and parallel to the joists, and also in rotation (cases A, B, and C of Fig. 3.2, respectively). After characterizing these extracted samples, the same tests were conducted also on the replicated ones: the timber structural elements ordered according to the measured material properties were used to build each diaphragm, from which plank-joint connection specimens were extracted. Seven tests were performed for cases A and C, four for configuration B. The fasteners used for the construction of the replicated diaphragms had identical or, where not possible, similar characteristics in terms of diameter and yield strength to the ones found in the original samples from the Groningen area. In this way, as shown in Section 4.2.2, it was possible to compare the properties and the behaviour of the extracted samples with replicated ones: similar values in terms of strength and maximum displacement (with respect to the usual scatter which affects the tests performed on timber joints) were found, thus no adjustment factors were needed.

3.3.5 Extraction, characterization and replication of masonry samples

Given the large amount of URM buildings in the Groningen area and the variations in masonry unit types and construction techniques, an extensive survey was conducted prior to the extraction of relevant specimens. These samples were taken from both residential buildings and schools, dating from the 1920s up to 2013 [139]. The predominant masonry units were found to be clay bricks (mainly solid, but also perforated and frogged); several samples also featured calcium silicate bricks, concrete blocks, or calcium silicate elements. A total of 318 samples were extracted from 19 different locations, and then shipped to TU Delft Stevin II Laboratory. Unfortunately, several samples arrived in such degree of damage or disintegration that it was not possible to destructively test them.

The following relevant material properties were tested, and constituted the basis for the replication of masonry:

- Compressive strength of masonry units according to EN 772-1 [140];
- Flexural strength of masonry units according to NEN 6790 [141];

- Compressive strength of masonry parallel and perpendicular to bed joints according to EN 1052-1 [142];
- Bending strength of masonry according to EN 1052-2 [143];
- Bond strength of masonry according to EN 1052-5 [144];
- Shear strength of masonry according to EN 1052-3 [145].

Because of the different masonry types and their quality, a large variation in the experimental results was observed, even within the same type. Therefore, both masonry units and mortars were selected to obtain material properties representing low-quality masonry, in favour of safety. For further details, the reader is referred to JAFARI et al. [139]. The replication process for masonry did not only involve TU Delft, but also EUCENTRE and LNEC laboratories [146], in which both full-scale tests on components, and shaking-table tests on representative building prototypes, were conducted.

3.4 Definition of the full-scale specimens to be tested

3.4.1 Timber diaphragms

In order to assess the in-plane response of as-built and strengthened timber diaphragms with Dutch features, a testing campaign was conducted on full-scale floors that were replicated based on the material properties of the original samples extracted from existing buildings (Section 3.3.2). The target of the experimental tests was to firstly perform a seismic assessment of the as-built floors. Subsequently, a light, reversible and adaptable retrofitting technique was developed, aiming at increasing the in-plane strength, stiffness and energy dissipation of the diaphragms [132]. Based on the literature review on past investigations on the seismic performance of timber diaphragms (Section 2.4), the experimental campaign was arranged considering the following aspects:

- As-built diaphragms had to be tested in two directions, because of their potentially orthotropic behaviour [25]. Besides, little information on the seismic behaviour of timber roofs was present in literature, thus a specimen representing a roof pitch was built, according to the characteristics of extracted sample G2.
- The adopted retrofitting technique consisted of an overlay of plywood panels (thickness $t_p = 18$ mm) screwed along their perimeter to the existing floor sheathing. This light, wood-based strengthening method was chosen because of its reversibility, adaptability, ease of installation, and above all its effectiveness in enhancing all in-plane properties of the diaphragms [23]-[26], including energy dissipation.
- Since the experimental campaign on the diaphragms took part contemporarily to that on masonry walls, it was decided to adopt the same test setup for both types of structural components (Section 3.5). Therefore, the diaphragms were tested in a vertical configuration, and the replicas represented half of a floor, or a single roof pitch, according to the principles described in Section 3.5.1. The tested specimens had all similar width B and span L .

Table 3.2: Geometrical characteristics of the five tested diaphragms, reported for their as-built configurations.

Properties of as-built diaphragms					
Specimen	DFpar-1 (floor)	DFpar-2 (floor)	DFper-3 (floor)	DFper-4 (floor)	DRpar-5 (roof)
Loading direction	Parallel to the joists		Perpendicular to the joists		Parallel to purlins
L (mm)	2400	2400	2300	2300	2730
B (mm)	3800	3960	3800	3800	3800
w (mm)	165	165	165	165	165
t (mm)	18	24	18	18	18
h (mm)	130	130	110	110	105
b (mm)	60	60	50	50	50
a (mm)	650	650	750	750	925
h' (mm)	N. A.	N. A.	N. A.	N. A.	35
b' (mm)	N. A.	N. A.	N. A.	N. A.	60
a' (mm)	N. A.	N. A.	N. A.	N. A.	820
Fasteners	- Two 3×55 mm nails at every intersection plank/purlin;				
	- One 5×110 mm nail at every intersection purlin/rafter				
	Two 3×65 mm nails at every intersection plank/joist				

The geometrical properties of the replicated diaphragms were determined according to the features of the extracted samples. Tables 3.2 and 3.3 present the characteristics of the as-built and retrofitted replicated diaphragms, and in Figures 3.4 to 3.6 their configurations are shown. The five diaphragms were labelled with the initials *DF* (*Detached house Floor*) or *DR* (*Detached house Roof*), followed by *-par* or *-per* (loading *parallel* or *perpendicular* to the joists, respectively), and by the progressive number. After testing each as-built diaphragm, the retrofitting interventions took place, and the specimens were subsequently retested: to identify these *strengthened* samples, letter *s* was added at the end of the specimen name.

Based on the material of the extracted samples, all structural elements were made of spruce (*Picea abies*) timber with strength class C24 [44], and the planks presented a tongue and groove configuration, as in original specimens. In order to represent the situation observed in reality, and in agreement with good practice, the tongues were not fully pushed to the side of the next plank, leaving a gap of ≈ 2 mm.

Table 3.3: Characteristics of the strengthened versions of the five tested diaphragms.

Additional properties of strengthened diaphragms					
Specimen	DFpar-1s	DFpar-2s	DFper-3s	DFper-4s	DRpar-5s
l_p (mm)	1200	1200	1200	1200	820
b_p (mm)	600	670	770	770	760
t_p (mm)	18	18	18	18	18
Screws	4.5×40 mm	5×60 mm	5×60 mm	5×70 mm	4.5×40 mm
Spacing	100 mm along the perimeter of each panel				
Other remarks	5×70 mm screws used for			Between the	75×150×8 mm steel angle
	top row		N. A.	joists: top	fastened at roof bottom
	at 150 mm spacing			60×130 mm	with 6×70 mm screws at
				blocks	150 mm spacing

When loading the specimens perpendicular to the joists, their connection to a (masonry) wall was also simulated by means of tropical hardwood elements, shown in the detail of Fig. 3.5. Two configurations were considered:

1. If the masonry pocket is totally void of mortar, then a hinged configuration can be assumed (specimens DFper-3 and 3s, Fig. 3.5);
2. If the joist is inserted in the masonry pocket and mortar is present, a slight clamping effect might be introduced (specimens DFper-4 and 4s, Fig. 3.5).

The structure of the roof pitch was slightly more complex than that of the floor, according to the configurations found in practice: between the wall plate and the top main beam of the roof, rafters were arranged, to which the purlins (supporting in turn the planks) were connected (Fig. 3.6).

For the retrofitted diaphragms, it was chosen not to cut the plywood panels in too large dimensions, to guarantee an easier installation of them in practice. In the very first strengthening (specimen DFpar-1s), approximately $b_p \times l_p = 600 \times 1200$ mm panels were used, which were positioned and screwed without taking into account the underlying layer of existing planks. Instead, from the second diaphragm on, the panels were cut, placed and screwed in such a way that all fasteners were always crossing the total thickness of the plywood panels and the planks, while for the first sample in some cases the screws were crossing the existing sheathing in the tongue between two planks. The position of underlying joists was not considered for cutting and placing the plywood panels and the screws, except for the top joist (Fig. 3.4) and the additional timber blocks of sample DFper-4s (Fig. 3.5).

The plywood panels were fastened to the sheathing along their perimeter with different screws depending on the specimen (see Table 3.3). In addition to that, in four specimens further strengthening elements were applied:

- For specimens DFpar-1s and DFpar-2s, the upper row of screws corresponded

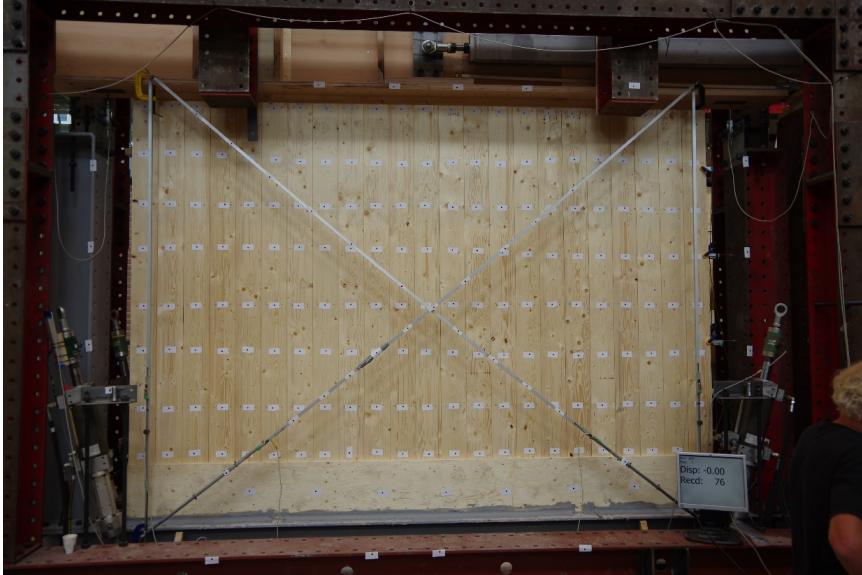
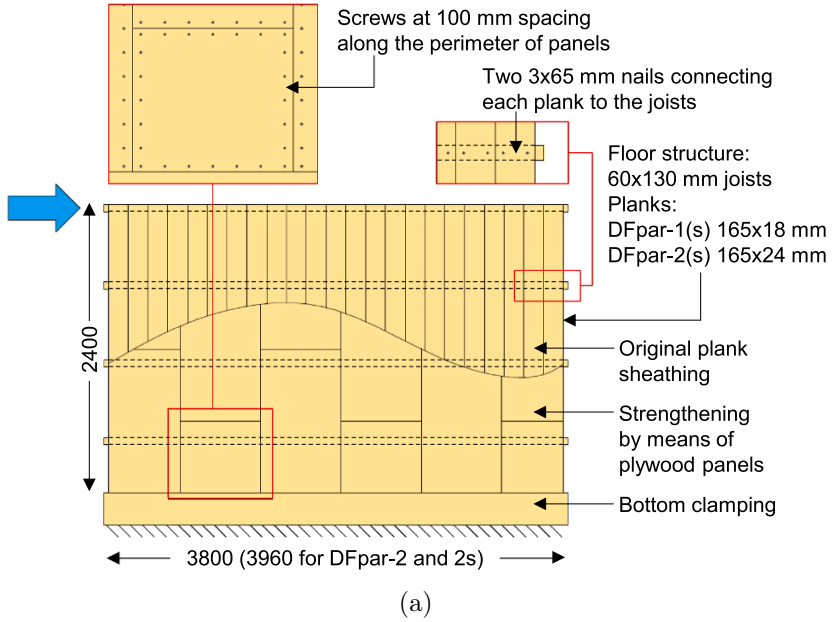


Figure 3.4: (a) Schematic representation of the diaphragms tested parallel to the joists (specimens DFpar-1 and 1s, DFpar-2 and 2s, view from decking side); dimensions in mm; (b) sample DFpar-1 positioned in the test setup.

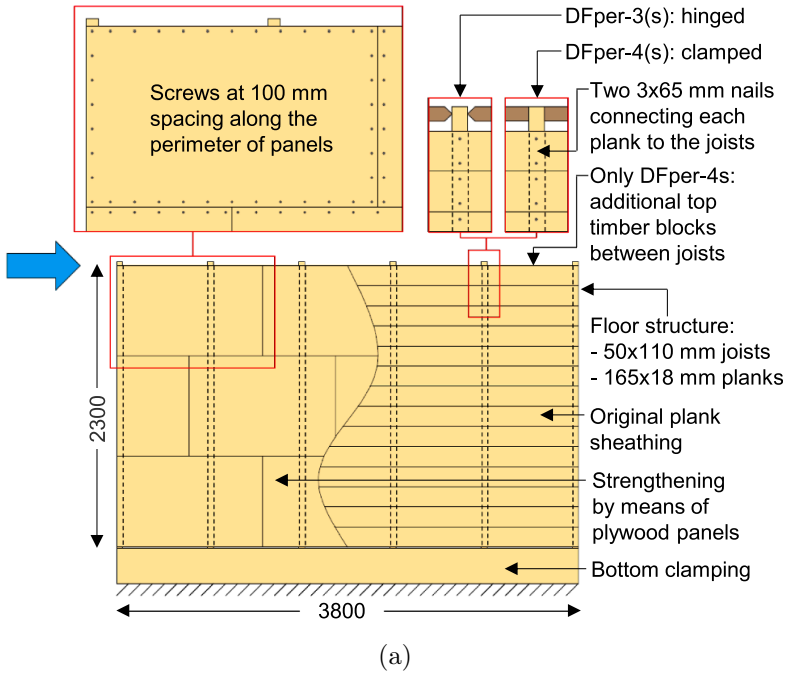


Figure 3.5: Schematic representation of the diaphragms tested perpendicular to the joists (specimens DFper-3 and 3s, DFper-4 and 4s, view from decking side); (b) sample DFper-3 positioned in the test setup.

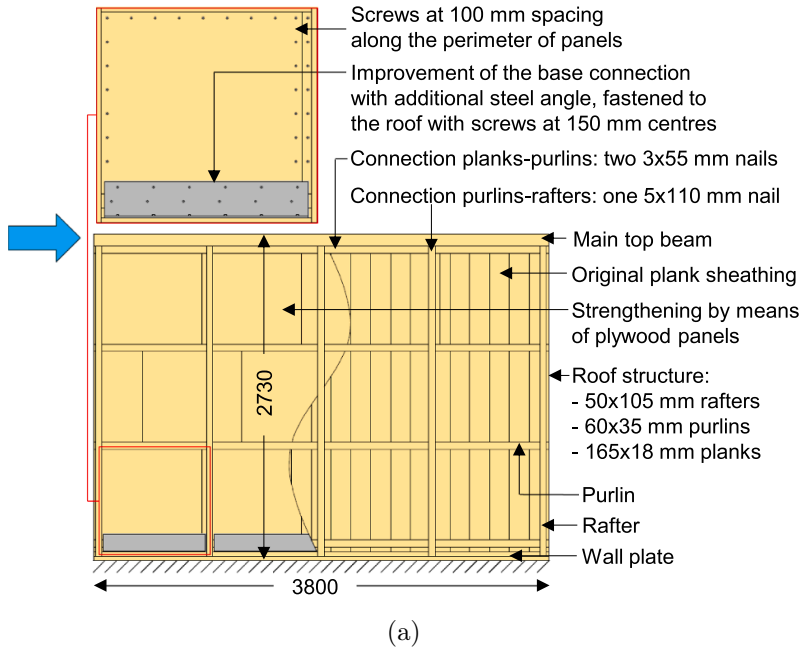


Figure 3.6: Schematic representation of the tested roof pitch (specimens DFpar-5 and 5s, view from the inner side); dimensions in mm; (b) sample DRpar-5 positioned in the test setup.



Figure 3.7: Replicated roof specimen from a terraced house tested at LNEC laboratories. From [147].

to the fastening of the strengthening panels directly to the top joist of the floor: hence, to improve the shear transfer in this area, 5×70 mm screws were used;

- In specimen DFper-4s, additional 60×130 mm timber blocks were placed on top of the floor between each couple of joists; this configuration allows to not only improve the in-plane stiffness of the floor through a better fastening of the panels, but can also be a possible solution to realize a diffused connection between diaphragm and wall in practice, by anchoring these blocks to the latter;
- In the extracted roof samples, the rafters supporting the pitch were fastened to the wall plate with only one 5×110 mm nail: this situation was replicated also in specimen DRpar-5. Because this was the only connection between the whole structure of the roof and the walls, it was chosen to not only improve the stiffness of the diaphragm, but to make the transfer of horizontal forces more effective as well. Therefore, between the rafters $75 \times 150 \times 8$ mm steel angles were fastened to both the roof structure and the wall plate with 6×70 mm screws at 150 mm centres. Besides, the plywood panels were cut in such a way that they could be inserted between the purlins and behind the rafters, allowing to perform an intervention from the inner part of the roof.

Appendix A reports the pictures of all tested samples in their as-built and strengthened configurations. Besides the experimental campaign on timber diaphragms conducted at TU Delft, another replicated roof sample was also tested at LNEC laboratories: for further information, the reader is referred to CORREIA et al. [147].

3.4.2 Timber-masonry connections

One of the main vulnerabilities of existing structures in the Groningen region appeared to be the presence of relatively poor connections between timber floors and masonry walls. Firstly, as-built joints were characterized: visual inspections in existing buildings allowed to select the most widespread configurations to be replicated and tested. Subsequently, retrofitting methods for the existing connections were designed in cooperation with local engineering consultants.

The large-scale testing campaign was arranged accounting for the knowledge of previous research studies [54]-[57], but overcoming the limitations highlighted in Section 2.5. Firstly, the size of the samples was defined in order to study the behaviour of the whole portion of wall around the timber joist; secondly, dynamic tests with a signal of an induced Groningen earthquake were performed, besides the usual quasi-static monotonic and cyclic ones. This enabled the characterization, under this specific seismic loading, of both the connections response and the damage on the masonry walls.

The experimental campaign was subdivided in two phases:

1. A first pilot study, focusing more on as-built connections, in which only quasi-static tests were performed [148];
2. A second, more extensive phase, which included dynamic tests and focused more on retrofitted configurations [149]-[151].

A frequent timber-masonry connection found in existing buildings in the Groningen area is the insertion of the joists in pockets in the masonry. The support length of the joist in the masonry wall normally corresponds to the width of a brick: thus, a joist is supported over the entire wall thickness, for single-leaf masonry (Fig. 3.8a); only over half of the wall thickness, for double-wythe masonry (Fig. 3.8b). Another frequent existing floor-to-wall connection type is realized by means of an hook anchor (Fig. 3.8c) nailed to the timber joist; this detail is found in terraced houses, and also in detached houses, in the form of an anchor plate. In single-leaf walls, the hook anchor is behind the leaf itself (Fig. 3.8d), while for double-wythe walls it is masoned in them (Fig. 3.8e). In the tested samples, the hook anchor measured $240 \times 240 \times 14$ mm, and was fastened to the timber joist with three 4×55 mm nails.

Within the pilot study, two types of masonry walls were considered: a clay brick, double-wythe wall, and a calcium silicate brick, single-leaf one (used in terraced houses). Besides the two aforementioned as-built configurations (CLAY-A and -B; CS-A and -B in Fig. 3.9), also a simple retrofitting intervention was tested: this consisted of a steel angle fastened to the joist with four 5×60 mm screws and to the masonry with two 10×95 mm mechanical anchors (configurations CLAY-C and CS-C in Fig. 3.9). In all configurations, the connection at roof level was studied, because this constitutes a very weak part of existing buildings, due to the absence of ongoing masonry on top, and the frequent presence of low-quality or damaged masonry. Within this pilot study, only one sample per configuration was tested.

The specimens consisted of approximately 980×600 mm masonry wall elements; a 65×170 mm (65×150 mm for CS configurations) timber joist was inserted orthogonally to the wall, with a length of approximately 1600 mm (Fig. 3.10). The masonry walls were glued at the bottom and at the two top corners to a steel frame, to ensure that the behaviour of the joist-masonry connection was studied, accounting for the portion of wall around it.

In the second phase of the experimental campaign, the connection of a timber joist with a single-leaf clay brick masonry wall was investigated. This situation, with reference to the Groningen region, is representative for a leaf of a cavity wall structure at roof level, or for a gable. The specimens had the same characteristics as in the pilot study, therefore they were composed of a 980×600 mm masonry wall, and a $65 \times 170 \times 1600$ mm timber joist.

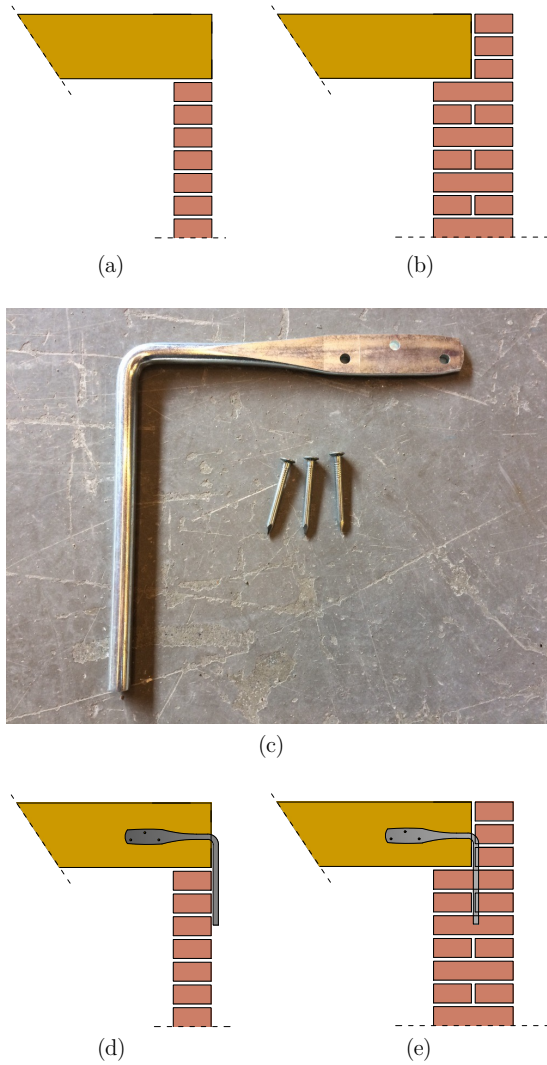


Figure 3.8: As-built timber-masonry connections typical of the Groningen area: masonry pocket in a single-leaf wall (a); masonry pocket in a double wythe wall (b); example of hook anchor (c); hook anchor in a single-leaf wall (d); hook anchor masoned in a double-wythe wall (e).

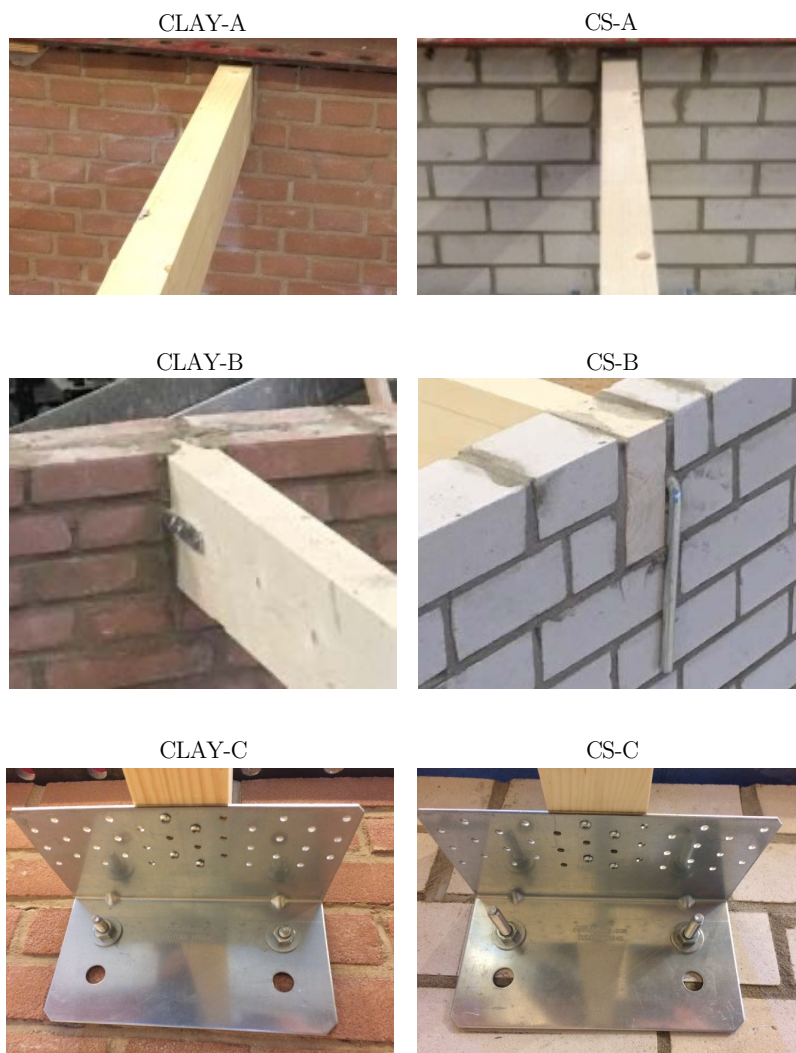


Figure 3.9: Configurations of timber-masonry connections tested within the pilot study: as-built with masonry pocket (CLAY-A and CS-A), as-built with hook anchor (CLAY-B and CS-B), strengthened with steel angle (CLAY-C and CS-C).

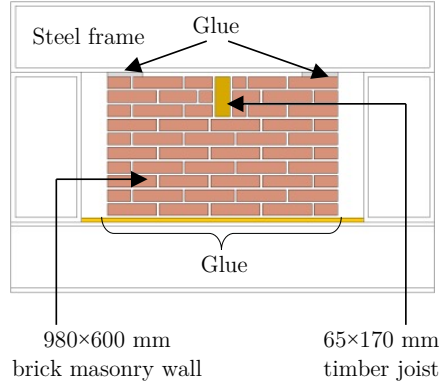


Figure 3.10: Principle of the tested sample representing a timber-masonry connection.

In total, seven configurations were studied (Fig. 3.11), two as-built ones (A, B) and five strengthened ones (C-G). Seven samples were tested for each option, as described in section 3.5.2, resulting in a total number of 49 tests. The two as-built connections consisted again of the simple masonry pocket with mortar (A), and the hook anchor (B).

Strengthening options C and D were tested by reusing the specimens realized for the as-built connections, so that they were in fact retrofitted samples. The first proposed retrofitting solution (C) was the same realized in configurations CLAY-C and CS-C of the pilot study. This strengthening option was applied on the tested samples representing the as-built masonry pocket connection (A), because the weakness of the joist-masonry interface prevented the masonry from being damaged.

Retrofitting method D was, instead, developed for masonry damaged around the joist, which may also be representative for low-quality masonry at the top of a wall. Therefore, for this option a further 80×80 mm joist was attached with 10×165 mm anchors only to sound masonry below the existing joist, and then fastened to it by means of two $90 \times 90 \times 3$ mm steel brackets and four 5×60 mm screws for each of them. In this case, the samples from configuration B were reused, because the presence of the hook anchor was expected to damage the masonry around the joists while testing, as it happened. It should be noted that, before strengthening these samples, the hook anchor was disconnected from the timber joist.

Strengthening options E, F and G were tested on newly-built replicated walls. Configuration E consisted of a $240 \times 240 \times 14$ mm hook anchor fastened to the joist with three 4×55 mm nails and then glued with epoxy to a $25 \times 40 \times 240$ mm incision realized on the front side of the wall.

Retrofitting method F was realized by connecting the joist to the wall with two inclined 7×180 mm screws. These were inserted into the joist after drilling holes of 10 mm diameter in the masonry and filled with injected epoxy: the screws were, therefore, partly embedded in the epoxy, and partly inserted in the joist. This intervention can be realized from the outside of a building: directly, when the measure is applied to gables, or by removing a limited number of bricks from the outer leaf, for the inner leaf of a cavity wall.

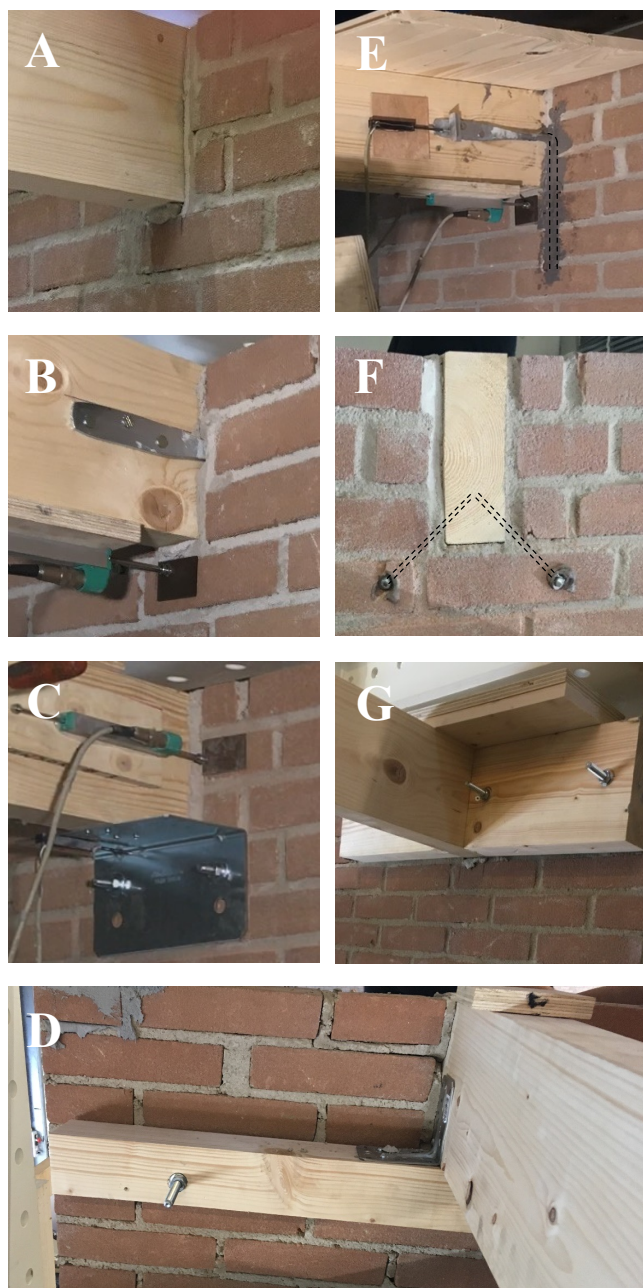


Figure 3.11: Overview of the seven configurations tested in the second phase: as-built with mortar pocket (A); as-built with hook anchor (B); strengthened with steel angle (C); strengthened with additional joist and steel brackets (D); strengthened with hook anchor glued into the wall (E); strengthened with two screws glued into the wall (F); strengthened with timber blocks (G).

Configuration G was realized with 65×170 mm timber blocks placed on both sides of the joist (in practice they would be positioned between each couple of joists). This option was also part of the floor strengthening intervention of sample DFpar-4s (Section 3.4.1). The blocks were firstly fixed to the existing joist by means of two 5×70 mm screws drilled at an angle of 45 degrees, and then fastened to the masonry with two 10×165 mm mechanical anchors each. However, since this intervention would in practice involve also the timber diaphragm, it was important to recreate the same conditions: hence, besides the presence of a 18×165 mm plank, fixed to the joist with two 3×65 mm nails, also an additional 18-mm-thick plywood panel overlay was fastened to the plank and inside the blocks with five 5×70 mm screws. While for configurations E and F the goal was the achievement of a much higher strength and stiffness compared to the as-built situation, even if renouncing to ductility, with strengthening option G this latter aspect was privileged.

Appendix B reports the drawings of all tested configurations, including the details of the retrofitting methods, for both the pilot study (Section B.1) and the second phase (Section B.2).

With regard to the material characterization of the tested samples, in both campaigns C24 timber [44] was used, namely spruce (*Picea Abies*) [149]; the material properties of wood determined were the same as for timber diaphragms, thus density, elastic modulus, and moisture content. For characterizing the masonry and the mechanical anchors, specific companion tests were performed to determine several relevant material properties:

- Compressive and flexural strength of mortar according to EN 1015-11 [152];
- Density of masonry;
- Compressive strength, elastic modulus, Poisson ratio and peak strain in compression according to EN 1052-1 [142];
- Flexural bond strength according to EN1052-5 [144];
- Shear strength and friction coefficient for masonry triplets according to EN 1052-3 [145].

Besides, since standard pull-out and shear strength values for mechanical anchors are commonly reported in producers' catalogues with reference to C20/25 concrete [153], the adopted mechanical anchors were tested to assess these properties for masonry, following the testing protocol of EN 846-5 [154]. For both pull-out and shear tests, a rate of 0.1 mm/s was applied and the anchors were fastened to the centre of a brick with a penetration length of 70 mm. A specimen before and after the test is shown in Fig. 3.12.

The results of the material characterization are reported in Section 4.2.3, while the outcomes of the two experimental campaigns on full-scale timber-masonry connections are presented in Section 4.4.

3.4.3 Masonry walls

Based on the extracted masonry samples (Section 3.3.5), an extensive campaign on full-scale walls was arranged [155]: both in-plane tests [156, 157] and out-of-plane tests

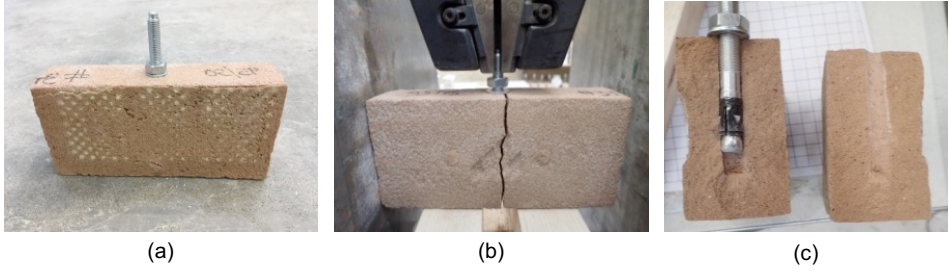


Figure 3.12: Example of specimen prepared for testing pull-out and shear strength of mechanical anchors in masonry: sample before (a) and after testing (b); specimen after removal from test setup (c). From [151].

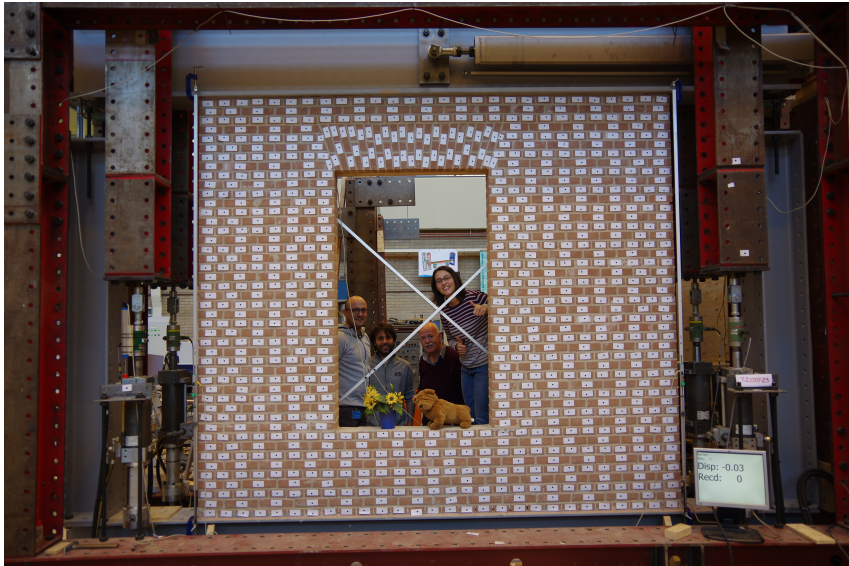


Figure 3.13: Wall TUD_COMP23 (sample with asymmetric opening). From [157].

[104, 158] were performed. The experimental programme on masonry components did not only involve TU Delft, but also EUCENTRE laboratory in Pavia (Italy) [159].

With regard to the walls tested at TU Delft, a summary of their main properties is reported in Tables 3.4 (in-plane tests) and 3.5 (out-of-plane tests). As can be noticed, all masonry types typical of the Groningen region were considered when constructing the structural components. The effect of openings was also taken into account in both loading directions (samples TUD_COMP12 [104] and TUD_COMP23 [158], Fig. 3.13). Besides, the out-of-plane tests were conducted in one-way and two-way bending, to cover both failure mechanisms [103]. For both in-plane and out-of-plane tests, a versatile test setup was designed (Section 3.5.3), adopted also for testing timber diaphragms (Section 3.5.1).

Should the readers be interested in exploring further the characteristics of the tested configurations, they can refer to RAVENSHORST and MESSALI [104], and ESPOSITO

3.4. Definition of the full-scale specimens to be tested

Table 3.4: Characteristics of the masonry walls tested in plane.

Sample name	Dimensions	Vertical pressure (MPa)	Material
	L_w (m) \times H_w (m) \times t_w (m)		
TUD_COMP-0a	$1.1 \times 2.76 \times 0.102$	0.71	Calcium silicate bricks (single-leaf)
TUD_COMP-1	$1.1 \times 2.76 \times 0.102$	0.7	Calcium silicate bricks (single-leaf)
TUD_COMP-2	$1.1 \times 2.76 \times 0.102$	0.51	Calcium silicate bricks (single-leaf)
TUD_COMP-3	$1.1 \times 2.76 \times 0.102$	0.4	Calcium silicate bricks (single-leaf)
TUD_COMP-4	$4.0 \times 2.76 \times 0.102$	0.5	Calcium silicate bricks (single-leaf)
TUD_COMP-5	$4.0 \times 2.76 \times 0.102$	0.3	Calcium silicate bricks (single-leaf)
TUD_COMP-6	$4.0 \times 2.76 \times 0.102$	0.5	Calcium silicate bricks (single-leaf)
TUD_COMP-20	$1.1 \times 2.76 \times 0.102$	0.63	Calcium silicate bricks (single-leaf)
TUD_COMP-21	$3.1 \times 2.71 \times 0.100$	0.36	Solid clay bricks (single-leaf)
TUD_COMP-22	$3.0 \times 2.71 \times 0.210$	0.36	Solid clay bricks (double-wythe)
TUD_COMP-23	$3.1 \times 2.71 \times 0.210$	0.36	Solid clay bricks (double-wythe)
TUD_COMP-24	$1.0 \times 2.74 \times 0.100$	0.6	Calcium silicate elements (single-leaf)
TUD_COMP-25	$1.0 \times 2.74 \times 0.100$	0.6	Calcium silicate elements (single-leaf)

Table 3.5: Characteristics of the masonry walls tested out of plane.

Sample name	Dimensions	Vertical pressure (MPa)	Material
	L_w (m) \times H_w (m) \times t_w (m)		
TUD_COMP-0b	$1.4 \times 2.75 \times 0.102$	0.2 (one-way bending)	Calcium silicate bricks (single-leaf)
TUD_COMP-7	$1.4 \times 2.75 \times 0.102$	0.2 (one-way bending)	Calcium silicate bricks (single-leaf)
TUD_COMP-10	$4.0 \times 2.75 \times 0.100$	0.05 (two-way bending)	Solid clay bricks (single-leaf)
TUD_COMP-11	$3.9 \times 2.76 \times 0.102$	0.05 (two-way bending)	Calcium silicate bricks (single-leaf)
TUD_COMP-12	$4.0 \times 2.76 \times 0.102$	0.05 (two-way bending)	Calcium silicate bricks (single-leaf)
TUD_COMP-26	$4.0 \times 2.71 \times 0.100$	0.06 (two-way bending)	Solid clay bricks (single-leaf)
TUD_COMP-27	$3.8 \times 2.71 \times 0.210$	0.06 (two-way bending)	Solid clay bricks (double-wythe)
TUD_COMP-28	$1.4 \times 2.72 \times 0.120$	0.25 (one-way bending)	Calcium silicate elements (single-leaf)
TUD_COMP-29	$3.6 \times 2.72 \times 0.120$	0.06 (two-way bending)	Calcium silicate elements (single-leaf)

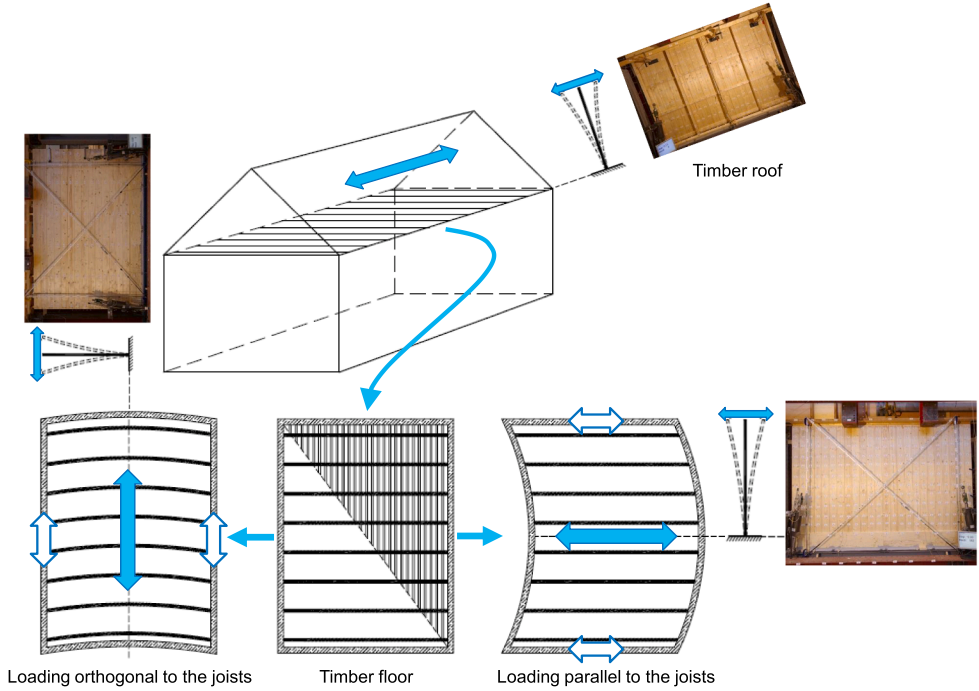


Figure 3.14: Principle for the adopted test configuration of floors and roofs. From [132].

and RAVENSHORST [157] for in-plane tests; RAVENSHORST and MESSALI [156], and DAMIOLA et al. [158] for out-of-plane tests.

3.5 Adopted test setups and testing methods for structural components

3.5.1 Timber diaphragms

In order to make economic use of the versatile setup designed for in-plane tests on timber diaphragms, and in-plane and out-of-plane tests on masonry walls, it was chosen to test in a vertical configuration half of the diaphragm, according to the principle shown in Fig. 3.14. Considering the structural behaviour of the planks (or of the joists), it is possible to test only one half of the diaphragm by clamping its bottom part (centre of symmetry of the floor): in this way, the applied force corresponds to the reaction that the floor is able to bear.

Each tested diaphragm was glued to a bottom HEB 300 steel beam, which was bolted to the part of the test setup connected to the laboratory floor (Fig. 3.15). The horizontal load was introduced by means of an LVL I-beam, fastened to the top joist (or to the wooden blocks shown in Fig. 3.5, when loading orthogonally to the joists) with screws having a diameter of 10 mm and spaced 150 mm. Lateral out-of-plane displacement of the LVL I-beam during the test was prevented by applying vertical

steel elements, covered with Teflon to allow low-friction sliding. In order to ensure the cantilever scheme assumed for the tests, the floors were clamped on the bottom part using two layers of plywood elements glued together and screwed on both sides. With regard to the roof, since only one of the two pitches was tested, the clamping was not necessary, as this was already provided by the wall plate.

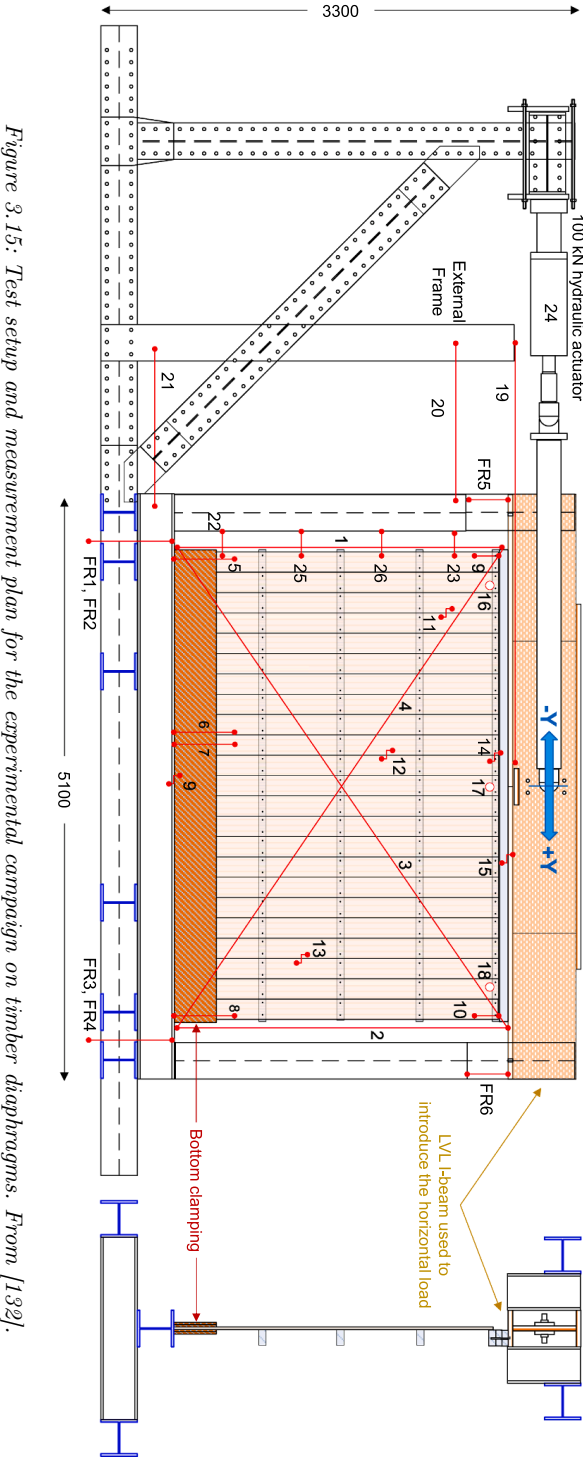
The measurement plan is given again in Figure 3.15: depending on the configuration of the specimens, the position of the sensors was slightly adapted for the different tests. For the strengthened versions of each diaphragm, extra sensors were positioned to record also the horizontal and vertical sliding of the plywood panels. All sensors consisted of LVDTs, except for the ones used to record the out-of-plane displacements of each diaphragm, which were lasers.

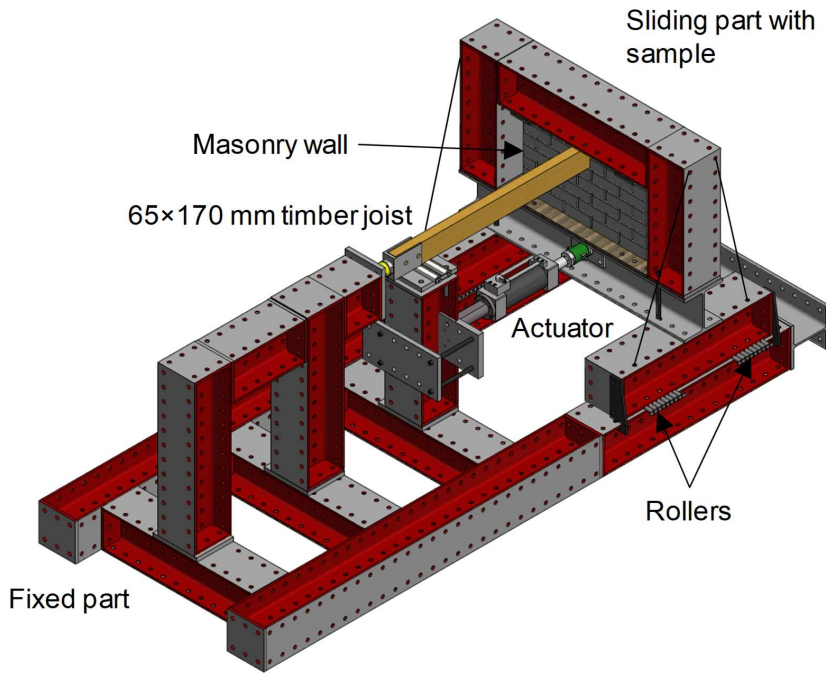
In-plane quasi-static reversed-cyclic tests were performed, according to the loading protocol of ISO 21581 [160]. A variable rate to achieve the ultimate displacement of the diaphragms between 1 and 30 minutes was adopted, in agreement with the provisions of this standard. The test results from this experimental campaign are reported in Section 4.3.

3.5.2 Timber-masonry connections

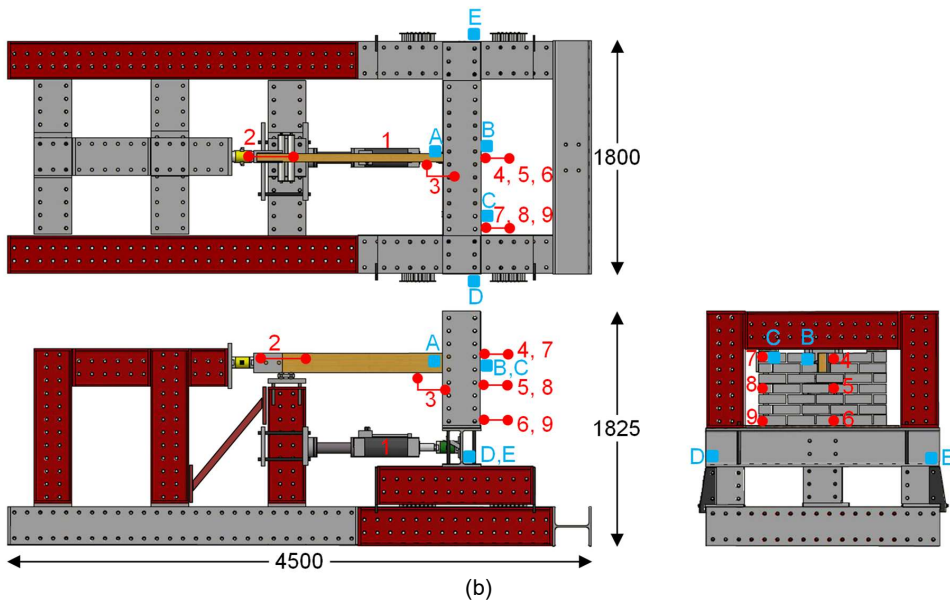
For the experimental campaign on timber-masonry connections, an innovative, versatile setup was designed, allowing to perform monotonic, cyclic and dynamic tests. A 3D view of the test setup is shown in Fig. 3.16a: this was composed of a static part, fastened to the laboratory floor, and a moving part on top of which each specimen was placed. Sliding of the moving part was ensured by rollers, while its possible rotations were prevented by plates and wheels close to the rollers. In this way, it was possible to enable only the axial horizontal displacements transmitted by the actuator, connecting the static part of the setup to the bottom beam on which each wall was built. Every sample was confined by a steel frame, to guarantee its stability; this frame was also further connected with bracings to the edges of the two horizontal steel beams sliding on rollers, in order to ensure an optimal stability against possible vibrations. A weight of 100 kg was hanged with a rope at mid span on the wooden joist, so that a vertical load of 0.5 kN was transferred to the connection, to represent the weight of the portion of floor around the joint in practice. In order to guarantee an effective action of the hydraulic actuator, the column on which it was clamped was further braced to the bottom frame. This bracing, not shown in Fig. 3.16a, is represented in Fig. 3.16b. The displacements were not imposed directly to the joist, but to the bottom part of the wall. In this way, it was possible to use a single, versatile setup with a realistic load application for all the three test typologies. In order to record the force transferred by the connections, a load cell was positioned between the timber joist and a stiff frame in the rear part of the setup.

Fig. 3.16b shows the adopted measurement plan: for monotonic and quasi-static tests, potentiometers were used (sensors 1-9). Only for dynamic tests, accelerometers were also placed (sensors A-E, with maximum capacity 2.5g), to have a more accurate detection of the connections response due to a sudden solicitation. Sensor 3 was the most meaningful source of information, because it measured the relative displacement between joist and wall. Sensors 4 to 9 recorded the out-of-plane displacements of the wall, and they were fastened to a wooden structure clamped in front of it. Furthermore,





(a)



(b)

Figure 3.16: Test setup (a) and measurement plan (b) for the experimental campaign on timber-masonry connections. From [151].

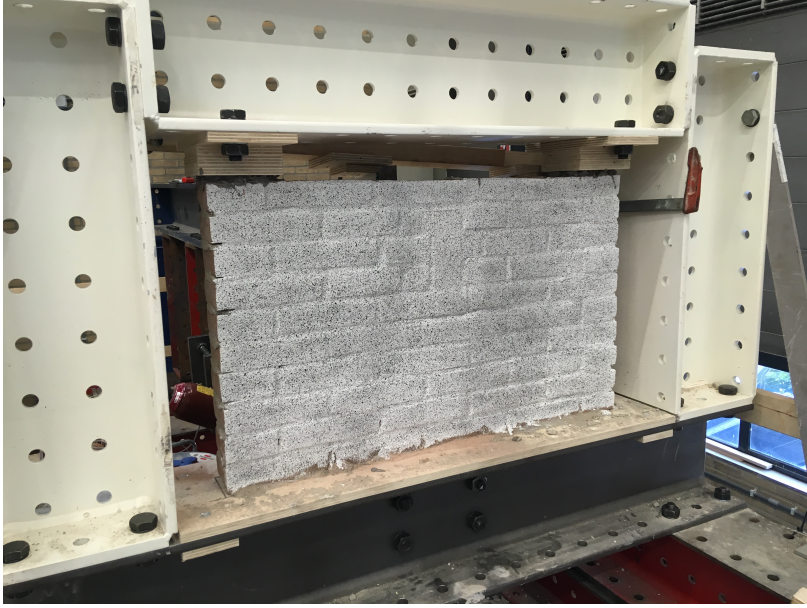


Figure 3.17: Pattern applied to a sample to detect out-of-plane displacements of the masonry wall with DIC technique. From [150].

for strengthened configurations a larger number of sensors were adopted, to detect also local mechanisms, such as deformation of steel angle or brackets, slip of screws, and sliding between timber elements [148, 149]. The following sign convention was adopted:

- A positive displacement sign corresponds to a pulling force on the connection (and therefore to a pushing action of the actuator at the bottom of the sample);
- A negative displacement sign corresponds to a pushing force on the connection (and therefore to a pulling action of the actuator at the bottom of the sample).

Besides the adopted sensors, for the two stiffest configurations (E and F), for which small displacements were expected, also *digital image correlation* (DIC) technique was employed, to have a complete coverage of the samples' response. The DIC system consisted of two cameras, placed at 700 mm from the wall's front side, having a resolution of 4096×3000 pixels each, and a frame rate up to 100 fps: this enabled the detection of out-of-plane and three-dimensional mechanisms, also for dynamic tests. A random pattern with matt black colour was applied to the front side of the walls for detecting their displacements (Fig. 3.17).

During the preliminary pilot study [148], only quasi-static reversed-cyclic tests were performed according to ISO 16670 [138], and one sample was built per each tested configuration. Instead, in the second testing phase [149], seven tests were performed for each configuration under displacement control: one monotonic test (M) to determine the ultimate displacement, three quasi-static reversed-cyclic tests (QS), and three high-frequency dynamic tests (HFD). Tables 3.6 and 3.7 report an overview of the performed tests and the adopted nomenclature.

Table 3.6: Overview of the tests performed in the preliminary pilot study and adopted nomenclature.

Configuration	Description	Test types	Specimen name(s)
CLAY-A	As-built joist-wall connection. Clay bricks double-wythe wall with the joist in a mortar pocket.	1 quasi-static cyclic test	CLAY-A-1
CLAY-B	As-built joist-wall connection. Clay bricks double-wythe wall with hook anchor masoned in the wall.	1 quasi-static cyclic test	CLAY-B-1
CLAY-C	Clay bricks double-wythe wall. Strengthening option for joist-wall connections in sound masonry. Retrofitting with an angle bracket screwed to the joist and anchored to the wall.	1 quasi-static cyclic test	CLAY-C-1
CS-A	As-built joist-wall connection. Calcium silicate bricks single-leaf wall with the joist in a mortar pocket.	1 quasi-static cyclic test	CS-A-1
CS-B	As-built joist-wall connection. Calcium silicate bricks single-leaf wall with hook anchor.	1 quasi-static cyclic test	CS-B-1
CS-C	Calcium silicate bricks single-leaf wall. Strengthening option for joist-wall connections in sound masonry. Retrofitting with an angle bracket screwed to the joist and anchored to the wall.	1 quasi-static cyclic test	CS-C-1

Monotonic and quasi-static reversed-cyclic tests were performed also for this second phase according to ISO 16670 [138]. Therefore, after determining the ultimate displacement of each configuration with monotonic tests, the amplitudes of the cycles were defined accordingly, and each cycle consisted of three runs in agreement with the standard. A rate of 0.3 mm/s was adopted.

Dynamic tests were performed by applying to the specimen a specific high-frequency signal generated by the hydraulic actuator. This dynamic signal was chosen starting from shaking table tests on typical Dutch buildings: it consisted of a recorded displacement history of a timber-masonry connection at roof level during a shaking table test performed at EUCENTRE [161], and it is shown in Fig. 3.18 together with the performed runs. This reference signal was induced in the joint by an input seismic accelerogram from the Groningen area, corresponding to 133% of the estimated reference response spectrum of that region, for a 2475 years return period [161]. It should be noticed that such an earthquake has never occurred in that region, therefore no comparison with damage observed in practice until recently can be made. The dynamic tests were conducted starting from a very small-amplitude signal (2.5% of the reference one from [161], Fig. 3.18), and then repeating it, progressively increasing the amplitude until collapse

Table 3.7: Overview of the tests performed in the second large-scale campaign and adopted nomenclature.

Configuration	Description	Test types	Specimen name(s)
A	As-built joist-wall connection. Clay bricks single-leaf wall with the joist in a mortar pocket.	1 quasi-static monotonic test	A-M-1
		3 quasi-static cyclic tests	A-QS-1, A-QS-2, A-QS-3
		3 high-frequency dynamic tests	A-HFD-1, A-HFD-2, A-HFD-3
B	As-built joist-wall connection. Clay bricks single-leaf wall with hook anchor.	1 quasi-static monotonic test	B-M-1
		3 quasi-static cyclic tests	B-QS-1, B-QS-2, B-QS-3
		3 high-frequency dynamic tests	B-HFD-1, B-HFD-2, B-HFD-3
C	Strengthening option for joist-wall connections in sound masonry. Configuration A retrofitted with an angle bracket screwed to the joist and anchored to the wall.	1 quasi-static monotonic test	C-M-1
		3 quasi-static cyclic tests	C-QS-1, C-QS-2, C-QS-3
		3 high-frequency dynamic tests	C-HFD-1, C-HFD-2, C-HFD-3
D	Strengthening option for joist-wall connections in damaged or low-quality masonry. Configuration B retrofitted with a further joist anchored to sound masonry and fixed to the existing joist with steel brackets. The hook anchor is disconnected.	1 quasi-static monotonic test	D-M-1
		3 quasi-static cyclic tests	D-QS-1, D-QS-2, D-QS-3
		3 high-frequency dynamic tests	D-HFD-1, D-HFD-2, D-HFD-3
E	Clay bricks single-leaf wall. Strengthening with an hook anchor nailed to the joist and glued to the wall after being placed in a previously realised incision on it.	1 quasi-static monotonic test	E-M-1
		3 quasi-static cyclic tests	E-QS-1, E-QS-2, E-QS-3
		3 high-frequency dynamic tests	E-HFD-1, E-HFD-2, E-HFD-3
F	Clay bricks single-leaf wall. Strengthening with two inclined screws inserted into the joist after drilling in the masonry proper holes, filled with epoxy.	1 quasi-static monotonic test	F-M-1
		3 quasi-static cyclic tests	F-QS-1, F-QS-2, F-QS-3
		3 high-frequency dynamic tests	F-HFD-1, F-HFD-2, F-HFD-3
G	Clay bricks single-leaf wall. Strengthening with timber blocks placed on both sides of the existing joist, screwed to it and to timber floor, and anchored to the wall.	1 quasi-static monotonic test	G-M-1
		3 quasi-static cyclic tests	G-QS-1, G-QS-2, G-QS-3
		3 high-frequency dynamic tests	G-HFD-1, G-HFD-2, G-HFD-3

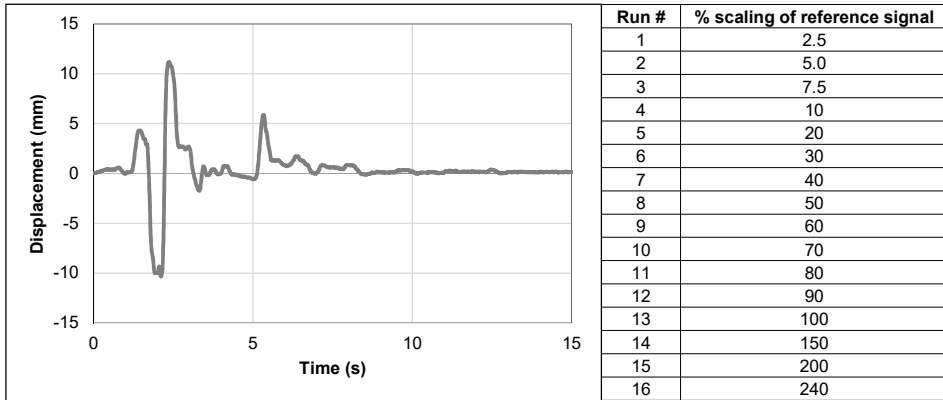


Figure 3.18: Adopted signal for HFD tests and performed runs; for as-built configurations A and B the maximum reached amplitude was 150% of the reference signal, linked to a 2475 years return period.

(or maximum applied displacement) was reached. In this way, a procedure similar to nonlinear incremental dynamic analyses was followed. It should be noticed that for as-built configurations A and B the largest reached amplitude was 150 mm, while for strengthened configurations C to G displacements up to 240 mm were applied, corresponding to the maximum actuator capacity. The reduced amplitude for as-built connections was adopted in order not to excessively damage the samples, enabling their reuse afterwards for testing configuration C and D (Section 3.4.2).

All test results from the experimental campaign on timber-masonry connections are reported in Section 4.4.

3.5.3 Masonry walls

For both in-plane and out-of-plane tests, the adaptable setup used for timber diaphragms was adopted, with a number of adjustments [104], [156]-[158], [162].

For the experimental campaign on the in-plane response of masonry walls, the test setup consisted of a steel frame with horizontal and vertical actuators (Fig. 3.19): the horizontal actuator for introducing in-plane displacements had a capacity of 400 kN; the vertical actuators for introducing axial pre-compression had a capacity 100 kN each. The vertical loading in the actuators could be differentiated to achieve two different boundary conditions, i.e. cantilever or double-clamped configuration. All actuators were computer-controlled. The specimens were glued to a steel beams at the bottom and the top, to prevent sliding shear failure and tension failure at the steel-masonry contact layer. Failures due to tensile bending stresses or shear could therefore occur only in the masonry and not at the steel-masonry contact layer. The bottom steel beam was attached to the frame anchored to the laboratory floor, while a steel girder, connected to the horizontal actuator, was bolted to the top steel beam. Out-of-plane rotations or displacements of the wall samples were prevented with vertical beams and bracings. With respect to the test set-up for the slender walls, on the squat walls the vertical actuators were moved outwards to create a larger lever arm; consequently, two extra

steel beams were added above the top steel girder, to ensure a uniform spreading of the vertical load on the top of the masonry wall. With regard to the loading protocol, each wall was cyclically tested in displacement control under quasi-static conditions. Each specimen was initially subjected to the targeted level of vertical pre-compression, which remained constant and equally distributed on top of the wall throughout the whole duration of the test. Then, horizontal displacements were applied to the top of the specimen through the software-controlled actuator, with cycles of increasing amplitude. An initial cycle in load control was performed up to 20% of the expected peak lateral force of the wall, and the corresponding displacement was measured. The amplitude of the following cycles was then determined as multiple of this displacement. Each cycle was composed of three repetitions, and an increasing displacement rate was adopted, so that every cycle lasted about 10 min, until a maximum rate of 1.5 mm/sec was achieved.

For the experimental campaign on the out-of-plane response of masonry walls, the test set-up featured a system of coupled airbags on both sides of the specimens, to apply uniform horizontal loads (Figs. 3.20 and 3.21). The airbags were supported by a timber sandwich reaction frame: load cells on both sides of this frame provided the activated loads; the difference between the loads measured on both sides was thus the net force taken up by the wall. The test was performed under displacement control, by adjusting the pressure in the airbags until the achievement of the desired deformation. During the test most of the walls were not visible, so the crack pattern had to be visually examined after the test. Similarly to the in-plane experimental campaign, both slender and squat walls were tested: the former were subjected to one-way bending, the latter to two-way bending. The walls were glued on wooden strips bolted to a top and a bottom steel beam. These two beams were connected by four springs (two per side), having a stiffness of 50 kN/m each. The springs allowed to apply a pre-compression force on the samples, which was measured by load cells. After establishing the initial pressure on the airbags, every deformation step was applied three times in the positive and negative direction. The deformations were increased each step by 0.5 mm in the first stages, and by up to 10 mm in the final stages; the displacement at midspan was controlled.

A summary of the results on component tests is reported in Section 4.5. For further details on the large-scale experimental campaign performed at TU Delft for characterizing the seismic performance of Dutch masonry walls, the reader is referred to [104], [156]-[158], [162].

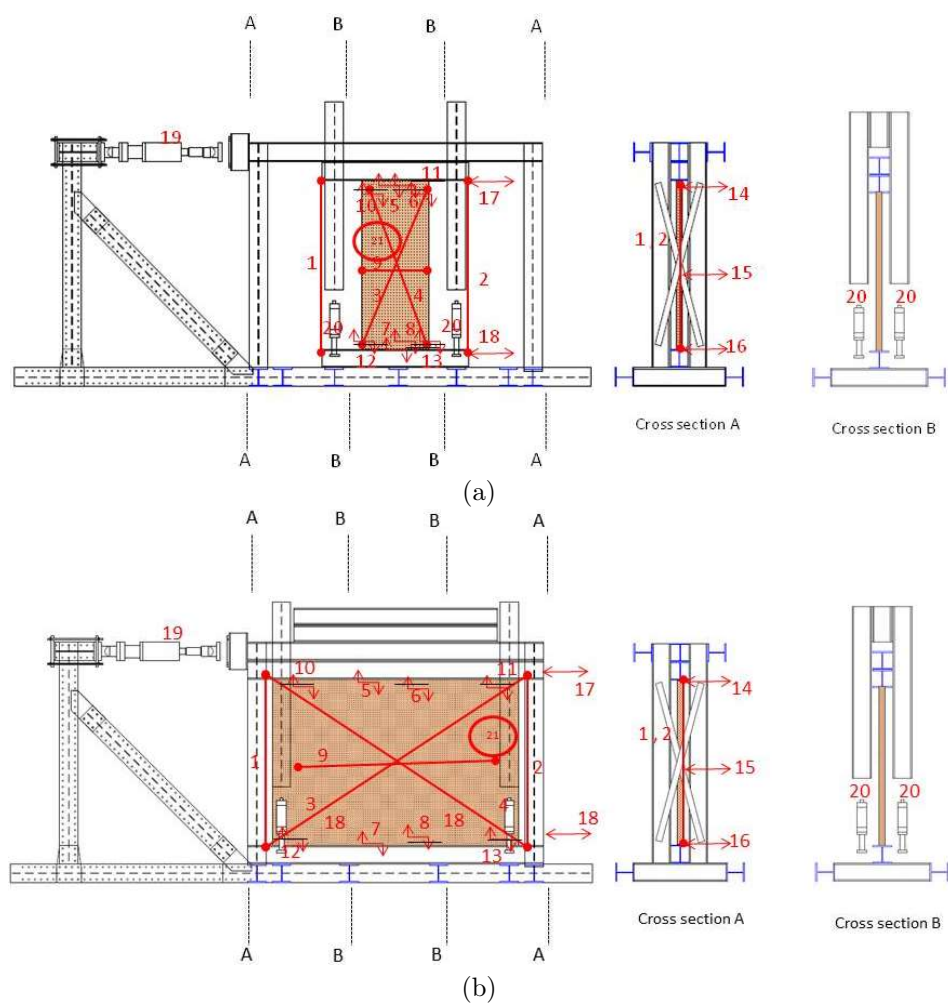
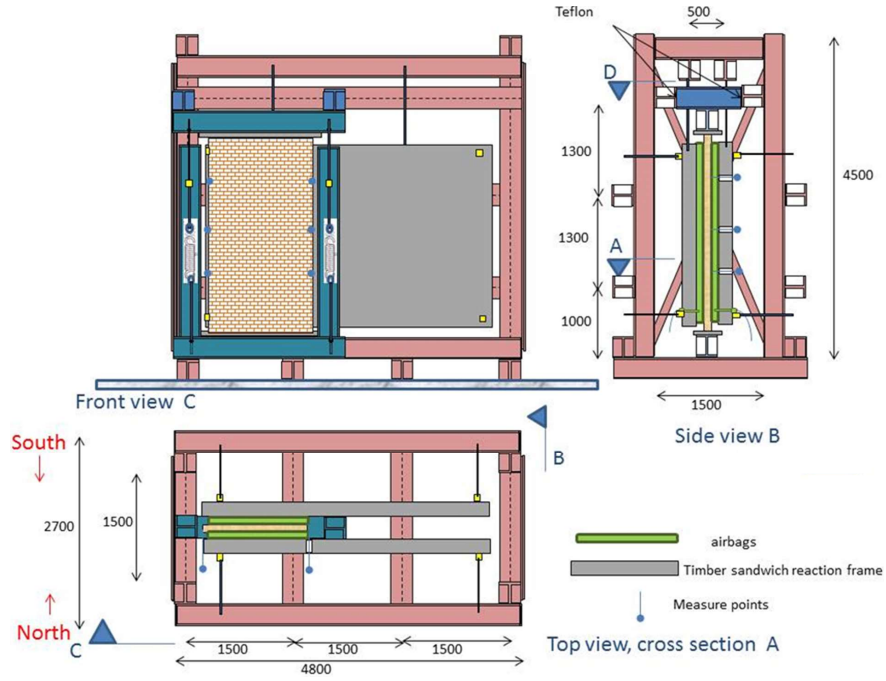
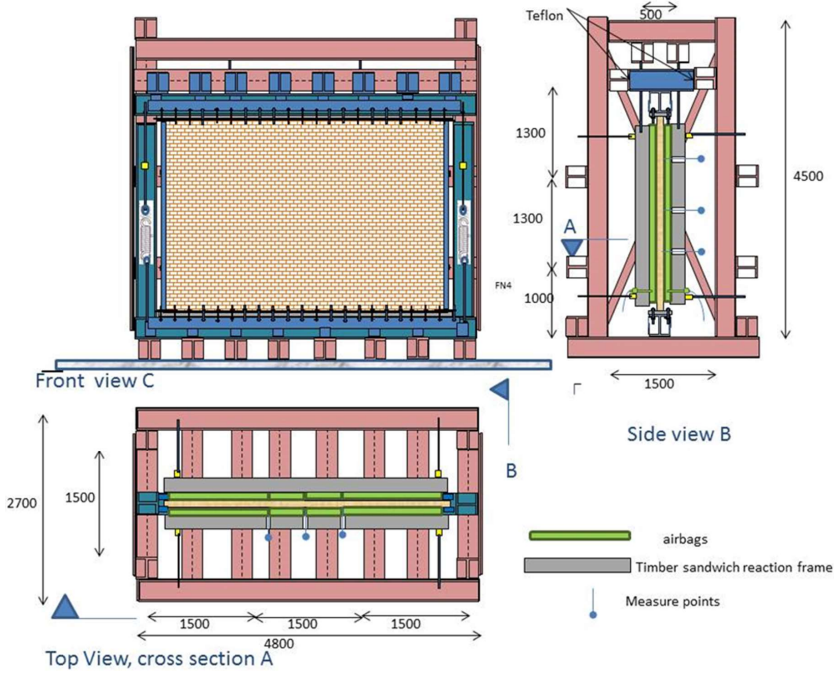


Figure 3.19: Test setup and measurement plan adopted for the in-plane tests on slender (a) and squat walls (b). From [156].



(a)



(b)

Figure 3.20: Test setup adopted for the out-of-plane tests on slender (a) and squat walls (b). From [104].

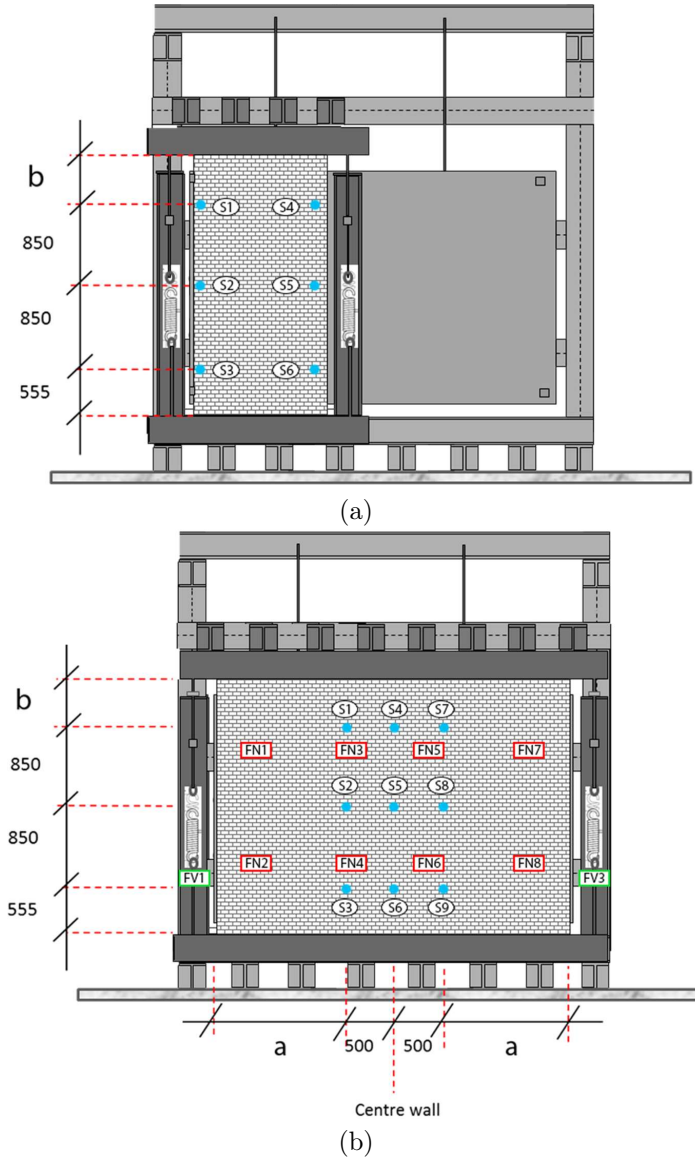


Figure 3.21: Measurement plan adopted for the out-of-plane tests on slender (a) and squat walls (b); both load cells (FN or FV) and sensors (S) are highlighted. From [158].

Chapter 4

Experimental results

4.1 Introduction

This chapter firstly addresses the outcomes of the replication process (Section 4.2), focusing in detail on material properties of timber diaphragms and timber-masonry connections. Secondly, the results from the experimental campaign on timber diaphragms are presented and thoroughly discussed in Section 4.3, characterizing also their dissipative role in terms of an equivalent hysteretic damping ratio. Furthermore, in section 4.3.7 the outcomes of the performed experimental tests on timber diaphragms will be compared to similar literature studies (Chapter 2) in terms of equivalent in-plane shear stiffness evaluated at different drift limits.

Then, Section 4.4 reports and discusses the results obtained from the tests conducted on timber-masonry connections. Finally, to complete the overview on the seismic characterization of structural components, a summary of the results from the experimental campaign on masonry components, conducted by a different research group, is provided in Section 4.5.

4.2 Results from material characterization

4.2.1 Material properties of extracted and replicated timber samples and fasteners

With reference to the methodology described in Section 3.3.3, Tables 4.1 and 4.2 show the results in terms of material properties of timber structural elements and fasteners, respectively, and provide a comparison between the characteristics of original and replicated samples. The two tables report the number n of tested samples, the average value of the parameter of interest (Av.), and the corresponding coefficient of variation (CoV).

On the basis of the obtained results, the replication was regarded as sufficiently accurate, leading to similar properties for replicated samples with respect to the extracted ones. A slightly larger difference was detected for the fasteners, essentially because of two reasons:

Table 4.1: Comparison of the material properties of timber joists and planks from extracted and replicated samples.

Property	Extracted specimens			Replicated specimens		
	n	Av.	CoV (%)	n	Av.	CoV (%)
ρ (kg/m ³)	27	481	9.6	35	474	10.2
E_{dyn} (N/mm ²)	27	12990	18.3	35	11830	21.2
$m.c.$ (%)	21	9.2	2.0	39	11.3	16.2

Table 4.2: Comparison of the characteristics of fasteners (3×65 mm nails) from extracted and replicated samples.

Property	Extracted specimens			Replicated specimens		
	n	Av.	CoV (%)	n	Av.	CoV (%)
T (MPa)	28	655	14.8	8	792	2.0
M_p (kNmm)	23	3.2	10.1	8	3.9	3.2

1. Newly produced nails are characterized by higher quality and better, standardized properties compared to older ones;
2. The majority of the extracted nails were slightly rusty.

However, it is worth remarking that, although this difference in terms of material properties was detected for the single fasteners, the behaviour of the whole plank-joint connections proved to be similar, as noticeable in Section 4.2.2. This phenomenon can be explained considering an extensive research study of VAN DE KUILEN [163], in which it is demonstrated that timber joints with rusty nails can show an increase of 20-25% in capacity compared to normal ones, because of the higher friction between wood and steel that could develop. This increase is within the same range as the recorded difference in properties between extracted and replicated samples: the higher values obtained for the new nails are therefore compensated in the whole plank-joint connections by the improvement in capacity given by rusty nails. For further information on the material properties of timber elements and fasteners, the reader is referred to [164].

Additionally, material properties of the plywood panels used for strengthening the diaphragms were determined (Table 4.3). The dynamic elastic modulus was measured in the direction parallel and perpendicular to the face grain of the panels.

4.2.2 Cyclic behaviour of extracted and replicated plank-joint connections

The response of plank-joint connections under quasi-static cyclic loading was determined as described in Section 3.3.4. Fig. 4.1 shows a typical example for comparison: the two cyclic responses are practically coincident until an already large displacement (10 mm), and display sufficiently similar values of strength and stiffness, considering the

Table 4.3: Material properties of the plywood panels used for strengthening the diaphragms.

Property	n	Av.	CoV (%)
ρ (kg/m ³)	39	473	3.5
$E_{dyn,0}$ (N/mm ²)	5	7130	6.8
$E_{dyn,90}$ (N/mm ²)	5	6310	11.2
$m.c.$ (%)	29	9.2	19.3

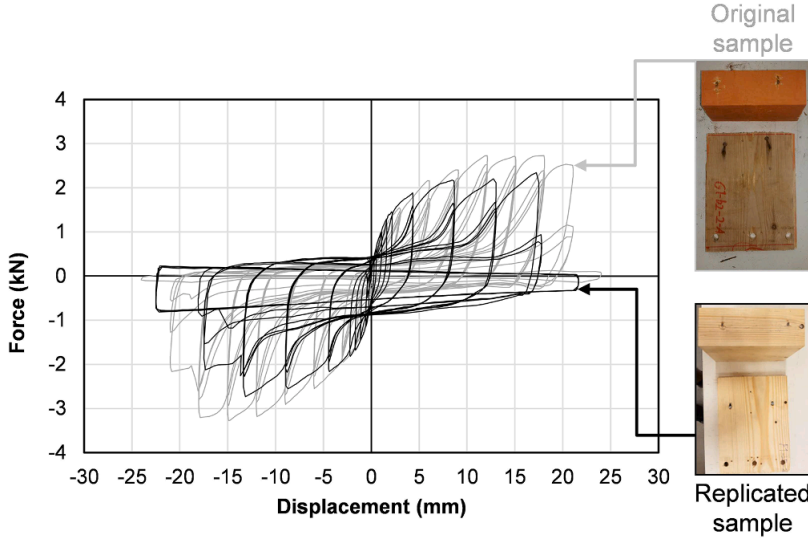


Figure 4.1: Comparison between the cyclic response of original and replicated plank-joint connections. From [132].

scatter that normally affects tests on timber joints. Furthermore, by visual observation, the shape of the hysteretic cycles appears to be similar as well.

From the performed tests, it was concluded that the replicated samples were able to show a comparable response under cyclic loading with respect to the extracted ones, and were therefore regarded as adequately representative for them. For an overview on all test results on plank-joint connections, the reader is referred to [165].

4.2.3 Material properties of replicated timber-masonry connections

The material characterization of timber-masonry connections took place according to the methodology described in Section 3.4.2. The properties of the timber joists used for the construction of the specimens are reported in Table 4.4. As can be noticed, the obtained values are in line with those measured for timber diaphragms (Table 4.1), thus confirming the accuracy of the replication process also for the timber-masonry connections samples.

Table 4.4: Material properties of the timber joists used for the construction of timber-masonry connection samples.

Property	n	Av.	CoV (%)
ρ (kg/m ³)	21	477	11.0
E_{dyn} (N/mm ²)	21	12216	16.0
$m.c.$ (%)	36	13	6.0

Table 4.5: Material properties of clay brick masonry used for the construction of timber-masonry connection samples, determined according to Section 3.4.2.

Property	n	Av.	CoV (%)
Compressive strength of mortar (MPa)	48	4.84	11.0
Flexural strength of mortar (MPa)	24	2.05	15.0
Density of masonry (kg/m ³)	43	1602	5.0
Compressive strength of masonry (MPa)	6	11.87	9.0
Average elastic modulus of masonry (MPa)	6	3278	17.0
Poisson ratio of masonry	6	0.15	17.0
Flexural bond strength (MPa)	28	0.11	51.0
Shear strength (MPa)	18	0.15	10.0
Friction coefficient	18	0.78	10.0

The characterization of masonry walls was conducted in cooperation with the *Applied Mechanics* Section of TU Delft. The same principles and methodology adopted for all construction campaigns of replicated masonry components were followed. The main material properties of both clay and calcium silicate masonry used to build the connection samples are reported in Tables 4.5 and 4.6, respectively, and were derived according to standardized companion tests. These properties were in line with those obtained from past construction phases, and thus constituted a fair and safe replication of existing low-quality masonry typical of the Groningen area [166].

Finally, also the peak strength and stiffness of the mechanical anchors in pull-out and shear load were determined: the results are reported in Table 4.7. This characterization was necessary because little information is available on the performance of such connectors in masonry, since their strength is normally evaluated and reported for their use in concrete [153].

Interestingly, it can be noticed that the pull-out load is halved compared to that referred to concrete, while in shear the obtained resistance in masonry is much lower, due to the weak and brittle behaviour of bricks. However, since the shear resistance is in practice already provided by the presence of joists in the masonry pockets, the most

Table 4.6: Material properties of calcium silicate brick masonry used for the construction of timber-masonry connection samples, determined according to Section 3.4.2

Property	n	Av.	CoV (%)
Compressive strength of mortar (MPa)	12	8.76	10.1
Flexural strength of mortar (MPa)	6	3.55	9.8
Density of masonry (kg/m ³)	15	1819	1.8
Compressive strength of masonry (MPa)	3	6.42	3.8
Average elastic modulus of masonry (MPa)	3	4586	23.6
Poisson ratio of masonry	3	0.16	20.0
Flexural bond strength (MPa)	15	0.39	25.6
Shear strength (MPa)	9	0.18	7.1
Friction coefficient	9	0.46	7.2

Table 4.7: Pull-out, shear strength and stiffness of mechanical anchors; the obtained values for clay brick masonry are also compared to the characteristic values reported by the producer with reference to C20/25 concrete [153].

Test type	Property	n	Av.	CoV (%)	Producer's value for C20/25 concrete
Pull-out	Pull-out strength (kN)	7	6.14	19.0	13.0
	Initial stiffness (kN/mm)	7	8.27	32.0	Not reported
Shear	Shear strength (kN)	8	2.68	16.0	21.4
	Initial stiffness (kN/mm)	8	1.19	40.0	Not reported

relevant property remains the axial capacity of the anchors, essential to guarantee the load transfer between floor joists and out-of-plane walls, and to prevent their collapse. These results enabled a better characterization of the structural capacity of mechanical anchors to be used for retrofitting of masonry buildings.

4.3 Analysis of test results for timber diaphragms

4.3.1 General

This section presents the results of the quasi-static cyclic in-plane tests conducted for the replicated as-built and strengthened timber diaphragms. The hysteretic cycles depicted in the graphs refer to the horizontal deflection of the diaphragms measured at their top (sensor 19 in Fig. 3.15). The experimental outcomes are discussed separately

for the samples loaded parallel to the joists (DFpar-1 and -1s, DFpar-2 and -2s, Section 4.3.2) and perpendicular to the joists (DFper-3 and -3s, DFper-4 and -4s, Section 4.3.3), and for the tested roof pitch (DRpar-5 and -5s, Section 4.3.4). A number of relevant outcomes from these tests are then summarized in Section 4.3.5. Besides, because of the high energy dissipation provided by the retrofitted diaphragms, their dissipative properties are investigated (Section 4.3.6). Finally, the obtained results in terms of in-plane stiffness are compared to similar outcomes from literature, and a simple, uniform criterion for this comparison is defined 4.3.7.

4.3.2 Specimens loaded parallel to the joists

The cyclic response obtained for specimens DFpar-1 and -1s, and DFpar-2 and -2s is shown in Fig. 4.2. Both as-built diaphragms displayed a flexible in-plane behaviour, with very limited energy dissipation. The small scatter in stiffness between the two floors was given by the different thicknesses of the planks (18 mm for sample DFpar-1, 24 mm for sample DFpar-2). No signs of global failure of the diaphragms were present after the end of the tests, so the plywood panels retrofitting could be subsequently applied.

The first strengthened floor (DFpar-1s) showed a strong improvement in stiffness and strength with respect to the original configuration. At large displacement values, failure of nails and screws was observed on top of the floor, together with an overall plasticization of fasteners across the diaphragm. This can also be noticed from the large amount of dissipated energy visible in the graph of Fig. 4.2, which was greatly enhanced compared to the as-built sample.

The second strengthened floor (DFpar-2s) was characterized by an even stronger and stiffer response, probably because of the more accurate positioning of the plywood panels on the existing sheathing (Section 3.4.1). Similarly to the previous case, high energy dissipation took place in the fasteners. Unfortunately, it was not possible to test this floor until large displacements, due to the sudden failure of the bottom epoxy layer. Despite this inconvenience, the reached level of displacement was still sufficient to characterize the in-plane behaviour of this retrofitted diaphragm.

4.3.3 Specimens loaded perpendicular to the joists

The in-plane cyclic behaviour obtained for specimens DFper-3 and -3s, and DFper-4 and -4s is depicted in Fig. 4.3. In as-built floors, very flexible in-plane behaviour and low energy dissipation were observed, and the difference in the response between the hinged (DFper-3) and the clamped (DFper-4) configuration displayed in Fig. 3.5 was negligible. Because of the very low stiffness of these samples, the contribution of friction among the planks was not negligible in comparison to the other loading direction: also for Dutch timber diaphragms, an orthotropic behaviour of the floors was observed, thus confirming the outcomes of WILSON et al. [25]. No signs of global failure of the diaphragms were present after both tests, and therefore the samples were strengthened afterwards.

The first retrofitted floor (DFper-3s) displayed a great improvement in strength, stiffness and energy dissipation. After 30-40 mm displacement a softening phase took place, initiated by the progressive plasticization and failure of the top nails. This fact

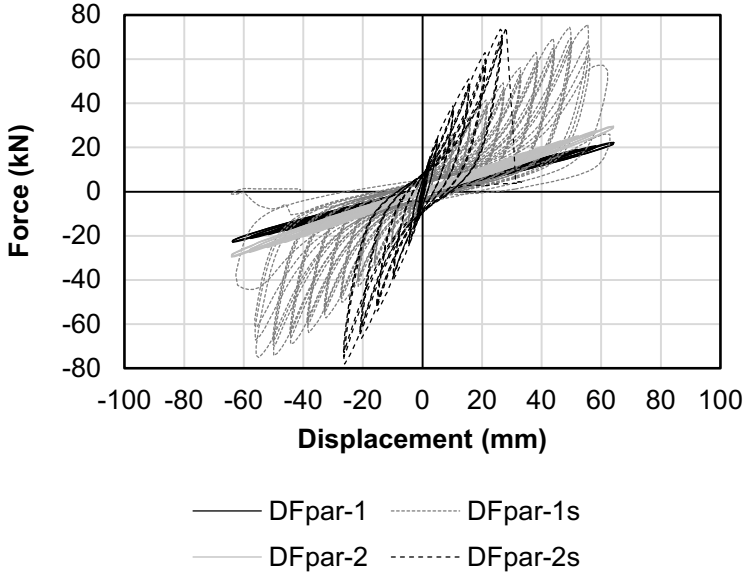


Figure 4.2: Experimental cyclic in-plane response of the as-built and retrofitted timber diaphragms tested parallel to the joists.

caused the joists to move independently of the sheathing, and therefore the whole resistance of the floor could not be activated.

For sample DFper-4s, the insertion of timber blocks in between the joists allowed for a better transmission of shear forces. This additional measure led to an overall much stiffer behaviour, and the diaphragm could deflect as a whole shear wall, unlike the previous strengthened case. The consequence was an improvement in strength and stiffness, but also in the capacity to withstand high lateral forces at large levels of displacement. As can be noticed, compared to sample DFper-3s, specimen DFper-4s is characterized by a much smoother softening phase (less than 20% of the peak value), although widespread plasticization in the fasteners and cracks in timber at large displacements occurred. This is also the reason of the high energy dissipation noticeable from the graph. Apart from plastic behaviour, few screws were also subjected to tensile failure.

4.3.4 Roof pitch specimen

The cyclic response of the tested roof specimen is reported in Fig. 4.4. In this case, because of the very flexible connection between each rafter and the wall plate, the roof was almost not able to withstand horizontal forces, confirming that this diaphragm type could be very vulnerable to seismic actions. No signs of global failure of the diaphragm were observed after the end of the test, so the specimen was subsequently retrofitted with the plywood panels overlay and the bottom steel angles for improving the shear transfer to the wall plate. This strengthening measure allowed to strongly improve the behaviour of sample DRpar-5s, in terms of in-plane strength, stiffness and energy dissipation. The test was stopped after the pull-out failure of top nails and of few bottom screws of the steel angle was observed.

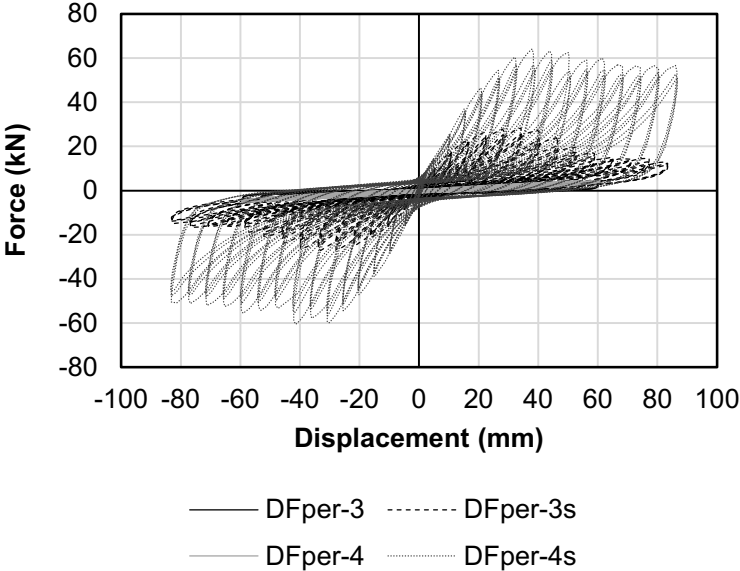


Figure 4.3: Experimental cyclic in-plane response of the as-built and retrofitted timber diaphragms tested perpendicular to the joists.

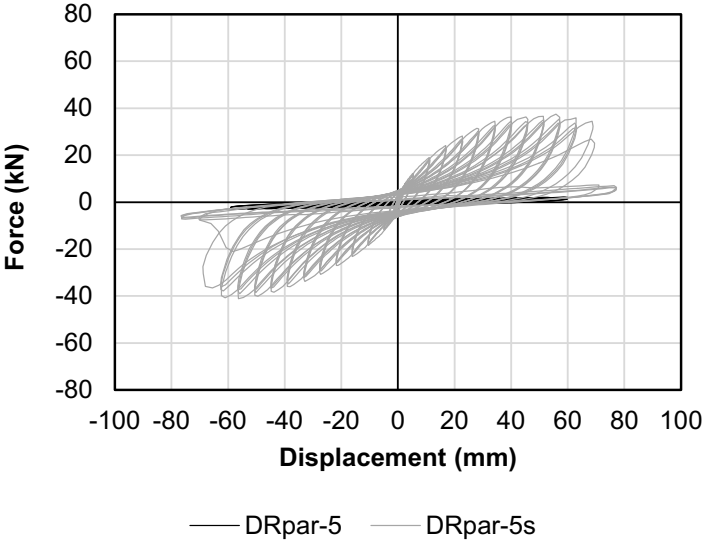


Figure 4.4: Experimental cyclic in-plane response of the as-built and retrofitted sample representing a roof pitch.

4.3.5 Discussion

From the reported test results on timber diaphragms, some important aspects can be highlighted. Firstly, all as-built timber diaphragms appeared to be very flexible, and especially in the direction orthogonal to the joists. With the applied strengthening technique, on the contrary, strength and stiffness of the diaphragms were largely improved. Furthermore, another interesting benefit of such retrofitting intervention is related to energy dissipation. In fact, refurbishment techniques such as use of FRP strips or RC slabs lead to high stiffening of floors, but normally the amount of dissipated energy is limited [16]. Instead, with the adopted reversible strengthening method, the floor is at the same time stronger, stiffer and also able to helpfully dissipate part of the energy provided by the earthquake. The goal of enhancing the beneficial damping properties of the diaphragms, highlighted in Section 3.4.1, was therefore achieved.

The aforementioned improved characteristics were noticed in all tested diaphragms, but are of importance especially for the roof sample. Strengthening a roof is a delicate intervention, because on the one hand an excessive flexibility may cause the whole building to be locally or globally damaged; on the other hand, if the stiffening method is associated with a not negligible increment of mass and/or lack of dissipative properties, the overall performance of the building can even be worsened. This is because the highest load provided by the earthquake occurs on top of the building, and the presence there of a too stiff and heavy structural element increases the horizontal load transferred to the walls. On the contrary, the proposed strengthening technique allows to maintain at the same time light and sufficiently stiff diaphragms, which are also able to beneficially dissipate energy.

Besides, the tested as-built diaphragms clearly showed a difference in their response depending on the loading direction. Yet, after strengthening, this orthotropic behaviour was much more mitigated if compared to the scatter observed for the as-built diaphragms: especially when besides the plywood panels timber blocks were placed (sample DFper-4s), the response in the two loading directions was very similar.

A last consideration involves the observed way of deflecting of the floors: the differences in deformed shapes between as-built and strengthened timber diaphragms were evaluated at 10 and 30 mm displacement. For as-built floors, a behaviour dominated by bending stiffness was noticed, while for their strengthened versions the response was shear-related (Fig. 4.5). The only specimen showing a shear behaviour also for its as-built configuration was the roof pitch (sample DFpar-5, Fig. 4.6), because of the weak and flexible connection between wall plate and rafters. It is interesting to notice that in strengthened samples, for larger displacement, it is also possible to perceive the mutual sliding of the panels (Fig. 4.5b-d). This fact can be recognized also for the roof sample (Fig. 4.6b), in which the panels undergo slightly larger displacements than the purlins. The flexural response of as-built samples appears to be in line with the outcomes of BRIGNOLA et al. [24], and highlights that the use of an equivalent shear stiffness to describe these types of diaphragms may be not appropriate, because this parameter cannot be size- or direction-independent for as-built floors.

4.3.6 Dissipative properties of the retrofitted diaphragms

The tested as-built samples exhibited an approximately linear elastic response, with limited energy dissipation and a low in-plane stiffness. On the contrary, all strengthened

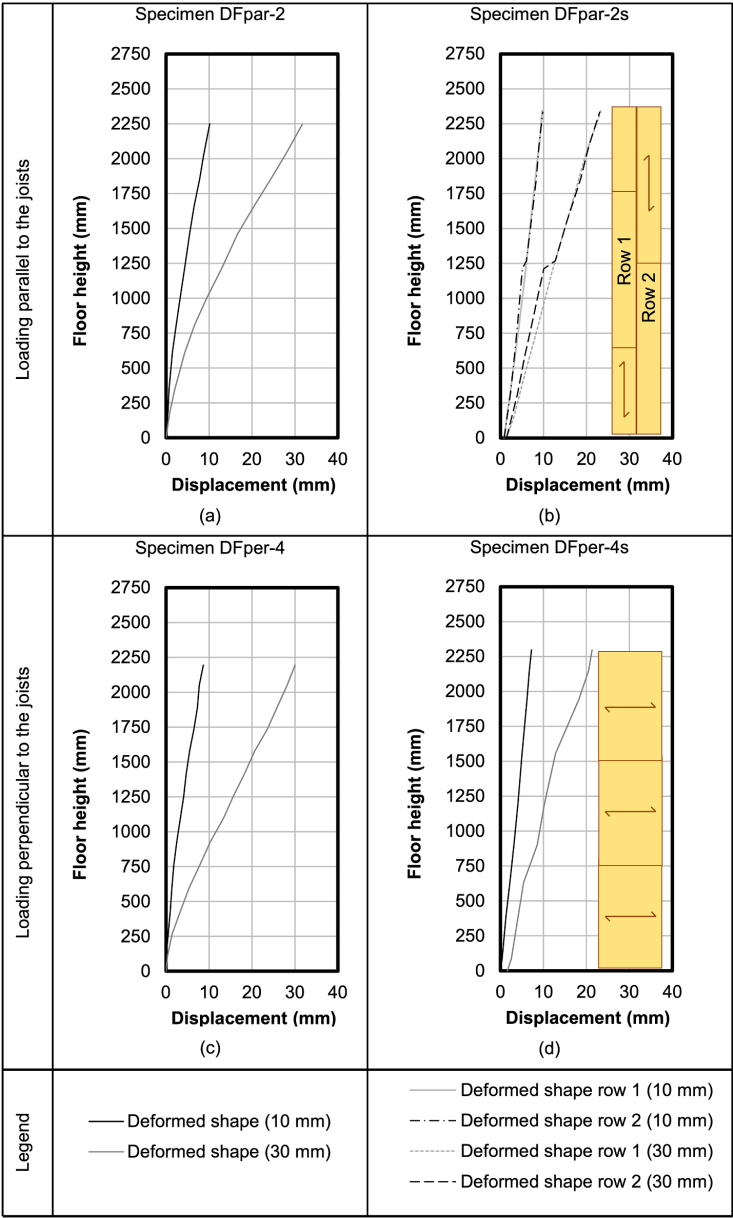


Figure 4.5: Examples of in-plane deformed shape: as-built (a) and strengthened (b) floors loaded parallel to the joists (reported for two adjacent rows of panels); as-built (c) and strengthened (d) floors loaded perpendicular to the joists. From [132].

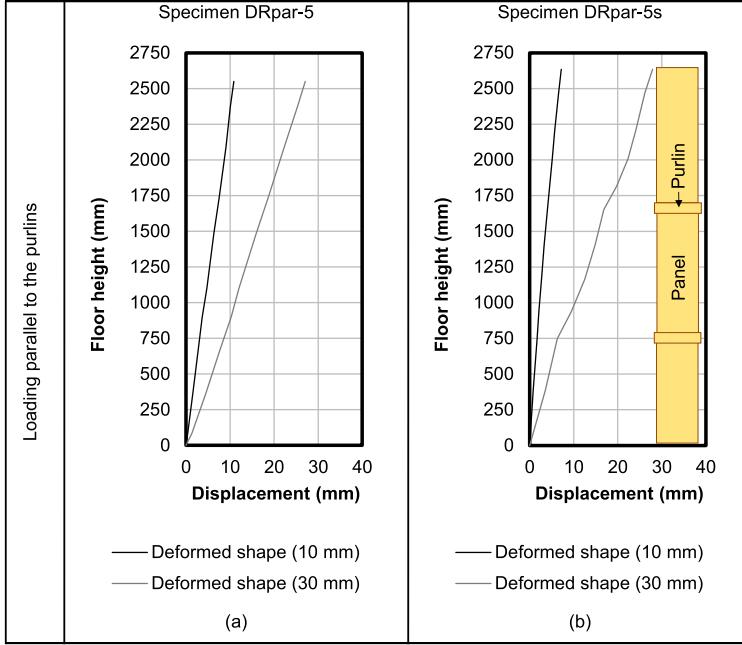


Figure 4.6: In-plane deformed shape of as-built (a) and strengthened roof sample (b). From [132].

diaphragms displayed a relevant improvement in all these characteristics. The potential beneficial effect of dissipative retrofitted floors was therefore quantified in terms of an equivalent damping ratio ξ , evaluated with the energy loss per cycle method [167]:

$$\xi = \frac{E_d}{2\pi E_e} \quad (4.1)$$

In the former equation, E_d is the energy dissipated in one full cycle, i.e. the area enclosed in it, and E_e is the corresponding elastic energy, as shown in Fig. 4.7. The adopted testing protocol for evaluating the in-plane response of the diaphragms [160] consisted of several displacement steps to be applied, each one composed of three cycles. In order to thoroughly characterize the dissipative properties of the floors, E_d was evaluated for all three cycles, and for each step until a drift $\gamma = \delta/L$ of approximately 1%, corresponding to a deflection δ of about 25 mm given the span $L = 2.3 \div 2.7$ m of the tested diaphragms. This allowed to analyze, within a limited drift range, the effect of progressive strength and stiffness degradation on ξ . Besides, the ISO 21581 testing protocol [160], with the application of several displacement steps very close to each other, led to a conservative estimation of ξ , because during a short, induced earthquake, a timber diaphragm is expected to undergo only a limited number of large-amplitude cycles, thus with lower degradation compared to the performed quasi-static tests.

The graphs of Fig. 4.8 show the evolution of ξ , calculated with Eq. 4.1, in relation to the drift for each cycle. As can be noticed, the dissipative contribution of the diaphragms is relevant, and especially in the initial displacement range, which can be of interest for buildings subjected to light, human-induced earthquakes. Values of ξ from 0.10 to 0.20

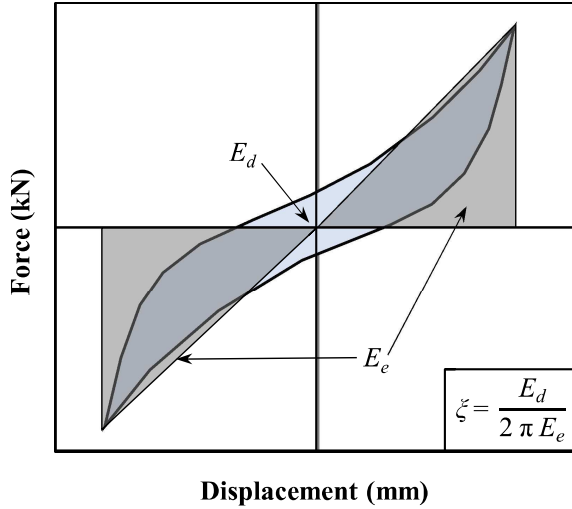


Figure 4.7: Determination of the equivalent damping ratio from the energy dissipated in one full cycle and the corresponding elastic energy. From [168].

were calculated, with the effect of degradation becoming noticeable after 0.5% drift: ξ decreases not only by further increasing the drift, but also among the three cycles within a same step.

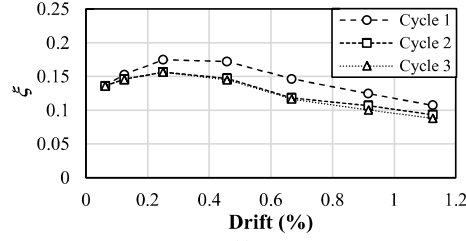
On the basis of the chosen displacement range, it was possible to define reference average values, displayed in Fig. 4.9: up to 0.5% drift, $\xi = 0.15$ can be assumed, while up to 1% drift, a very close value of $\xi = 0.14$ was obtained, due to the slightly larger effect of cyclic strength and stiffness degradation. Interestingly, these reference values are 2.5 times higher compared to those proposed by NPR 9998 for timber structural members [27], because dissipative seismic strengthening techniques were initially not considered in the guidelines: the large number of fasteners in the retrofitted diaphragms induces a much larger dissipation compared to as-built floors, for which the present values could be more appropriate.

The dissipative potential of timber diaphragms retrofitted with the proposed technique is therefore relevant. Besides the simplified characterization of energy dissipation provided by the floors by means of an equivalent hysteretic damping, the full cyclic response of the diaphragms will be investigated analytically and numerically in Chapter 5.

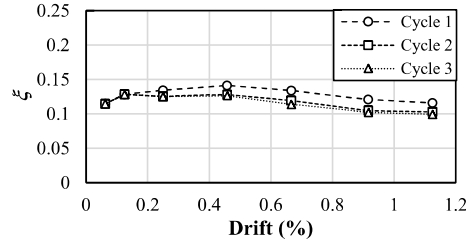
4.3.7 Comparison of the results with similar research studies from literature

This section investigates how as-built and retrofitted timber diaphragms with Dutch features relate to previous research studies from literature. The comparison is presented in terms of both in-plane stiffness and equivalent hysteretic damping of the floors.

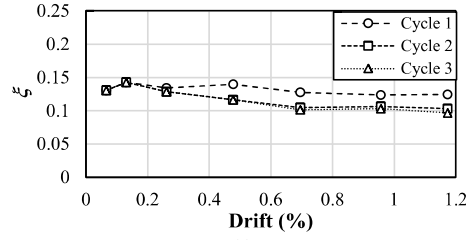
Chapter 2 showed that several retrofitting methods for timber floors have been developed in the recent years, and even for the same strengthening technique the outcomes are in general not comparable due to the use of different standards or



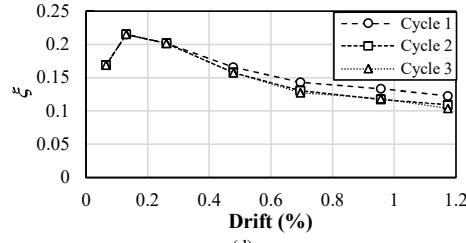
(a)



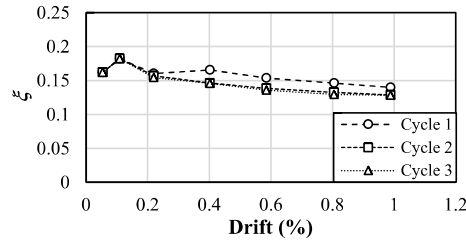
(b)



(c)

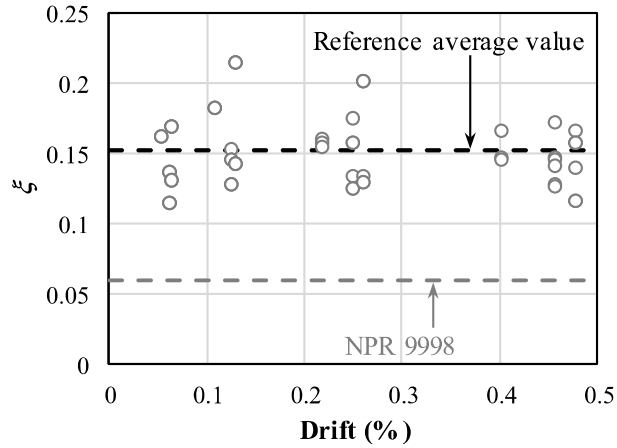


(d)

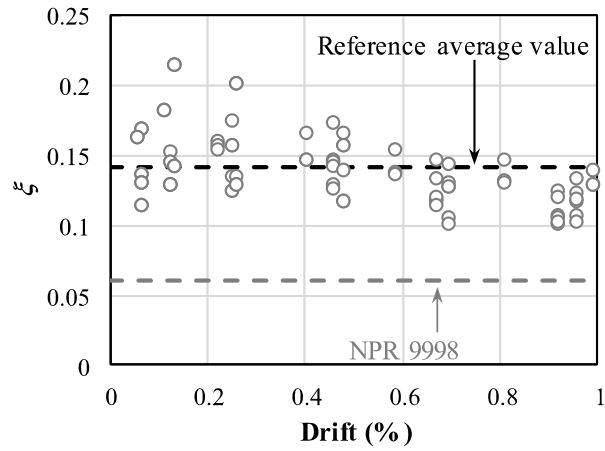


(e)

Figure 4.8: Evaluation of the equivalent damping ratio for the retrofitted timber diaphragms as a function of drift: sample DFpar-1s (a), DFpar-2s (b), DFper-3s (c), DFper-4s (d), DRpar-5s (e). From [168].



(a)



(b)

Figure 4.9: Estimation of a reference average value of equivalent damping ratio up to 0.5% (a) and 1% drift (b), in comparison to the present value proposed in NPR 9998 for general timber structural members; the dots correspond to analytically calculated values. From [168].

assumptions for calculating the in-plane stiffness of the diaphragms. Besides, the definition of the equivalent shear stiffness G_d appeared to be not always suitable for as-built diaphragms, because of their flexural and orthotropic behaviour. On the contrary, strengthened diaphragms can be properly characterized with this quantity, because of their shear-related response. However, because of the nonlinear in-plane behaviour of the floors, a single value of G_d cannot fully represent the in-plane properties of the diaphragms depending on the reached deflection.

Taking into account all aforementioned aspects, a simple, uniform criterion was formulated to compare the test results. Among the studies presented in Section 2.4, only those focusing on light, reversible, wood-based techniques similar to the one applied for the tested diaphragms will be considered for comparison, and namely:

- Superposition of an additional layer of planks arranged at an angle of 45° with respect to the original sheathing [19, 20];
- Superposition of an additional layer of planks arranged at an angle of 90° with respect to the original sheathing [18, 21];
- Overlay of OSB panels [22];
- Overlay of plywood panels (the most similar to the applied and tested strengthening technique) [23]-[26];

Fig. 4.10 provides an overview of the selected reference research studies on the in-plane response of diaphragms, and includes the specimens tested at TU Delft [132]. A complete, detailed summary of the properties of the compared samples is reported in Appendix C, subdivided by author. It is worth noticing that the experimental results of PIAZZA et al. [15] and BALDESSARI [16], although relevant for the subject, are not included in the comparison, due to the large size of the structural elements, and because all tested diaphragms were surrounded by a continuous steel plate, fastened along the floor perimeter to simulate the presence of an improved connection to the masonry walls; this structural element remarkably increased the stiffness of the diaphragms, up to two times [16]. On the contrary, the chosen floor samples were all strengthened with only timber-based techniques, and more similar to those with Dutch features, in terms of structural elements size (e.g panels), and fasteners dimensions, position and spacing.

The simple, uniform comparison method consisted of the definition of a secant stiffness intersecting the backbone curve of the floors at specific *drift* limits [169], where the drift of the floor is defined as the in-plane shear-related angular strain γ at the floor support (Fig. 4.10). Therefore, following this definition, the equivalent shear stiffness can be calculated as:

$$G_d = \frac{V}{\gamma \cdot B} \quad (4.2)$$

In the former equation, V is the shear load acting on the floor according to its static scheme (Fig. 4.10), while B is the length of the supported side of the floor, parallel to the in-plane load. From the experimental data no influence of initial stages with low stiffness due to e.g. presence of gaps in wooden joints was noticed, thus the use of drift limits was suitable to identify the secant stiffness on the backbone curves of the tested floors.

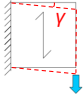
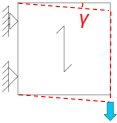
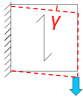
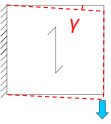
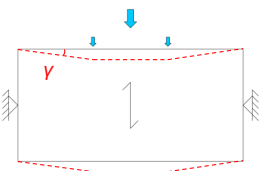
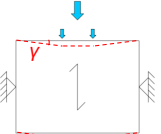
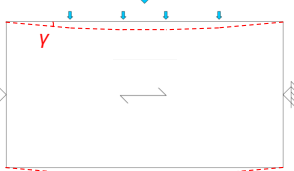
Static scheme	Sample dimensions [mm]	Loading direction	Sample name(s)	Strengthening technique(s)
	2120×2120	Parallel to joists	<i>FM</i> (as-built); <i>FMSB</i> (as-built); <i>FM+45°SP(A)</i> ; <i>FM+45°SP(B)</i>	Overlay of planks arranged at 45° with respect to existing boards [8, 9]
	3000×3000	Parallel to joists	<i>01-T2-OR</i> (as-built); <i>02-T6-OR</i> (as-built); <i>03-T4-T6</i>	Overlay of planks arranged at 90° with respect to existing boards [7]
	2125×2125	Parallel to joists	<i>S</i> (as-built); <i>SS</i>	Overlay of planks arranged at 90° with respect to existing boards [10]
	3160×3000	Parallel to joists	<i>UR-2</i> (as-built); <i>OSB90-R-2</i> ; <i>OSB0-S-2</i>	Overlay of OSB panels arranged parallel or perpendicular to joists [11]
	7320×3660	Parallel to joists	<i>MAE-2</i> (as-built); <i>MAE-2B</i> ; <i>MAE-2C</i>	Overlay of plywood panels [12]
	4000×3000	Parallel to joists	<i>AB-1</i> (as-built); <i>R-1</i>	Overlay of plywood panels [13]
	9600×4700	Orthogonal to joists	<i>26_B_asB</i> (as-built); <i>35_B_Plyw</i>	Overlay of plywood panels [15]

Figure 4.10: Overview of the timber diaphragms examined in the comparison. For visual comparison, the static schemes are reported at the same scale, along with in-plane deformed shapes and drifts γ . The first given dimension is always the one orthogonal to the load; sample names are reported according to the authors' nomenclature. From [169].

Static scheme	Sample dimensions [mm]	Loading direction	Sample name(s)	Strengthening technique(s)
	10400×5500	Parallel to joists	1a-PARA (as-built); 1b-PARA	Overlay of plywood panels [14]
	5500×10400	Orthogonal to joists	1a-PERP (as-built); 1b-PERP	Overlay of plywood panels [14]
	2400×3800	Parallel to joists	DFpar-1 (as-built); DFpar-1s	Overlay of plywood panels [129]
	2400×3960	Parallel to joists	DFpar-2 (as-built); DFpar-2s	Overlay of plywood panels [129]
	2300×3800	Orthogonal to joists	DFper-3 (as-built); DFper-4 (as-built); DFper-3s; DFper-4s	Overlay of plywood panels [129]
	2730×3800	Orthogonal to rafters	DRpar-5 (as-built); DRpar-5s	Overlay of plywood panels [129]

Figure 4.10: Continued. From [169].

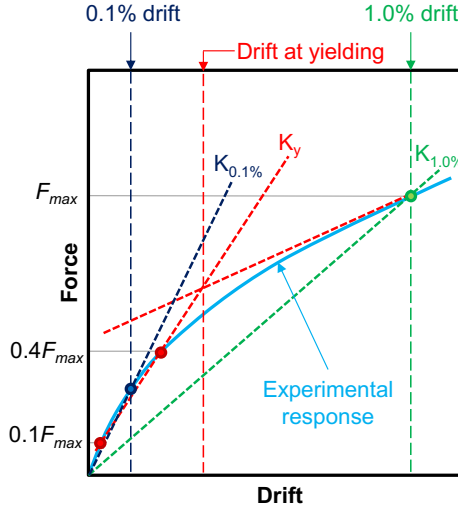


Figure 4.11: Derivation of the stiffness K at different drift levels: 0.1%, 1.0% and at a conventional yielding point, defined as the intersection between an initial stiffness determined according to EN 12512 [45], and the tangent to the experimental curve at 1.0% drift. From [169].

The equivalent shear stiffness values were derived from the experimental results at defined drifts, for both as-built and strengthened floors. Although this quantity is size- and direction-dependent for as-built floors, G_d was always calculated also for them. This allowed to compare the existing diaphragms to the strengthened ones, and to quantify the improvement in in-plane stiffness between the two configurations.

The stiffness of all reference diaphragms was evaluated at an initial phase (0.10% drift), and at a higher but not excessive level of drift (1.00%), when nonlinear behaviour is dominant. Additionally, a third value of stiffness was calculated, with reference to a *conventional yielding point* of the floor: this was defined as the intersection between the following two lines (Fig. 4.11):

- An initial stiffness, determined according to EN 12512 [45], and taking as F_{max} the value of total in-plane load at 1.00% drift;
- The tangent to the experimental curve determined at the maximum considered drift of 1.00%.

It should be noticed that other reference drift values for calculating the secant stiffness could also be adopted; in this comparison it was chosen to examine a range that is of interest for masonry structures, for which an excessive deflection of floors is not desirable due to the potential out-of-plane collapse of the walls. All values of stiffness were calculated based on the graphs and hysteretic cycles available in each reference publication.

In all selected research studies, as-built diaphragms displayed in general a very flexible response, and for certain configurations the floors were almost not able to withstand in-plane loads without large deformations (samples FMSB [19, 20], FM [19, 20], S [21], UR-2 [22], DRpar-5 [132]), especially due to low rotational stiffness of

the nail couples. Furthermore, an orthotropic response was observed when considering the two directions of loading (samples 1a-PARA [25], 1a-PERP [25], DFpar-1 [132], DFpar-2 [132], DFper-3 [132], DFper-4 [132]). This property of floors has therefore to be considered, when modelling them with the purpose of the seismic assessment of existing buildings. Table 4.8 summarizes the values of stiffness calculated by the authors and with the proposed method for each research study; in the table, as-built (original) samples are identified by letter (O), strengthened ones by letter (S), and their names are according to the notation used by the authors. It should be noticed that, since for several as-built floors G_d is size-dependent, a comparison between original and strengthened diaphragms is either possible for the same authors, or for floors having similar dimensions or aspect ratio. Instead, the equivalent shear stiffness values of strengthened diaphragms can be compared among each other, because of their more shear-related response: this comparison is visually shown in Fig. 4.12.

Strengthening with a superposition of planks arranged at an angle of 45° with respect to the original sheathing already constitutes a remarkable improvement in stiffness compared to the as-built condition (up to ten times). Specimens FM+45°SP(A) and FM+45°SP(B) [19, 20] displayed approximately the same stiffness and a large enhancement of their in-plane properties.

Slightly less effective is the retrofitting with a superposition of planks arranged at an angle of 90° with respect to the original sheathing. Sample 03-T4-T6 [18] displayed a very high stiffness at initial stages, while at larger drifts a reduction until a value in line with other floors is observable. This response could depend on the structure of the floor as well, characterized by a double warping of main and secondary joists. Instead, specimen SS [21] showed the lowest stiffness among the selected diaphragms. With this technique, the in-plane stiffness could be increased by up to 4 times.

Considering the OSB panels overlay, samples OSB90-R-2 and OSB0-S-2 [22] show that the direction in which OSB panels are arranged with respect to the sheathing can have a strong influence on the response. With panels placed perpendicular to the joists, only half of the stiffness is obtained at every reference drift, with respect to the configuration having panels positioned parallel to the joists. This can be attributed to the larger lever arm of the rocking panels in the latter configuration. In any case, the improvement in in-plane stiffness is considerable compared to the as-built situation (Table 4.8), with an increase of approximately 5 and 10 times for panels arranged perpendicular and parallel to the joists, respectively. As noticeable from Fig. 4.12, this technique can be considered equivalent to the plywood panels overlay. Thus, similarly to a plywood panel retrofitting, the arrangement of OSB panels could be optimized in order to make the floor isotropic after strengthening, similarly to the aforementioned interlocked overlay proposed by GIONGO et al. [26].

Retrofitting with a plywood panels overlay appears to provide similar results in terms of shear stiffness, at least for strengthened floors having a total sheathing thickness (very common in practice) between 30 and 40 mm, like the considered ones. Unblocked and blocked plywood panels, present in sample MAE-2B and MAE-2C (Section 2.4, [23]), respectively, could be both recommendable interventions depending on the specific situation: in the blocked layout, the stiffness is doubled compared to the unblocked strengthening option. Specimen R-1 [24] was strengthened with an unblocked plywood panels overlay as well, and the value of stiffness is thus similar to floor MAE-2B [23]. The same applies to samples 1b-PARA and 1b-PERP [25], even if an orthotropic

behaviour is present, with a lower stiffness for the direction perpendicular to the joists. On the contrary, in floor 35_B_Plyw [26], also tested orthogonally to the joists, an increased stiffness was obtained, which is very close to that of specimens tested parallel to the joists (Fig. 4.12). This result is because of the more interlocked plywood panels overlay, along with the presence of the timber blocking elements at the floor edges: the orthotropic behaviour is in this case fully mitigated.

The diaphragms tested at TU Delft [132] generally reflected the values obtained when strengthening with an unblocked plywood panels overlay, including again the orthotropic response, detected in sample DFper-3s. The only exception is represented by specimen DFper-4s that can be regarded as an example of partially blocked panels overlay: the blocks were placed between the joists at their end supports, similarly to the intervention realized by GIONGO et al. [26]. The floor, tested perpendicular to the joists, showed in-plane stiffness values comparable to the diaphragms tested parallel to the joists. Furthermore, it was possible to double its stiffness with respect to the unblocked specimen DFper-3s. Even the roof sample DRpar-5s displayed a great improvement in in-plane stiffness, especially when compared to the as-built situation (Table 4.8).

This comparison proves the effectiveness of the plywood panels overlay as a seismic retrofitting technique, with respect to other wood-based strengthening methods, because also Dutch timber diaphragms with small and light structural elements are able to reach in-plane stiffness values comparable to those of all other reported floors strengthened with the same technique. Furthermore, the use of a uniform criterion enabled a more detailed characterization of the diaphragms, accounting also for their nonlinear behaviour through the use of different drift limits. The proposed strengthening technique with unblocked plywood panes can be conservatively characterized by means of approximately $G_d = 3000$ N/mm at 0.1% drift, and $G_d = 1200$ N/mm at 1% drift [169]. As a result of the experimental study and the performed uniform comparison, the Dutch seismic guidelines were updated with these outcomes, suggesting the plywood panels overlay as an advantageous retrofitting option for the Groningen area.

However, in-plane stiffness in itself is not the only relevant parameter influencing the seismic response of the diaphragms. For the adopted technique, a highly dissipative behaviour was recognized (Section 4.3.6), with an average equivalent hysteretic damping for all tested floors of $\xi = 0.14$ at 1.0% drift. By calculating ξ at the same drift value by means of Eq. 4.1 for cyclically tested floors retrofitted with plywood panels from literature, values between 0.11 and 0.14 were obtained [168], and more specifically:

- $\xi = 0.14$ for sample MAE-2B [23];
- $\xi = 0.11$ for sample R-1 [24];
- $\xi = 0.14$ for sample 1b-PARA [25];
- $\xi = 0.12$ for sample 1b-PERP [25].

This is a further proof of the effectiveness and reliability of the plywood panels overlay retrofitting technique, which can truly boost the dissipative properties of the diaphragms. This aspect is even more relevant for the light and flexible existing Dutch floors, which can be strongly improved in their global in-plane characteristics.

As can be noticed, a characterization by fixed values of in-plane stiffness and damping can already provide a first picture on the seismic response of the (retrofitted)

4.3. Analysis of test results for timber diaphragms

Table 4.8: Overview of in-plane stiffness values for the as-built (O) and strengthened (S) timber diaphragms selected for comparison. Values of equivalent shear stiffness that are size-dependent because of the flexural properties of as-built floors are reported in *italic*, while the symbol (*) denotes values obtained from an extrapolation of the experimental curve and not directly from it, because the test was stopped slightly before reaching this drift value.

Authors	Standards adopted by Authors for stiffness evaluation	Sample names	K [kN/mm]				G_d [N/mm]			
			From Authors	0.1% drift	1.0% drift	Yielding (drift)	From Authors	0.1% drift	1.0% drift	Yielding (drift)
VALLUZZI et al. [19, 20]	EN 12512 [45], with F_{max} at 30 mm displacement	<i>FMSB (F1.M)</i> (O)	0.08	0.15	0.04	0.1 (0.12%)	81	152	43	100 (0.12%)
		<i>FM (F2.M)</i> (O)	0.29	0.31	0.06	0.33 (0.12%)	288	313	62	330 (0.12%)
		<i>FM+45°SP(A)</i> (S)	1.18	2.06	0.71	1.89 (0.3%)	1176	2065	707	1890 (0.3%)
		<i>FM+45°SP(B)</i> (S)	1.25	2.13	0.72	1.89 (0.3%)	1247	2128	719	1890 (0.3%)
CORRADI et al. [18]	ASTM E 519-81 [48]	<i>01-T2-OR</i> (O)	0.47	0.71	0.13	0.23 (0.07%)	470	710	128	230 (0.07%)
		<i>02-T6-OR</i> (O)	0.28	0.77	0.20	0.26 (0.08%)	280	771	204	255 (0.08%)
		<i>03-T4-T6</i> (S)	1.71	2.19	0.40	2.19 (0.1%)	1710	2190	400	2190 (0.1%)
		<i>S</i> (O)	0.05	0.15	0.05	0.16 (0.14%)	55	153	53	165 (0.14%)
BRANCO et al. [21]	EN 12512 [45], with F_{max} at 100 mm displacement	<i>SS</i> (S)	0.13	0.61	0.16	0.61 (0.1%)	132	609	165	609 (0.1%)
GUBANA and MELOTTTO [22]	EN 12512 [45] as such	<i>UR-2</i> (O)	0.53	0.55	0.09	0.55 (0.1%)	560	582	97	582 (0.1%)
		<i>OSB90-R-2</i> (S)	1.77	2.55	0.57	3.12 (0.07%)	1870	2691	606	3290 (0.07%)
		<i>OSB0-S-2</i> (S)	1.97	5.05	1.19	4.27 (0.13%)	2080	5320	1259	4496 (0.13%)
PERALTA et al. [23]	FEMA 273 [49], FEMA 356 [50]	<i>MAE-2</i> (O)	1.80	5.84	1.42	5.84 (0.1%)	600	1949	475	1949 (0.1%)
		<i>MAE-2B</i> (S)	8.40	10.96	2.34	7.76 (0.12%)	2800	3653	780*	2400 (0.12%)
		<i>MAE-2C</i> (S)	11.30	17.96	5.22	13.93 (0.18%)	3767	5990	1743*	4644 (0.18%)
		<i>AB-1</i> (O)	1.36	3.06	1.16	3.02 (0.18%)	<i>340</i>	<i>769</i>	<i>290</i>	<i>756</i> (0.18%)
BRIGNOLA et al. [24]	None, secant stiffness calculation at 12 mm displacement	<i>R-1</i> (S)	6.65	14.70	5.20	12.40 (0.16%)	1665	3675	1300	3102 (0.16%)
GHONGO et al. [26]	None, secant stiffness calculation at various drifts	<i>26_B_asB</i> (O)	-	1.16	0.65	1.00 (0.25%)	190	302	169	260 (0.25%)
		<i>35_B_Plyw</i> (S)	-	10.70	3.69	10.70 (0.1%)	1343	2783	961	2783 (0.1%)
WILSON et al. [25]	FEMA 273 [49], FEMA 356 [50], ASTM E 2126 [51]	<i>1a-PARA</i> (O)	0.64	2.06	0.47	2.06 (0.1%)	198	637	148	637 (0.1%)
		<i>1b-PARA</i> (S)	14.52	19.55	3.66	15.00 (0.15%)	4459	3294	1140	2533 (0.15%)
		<i>1a-PERP</i> (O)	1.61	5.34	1.54	3.75 (0.14%)	<i>134</i>	<i>441</i>	<i>128</i>	<i>313</i> (0.14%)
		<i>1b-PERP</i> (S)	22.41	30.89	7.15	30.89 (0.1%)	1864	1402	595	1402 (0.1%)
		<i>DFpar-1</i> (O)	-	0.74	0.36	0.48 (0.28%)	-	<i>467</i>	<i>227</i>	<i>303</i> (0.28%)
MIRRA et al. [132]	None, secant stiffness calculation at various drifts	<i>DFpar-2</i> (O)	-	0.86	0.47	0.57 (0.16%)	-	<i>521</i>	<i>285</i>	<i>345</i> (0.16%)
		<i>DFper-3</i> (O)	-	0.33	0.11	0.25 (0.15%)	-	<i>200</i>	<i>67</i>	<i>151</i> (0.15%)
		<i>DFper-4</i> (O)	-	0.21	0.10	0.21 (0.1%)	-	<i>127</i>	<i>60</i>	<i>127</i> (0.1%)
		<i>DRpar-5</i> (O)	-	0.15	0.06	0.15 (0.1%)	-	108	41	108 (0.1%)
		<i>DFpar-1s</i> (S)	-	5.45	2.02	5.70 (0.09%)	-	3441	1277	3600 (0.09%)
		<i>DFpar-2s</i> (S)	-	6.32	2.83	5.61 (0.15%)	-	3832	1717	3403 (0.15%)
		<i>DFper-3s</i> (S)	-	1.88	1.21	1.56 (0.45%)	-	1136	735	946 (0.45%)
		<i>DFper-4s</i> (S)	-	5.28	2.93	4.11 (0.26%)	-	3196	1773	2488 (0.26%)
		<i>DRpar-5s</i> (S)	-	3.42	1.31	2.57 (0.4%)	-	2457	940	1848 (0.4%)

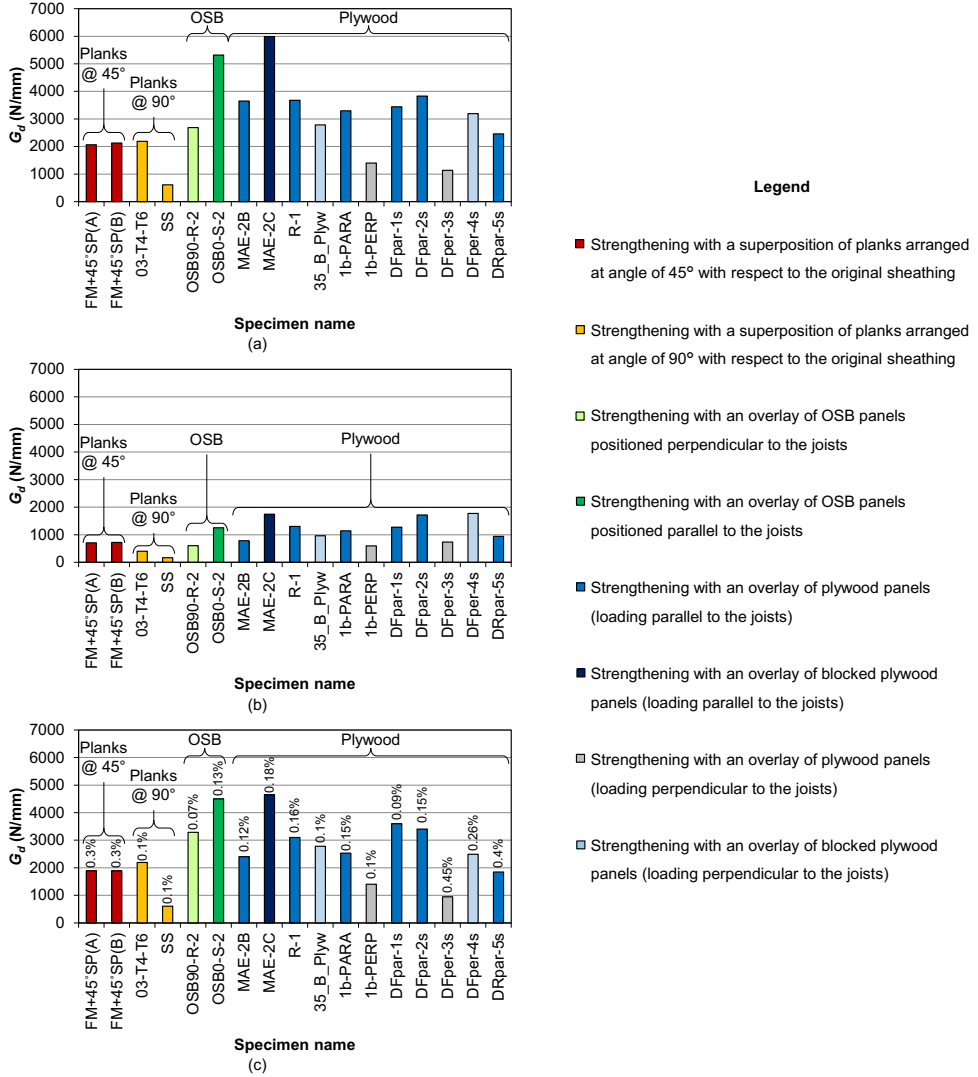


Figure 4.12: Comparison of the equivalent shear stiffness of strengthened diaphragms at 0.1% (a) and 1.0 % (b) drift, and at yielding (c); in the latter case the corresponding drift is also indicated. The retrofitting techniques are divided by groups, and colors identify specific strengthening characteristics. From [169].

diaphragms. Yet, to account for the highly nonlinear response of the floors, and their specific pinching behaviour, typical of timber structures, a further step is necessary. Therefore, in Chapter 5 the comprehensive analytical characterization of the diaphragm will be presented.

4.4 Analysis of test results for timber-masonry connections

4.4.1 Results from pilot study

This section reports the results of the conducted preliminary pilot study on both double-wythe clay brick walls and single-leaf calcium silicate brick walls (Section 3.4.2). In this testing phase, quasi-static cyclic tests were performed on six samples (see Section 3.5.2). Fig. 4.13 provides an overview of the cyclic response of the timber-masonry joints recorded by sensor 3 in Fig. 3.16.

The as-built configuration CLAY-A showed a non-symmetric behaviour because of the particular configuration of the masonry pocket. When the joist is pulled from the wall, the horizontal load can be transferred only by friction between timber and mortar, and this governing frictional response is observable also in Fig. 4.13a. On the contrary, when pushing the joist towards the wall, the second leaf of bricks can give a contribution in the resistance, resulting in a much stiffer behaviour and a higher strength. After the peak force, a softening phase took place, because of the sliding of part of the second leaf of bricks during the test (Fig. 4.14a).

Specimen CLAY-B, representing the hook anchor as-built connection, also showed a non-symmetric behaviour. When the joist pushed the wall, also the second leaf of bricks could play a role in resisting the horizontal load, while in the opposite direction the shear transfer could only be provided by the masoned-in anchor. The cyclic response of this sample is shown in Fig. 4.13b. At large displacements, several cracks developed, together with the sliding of part of the second leaf during the test (Fig. 4.14b). Besides this visible damage on the wall, also the nails connecting the masoned-in anchor to the joist were slightly bent, causing wood embedment and small energy dissipation.

Strengthening option CLAY-C showed a large improvement in shear transfer (Fig. 4.13c), without causing significant damage to the wall up to the peak load. After reaching this strength, the wall started to be more and more cracked, with also a significant sliding of bricks in the area around the joist (Fig. 4.14c).

The stiffness of the joint was radically improved compared to the as-built configurations: 5 times higher than the one measured for sample CLAY-B, and almost 9 times higher than the one of specimen CLAY-A. Besides the out-of-plane damage, also some cracks in the vicinity of the mechanical anchors were observed, along with an incipient pull-out failure of the anchors and bending of the steel angle. Furthermore, a fairly high embedment in the timber joist was observed, with bending and yielding of the screws connecting the steel angle to it. This led to energy dissipation and plastic behaviour.

With regard to the calcium silicate walls, specimen CS-A showed a symmetric frictional behaviour (Fig. 4.13d). The shear force transferred by this joist-masonry connection was thus very low. The timber-mortar friction coefficient could be quantified as 0.75, a value that was confirmed also in the second testing phase (Section 4.4.2).

Table 4.9: Peak strength in pulling and pushing, and stiffness evaluated at 2 mm for the joints tested within the pilot study.

Configuration	Peak force (kN)		Stiffness at 2 mm displacement (kN/mm)	
	Pulling	Pushing	Pulling	Pushing
CLAY-A	0.69	6.31	0.28	2.62
CLAY-B	5.03	12.93	1.39	4.05
CLAY-C	10.35	15.47		4.10
CS-A	0.46	0.62		0.22
CS-B	5.27	1.43		0.58
CS-C	5.66	10.54		3.46

During the test, the sample showed practically negligible movements of the wall, also when the largest displacements were applied: the joist was simply sliding through the masonry pocket (Fig 4.14d).

Specimen CS-B exhibited a non-symmetric behaviour: when pushing the joist towards the wall a frictional behaviour occurred (similarly to sample CS-A); in the pulling phase, the shape of the anchor could instead involve also the wall in the resisting process. The obtained cyclic response is reported in Fig. 4.13e. At the end of the test, the wall showed cracks induced by the action of the hook anchor (Fig. 4.14e). Furthermore, a slight embedment in the timber joist was observed, together with a small bending of the nails connecting the anchor to it.

The retrofitted configuration tested in sample CS-C greatly improved the shear transfer of the joint, with a stiffness 8 times higher than that of specimen CS-B, and more than 12 times higher than that of sample CS-A. The cyclic response of this timber-masonry connection is depicted in Fig. 4.13f. The damage state of the wall after the test is shown in Fig. 4.14f. Besides the cracks occurred to masonry, a slight embedment in the timber joist was observed, along with limited yielding of screws.

A summary of the peak forces in pulling and pushing, and the secant stiffness value at 2 mm displacement is reported in Table 4.9. The stiffness was evaluated from the experimental backbone curves at that displacement level, so that the large scatter in stiffness of the very initial cycles could be mitigated, while still obtaining values representative for an approximately linear elastic behaviour of the joints.

4.4.2 Quasi-static monotonic and cyclic tests

In the second testing phase, conducted after the pilot study, more retrofitting configurations were studied and single-leaf clay brick walls were considered (Section 3.4.2). The response under monotonic and quasi-static reversed-cyclic loading is shown

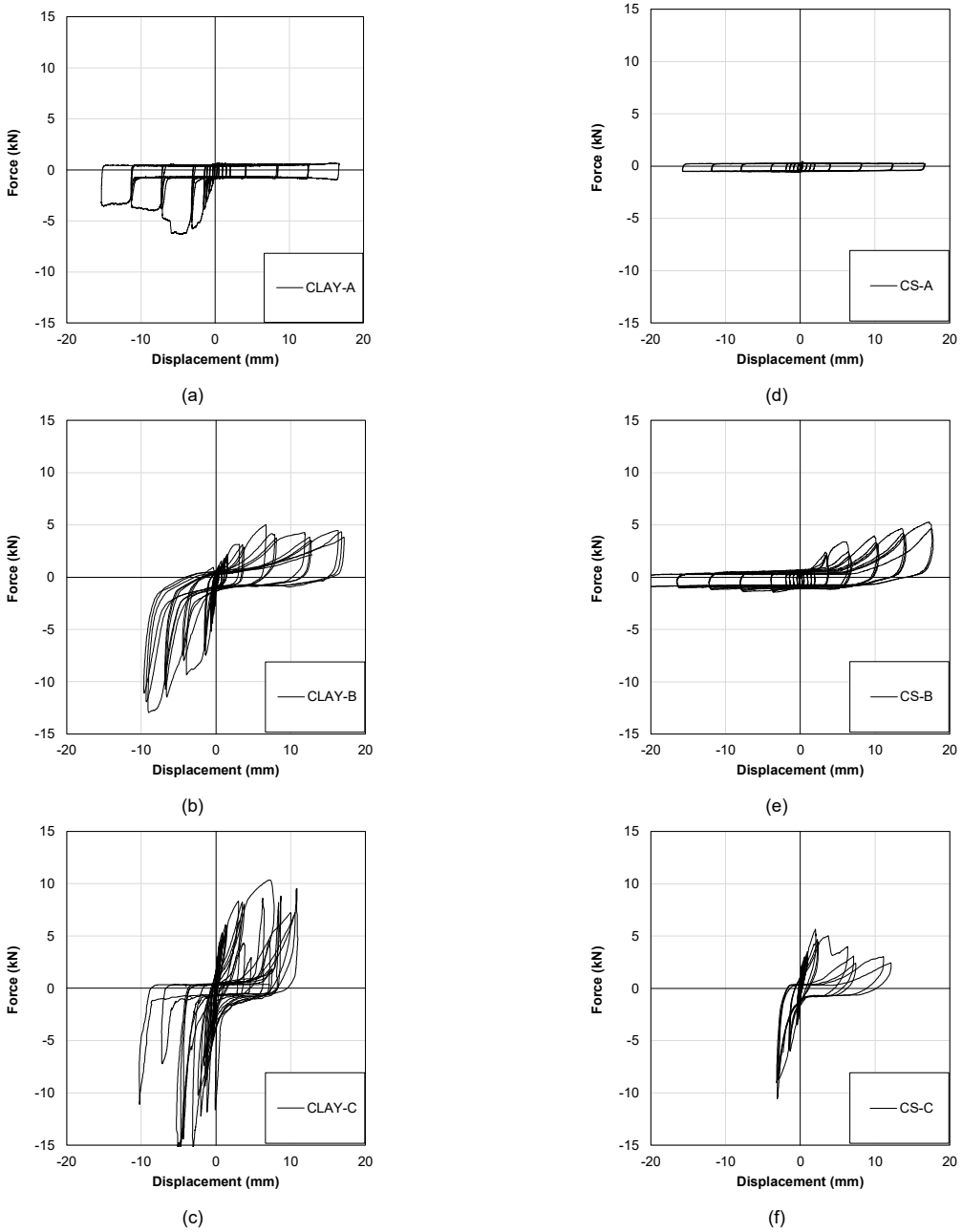


Figure 4.13: Cyclic response of the timber-masonry connections tested within the pilot study: samples CLAY-A (a), CLAY-B (b), CLAY-C (c), CS-A (d), CS-B (e), CS-C (f).



(a)



(d)



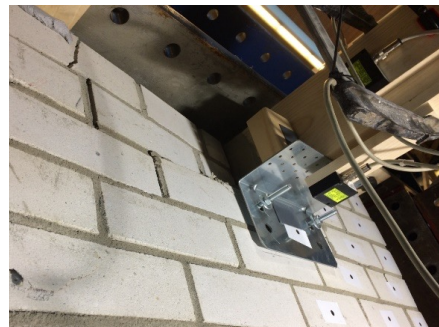
(b)



(e)



(c)



(f)

Figure 4.14: Damage and cracks on walls occurred after testing to samples CLAY-A (a), CLAY-B (b), CLAY-C (c), CS-A (d), CS-B (e), CS-C (f). From [148].

in Fig. 4.15 for all configurations. As in the previous case, the reported displacement is the joist-wall one, recorded by sensor 3. From monotonic tests (Fig. 4.15a), the difference in terms of stiffness and ductility among the seven tested configurations is already evident; these results are further confirmed by quasi-static cyclic tests.

Configuration A (Fig. 4.15) showed a purely frictional behaviour and a very low force transfer between joist and wall, as expected. The strength might be increased if the joist in the mortar pocket is slightly tilted, as observed for sample A-QS-3. The timber-mortar friction coefficient was quantified as $0.6 \div 0.8$, thus confirming the result from the pilot study.

Configuration B also showed a frictional behaviour when pushing the connection, because the hook anchor was free to move, while in the opposite loading direction the wall was also involved in the resisting process, triggered by the vertical part of the anchor. It is interesting to notice that a reasonably high strength can be achieved even by an as-built configuration, although in one of the two loading directions only. The observed behaviour was similar to that of configuration CS-B. As a last remark, sample B-QS-3 showed a more symmetric response because, after the first initial cycles with frictional behaviour in the pushing direction, a mortar particle detached from the pocket and remained clamped between the anchor and the wall, causing an increase in the transferred load (Fig. 4.15c).

Configuration C represented a good compromise among strength, stiffness and ductility. With this first retrofitting method, the capacity was increased more than tenfold compared to configuration A. The main failure modes were related to slight yielding of the screws, together with bricks or anchors extraction from the wall, which displayed many cracks after testing (Fig. 4.15d). In the initial phases a quite uniform behaviour among the three tested configurations was observed.

Configuration D (Fig. 4.15e) displayed moderately high values of strength and stiffness, especially when considering that this option was applied to the walls of configuration B already damaged by the testing. Bending and yielding of screws and steel brackets were observed, and cracks on the walls occurred as well for very large displacements (approximately 10 mm), leading to a non-symmetric behaviour. Depending on the larger or smaller play in all components of this connection type, a scatter in stiffness was observed during the initial cycles.

Configuration E was developed in order to obtain a rigid connection, even if not ductile. This objective was appropriately reached, as can be noticed from Fig. 4.15f. The initial response was uniform, with the exception of sample E-QS-2 that was, however, already slightly cracked around the connection. The main failure mode was the detachment from the wall of the glued part of the hook anchor, with also limited yielding of the nails connecting it to the joist. It should be noticed that the failure was not related to the glue itself, but to the cracking of bricks and mortar around it.

Configuration F was designed with the same purpose as option E. In this case, even more strength was achieved because of the efficient load transfer between joist and wall, and the three specimens exhibited in general a very similar response (Fig. 4.15g). No failure of screws and timber joist was observed, but a large and distributed crack pattern was visible in the tested samples.

In configuration G, developed to be a dissipative option, the specimens showed high strength linked with ductility and energy dissipation, due to yielding and bending of screws and nails and, for large displacements, also cracking in the walls. Furthermore,

the three tested samples displayed very similar hysteretic cycles, in both initial and overall behaviour (Fig. 4.15h).

4.4.3 Dynamic tests

Similarly to quasi-static cyclic tests, Fig. 4.16 shows the hysteretic cycles obtained with the incremental dynamic tests for all samples. As a general remark, the load-displacement response of the specimens under a short sudden earthquake loading did not largely differ from that of the quasi-statically tested ones, apart from specific aspects discussed in more detail in Section 4.4.4.

Fig. 4.16a shows an example of the acceleration signal applied to the connection, selected to replicate the seismic motions that may take place in Groningen, characterized by a short duration shock. The acceleration, recorded by the accelerometers on the connection, represents 100% of the reference signal (10 mm displacement amplitude).

Configuration A (Fig. 4.16b) displayed again a frictional response, with slightly larger transferred forces induced by the dynamic nature of the signal.

Configuration B (Fig. 4.16c) showed a frictional behaviour when pulling the connection, as it was observed for quasi-static tests, and an increase in strength when pushing the anchor. However, this increase occurred more gradually compared to the quasi-static cyclic response, probably because of the higher play in the connection induced by sudden loading.

Configuration C (Fig. 4.16d) exhibited a response similar to that observed under quasi-static loading for the pulling direction, but not for the pushing direction, in which higher peak forces were reached due to the aforementioned impact effect. The failure modes were also very similar, although less damage was observed in the samples subjected to the dynamic loading.

For configuration D (Fig. 4.16e) the same remarks apply as for configuration C, yet it is also important to notice that a slightly more flexible and less resistant behaviour was observed when pulling the joint.

Configuration E (Fig. 4.16f) was also very similar in terms of response to the quasi-static test results, but the impact effect when pushing determined once more higher peak forces in this loading direction.

Configuration F (Fig. 4.16g) showed higher force transfer when pushing as well; interestingly, under dynamic loading this connection type became approximately symmetric in terms of peak forces and stiffness. This behaviour could be explained considering that the load transfer is slightly less efficient in pushing, and this is counterbalanced by the impact effect in dynamic tests.

Configuration G (Fig. 4.16h) showed a hysteretic behaviour similar to that of quasi-static tests, but higher loads in both directions were reached. The overall dissipative and ductile behaviour was therefore again present, but with an improved transfer of force in the connection. Besides the aforementioned impact effect, a possible explanation for the higher peak strength in both loading directions could be the lower damage occurred on the top part of the masonry walls, compared to quasi-static tests.

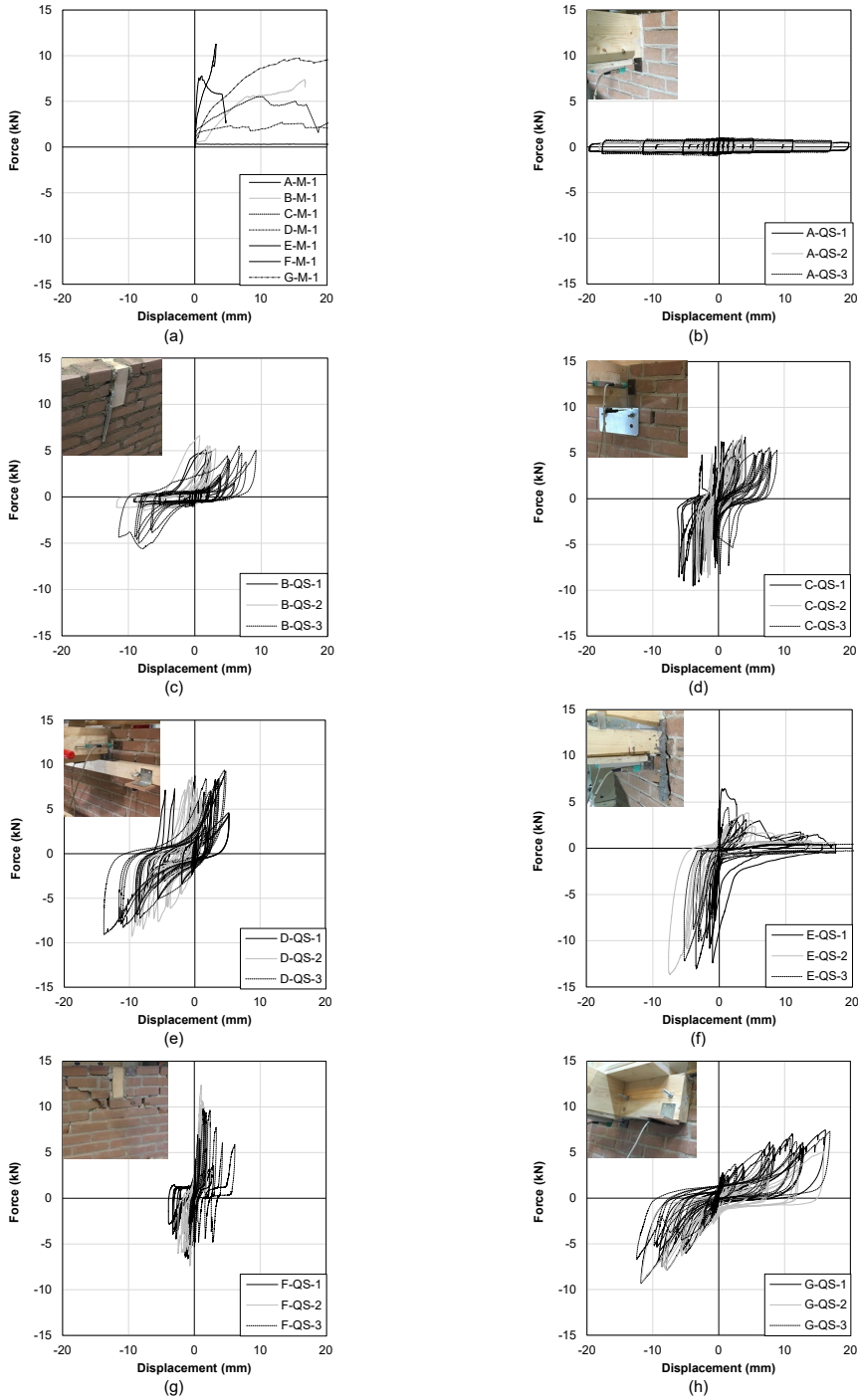


Figure 4.15: Summary of monotonic (a) and cyclic test results for configurations A (b), B (c), C (d), D (e), E (f), F (g), and G (h). A representative picture of a sample after testing is also shown. From [151].

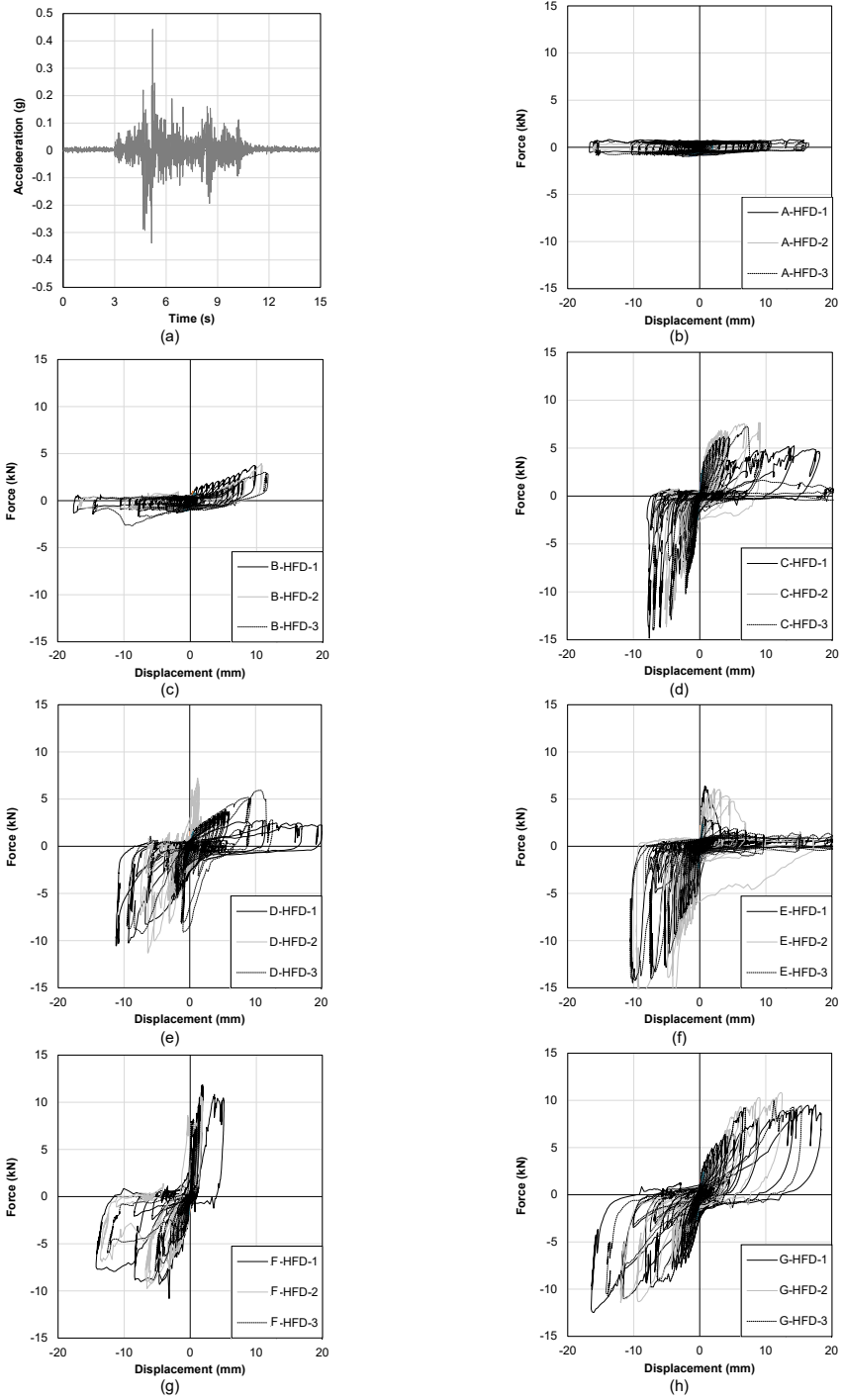


Figure 4.16: Example of acceleration response measured at 100% signal amplitude on sample G-HFD-1 (a); dynamic test results for configurations A (b), B (c), C (d), D (e), E (f), F (g), G (h). From [151].

4.4.4 Comparison between quasi-static and dynamic tests

Table 4.10 shows a comparison between quasi-static and dynamic tests in terms of peak force measured for pulling and pushing forces, as well as of secant stiffness evaluated at 2 mm displacement, similarly to the pilot study. As can be noticed, at least for short-duration shallow earthquakes such as the ones in Groningen, quasi-static tests can be considered reliable for assessing the response of connections similar to those investigated in this study: tests with such loading protocol are in general slightly more conservative, even if they cannot show phenomena such the impact effect or the higher play (and therefore a more flexible behaviour, as observed in configurations B and D) induced by the sudden loading in the connection.

The reason for the generally larger strength values obtained with the high-frequency dynamic tests could be related to the sudden nature of the signal, and to the lower number of cycles applied to the connections in comparison to quasi-static cyclic tests. This fact could also explain the more limited damage on the walls, despite the sudden dynamic loading. To further investigate these aspects, firstly the crack pattern developed at peak force was compared, which for options E and F was also recorded with DIC in quasi-static and dynamic tests. Secondly, a long-duration tectonic earthquake signal (Irpinia, Italy, 1980 [170]) was applied to an additionally built sample representing configuration C: a different and longer dynamic loading representative of a tectonic earthquake was expected to cause way more damage compared to an induced earthquake's one.

With regard to the crack pattern, a visual inspection of the samples (Fig. 4.17) already showed that the walls were less damaged when subjected to the induced earthquake loading with respect to the quasi-static tests (at the same displacement amplitude). This is confirmed with the more detailed information on cracks opening retrieved from DIC for options E and F (Fig. 4.18): this technique enabled to detect also the presence of small cracks, which appeared to be way more spread on the surface of the sample during quasi-static tests. This additional piece of information is of importance, confirming once more that quasi-static tests can be regarded as conservative for evaluating the response of the tested connections. Besides, according to the obtained results, a masonry building in the Groningen area subjected to a single induced earthquake could undergo much less damage, compared to the same construction in a region where tectonic earthquakes occur.

To have more insight into this last aspect, an additional sample with configuration C was constructed, and then subjected to the Irpinia earthquake signal (1980), having a much longer duration compared to that of the adopted induced signal from Groningen (86 s vs 14 s). The Irpinia signal was scaled to the same displacement amplitudes as the induced one (refer to Fig. 3.18), to have a consistent comparison. As can be noticed from Fig. 4.19a-b, the hysteretic behaviour of the connection under the tectonic earthquake signal was similar to the one recorded with the induced ground motion, also in terms of strength and stiffness. Yet, a much more extensive damage was observed on the sample subjected to the tectonic earthquake, which almost collapsed during the last run (Fig. 4.19d), although subjected to the same displacement amplitudes in each run. A less evident impact effect was also present, due to the slightly lower frequency of the tectonic signal compared to the induced one. The proposed retrofitting options could greatly improve the seismic response of the building stock in the Groningen area. The strengthened joints are beneficial at structural level, because they can provide the building with a box-like behaviour, but also at material level, since lower damage is


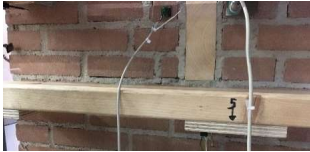












Configuration	Quasi-static cyclic tests	Dynamic tests
A		
B		
C		
D		
E		
F		
G		

Figure 4.17: Visual comparison of damage and cracks occurred to the walls under quasi-static cyclic and dynamic loading after the tests. From [151].

Table 4.10: Comparison between quasi-static and dynamic tests in terms of peak force in pulling and pushing, and stiffness evaluated at 2 mm displacement. Both average values and, in brackets, their standard deviations are reported.

Configuration	Peak force in pulling (kN)		Peak force in pushing (kN)		Secant stiffness at 2 mm displacement (kN/mm)	
	QS tests	HFD tests	QS tests	HFD tests	QS tests	HFD tests
A	0.7 (0.3)	0.6 (0.2)	0.7 (0.3)	0.8 (0.3)	0.4 (0.2)	0.3 (0.1)
B	5.8 (0.8)	3.5 (0.5)	1.2 (0.2)	1.6 (0.9)	0.5 (0.1)	0.5 (0.2)
C	6.4 (0.7)	6.7 (1.3)	8.9 (0.7)	14.1 (0.6)	2.6 (0.4)	3.3 (0.3)
D	8.9 (0.4)	5.6 (1.8)	8.7 (0.9)	10.4 (1.0)	1.6 (0.6)	1.9 (0.5)
E	4.9 (1.4)	5.2 (1.8)	11.6 (2.4)	14.8 (0.7)	2.8 (1.2)	2.9 (0.7)
F	10.1 (2.1)	10.7 (1.1)	6.4 (1.1)	9.5 (1.5)	3.6 (0.1)	4.3 (0.4)
G	6.6 (1.3)	10.1 (0.7)	8.4 (1.5)	11.6 (0.9)	1.4 (0.2)	2.4 (0.2)

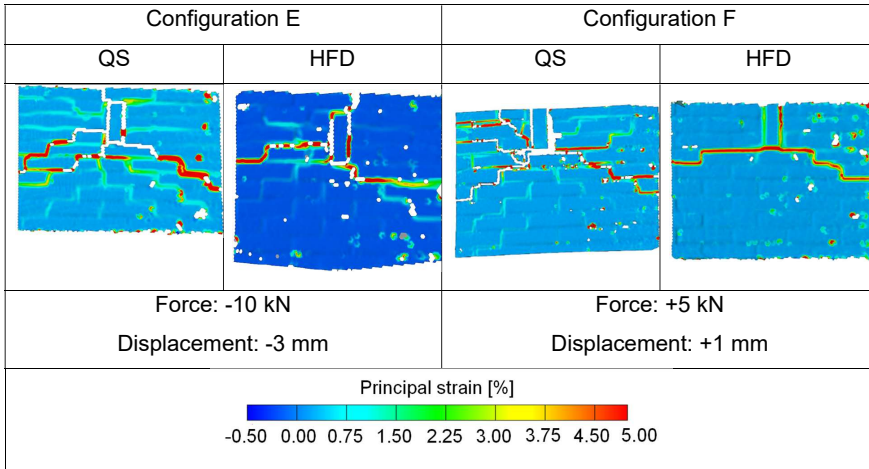


Figure 4.18: Comparison of crack pattern under the same displacement amplitude at peak strength detected by DIC for configurations E and F in quasi-static cyclic and dynamic tests. From [151].

underwent by the masonry. Finally, some of the connections can also activate energy dissipation, as discussed in Section 4.4.6.

4.4.5 Failure modes of the connections

In this section, the failure modes observed while testing the joints are discussed; in addition to that, other failure types are included because they may occur in presence of more deteriorated structural elements and materials. Fig. 4.20 displays the configurations tested in the second phase with the respective failure modes and the description of the main outcomes from the tests. Configurations A, B and C were also tested within the pilot study, although with different masonry wall types, but the same failure modes were observed.

With regard to as-built configurations, the frictional behaviour of joint type A does not lead to a real failure mode with damage at connection level. At structural level, a detachment of the wall from the joists could occur instead, with the consequent out-of-plane collapse of the wall. The same consideration applies for configuration B in the pushing direction, while the presence of the hook anchor may cause cracking in the masonry and yielding of nails when pulling.

When considering the strengthened configurations, a larger number of failure mechanisms can occur for the same configuration. In configurations C and D, bending and yielding of screws and steel angles were observed, as well as cracks in the walls around the joints. For large displacements, but not in all cases, the pull-out failure of one mechanical anchor occurred as well. Configuration E was characterized by yielding of the nails connecting the hook anchor to the joist and by the detachment of the glued interface from the wall, a brittle and less desirable failure mode; cracks on the walls were also detected. In configuration F, the main failure mode was related to the damage on the walls and the brick sliding or extraction due to the screws' action. Ideally, also bending and yielding of the screws could potentially occur, but they were not observed during the performed tests due to the large diameter adopted for the screws. Finally, for configuration G, yielding of nails and screws was noticed, together with cracks on the walls and, for very large displacements, the pull-out failure of one or two mechanical anchors.

The description of the failure modes and the test results will contribute to the definition of calculation models of the tested timber-masonry connections, reported in Chapter 5.

4.4.6 Dissipative properties of the connections

The energy dissipation provided by each configuration was quantified in terms of an equivalent damping ratio, evaluated at the cycle corresponding to half of the peak force. For configuration A, for which the peak force was constant due to the frictional response, the damping ratio was evaluated at half of the maximum applied displacement.

The damping ratio was calculated by adopting the energy loss per cycle method (Eq. 4.1); the results of this analysis are reported in Table 4.11. Configuration A showed the highest damping value because of its frictional behaviour and displacement capacity, but its limited shear transfer would not be sufficient to prevent the walls from out-of-plane collapses. For this reason, when this component is evaluated as part of a whole building,

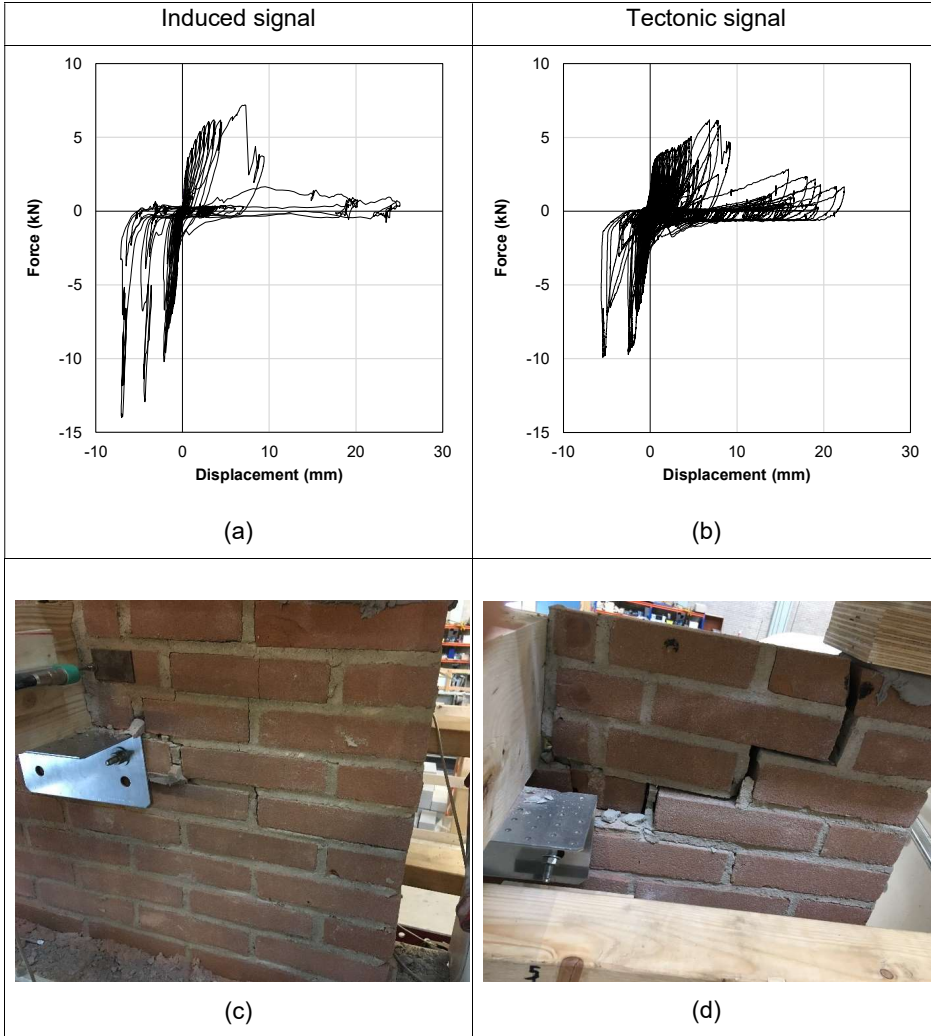


Figure 4.19: Comparison between the hysteretic response of configuration C under an induced (a) or tectonic (b) signal; damage on the masonry wall and the joint after the tests with induced (c) and tectonic signal (d). From [151].







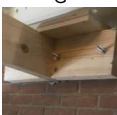
Joint type	Failure mechanisms	Remarks from quasi-static tests	Remarks from dynamic tests
<p>A</p> 	Friction on the joist-mortar interface	Frictional response	Higher strength values due to sudden load relatively to quasi-static tests, but absolute strength values still low
<p>B</p> 	<ul style="list-style-type: none"> • Friction on the joist-mortar interface • Yielding of nails • Cracking of masonry 	Whole wall activated in pulling after frictional behaviour	Higher play and lower stiffness
<p>C</p> 	<ul style="list-style-type: none"> • Yielding of screws • Cracking of masonry or bricks' extraction • Bending and yielding of the steel angle • Pull-out failure of the mechanical anchors 	Whole wall activated in both directions with effective transfer of load; yielding of screws and steel angle	Same stiffness, higher pushing strength due to impact effect
<p>D</p> 	<ul style="list-style-type: none"> • Yielding or pull-out failure of screws • Cracking of masonry or bricks' extraction • Bending and yielding of the steel brackets • Pull-out failure of the mechanical anchors 	Whole wall activated in both directions with effective transfer of load; yielding of screws and angle brackets	Higher play, lower stiffness; lower pulling strength and higher pushing strength due to impact effect
<p>E</p> 	<ul style="list-style-type: none"> • Yielding of nails • Cracking of masonry • Detachment of glue pocket with extraction of the hook anchor 	Whole wall activated in both directions with effective transfer of load until detachment of glued interface	Slightly higher pushing strength due to impact effect
<p>F</p> 	<ul style="list-style-type: none"> • Cracking of masonry or bricks' extraction • <i>Yielding or pull-out failure of screws</i> 	Whole wall activated in both directions with effective transfer of load and a very stiff behaviour	Higher play and lower stiffness, higher strength
<p>G</p> 	<ul style="list-style-type: none"> • Yielding or pull-out failure of screws and nails • Cracking of masonry or bricks' extraction • Pull-out failure of the mechanical anchors 	Whole wall activated in both directions with effective transfer of load and with a very ductile behaviour	Slightly higher strength and stiffness

Figure 4.20: Summary of the possible failure modes (in italic those not observed in the tests, but possible in practice) and main outcomes from the tests for each connection type. From [151].

Table 4.11: Values of equivalent damping ratio evaluated for each tested connection configuration. Both average values and, in brackets, their standard deviations are reported.

Configuration	Equivalent damping ratio evaluated at half of peak force
A	0.59 (0.03)
B	0.23 (0.03)
C	0.20 (0.08)
D	0.23 (0.05)
E	0.08 (0.02)
F	0.14 (0.02)
G	0.18 (0.03)

its performance would be insufficient. The values determined for the other connections show two distinct groups: configurations B, C, D and G, thus the most ductile ones, exhibited remarkable damping values, besides improving the stiffness and strength of the as-built configurations. Connection types E and F showed lower damping values, because these strengthening methods privileged strength and stiffness rather than energy dissipation, which is mainly provided by cracking of masonry.

The damping properties of the connections are useful to complete their characterization, but the role of this dissipative contribution is less relevant than that of the (retrofitted) diaphragms. This is because a sufficiently stiff joint can be considered as approximately continuous (and therefore it could be designed based on strength) as noticeable from Chapters 5 and 7, thus not bringing into play high dissipation. Furthermore, the shear transfer of a single connection is only a fraction of that provided by the floor, for which a larger energy dissipation is therefore activated in the context of the global response of timber buildings.

4.5 Summary of test results for masonry walls

4.5.1 General

In the following sections, the test results on masonry structural components will be briefly summarized. Since, as already stated, this experimental campaign was conducted by a different research group at TU Delft, for further information the reference to the relevant test reports will be provided.

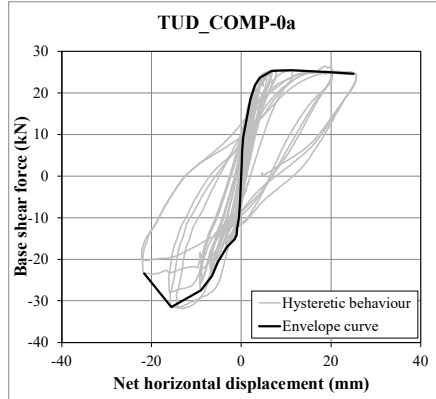


Figure 4.21: Cyclic response of sample TUD_COMP-0a. From [156].

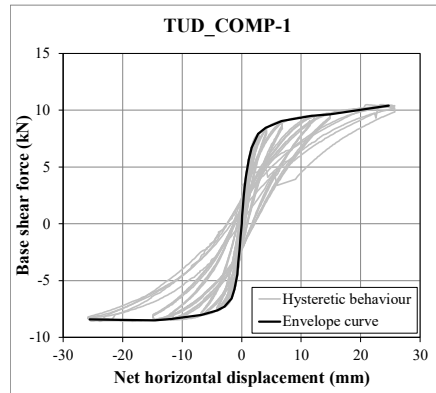


Figure 4.22: Cyclic response of sample TUD_COMP-1. From [156].

4.5.2 In-plane tests on masonry walls

Figs. 4.21 to 4.34 report the cyclic in-plane responses of all tested walls, while Table 4.12 summarizes the observed failure modes: as can be noticed, all in-plane failure mechanisms were obtained. For further information, the reader is referred to [156, 157].

From these tests, a thorough characterization of the cyclic in-plane response of walls with Dutch features was possible, and based on that, conventional drift limits identifying their failure could be retrieved (Section 5.6.2).

4.5.3 Out-of-plane tests on masonry walls

Figs. 4.35 to 4.41 report the cyclic out-of-plane responses of all tested walls: the difference between the walls tested in one-way and two-way bending (Table 3.5) is noticeable. The response of sample TUD_COMP-29 is not reported, because due to a technical issue the wall could not be characterized until failure, but only in the initial cycle [158]. For further information, the reader is referred to [104, 158].

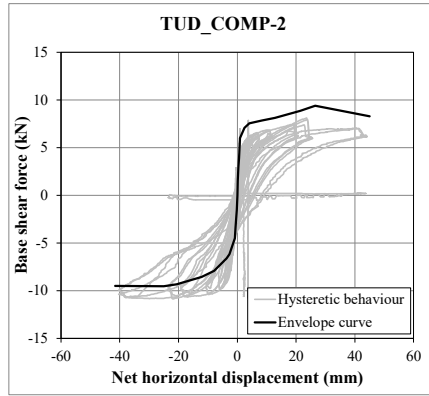


Figure 4.23: Cyclic response of sample TUD_COMP-2. From [156].

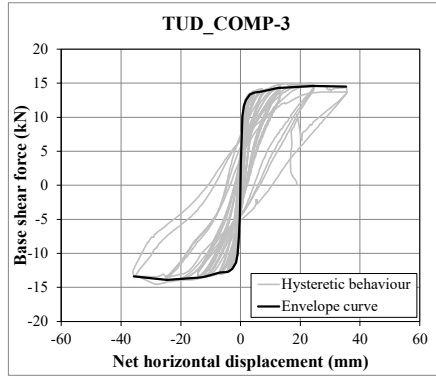


Figure 4.24: Cyclic response of sample TUD_COMP-3. From [156].

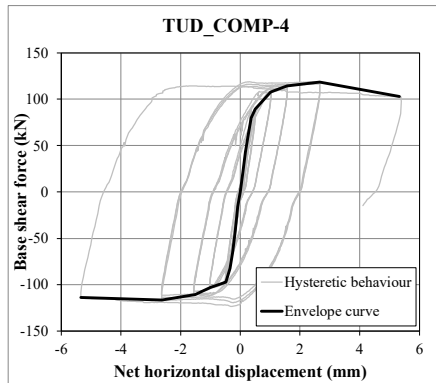


Figure 4.25: Cyclic response of sample TUD_COMP-4. From [156].

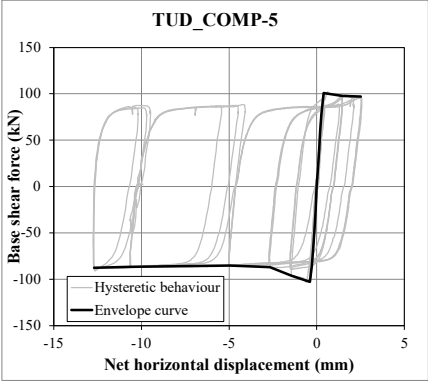


Figure 4.26: Cyclic response of sample TUD_COMP-5. From [156].

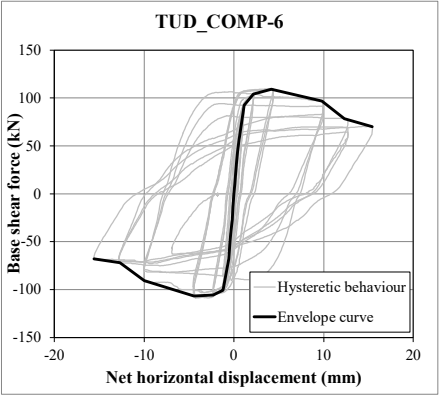


Figure 4.27: Cyclic response of sample TUD_COMP-6. From [156].

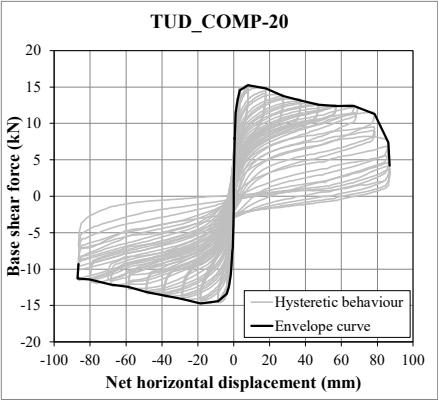


Figure 4.28: Cyclic response of sample TUD_COMP-20. From [157].

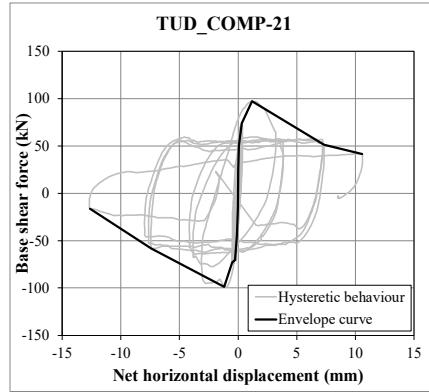


Figure 4.29: Cyclic response of sample *TUD_COMP-21*. From [157].

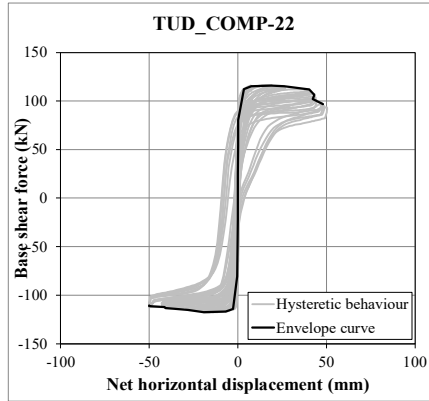


Figure 4.30: Cyclic response of sample *TUD_COMP-22*. From [157].

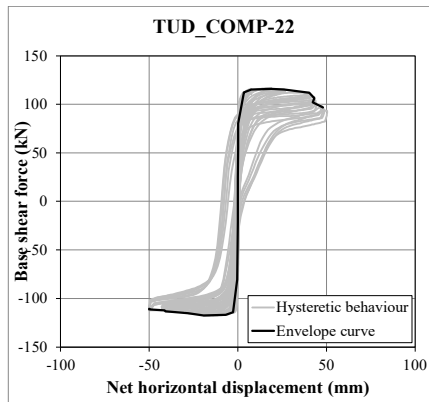


Figure 4.31: Cyclic response of sample *TUD_COMP-22*. From [157].

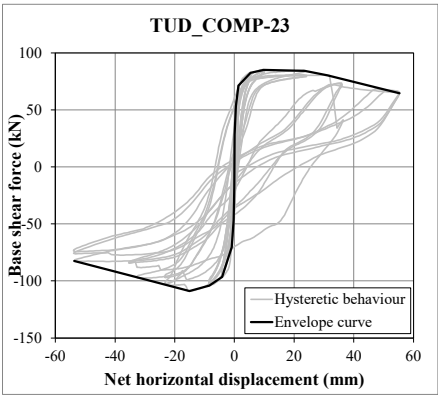


Figure 4.32: Cyclic response of sample TUD_COMP-23. From [157].

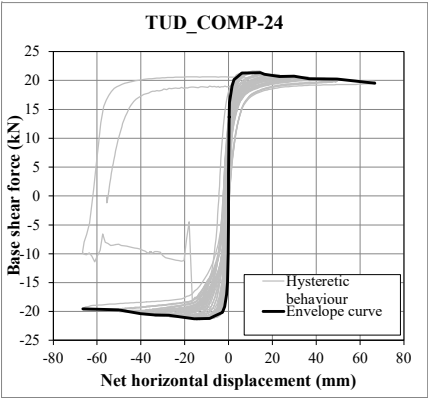


Figure 4.33: Cyclic response of sample TUD_COMP-24. From [157].

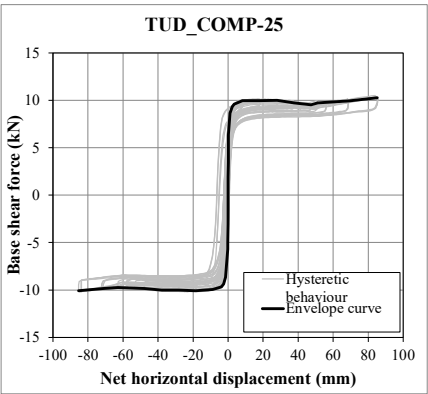


Figure 4.34: Cyclic response of sample TUD_COMP-25. From [157].

Table 4.12: Summary of the failure modes of the tested in-plane walls.

Sample name	Failure modes
TUD_COMP-0a	Rocking, toe crushing and sliding
TUD_COMP-1	Rocking, toe crushing and sliding
TUD_COMP-2	Rocking and sliding
TUD_COMP-3	Rocking and toe crushing
TUD_COMP-4	Diagonal shear failure
TUD_COMP-5	Sliding
TUD_COMP-6	Diagonal cracking and toe crushing
TUD_COMP-20	Rocking and toe crushing
TUD_COMP-21	Diagonal shear failure
TUD_COMP-22	Sliding and toe crushing
TUD_COMP-23	Rocking of two wall parts
TUD_COMP-24	Rocking and splitting of the bottom unit
TUD_COMP-25	Pure rocking

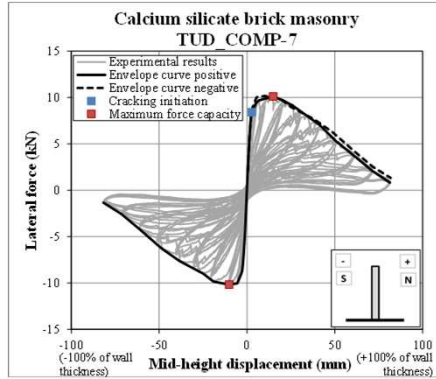


Figure 4.35: Cyclic response of sample TUD_COMP-7. From [104].

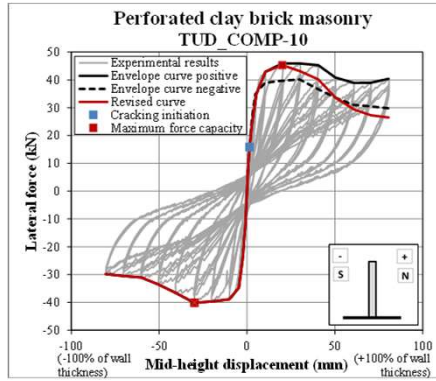


Figure 4.36: Cyclic response of sample TUD_COMP-10. From [104].

From these tests, a through characterization of the cyclic out-of-plane response (in one-way or two-way bending) of walls with Dutch features was possible, and based on that, conventional drift limits identifying their failure could be retrieved (Section 5.6.2).

4.5.4 Interaction between masonry structural components

Besides characterizing the single masonry components, a full-scale portion of building representing a Dutch terraced house [171] was also realized (Fig. 4.42). The house prototype was subjected to a displacement-controlled cyclic loading in order to retrieve its capacity curve (Fig. 4.42c), and the test allowed to characterize the interaction between in- and out-of-plane calcium-silicate brick masonry walls, and concrete floors. This same test was also taken as reference to validate the modelling strategy for masonry implemented in DIANA FEA (Chapter 5).

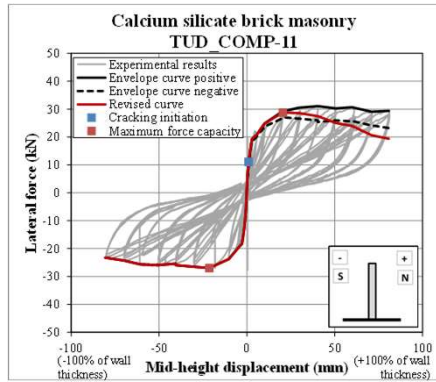


Figure 4.37: Cyclic response of sample TUD_COMP-11. From [104].

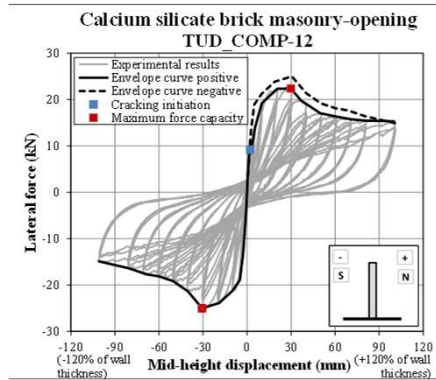


Figure 4.38: Cyclic response of sample TUD_COMP-12. From [104].

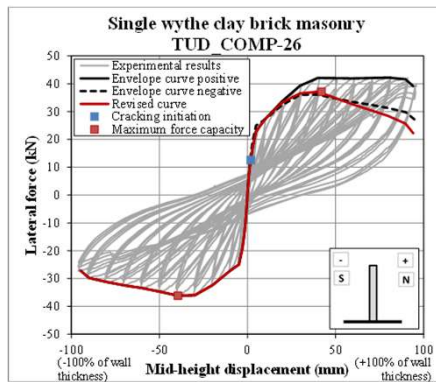


Figure 4.39: Cyclic response of sample TUD_COMP-26. From [158].

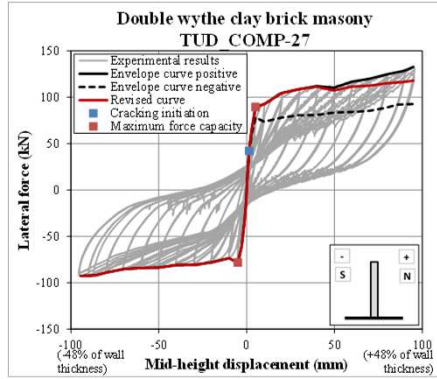


Figure 4.40: Cyclic response of sample TUD_COMP-27. From [158].

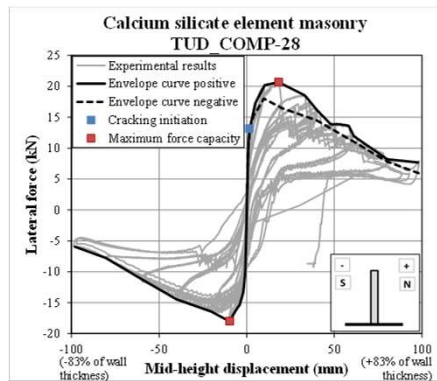


Figure 4.41: Cyclic response of sample TUD_COMP-28. From [158].

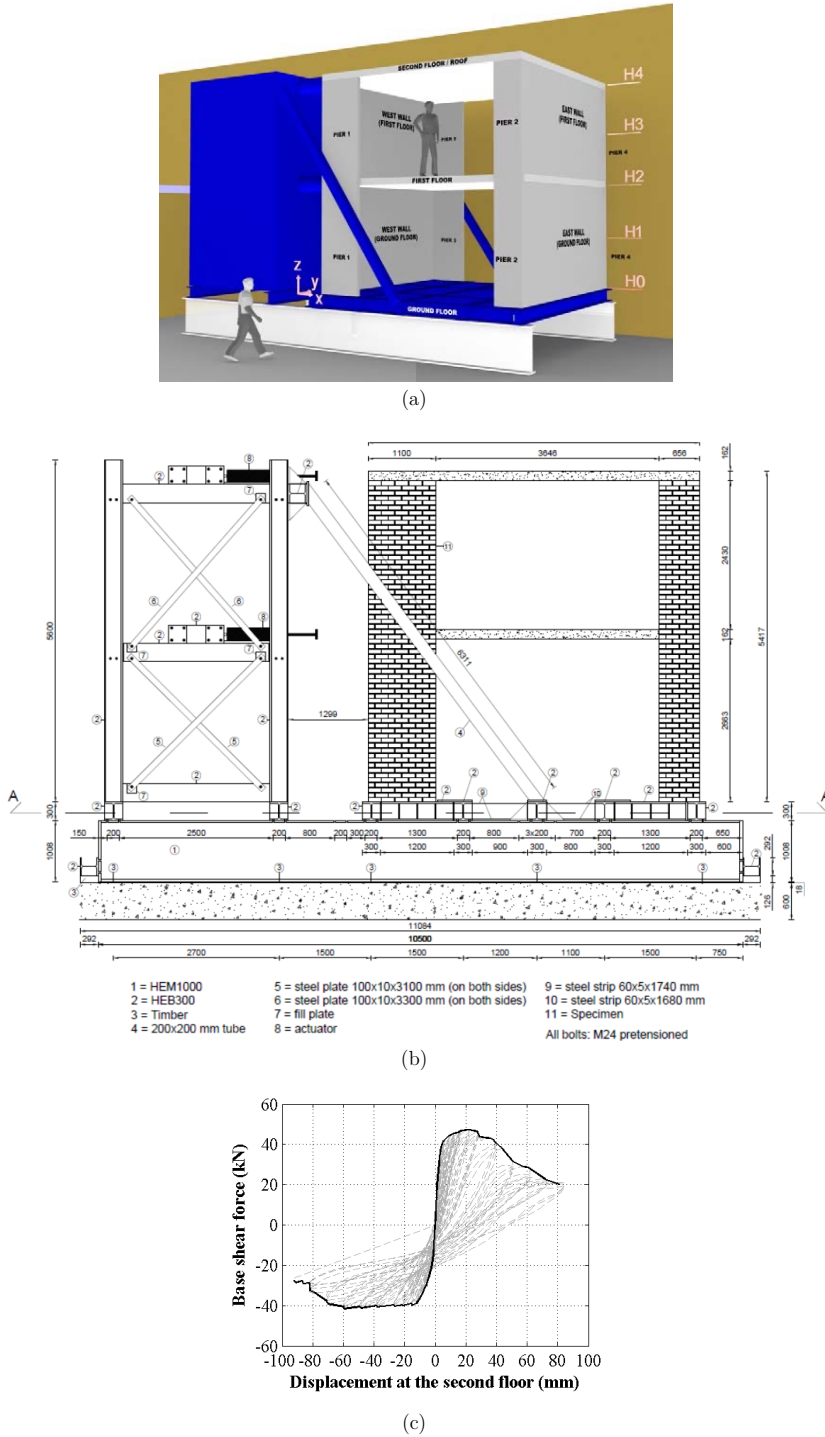


Figure 4.42: Cyclic pushover test on a full-scale clay brick masonry assemblage representing a terraced house unit: 3D view of the building (a); test setup and measurement plan (b); capacity curve (c). From [171].

Chapter 5

Modelling the seismic response of structural components

5.1 Introduction

In order to broadly apply in the seismic assessment and retrofitting of existing buildings the experimental results presented in Chapter 4, analytical and/or numerical models have to be derived, which can describe the seismic behaviour of floors, connections, and walls more generally. This is another knowledge gap found in Chapter 2, where the lack of models or general equations to calculate as-built and retrofitted timber diaphragms and timber-masonry connections was highlighted, from the analytical and numerical point of view.

Starting from this framework, and aided by the obtained test results, this chapter presents the analytical and numerical models, as well as specific recommendations, to describe the seismic behaviour of structural components, with specific focus on timber diaphragms and their connections to masonry walls. Similarly to Chapters 3 and 4, the analytical and numerical modelling strategies are discussed separately for timber diaphragms, wall-to-floor timber-masonry connections and masonry walls.

An outline of the modelling approach followed in this chapter is shown in Fig. 5.1. First of all, the analytical and numerical characterization of as-built diaphragms will be addressed (Section 5.2), so that their seismic assessment can be properly performed (step 1 in Fig. 5.1). Secondly, the formulation of an advanced nonlinear model will be presented, accounting in detail for the cyclic, nonlinear in-plane response of the retrofitted diaphragms, and allowing to accurately design the strengthening interventions (Section 5.3). In addition to that, the implementation of the formulated model in two different software, widely adopted also for numerical analyses on masonry buildings, will be addressed in detail: a macro-element modelling approach will be followed, and specific modelling strategies will be provided in Section 5.4.

Timber-masonry connections will be analytically and numerically described as well (Section 5.5), by formulating calculation methods for determining their load-slip response, and recommending modelling approaches compatible with the numerical macro-element representation of the diaphragms. This analytical and numerical characterization of

retrofitted diaphragms and timber-masonry connections completes steps 2 and 3 of Fig. 5.1.

Finally, the usual approaches for modelling masonry structural components will be summarized, including the commonly adopted drift limits for identifying their in-plane or out-of-plane failures (Section 5.6).

5.2 Analytical and numerical models for as-built timber diaphragms

5.2.1 Analytical modelling of as-built diaphragms

For as-built flexible floors with continuous planks, such as the Dutch diaphragms, the use of an equivalent shear stiffness to quantify their in-plane response appears not to be suitable. This is because their behaviour is mostly flexural, and governed by bending of the main joists or boards, while the whole sheathing does not contribute to create sufficient shear rigidity. Thus, it was only possible to derive G_d for the tested samples at different drifts (Section 4.3.7), keeping in mind that this could not be fully representative for the observed behaviour, and also not size- or direction-independent (with the exception of the roof sample, which showed a shear-related response because of its specific configuration). This can immediately be noticed considering that in a cantilever static scheme, such as the test setup one, the flexural deflection is linked to the cube of the span, whereas the shear deformation is linearly related to it. Thus, a scale effect is present when bending deformation is governing, and the use of G_d could lead to wrong estimations of the actual in-plane stiffness and deflection of the diaphragms for other sizes than tested. Furthermore, it has to be considered that longer spans and/or smaller structural elements imply a more relevant contribution of resisting moments given by nail couples and friction effects [46, 47].

However, by applying relations from mechanics it is still possible to accurately represent the behaviour of these as-built floors. In the calculations, when loading parallel to the joists, friction in the planks as well as the small resisting bending moment given by each nail couple according to the applied rotation, were neglected given their limited contribution. This assumption is valid especially when the specimens undergo sufficiently high forces. For the other direction, however, the influence of friction was noticeable from the hysteretic cycles of the samples tested orthogonally to the joists (Section 4.3.3). In fact, in the loading and unloading phases an almost infinitely rigid behaviour occurred, before the stiffness related only to the geometry of structural elements composing the floor came into play.

The reason for this lies in the fact that the diaphragms were so flexible, that they could undergo only very limited horizontal loads (up to 4 kN), and therefore even this contribution from friction could play a non-negligible role. The same considerations can be drawn with regard to the resisting bending moment given by nail couples. The calculation in this case is slightly more complex, because these moments are nonlinearly depending on the rotation of the joists, which in turn is due to the moments themselves, leading to an iterative procedure [46]. Therefore, the calculation of the deflection of the diaphragms remains still possible. Together with the geometrical dimensions of each as-built sample, the following material properties were adopted based on the test results

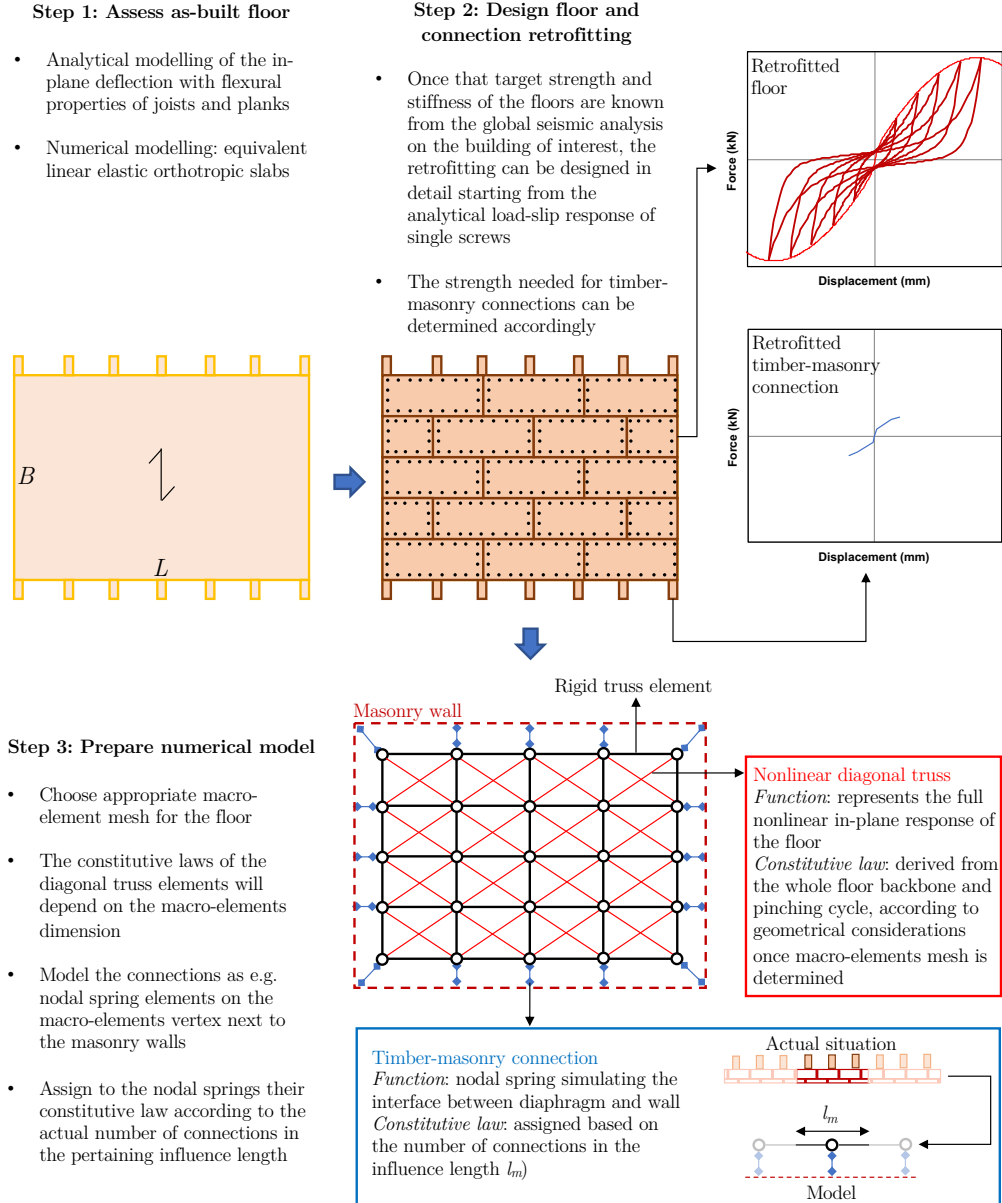


Figure 5.1: Summary of the adopted procedure for the analytical and numerical modelling of as-built and retrofitted timber-diaphragms and timber-masonry connections.

on replicated structural elements [132]:

- $E_{planks} = 11210 \text{ MPa}$;
- $E_{joists} = 13120 \text{ MPa}$;
- $I_{planks} = (t \cdot w^3/12) \cdot n_{planks}$ when loading parallel to the joists;
- $I_{joists} = (h \cdot b^3/12) \cdot n_{joists}$ when loading perpendicular to the joists;

In the former relations, E_{planks} , I_{planks} , n_{planks} , and E_{joists} , I_{joists} , n_{joists} are the elastic modulus, the moment of inertia, and the number of planks and joists in the diaphragm, respectively.

Then, considering the static scheme of the tested floors, the deflection δ on top of the floors induced by a load F can be obtained with the following relations:

- Loading parallel to the joists: $\delta = F \cdot L^3/(3 \cdot E \cdot I_{planks})$
- Loading perpendicular to the joists (see Figure 5.2 for better clarification):

$$\delta = F \cdot L^3/(3 \cdot E \cdot I_{joists}) - \sum_i [(M_i \cdot X_i^2)/(2 \cdot E \cdot I_{joists}) + (M_i \cdot X_i)/(E \cdot I_{joists})(L - X_i)] \cdot n_{joists}; \quad i = 1 \dots n_{couples}$$

In the former equation, the deflection is slightly decreased by the moments M_i induced in the $n_{couples}$ nail couples because of their rotation, depending on their coordinates X_i (Fig. 5.2). Besides, L identifies the span of the tested halved floor.

In Figs. 4.5-4.6 the deformed shape of the diaphragms was shown at 10 and 30 mm in-plane deflection: the in-plane forces obtained from the tests at these displacement values were substituted in the proposed analytical formulations. The results of these calculations are shown in Table 5.1. Only the four floor samples having a flexural response were considered, because the roof had a shear-related deflection: for this latter diaphragm type an average G_d value of 50 kN/mm was derived, which is in line with similar as-built floors from literature displacing in shear (Table 4.8).

As noticeable from Table 5.1, for both loading directions the flexural behaviour of the floor samples observed during the tests is also confirmed by these analytical calculations. For the specimens tested orthogonally to the joists, the values show a slight scatter, probably because for the calculation of the bending moments M given by single nail couples always the same average backbone curve was used (Fig. 5.2), derived from the rotational tests on plank-joist connections [132]. Nevertheless, the obtained values are still comparable to those experimentally recorded. The average backbone curve was calculated according to FOSCHI's exponential model [172] adapted for torsional behaviour, by means of the following equation calibrated on the whole set of results (10 reference backbones, $R^2 = 0.84$):

$$M = (M_0 + K_{1,rot}\varphi)[1 - \exp(-K_{0,rot}\varphi/M_0)] \quad (5.1)$$

with:

- φ rotation to which the single nail couple is subjected;

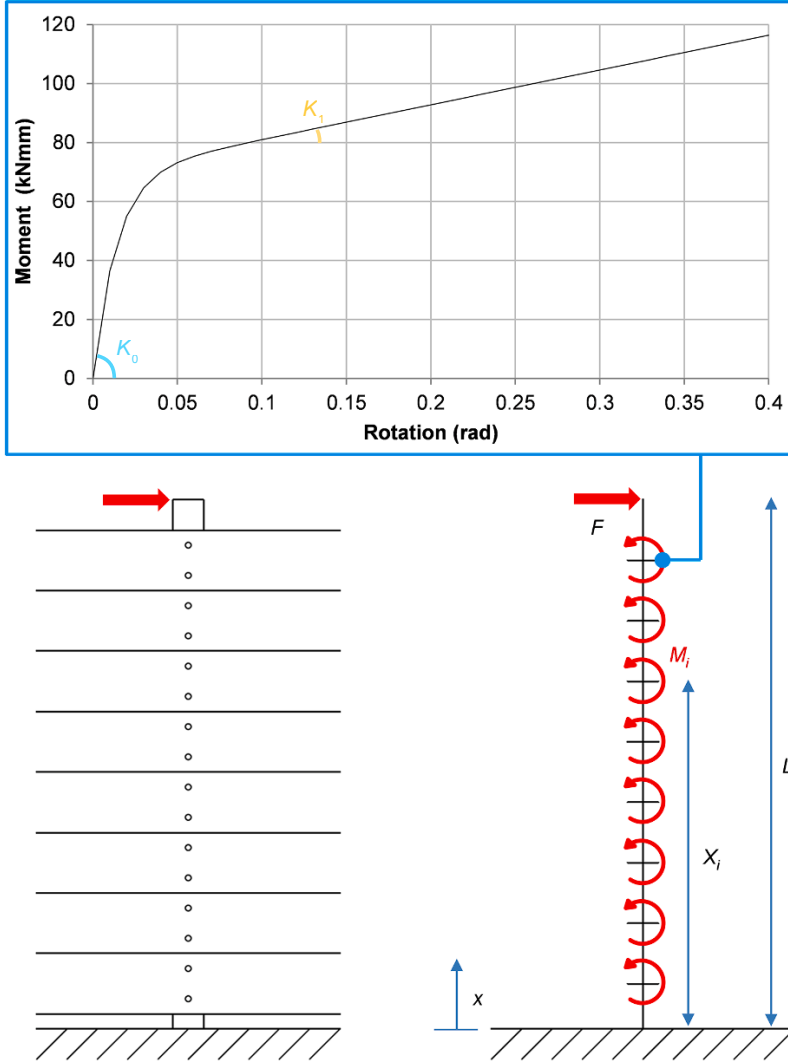


Figure 5.2: Scheme for the analytical calculation of the floor deflection in the direction orthogonal to the joists: for the moments given by nail couples, the shown average backbone curve calibrated from the conducted experimental tests in torsion on plank-joist connections was used. From [132].

Table 5.1: Comparison between the experimental and analytical values of displacement for as-built specimens loaded parallel and perpendicular to the joists. The symbol (*) refers to a load value obtained after subtracting the contribution of friction between planks, equal to ≈ 0.9 kN for sample DFper-3 and to ≈ 0.5 kN for specimen DFper-4.

Specimen name	Horizontal load (kN)	Experimental displacement (mm)	Analytical displacement (mm)
DFpar-1	4.0	10.1	10.6
	11.3	30.0	30.0
DFpar-2	5.0	9.5	9.6
	15.8	30.2	30.2
DFper-3	1.1*	10.3	11.1
	2.2*	30.0	29.7
DFper-4	1.0*	10.1	11.2
	2.5*	30.0	30.1

- Yielding torsional moment $M_0 = 69.2$ kNmm;
- Initial rotational stiffness of the single nail couple $K_{0,rot} = 5059.7$ kNmm/rad;
- Post-yielding rotational stiffness of the single nail couple $K_{1,rot} = 118.0$ kNm-m/rad.

This contribution of the resisting moments provided by the nail couples is of importance for floors with light, slender structural elements. In fact, for a certain deflection δ , the following load F is derived when accounting for this contribution:

$$F = \frac{6EI_{joists}\delta + 3 \sum_{i=1}^{n_{couples}} M_i X_i (2L - X_i) n_{joists}}{2L^3} = \frac{3\gamma_f EI_{joists}}{L^3} \quad (5.2)$$

Therefore, the resisting action of the nail couples moments is considered by adopting a factor γ_f , which increases the global flexural stiffness of the diaphragm. If several cross sections are considered, the curve in Fig. 5.3 is obtained: as can be noticed, the contribution of the moments becomes almost not relevant as soon as the in-plane inertial properties increase. The curve can be interpolated with the following simplified equation for calculating γ_f :

$$\gamma_f = 1 + \frac{3 \cdot 10^6}{I} \quad (5.3)$$

with I moment of inertia of a single structural element (e.g. a joist), in mm^4 . It should be noticed that this expression is valid for floor configurations very similar to the tested ones, and refers to 3×65 mm nails (commonly found in practice).

The conducted experimental and analytical research contributed to the update of the Dutch seismic standard NPR 9998 [27], providing guidelines on the seismic assessment of as-built diaphragms and the calculation of their in-plane deflections (flexural, for

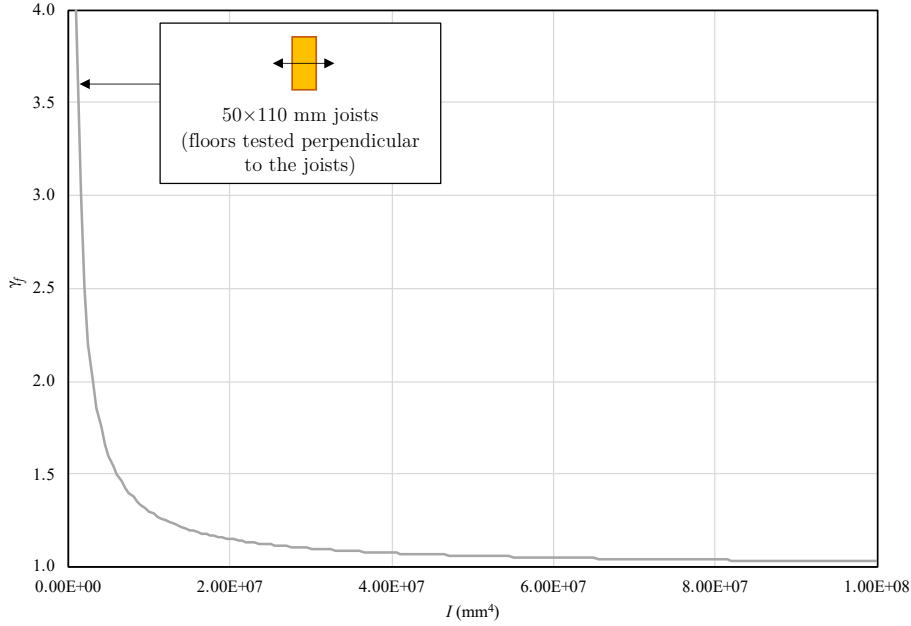


Figure 5.3: Value of the factor γ_f increasing the global flexural stiffness of the diaphragms as a function of the moment of inertia I of a single structural element of the floor.

whole floors with continuous planks, and shear-related for roof pitches, as shown in Fig. 5.4).

5.2.2 Numerical modelling of as-built diaphragms

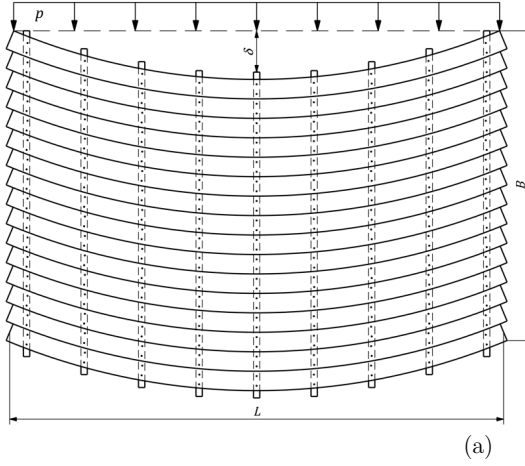
The response of as-built diaphragms with Dutch features proved to be approximately elastic and orthotropic. Therefore, in order to model the global behaviour of the diaphragms, the use of orthotropic shell elements can be a reasonable option, which is already adopted for numerical studies on existing URM buildings [129, 173]. The properties to be attributed to the elements are calibrated to reflect both the static and the seismic response of the floors.

The static behaviour under vertical loads (acting along the z -axis), such as the self-weight, is considered by means of an equivalence of the structural properties:

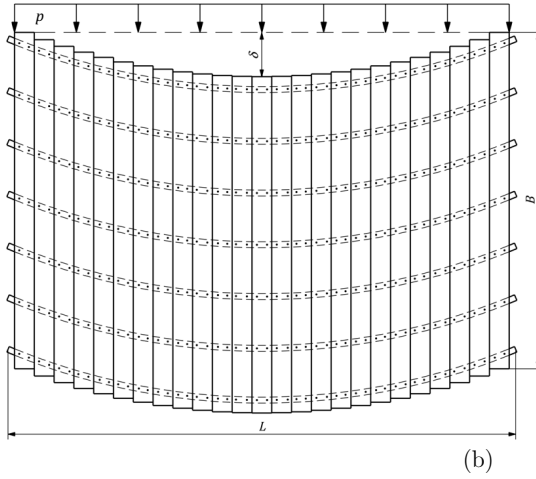
$$E_{eq} = E_{timber} I_{joists} / I_{slab} \quad (5.4)$$

In the former equation, I_{joists} is the sum of the moments of inertia (referred to the vertical load-bearing direction) of the single joists, and I_{slab} is the moment of inertia of the equivalent slab, determined by attributing a thickness t of the shell elements equal to that of the sheathing. Because no slab effect is present for these diaphragms, the Poisson coefficient $\nu = 0$.

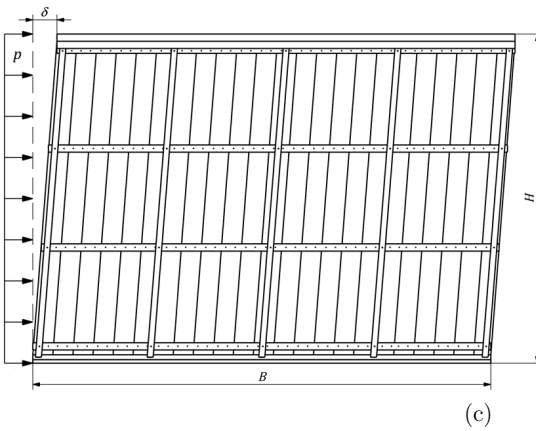
The seismic response is considered by means of an equivalent shear modulus to be attributed to the in-plane loading direction (xy plane). The equivalent shear modulus is evaluated by means of a flexural equivalence as follows [47]:



$$\delta = \frac{5pL^4}{384EI_{planks}}$$



$$\delta = \frac{5pL^4}{384\gamma_f EI_{joists}}$$



$$\delta = \frac{pH^2}{2G_d B}$$

$G_d = 30 \div 80 \text{ N/mm}$

Figure 5.4: Static schemes for calculating the in-plane deflections of whole diaphragms loaded parallel (a) or perpendicular (b) to the joists, and of roof pitches (c). From [27].

$$G_{xy} = \frac{48 \cdot E \cdot I_{in-plane}}{5 \cdot B \cdot L^2 \cdot t} \quad (5.5)$$

where $I_{in-plane} = I_{planks}$ or I_{joists} , depending on the loading direction.

Instead, the two shear moduli G_{xz} and G_{yz} , which involve again the static response under vertical loads, are determined as $E_{eq}/16$, similarly to timber structural elements.

This modelling strategy for as-built timber diaphragms is also adopted to model the retrofitted floors, but with a number of variations to fully account of their in-plane nonlinear, dissipative in-plane response (Sections 5.3 and 5.4).

5.3 Analytical models for retrofitted timber diaphragms

5.3.1 Introduction

The objective of this section is to analytically describe the in-plane response in terms of strength, stiffness, and energy dissipation of timber floors strengthened with plywood panels screwed along their perimeter to the existing sheathing. As starting point, the load-slip behaviour of the screws fastening planks and plywood panels was evaluated (Section 5.3.2): based on this, the global in-plane response of the diaphragm was then derived analytically (Section 5.3.3). Although the analytical model has been formulated to predict the response of floors with Dutch features, its definition is general and can be applied to other contexts as well, provided that the proposed retrofitting method is used, and an efficient shear transfer is ensured on the diaphragms sides, and to the walls (e.g. with timber blocks, steel angles, additional fasteners, etc.). The behaviour of the diaphragms is analysed when loading them both parallel and perpendicular to the joists, as in the testing phase (Section 3.5.1), according to the principles of Fig. 5.5.

In order to generalize the formulated model, the methodology adopted to derive the expression defining the load-slip behaviour of screws is presented in two cases:

1. Derivation from performed tests on plank-plywood panel connections;
2. Derivation through equations from current standards or literature.

The main assumptions at the basis of the proposed model are as follows:

- The shear load between panels can be transferred by the underlying planks to which they are screwed;
- Contact between plywood panels is taken into account as an increase in stiffness, according to the findings of RIZZI et al. [175];
- The rows of screws that are parallel to the load oppose to the panels sliding, while the ones that are perpendicular to the load have to withstand the panels rotation.

The derived formulation was validated by comparing the response predicted with the analytical model to the one of tested diaphragms.

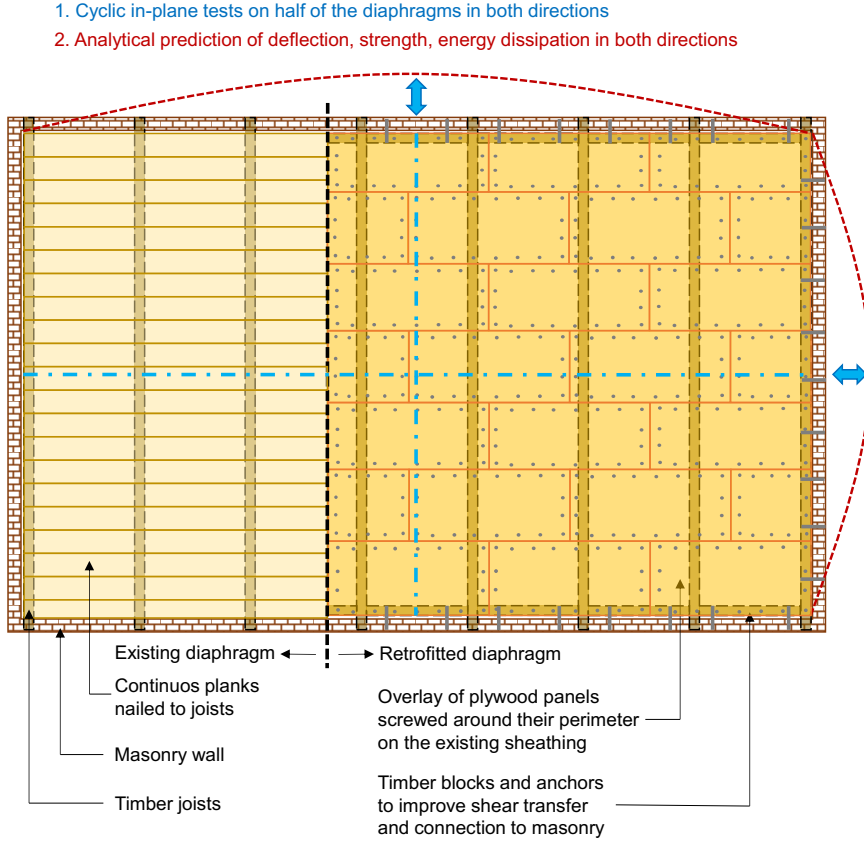


Figure 5.5: Example of timber diaphragms retrofitted with a plywood panels overlay, and basic principles for the conducted tests and the formulation of the analytical model. From [174].

5.3.2 Definition of the load-slip behaviour of fasteners

Since the proposed model aims to describe, starting from the single fasteners, the global in-plane behaviour of floors strengthened with plywood panels, the properties of these connectors have to be accurately defined.

Before arranging the experimental campaign on full-scale strengthened floors [132], tests were performed on fourteen small-size replicates to assess the properties of the fasteners connecting the plywood panels to the planks. These specimens consisted of a portion of plank, to which part of a plywood panel was fastened by means of two screws, as shown in Fig. 5.6. The main direction of the panel was arranged parallel to that of the plank, as it was done for the full-scale tests on floors. The adopted material was the same used for the construction of the whole diaphragms, therefore it represented an accurate replication of existing floors (Section 4.2.1). Both plywood panels and planks were made of spruce (*Picea Abies*), and had a thickness of 18 mm, while the screws had a diameter of 4.5 mm and a length of 40 mm.

Quasi-static reversed-cyclic shear tests were performed according to ISO 16670 [138]: seven replicates were tested parallel to the main direction of the plank, and the other

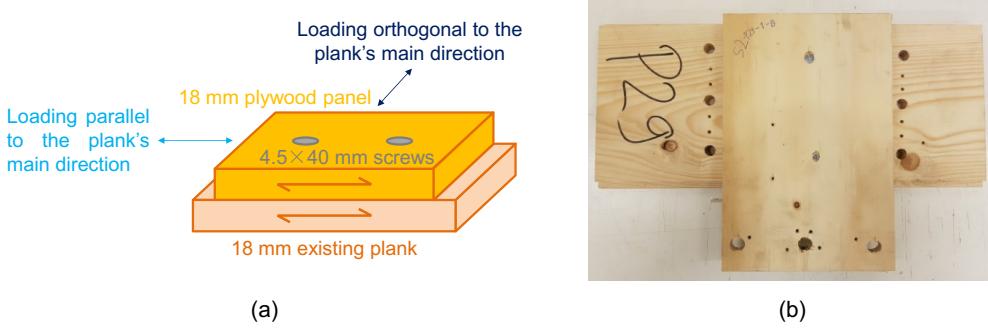


Figure 5.6: Samples prepared for the tests on screws fastening the plywood panels to the existing sheathing: schematic description (a) and example of specimen (b). From [174].

Table 5.2: Variations in the characteristics of the full-scale tested diaphragms with respect to the small-size tests on screws fastening plywood panel and plank.

Full-scale sample	Variations with respect to small-size plank-plywood tests
DFpar-1s	None
DFpar-2s	Planks (24 mm), Screws (d = 5 mm)
DFper-3s	Screws (d = 5 mm)
DFper-4s	Screws (d = 5 mm)
DRpar-5s	None

seven orthogonal to it (Fig. 5.6a). The obtained load-slip curves were similar between the two loading directions, as will later be shown.

However, some of the full-scale strengthened floors did not present the same characteristics as the small-size replicates: sample DFpar-2s featured 24 mm planks, and in specimens DFpar-2s, DFper-3s, DFper-4s screws with a 5 mm diameter were used (Section 3.4.1); these variations are summarized in Table 5.2. Thus, to predict the behaviour of all the diaphragms and to account for these variations, the derivation of the equation for the fasteners response was generalized: in this way, if tests are available, the expression can be derived according to the same procedure described in the following; otherwise, the direct estimation of the load-slip behaviour remains still possible with the knowledge of basic material properties of timber and fasteners.

The determination of the load-slip curve for the screws is of fundamental importance for the description of the overall behaviour of the diaphragms: starting from an appropriate representation of the nonlinear behaviour of the fasteners, it is then possible to extend it to the whole system. To determine the load-slip curve from the performed tests, firstly the backbone curves were constructed from the hysteretic cycles, following the procedure of ISO 16670 [138]. Secondly, the curves corresponding to the third stabilized envelope were considered; the procedure was carried out separately for each loading direction [174]. The negative backbones were included in the positive side

of the graph: in total, 14 backbone curves were thus available for each loading direction. As a consequence, a possible asymmetric behaviour was not taken into account; yet, this assumption still allows to accurately capture the whole response of the diaphragms, as shown in Section 5.3.4.

It was chosen to model the load-slip response by means of a linear and a parabolic branch, representing the initial stiffness and the global behaviour, respectively. This procedure was followed for screws tested both parallel and orthogonally to the main direction of the planks, as shown in Fig. 5.7. The threshold for the choice of the experimental points representing the initial stiffness was fixed at a displacement of approximately 1 mm.

After determining these two branches (initial stiffness and global backbone), for a better representation, a continuous curve was created with an extension of FOSCHI's load-slip model for nails [172]. This consisted of an exponential curve linking together two straight lines, representing the initial and the post-yielding stiffness. The same principle was, thus, followed for the construction of the curve linking the initial stiffness line and the parabola representing the global response. By adopting this model, it is possible to take into account both post-yielding and softening behaviour of the fasteners. The equation of the curve is defined as:

$$F_s = (F_0 + a \cdot d_s + b \cdot d_s^2) \left[1 - \exp \left(-\frac{K_0}{F_0} d_s \right) \right] \geq 0; \text{ with } a > 0, b < 0 \quad (5.6)$$

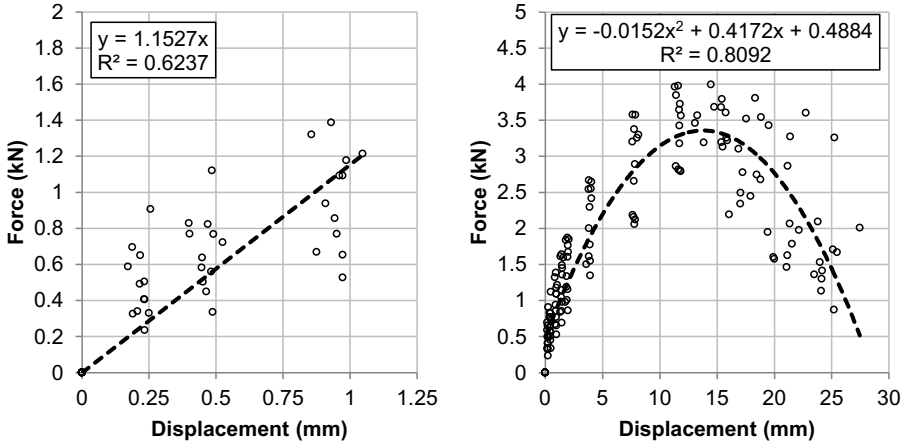
In the former equation, F_s and d_s are the force and displacement of the screw, respectively; F_0 , a and b are the coefficients of the parabola representing the global behaviour, while K_0 is the slope of the line representing the initial stiffness. This curve (Fig. 5.8) fits the experimental points with $R^2 = 0.83$ when the panel is loaded parallel to the plank, and with $R^2 = 0.95$ if the force is applied perpendicular to it. As a failure criterion for the softening phase, the ultimate displacement can be considered as the one at which the maximum load has decreased by 20% after the peak, in agreement with the provisions of ISO 16670 [138] and EN 12512 [45]. As it is usually observed when analysing tests on timber joints, a scatter is present in the data points and the backbones: however, since a large number of screws is used in the whole floor, the global behaviour will tend to the average trend.

When tests are not available for determining the parameters K_0 , F_0 , a and b , an estimation of them with equations present in standards or literature is proposed as follows:

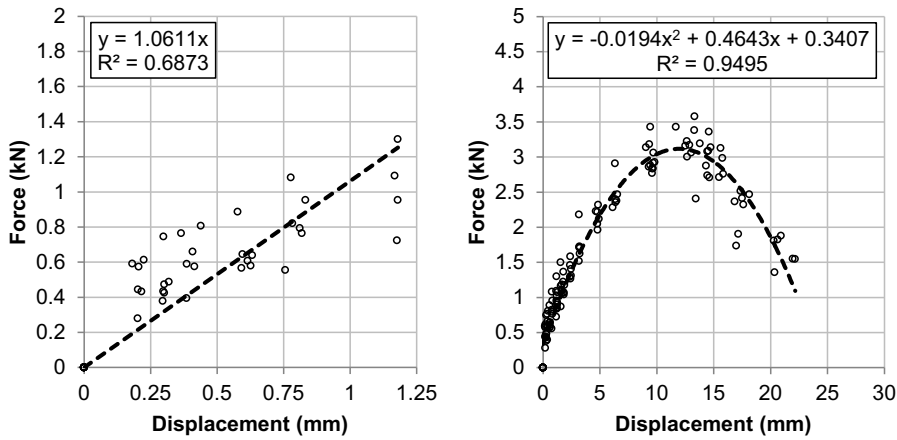
- K_0 can be determined with the expression provided by DUBAS et al. [176] for non-predrilled nails, using the nominal diameter d of the screw:

$$K_0 = 50d^{1.7} \quad (5.7)$$

This equation was chosen for its simplicity and very good agreement with the test results on plank-panel replicates. Instead, relations provided by EN 1995 [1] and DIN 1052 [177] tended to overestimate K_0 : Table 5.3 reports a comparison between the experimental values and the ones calculated adopting the aforementioned equations.



(a)



(b)

Figure 5.7: Determination from experimental tests of the branches representing the initial stiffness (linear branch of Eq. 5.6) and the global response (parabolic branch of Eq. 5.6) of the screws when loading the plywood panel parallel to the plank (a) and perpendicular to it (b). Experimental data points correspond to the amplitudes of each cycle on the various backbones. From [174].

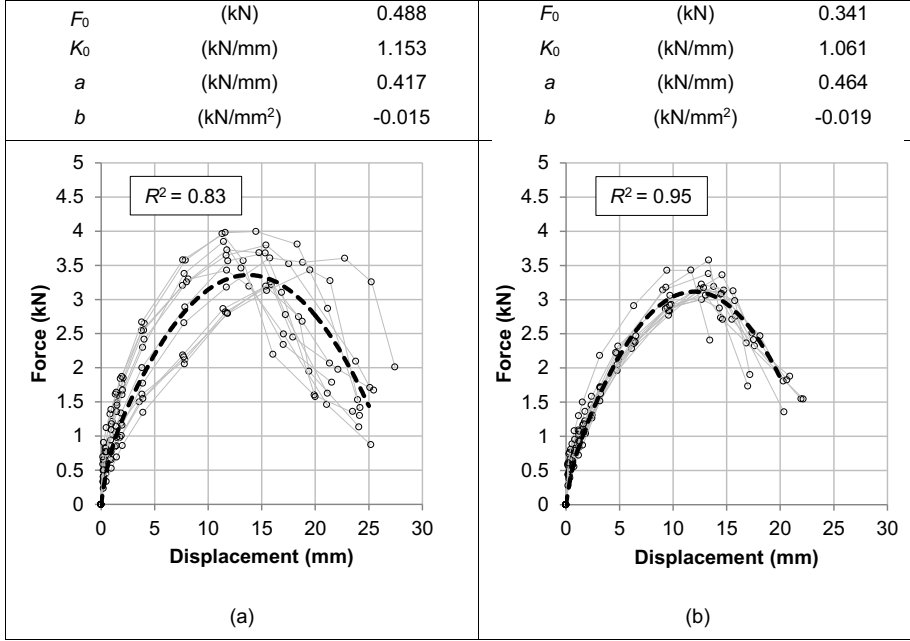


Figure 5.8: Proposed load-slip curve (dashed) in comparison to the experimental data points and backbones for the direction parallel to planks (a) and perpendicular to them (b). The main parameters of the curve equation are also reported. From [174].

- F_0 can be predicted starting from the knowledge of the maximum force F_{max} determined according to EN 1995 [1] and JOHANSEN's theory [178] for timber-to-timber joints, and with a screw sufficiently slender to develop two plastic hinges (this was also the failure mode observed in the tests):

$$F_{max} = \sqrt{\frac{2\beta}{1+\beta}} \sqrt{2Mf_{h,1}d} + \frac{F_{ax}}{4} \quad (5.8)$$

In the former equation, the usual factor 1.15 of the design expression in EN 1995 was neglected, because the average material characteristics were used. The other parameters have the same meaning as in EN 1995, thus M is the plastic bending moment of the screw, $f_{h,1}$ is the embedment strength of the first member of the joint, β is the ratio between the embedment strengths of the second and of the first member, d the nominal diameter of the screw, and F_{ax} the axial force developed because of the rope effect, determined in this case as [179]:

$$F_{ax} = f_{ax} \cdot d \cdot l_{ef} \left(\frac{\rho_n}{\rho_a} \right)^{0.8} \quad (5.9)$$

with f_{ax} withdrawal resistance parameter referred to a density $\rho_a = 350 \text{ kg/m}^3$ [179]; ρ_n is the density of the plywood panels or the planks, l_{ef} the effective

Table 5.3: Comparison among the values of initial stiffness K_0 for a single screw obtained experimentally and calculated according to equations from standards or literature.

Equation for K_0	Source	Stiffness (kN/mm)
$50d^{1.7}$	DUBAS et al. [176]	0.64
$\rho^{1.5}d^{0.8}/30$	EN 1995 [1]	1.08
$\rho^{1.5}d^{0.8}/25$	DIN 1052 [177]	1.30
-	Value from tests, // to plank	0.58
-	Value from tests, \perp to plank	0.53

threaded length, corresponding in this case to the thickness of the plywood panels or the planks.

The plastic bending moment is calculated with the screws shank or inner diameter d_1 , while for the embedment strength evaluation the nominal one is adopted. Then, F_0 can be estimated as $F_{max}/8$.

- To determine the parameters a and b , it is necessary to identify three points crossed by the parabola. The last quantity to be estimated is, then, the slip d_{max} of the screw at F_{max} . To this end, firstly the expression of EN 409 [137] can be used for determining the angle α at which the plastic bending moment of the screws is evaluated, and adopting for its calculation their shank or inner diameter d_1 (Eq. 5.10). Secondly, the distance $(b_1 + b_2)$ between the two plastic hinges according to JOHANSEN's theory [178] is determined (Eq. 5.11). By combining these two quantities, the slip d_{max} can be estimated (Eq. 5.12). Thus:

$$\alpha = \frac{110}{d_1} \quad (5.10)$$

$$b_1 = \sqrt{\frac{2\beta}{1+\beta}} \sqrt{\frac{2M}{f_{h,1}d}} \text{ and } b_2 = \frac{b_1}{\beta} \quad (5.11)$$

$$d_{max} = (b_1 + b_2) \tan \alpha \quad (5.12)$$

After calculating the slip at F_{max} , the parabola is univocally determined by the three points $(0, F_0)$, (d_{max}, F_{max}) , and $(2d_{max}, F_0)$. The two coefficients are then calculated as:

$$a = 2(F_{max} - F_0)/d_{max} \quad (5.13)$$

$$b = -(F_{max} - F_0)/d_{max}^2 \quad (5.14)$$

The aforementioned procedure led to obtain an estimated load-slip behaviour very close to the experimental ones: the comparison is shown in Fig. 5.9, together with a summary of the estimated parameters. The properties of the tested plank-plywood panel samples, used for the derivation of the load-slip analytical curve, are reported in Table

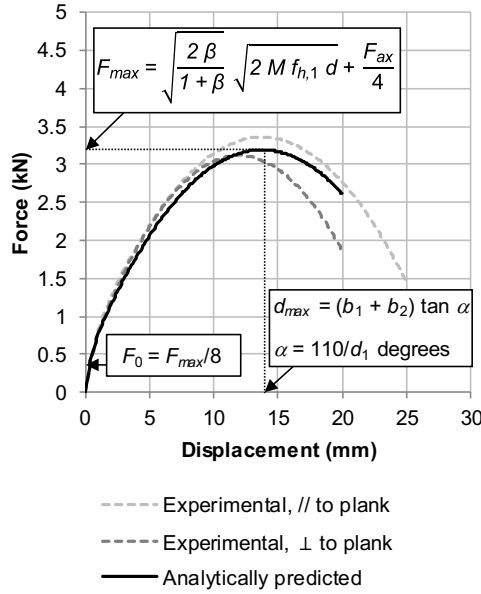


Figure 5.9: Comparison between the analytically derived curve and the two obtained from the experimental data. From [174].

5.4. With this prediction, it was also possible to account for the different diaphragms configurations (Table 5.2), for which specific companion tests on plank-plywood panel joints were not performed. The results from these calculations are reported in Table 5.5: as can be noticed, the increase in screws diameter has a greater influence on the peak force than the presence of thicker planks (sample DFpar-2s).

Therefore, by adopting this procedure, it is possible to generalize the proposed expression also when tests are not available or material properties cannot be measured. It is sufficient to know, for instance, the properties of screws according to the producers, and the strength classes of planks and plywood.

5.3.3 Prediction of the global behaviour of diaphragms

The proposed analytical model was developed by taking into account the stiffening intervention adopted for the experimental tests presented in Section 3.4.1. In the following, the direction orthogonal to the in-plane load is identified as *vertical*, the one parallel to it as *horizontal*.

As previously shown, the retrofitting took place by screwing plywood panels along their perimeter to the sheathing of the as-built existing floor, without having to consider the position of the underlying joists, but only with respect to the planks arrangement. This type of refurbishment is particularly advantageous, because the screws are placed in such a way that it is possible to identify their specific contribution to the overall resisting mechanism.

This aspect is more clearly depicted in Fig. 5.10a: when the strengthened floor is subjected to a horizontal load and the panels are vertically arranged, the force

Table 5.4: Material properties of the tested plank-plywood panel joints used for the derivation of the analytical curve.

Property	Value
Average density of plank ρ_1 (kg/m ³)	444
Average density of plywood panel ρ_2 (kg/m ³)	469
Nominal screw diameter d (mm) from producer	4.5
Screw's shank diameter d_1 (mm) from producer	3.1
Tensile strength of screws f_u (MPa) from producer	1000
Withdrawal resistance parameter f_{ax} (MPa) from producer	17

Table 5.5: Calculated parameters based on diaphragms configurations of Table 5.2. The variation in results compared to samples DFpar-1s and DRpar-5s, having the same properties as the reference tests on plank-plywood panel joints, is noticeable.

Property	Calculated value				
	DFpar-1s	DFpar-2s	DFper-3s	DFper-4s	DRpar-5s
Distance plastic hinge-plank's edge b_1 (mm)	11.3	13.7	13.7	13.7	11.3
Distance plastic hinge-panel's edge b_2 (mm)	7.9	9.6	9.6	9.6	7.9
Estimated bending angle (°)	35.5	29.7	29.7	29.7	35.5
Shear strength for 2 screws F_{max} (kN)	3.2	4.0	3.9	3.9	3.2
Estimated slip at peak force d_{max} (mm)	13.7	13.3	13.3	13.3	13.7

is subdivided among the columns of panels, and the screws are opposing to it with their stiffness. Each column of panels is subjected to rotation and sliding: the rocking behaviour is taken into account by considering the vertical screws, while the (very limited) slip is evaluated through the horizontal screws. More precisely, because of the alternate configuration of the panels, the vertical number of screws is always fixed, while the horizontal one is considered as an average of two columns, as shown again in Fig. 5.10a.

When the pattern of the panels is composed of horizontal rows, a similar procedure can be followed, remembering that now the number of horizontal screws remains always the same, and a calculation has to be performed for the average number of vertical ones: this aspect is shown in Fig. 5.10b. In this case, consider for the same floor a vertical column composed of two whole panels and two halves of them, and another column in which the opposite situation is present (four halves and only one whole panel): as can be observed, the total number of horizontal screws remains the same independently from the considered column. This statement is valid also for the vertical screws, because when they are positioned at half of the width of the column, their number is doubled and their lever arm is half of the one of the vertical screws at the edges of the column. Therefore, the number of the central screws gives the same contribution as the one of the screws on the edges. Then, independently from the chosen way to consider a column, always the same number of screws is calculated. It is only important to count the number of columns needed to cover the whole floor coherently with the assumed configuration for the determination of one column (in this example *whole panel – two halves – whole panel* or *two halves – whole panel – two halves*).

Starting from these assumptions, the global in-plane response of the diaphragms can be predicted. When knowing the load-slip behaviour of screws (Section 5.3.2), for a certain displacement d_s of the fastener, a value F_s of force corresponds. Starting from these two parameters, it is possible to calculate the global deflection of the diaphragm according to the principle shown in Fig. 5.11, for vertically arranged panels.

The total horizontal load induces a rotation ϑ of each column of plywood panels, given by:

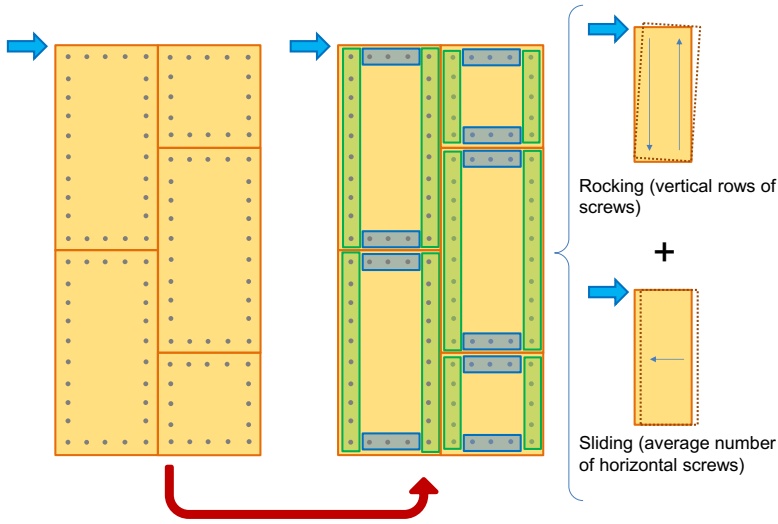
$$\vartheta = \frac{d_{s,v}}{w_c - e} \quad (5.15)$$

where $d_{s,v}$ is the displacement of one vertical screw, w_c is the width of the panels column, and e is the distance of the solicited vertical screws from the edge. The rotation point is considered to be at each panel corner because of the way of deflecting of a whole diaphragm, with contact among panels (Fig. 5.11), as was observed during the tests as well. This interlocking effect is then taken into account as an increment in horizontal load, as will be shown later. Should the panels be able to rotate more freely, for instance if a gap among them is left on purpose, the lever arm to be adopted would be $w_c - 2e$.

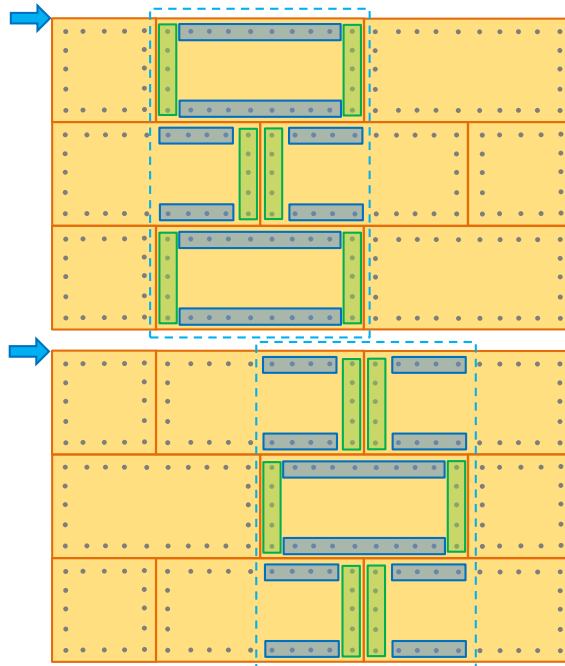
The horizontal displacement d_c reached on top of the column of panels (corresponding to the middle of the floor) is, thus:

$$d_c = \vartheta \cdot l_c \quad (5.16)$$

where l_c is the length of the panels column covering half of the diaphragm. Besides the displacement, also the horizontal load can be calculated by applying equilibrium, and starting from the force $F_{s,v}$ on a single vertical screw:



(a)



(b)

Figure 5.10: Principle of the analytical model formulated for the seismic design of the proposed strengthening technique, when the panels are arranged vertically (a); individuation of the horizontal and vertical screws columns when the panels are arranged horizontally (b). From [174].

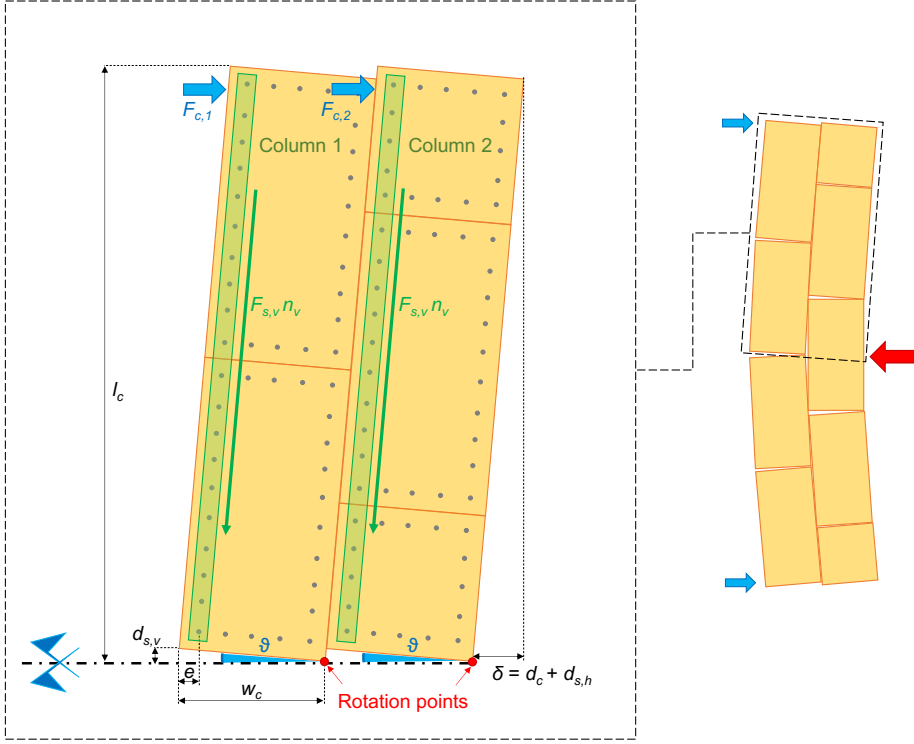


Figure 5.11: Principle for the calculation of the global deflection of the floor from each column of panels. From [174].

$$F_c = \frac{F_{s,v} \cdot n_v \cdot (w_c - e)}{l_c} \quad (5.17)$$

where n_v is the number of solicited vertical screws in a column and F_c the horizontal force activated in one column. Again, with panels able to rotate freely, the lever arm to be adopted is $w_c - 2e$.

After this step, by knowing the number of columns n_c , the total horizontal load F is calculated as:

$$F = n_c F_c \quad (5.18)$$

This force is referred to half of the diaphragm, and it therefore represents the shear that is transferred to the walls, while the resistance of the floor is given by $2F$. Furthermore, to account for panels interlocking due to the deflection of the diaphragm (Fig. 5.11), results from sensitivity analyses on several diaphragms configurations reported in RIZZI et al. [175] were considered. With a load parallel to the panels (e.g. as in Fig. 5.10b), a negligible interlocking effect was noticed. Instead, with the alternate disposition of Fig. 5.11 and a load orthogonal to the panels, a drift-dependent not negligible increment in stiffness was observed. From the results of RIZZI et al. [175], the following simplified expression was formulated to account for a drift-dependent force

increment F due to panels interlocking, to be used when the load is orthogonal to the panels and they have an alternate disposition (thus, only for samples DFpar-1s and DFpar-2s, in this case):

$$\Delta F = 1.05 + 10 \frac{d_c}{l_c} \quad (5.19)$$

Thus, if panels interlocking is present:

$$F = \Delta F \cdot n_c \cdot F_c \quad (5.20)$$

Now, the slip of the column can be determined by considering the horizontal screws; the load $F_{s,h}$ on each one of them is given by:

$$F_{s,h} = \frac{F}{n_c n_h} \quad (5.21)$$

where n_h is the total (or average, if the case) number of horizontal screws in a column of panels. From this value of $F_{s,h}$, the corresponding displacement $d_{s,h}$ is known, and consequently also the panels' slip. Compared to the displacement due to rocking, this sliding is very limited (up to 1.8% of d_c for the analysed diaphragms). The total deflection of the floor is equal to:

$$\delta = d_c + d_{s,h} \quad (5.22)$$

The values of the aforementioned parameters for each tested diaphragm are reported in Table 5.6, and this procedure was followed for the determination of the in-plane deformation of the floor. The results of this calculation are coherent with the static scheme that was adopted in the full-scale experimental tests. However, in practice the load is not punctually applied in the middle of the floor, but distributed: to account for this, it is necessary to consider the pertaining static scheme. As an example, if a diaphragm with dimensions $B \times L \times t$ and shear modulus G can be regarded as a simply supported beam, then a distributed in-plane load $p = F/L$ would cause a deflection $\delta_q = p \cdot L^2 / (8 \cdot G \cdot B \cdot t) = F \cdot L / (8 \cdot G \cdot B \cdot t)$ instead of $\delta_F = F \cdot L / (4 \cdot G \cdot B \cdot t)$. This means that the force-displacement relation of the floor, calculated with the analytical model, has to be modified by considering a halved deflection.

The above presented procedure allows to determine, starting from the proposed analytical curve representing the load-slip response of screws (Section 5.3.2), the global force-displacement backbone of the diaphragms. In addition to that, an estimation of the internal pinching cycles is of importance for both assessing the dissipative properties of the floors, and implementing their full response in a numerical model.

Therefore, a method was developed to estimate the pinching cycles from the proposed curve. The procedure starts from identifying a succession of linear branches, similarly to the **Pinching4** material [180] implemented in the software *OpenSees* [181] (Section 5.4), used also in past studies for modelling the dissipative response of timber diaphragms (see, for instance, [9, 10, 13]). The reference points are defined according to the procedure shown in Fig. 5.12, on the basis of geometrical considerations.

The pinching behaviour implies the presence of a residual force at zero displacement: this load is in general approximately corresponding to the force that leads to the very first yielding of the tested sample. In the analytical curve equation, F_0 is the intercept

Table 5.6: Values of the parameters used to predict the global in-plane response of the diaphragms according to the properties of tested samples.

Parameter	DFpar-1s	DFpar-2s	DFper-3s	DFper-4s	DRpar-5s
w_c (mm)	670	670	1200	1200	825
e (mm)	50	50	50	50	50
l_c (mm)	2400	2400	2300	2300	2730
n_v	23	24	23	23	20
n_c	6	6	3	3	4.5
n_h	25	25	60	60	36

on the y -axis (force) of the parabola representing the global response of the specimens: in order to capture the very first yielding on the analytical curve, the intercept on the y -axis assumed for the pinching cycle is $2F_0/3$, a value around which the initial slope of the curve starts to change.

After having considered this first intercept, the pinching cycle can be determined for a certain amplitude identified by a point $(\delta_C, F_C(\delta_C))$ on the curve. As a first step, two lines are determined: one joining the points $(0, 2F_0/3)$ and $(\delta_C, F_C(\delta_C))$, and one crossing the point $(\delta_C, F_C(\delta_C))$ with slope K_0 (Fig. 5.12, step 1). Then, the bisector of these two lines is found (step 2). In step 3, the remaining part of the cycle is defined: firstly, the line joining $(0, 2F_0/3)$ and the point on the bisector having x -coordinate equal to $\delta_C/2$ is determined; secondly, a line parallel to the former one intersects the branch having slope K_0 , starting from the point $(0, -2F_0/3)$.

In step 4, the whole multilinear cycle is thus determined by the following points, identified by the previous branches and reported clockwise (Fig. 5.12):

- A. $(0, 2F_0/3)$;
- B. $(\delta_C/2, \text{intersection between bisector, and line joining } 2F_0/3 \text{ with the bisector at } \delta_C/2)$;
- C. $(\delta_C, F_C(\delta_C))$;
- D. Intersection between the line passing through $-2F_0/3$ parallel to the one individuating point B, and the branch with slope K_0 ;
- E. $(0, -2F_0/3)$.

The negative part of the pinching cycle (points B', C', D' of Fig. 5.12) is antisymmetric to the positive one, as defined for the equation of the backbone curve. The reference points can be directly adopted for implementation (for instance, when using **Pinching4** material in *OpenSees*; see Section 5.4).

For a more refined analytical evaluation of both pinching and damping properties of the diaphragms, the multilinear cycle is used in step 5 to construct four exponential branches smoothening the straight lines. The equations link these straight lines similarly

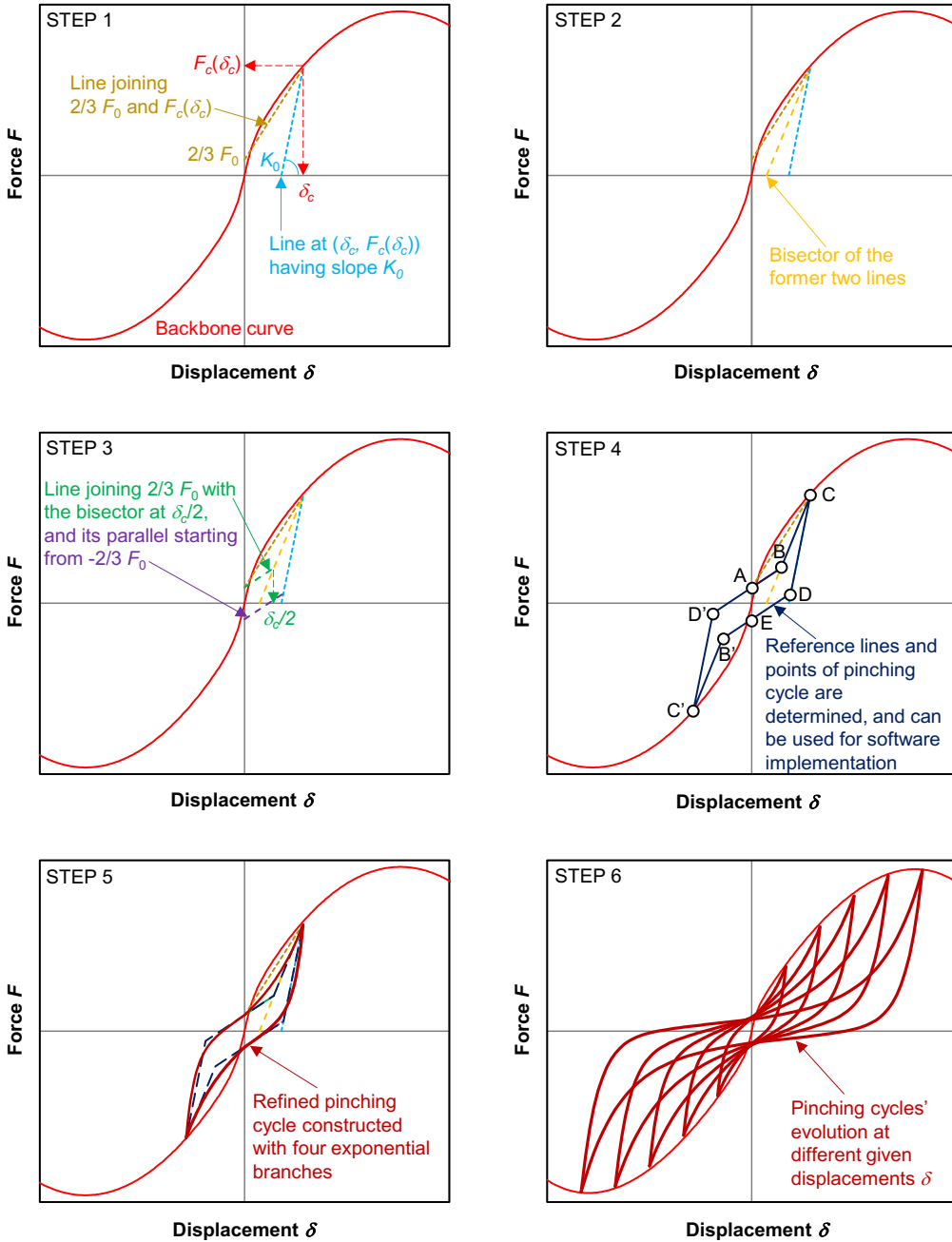


Figure 5.12: Procedure for the determination of the pinching cycles from the analytical backbone curve. From [174].

to FOSCHI's formulation [172]. Considering, for more simplicity in deriving the expressions and aided by Fig. 5.12, the negative part of the pinching cycle ($\delta_{C'} \leq \delta \leq 0$), the equations are:

- Negative loading (NL):

$$F_{NL} = F_{C'} + \left[\left(F_E - F_{C'} + \frac{F_E - F_{B'}}{\delta_E - \delta_{B'}} \delta_{C'} \right) + \frac{F_E - F_{B'}}{\delta_E - \delta_{B'}} (\delta - \delta_{C'}) \right] \cdot \left[1 - \exp \left(- \frac{D_p \frac{F_{B'} - F_{C'}}{\delta_{B'} - \delta_{C'}}}{F_E - F_{C'} + \frac{F_E - F_{B'}}{\delta_E - \delta_{B'}} \delta_{C'}} (\delta - \delta_{C'}) \right) \right] \quad (5.23)$$

- Negative unloading (NU):

$$F_{NU} = F_{C'} + \left[\left(F_A - F_{C'} + \frac{F_A - F_{D'}}{\delta_A - \delta_{D'}} \delta_{C'} \right) + \frac{F_A - F_{D'}}{\delta_A - \delta_{D'}} (\delta - \delta_{C'}) \right] \cdot \left[1 - \exp \left(- \frac{2 \frac{F_{D'} - F_{C'}}{\delta_{D'} - \delta_{C'}}}{F_A - F_{C'} + \frac{F_A - F_{D'}}{\delta_A - \delta_{D'}} \delta_{C'}} (\delta - \delta_{C'}) \right) \right] \quad (5.24)$$

In Eq. 5.23, $D_p = 1 + (\delta_{C'}/\delta_{max})^3$ is a factor accounting for pinching stiffness degradation, dependent on the displacement δ_{max} at which the peak force of the diaphragm is reached. This factor implies that the loading branch follows the bisector slope (segment C'-B') for small displacements, but then its slope increases up to two times the bisector one at δ_{max} . With this additional factor, it is therefore possible to account for stiffness degradation depending on the reached displacement.

Then, for the positive part of the pinching cycle ($0 \leq \delta \leq \delta_C$), the other two curves F_{PL} (positive loading) and F_{PU} (positive unloading) are antisymmetric to the aforementioned ones. Since the initial unloading stiffness of pinching cycles is usually quite high, this was taken as $2K_0$, as can be noticed in Eq. 5.24. Finally, each curve is asymptotic, thus in $\delta = 0$ continuity would not be guaranteed. To adjust for this, the curves F_{PL} and F_{NU} are translated along the y -direction by the quantity $[F_{PL}(0) - F_{NU}(0)]/2$, to have a common $F(0)$ at $[F_{PL}(0) + F_{NU}(0)]/2$; the curves F_{PU} and F_{NL} are translated along the y -direction by the quantity $[F_{PU}(0) - F_{NL}(0)]/2$, to have a common $F(0)$ at $[F_{PU}(0) + F_{NL}(0)]/2$.

This completes the analytical derivation of the pinching cycle. The advantage of this geometrical procedure is that the pinching cycle can follow the nonlinear behaviour of the backbone curve, because of the progressive change of slope of the bisector (Fig. 5.12, step 6). This estimation of the pinching cycle proved to be reliable, as will be shown in Section 5.4.

5.3.4 Application of the analytical model for the tested floors

The combination of the derived analytical curve and of the pinching cycle estimation enables the prediction of the in-plane response of the tested floors, in order to assess the accuracy of the developed model. Therefore, this section presents a comparison of the analytical backbone (always depicted in red) and an estimated representative

pinching cycle (always shown in dark blue), with the experimental hysteretic cycles (light blue). The results are presented in Figs. 5.13-5.15: for each diaphragm, both the global behaviour and the initial response (up to 20 mm displacement) are shown. As can be noticed, the analytical model proves to well predict the in-plane behaviour of the diaphragms, also when variations are present with respect to the reference tests on plank-plywood panel joints.

For sample DFpar-1s (Fig. 5.13a), the initial stiffness and pinching response are fully captured by the model. Besides, the fact that panel interlocking is taken into account enables the correct prediction of both strength and displacement at failure of the specimen. The softening behaviour was not fully achieved during the test, because of premature failure of the screws and nails enabling the shear transfer on the floor side. By adopting more fasteners, the failure would have been distributed only among the panels screws, leading to the behaviour described by the model.

In sample DFpar-2s (Fig. 5.13b), both initial stiffness and pinching behaviour are well predicted by the developed model, with a slight load underestimation, especially for the negative backbone. Nevertheless, the global response appears to be properly captured, but in this case the diaphragm was not tested until capacity, because of the failure of the bottom glue layer anchoring it to the laboratory floor (Section 4.3.2).

Sample DFper-3s was characterized by the failure of the nails connecting joists and planks on the top part of the floor, leading to a decrease in stiffness and a softening phase (Section 4.3.3): this failure caused the joists to move independently from the sheathing, which underwent a lower deflection. The global response of the specimen is depicted in grey in Fig. 5.14a and seems not to be represented by the model. However, this overall response recorded by reference sensor 19 of Fig. 3.15 included the independent movement of the joists: instead, when considering sensor 23, recording only the sheathing behaviour (planks and plywood system, light blue), the latter is again correctly predicted in terms of initial stiffness and pinching behaviour.

This is even more evident in sample DFper-4s, identical to DFper-3s, but in which timber blocks were placed to prevent the aforementioned independent movement of the joists. In this case, both initial and the global behaviour of the floor are predicted by the model, including peak force and displacement at which this takes place. During the test, after beginning the softening phase, besides yielding of the screws, also cracking of the plywood panels and planks along one row of fasteners occurred (Fig. 5.14c): this led to a free sliding of the sheathing for larger drifts, thus Fig. 5.14b shows the floor's hysteretic cycles up to the displacement at which the crack occurred.

Finally, the model proved to be effective also for the roof pitch (sample DFpar-5s, Fig. 5.15), again for both initial response and global behaviour, including failure of the sample. The pinching response is properly captured as well.

The graphical comparison of Figs. 5.13-5.15 is completed by Table 5.7, in which the values of initial stiffness, peak force and its corresponding displacement of the diaphragms are reported, from both experimental tests and analytical calculations; the observed failure modes are also summarized. The bottom glue layer failure in sample DFpar-2s would not occur in practice, because it would not be part of the retrofitting: it was only needed to complete the bottom clamping of the floors for the tests [132]. Instead, boundary conditions have to be appropriately designed, to achieve a more gradual and global failure of the retrofitted diaphragms, as obtained for instance with sample DFpar-5s.

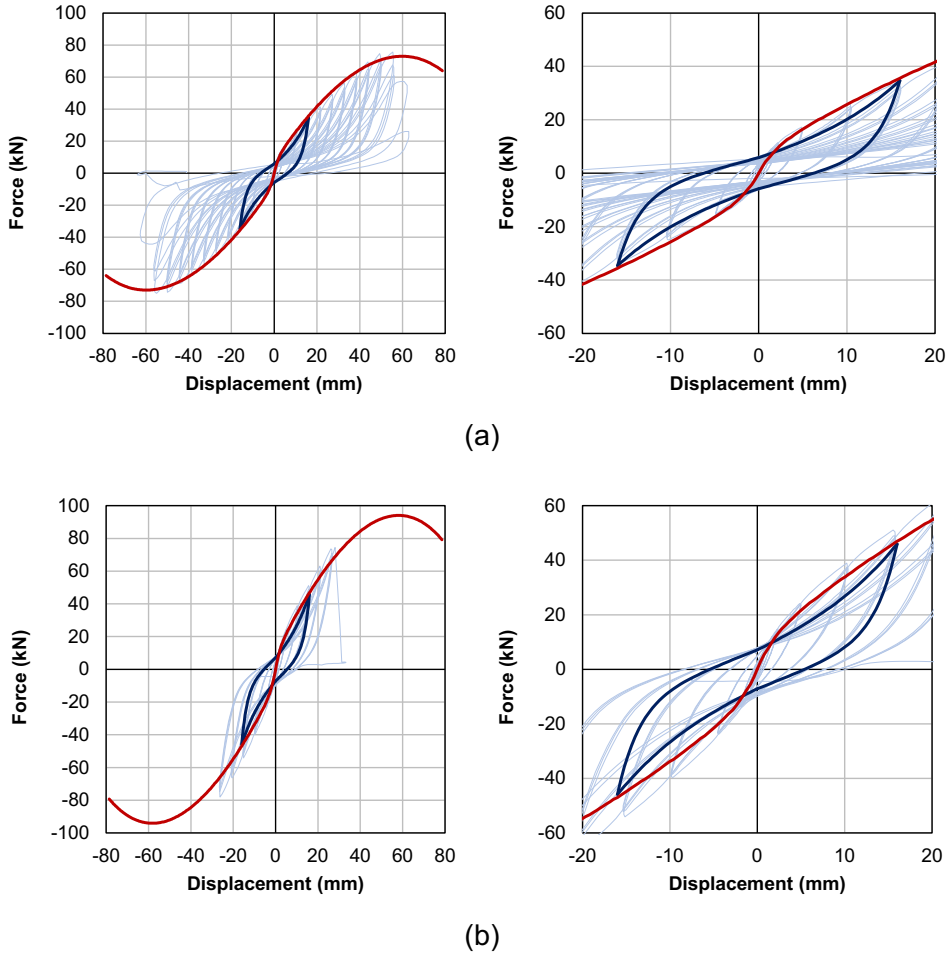


Figure 5.13: Comparison between analytical backbone (red) and estimated pinching cycle (dark blue) with the experimental hysteretic response (light blue) for the floors tested parallel to the joists: global (left) and initial (right) response of samples DFpar-1s (a) and DFpar-2s (b). From [174].

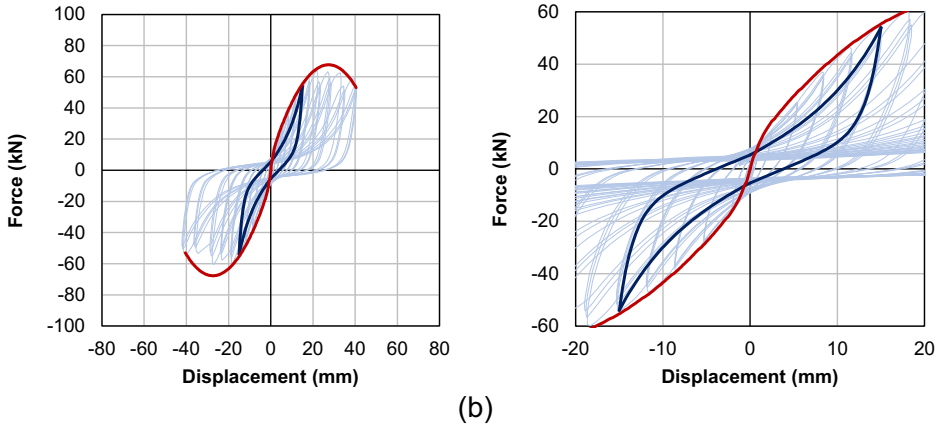
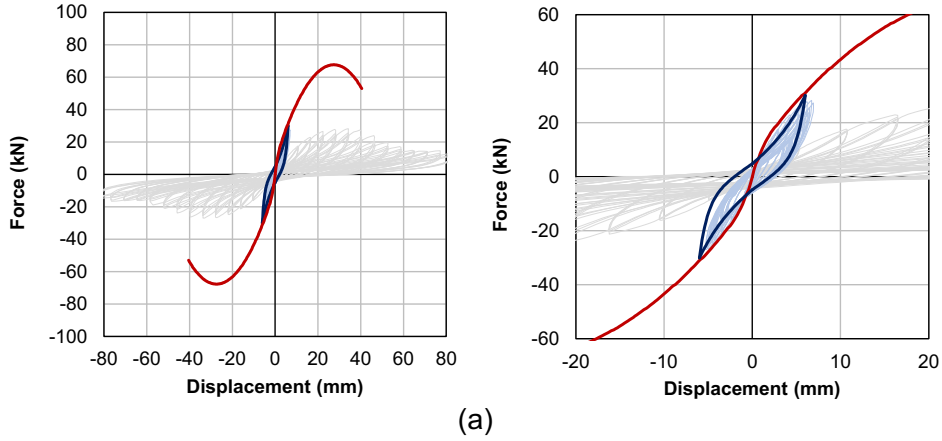


Figure 5.14: Comparison between analytical backbone (red) and estimated pinching cycle (dark blue) with the experimental hysteretic response (light blue) for the floors tested perpendicular to the joists: global (left) and initial (right) response of samples DFper-3s (a, with in grey the overall recorded cycle and light blue the sheathing's one) and DFper-4s (b); crack opening in a plank during softening phase of sample DFper-4s (c). From [174].

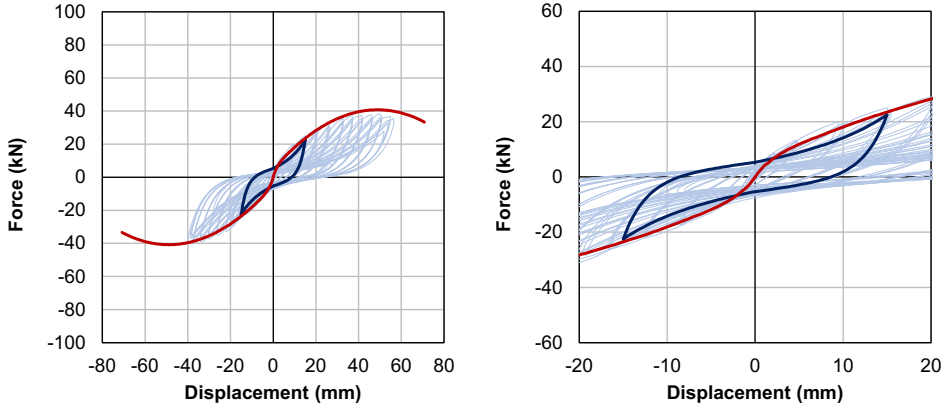


Figure 5.15: Comparison between analytical backbone (red) and estimated pinching cycle (dark blue) with the experimental hysteretic response (light blue) for the roof pitch [14]: global (left) and initial (right) response of sample DFpar-5s. From [174].

Table 5.7: Comparison between initial stiffness K_0 , peak force F_{max} and corresponding displacement d_{max} obtained from test results and calculated with the analytical model. The cause of failure observed during the tests is also reported for each sample.

Sample	Cause of failure	Test results			Results from analytical model		
		K_0 (kN/mm)	F_{max} (kN)	d_{max} (mm)	K_0 (kN/mm)	F_{max} (kN)	d_{max} (mm)
DFpar-1s	Top row of screws, global plasticization	5.4	75.6	55.5	5.2	73.0	59.9
DFpar-2s	Bottom glue layer	6.3	Not reached		6.6	94.1	58.1
DFper-3s	Joists nails	10.8	Not reached		11.2	67.7	27.3
DFper-4s	Yielding of screws, splitting in a plank	11.8	64.1	22.0	11.2	67.7	27.3
DRpar-5s	Bottom bolts, global plasticization	3.5	38.4	49.6	3.8	40.8	48.8

Furthermore, in the context of the global seismic response of existing buildings, out-of-plane walls cannot be subjected to excessive deflections. Thus, an accurate characterization of the floors behaviour until moderate drift limits is of importance, and the proposed analytical model proved to be suitable for this purpose, as can also be noticed by the good estimation of the initial stiffness K_0 in Table 5.7.

In terms of energy dissipation, pinching cycles are well predicted for all samples, and provide equivalent damping ratio (ξ) values close to experimental ones (Fig. 5.16), as determined in Section 4.3.6 by means of the energy loss per cycle method [167]. It can be noticed that the use of the simplified multilinear pinching cycle tends to underestimate the dissipative contribution of the floor, while the refined one provides more reliable results, especially for drifts δ/L larger than 0.4%.

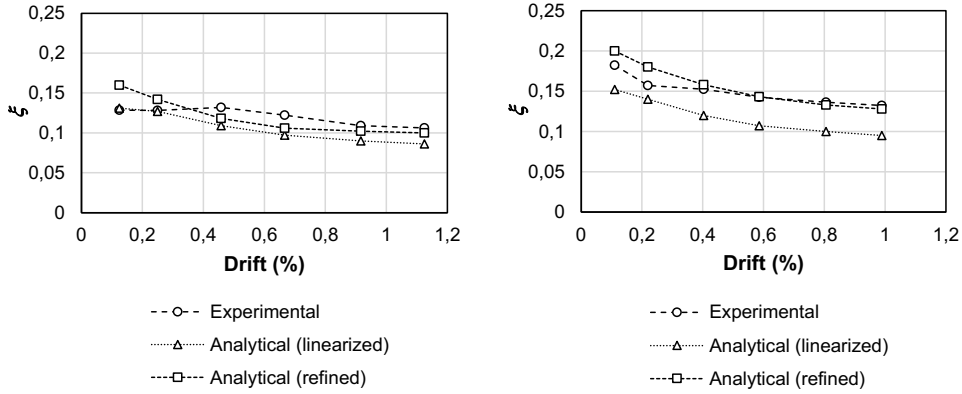


Figure 5.16: Example of comparison, for (a) a floor (DFpar-2s) and (b) a roof sample (DRpar-5s), between the analytically predicted equivalent damping ratio (adopting both the linearized and the refined pinching cycle) and the one calculated in Section 4.3.6. From [174].

5.4 Numerical modelling approach for retrofitted diaphragms

5.4.1 Introduction

As already stated in Chapter 2, the fact that one of the main aims of past seismic retrofitting strategies was only the floors stiffening, did not open up the opportunity to model the cyclic response and dissipative behaviour of the diaphragms, because they were designed and regarded as linear, infinitely stiff slabs with no dissipative behaviour [15, 16, 17, 18]. When the pushover analysis for existing URM building started to be widely adopted, the modelling of as-built flexible diaphragms was also enabled, generally by means of linear elastic orthotropic slabs [125, 129], as also shown in Section 5.2.2. Yet, in both cases the beneficial dissipative contribution of the (retrofitted) diaphragms is not taken into account, and a computationally efficient modelling of these structural components is not featured by the commonly adopted software for seismic analyses of URM buildings.

However, the open source software *OpenSees* [181], specifically developed for advanced nonlinear seismic analyses, allows to model several material types by means of uniaxial elements. Among these materials, the **Pinching4** one (Fig. 5.17, [180]) is particularly suitable for modelling the in-plane response of timber diaphragms through macro-elements, and it has already been adopted in past analyses [10, 13] to account for the cyclic and dissipative behaviour of the floors. Yet, in those research studies, the material was calibrated based on test results only, thus without following an analytical procedure. For this reason, Section 5.4.2 provides a number of recommendations for implementing the in-plane response of the diaphragms according to the formulated analytical model. Unfortunately, one of the main drawbacks of *OpenSees* is the lack of a graphical user interface, and the absence of a fast, efficient modelling strategy for complex masonry structures (Section 5.6): both floors and walls can be modelled by means of macro-elements, but only relatively simple buildings could be considered

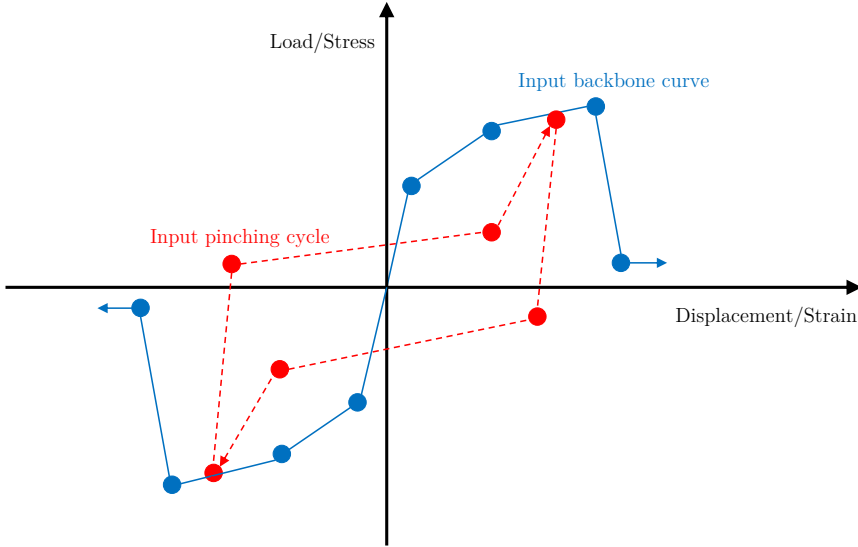


Figure 5.17: Schematic representation of the *OpenSees Pinching4* material [180]: the input backbone curve and pinching cycle are highlighted.

[10]-[14]. Besides, the out-of-plane response of masonry is not easily simulated with this approach (Section 5.6).

Therefore, besides providing suggestions on how to calibrate an existing material to be suitable for representing the seismic response of timber diaphragms in *OpenSees*, a user-supplied subroutine was implemented (Section 5.4.3), to be used in the software DIANA FEA, version 10.4 [182]. This software already features an advanced nonlinear model for masonry (Section 5.6), but lacks suitable materials and constitutive laws for simulating timber floors. The combination of both modelling strategies can instead enable an efficient and complete numerical simulations of the global seismic response of URM buildings, accounting for the nonlinear, cyclic and dissipative behaviour of all structural components.

5.4.2 Implementation of the floors response in *OpenSees* based on the analytical model

Based on the developed analytical procedure, the in-plane response of timber diaphragms can be easily implemented in advanced numerical models in *OpenSees*, and in particular the following applications can be of interest:

- Seismic assessment of the overall in-plane response of the diaphragms, up to failure;
- Numerical analyses for which the target is the global seismic behaviour of a URM building.

Recommendations for these two applications are presented in the following, taking into account the implementation procedure of the *Pinching4* material type, which proves

to be quite accurate for these applications [10]. The input pinching cycle is identified as a succession of linear branches at a desired amplitude, as was already considered for the analytical model (Fig. 5.12, step 4), but the backbone curve has to be constructed with four points per loading direction (Fig. 5.17). Therefore, from the analytical curve a proper implementation of the backbone one has to be carried out.

In the first case, when the total deflection range of the floor is of interest (Fig. 5.18a), the backbone curve can be constructed considering the whole analytical curve, as can be noticed. The ultimate displacement d_3 corresponds to the failure of the diaphragm ($F_3 = 0.8F_{max}$). In order to obtain a reliable result, since *OpenSees* creates by default a drift-dependent evolution in terms of stiffness and enclosed area for pinching, it is advised to estimate the input cycle at d_1 . In this way, it is possible to avoid an overestimation of the floor energy dissipation due to the choice of a reference cycle too close to the beginning of the load-displacement history.

When, instead, the target is the seismic assessment of a whole building, it is important to well characterize the floor until the expected drift, beyond which, for instance, the out-of-plane failure of the wall may occur. In this case, the response of the diaphragms has to be modelled thoroughly in terms of stiffness and energy dissipation, but only for a limited initial part of the backbone curve (Fig. 5.18b), as derived according to the storey seismic shear when designing the retrofitted floor and its connections to the walls. Therefore, after having determined the limit out-of-plane displacement for the wall ($d_{u,wall}$), the remaining part of the backbone can be constructed. As a final step, for the same reason as in the previous case, it is advised to estimate the input pinching cycle at d_2 .

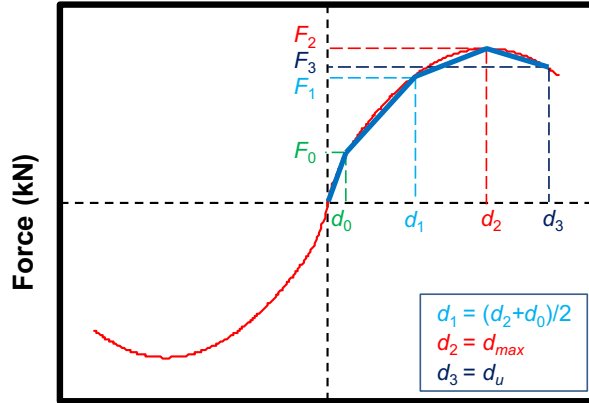
The two aforementioned procedures were both applied to sample DFpar-1s, as a representative example. The adopted modelling strategy, consisting of a macro-element approach, is shown, together with the results, in Fig. 5.19. The numerical model was composed of a grid of infinitely stiff truss elements, in which diagonal nonlinear springs were inserted, with the **Pinching4** material implemented in them, according to the indications given for either the global or the initial response of the floor. Starting from the backbone curve of the whole retrofitted diaphragm, determined through the analytical model, it is possible to define the constitutive law for the single spring according to geometrical considerations. The displacement δ_{sp} of the spring is given by:

$$\delta_{sp} = \frac{\delta}{m} \cos \alpha_s \quad (5.25)$$

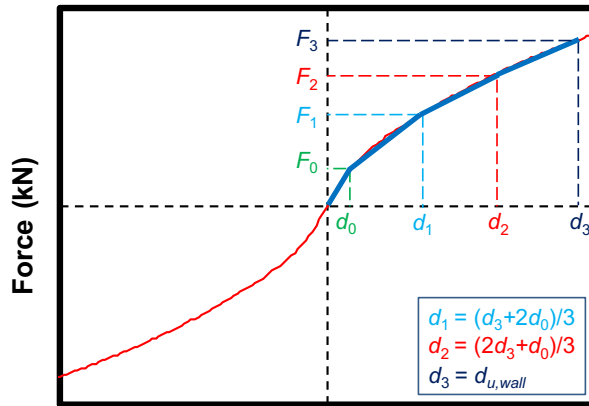
In the former equation, α_s is the angle between the spring and the loading direction (Fig. 5.19a) and m the number of macro-elements rows parallel to the applied load (in this case, $m = 2$). The shear force F is then subdivided among the s springs and transformed into an axial force N on a single one:

$$N = \frac{F}{s \cos \alpha_s} \quad (5.26)$$

Cyclic displacement-based analyses were performed, by applying the same steps as in the experimental tests: the results confirm that the analytical model can be reliably adopted as an input for the numerical one, and the two proposed procedures can be suitably applied to determine the global or initial behaviour of the diaphragms. In the proposed example, since the analytical model slightly underestimates the peak force,



(a)



(b)

Figure 5.18: Implementation procedure of the analytical model based on OpenSees *Pinching4* material [180] when the aim is to model the global response of the floors (a) or their nonlinear behaviour in an entire building (b). From [174].

this is reflected in the numerical model as well. However, the overall response appears still to be well captured (Fig. 5.19b). An even better result is achieved for the initial behaviour of the floor, due to the accuracy of the model in predicting the beginning of the load-displacement curve (Fig. 5.19c).

5.4.3 Implementation of a user-supplied subroutine simulating the seismic response of floors in DIANA FEA

In order to properly capture the in-plane (seismic) and out-of-plane (static) behaviour of the diaphragms, while simultaneously implementing the analytical model, a macro-element strategy was also adopted in DIANA FEA (Fig. 5.20). The floors were modelled by combining linear elastic shell elements, for representing the out-of-plane behaviour under static vertical loads, and nonlinear macro-elements overlapped to them for describing the in-plane behaviour. These macro-elements consisted of six truss elements: four rigid trusses connected to form a quadrilateral, and two nonlinear trusses placed diagonally (Fig. 5.20), in which the nonlinear in-plane behaviour of the floor was implemented adopting the proposed analytical model. Therefore, starting from a retrofitted diaphragm designed through the formulated analytical procedure, its cyclic in-plane response is modelled by creating a mesh of macro-elements, whose size determines the constitutive laws of the diagonal trusses. On the contrary, the behaviour under vertical loads is simulated through the linear elastic orthotropic shells: similarly to the approach presented in Section 5.2.2, the flexural characteristics were assigned considering an equivalence between the actual inertial properties of the joists, and those of the slab, so that the same vertical deflection could be achieved.

In order for the user-supplied subroutine to be compatible with the DIANA FEA environment, the constitutive laws for the diagonal trusses of the macro-elements were implemented adopting the FORTRAN 90 programming language. For this application, two types of input variables are required by the software: user-specified initialization parameters (not changing within the subroutine calculations), and initial state variables (varying during subroutine calculations, e.g. for determining loading and unloading points). The user-supplied subroutine subsequently provides the stress-strain relation, to be adopted at every calculation step.

Three relevant parameters for initialization were needed (Fig. 5.21):

- the strain ε_{max} at peak stress σ_{max} ;
- the peak stress σ_{max} itself;
- the initial elastic modulus K_0 .

These parameters are known, once the retrofitting of the diaphragm is designed through the analytical model, according to the expected seismic loads. Besides, ten initial state variables were adopted, necessary for describing all loading and unloading branches, and their initial value was set to 0. With reference to Fig. 5.21, these variables are:

- the maximum strains ever reached in tension and compression ($\varepsilon_{t,max}$ and $\varepsilon_{c,max}$, respectively)
- the stress-strain coordinates identifying the end of the loading and unloading branches in tension (points $(\varepsilon_{t,l}, \sigma_{t,l})$ and $(\varepsilon_{t,ul}, \sigma_{t,ul})$, respectively)

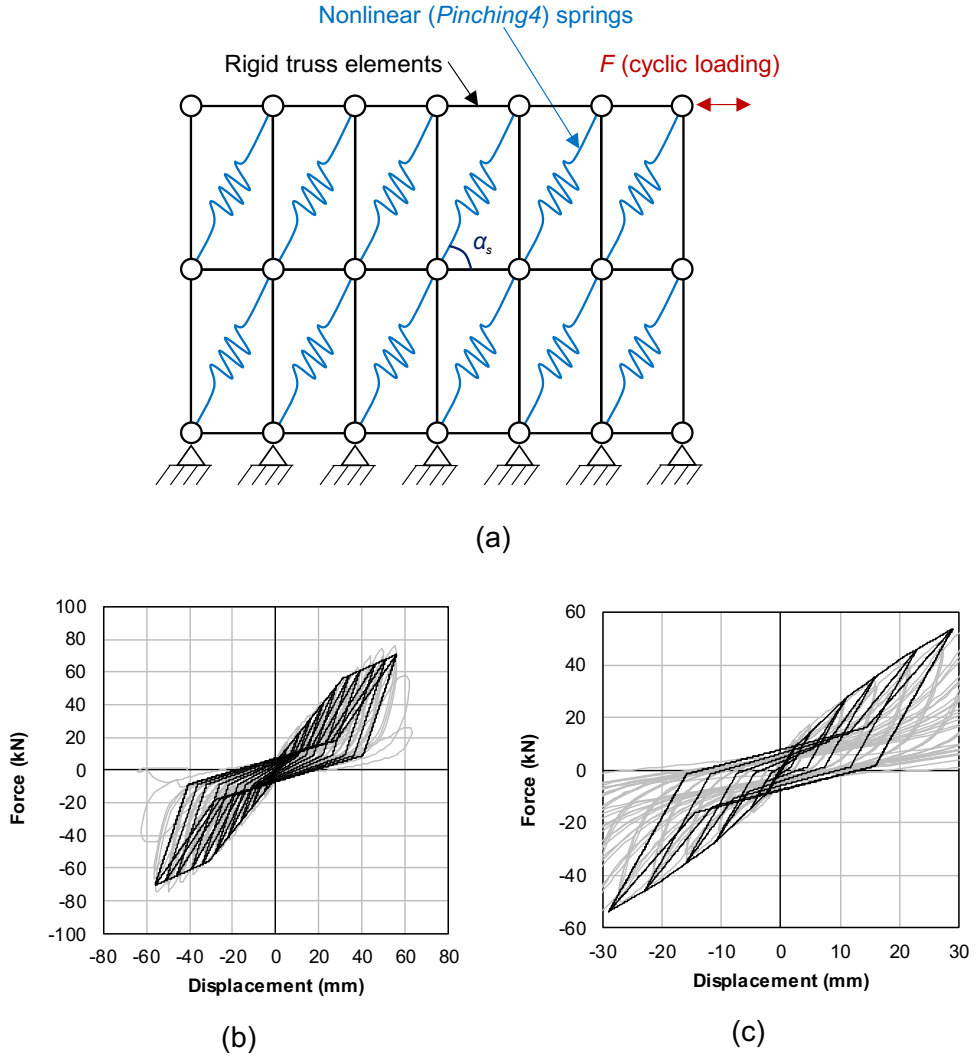


Figure 5.19: Numerical model for the diaphragm representation (a); results of the numerical analysis when implementing the analytical model to assess the global (b) and initial (c) response of the diaphragms. The experimental cycle (grey) refers to sample DFpar-1s, the numerical cycle is depicted in black. From [174].

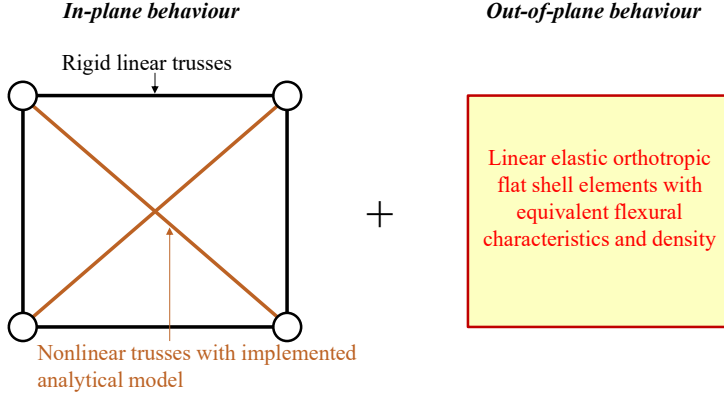


Figure 5.20: Adopted strategy for modelling in-plane and out-of-plane behaviour of timber diaphragms in DIANA FEA, with a mesh of macro-elements overlapped to linear elastic orthotropic shell elements. From [183].

- the stress-strain coordinates identifying the end of the loading and unloading branches compression (points $(\varepsilon_{c,l}, \sigma_{c,l})$ and $(\varepsilon_{c,ul}, \sigma_{c,ul})$, respectively).

Through these variables, the pinching behaviour during unloading and reloading can be defined. The constitutive laws implemented through the user-supplied subroutine are now presented for the tensile branch only, since the compressive one follows antisymmetric relations.

The constitutive law follows the tensile loading branch as long as $\varepsilon > 0$ and $\varepsilon > \varepsilon_{t,max}$, with the constitutive law of Eq. 5.27, based on the same principle of the load-slip curve of Eq. 5.6 (Fig. 5.22, blue branch):

$$\sigma = (\sigma_y + a\varepsilon + b\varepsilon^2) \left[1 - \exp \left(-K_0 \frac{\varepsilon}{\sigma_y} \right) \right] \quad (5.27)$$

In Eq. 5.27, $\sigma_y = \sigma_{max}/8$, following the analytical derivation presented in Section 5.3.2. Furthermore, a conventional yielding strain, necessary for defining elastic unloading and reloading, is also assumed as $\varepsilon_{t,y} = 2\sigma_y/K_0$.

After reaching $\varepsilon_{t,max}$, the tensile unloading phase is defined if $\varepsilon > 0$, $\varepsilon < \varepsilon_{t,max}$, and $\varepsilon < \varepsilon_0$, with ε_0 initial strain at the beginning of the current step. If $\varepsilon_{t,max} < \varepsilon_{t,y}$, the unloading is still elastic and follows Eq. 5.27. If, instead, the yielding has already occurred, the nonlinear unloading laws come into play. In this case, the response is distinguished between the case in which the unloading starts from the envelope curve (at $\varepsilon_{t,max}$, yellow branch of Fig. 5.22), and when the unloading occurs after a reloading phase (red branch of Fig. 5.22). In the first case, $\varepsilon_{t,l} \equiv \varepsilon_{t,max}$, and the constitutive law is formulated as (see Fig. 5.22 for the meaning of the various parameters, based on Eqs. 5.23-5.24):

$$\sigma = f_{t,ul} = \sigma_{t,max} [\sigma_{t,max} - p_{0,ul} - K_4(\varepsilon - \varepsilon_{t,max})] \cdot \left[1 - \exp \left(2K_0 \frac{\varepsilon - \varepsilon_{t,max}}{\sigma_{t,max} - p_{0,ul}} \right) \right] \quad (5.28)$$

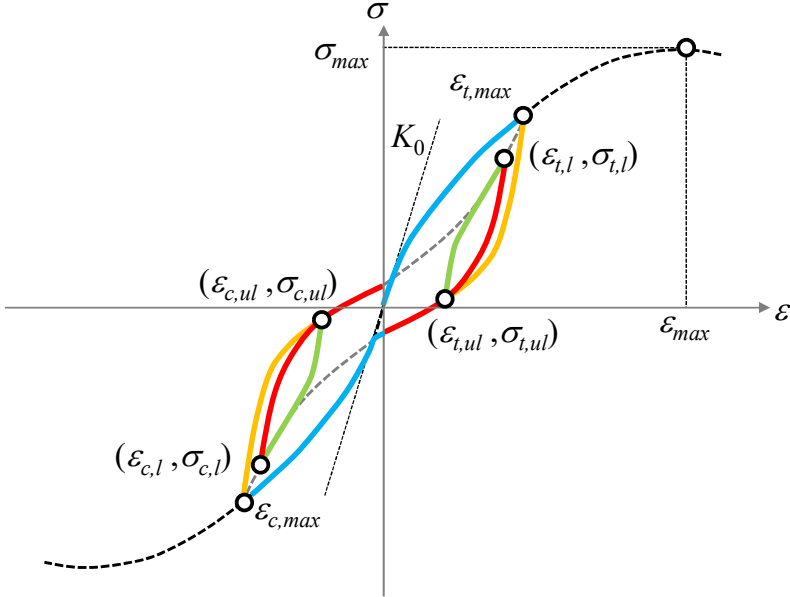


Figure 5.21: Representation of the input parameters for the user-supplied subroutine. From [183].

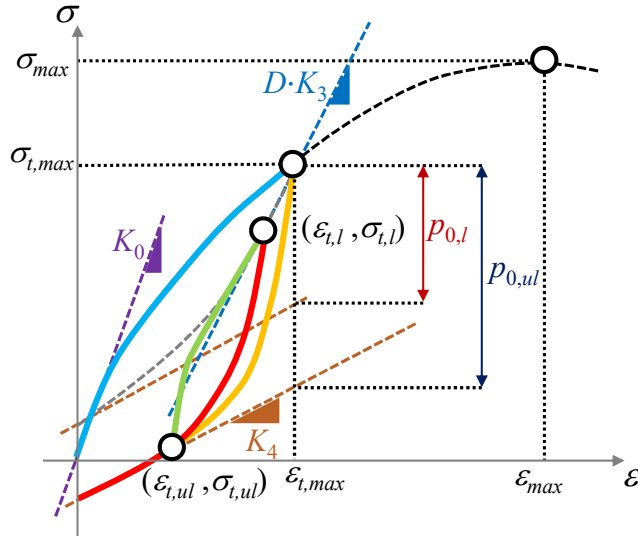


Figure 5.22: Loading, unloading and reloading branches implemented in the user-supplied subroutine.

In the second case, the relation is ($\varepsilon_{t,l} \neq \varepsilon_{t,max}$):

$$\sigma = \sigma_{t,l} - (\sigma_{t,l} - f_{t,ul}) \left[1 - \exp \left(2K_0 \frac{\varepsilon - \varepsilon_{t,l}}{\sigma_{t,l} - f_{t,ul}} \right) \right] \quad (5.29)$$

Finally, the tensile reloading phase is defined if $\varepsilon > 0$, $\varepsilon < \varepsilon_{t,max}$, and $\varepsilon > \varepsilon_0$. Again, if $\varepsilon_{t,max} < \varepsilon_{t,y}$, the unloading is still elastic and follows Eq. 5.27. Otherwise, the nonlinear reloading phase takes place according to the following constitutive law:

$$\sigma = \sigma_{t,ul} + (f_{t,l} - \sigma_{t,ul}) \left[1 - \exp \left(-2K_0 \frac{\varepsilon - \varepsilon_{t,ul}}{f_{t,l} - \sigma_{t,ul}} \right) \right] \quad (5.30)$$

with:

$$f_{t,l} = \sigma_{t,max} - [\sigma_{t,max} - p_{0,l} - K_4(\varepsilon - \varepsilon_{t,max})] \left[1 - \exp \left(D \cdot K_3 \frac{\varepsilon - \varepsilon_{t,max}}{\sigma_{t,max} - p_{0,l}} \right) \right] \quad (5.31)$$

and:

$$D = 1 + \left(\frac{\varepsilon_{t,max}}{\varepsilon_{max}} \right)^3 \quad (5.32)$$

With reference to Eq. 5.32, the parameter D is a factor accounting for the stiffness degradation of the pinching cycles, becoming progressively narrower when the floor drift increases (Fig. 5.12, step 6). This quantity is equivalent to the parameter D_p in Eq. 5.23, with the only difference that D is based on a ratio between strains.

As already presented in section 5.3.4, the analytical model proved to be accurate for predicting the global in-plane response of the retrofitted timber diaphragms. Since the model was implemented in the user-supplied subroutine, very close results were expected, useful to validate both the subroutine itself, and the adopted modelling strategy for timber diaphragms. As a first trial and validation example, a retrofitted timber diaphragm with similar characteristics to sample DFpar-1s was modelled. A 4×6 m floor was considered, supported on the long sides, having as in-plane properties an initial stiffness of 10 kN/mm, and a strength of 150 kN activated at 60 mm displacement. The floor featured 60×130 mm joists at a heart-to-heart distance of 500 mm, while the thickness of both plywood panels and planks was 18 mm. The elastic modulus of timber was assumed to be 10000 MPa. On the basis of these characteristics, equivalent input properties were determined for the elements in the numerical model.

The modelled diaphragm consisted of a mesh of 1×1 m macro-elements (capturing the in-plane response), overlapped to flat shell elements (accounting for the out-of-plane behaviour), as shown in Fig. 5.23. The three initial parameters, required by the user-supplied subroutine for determining the constitutive law of the nonlinear diagonal trusses, can be derived from geometrical considerations, once the macro-elements mesh is defined. Starting from the whole floor deflection δ , the displacement u of a diagonal truss is given by:

$$u = \frac{\delta \cos \alpha_s}{m} \quad (5.33)$$

where α_s is the angle between the truss and the loading direction (Fig. 5.23), and m the number of macro-elements rows parallel to the applied load in half of the floor

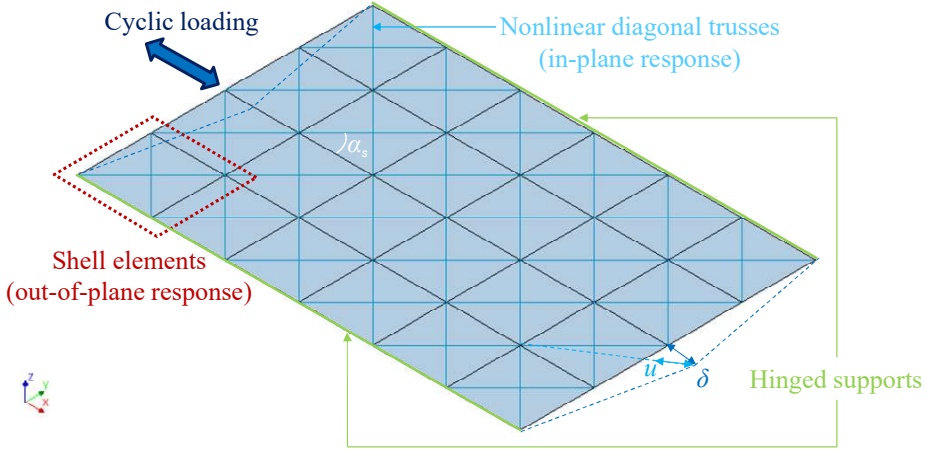


Figure 5.23: Model of the retrofitted diaphragm for the validation of the user-supplied subroutine. From [183].

(in this case, $m = 2$). The strain values to be adopted as input for the user-supplied subroutine are finally derived by dividing u by the length of the single diagonal truss. The shear force $F/2$ is then subdivided among the s trusses in one macro-elements row, and transformed into an axial force N on a single one:

$$N = \frac{F}{2s \cos \alpha_s} \quad (5.34)$$

From the knowledge of the geometrical relations for N and δ , also the initial stiffness of the diagonal trusses can be calculated. For convenience, a unitary section was adopted for the truss elements, so that force and stress could be coincident in their values.

After defining the nonlinear constitutive laws for the macro-elements, also the properties of the shell elements were derived, considering an equivalence in flexural properties between the joists and the slab, and defining an equivalent elastic modulus E_{eq} according to Eq. 5.4. A thickness of 36 mm (18 mm for planks and 18 mm for plywood panels) was attributed to the planks. According to the reference system of Fig. 5.23, the elastic modulus E_{eq} was assigned to all directions, while the shear moduli were different: a value of 0.1 MPa was assigned to G_{xy} , because the in-plane behaviour was already described by the macro-elements, while $G_{xz} = G_{zy} = E_{eq}/16$ (similarly to an actual timber material, and to the procedure for modelling as-built diaphragms presented in Section 5.2.2). The main material properties assigned to the model are summarized in Table 5.8, while their calculation is reported in Appendix D. Hinged supports were placed to the two lateral edges parallel to the application of the in-plane load (Fig. 5.23).

The floor was firstly subjected to a linear static analysis to verify the equivalence in flexural properties between the slab and the joists (Fig. 5.24a). Both the self-weight and a vertical load of 1.5 kN/m² were applied.

Then, two in-plane cyclic analyses were performed, one to assess the global cyclic behaviour (Fig. 5.24b), and one in which local loops were imposed (Fig. 5.24c). These

Table 5.8: Properties adopted in the trial retrofitted floor model.

Function	Element type	Property	Value
Macro-elements representing the in-plane behaviour of the floor	Rigid trusses	Elastic modulus E_t (MPa)	10^{10}
		ϵ_{max}	0.015
	Diagonal trusses	σ_{max} (MPa)	8840
		K_0 (MPa)	2360000
Shell elements describing the out- of-plane response of the floor	Shell elements	Elastic moduli E_x, E_y, E_z (MPa)	61200
		In-plane shear modulus G_{xy} (MPa)	0.1
		Shear moduli G_{xz}, G_{zy} (MPa)	3820

analyses were displacement-based, and the displacement was applied at the floor midspan (Fig. 5.23).

Finally, a time-history analysis was conducted (Fig. 5.24d), subjecting the floor to a scaled seismic signal (Fig. 5.25), representative for the Groningen area.

As can be noticed (Fig. 5.24), both out-of-plane and in-plane behaviour of the floor are properly captured by the adopted modelling strategy and the implemented subroutine. The deflection under vertical loads proved the correct application of the flexural properties to the shell elements: the obtained displacement was practically coincident with the one calculated analytically by considering the floor joists. With regard to the in-plane response, strength, stiffness, energy dissipation and pinching behaviour are well described in all in-plane analyses, with a response quite close to that of reference sample DFpar-1s (Fig. 5.13).

Besides the analyses conducted for this first trial model, the subroutine was also validated against a sample tested parallel to the joist (DFpar-1s), a specimen tested perpendicular to the joists (DFper-4s), and the roof pitch (DRpar-5s). As can be noticed from Fig. 5.26, in all cases the cyclic and dissipative behaviour was well captured, and the adopted modelling strategy accurately simulated the response of the tested floors.

Therefore, the developed macro-element modelling approach for timber floors retrofitted with the proposed technique proves to be efficient and with relatively low computational cost. This is essentially because of two reasons:

1. The macro-element strategy allows to model the global response of the diaphragms without having to use a large number of elements, e.g. as in numerical simulations where the single planks, joists, plywood panels and fasteners are modelled in detail.
2. The complex, nonlinear constitutive laws are attributed to uniaxial elements, while the shell elements (requiring a larger computational effort) feature only linear properties.

This user-supplied subroutine is thus an efficient tool for modelling the seismic response of retrofitted dissipative diaphragms, and constitutes a key step towards the quantification of the beneficial effect of timber floors in existing URM buildings (Chapter 7). The listing of the implemented subroutine USRMAT is reported in Appendix E.

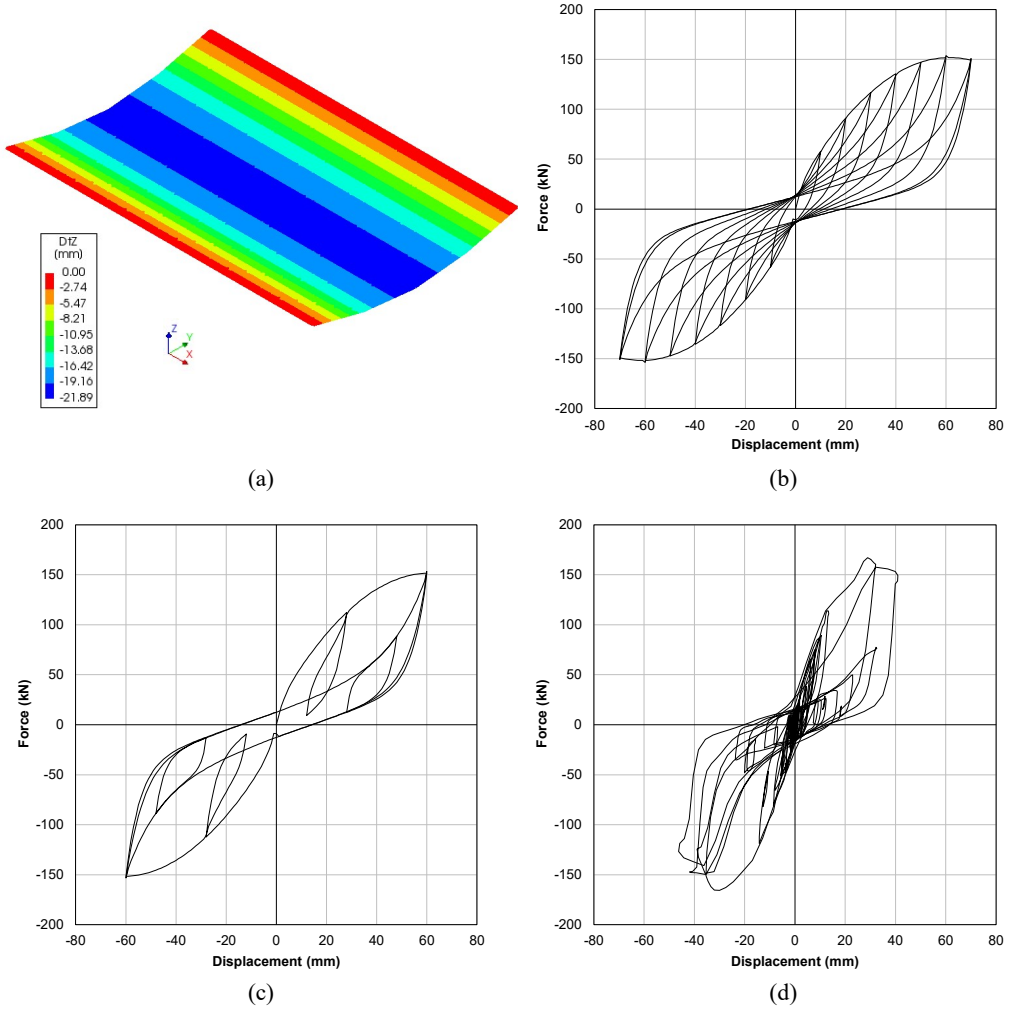


Figure 5.24: Results from the analyses conducted for the validation of the user-supplied subroutine and the overall modelling strategy for timber floors: out-of-plane static analysis under vertical loads (a); complete displacement-based in-plane cyclic analysis (b); displacement-based in-plane cyclic analysis with local loops (c); in-plane time-history analysis under an induced Groningen earthquake accelerogram (d). From [183].

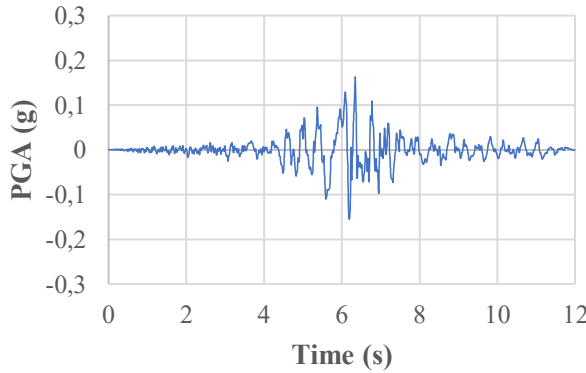


Figure 5.25: Seismic signal used for the time-history analysis of the trial retrofitted diaphragm model. From [183].

5.5 Analytical and numerical models for timber-masonry connections

5.5.1 Introduction

This section addresses the numerical and analytical modelling approaches for floor-to-wall timber-masonry connections. In both cases, from the seismic point of view, strength and stiffness of the connections are essential parameters to predict. The knowledge of the strength is of importance, because the connections can be subsequently designed to be sufficiently resistant compared to the other structural components, so that for instance out-of-plane collapses of walls can be prevented. On the contrary, the stiffness of the joint determines how large is the mutual sliding between a floor and the surrounding walls: a reasonably high value of stiffness allows to approximate the connection as practically continuous (Chapter 7), while the response of a flexible joint has to be fully taken into account.

In Section 5.5.2 calculation models are formulated for the analyzed connections (Section 3.4.2), and validated against the obtained test results (Section 4.4). Based on these analytical formulation, the topic of numerical modelling of these joints is discussed in Section 5.5.3. The approach followed is based on Fig. 5.1: the proposed analytical calculations refer to the single connections, while in the numerical model the joints are simulated as, for instance, nodal springs, to which the constitutive law is assigned based on the dimensions of the macro-element mesh representing the retrofitted floors.

5.5.2 Analytical modelling of timber-masonry connections

In this section, calculation models are formulated for determining the strength and stiffness of the tested configurations, assuming for the connections a uniaxial behaviour along the longitudinal axis of the joist.

In the case of a joist simply inserted in a mortar pocket (**configurations CLAY-A, CS-A, A**), the response is dominated by friction (Section 4.4). Given such frictional

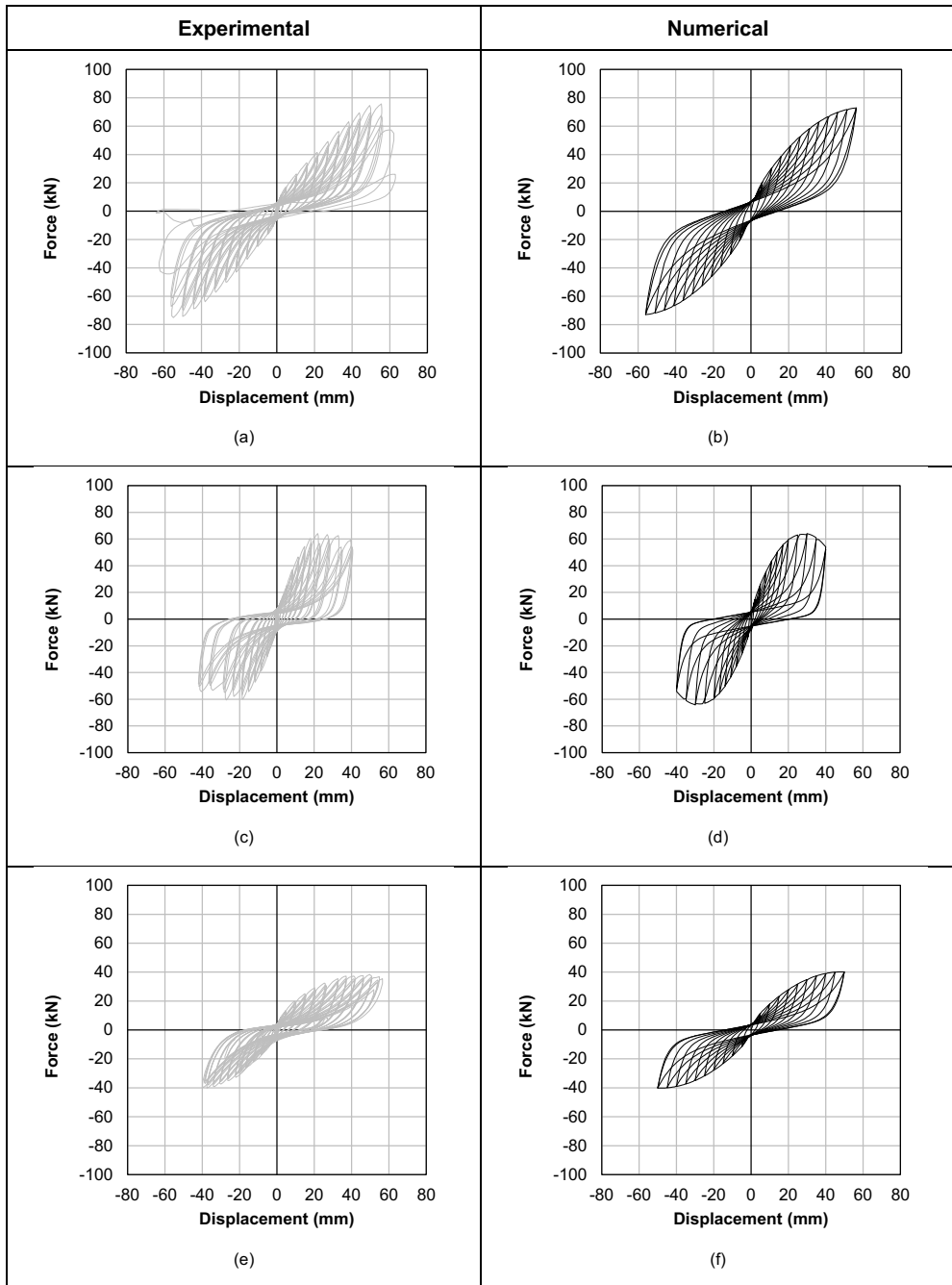


Figure 5.26: Validation of the user-supplied subroutine against the tested diaphragms: experimental (a) and numerical (b) response of sample DFpar-1s; experimental (c) and numerical (d) response of sample DFper-4s; experimental (e) and numerical (f) response of sample DRpar-5s.

nature of the load transfer for this connection type, the peak and residual horizontal load (F_p and F_{res} , respectively) can be safely estimated as:

- $F_p = \mu_p F_v$ for peak friction (before sliding of the connection);
- $F_{res} = \mu_{res} F_v$ for post-peak friction (sliding of the connection).

In the former equations, F_v is the vertical load acting on the connection (equal to 0.5 kN during the tests), μ_p is the static friction coefficient and μ_{res} is the residual one, when the connection starts sliding. A safe estimation can be achieved with $\mu_p = 0.8$ and $\mu_{res} = 0.6$ (derived from monotonic test), bearing in mind that other effects, such as a further contribution to the final strength of a slightly tilted joint (sample A-QS-3, see Section 4.4), are not considered. Figure 5.27a depicts a comparison between the quasi-static cyclic tests on configuration A and the presented frictional model. However, only for double-wythe walls (configuration CLAY-A), a further contribution to the strength is given by the leaf behind the joist, when the latter is pushing against the former. This increase can be quantified by considering the sliding of the bricks hit by the joists. For the tested configuration, this leaf portion is shown in Fig. 5.27b: the sliding bed joints are also highlighted (the vertical ones are not considered, because of the often poor or absent bond provided). The strength F_{leaf} of the leaf portion is determined as:

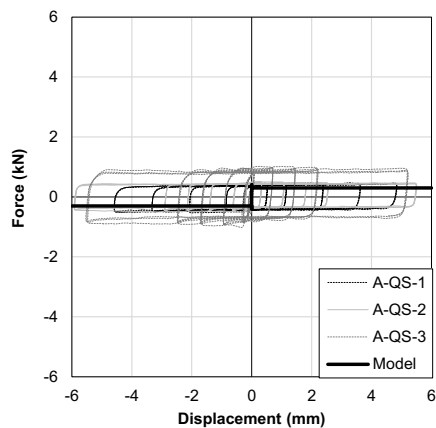
$$F_{leaf} = f_v A_s = f_{v,0} A_s + \mu_s W \quad (5.35)$$

In the former equation, f_v is the total shear strength of masonry, $f_{v,0}$ is the shear strength at no pre-compression, A_s is the total area of the sliding part, μ_s is the shear friction coefficient, W is the pre-compression acting on the sliding portion. In the case of the tested configuration, W is approximately absent, because the masonry leaf is at roof level, therefore $F_{leaf} = f_{v,0} A_s$. With $f_{v,0} = 0.15$ MPa (Table 4.5) and $A_s = 41000$ mm², $F_{leaf} = 6.1$ kN, a value very close to the obtained strength of 6.3 kN (Table 4.9). The stiffness of this joint type is more difficult to quantify, because it can be affected by the joist position, adjacent or not to the masonry leaf behind it, in the mortar pocket. For the tested configuration, if until the pushing peak force a load-slip exponential relation is adopted, then the force transferred by the joint is:

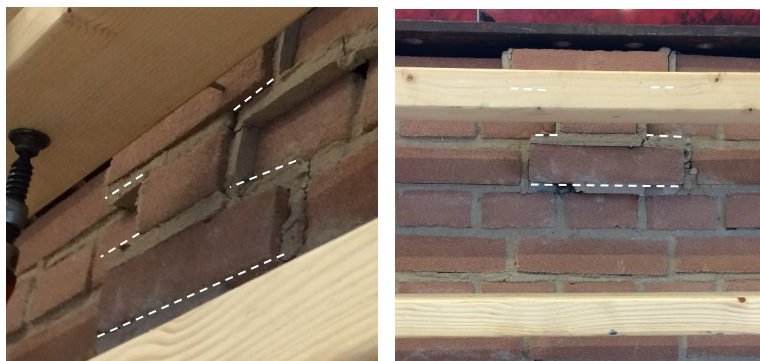
$$F = F_{leaf} \left[1 - \exp \left(-\frac{K_s}{F_{leaf}} \delta_c \right) \right] \quad (5.36)$$

In the former equation, δ_c is the connection displacement, while K_s is the load-slip stiffness observed during companion shear tests [166], having a value of approximately 6.3 kN/mm. Although this parameter is affected by large dispersion, the proposed equation appears to reasonably predict the joint response (Fig. 5.27c). In any case, even considering the increase in strength provided by a second leaf, this connection type proves to be a vulnerable joint in existing buildings, because the risk of mutual sliding and (partial) detachment of out-of-plane walls is very high (Chapter 7).

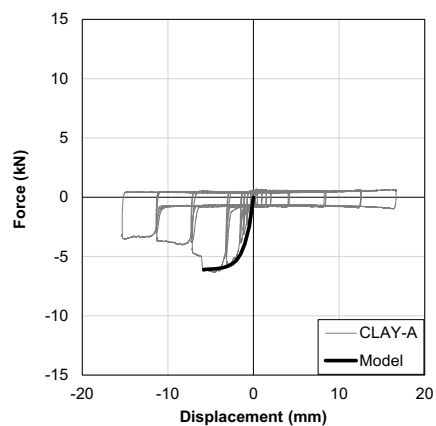
With regard to the as-built joints with hook anchors, **configurations CS-B and B** followed a frictional response in the pushing direction, while in the pulling one also a portion of the wall was involved in the resisting process (Section 4.4). **Configuration CLAY-B** showed a very similar response in the pulling direction, but for the pushing



(a)



(b)



(c)

Figure 5.27: Comparison between the experimental cyclic response of configuration A and the proposed frictional model (a); sliding of bricks in the masonry leaf behind the timber joist (b); prediction of the strength increase because of the additional masonry leaf behind the joist according to Eq. 5.36 (c).

one the presence of the additional masonry leaf led to higher strength, given by a combination of the hook anchor action and the leaf portion behind the joist.

When frictional behaviour is present in the pushing direction, the contribution to the strength is in this case given not only by the friction between joist and mortar pocket, but also by the sliding between the hook anchor and the mortar. For the first mechanism, the previously defined model for configuration A can be adopted, while for an estimation of the effect of the second one, the expression to calculate the adherence stress of smooth bars embedded in concrete can be used [184]:

$$\tau_b = 0.15\sqrt{f_{c,k}} \quad (5.37)$$

with τ_b adherence shear stress and f_{ck} cylindrical compressive strength of concrete. In this case, since only half of the hook anchor bar is embedded in the mortar pocket, while the other one is in contact with the timber joist, the developed adherence force F_b can be assumed as:

$$F_b = \left(0.15\sqrt{0.83f_m}\right) \pi r_b l_b \quad (5.38)$$

where f_m is the cubic compressive strength of mortar (transformed in cylindrical one with the coefficient 0.83, as it is done for concrete), and r_b and l_b are the radius and the embedded length of the hook anchor bar, respectively. For the tested samples, $f_m = 4.84$ MPa for clay bricks, and $f_m = 8.76$ MPa for calcium silicate bricks (Tables 4.5-4.6), while $r_b = 7$ mm and $l_b = 100$ mm (the leaf thickness). Therefore:

- $F_b = 0.7$ kN for clay brick masonry, with a total transferred load of $F_B = F_b + F_{res} = 1.0$ kN
- $F_b = 0.9$ kN for calcium silicate masonry, with a total transferred load of $F_B = F_b + F_{res} = 1.2$ kN

As can be noticed, both values are in line with the observed pushing strength of the joint for configurations CS-B and B (Tables 4.9-4.10). Besides, the initial stiffness K_i can be estimated as the one of the nails connecting the hook anchor to the joist, since these are the main elements determining the play in the connection. The definition of K_{ser} following EN 1995 [1] was adopted for a steel-to-timber joint with three not predrilled nails, considering the mean value of density for timber (Table 4.4) and obtaining a value of $K_i = 6.32$ kN/mm.

With regard to the pulling direction, a force-displacement function having two branches can be defined:

$$F = \begin{cases} K_i \delta_c & \delta_c \leq F_B/K_i \\ (F_w - F_B) \left\{ 1 - \exp \left[-\frac{K_i}{F_w - F_B} \left(\delta_c - \frac{F_B}{K_i} \right)^2 \right] \right\} + F_B & \delta_c > F_B/K_i \end{cases} \quad (5.39)$$

The first branch is symmetric to the one of the opposite loading direction, while the second branch starts from the calculated value of F_B , and has a parabolic beginning after which it is asymptotic to the maximum force F_w that the portion of wall involved by the anchor is able to transfer before cracking (Fig. 5.28a). F_w can be estimated

by considering the bond strength of the masonry portion involved by the anchor and having length l_{ef} , according to Figure 5.28a:

$$F_w = f_w t_w l_{ef} \quad (5.40)$$

with f_w bond strength of masonry, and t_w thickness of the wall. In the case of the tested samples, $l_{ef} = 512$ mm. The function of Eq. 5.39 was chosen because it can well schematize the transition between the frictional behaviour and the resistance of the wall through the sliding of the nails of the anchor. Fig. 5.28b shows the comparison between the experimental backbone curves and the presented analytical prediction, which appears to be a fair estimation of the connection behaviour, with the slope of the second branch in the pulling direction approximately following that of the tested samples. This prediction appears to be conservative and well describing the behaviour of the joint also for monotonic and dynamic loading. It is finally important to underline that the proposed calculation method refers to conditions similar to the tested ones, i.e. a connection at roof level. Higher strength can be expected at a normal floor level, because a much larger amount of masonry can be involved: in that case, the nail strength could for instance become governing. Although this is an as-built configuration, it does not appear to be as vulnerable as the mortar pocket case, because a certain continuity is guaranteed between joist and wall.

In **configurations CLAY-C, CS-C and C**, the response was mainly influenced by the slip of the mechanical anchors and the screws. From the performed companion tests, peak force and stiffness values are known for the anchors, but they should be compared to another failure mechanism that could occur and was also observed during the tests, and namely the extraction of bricks, in which the anchors are fastened, below the joists. This phenomenon is very likely to occur at roof level and is linked to the shear strength f_v of masonry. In particular, the force that can be expected depends on the number n_b of bricks below the joists involved, on their area A_b and on the weight W that the connection transfers to the bricks.

$$F_e = f_v A_b = f_{v,0} n_b A_b + \mu_s W \quad (5.41)$$

In this case, $n_b = 2$, $A_b = 210 \times 100$ mm² and $W = 0.5$ kN, therefore $F_e = 7.1$ kN. This constitutes an upper load limit, and is lower than the peak strength of two anchors, as can be noticed from the data in Table 4.7. Therefore, the value of F_e should always be checked, especially at roof level, because depending on the dispersion of the results for masonry and anchors, also bricks extraction can become governing, as it also happened in the tests. For this connection type, a function linking the initial stiffness K_a of the anchors and the strength limit F_e can be defined as follows:

$$F = F_e \left[1 - \exp \left(-\frac{n_a K_a}{F_e} \right) \delta_c \right] \quad (5.42)$$

with n_a number of mechanical anchors in the connection. To the load-slip law that has just been defined, the displacement induced by F on the screws needs to be computed as $\delta_{screws} = F/K_{screws}$, where K_{screws} can be again determined from the definition of K_{ser} [1]. Thus, the total displacement is calculated as $\delta^* = \delta_c + \delta_{screws}$; the equation can be adopted for both positive and negative branch. Figure 5.29 shows the comparison between the predicted and experimental response, which appears to be well captured,

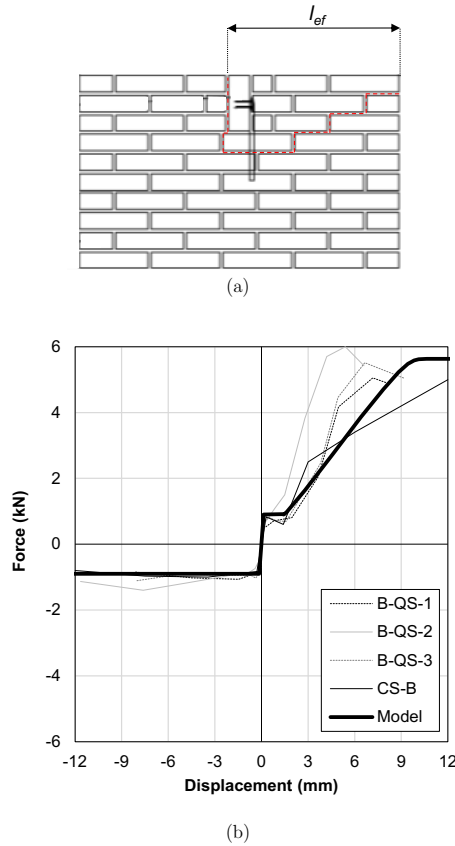


Figure 5.28: Analytical response of the hook anchor connection type: determination of the effective length of the resisting wall portion (a); comparison between the analytical expression of Eq. 5.39 and the backbone curves of the tested samples.

especially in terms of initial stiffness and peak force; a slight underestimation of the pushing load is observable, because in this direction the brick extraction or anchor sliding are partly impeded by the steel angle, which involves a larger portion of the wall in the resisting process. In any case, a continuous, stiff connection is realized with this configuration.

Configuration D was applied to already damaged masonry (Section 3.4.2), thus a large variation in the experimental response was observed (Section 4.4). This configuration can be modelled by considering three contributions to the global initial stiffness of the joint:

- Stiffness of the mechanical anchors in the single connection $n_a K_a$;
- Stiffness of the screws connecting the existing joist to the steel angles, K_1 ;
- Stiffness of the screws connecting the steel angles to the additional joist, placed below the existing one, K_2 ;

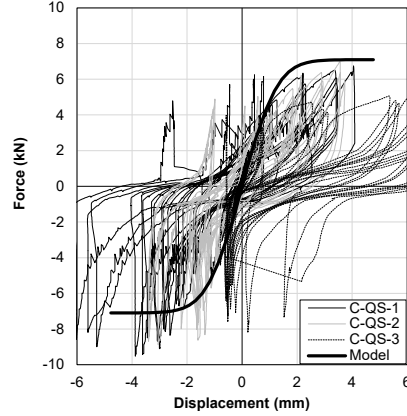


Figure 5.29: Comparison between the analytically predicted and experimental behaviour of strengthened configuration C.

All three components are responsible for a slip in the connection, and the system can be considered as a series of springs; the global equivalent stiffness K_{eq} is determined as:

$$K_{eq} = \left(\frac{1}{n_a K_a} + \frac{1}{K_1} + \frac{1}{K_2} \right)^{-1} \quad (5.43)$$

For the tested connections, K_a was determined according to Table 4.7, while K_1 and K_2 are quantifiable according to EN 1995 [1], following the same calculations performed in the previous configurations; both stiffness values refer to four screws (Section 3.4.2), thus $K_1 = K_2 = 10.1$ kN/mm and $K_{eq} = 3.8$ kN/mm. The upper strength limit can be conservatively estimated as F_e (Eq. 5.41), thus again 7.1 kN for the tested sample, similarly to the previous case. The load-slip response can be modelled as:

$$F = F_e \left[1 - \exp \left(-\frac{K_{eq}}{F_e} \right) \delta_c \right] \quad (5.44)$$

The proposed calculation method allows to conservatively schematize the connection response, as can be noticed from Figure 5.30. The curve is shown for the negative branch, where a more stable behaviour was observed: especially in the pulling direction, the recorded cycles are not always symmetric because the already damaged wall moved together with the sensor, leading to a not self-centering behaviour.

Configuration E featured a hook anchor glued with epoxy into an incision in the masonry walls (Section 3.4.2). This joint is characterized by an initial stiffness K_i given by the nails of the hook anchor and a response that is different for pulling and pushing loading direction: for the former, the detachment of the bricks around the glue has to be considered; for the latter, the strength of the wall is brought into play. For the pulling direction, the following load-slip equations can be formulated, based on the observed experimental response:

$$F = \begin{cases} K_i \delta_c & \delta_c \leq \delta_g = F_g / K_i \\ F_{res} + \frac{F_g}{\delta_c - \delta_g + F_g / (F_g - F_{res})} & \delta_c > F_g / K_i \end{cases} \quad (5.45)$$

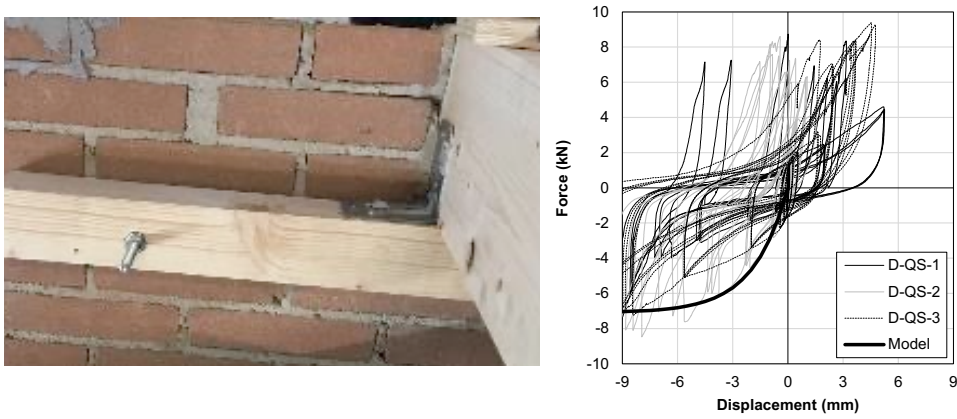


Figure 5.30: Comparison between the analytically predicted and experimental behaviour of strengthened configuration D.

In the former equation, F_{res} is the previously defined frictional force, and F_g is the load leading to detachment of the bricks around the epoxy (Section 4.4). As can be noticed, the second branch is derived as an hyperbole connecting F_g and F_{res} . F_g can be computed as $F_g = \tau_g A_i$, with τ_g detachment tangential stress and A_i area of the incision. The incision area was equal to $(40+40+25) \times 240 \text{ mm}^2$ (Section 3.4.2), while from performed tests a value of $\tau_g = 0.17 \pm 0.05 \text{ MPa}$ was obtained. Thus, for the present case $F_g = 4.3 \text{ kN}$ is obtained, and thus a conservative value in line with the obtained pulling strength (Table 4.10).

For the pushing direction, instead, the response is modelled as:

$$F = F_w \left[1 - \exp \left(-\frac{K_i}{F_w} \delta_c \right) \right] \quad (5.46)$$

In this case, the equation constitutes an exponential branch linking the initial stiffness of the nails, determined in the same way as configuration B, and the flexural bond strength F_w of the whole wall (thus, in Eq. 5.40, $l_{ef} = 980 \text{ mm}$), equal to 11.3 kN. It should be noticed that this value refers to the tested samples, but in practice l_{ef} would correspond to the joists spacing. The comparison between the experimental and analytically predicted behaviour is depicted in Fig. 5.31: as can be noticed, the initial stiffness is slightly underestimated, but this appears to be conservative, because it can cover also cases in which small cracks are already present, as it happened for sample E-QS-2.

Configuration F was also a very stiff connection type (Section 3.4.2), in which the response was influenced by the axial stiffness K_{ax} of the screws and the phenomenon of brick extraction, similarly to joint types C and D. The axial slip modulus can be determined according to the European Technical Assessment of the screws producer [179], with an effective threaded length of the 7-mm-diameter screws in the timber member l_{thread} of 90 mm, resulting in a value of $K_{ax} = 25 \cdot d \cdot l_{thread} = 31.5 \text{ kN/mm}$. Therefore, the load-slip relation is formulated as:

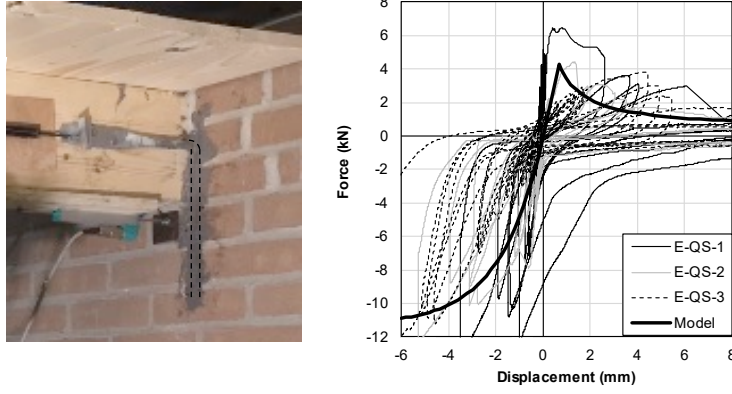


Figure 5.31: Comparison between the analytically predicted and experimental behaviour of strengthened configuration E.

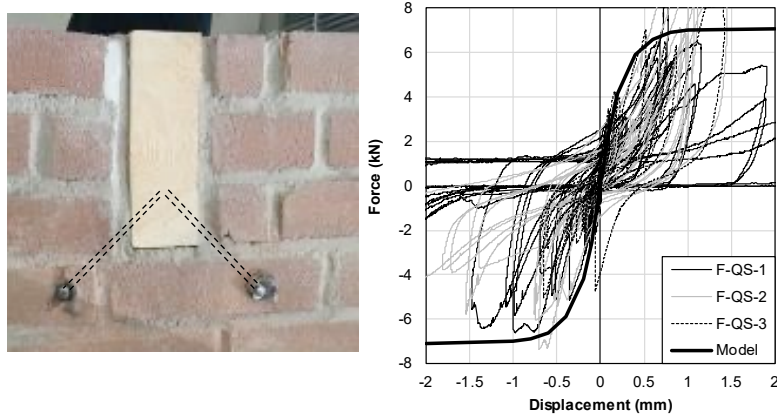


Figure 5.32: Comparison between the analytically predicted and experimental behaviour of strengthened configuration F.

$$F = F_e \left[1 - \exp \left(-\frac{n_{screws} K_{ax}}{F_e} \delta_c \right) \right] \quad (5.47)$$

In the tested samples, $n_{screws} = 2$. The proposed relation enables a good prediction of the behaviour of this connection until the peak force (Fig 5.32). Because of the high variability of the softening phase and the fact that this joint is intended to be stiff and not ductile, it was chosen not to propose an equation for post-peak response.

Finally, **configuration G** was the option developed based on the retrofitting of the diaphragms as well (Section 3.4.2): timber blocks were placed on both sides of the joists, and also the sheathing and the plywood panels were present in the tested samples. The total slip of the connection is, thus, given by the following contributions from the various fasteners, according to the way in which the load is transferred from the wall to the joist (Fig. 5.33):

- Stiffness of the mechanical anchors in the single connection $n_a K_a$;
- Stiffness of the screws connecting the timber blocks to sheathing and plywood panels, K_b ;
- Stiffness of the screws and the nails connecting the plywood panel and the sheathing to the joist, K_j ;

In the tested samples, four anchors were present; four were also the screws fastening the timber blocks to sheathing and plywood panels. The plywood-sheathing-joist interface was, instead, connected by means of one screw and two nails (see Appendix B and Fig. 5.33). The stiffness of screws and nails was calculated according to EN 1995 [1], analogously to the previous cases. After determining all contributions to the connection slip, a global, equivalent stiffness of the joint can be defined, again representing the system as a series of springs:

$$K_{eq} = \left(\frac{1}{n_a K_a} + \frac{1}{K_b} + \frac{1}{K_j} \right)^{-1} \quad (5.48)$$

For the specific configuration of the tested samples, $K_{eq} = 1.8 \text{ kN/mm}$. The load-slip equation is then defined as:

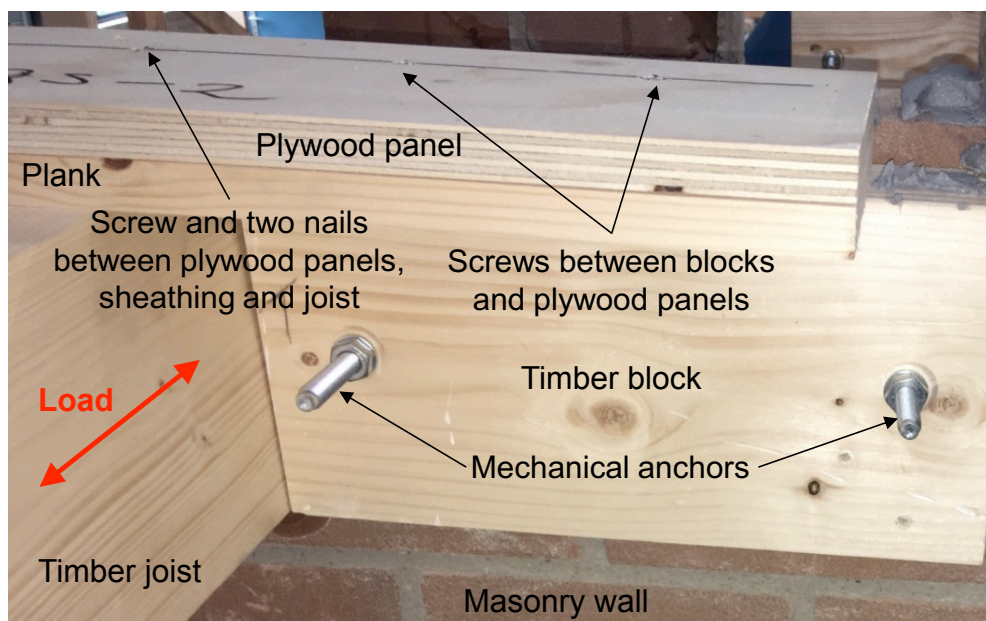
$$F = F_w \left[1 - \exp \left(-\frac{K_{eq}}{F_w} \delta_c \right) \right] \quad (5.49)$$

in which F_w is determined according to Eq. 5.41, with $l_{ef} = 980 \text{ mm}$, similarly to configuration E. Figure 5.33b shows the comparison between the experimental and analytical response: the proposed equation is able to properly capture the observed behaviour.

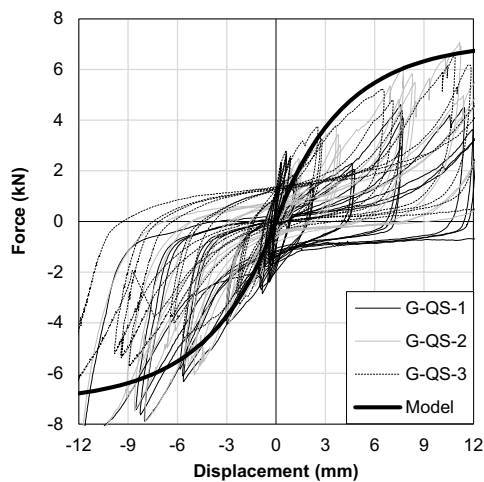
All calculation models developed in this section were derived and validated based on the tested configurations, representing timber-masonry joints at roof level: for other positions in the building, the strength and stiffness may be different. The proposed expression can be used to estimate a strength value for a specific as-built or retrofitted configuration, as well as their stiffness. Yet, as will be noticeable in Chapter 7, when the stiffness is reasonably high, and the connection has sufficient (over)strength, a continuous behaviour between floor and wall can be assumed.

5.5.3 Numerical modelling approaches for timber-masonry connections

A convenient modelling strategy for simulating the seismic response of timber-masonry connections is to adopt spring elements for them, in which the constitutive laws developed in the previous chapter can be implemented. If the stiffness of the connection is high enough, for a simplified modelling a continuous interface can also be reasonably assumed between floors and walls, as will be shown in Chapter 7. This section focuses on the implementation of spring elements for modelling the connections, by considering a widely adopted software for nonlinear seismic analysis, such as *OpenSees*, and an advanced commercial software, such as DIANA FEA, similarly to the recommendations given for the strengthened timber diaphragms (Section 5.4). The numerical modelling approach is based on the knowledge of the backbone curve of the single connection,



(a)



(b)

Figure 5.33: Main contribution to connection slip from the various fasteners (a); comparison between the analytically predicted and experimental behaviour of strengthened configuration G (b).

determined either analytically or experimentally. Then, depending on the dimensions of the macro-elements used for simulating the response of timber diaphragms, the constitutive law is assigned to the springs depending on the actual number of connections pertaining to the macro-element width l_m , as it has been shown in Fig. 5.1.

When modelling timber-masonry connections as spring elements in *OpenSees*, the nonlinear cyclic response of the joints can be simulated by adopting the uniaxial **Hysteretic** material [180]. Only for the mortar pocket configuration, characterized by a purely frictional behaviour, a simpler strategy can be the use of the uniaxial **Steel01** material [180]. For all configurations, displacement-based cyclic analyses were performed. In general, for modelling timber-masonry joints, **zeroLength** elements are recommended [180], and they were also used in the presented implementation procedure. These elements are to be applied between two coincident nodes, and three different uncoupled uniaxial responses can be assigned to each direction x , y or z . This is particularly convenient, because the connection can be nonlinearly modelled only in the direction of interest, while for the other two can be represented as stiff or hinged.

Therefore, for configuration A (mortar pocket), to simulate the cyclic frictional response, the following parameters need to be specified for implementing the **Steel01** material (Fig. 5.34a):

- A yielding force **\$Fy**, corresponding to the peak friction load according to the pre-compression applied to the connection;
- An initial stiffness **\$E0**, that theoretically could be infinite for purely frictional response. In the calibrated connection, having fixed a maximum displacement **\$dmax** of 20 mm, the stiffness was assumed to be equal to $100 \cdot Fy / dmax$;
- A parameter **\$b** determining the post-yielding hardening; in a frictional behaviour this phenomenon is almost absent, thus **\$b** was assumed to be 0.001.

For all other connection types, the uniaxial **Hysteretic** material needs the following input parameters to be specified (Fig. 5.34b-c):

- **\$s1p**, **\$e1p**: stress and strain (or force and deformation) at first point of the envelope in the positive direction;
- **\$s2p**, **\$e2p**: stress and strain (or force and deformation) at second point of the envelope in the positive direction;
- **\$s3p**, **\$e3p**: stress and strain (or force and deformation) at third point of the envelope in the positive direction (optional);
- **\$s1n**, **\$e1n**: stress and strain (or force and deformation) at first point of the envelope in the negative direction;
- **\$s2n**, **\$e2n**: stress and strain (or force and deformation) at second point of the envelope in the negative direction;
- **\$s3n**, **\$e3n**: stress and strain (or force and deformation) at third point of the envelope in the negative direction (optional);
- **\$pinchx**: pinching factor for strain (or deformation) during reloading;

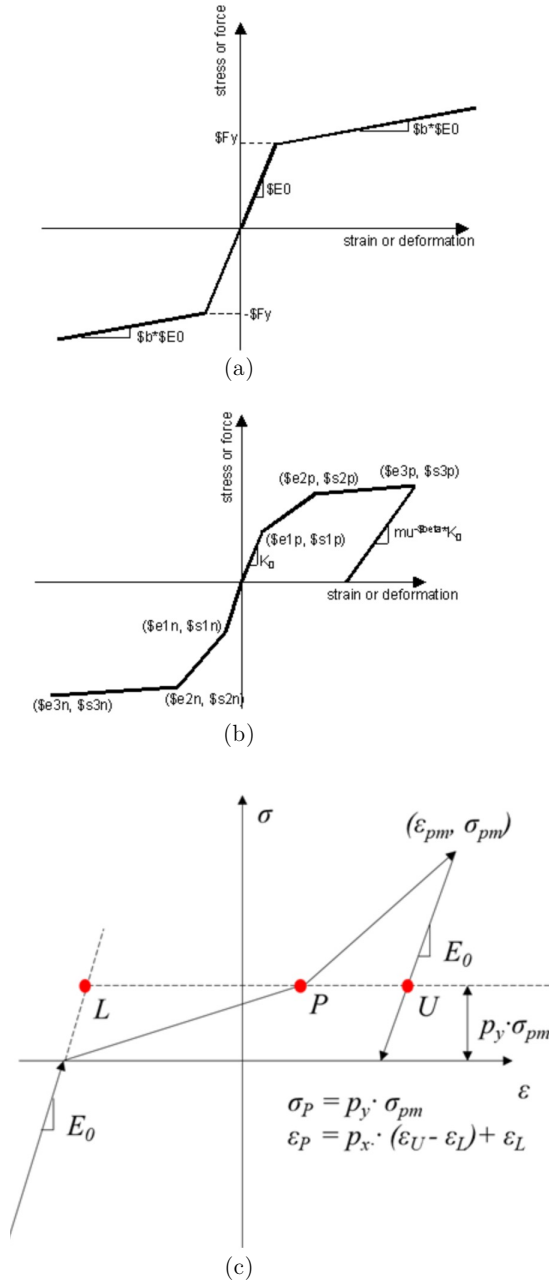


Figure 5.34: Main parameters of the **Steel01** material (a) in **OpenSees**; stress, strain, damage (b) and pinching (c) parameters of the **Hysteretic** material. From [180].

Table 5.9: Values of the parameters `$pinchx` and `$pinchy` adopted for the implementation of the timber-masonry connections in OpenSees.

Connection type	<code>\$pinchx</code>	<code>\$pinchy</code>
B	0.8	0.5
C	0.6	0.1
D	0.7	0.4
E	0.6	0.1
F	0.6	0.2
G	0.7	0.2

- `$pinchy`: pinching factor for stress (or force) during reloading;
- `$damage1`: damage due to ductility;
- `$damage2`: damage due to energy;
- `$beta`: power used to determine the degraded unloading stiffness based on ductility (optional parameter, set as zero by default).

While the first six parameters couples directly derive from the experimental or analytical load-slip backbone curves of the joints, a calibration of the non-dimensional pinching parameters `$pinchx` and `$pinchy` is necessary to well reproduce the behaviour of tested connections B-G, which showed this phenomenon. The two damage parameters and the optional one were all set to zero. Table 5.9 reports the recommended parameters to be used for the specific tested configurations, and the results of this implementation are shown in Fig. 5.35.

The implementation of the constitutive laws of the connections is also possible in DIANA FEA, and was adopted for the second case-study building presented in Chapter 7. A convenient element, with a behaviour equivalent to the `zeroLength` one of OpenSees, is the nodal spring [182], for which coupled or uncoupled force-displacement and moment-rotation (nonlinear) relations can be assigned. In the case of timber-masonry connections, a user-specified nonlinear diagram can be assigned to the nodal springs (see Fig. 5.36 as an example), in the working direction of interest for the joint, similarly to the uniaxial `Hysteretic` material of OpenSees. In other words, the experimentally or analytically determined (see the previous section) backbone curves of the joints can be used for constructing the nonlinear diagram. The full cyclic behaviour cannot be taken into account in detail as in OpenSees, but the nonlinear response of the connection is still represented, allowing to capture the mutual displacements between floors and walls. Further details are reported while presenting the case-study buildings in Chapter 7.

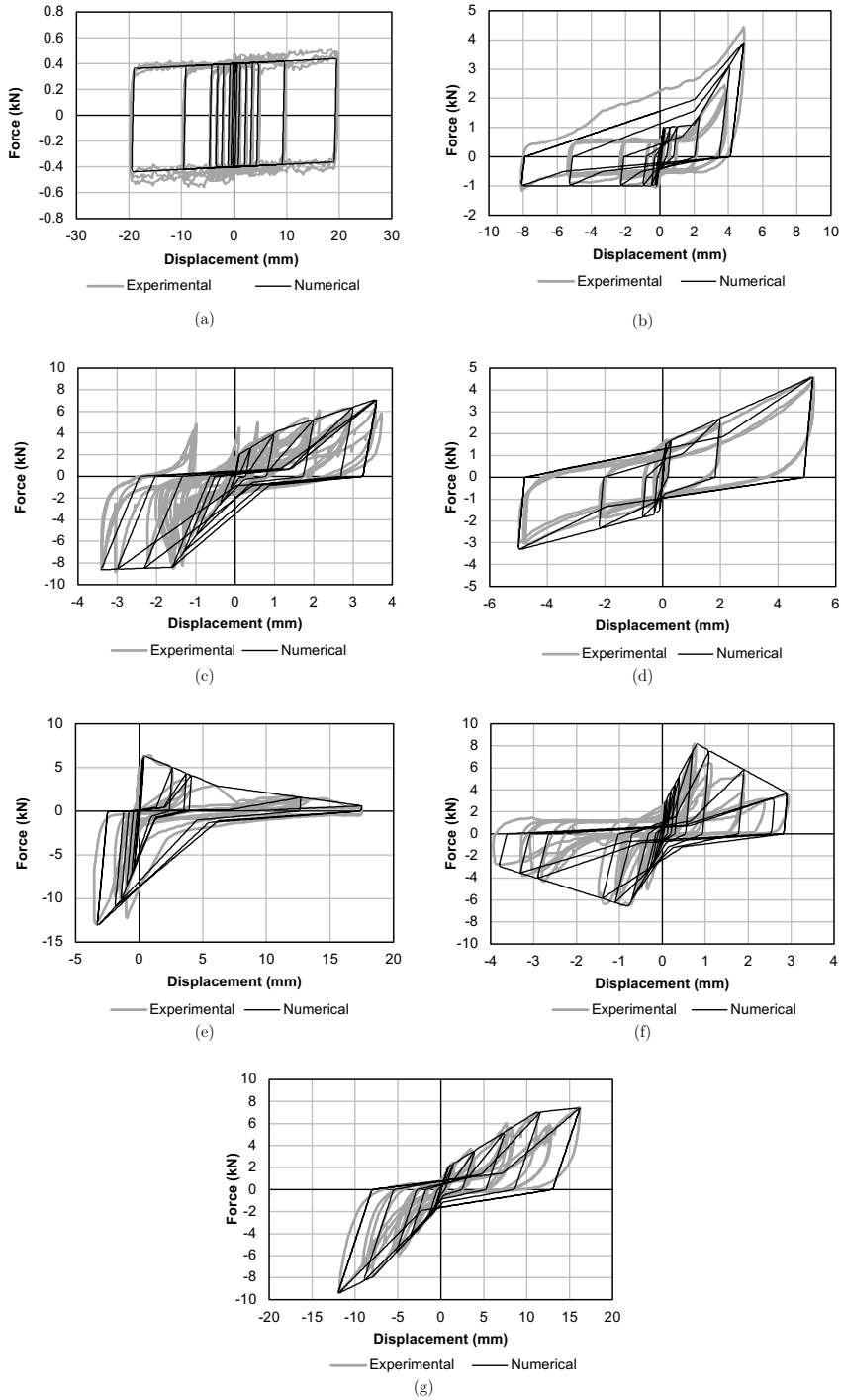


Figure 5.35: Comparison between the numerically implemented connection in OpenSees and representative experimental results: configurations A (a), B (b), C (c), D (d), E (e), F (f), and G (g).

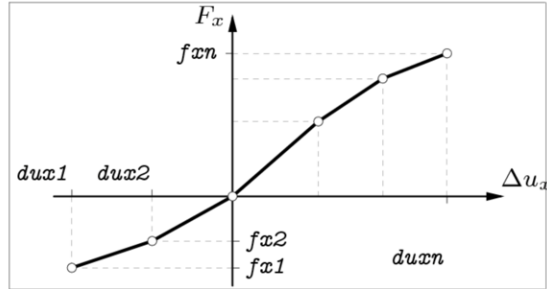


Figure 5.36: Force-elongation diagram for spring elements in DIANA FEA. From [182].

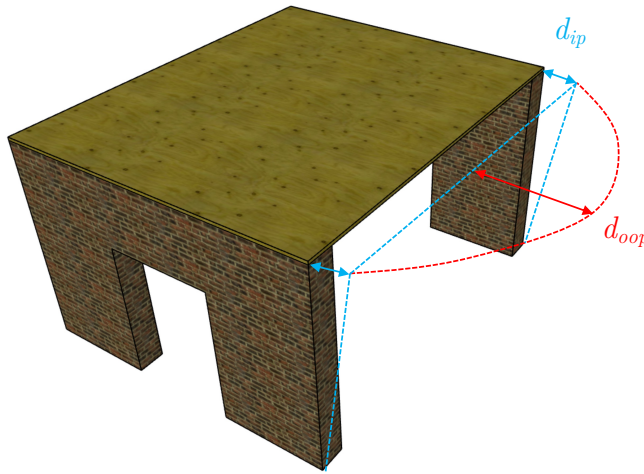


Figure 5.37: Representation of the in-plane and out-of-plane drift limits in a basic masonry building with a timber diaphragm.

5.6 Drift limits and numerical modelling strategies for masonry walls

5.6.1 General

When modelling the seismic response of URM buildings, the nonlinear behaviour of masonry can be simulated in several ways. When a failure is not clearly recognizable by numerical issues (e.g. instability or divergence because of too damaged or collapsed structural components), the use of *drift limits* (ratio between top displacement and deformable height of the wall, Fig. 5.37) is a common way of assessing the damage state of URM walls. Therefore, this section firstly focuses on the usually adopted drift limits at both in-plane and out-of-plane collapse (Sections 5.6.2 and 5.6.3, respectively). Then, the main numerical modelling approaches for masonry will be briefly summarized (Section 5.6.4), and the motivation behind the software adopted for the numerical analyses on whole URM buildings will be presented.

5.6.2 Drift limits for in-plane loaded masonry walls

The usually adopted drift limits d_{ip} (Fig. 5.37) for in-plane failures of masonry walls depend on the collapse mechanism: shear-related failures are associated to collapses at smaller drifts than for rocking responses.

- For shear failures, an in-plane inter-storey drift of 0.53% can be assumed as failure criterion [4]; this is also confirmed by relevant experimental research [185].
- For flexural failures, an in-plane inter-storey drift of 1.0% of the pier height can be assumed as failure criterion [4]; however, for Dutch masonry, based on a large database of experimental tests on rocking piers, the following empirical equation can be adopted [186]:

$$d_{ip,rocking\ failure} = 0.9\% \cdot \left(1 - 2.6 \frac{\sigma_0}{f_c}\right) \cdot \sqrt{\frac{H}{L}} \cdot \frac{H_{ref}}{H} \quad (5.50)$$

In the former equation, σ_0/f_c is the axial load ratio between pre-compression on the pier and compressive strength, H/L is the aspect ratio of the wall, and H_{ref}/H accounts for a size effect, with H_{ref} set equal to a typical reference storey height of 2.4 m [186].

5.6.3 Drift limits for out-of-plane loaded masonry walls

As an out-of-plane drift limit d_{oop} (Fig. 5.37), a conservative value of 2.0% of the wall height can be assumed, independently of the (local) failure mechanism. This value derives from the provisions of the New Zealand standard NZS 1170.5 [187, 188], which suggests a global drift limit of 2.5% for a building under seismic action. Because of the slenderness of Dutch masonry, and in agreement with the performed experimental tests, a more conservative value was assumed. Furthermore, in any case the out-of-plane displacement should not exceed 50% of the wall thickness [100].

5.6.4 Numerical modelling approaches for masonry structures

Different numerical modelling approaches are proposed to simulate masonry structures: the differences lie on the scale of analysis and how masonry is described. The main modelling approaches can be categorized as follows [189] (Fig. 5.38):

- Block-based models (BBM);
- Continuum models (CM);
- Geometry-based models (GBM).
- Macro-element models (MM) or equivalent-frame models (EFM).

In BBM, masonry is modeled in a block-by-block fashion and, therefore, the actual masonry texture can be accounted for. The block behaviour can be considered rigid or deformable, whereas the interaction among blocks can be mechanically represented by means of several suitable formulations.

In CM, the masonry material is modelled as a continuum deformable body, without distinction between blocks and mortar layers. The constitutive laws adopted for the

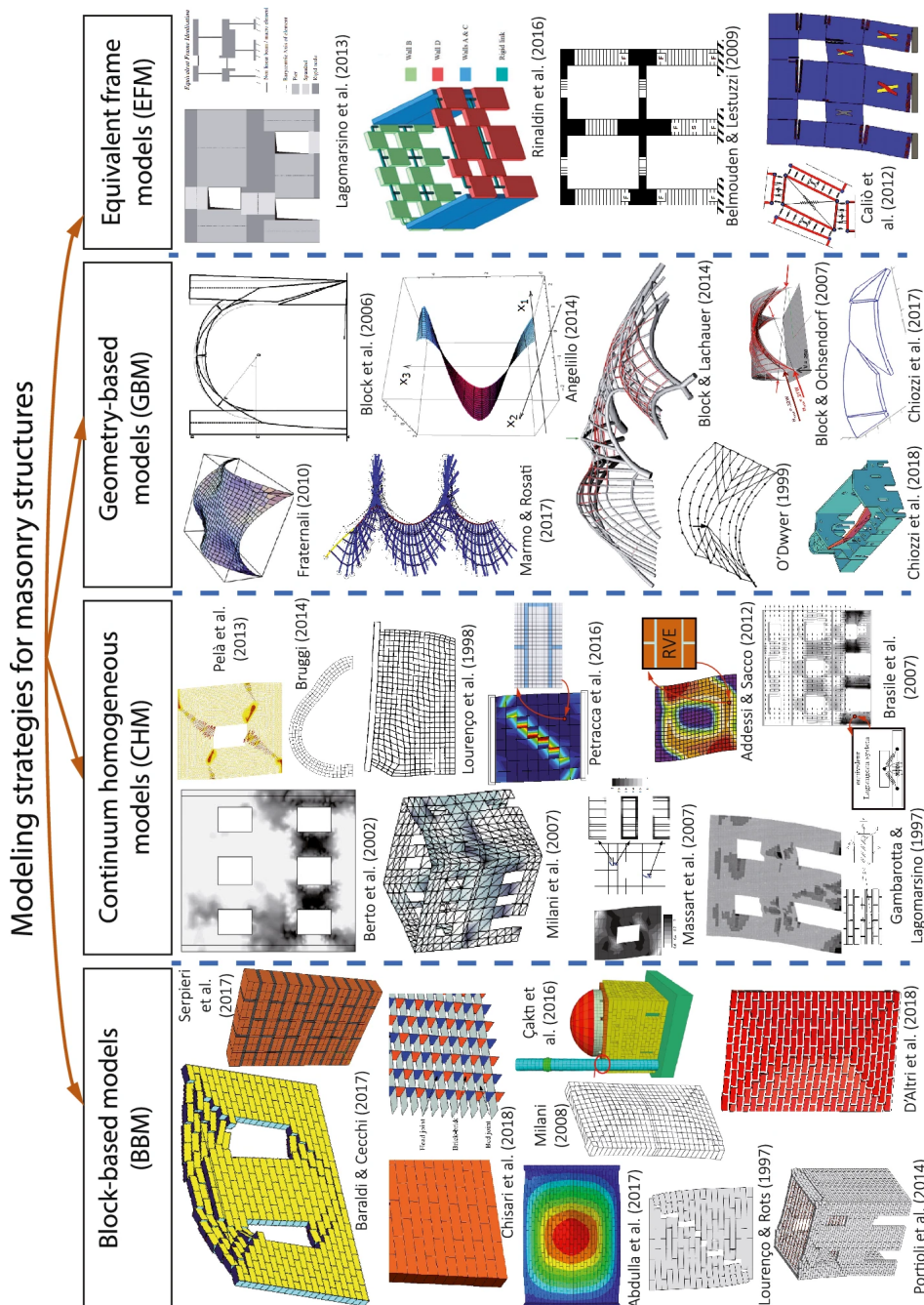


Figure 5.38: Numerical modelling strategies for masonry structures. From [189].

material can be defined either through direct approaches or through homogenization procedures and multi-scale approaches. In the first case, for instance, constitutive laws are formulated and calibrated on the basis of experimental tests. In the second approach, instead, the constitutive law of the material (considered as homogeneous in the structural-scale model) is deduced from a homogenization process which relates the structural-scale model to a material-scale model (representing the main masonry heterogeneities) of a representative volume element (RVE) of the structure [189]. With this approach, the solution of structural-scale problems could be formulated in a multi-scale framework.

In GBM, the structure is modelled as a combination of rigid bodies. The geometry of the structure represents the main (or even the only) input of these modelling strategies; the structural equilibrium and/or collapse are investigated through different procedures. Typically, these methods implement limit analysis-based solutions, which can be based on either static or kinematic theorems. Although these models could, in some respects, be considered as continuum models, it should be remarked that the present category is based on the assumption of rigid body.

In MM or EFM, the structure is idealized into panel-scale structural components (macro-elements) with a phenomenological or mechanical-based response. Typically, two main structural components may be identified: piers and spandrels. The subdivision of the structure into panel-scale portions is an a-priori operation made by the analyst who interprets the structural conception of the building. Although these models could, in some respects, be considered continuum approaches, the main difference with CM is that the constitutive law of macro-elements attempts to reproduce the mechanical response of panel-scale structural components, while the constitutive laws of the models in CM try to reproduce the mechanical behavior of the masonry material.

The first modelling strategy (BBM), although theoretically possible for large-scale seismic analyses, requires a considerably high computational effort when modelling whole masonry structures [189]. On the contrary, GBM are very powerful for a fast and effective evaluation (with kinematic limit analysis) of the main vulnerabilities of a masonry building in terms of local collapses, such as those of (portions of) out-of-plane walls or gables, but do not provide information on the displacement capacity. For these reasons, the most widely adopted approaches for the numerical modelling of the seismic response of masonry structures are the CM and MM/EFM. The computational demand of the former modelling strategy is higher, but it can account for damage cracks and smeared failure models of all masonry components. On the contrary, MM/EFM are computationally faster, and specifically devoted to the global seismic response of masonry buildings, but also present some drawbacks. In particular, they usually assume that any activation of local (out-of-plane) failure modes is prevented. This decoupling assumption, although local failure modes can be separately assessed through kinematic limit analysis (e.g. with GBM), could lead to conventional estimates of the seismic capacity, as in reality out-of-plane and in-plane damages might simultaneously arise [189]. Additionally, macro-element models cannot always precisely account for structural details, such as the interlocking between orthogonal walls. Finally, the a-priori idealization of the structure in piers and spandrels could cause the modelled mechanical system to be far from the actual one, particularly for the case of irregular opening layouts. Yet, for regular buildings with not too flexible diaphragms, MM/EFM are suitable strategies for assessing the seismic response of URM structures [129].

With reference to CM approaches, one of the most advanced software accounting for the nonlinear response of masonry is DIANA FEA [182], with its implemented *Engineering Masonry Model* (EMM) [190]. The EMM is a smeared failure model and can be applied in combination with regular plane stress (membrane) and curved shell elements for modelling seismic response of masonry walls. This implemented model is a total-strain based continuum model having the following features [190]:

- It covers tensile, shear and compression failure modes. More specifically, the failure mechanisms considered in EMM are tensile cracking of the bed joint, compressive crushing in the direction normal to the bed joint, tensile cracking of the head joint, compressive crushing in the direction normal to the head joint, cracking in the direction normal to the diagonal staircase cracks, frictional shear sliding, and out-of-plane shear failure.
- It is equipped with adequate secant, elastic and mixed hysteresis loops for the different failure modes, including orthotropy, by using different properties for elasticity, strength and softening for the two directions;
- The anisotropy of the masonry resulting from different stiffness in the direction of the bed and head joints is considered;
- The element x -direction is aligned with the bed joints and is normal to the head joints, which are oriented along the element y -direction.
- There are four predefined crack directions in the plane of the element, in the direction of the bed joint, in the direction of the head joint, and in two diagonal directions at a user-defined angle, respectively.

The EMM has been validated to several performed tests, and has shown in general from a reasonable to a very good agreement with the experimental results, in terms of both the representation of crack pattern and the cyclic hysteretic response (Fig. 5.39). Besides, it has also been proved that the interaction between in- and out-of-plane walls can be reliably predicted [191], by creating a numerical model simulating the cyclic pushover test conducted at TU Delft on a prototype representing a terraced house [171], presented in Section 2.7 and shown in Fig. 4.42. As can be noticed from Fig. 5.40, the numerical capacity curve shows good agreement with the experimental one.

Hence, when this advanced model for masonry is coupled with the user-supplied subroutine representing the nonlinear, dissipative response of the timber diaphragms (Section 5.4.3), all relevant contributions to the global seismic response of URM buildings can be reliably taken into account in the numerical analyses.

However, for preliminary analyses on simple buildings, it has been shown that a macro-element approach is particularly suitable for modelling timber diaphragms (Section 5.4.2). This same strategy was also adopted in past research studies [9, 10, 13], and was applied to masonry walls as well. In those studies, the first to consider the dissipative behaviour of the diaphragms, *OpenSees* software [181] was used, because of the large number of available nonlinear, advanced materials, for both masonry and floors.

In fact, other macro-element-based commercial software, such as TREMURI [129] or 3D-MACRO [192], although very efficient for nonlinear analyses on masonry piers,

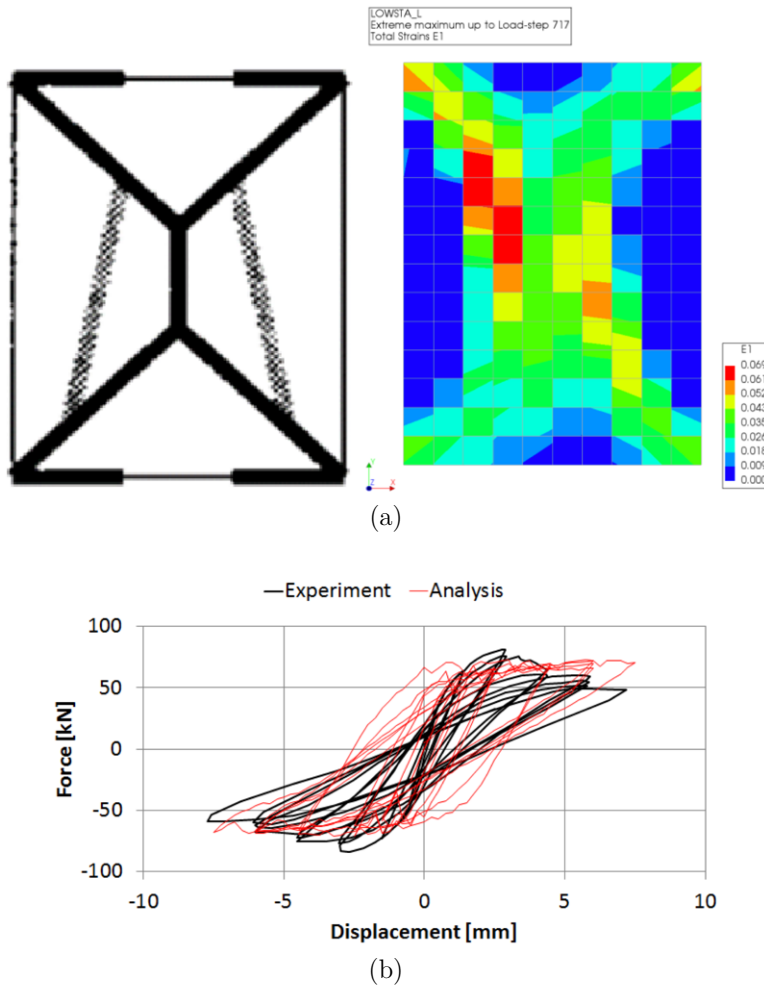


Figure 5.39: Comparison between the experimental and numerical crack pattern (a) and cyclic load-displacement response (b) of the squat wall tested in [75]. From [190].

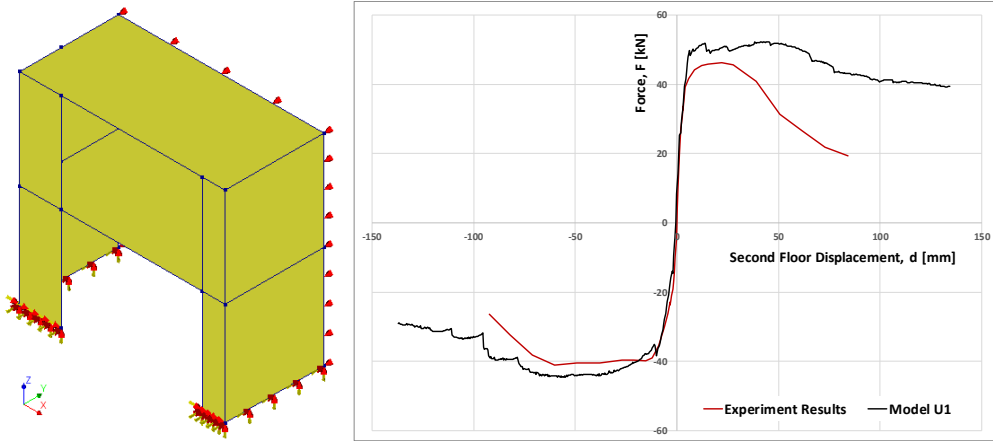


Figure 5.40: Comparison between the experimental and numerical capacity curve of the prototype simulating a terraced house tested at TU Delft [171]. Adapted from [191].

do not allow to account for dissipative timber diaphragms, because the only options available to model them is the use of a linear elastic orthotropic membrane, as is the case for DIANA FEA [182]. For this reason, specific implementation procedures were developed to simulate the dissipative behaviour of timber diaphragms based on the formulated analytical model in both *OpenSees* (Section 5.4.2) and DIANA FEA (Section 5.4.3).

Because of the computationally efficient macro-element modelling strategy adopted in *OpenSees* for masonry and diaphragms [9, 10, 13], this method will also be used for preliminary analyses on basic URM structures to validate the proposed extended approach for evaluating their seismic capacity (Chapter 6), prior to the extensive numerical modelling in DIANA FEA of three case-study buildings (Chapter 7).

The adopted macro-element strategy for masonry in *OpenSees* allows to well represent the in-plane behaviour of piers (Fig. 5.41): the walls are subdivided into smaller quadrilaterals of rigid trusses, with two inner diagonal springs (simulating the hysteretic shear-diagonal failure), and outer vertical and horizontal springs, for modelling rocking and sliding behaviour, respectively. For all nonlinear springs, the uniaxial **Hysteretic** material can be adopted [180], which is particularly suitable for describing especially shear failures (Fig. 5.41b)

This modelling strategy allows to describe all nonlinear in-plane failure mechanisms of masonry walls by defining sub-modules for both piers and spandrels (Fig. 5.41a), and obtaining very good agreement with experimental tests (Fig. 5.41b). Yet, two main limitations can be identified:

- The lack of a graphical user interface in *OpenSees* allows to only model relatively simple buildings, since the geometry and definition of each element, the constitutive laws, and the analyses types have to be manually implemented by means of a listing in `.tcl` (*tool command language*) format.
- The difficulty in fully modelling out-of-plane walls and their failure mechanisms, for which a very fine mesh of macro-elements would be necessary: this is also

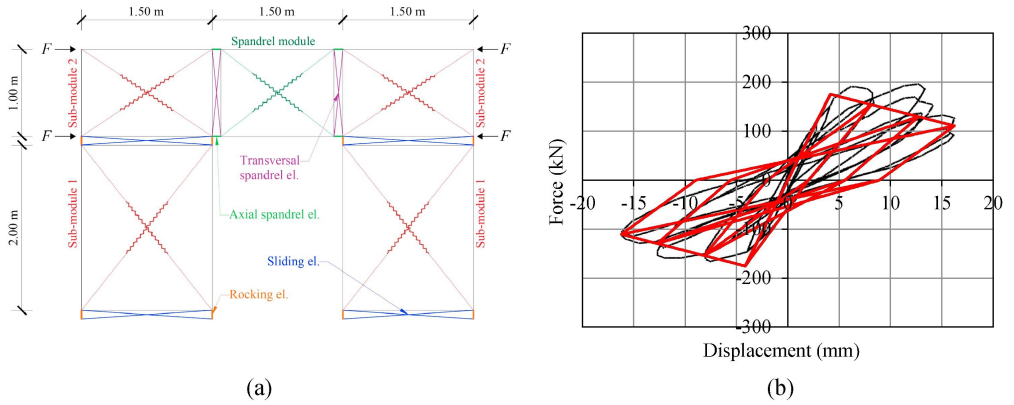


Figure 5.41: Example of a masonry macro-model implemented in OpenSees (a): sub modules, elements connecting wall sub-modules and equivalent external compression forces because of steel ties (F); numerical validation of the macro-model against the test results of [77] (b). From [11].

the reason why DIANA FEA was adopted for the analyses on whole case-study buildings.

Chapter 6

Seismic capacity of URM buildings and its optimization

6.1 Introduction

This chapter constitutes a linking element between the assessment of the seismic response of structural components, performed both experimentally (Chapters 3-4) and analytically (5), and the optimization of the global seismic behaviour of URM buildings through the dissipative retrofitting of their timber diaphragms (Chapter 7). More specifically, the knowledge gap related to the physical point of view is addressed in the following, focusing on the need of a more general approach for evaluating seismic capacity, not based on PGA only, but that can account more in depth for load duration, energy dissipation and structural damage.

Therefore, in order to consider the aforementioned factors, a more generalized, energy-based approach is proposed. First of all, an analytical strategy to estimate energy dissipation and damage for URM buildings will be presented (Section 6.2), starting from linear SDOF systems and extending the formulation for nonlinear MDOF structures. This formulation intrinsically account for (strong motion) load duration, and allows to assess the structural damage in terms of number of cycles underwent by the system. The prediction of the dissipated hysteretic energy starts from the estimation of the effective period at collapse of the structure, from which its pseudo-velocity can be determined from the relative response spectrum. Then, the hysteretic energy is calculated by knowing the strong motion duration of the input seismic signal.

The analytical prediction of hysteretic energy is of particular interest, because with this approach it is also possible to quantify the behaviour factor of URM buildings having dissipative retrofitted diaphragms. In fact, the behaviour factor is directly linked to the estimation of the effective period at collapse: under a same seismic signal, the analytically predicted hysteretic energy can be associated to a specific range of effective periods (and thus to a specific range of behaviour factors), and can be compared to the hysteretic energy obtained from numerical time-history analyses, thus validating the assumed range. Therefore, this strategy enables the quantification and validation of increased behaviour factors for URM buildings with optimized diaphragms: in order to

validate this approach, numerical analyses on two basic URM buildings are conducted (Section 6.3), evaluating also the influence of timber diaphragms stiffness and dissipation on their seismic response.

This allows to identify an optimal retrofitting intervention, enabling a maximization of the seismic capacity of the building. With the proposed strategy, this optimized strengthening can be preliminarily quantified in terms of activated hysteretic energy, damping contribution, and behaviour factor, as summarized in Section 6.4. The outcomes from these first analyses will finally constitute the basis for the extensive numerical analyses on three case-study buildings (Chapter 7), in which the optimization strategy will be further validated.

6.2 Estimating energy dissipation and damage

6.2.1 General

In order to better clarify the impact of well-retrofitted and dissipative timber diaphragms on the structural response to earthquakes of existing URM buildings, an extension of the concept of seismic capacity is needed. A common way to assess in detail the seismic behaviour of URM buildings is by performing nonlinear incremental dynamic analyses, often resulting in PGA vs. (inter-storey) displacements curves (see Chapter 2). However, the use of PGA only can lead to not complete conclusions on the seismic capacity of a building [28]: it is important, when evaluating the best retrofitting option, to extend this concept in such a way that damage and potential earthquake duration are also considered [193]. In fact, two earthquakes with the same PGA but with different durations can cause different effects and damage on a structure (Section 2.3). Furthermore, the retrofitting of the diaphragms has direct consequences in changing the fundamental period of the building, and thus the amplification effect on the structure.

Therefore, for a more detailed seismic assessment and retrofitting of existing URM buildings, other parameters have to be taken into account, having a better correlation with damage and load duration influence on the structures. In order to define these indicators, it is worth recalling how the energy imparted by an earthquake is absorbed or stored in a structure [194].

6.2.2 Energy components in linear elastic SDOF systems

In Chapter 2, the dynamic response of a linear elastic SDOF system subjected to seismic excitation was presented (Eqs. 2.1-2.2):

$$\ddot{x} + 2\omega_n\xi\dot{x} + \omega_n^2x = -\ddot{x}_g \quad (6.1)$$

Starting from Eq. 6.1, the work (per mass unit and relatively to the ground) performed by the system can be calculated as [194]:

$$\int \ddot{x}dx + 2\omega_n\xi \int \dot{x}dx + \omega_n^2 \int xdx = - \int \ddot{x}_gdx \quad (6.2)$$

The equation above can be rewritten by identifying the various energy contributions as:

$$E_k + E_d + E_e = E_i \quad (6.3)$$

Therefore, the sum of the kinetic energy E_k , the energy given by viscous damping E_d , and the elastic energy E_e , equals the total energy E_i imparted by the earthquake.

In order to identify the role of the single equation members, consider a simple example of an SDOF system, initially undamped, with a mass of 30000 kg and a stiffness of 11667 N/mm, subjected to the 2018 Zeerijp induced earthquake signal [195] (Fig. 6.1a). The response is shown in Fig. 6.1b-c: as can be noticed, the input energy equals the sum of the kinetic and elastic energy, which are always out of phase, and at the end of the earthquake the oscillation continues due to the absence of damping. The energy is thus never accumulated in the system, since it is linear and undamped, but is alternatively exchanged in the form of kinetic and elastic energy.

If damping is also present in the considered SDOF oscillator, with for instance $\xi = 0.05$, then viscous energy is progressively stored in the system, and the damping softens the vibrations of the oscillator after the earthquake strong motion ends. Therefore, in this case, at the end of the seismic event the imparted energy is equal to the viscous one, while during the earthquake part is stored because of damping, and part exchanged between kinetic and elastic energy (Figure 6.2).

6.2.3 Energy components in nonlinear SDOF systems

After examining linear elastic SDOF system, the further contribution of the inelastic energy dissipated through nonlinearities is now considered. The equation is thus rewritten in a more general form, referred to a nonlinear system in which hysteretic cycles take place after yielding of the structural material. Under this hypothesis, the energy balance becomes:

$$E_k + E_d + E_e + E_{hys} = E_i \quad (6.4)$$

where E_{hys} is the hysteretic energy. This additional contribution is another important source of energy absorption, besides the one linked to viscous damping. This is also a reason why hysteretic energy is often associated to an equivalent damping ratio accounting for this further dissipative capacity [32, 167], as was also done for the timber diaphragms characterization (Section 4.3.6). Figure 6.3 shows the dynamic response of a nonlinear system made of elasto-plastic S235 steel, with a mass of 30000 kg and an initial stiffness of 10334 N/mm, subjected to the 2018 Zeerijp earthquake, scaled up to plasticization of the system. As can be observed, in this case the system stores the input energy in the form of viscous and deformation hysteretic energy, while the recoverable contributions remain those of elastic (when the oscillations are below yielding of steel) and kinetic energy.

At the end of the ground motion, therefore, a large part of the energy imparted by the earthquake is dissipated by the system through nonlinear hysteretic cycles, connected to a progressive yielding and deterioration in the material. From the presented graphs, it can be noticed how the duration of the earthquake can play a crucial role in the level of damage underwent by a structure [28]. Hence, an extension of the current seismic assessment methods based only on PGA would allow to characterize more completely the optimal retrofitting of existing buildings, from a force-based design to an energy-related perspective. To make this transition possible, a parameter identifying the structural response to earthquakes has to be considered, and namely the spectral velocity S_v (Section 2.3).

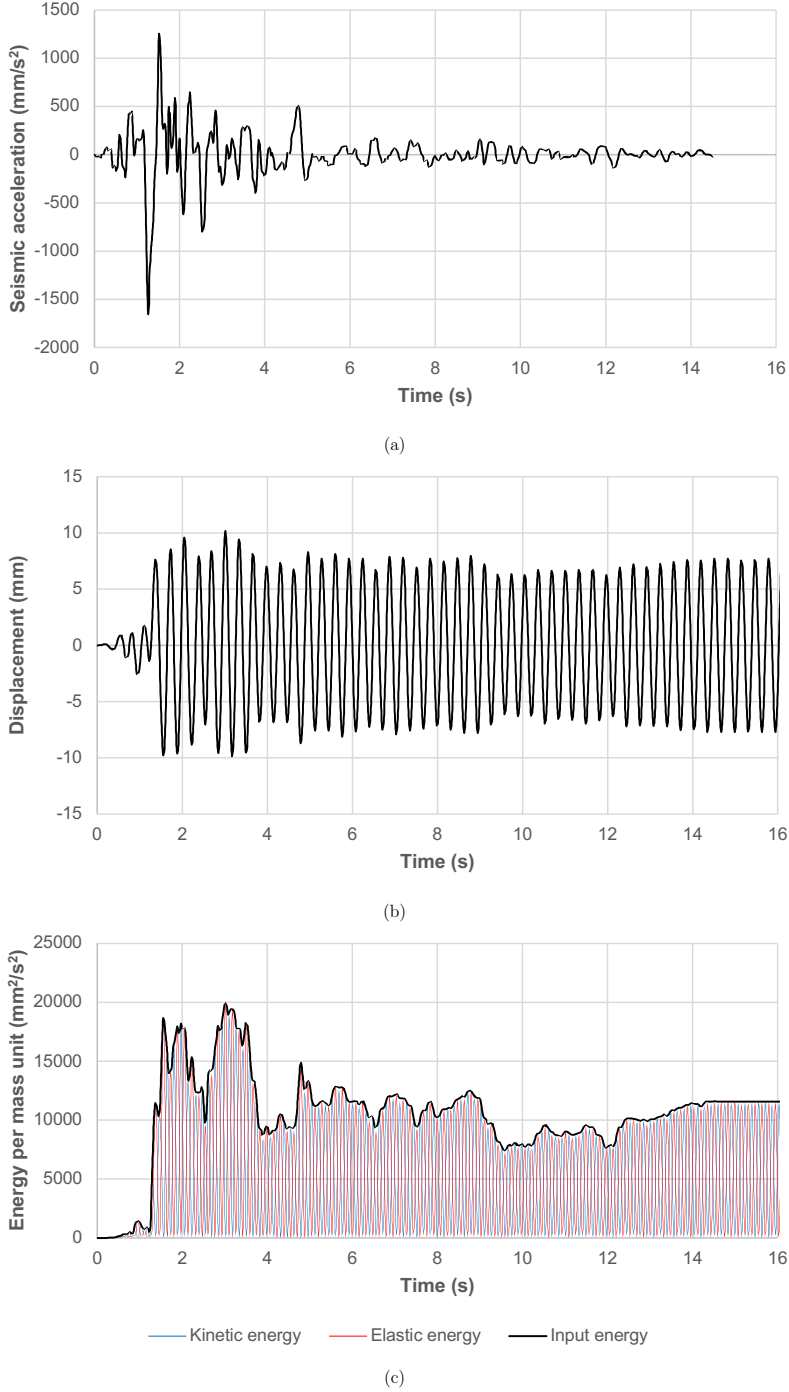


Figure 6.1: Dynamic response of an linear elastic, undamped SDOF system subjected to the 2018 Zeerijp induced earthquake: seismic input acceleration \ddot{x}_g (a); displacement time-history of the system x (b); overview of the single energy components (c).

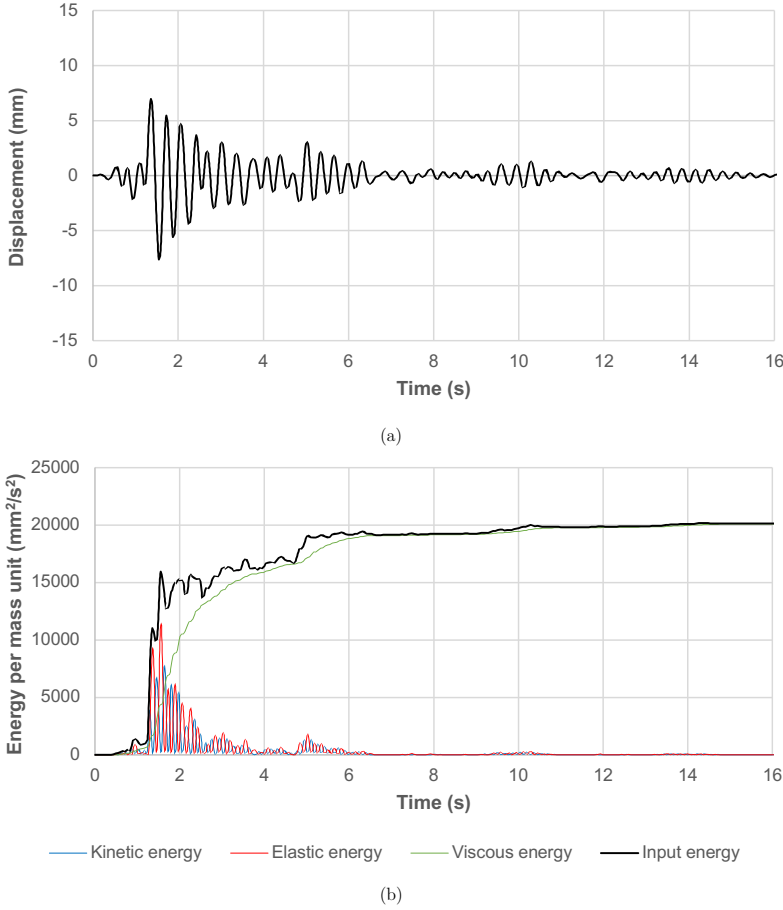


Figure 6.2: Dynamic response of a linear elastic, damped elastic SDOF system ($\xi = 0.05$) subjected to the 2018 Zeerijp induced earthquake signal of Fig. 6.1a: displacement time-history of the system x (a); overview of the single energy components (b).

6.2.4 The role of spectral velocity

The spectral velocity S_v allows to identify the energy contribution of earthquakes, from both the *seismic demand* and the *structural response* point of view.

Considering the seismic demand, HOUSNER [196] gave a definition of the maximum input energy of an elastic SDOF system on the basis of the pseudo-velocity spectrum. In fact, the spectral velocity reflects the energy demand per mass unit E_v of an elastic SDOF system as follows [28, 196]:

$$E_v = \frac{1}{2} S_v^2 \quad (6.5)$$

Therefore, this parameter can be used to estimate the earthquake *damaging potential* from an energy perspective, because the pseudo-velocity spectrum constitutes the lower bound of the input energy spectrum [28, 194]. In fact, in a linear, undamped SDOF

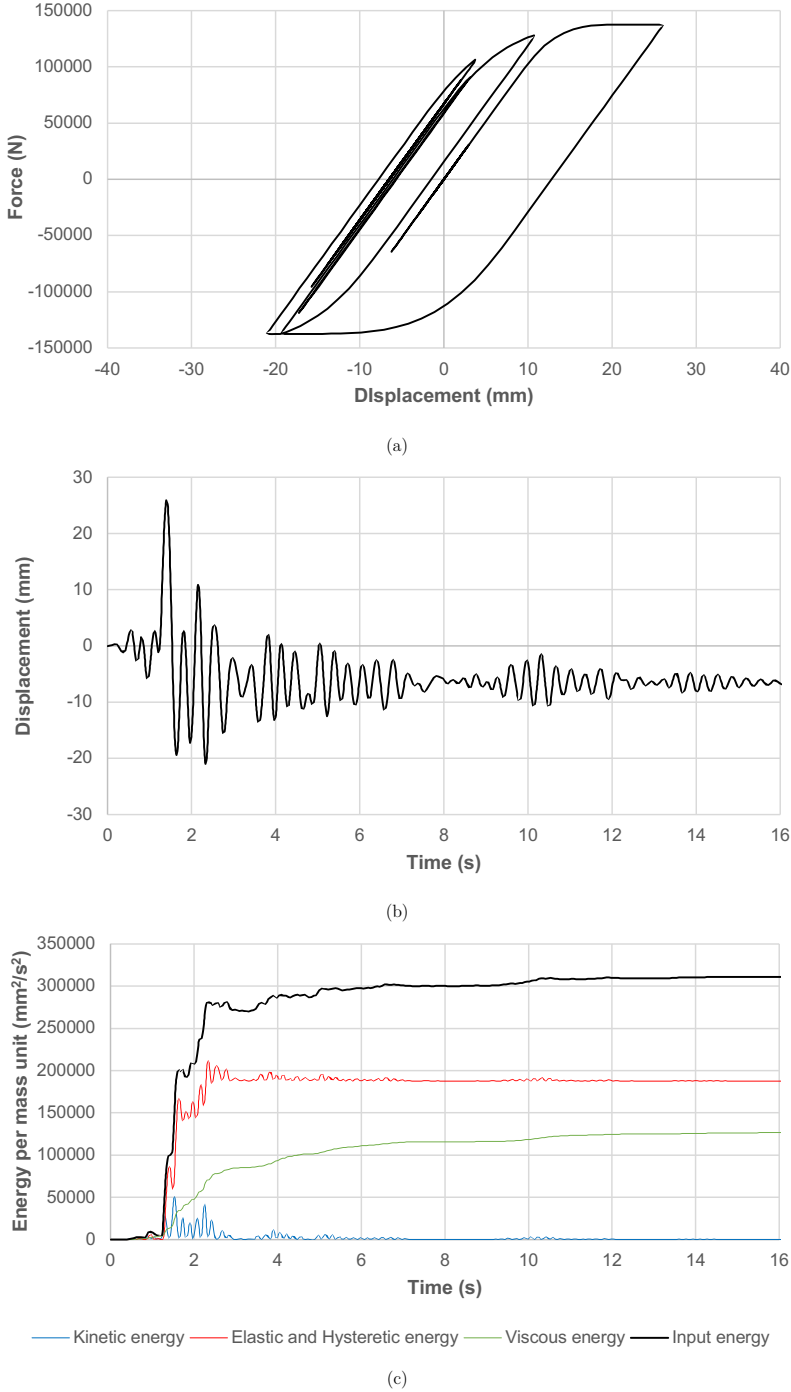


Figure 6.3: Dynamic response of a damped nonlinear SDOF system ($\xi = 0.05$) subjected to the 2018 Zeerijp earthquake of Fig. 6.1a amplified up to plasticization of the system: load-displacement response (a); displacement time-history of the system x (b); overview of the single energy components (c).

system, such as that analyzed in the previous section, the input energy can only be transferred in the structure by means of a continuous exchange of kinetic and elastic energy, which are directly related to the square of spectral velocity. The presence of other sources of energy absorption in the structure (e.g. viscous or hysteretic) can only increase the input energy that can be imparted to the system, and this is the reason why with the square of spectral velocity the lower bound of input energy can be described.

As an example for this concept, it is worth recalling that in Section 2.3.3 it has been shown how relatively short, high-frequency earthquake signals (such as induced ones) can cause much less damage compared to long, low-frequency ground motions (such as tectonic ones), despite having similar PGA values. With the use of S_v^2 , an already clearer picture can be obtained: as an example, Fig. 6.4 compares the 2018 Zeerijp induced earthquake [195] (14 s duration, $M_L = 3.4$) and the 1980 Irpinia tectonic earthquake [170] (86 s duration, $M_L = 6.9$) in terms of acceleration and velocity response spectrum: the PGA of both signals is similar, but the difference in frequency content highlights a way higher potential damaging effect of the Irpinia earthquake through the lower-bound input energy spectrum, represented by S_v^2 (Fig. 6.4b). The increased damaging potential of Irpinia earthquake is in fact also confirmed by the large difference in magnitude with respect to the Zeerijp induced seismic event.

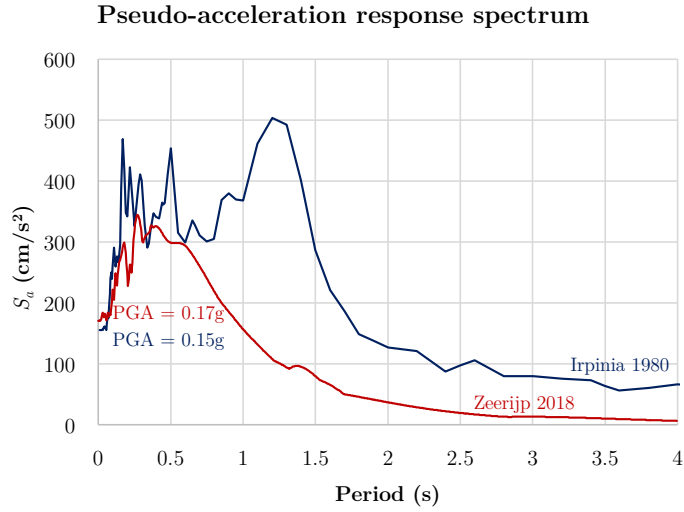
The former example already highlighted the potential use of S_v^2 for estimating the lower bound of input energy from the demand side. However, this indicator has an important meaning from the structural response point of view as well. Following the definitions given in Section 2.3, the maximum elastic energy (per mass unit) of a linear SDOF system, linked to the maximum solicitation (and, thus, potential damage) during the earthquake is [32]:

$$E_e = \frac{1}{2} \frac{k}{m} x_{max}^2 = \frac{1}{2} \omega_n^2 x_{max}^2 = \frac{1}{2} S_v^2 \quad (6.6)$$

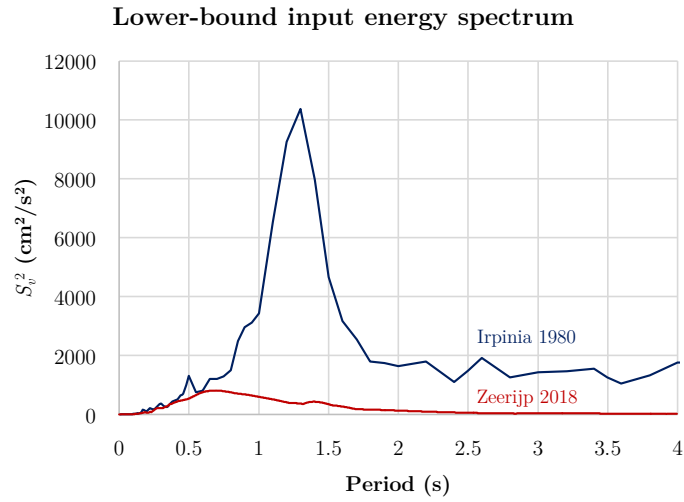
Thus, the spectral velocity appears as an immediate, intuitive quantity for identifying the deformation energy of the system, which can be directly linked to structural damage.

As an example for this, consider the three basic URM buildings with timber diaphragms shown in Fig. 6.5. These structures can be considered as simple nonlinear SDOF systems. If, firstly, a pushover analysis (Section 2.3) is performed for the building in its existing configuration, with a very flexible floor and poor connections to the walls (Fig. 6.5a), the out-of-plane (OOP) collapse of the walls is soon reached, without involving other structural components in the resisting process. Yet, a positive aspect is that the period of this building is high, because of the low stiffness of the floor, and this might correspond to a slightly reduced amplification of the seismic signal.

If now a retrofitting intervention on the floor (Fig. 6.5b), such as the cast of a concrete slab, is performed, the diaphragm becomes infinitely stiff. This strengthening method has been widely applied in the past to enhance the box-like behaviour of URM buildings (Section 2.7). In this case, the seismic response changes from out-of-plane to in-plane (IP) dominated; the maximum base shear F_u is reached, but with limited displacement capacity (d_u) and a lower fundamental period compared to the previous case. If, finally, an optimized dissipative retrofitting of the diaphragms is applied (Fig. 6.5c), it could be possible to keep a high displacement capacity without causing out-of-plane collapse of the walls, and at the same time to involve at a later stage the in-plane capacity of walls, because of the beneficial, dissipative effect of the diaphragms.



(a)



(b)

Figure 6.4: Comparison between the 2018 Zeerijp earthquake and the 1980 Irpinia earthquake in terms of pseudo-acceleration (a) and lower-bound input energy S_v^2 (b) response spectra.

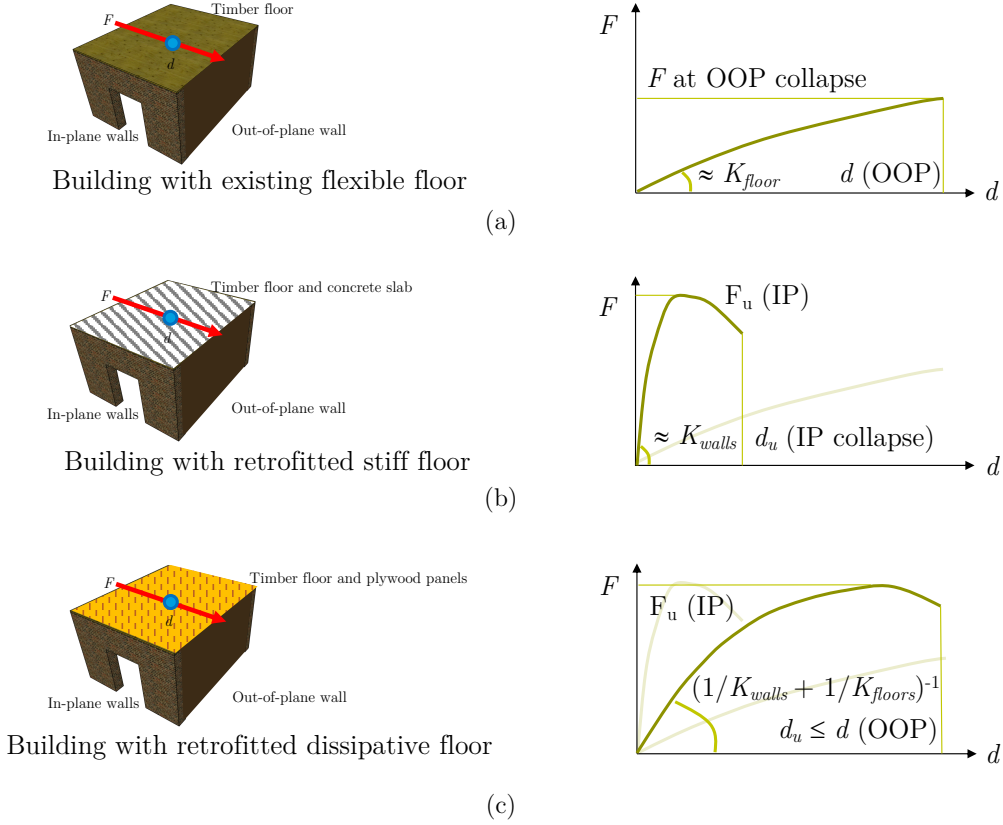


Figure 6.5: Example of pushover analyses on basic URM buildings with a flexible (a), retrofitted stiff (b), and retrofitted dissipative (c) timber floor. The control node corresponds to the centre of mass of the floor.

Therefore, the goal of an optimal retrofitting intervention is to retrieve from the structure the maximum base shear, while achieving the maximum displacement capacity within walls drift limits. Maximizing these two parameters also means maximizing the (equivalent) deformation energy of the system, which is directly correlated with the pseudo-velocity. When the (equivalent) deformation energy is combined with hysteretic energy and nonlinearities, the prediction is not as immediate as in the former equivalence anymore. However, S_v can still represent a good indicator for the maximum potential energy dissipation that could be retrieved from a system [197], as shown in the next section.

6.2.5 Predicting seismic energy dissipation of SDOF systems with spectral velocity

This section presents the procedure for estimating the energy dissipated during an earthquake for linear elastic SDOF system, according to NURTUĞ and SUCUOĞLU [197]. This formulation allows to account for seismic load duration and will be, then, extended

for analyzing the seismic response of MDOF URM structures. The proposed analytical procedure starts with the expression of the energy dissipated by a viscous damper under harmonic excitation E'_d :

$$E'_d = \int_0^{T_n} f_d dx \quad (6.7)$$

where $f_d = c(du/dt)$ is the damping force, $c = 2\xi m\omega_n$ is the viscous damping coefficient, and x is the harmonic displacement response function expressed by:

$$x = \varrho \sin(\bar{\omega}t) \quad (6.8)$$

In the above expressions, ω_n and $\bar{\omega}$ are the natural and excitation frequencies, respectively, T_n is the natural period, and ϱ is the harmonic displacement amplitude. By substituting the expression for x into Eq. 6.7 and performing the integration, the energy E'_d dissipated in each cycle can be obtained as:

$$E'_d = 2\pi\xi m\omega_n \bar{\omega} \varrho^2 \quad (6.9)$$

When a linear SDOF system is subjected to an earthquake ground motion, it is mainly excited by those frequencies close to its natural frequency. Consequently, its response distribution in the frequency domain exhibits significant amplification around its natural frequency. In the former equation, the excitation frequency can therefore be replaced by the natural frequency of the system [197]. Hence:

$$E'_d = 2\pi\xi m\omega_n^2 \varrho^2 \quad (6.10)$$

This is the energy dissipated by the system in a single cycle, therefore the total energy E_d absorbed under n_{cyc} cycles can be represented as:

$$E_d = \sum_{i=1}^{n_{cyc}} E'_{d,i} = 2\pi\xi m\omega_n^2 \sum_{i=1}^{n_{cyc}} \varrho_i^2 \quad (6.11)$$

Alternatively, the expression can be rewritten as follows:

$$E_d = 2\pi\xi m\omega_n^2 n_{cyc} (\bar{\varrho}^2 + \sigma_{\varrho}^2) \quad (6.12)$$

in which $\bar{\varrho}$ is the average value of all displacement amplitudes, and σ_{ϱ} is their standard deviation. Considering the maximum (or spectral) displacement S_d , and defining:

$$\alpha = \frac{\bar{\varrho}}{S_d} \quad (6.13)$$

$$\beta = \frac{\sigma_{\varrho}}{S_d} \quad (6.14)$$

the former equation can be reformulated as:

$$E_d = 2\pi\xi m\omega_n^2 n_{cyc} S_d^2 (\alpha^2 + \beta^2) \quad (6.15)$$

The quantity $S_d^2(\alpha^2 + \beta^2)$ denotes the mean value of the squares of response displacement amplitudes:

$$(\alpha^2 + \beta^2) = \frac{(\varrho^2)_{average}}{S_d^2} \quad (6.16)$$

After analyzing an extensive database of ground signals, NURTUĞ and SUCUOĞLU [197] noticed that the non-dimensional parameter $\alpha^2 + \beta^2$ for SDOF systems is not sensitive to damping ratio or to ground motion type and duration, but only to period. Based on this outcome, an equation was proposed for estimating this parameter [197]:

$$\alpha^2 + \beta^2 = 0.25T_n^{1/3} \quad (6.17)$$

With regard to the number of response displacement cycles n , this can be expressed as the ratio of response duration and vibration period T_n . Yet, not the whole duration of the seismic response is relevant for energy dissipation, therefore an effective response duration should be identified.

TRIFUNAC and BRADY [198] defined the earthquake strong motion duration Δt_e as the time interval where 90% contribution to the accelerogram intensity takes place. Based on this, an analogous energy-related quantity can be defined as Δt_e^r , i.e. the duration within which 90% of the energy dissipation takes place [197]. Hence, the number n_{cyc} of displacement cycles during the effective response duration is:

$$n_{cyc} = \frac{\Delta t_e^r}{T_n} = \omega_n \frac{\Delta t_e^r}{2\pi} \quad (6.18)$$

From the extensive analyses conducted in [197], it appeared that the effective response duration increases with vibration period, but decreases with the amount of damping. A simple relationship was formulated to express the variation of the effective response duration with the effective strong motion duration, the vibration period, and the damping ratio:

$$\Delta t_e^r = \Delta t_e + 3.3 \frac{T_n}{6\xi} \quad (6.19)$$

This relationship satisfies several physical limitations, such as that the effective response duration should approach the effective strong motion duration for both short-period systems and systems with high damping, and it approaches infinity for undamped systems which dissipate no energy. Finally, considering all previously defined quantities, and remembering that $\omega_n^2 S_d^2$ equals the square of the spectral pseudo-velocity S_v^2 , the energy dissipated by the system can be calculated as:

$$E_d = \xi m \omega_n \Delta t_e^r S_v^2 (\alpha^2 + \beta^2) \quad (6.20)$$

Although the damping ratio appears explicitly in the former equation, the dissipated energy is relatively insensitive to it, because an increase in damping corresponds to a decrease in pseudo-velocity and effective duration [197]. Furthermore, since Δt_e^r refers to 90% of the dissipated energy, the derived expression should be multiplied by the factor 10/9.

It should be noticed that the aforementioned expressions were derived for SDOF linear systems, but the formulation can be extended also for MDOF nonlinear systems.

The extension of Eq. 6.20 for MDOF systems can be carried out analogously to the principles of pushover analysis (Section 2.3): if an MDOF building is sufficiently

regular, it can be transformed into an equivalent SDOF system by means of a factor Γ_n (Eq. 2.14). Following this assumption, the building can be characterized by means of its (first-mode) pseudo-velocity $S_v^* = S_v/\Gamma_n$. Thus, the energy estimation for MDOF systems can be obtained in a simplified way by reformulating for an equivalent SDOF system Eq. 6.20 as follows [199]:

$$E_d = \xi m^* \omega_n \Delta t_e^r \Gamma_n^2 S_v^{*2} (\alpha^2 + \beta^2) \quad (6.21)$$

When now nonlinearities are taken into account, it is important to notice that Eq. 6.20 is insensitive to damping ratio. On the contrary, the most relevant quantity determining E_d is the fundamental period T_n , on which all other quantities depend. Since T_n progressively increases because of nonlinearities and damage (e.g. strength and stiffness degradation), it is in principle not possible to define a single precise value of dissipated energy (also keeping in mind the intrinsic uncertainties in the equations for Δt_e^r and $\alpha^2 + \beta^2$). Yet, a range in which the nonlinear system will fall can still be identified, depending on the ductility of the system at a near-collapse situation.

This strategy is particularly advantageous, because besides predicting the dissipated energy, it allows to compute the behaviour factor of buildings (Section 2.3). Although the behaviour factor is meant for linear analyses with the lateral force method, it has an important advantage, because it allows to quantify the potentially beneficial effect of dissipative timber diaphragms by means of a single parameter. The behaviour factor q for URM buildings is linked to the ductility μ by means of the following expression [185]:

$$q = \sqrt{2\mu - 1} \quad (6.22)$$

In the same way, an effective period $T_{n,eff}$ of a system *linearly equivalent* to the nonlinear one at collapse can be expressed as a function of the ductility and the initial period T_n , independently of the type of hysteretic behaviour [200, 201]:

- For $1 < \mu < 4$:

$$T_{n,eff} = [0.167(\mu-1)^2 - 0.031(\mu-1)^3 + 1] T_n \quad (6.23)$$

- For $4 \leq \mu \leq 6.5$:

$$T_{n,eff} = [0.283 + 0.129(\mu-1) + 1] T_n \quad (6.24)$$

- For $\mu > 6.5$:

$$T_{n,eff} = \left\{ 0.89 \left[\sqrt{\frac{\mu - 1}{1 + 0.05(\mu - 2)}} - 1 \right] + 1 \right\} T_n \quad (6.25)$$

It is expected that the presence of dissipative timber diaphragms can increase the ductility (and thus the behaviour factor) of URM buildings. Therefore, before performing extensive numerical analyses on the three case-study buildings (Chapter 7), a preliminary study is conducted in this chapter on basic SDOF URM structures, to evaluate the potential of this characterization in terms of spectral velocity and energy prediction, and to quantify the increase in E_d , μ and q given by dissipative diaphragms.

6.3 Analyses on SDOF URM buildings

6.3.1 General

This section presents the results of preliminary numerical analyses performed to validate the previously described criteria for determining the seismic capacity of URM buildings from an energetic point of view, so that the optimal retrofitting intervention choice is not driven by a PGA-based assessment only. The approach was validated with two basic SDOF URM buildings:

1. A building with Dutch features, subjected to induced earthquakes;
2. A building with Italian features, subjected to tectonic earthquake.

The use of earthquake types and building properties according to different contexts allows for a generalization of the criteria for an optimal retrofitting. In particular, the building with Italian features presented thicker walls and timber floors built with more massive structural elements, thus an increased seismic mass with respect to the structure representative for the Dutch context.

For both cases, the macro-element modelling approach for masonry walls and timber diaphragms was adopted in *OpenSees* software (Section 5.6.4). In the next sections, the characteristics of the buildings and the adopted modelling strategy are presented, as well as the results from the numerical analyses.

6.3.2 Characteristics of the analyzed SDOF URM buildings

The extension of the approach for evaluating seismic capacity for URM buildings from an energy perspective was validated in the two basic SDOF structures shown in Fig. 6.6. As can be noticed, the adopted macro-element approach for both floors and walls was implemented in *OpenSees* according to specific experimental results on structural components:

- For building A (Fig. 6.6b), representing the Dutch context with induced earthquakes, the in-plane behaviour of the floor was calibrated based on the response of sample DFpar-1s (Section 5.4.2), while the in-plane walls featured the properties of specimen TUD_COMP-22 (Section 4.5) [202], thus with a rocking-related behaviour;
- Building B (Fig. 6.6c), representing the Italian context with tectonic earthquakes, presented the same properties and modelling strategy as the URM structure analyzed in SCOTTA et al. [10]: the in-plane response of the diaphragms was based on the findings of PIAZZA et al. [15], while the walls had characteristics calibrated on the in-plane tests of MAGENES and CALVI [77], thus with a diagonal shear-related response.

In both cases, for these first analyses, the out-of-plane walls were not modelled, but the out-of-plane failure was considered when the drift $d_{oop} < 2.0\%$, according to Section 5.6.3. On the contrary, the in-plane response of masonry walls was modelled in detail: in the case of building A, the walls underwent a rocking behaviour, meaning that the vertical springs of each macro-element were firstly activated; in building B,

the geometry of the piers and the larger pre-compression on them led to a shear diagonal failure, involving the corresponding springs. The constitutive laws of the macro-elements representing the masonry were based on the experimentally obtained strength and displacement capacity, which also corresponds to the in-plane drift limits for rocking and shear provided in Section 5.6.2. For representing the in-plane response of timber diaphragms, the **Pinching4** material was implemented in their macro-elements, while for all nonlinear springs of the walls the **Hysteretic** material model was used [10, 180, 181, 202]. Floor-to-wall connections were considered as continuous for both buildings.

Besides verifying the proposed energy-based approach for characterizing seismic capacity of these buildings, a sensitivity study on the optimal retrofitting intervention for the timber diaphragms was conducted. As noticeable from Fig. 6.6, both buildings feature similarly dissipative diaphragms: thus, to study their beneficial impact, a range of their in-plane stiffness values was considered, while keeping the properties of the walls and the total mass unvaried. In this way, the backbone curve and pinching cycles were progressively scaled, so that for too deformable floors an out-of-plane collapse was more likely, for moderately flexible diaphragms the dissipation could be enabled, and for (very) stiff floors only the linear elastic field was involved. The scaling factors reported in Fig. 6.6 were applied to the in-plane load values, while the displacements were kept fixed; a scaling factor of 1.0 corresponded thus to the reported graphs referred to the floors. Following this sensitivity study, the obtained results will be illustrated as a function of a parameter R representing the ratio between the initial stiffness of the diaphragms and that of all in-plane walls:

$$R = \frac{K_{i, floor}}{\sum_j K_{i, wall, j}} \quad (6.26)$$

Time-history analyses were conducted by subjecting each configuration of the two buildings, corresponding to a value of in-plane stiffness of the timber floor, to seven accelerograms compatible with the expected response spectrum of a specific site, following the provisions of EN 1998 [3]: a total of 42 incremental dynamic analyses up to collapse were performed for each building. Fig. 6.7 shows the seven induced earthquake signals for building A referred to the site of Godlinze [203], while Fig. 6.8 depicts the seven tectonic accelerograms referred to the site of Naples [204], applied to building B. Among the tectonic earthquakes, three largely destructive events are also present: the 1979 Montenegro earthquake [118] (Signal 1), the 1980 Irpinia earthquake [170] (Signal 2), and the 1976 Friuli earthquake [205] (Signal 7). The two chosen sites of Godlinze and Naples are characterized by similar expected values of PGA (around 0.17g), but the damaging potential of the seismic signal can be very different, because of the noticeable variations in (effective) load duration. In this way, with the performed preliminary numerical analyses, it was possible to verify and generalize the extended concept of seismic capacity: the results are reported in the next section.

6.3.3 Results of the numerical analyses

This section presents the results obtained from the numerical sensitivity time-history analyses on buildings A and B, and the energy-based evaluation of seismic capacity for URM buildings.

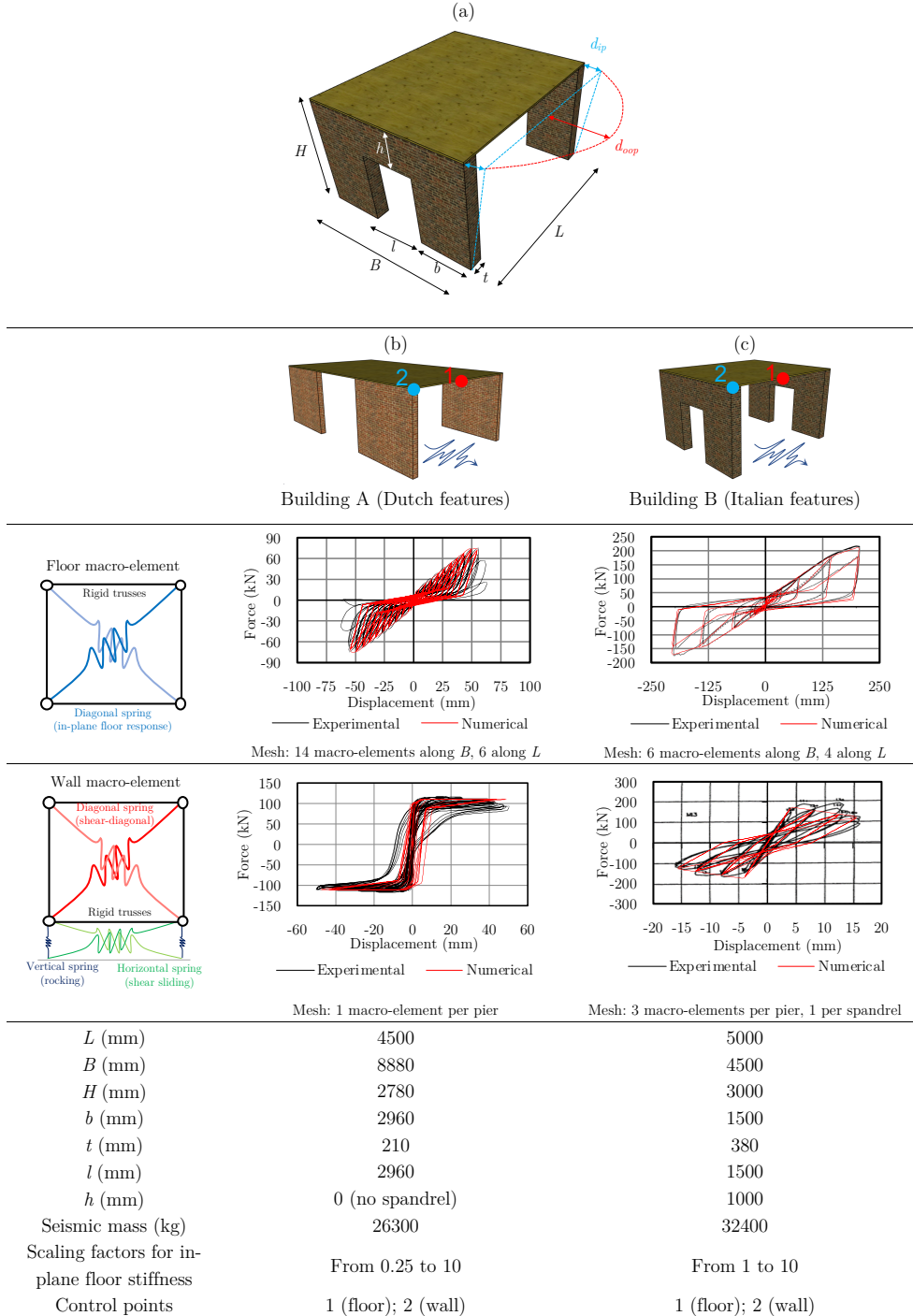


Figure 6.6: Relevant geometrical parameters (a) of the basic case-study buildings with Dutch (b) and Italian (c) features. The main properties of the models, as well as the macro-element calibration, are reported.

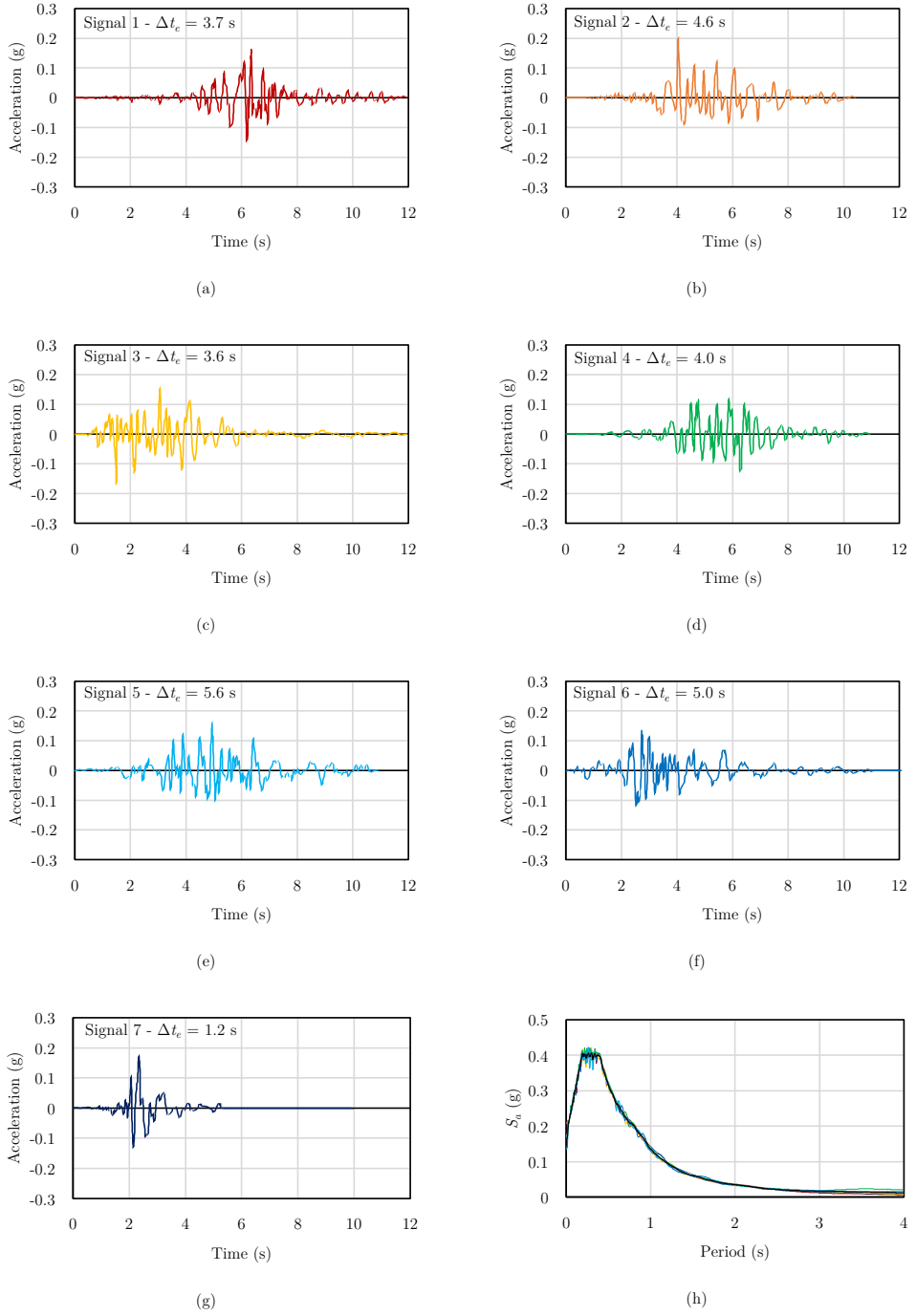


Figure 6.7: Induced seismic signals (a-g) and their average response spectrum (h) [203] adopted for the analyses on building A.

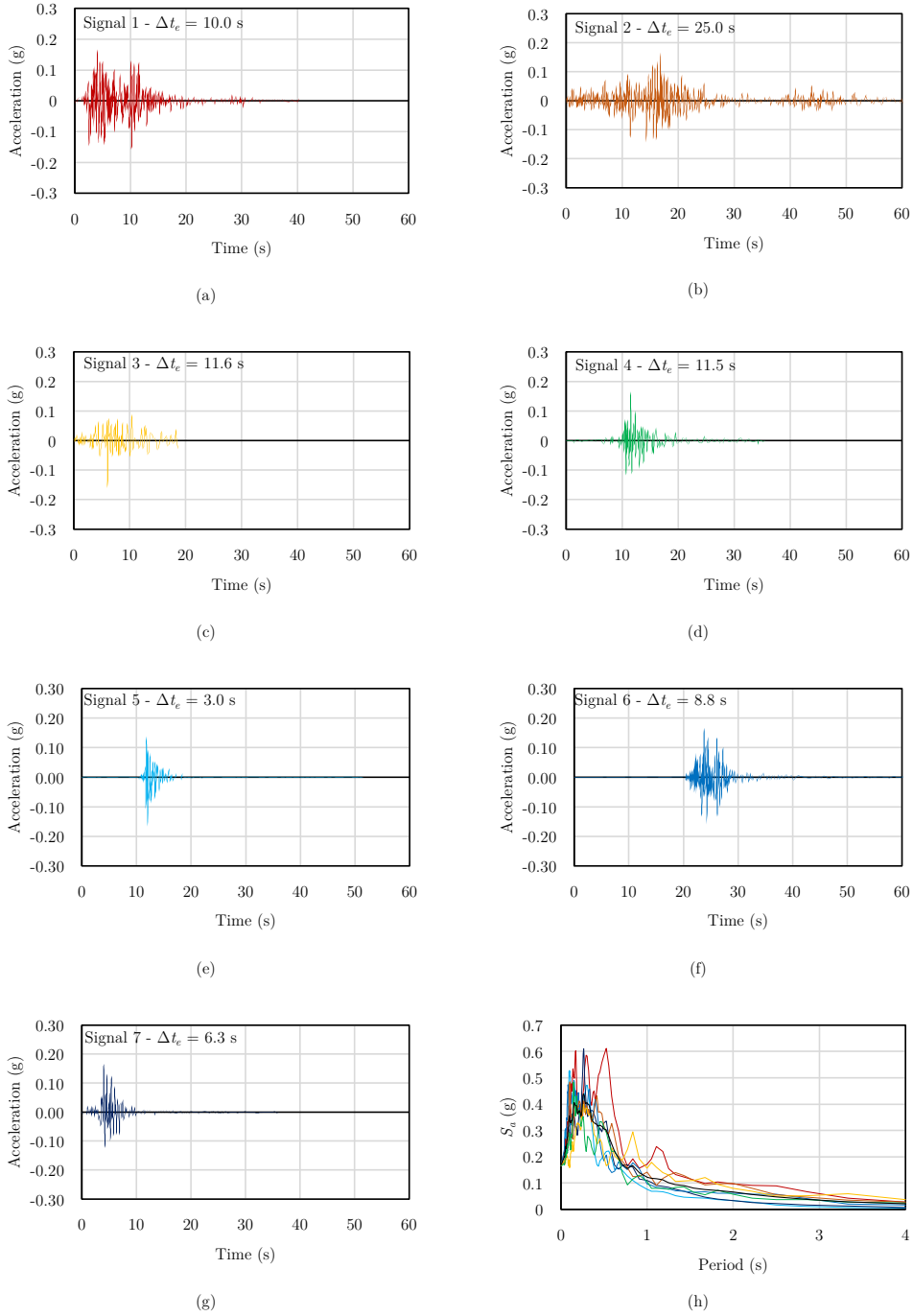


Figure 6.8: Tectonic seismic signals (a-g) and their average response spectrum (h) [204] adopted for the analyses on building B.

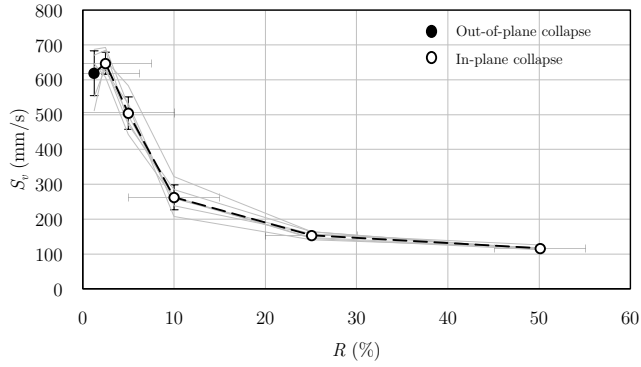
Starting firstly from building A, Fig. 6.9 shows the evolution of spectral velocity S_v , PGA at collapse and estimated behaviour factor q as a function of the stiffness ratio R (Eq. 6.26). As emerged from Section 6.2, S_v is directly linked to deformation energy and dissipation, and the results of the analyses confirm this: as soon as the floor stiffness is sufficient not to cause an out-of-plane collapse, then an in-plane failure of the walls is obtained, but with a large dissipation of the floors, because of their displacement capacity.

Therefore, for these dissipative floors, the maximum S_v is obtained within drift limits, and thus also the hysteretic energy dissipated by the building is maximum (Fig. 6.9a). When, instead, the floors are progressively stiffer and less dissipative, the values of S_v become lower, because this parameter is now linked to the displacement capacity of the walls only, with a smaller (or absent) contribution of the retrofitted timber diaphragms.

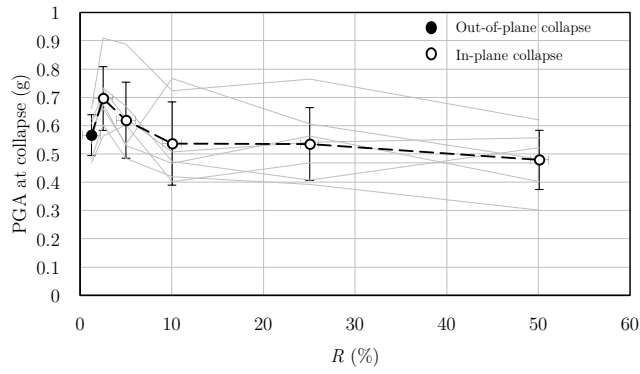
This outcome is reflected also when considering the evolution of the PGA at collapse with R (Fig. 6.9b). Although with this parameter it is not possible to account for load duration (Section 2.3), it can still be useful to identify an optimal retrofitting when comparing similar earthquakes, such as those adopted for the analyses. In fact, although with a larger dispersion compared to pseudo-velocity, the same optimal stiffness ratio between floor and walls can be identified: a URM structure with a retrofitting intervention designed for activating energy dissipation, is able to withstand a seismic signal with a larger imparted acceleration (thus, a potentially more damaging earthquake) with respect to a building with stiff floors.

A further confirmation of the crucial role played by a well-designed retrofitting intervention is provided by the evolution of the behaviour factor q as a function of R (Fig. 6.9c). The behaviour factor was estimated by combining Eq. 6.22 with Eqs. 6.23-6.25, and considering the value of the effective period at collapse $T_{n,eff}$ derived from the numerical analyses; this same period was then used to predict the hysteretic energy of the building, as will be later shown. Table 6.1 reports all values of T_n , $T_{n,eff}$ and q for building A. As can be noticed, the configurations with a stiffer floor are characterized by $q \approx 2.2$, a value that is in line with the recommended behaviour factor range for masonry structure of $1.5 \div 2.5$ [3]. This also means that the energy dissipation is only localized in the piers, because the floors cannot contribute to it due to their limited or absent displacement capacity. On the other hand, with dissipative retrofitted diaphragms, q could even reach a value of 4, provided that the floor is designed for a stiffness that is sufficient to avoid the out-of-plane collapse.

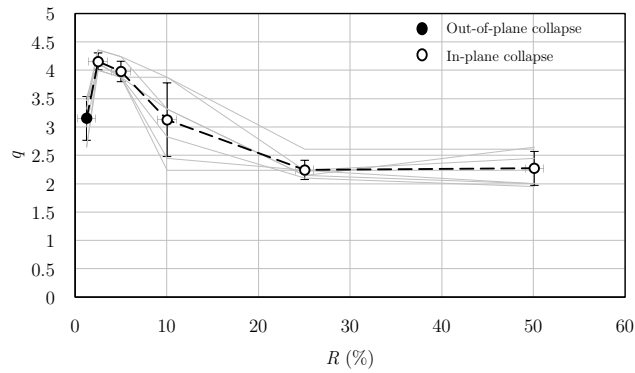
The beneficial effect of dissipative timber floors is also quantifiable in terms of energy and damage, as is noticeable from Fig. 6.10. The dissipative contribution of the floor becomes relevant when their maximum displacement capacity within masonry drift limits is brought into play (Fig. 6.10a), while with stiff floors the (limited) energy dissipated by the building is only provided by the piers. It is interesting to notice that for this basic SDOF building the prediction of the total hysteretic energy at $T_{n,eff}$ by means of Eq. 6.20 is reliable for all R values. Furthermore, since $T_{n,eff}$ increases with ductility, it could be expected that dissipative floors may represent an advantage for URM buildings, because a larger period could often correspond to a progressively lower amplification of the seismic signal, but also to a lower number of cycles n_{cyc} for masonry walls. This latter aspect is clarified in Fig. 6.10b, in which it is noticeable that with a stiff floor not only the energy dissipation is transferred exclusively to masonry



(a)



(b)



(c)

Figure 6.9: Spectral velocity (a), PGA at collapse (b) and estimated behaviour factor (c) as a function of the stiffness ratio R for building A.

Table 6.1: Values of initial period, effective period at collapse, and behaviour factor as a function of R of building A for each signal.

R (%)		1.25	2.5	5	10	25	50
T_n (s)		0.26	0.21	0.15	0.11	0.08	0.07
Signal 1	$T_{n,eff}$ (s)	0.43	0.47	0.33	0.18	0.11	0.10
	q	2.6	4.0	3.9	2.4	2.2	2.2
Signal 2	$T_{n,eff}$ (s)	0.50	0.50	0.36	0.24	0.11	0.09
	q	3.3	4.3	4.2	3.9	2.2	2.0
Signal 3	$T_{n,eff}$ (s)	0.46	0.48	0.33	0.24	0.13	0.11
	q	3.0	4.1	3.9	3.9	2.6	2.6
Signal 4	$T_{n,eff}$ (s)	0.51	0.50	0.36	0.22	0.11	0.09
	q	3.5	4.3	4.2	3.3	2.1	2.0
Signal 5	$T_{n,eff}$ (s)	0.52	0.48	0.33	0.21	0.11	0.11
	q	3.5	4.1	3.9	3.3	2.1	2.6
Signal 6	$T_{n,eff}$ (s)	0.43	0.48	0.33	0.16	0.12	0.11
	q	2.6	4.1	3.8	2.2	2.2	2.4
Signal 7	$T_{n,eff}$ (s)	0.51	0.47	0.33	0.19	0.11	0.09
	q	3.5	4.0	3.9	2.8	2.1	1.9

walls, but the piers have also to undergo a much larger number of cycles (thus with more damage) compared to the case of optimal retrofitting.

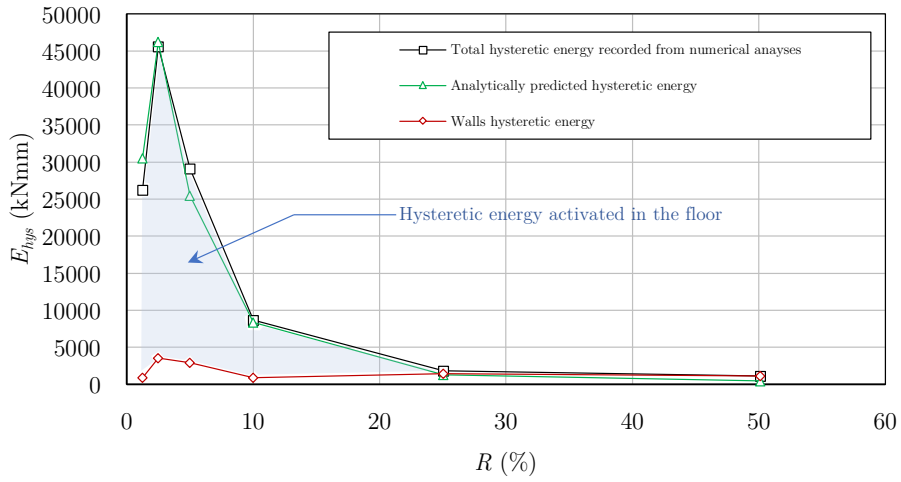
A final consideration is related to the role of PGA and S_v as seismic capacity indicators. In order to assess their reliability in identifying structural damage, both parameters were correlated to hysteretic energy. Because of the wide range of values for the latter quantity, it was chosen to perform the correlation by adopting normalized quantities, where the normalization X_n of a certain parameter X corresponds to:

$$X_n = \frac{X - X_{min}}{X_{max} - X_{min}} \quad (6.27)$$

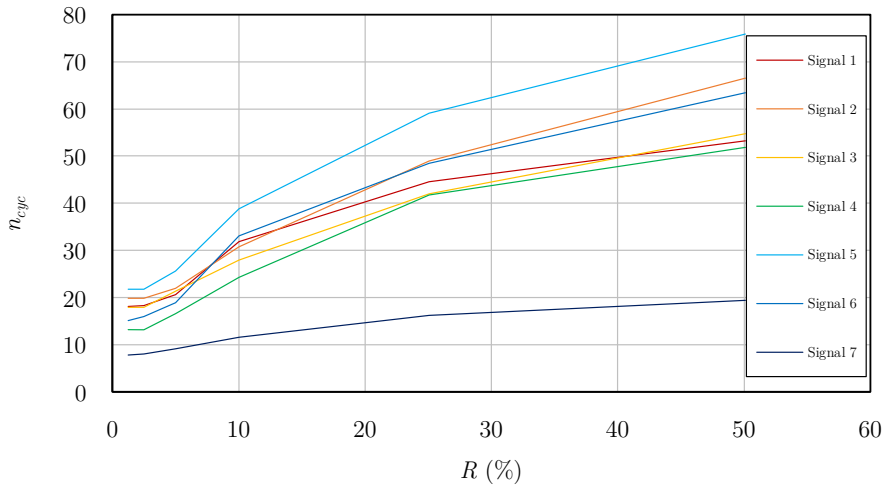
The use of normalized quantities is convenient for this case, also because non-dimensional graphs are obtained.

In Section 2.3 it has been shown that PGA cannot fully capture the energy-related aspects (damage or load duration), and this is further confirmed by the (moderate) correlation shown in Fig. 6.11a, in which normalized PGA values at collapse are plotted against normalized value of hysteretic energy. On the contrary, when the maximum recorded S_v^2 is considered (Fig. 6.11b), the correlation with the hysteretic energy is much clearer, confirming once more that the results of Eq. 6.20 can be extended to nonlinear systems as well.

The aforementioned outcomes can be also observed from the analyses on building B. Fig. 6.12 depicts the evolution of spectral velocity S_v , PGA at collapse and estimated behaviour factor q as a function of the stiffness ratio R . Similarly to building A, it is once more possible to identify an optimal retrofitting intervention from all graphs, corresponding to the maximum displacement capacity of the floor within masonry drift limits. For building B, a larger dispersion in the PGA values at collapse is noticeable, probably because of the wide range of durations of the adopted signals. Nevertheless, it

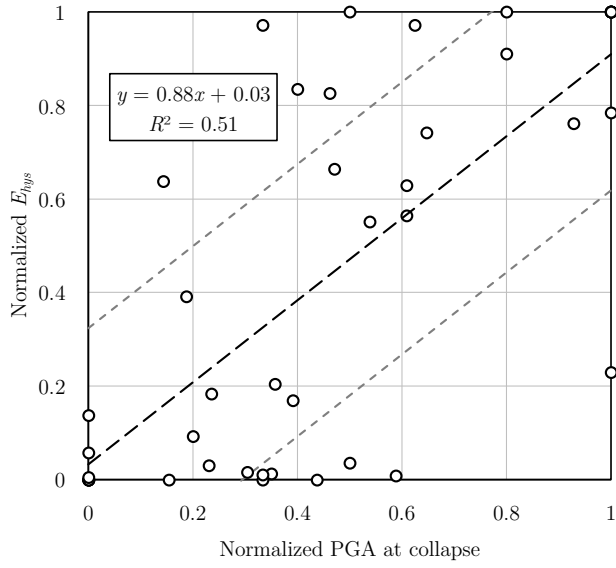


(a)

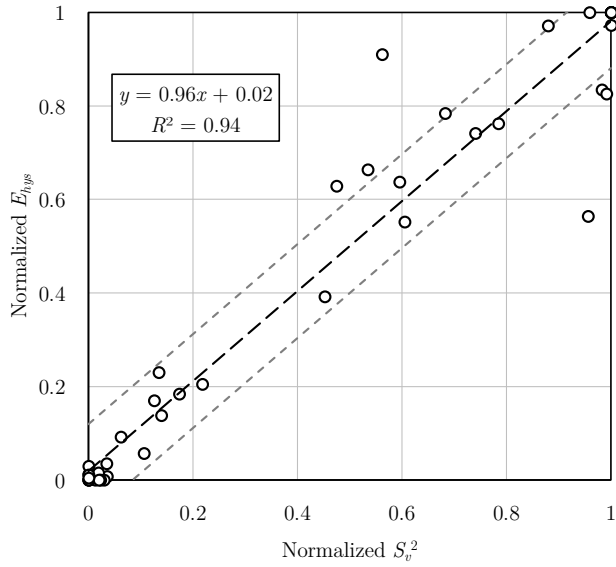


(b)

Figure 6.10: Recorded and predicted hysteretic energy dissipated by the building and its components (a) under signal 4; evolution of the number of cycles sustained by the walls with the increase in floor stiffness (b).



(a)



(b)

Figure 6.11: Correlations between normalized PGA (a) and normalized S_v^2 with normalized hysteretic energy for building A.

Table 6.2: Values of initial period, effective period at collapse, and behaviour factor as a function of R of building B for each signal.

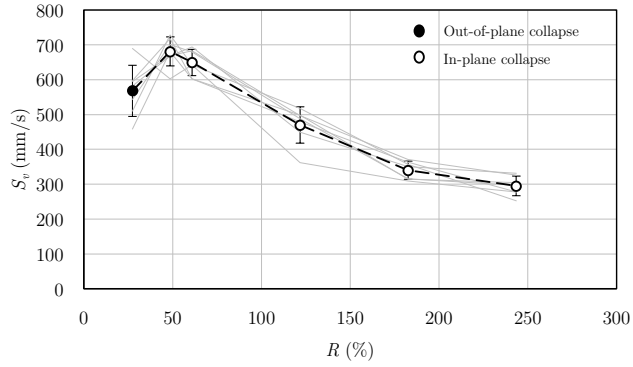
	R (%)	27	49	61	122	183	243
	T_n (s)	0.19	0.16	0.15	0.14	0.13	0.13
Signal 1	$T_{n,eff}$ (s)	0.39	0.38	0.35	0.25	0.17	0.15
	q	3.6	4.3	4.1	3.1	2.0	1.7
Signal 2	$T_{n,eff}$ (s)	0.39	0.36	0.31	0.25	0.22	0.20
	q	3.6	4.0	3.6	3.2	2.6	2.4
Signal 3	$T_{n,eff}$ (s)	0.41	0.38	0.29	0.23	0.17	0.18
	q	3.9	4.3	3.3	2.6	2.0	2.2
Signal 4	$T_{n,eff}$ (s)	0.40	0.39	0.31	0.23	0.17	0.14
	q	3.7	4.4	3.5	2.6	2.0	1.6
Signal 5	$T_{n,eff}$ (s)	0.37	0.39	0.28	0.19	0.15	0.15
	q	3.3	4.4	3.0	2.2	1.7	1.7
Signal 6	$T_{n,eff}$ (s)	0.37	0.36	0.29	0.25	0.21	0.20
	q	3.3	4.0	3.3	3.0	2.4	2.4
Signal 7	$T_{n,eff}$ (s)	0.34	0.32	0.31	0.24	0.22	0.18
	q	3.0	3.5	3.6	2.8	2.6	2.2

is still possible to identify an optimization point, as is noticeable when considering S_v as well.

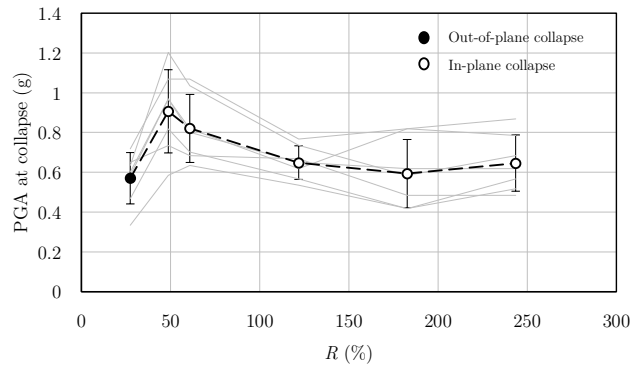
The dissipative role of well-retrofitted diaphragms is also confirmed by the evolution of the estimated behaviour factor with the floor in-plane stiffness, with values very similar to building A ($q \approx 4$ for an optimal strengthening, $q \approx 2$ for stiff floors and dissipation only activated in masonry piers). Table 6.2 reports all values of T_n , $T_{n,eff}$ and q for building B.

The conclusions from the previous case are also confirmed when analyzing the response of building B as a function of R with regard to activated hysteretic energy and damage on walls, expressed in terms of number of cycles. As noticeable from Fig. 6.13a, the optimal floor retrofitting corresponds to a remarkable dissipative contribution compared to configurations with stiff diaphragms. Once more, this larger displacement capacity is also linked to an increased $T_{n,eff}$, and thus to a reduction of the number of cycles to which the system is subjected (Fig. 6.13b), with respect to stiff floors. Although these outcomes confirm what has been obtained with the analyses on building A, an interesting difference is noticeable, in terms of the number of cycles to which the building is subjected: because of the longer duration and larger damaging potential of tectonic signals, n_{cyc} is on average higher for building B, and this is linked to a more extensive damage on walls compared to building A, subjected to induced earthquakes. This again denotes the importance of load duration, which can now be considered in the analyses with the presented approach.

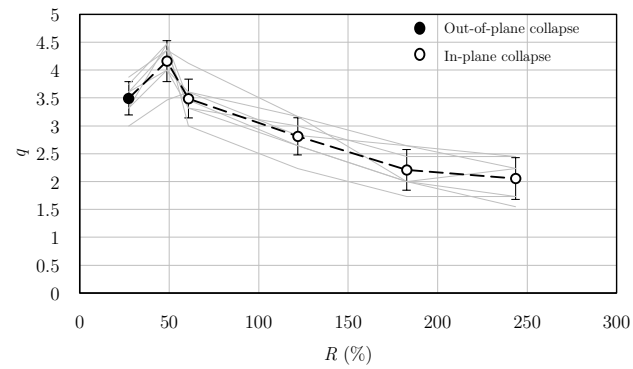
Finally, also for building B it is noticeable that S_v^2 has a much better correlation to hysteretic energy and damage compared to PGA (Fig. 6.14), thus confirming that the energy-based approach is general and suitable for both tectonic and induced earthquakes.



(a)

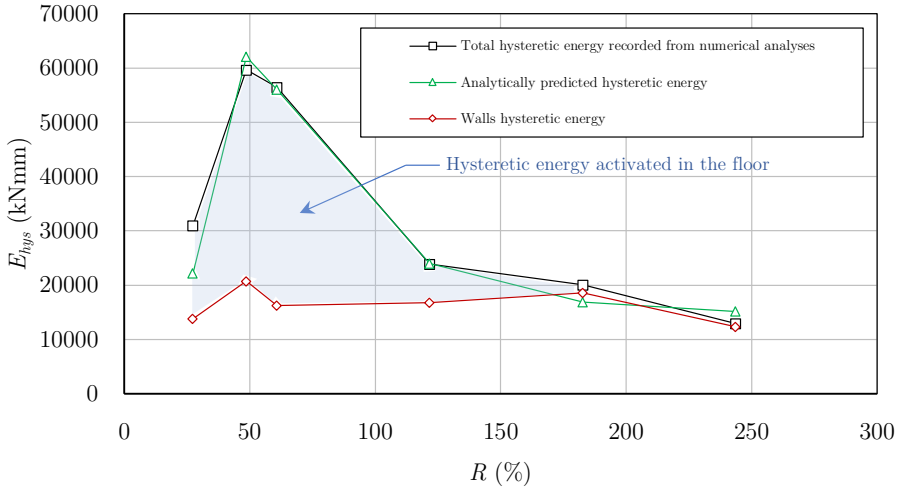


(b)

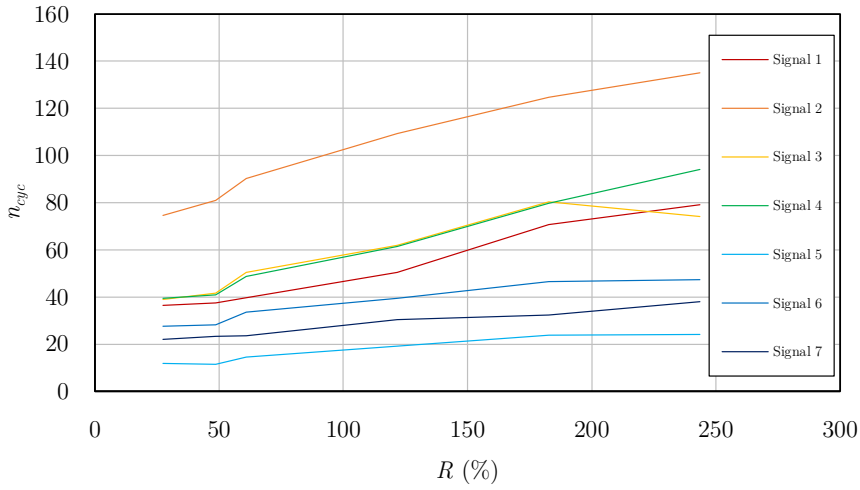


(c)

Figure 6.12: Spectral velocity (a), PGA at collapse (b) and estimated behaviour factor (c) as a function of the stiffness ratio R for building B.

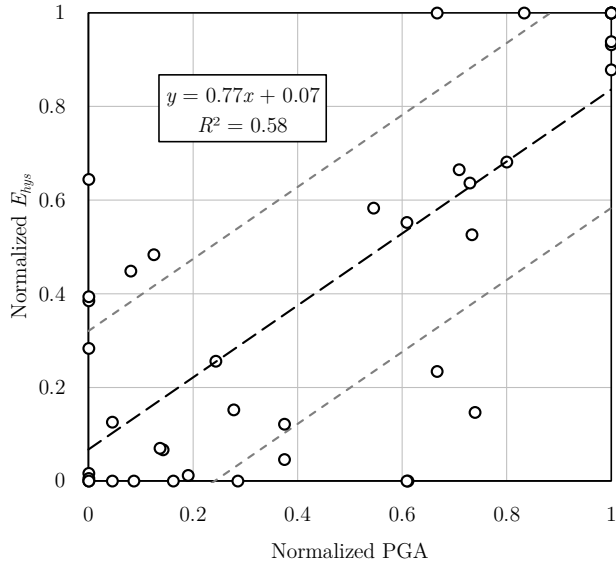


(a)

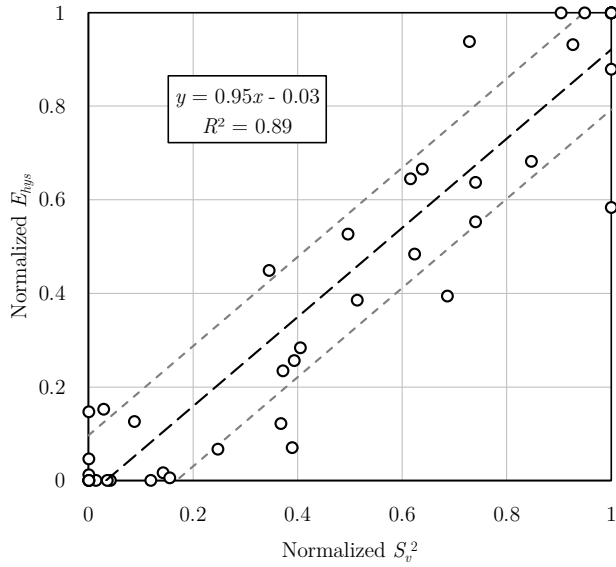


(b)

Figure 6.13: Recorded and predicted hysteretic energy dissipated by the building and its components (a) under signal 1; evolution of the number of cycles sustained by the walls with the increase in floor stiffness (b).



(a)



(b)

Figure 6.14: Correlations between normalized PGA (a) and normalized S_v^2 with normalized hysteretic energy for building B.

6.4 Summary

In the previous numerical analyses it has been shown that an extended and more complete assessment of seismic capacity can be achieved by means of an energy-based approach. In this context, it has been proved that the maximum S_v^2 for a building can be a reliable indicator, which immediately identifies its capacity in terms of maximum base shear and displacement within drift limits, and also maximum stored energy. The spectral velocity allows to better capture the structural response than a ground-motion-related parameter like PGA. Besides, it has been shown that a reliable prediction of hysteretic energy activated in the building by an earthquake can be obtained, provided that the effective strong motion duration of the seismic event is known, and that the buildings are sufficiently regular to be reasonably schematized as (equivalent) SDOF systems [3, 4]. This is possible when analyzing past signals, but could also be applied in practice if, in addition to response spectra, also design seismic durations are provided in the standards, based on available statistical data, and referred to a specific site and return period.

Furthermore, it has been demonstrated that the optimized floor retrofitting is beneficial not only in increasing the energy dissipated by the URM structure, but also in reducing the damage on the walls by decreasing the number of cycles on them. In fact, if the displacement capacity of the floor (within drift limits) is maximized, then also the (effective) period of the structure is maximum, and this can be even more convenient in presence of high-frequency induced earthquakes. Additionally, a light, dissipative strengthening can also be beneficial from an economic point of view, because it can constitute a more affordable intervention compared to hard floor stiffening. Thus, the main features of an optimized strengthening intervention are summarized as follows:

- The optimal retrofitted floor should be moderately flexible, so that in-plane and out-of-plane drift limits are respected, both at near-collapse limit state and at damage limit state.
- The optimized intervention maximizes, within the drift limits, the energy dissipation capacity of the building.
- The optimal floor retrofitting minimizes the damage on the whole system, making the masonry walls subjected to the minimum number of cycles for a certain prescribed earthquake duration.

With a strengthening of timber diaphragms able to activate their energy dissipation, the seismic capacity of URM buildings can therefore be optimized, because the floor can act as a damper, reducing the solicitations transferred to the walls. In fact, as shown in Fig. 6.15a, under the same seismic signal, the building featuring the optimized retrofitted floor displays still an approximately elastic response for the masonry walls. This means that less damage has occurred in the piers, which can thus sustain a more intense signal. The reduction in the forces acting on the structure, and induced by the dissipative floors, can be equivalently expressed by adopting an over-damped response spectrum, reduced by a factor η [3]:

$$\eta = \sqrt{\frac{10}{5 + \xi}} \quad (6.28)$$

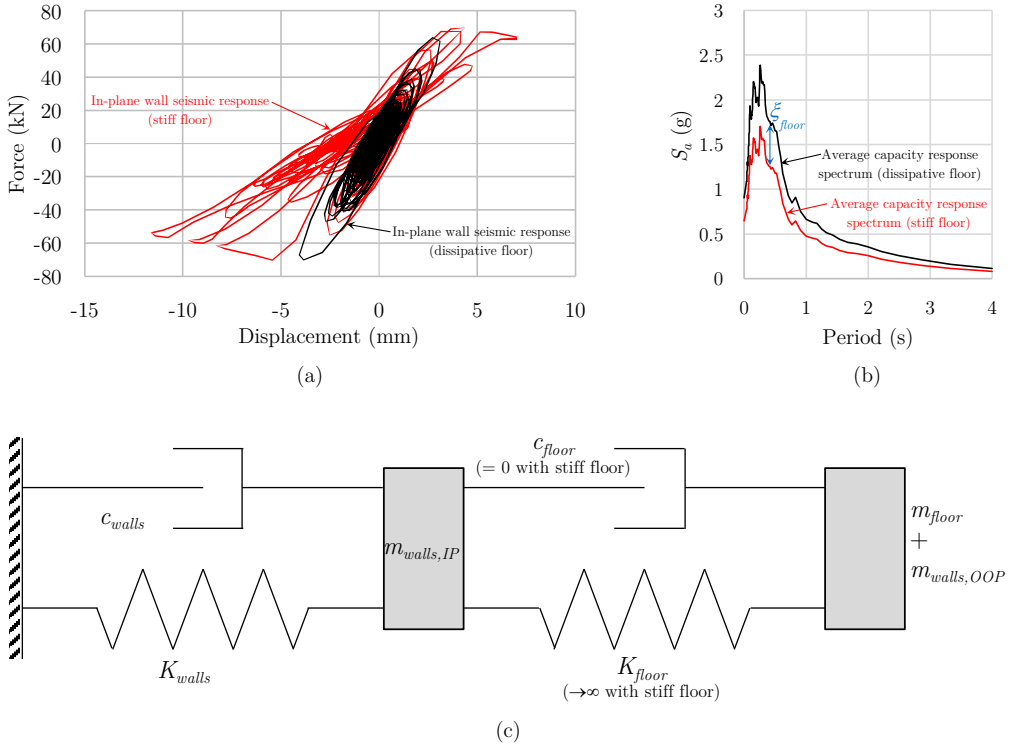


Figure 6.15: (a) in-plane response of a masonry wall of building B under signal 1 at the same amplitude for the optimal configuration with dissipative floor and that with stiff diaphragm: the damping contribution of the well-retrofitted floor is evident; (b) average capacity response spectra of the dissipative and stiff floor configurations; (c) rheological model schematizing the contributions in mass, stiffness and damping of masonry walls and timber floors.

From Fig. 6.15b, it appears that the dissipative floor allows the building to withstand a stronger seismic signal (and associated response spectrum), while the configuration with the stiff floor immediately brings the wall into play, with a corresponding 29% lower capacity response spectrum. The difference between the two capacity spectra is represented by the damping contribution of the retrofitted diaphragm: therefore, if a URM building with dissipative floors is modelled as a structure with stiff diaphragms, and the damping contribution is considered by means of η , that construction will be subjected to an over-damped response spectrum, reduced by 29%. This would correspond to $\eta = 0.71$, and thus to $\xi = 15\%$: it is interesting to notice that this additional damping contribution provided by the diaphragms is fully in line with the value obtained when investigating their dissipative properties (Section 4.3.6).

The dissipative contribution is also recognizable in the higher behaviour factor that characterizes the optimal, dissipative retrofitting compared to a rigid floor configuration: an increase of up to 80% can be noticed with respect to the usual values attributed to traditional URM structures. It is interesting to compare this large increase in q because of the dissipative diaphragms to the provisions of EN 1998 for timber structures [3]. In

the standard, a distinction is made between the behaviour factor of timber buildings with nailed wall panels and glued diaphragms, and that of structures having both floors and walls made of nailed elements. The former case can be assimilated to a masonry building with stiff and not dissipative floors, where the dissipation is localized only in the walls. The latter case, instead, can count on a further dissipative contribution, the one of the floors, increasing the behaviour factor by 60% (from 3.0 to 5.0 [3]). This increase in q related to the floors seems to be confirmed by the performed analyses also for URM structures with dissipative floors. Yet, because only basic buildings were investigated, the higher values of q have to be further validated when analyzing the case-study buildings (Chapter 7). In particular, although values of q up to 4 has been obtained, the following recommended range will be validated in the extensive numerical analyses:

$$q_{opt} = 2.5 \div 3.5 \quad (6.29)$$

where q_{opt} is the behaviour factor referred to the optimized retrofitting. This range is derived by considering the provisions for URM buildings ($q_{URM} = 1.5 \div 2.5$ [3]), and the additional damping contribution of the diaphragms ($\xi = 0.15$). In fact, because $\eta = 1/q$ [3], the behaviour factor of the diaphragms only can be quantified as $q_{floor} = 1.5$ with $\eta = 0.71$. Then, since the URM structure can be considered as a succession of two dampers (floors and walls, Fig. 6.15c), the seismic action A is firstly dissipated by the floors ($A' = A/q_{floor}$), and then the damped action A' is transmitted to the walls, which in turn dissipate energy ($A'' = A'/q_{URM}$). The behaviour factor q_{opt} is thus a combination of q_{floor} and q_{URM} :

$$q_{opt} = q_{URM} \cdot q_{floor} = \begin{cases} 2.25 & \text{if } q_{URM} = 1.5 \\ 3.75 & \text{if } q_{URM} = 2.5 \end{cases} \quad (6.30)$$

The obtained values were then rounded to 2.5 and 3.5 as a recommended, conservative range to be validated. These values have been confirmed by the performed analyses on SDOF buildings, but will be further confirmed, along with the energy-based approach, in Chapter 7.

As a final consideration, it should be noticed that with this broader approach for evaluating seismic capacity, contrarily to the use of PGA only, it is possible to link a still intuitive parameter (pseudo-velocity, available from response spectra) with the estimation of the effect of damage and load duration on URM buildings, thus allowing a more aware and optimized retrofitting of their timber diaphragms.

Chapter 7

Numerical modelling of the seismic response of existing URM buildings

7.1 Introduction

In this chapter, the extended approach for evaluating seismic capacity, and the analytical and numerical modelling approaches for single structural components presented in the previous chapters, are now adopted for characterizing the optimal performance of case-study existing and retrofitted URM buildings.

Before presenting the three analyzed case-study buildings, the modelling strategy adopted in this chapter for masonry walls and timber floors is evaluated (Section 7.2). Results from a shaking-table test performed on a small Dutch detached house are compared to the outcomes of numerical modal and time-history analyses performed after modelling this same building in DIANA FEA software. In this way, the reliability of the modelling strategy is assessed, both in terms of force-displacement response of the building and damage identification (e.g. cracks and their location), and of a realistic representation of the in-plane stiffness of the timber diaphragms.

Subsequently, an overview of the three case-study buildings is presented (Section 7.3). The first analyzed URM construction (Section 7.4) is a Dutch detached house in Godlinze, from which timber diaphragms samples were extracted for their replication (Chapter 3). The second case-study structure consists of a more monumental complex, resembling the former post office building in Loppersum (Section 7.5): since this construction is regular and features large dimensions, it was chosen to perform additional, specific studies for assessing the influence of timber-masonry connection types and interlocking among internal masonry walls on its seismic response. The third analyzed building resembles a typical country house of the Po Valley and Venetian Plain (Section 7.6). Thus, the characteristics of masonry and timber floors for this building were based on the Italian context.

The first two case-study buildings were subjected to induced seismic signals, the third to tectonic ones. The different contexts and earthquake types considered enabled

a generalization of the results, showing how an optimal seismic performance of URM buildings can be achieved, by means of an efficient retrofitting of floors and timber-masonry connections.

7.2 Evaluation of the modelling approach against an experimental shake-table test

7.2.1 Properties of tested prototype and numerical model

In order to evaluate the suitability of the adopted modelling strategies for timber floors and masonry walls, a numerical model was created, having the characteristics of the EUC-BUILD2 prototype, representing a typical Dutch double-wythe clay brick masonry detached house with non-strengthened timber diaphragms tested at the EUCENTRE shake table laboratory in 2016 [206]. The main characteristics of the prototype are shown in Fig. 7.1: the plan dimensions (5330×5770 mm) could not be excessively large because of intrinsic limitations in the shake-table area. The same geometrical properties were adopted in the numerical model; a comparison of this with the real building is depicted in Fig. 7.2.

Masonry structural components were modelled by means of a mesh of 300×300 mm 8-nodes shell elements featuring the DIANA FEA (version 10.4) Engineering Masonry Model [190]. The input parameters attributed to these shell elements were derived on the basis of both the final experimental report [206], and the masonry material properties determined at both EUCENTRE and TU Delft [166]. An overview of these parameters is reported in Table 7.1.

The diaphragms were simulated by means of linear elastic orthotropic 300×300 mm 8-nodes shell elements, featuring equivalent properties according to the modelling strategy presented in Section 5.2.2, and similarly to the example provided in Appendix D. The equivalent elastic moduli, reported in Table 7.2, were thus derived by considering an equivalence in the flexural properties between the joists and the shells. This resulted in a fictitious material featuring large equivalent elastic moduli, since the flexural properties of the joists were concentrated within the small thickness of the shell elements. These values refer to diaphragms composed of 80×180 mm joists at approximately 600 mm spacing and 24×200 mm planks, according to the experiment. The in-plane shear modulus G_{xy} of the floors is low, because of their flexible behaviour, and corresponds to an equivalent shear stiffness $G_{eq} = 120$ N/mm, similarly to the values observed in the experimental tests presented in Chapter 4. Besides the self-weight, the equivalent mass density included also the additional seismic masses (≈ 1.3 t) placed on the diaphragms [206]. In this specific case, because in the prototype the joists and the roof structure were well connected to the masonry walls, a continuous, hinged connection was assumed between horizontal and vertical structural components.

Three analysis types were performed:

1. A first, static analysis to check the correspondence between the mass of the numerical model and that of the tested building;
2. An eigenvalue analyses, to verify the correct input of mass and stiffness in the model, and compare the obtained first fundamental period to that of the prototype;

7.2. Evaluation of the modelling approach against an experimental shake-table test

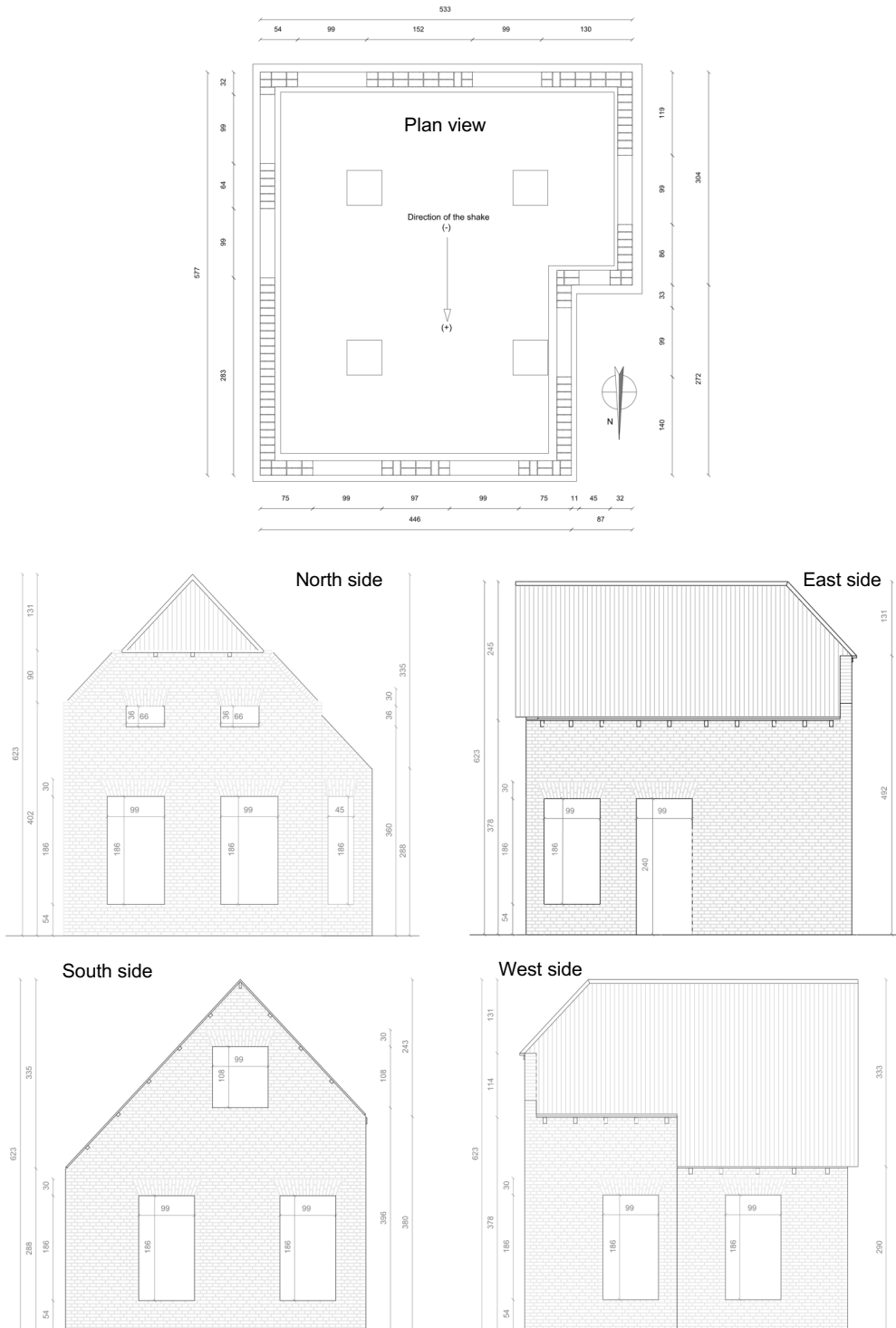


Figure 7.1: Prototype EUC-BUILD2 tested at EUCENTRE. Adapted from [206].



Figure 7.2: Real EUC-BUILD2 prototype (a) and realized numerical model in DIANA FEA (b).

Table 7.1: Material properties adopted for masonry shell elements (210 mm thickness) based on [166] and [206].

Property	Value
Young modulus E_x parallel to bed joint (MPa)	3000
Young modulus E_y perpendicular to bed joint (MPa)	6000
Shear modulus G_{xy} (MPa)	2400
Mass density ρ (kg/m ³)	1980
Bed joint tensile strength f_t (MPa)	0.15
Fracture energy in tension G_{F1} (N/mm)	0.01
Compressive strength f_c (MPa)	9.3
Fracture energy in compression G_c (N/mm)	20
Friction angle ($^\circ$)	29
Cohesion (MPa)	0.15
Fracture energy in shear (N/mm)	0.1

Table 7.2: Equivalent properties adopted for timber diaphragms shell elements (24 mm thickness), according to the modelling strategy presented in Section 5.2.2 and the example provided in Appendix D.

Property	Value
Equivalent Young modulus E_{eq} (MPa)	584922
In-plane shear modulus G_{xy} (MPa)	5
Out-of-plane equivalent shear moduli G_{xz} , G_{zy} (MPa)	36557
Equivalent mass density ρ (kg/m ³)	2840

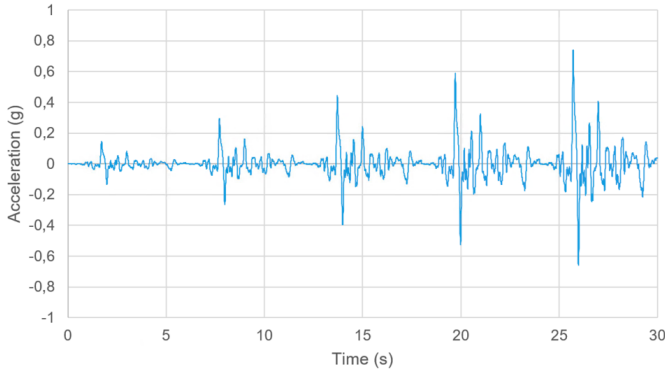


Figure 7.3: Seismic signal with increasing amplitude adopted for the time-history analyses on the EUCENTRE prototype model.

3. An incremental time-history analysis, by subjecting the building to a seismic signal (Fig. 7.3). The time-history analysis was performed by considering an intrinsic Rayleigh damping of 2% [32], and adopting the Quasi-Newton iterative method [182]. As convergence criterion, the energy norm was used, with a limit tolerance of 10^{-4} .

It should be noticed that, for the last analysis type, it was not possible to recreate exactly the same loading protocol as that of the tested sample. The prototype was subjected to a total of 36 shocks, which included two different signals and random vibrations for assessing the fundamental period and its evolution with damage. Therefore, with the incremental signal of Fig. 7.3 not the same level of degradation as that of the prototype could be reached. Yet, the objective of the performed time-history analysis was to assess whether the seismic response, the collapse earthquake intensity, and the damage in terms of crack pattern could be reasonably captured by the model under a similar seismic signal. This goal was achieved, and the adopted modelling strategy proved to be suitable for conducting the analyses on the other case-study buildings, as shown in the following.

7.2.2 Evaluation of seismic response

According to the experimental report [206], the total mass of the prototype was quantified as 32.61 t, while its fundamental period in the undamaged state was estimated as 0.11 s. As can be noticed from Fig. 7.4, these two relevant seismic properties are well represented by the created model, which was characterized by a total mass of 32.5 t and a fundamental period of 0.11 s, practically coincident to that of the prototype. The associated first mode shape, showing the weakest direction of the building and the vulnerability of the gables, was also representative for the experimental observations.

With regard to the time history analysis, as stated before, the same level of damage on the building could not be reproduced because of the lower number of incremental seismic signals applied. Yet, it was still possible to compare the seismic response between model and experiment in the initial, undamaged phases, and to verify the conditions at collapse.

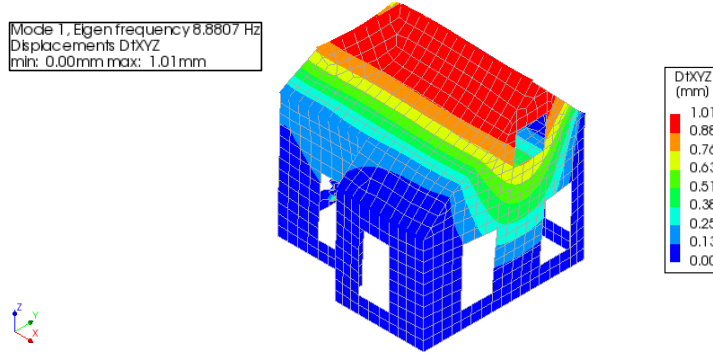


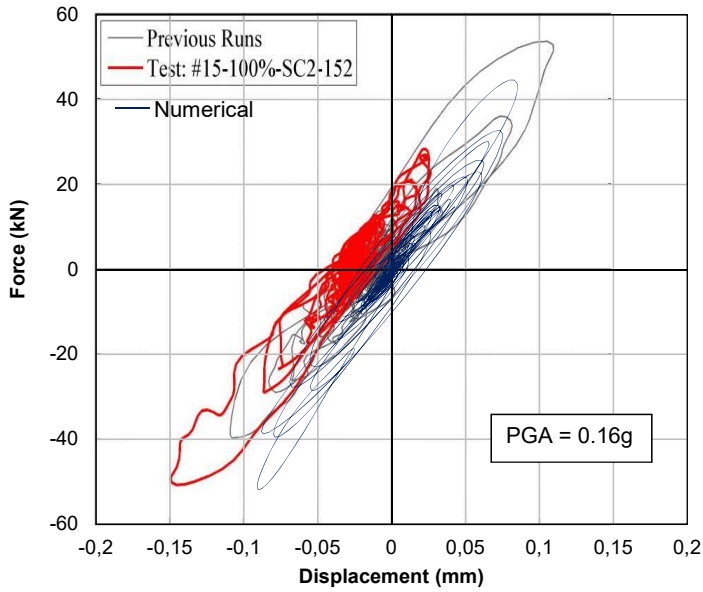
Figure 7.4: Results from eigenvalue analysis in terms of first fundamental frequency and associated mode shape.

With regard to the response of the building in its undamaged state, corresponding to the first applied signal amplitude ($\text{PGA} = 0.16\text{g}$), Fig. 7.5a shows the recorded experimental seismic behaviour and the numerically obtained one. As can be noticed, the response is well represented by the numerical model, and also the initial stiffness of the prototype is captured, confirming once more the obtained fundamental period. When considering the behaviour at collapse, the numerical model shows a higher base shear capacity, with a slightly stiffer response. This can be attributed to the more limited degradation of the building, because of the lower number of seismic sequences applied. Yet, the obtained PGA at collapse was very similar to the experimental one (0.7g vs. 0.66g , respectively, Fig. 7.5b). Besides, the overall stiffness after the in- and out-of-plane failures of masonry walls was also well captured, therefore it was expected that the damage identification in terms of crack pattern could have been very similar to that of the real prototype. This latter aspect was in fact confirmed, and is discussed in the next section.

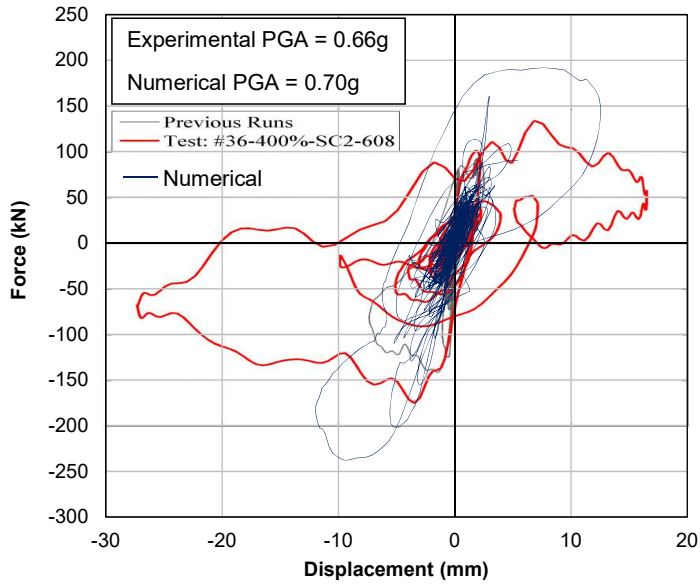
7.2.3 Evaluation of damage

From the previous section, it was already evident that the seismic behaviour of the prototype could be well captured by means of the adopted numerical modelling approach. This aspect was also confirmed when evaluating the damage at collapse in terms of crack pattern (represented by the principal crack opening width E_{cw1}) for both tested prototype and numerical model (Fig. 7.6). As can be noticed, the observed cracks and failure modes were correctly represented by the model, and in particular with regard to the following aspects:

- The model accurately highlighted the vulnerability of the gables because of the flexible roof structure, causing extensive damage to the north and south walls. The crack pattern around openings and in the gables is also well represented (Fig. 7.6a-c);
- The in-plane failure of the masonry piers in the west side was also captured, highlighting the slightly torsional behaviour of the building (Fig. 7.6b);



(a)



(b)

Figure 7.5: Experimental and numerical seismic response of the building prototype under the first applied signal in undamaged conditions (a) and at collapse (b). Adapted from [206].

- The presence of less damage in the more resistant east side is predicted as well, with the exception of the squat pier, in which additional cracks are present in the numerical model (Fig. 7.6d). However, this can also be related once more to the lower degradation of the numerical model with respect to the experiment: in the shake-table test, the large number of signals applied could have led to more damage of the weak west side, thus causing less cracks to the west one.

From the performed evaluation, it can be concluded that the adopted modelling approach appears to be suitable for assessing the seismic behaviour of URM buildings with a view to the optimal retrofitting of their timber diaphragms.

7.3 Overview of the analyzed case-study buildings and configurations

In order to prove the dissipative, beneficial effect of efficiently retrofitted and designed timber diaphragms on the seismic performance of existing buildings, several configurations and multiple contexts and earthquake types were covered in the analyses (Fig. 7.7). Because of the specific situation of the Groningen region, two case-study buildings presented characteristics typical of the Dutch context: therefore, both a detached house in the town of Godlinze, and a more monumental building located in Loppersum were modelled. A generalization of the conclusions obtained for the Dutch framework was then achieved by considering an Italian country house typical of the Po Valley and Venetian Plain.

In all cases, to retrieve a detailed picture of the seismic response of the analyzed configurations, nonlinear incremental dynamic analyses were performed. The first two case-study buildings were subjected to the seven induced signals already shown in Fig. 6.7; for the third, instead, the tectonic signals previously depicted in Fig. 6.8 were adopted. The seismic capacity of all configurations was characterized in terms of base shear-top floor (or roof) displacement responses, PGA at collapse, and for the retrofitted cases also by means of the hysteretic energy quantification and prediction according to Chapter 6. The latter procedure allowed, in particular, to both verify the optimal performance of masonry structures with moderately (and not infinitely) stiff but dissipative floors, and to assess the increased range of behaviour factor values ($q = 2.5 \div 3.5$), derived in the former chapter, in presence of URM buildings featuring these dissipative diaphragms.

In all cases, the effect of the diaphragms stiffness on the seismic performance of the buildings was evaluated. Besides the existing configurations, two retrofitting options were also considered, such as the cast of a concrete slab on the existing diaphragms, and the proposed strengthening technique with plywood panels screwed to the existing sheathing. In addition to that, for the first case-study building, also a detailed characterization of near-collapse and damage limit state of masonry was conducted; for the second case-study building, the influence of different as-built and retrofitted timber-masonry connections was evaluated, as well as the role of interlocking among masonry walls.

In the following sections, the properties of the numerical models and the results from the performed analyses will be presented and discussed. The nomenclature adopted to identify each configuration is reported in Fig. 7.7: it should be noticed that, in total, 13

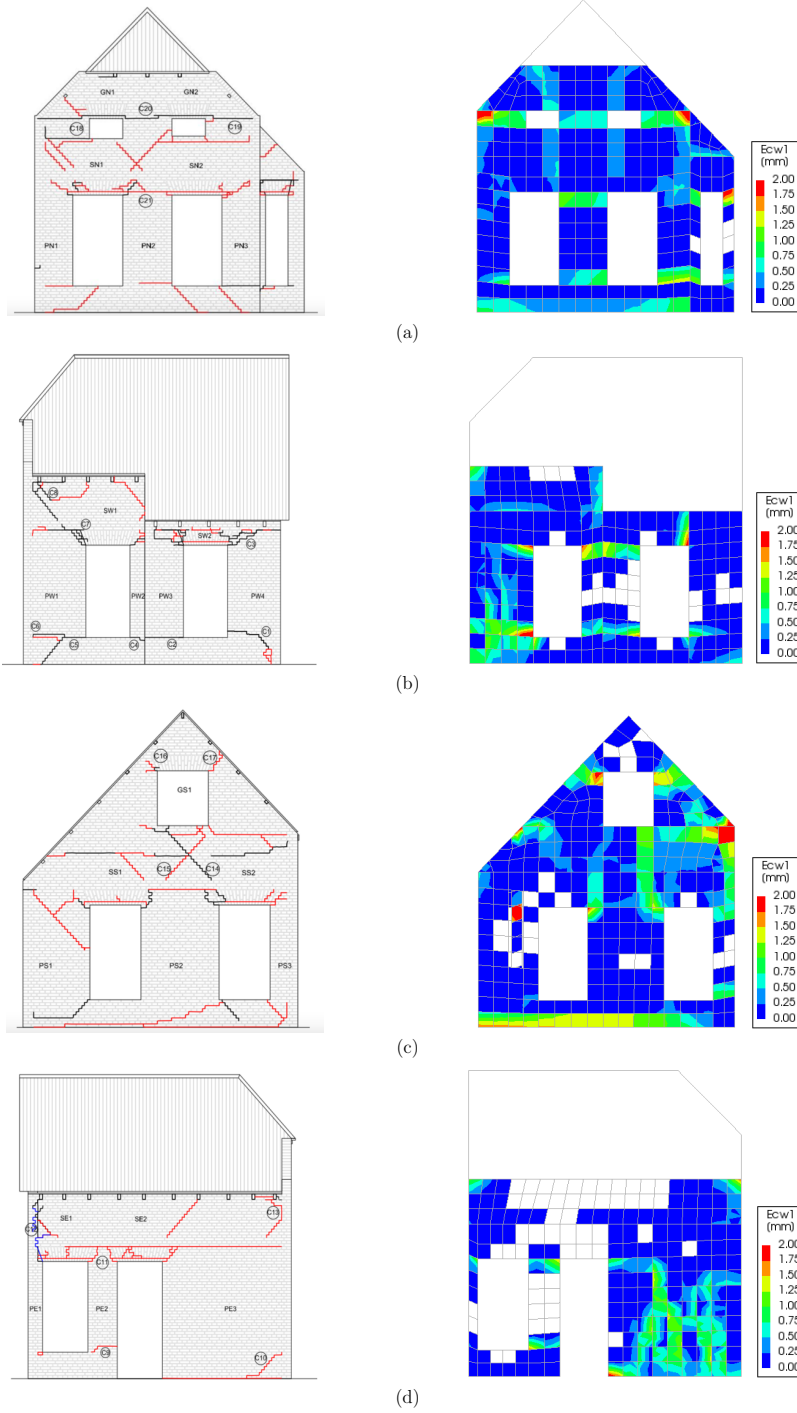


Figure 7.6: Comparison between the experimentally observed damage and the numerically obtained crack pattern (in terms of principal cracks E_{crw1}) at collapse for the north (a), west (b), south (c), and east (d) side.

Table 7.3: Material properties adopted for masonry shell elements (thickness = 210 mm) based on [166] and [207].

Property	Value
Young modulus E_x parallel to bed joint (MPa)	1500
Young modulus E_y perpendicular to bed joint (MPa)	2000
Shear modulus G_{xy} (MPa)	800
Mass density ρ (kg/m ³)	2000
Bed joint tensile strength f_t (MPa)	0.15
Fracture energy in tension G_{F1} (N/mm)	0.01
Compressive strength f_c (MPa)	14.0
Fracture energy in compression G_c (N/mm)	30
Friction angle (°)	34
Cohesion (MPa)	0.2
Fracture energy in shear (N/mm)	0.1

configurations were examined, and each one was subjected to 7 accelerograms in both x and y direction; this led to a total of 182 nonlinear time-history analyses conducted.

7.4 First case-study building (B1)

7.4.1 Model properties

A detached house typical of the Groningen area was selected as first case-study building (Fig. 7.8). This URM low-rise house has a relatively simple structure, but some irregularities are present, such as the position and shape of wall openings, and the thickness of the walls, not constant along the height, with gables featuring a single-leaf wall (100 mm thick) instead of the ground floor double-wythe walls (210 mm thick). Besides, one more single-leaf wall was present, supporting one of the floors approximately at midspan, in correspondence to the staircase (Fig. 7.8). Three configurations were studied: one represented the as-built house with flexible diaphragms (B1-AB); in the other two, the floors were retrofitted with plywood panels (B1-PP) or with a concrete slab (B1-RC).

The properties of masonry, reported in Table 7.3, were assumed to be the same for the three configurations. The adopted values are in line with the characteristics of medium-low quality masonry: these material properties fall on the conservative side with respect to experimental tests performed on both existing and replicated Dutch masonry [155], and were also defined according to calibration studies [207]. 300×300 mm shell elements with the implemented DIANA FEA (version 10.4) Engineering Masonry Model [190] were used for modelling the masonry.

While for the walls a density of 2000 kg/m^3 was assumed, for the diaphragms the density values included the self-weight of structural elements, a dead load of 1.00 kN/m^2 (accounting for further elements such as non-structural walls, finishes, plants, pipes), and 30% of the live load, equal to $0.3 \cdot 1.75 \text{ kN/m}^2$ for Dutch residential buildings [208].

Case-study building 1 (B1)	Case-study building 2 (B2)	Case-study building 3 (B3)
		
<ul style="list-style-type: none"> • Dutch features • Three configurations studied: <ol style="list-style-type: none"> 1. As-built (B1-AB) 2. Diaphragms retrofitted with concrete slabs (B1-RC) 3. Diaphragms retrofitted with plywood panels (B1-PP) • Continuous, hinged connections between diaphragms and walls assumed in the model, because of the presence of effective joints and wall plates in reality • Good interlocking among masonry walls • Subjected to 7 induced seismic signals per direction • Detailed analysis of in-plane and out-of-plane drifts at near-collapse limit state • Evaluation of the performance of the buildings also at damage limit state 	<ul style="list-style-type: none"> • Dutch features • Three as-built configurations studied: <ol style="list-style-type: none"> 1. As-built with mortar pocket timber-masonry connection (B2-AB-MP) 2. As-built with hook anchor timber-masonry connection (B2-AB-HA) 3. As-built with mortar pocket timber-masonry connection and no interlocking among walls (B2-AB-MP-NI) • Four retrofitted configurations studied: <ol style="list-style-type: none"> 1. Diaphragms retrofitted with concrete slabs and continuous timber-masonry joints (B2-RC) 2. Diaphragms retrofitted with plywood panels and wall-to-floor connections strengthened with timber blocks and mechanical anchors (B2-PP) 3. Diaphragms retrofitted with concrete slabs and continuous timber-masonry joints, but no interlocking among walls (B2-RC-NI) 4. Diaphragms retrofitted with plywood panels and wall-to-floor connections strengthened with timber blocks and mechanical anchors, but no interlocking among walls (B2-PP-NI) • Evaluation of the influence of masonry interlocking and timber-masonry connections • Subjected to 7 induced seismic signals per direction 	<ul style="list-style-type: none"> • Italian features • Three configurations studied: <ol style="list-style-type: none"> 1. As-built (B3-AB) 2. Diaphragms retrofitted with concrete slabs (B3-RC) 3. Diaphragms retrofitted with plywood panels (B3-PP) • Continuous, hinged connections between diaphragms and walls assumed in the model • Good interlocking among masonry walls • Subjected to 7 tectonic seismic signals per direction
		

Figure 7.7: Overview of the analyzed case-study buildings and nomenclature adopted for their configurations.

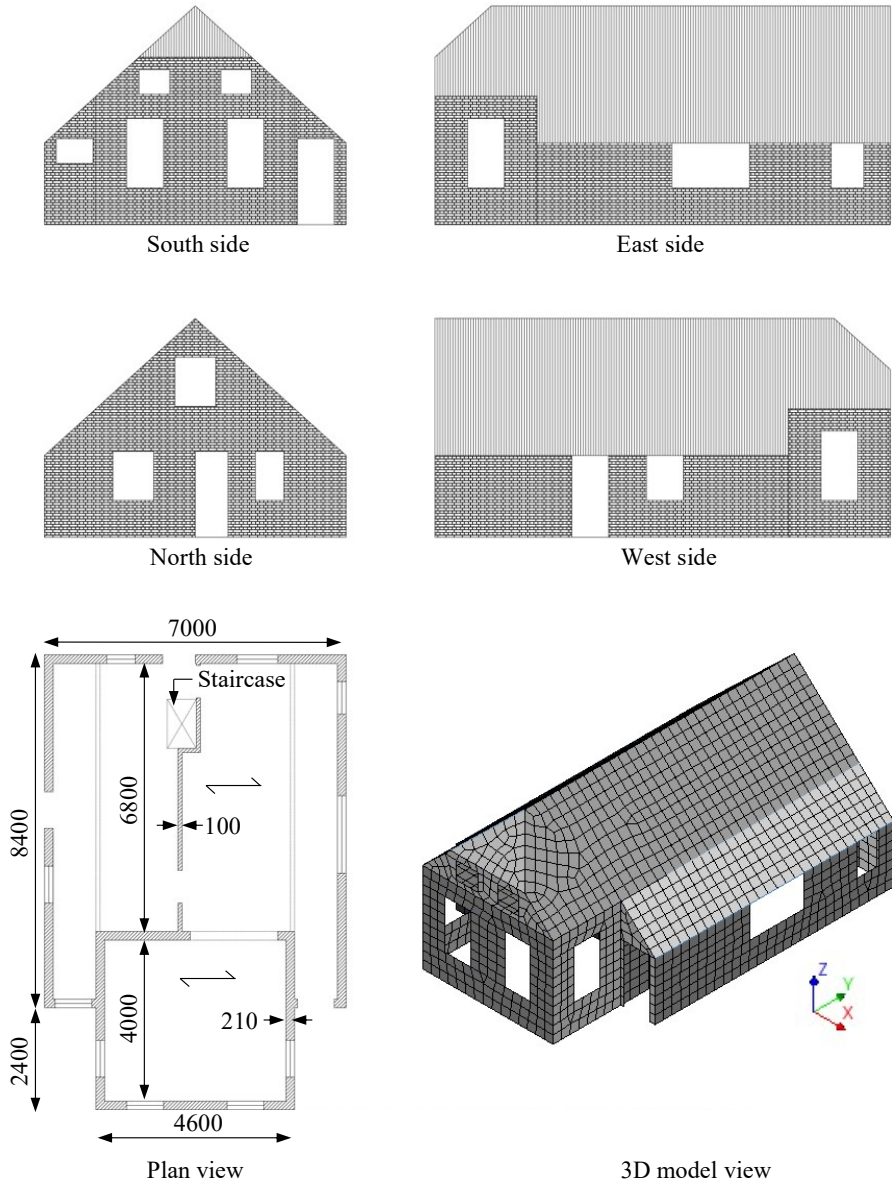


Figure 7.8: Main properties and geometry of the first case-study building B1; dimensions in mm. From [183].

Table 7.4: Equivalent properties adopted for the shell elements (thickness = 18 mm) representing the flexible diaphragms in configuration B1-AB, in agreement with the modelling strategy presented in Section 5.2.2 and the example provided in Appendix D.

Property	Value		
	4.0×4.6 m floor	4.6×6.8 m floor	Roof
Equivalent Young modulus E_{eq} (MPa)	978000	620000	405000
In-plane shear modulus G_{xy} (MPa)	12	7	6
Out-of-plane equivalent shear moduli G_{xz} , G_{zy} (MPa)	61125	38750	25312
Mass density ρ (kg/m ³)	9440	9270	6170

Configuration B1-AB featured flexible diaphragms, having the following characteristics with reference to Fig. 7.8:

- The 4.0×4.6 m floor presented 75×180 mm joists at 800 mm spacing;
- The 4.6×6.8 m floor had 60×160 mm joists arranged at 750 mm spacing;
- The roof presented 50×105 mm rafters at 900 mm spacing; on the rafters purlins were arranged, supporting in turn the planks, similarly to the tested roof pitch presented in Chapter 3;
- All diaphragms featured 18-mm-thick planks.

These structural properties of the diaphragms were translated in the numerical model by following the modelling strategy for as-built floors described in Section 5.2.2 and exemplified in Appendix D. Therefore, because of the very small energy dissipation observed from tests on replicated as-built floors [132], the diaphragms were modelled with linear elastic orthotropic shell elements, whose properties are reported in Table 7.4. The in-plane shear moduli of the diaphragms were derived by considering the flexural properties of the planks or the joists, according to the procedure presented in Section 5.2.2. It should be noticed that these values would correspond to equivalent shear stiffnesses of 108 to 216 kN/m, and are thus in line with other similar stiffness estimations for existing floors from literature [19]-[25], [132]. From an in-situ inspection, it was noticed that a timber wall plate surrounded the whole roof, and the floor joists were also connected to this structure. Therefore, a continuous hinged connection was assumed between diaphragms and walls at the floors supports. A continuous connection and good interlocking among masonry walls was considered as well. In general, the main elements of vulnerability due to the diaphragms flexibility, appeared to be related to the lack of seismic load redistribution among the walls in the x direction, and to the very low stiffness of the roof structure in the y direction, with possible local collapses of the north and south wall gables (Fig. 7.8).

In configuration B1-RC, featuring diaphragms retrofitted by casting a concrete slab on them, the floors were also modelled with linear elastic orthotropic shell elements, having the properties of structural reinforced concrete (Table 7.5). The thickness of the slab was 50 mm, as it would commonly be realized in practice [15, 17, 18].

For configuration B1-PP, having floors retrofitted with plywood panels, the modelling strategy discussed in Section 5.4.3 and exemplified in Appendix D was adopted: besides

Table 7.5: Material properties adopted for the shell elements (thickness = 58 mm) representing the concrete slabs in configuration B1-RC.

Property	Value		
	4.0×4.6 m floor	4.6×6.8 m floor	Roof
Young moduli E_x, E_y, E_z (MPa)	30000	30000	30000
Shear moduli G_{xy}, G_{xz}, G_{yz} (MPa)	12500	12500	12500
Mass density ρ (kg/m ³)	4336	4290	4250

the linear elastic orthotropic shell elements, also the nonlinear macro-elements were present, featuring the constitutive laws of the implemented user-supplied subroutine. As shown in Chapter 6, the optimized retrofitting interventions on the diaphragms should be able to retrieve the maximum in-plane strength of the walls, and at the same time be sufficiently flexible to dissipate energy, but sufficiently stiff to prevent out-of-plane collapse. Therefore, the strengthened floors were designed according to the global in-plane capacity of the piers, and conservative out-of-plane drift limits for the walls:

- The maximum base shear of the house (approximately 450 kN in the weak x direction) was evaluated through a preliminary pushover analysis applied to configuration B1-RC, and then the loads at floor and roof level were estimated through the lateral force method. The retrofitting intervention was designed accordingly, providing sufficient strength to activate in-plane failure mechanisms up to the expected 450 kN base shear capacity, but contemporarily deflection capacity.
- At the same time, to prevent out-of-plane walls failure, the maximum midspan displacement, at which the diaphragms reached their strength, was fixed at 2% of the out-of-plane walls (or gables, for the roof) height (Section 5.6.3). The potential stiffening effect of the out-of-plane walls was conservatively not taken into account, also because of the presence of large openings. Besides, use of dry screed made of loose material was assumed, so that the deflection of the floors could be enabled.

Table 7.6 reports the properties of the macro- and shell elements simulating the retrofitted diaphragms, while Appendix F reports the drawings and the main characteristics of the dissipative strengthening interventions for the floors in this case-study building. The macro-element mesh was defined in such a way that the 4.0×4.6 m floor was modelled with 4×4 macro-elements, the 4.6×6.8 m floor with 4×6 macro-elements, and each roof pitch with 3×8 macro-elements.

For all configurations, after a preliminary characterization of the vibration modes by means of eigenvalue analyses, nonlinear incremental dynamic analyses were performed, by subjecting the house to seven accelerograms of induced earthquakes (Fig. 6.7). The main loading directions x and y were studied separately, therefore a total of 42 analyses were performed. An intrinsic Rayleigh damping of 2% was considered [32], and the Newton-Raphson iterative method was adopted [182]. As convergence criterion, the force or displacement norms were used, with a limit tolerance of 10^{-2} .

Table 7.6: Equivalent properties adopted for the macro-elements and shell elements (thickness = 36 mm) representing the diaphragms retrofitted with plywood panels in configuration B1-PP, in agreement with the modelling strategy presented in Section 5.4.3 and the example provided in Appendix D.

Property	Value		
	4.0×4.6 m floor	4.6×6.8 m floor	Roof
<i>Macro-elements (in-plane response)</i>			
Young modulus of rigid trusses E_t (MPa)	10^{10}	10^{10}	10^{10}
Diagonal trusses max. strain ε_{max}	0.027	0.019	0.012
Diagonal trusses max. stress σ_{max} (MPa)	12700	21200	13700
Diagonal trusses initial stiffness K_0 (MPa)	2490000	5980000	5980000
<i>Shell elements (out-of-plane response)</i>			
Equivalent Young modulus E_{eq}	122000	77500	50700
In-plane shear modulus G_{xy} (MPa)	0.1	0.1	0.1
Out-of-plane equivalent shear moduli G_{xz} , G_{zy} (MPa)	7640	4840	3170
Mass density ρ (kg/m ³)	4940	4860	3310

7.4.2 Results from eigenvalue analyses

The preliminarily performed eigenvalue analyses on the three configurations were useful to characterize the fundamental periods and mode shapes in both the x and y directions, reported in Fig. 7.9. As can be noticed, already from these analyses the main vulnerabilities highlighted in the last section for B1-AB configuration are confirmed, especially with reference to the weakness of gables and poor overall load redistribution. Furthermore, the dissipative retrofitting intervention does not excessively increase the stiffness of the whole building, leading to a fundamental period falling in between that of B1-AB and B1-RC configurations. Starting from these initial fundamental periods, the effective periods at collapse will also be determined as a function of the behaviour factor, to assess and predict the hysteretic energy dissipation of the retrofitted configurations, as discussed in the next section.

7.4.3 Results from time-history analyses

The three configurations of the house were subjected to the seven induced signals of Fig. 6.7, by progressively scaling them until collapse. Firstly, the results are presented in terms of PGA at collapse of each configuration (Fig. 7.10). In fact, although such characterization is not fully representative of the energy and load duration characteristics, in Chapter 6 it has been demonstrated that, on average, the optimal performance of a URM building can still be identified with this parameter.

As can be noticed, as-built configuration B1-AB already collapsed at a low level of intensity under almost all signals, without needing to amplify them. This means that, for the areas within the Groningen region where more intense seismic events are expected, a retrofitting intervention would be necessary to increase the seismic performance of the house. In fact, when the floors are stiffened with a concrete slab

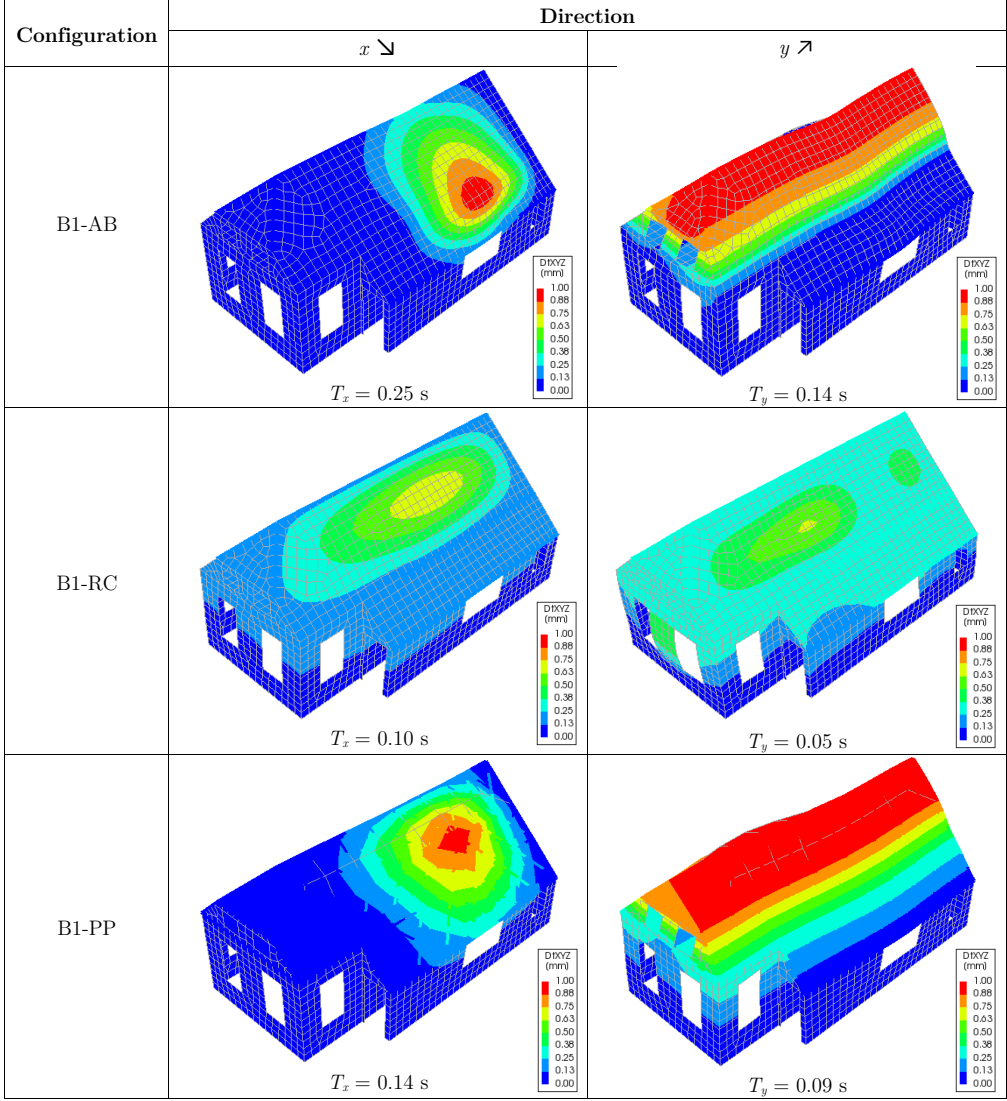


Figure 7.9: Results from eigenvalue analysis in terms of fundamental periods and associated mode shapes for the three configurations of case-study building B1.

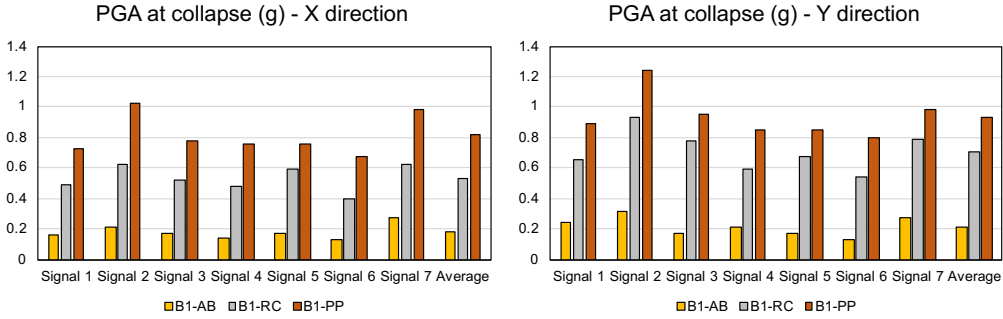


Figure 7.10: PGA at collapse for the three configurations in the x (left) and y direction (right).

(configuration B1-RC), a great improvement in the capacity of the building is obtained, mainly because of the enhanced box behaviour. Yet, the best performance is retrieved with the plywood panels overlay, in both loading directions (configuration B1-PP). The latter retrofitting intervention is easily applicable, light, reversible, and provides a beneficial energy dissipation to the diaphragms, improving even more the seismic capacity of the house.

The effect of the diaphragms on the response of the building is depicted in Fig. 7.11: the base shear-roof displacement curves are reported at collapse, and refer, as a representative example, to signal 1 applied in the x direction (the weakest); the control node for displacement corresponds to the centre of mass of the roof. For a clearer representation, also a trilinear backbone is shown, whose branches are determined on the basis of the global initial stiffness of the building until cracking, from cracking until the maximum displacement-force point is reached, and at ultimate displacement (collapse and no strength), according to the procedure by MESSALI et al. [209]. All other base shear-roof displacement curves, for each configuration and loading direction, are reported in Appendix H.

Configuration B1-AB shows a very flexible response: the floors undergo large displacements at an already limited signal amplitude, and the in-plane walls are not brought into play, with the exception of the very slender pier next to the staircase. Besides, the crack pattern (Fig. 7.11a) shows a partial out-of-plane collapse of the 100-mm-thick central wall, and of the north gable, probably due to torsional effects. A very different situation is noticeable in configuration B1-RC. In this case, the failure of the building is fully related to the in-plane walls, and a beneficial re-distribution of horizontal loads is achieved among the various walls; the force-displacement graph also confirms a typical in-plane failure of masonry (Fig. 7.11b).

A hybrid response between the first two configurations is obtained when the floors are retrofitted with plywood panels: a larger displacement capacity of the diaphragms together with an in-plane failure of the walls is noticeable (Fig. 7.11c). The crack pattern is similar to that observed for the concrete slab configuration, with a slightly higher amount of damage in the out-of-plane walls, because of the lower stiffness of the floors.

Yet, the beneficial, dissipative effect of the diaphragms leads to a 30% higher performance of the building in terms of PGA, confirming the result already obtained in the preliminary analyses of Chapter 6, and therefore also the 15% equivalent hysteretic damping value derived for the retrofitted floors. The three aforementioned responses

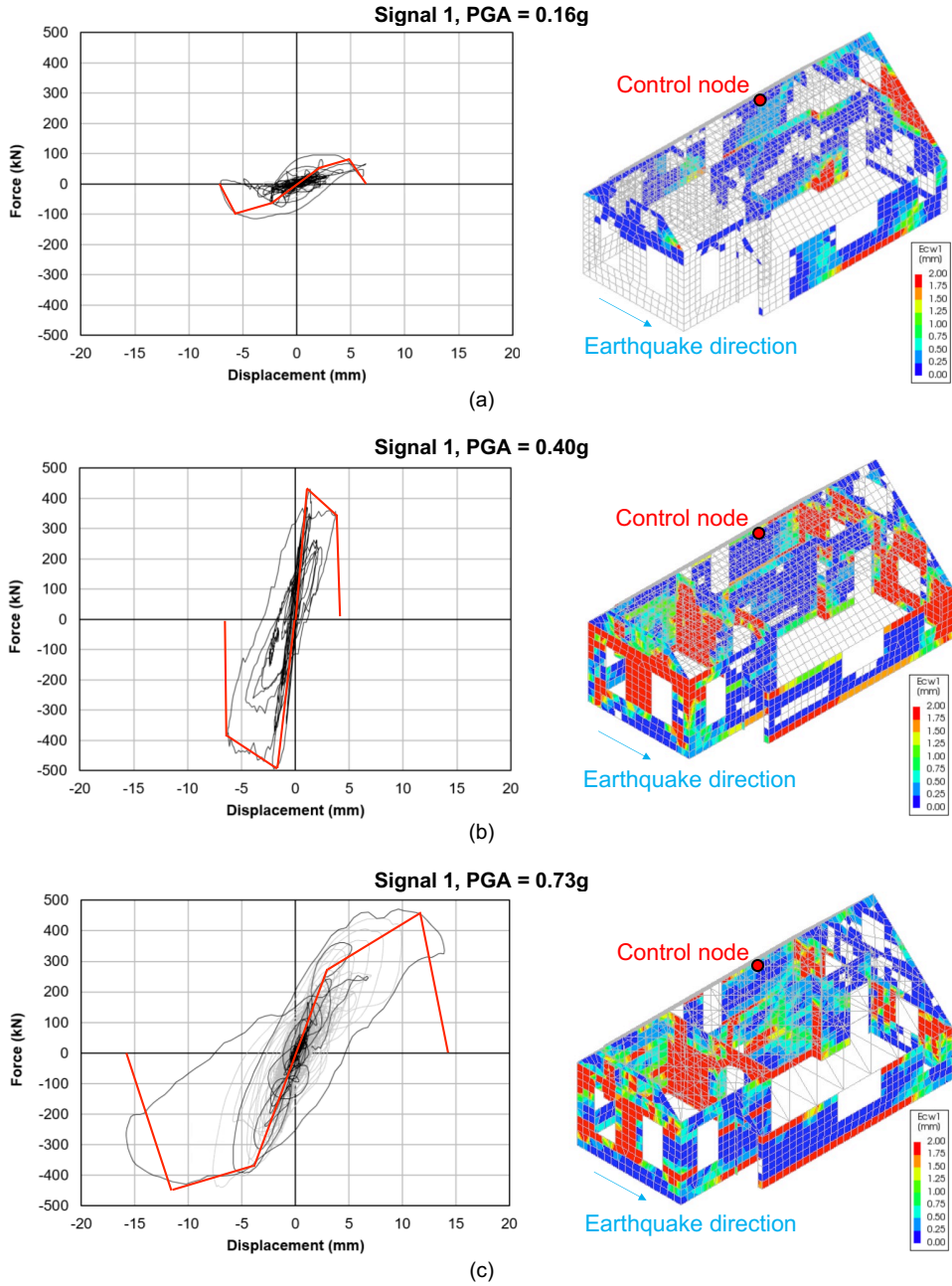


Figure 7.11: Base shear vs. roof displacement response, including trilinear backbone, and damage level in terms of principal crack opening ($Ecw1$) for the three configurations: B1-AB (a), B1-RC (b), B1-PP (c).

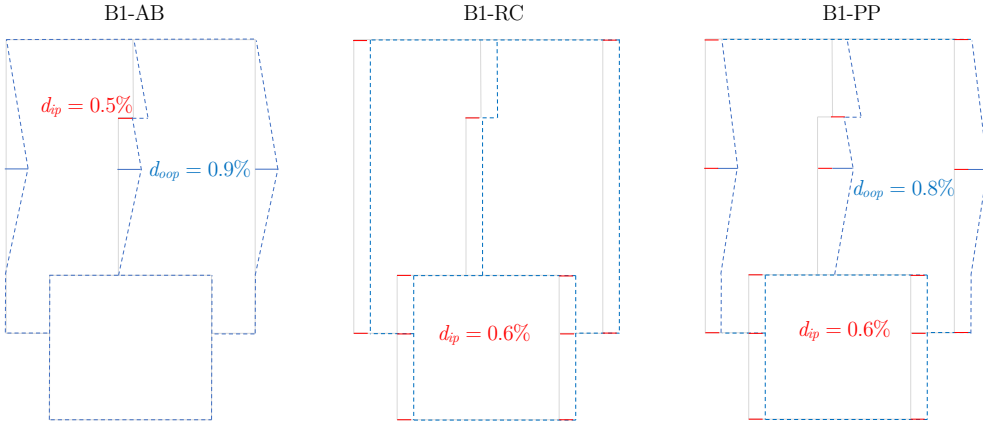


Figure 7.12: Schematic representation of the in-plane and out-of-plane drifts underwent by the masonry walls for the three configurations of building B1 under signal 1 (plan view).

of the analyzed configurations were also confirmed when considering the in-plane and out-of-plane maximum drifts of the walls recorded during the analysis. As an example, Fig. 7.12 shows a schematic representation of the drifts for the three configurations: as can be noticed, in the first case (B1-AB) the slender pier next to the staircase undergoes an in-plane drift of 0.5%, slightly lower but close to the limits specified in Section 5.6.2; for configurations B1-RC and B1-PP, in-plane drifts compatible with the observed shear-related failure of the central squat pier were obtained (0.6%), but for case B1-RC the floors behaved as infinitely stiff. In the configurations having deformable diaphragms (B1-AB and B1-PP) an out-of-plane displacement of the walls was also observed, but this was within the limit of 2% of the pertaining wall height. Therefore, a full out-of-plane collapse of a wall was not observed, even if damage and presence of cracks are still recognizable.

The possibility for configuration B1-PP of withstanding more intense earthquakes does not only depend on the lower seismic mass (with respect to case B1-RC) provided by the reversible retrofitting intervention, but also because of its energy dissipation capacity. In fact, first of all, the higher mass of the concrete slab has a beneficial effect on the in-plane capacity of the wall, which is increased due to the larger vertical pre-compression applied. Secondly, from the performed eigenvalue analysis, the first fundamental period resulted as 0.1 s for configuration B1-RC, and 0.14 s for B1-PP. In both cases, the structure in the elastic phase is stiff, as expected when studying a low-rise masonry building; however, the plateau of the average response spectrum of the adopted signals starts at a period of 0.19 s (Fig. 6.7). Since the displacement capacity of building B1-PP immediately brings into play the nonlinearity of the floors (including pinching cycles and energy dissipation), this configuration experiences a rapid increase of its period, and becomes quickly subjected to the maximum spectral acceleration. Instead, when concrete slabs are present (B1-RC), the diaphragms can be regarded as infinitely stiff, thus the response is approximately linear elastic until the in-plane capacity of the weakest wall is reached.

The combination of a higher pre-compression on the walls with a limited in-plane displacement capacity, compared to configuration B1-PP, implies a slower evolution of

Table 7.7: Effective periods at collapse for the retrofitted configurations B1-RC and B1-PP as a function of their behaviour factor ranges.

Configuration	Excited seismic mass (kg)	Direction	$T_{n,eff}$ (s)		
B1-RC	55577	x	0.11 ($q = 1.5$)	0.13 ($q = 2.0$)	0.16 ($q = 2.5$)
		y	0.06 ($q = 1.5$)	0.07 ($q = 2.0$)	0.09 ($q = 2.5$)
B1-PP	43267	x	0.22 ($q = 2.5$)	0.25 ($q = 3.0$)	0.28 ($q = 3.5$)
		y	0.16 ($q = 2.5$)	0.18 ($q = 3.0$)	0.20 ($q = 3.5$)

the period due to nonlinearities, and the spectral plateau is reached at a later stage. Nevertheless, the reversible, dissipative retrofitting still shows a higher capacity.

This latter aspect is even more evident when characterizing the two retrofitted configurations in terms of energy (Fig. 7.13). The hysteretic energy provided by configuration B1-PP is remarkably larger than that of building B1-RC: more than six times in the x direction, and twenty times in the y direction. Besides, it can be noticed that the prediction of dissipated energy by means of Eq. 6.20 proves to be accurate:

- The usual behaviour factor range of $q = 1.5 \div 2.5$ for masonry structures is confirmed when considering configuration B1-RC, but because of the less ductile response in the y direction, it appears to be more conservative to limit it up to $q = 2.0$ for this specific building;
- The increased behaviour factor range for URM buildings with dissipative diaphragms ($q = 2.5 \div 3.5$) is confirmed and falls in most cases on the conservative side of the hysteretic energy capacity prediction at collapse.

For this prediction, the periods at collapse $T_{n,eff}$ were determined as a function of the behaviour factors q (Eqs. 6.23-6.25), and are reported in Table 7.7. By knowing the values of $T_{n,eff}$ corresponding to each q , the hysteretic energy can be estimated with Eq. 6.20, by using the pseudo-velocity response spectrum, as was done in the preliminary analyses presented in Chapter 6. An example for this calculation is reported in Appendix G. It can be noticed that the dissipative retrofitting of the floors proves to be particularly beneficial in the y direction, because it can increase the displacement capacity of the whole system, compared to the very stiff and much less ductile response of B1-RC configuration.

Further considerations on the dissipative role of the floors will be provided in Section 7.7.

7.4.4 Assessment of building B1 at damage limit state

To conclude the analysis of this first case-study building, a characterization of the house at damage limit state was also conducted. This was necessary to prove that, although the timber diaphragms retrofitted with the proposed dissipative technique are not infinitely stiff, the damage due to frequent, low-intensity earthquakes is still limited. The damage to be assessed especially involves the out-of-plane walls: on the one hand,

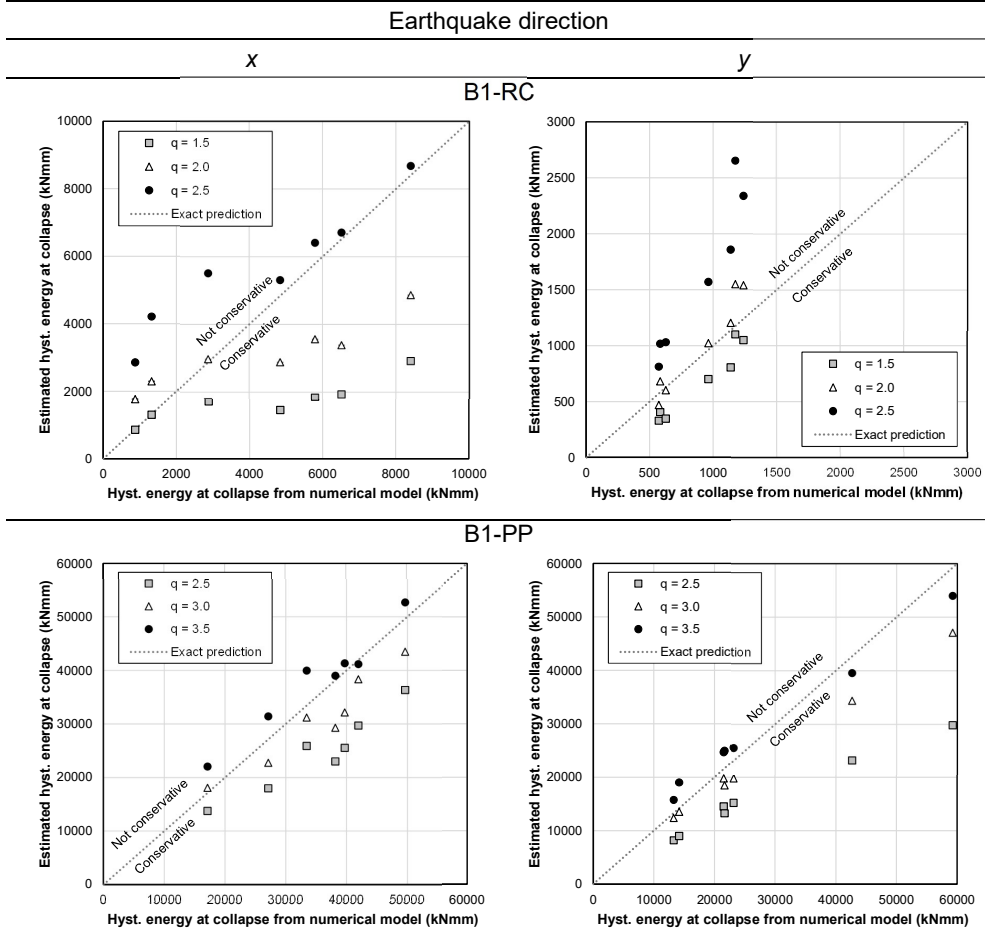


Figure 7.13: Recorded and predicted hysteretic energy of retrofitted configurations B1-RC and B1-PP as a function of the proposed behaviour factor ranges.

the in-plane deflection of each floor can activate its energy dissipation; on the other hand, this displacement capacity may not induce widespread cracks on the walls under a low-intensity seismic events. In fact, in the latter case, the intervention would only be beneficial for the near-collapse limit state, but not economically convenient throughout the service life of the building, because it would require numerous retrofitting actions on masonry.

The configurations of building B1 at damage limit state were analyzed by considering a return period of 95 years, in agreement with NPR 9998 [27]. This corresponds to an expected PGA of $0.07 \div 0.08g$ [203], and thus to approximately half of the amplitude of the applied signals of Fig. 6.7. Time-history analyses were performed with these downscaled signals, and the response of the building was evaluated in terms of cracks extension and maximum displacements (in the direction of the earthquake) recorded in the analyses. In particular, starting from these displacements, it is possible to evaluate

whether the structure meets the (inter-storey) drift requirements for damage limit state, prescribed as 0.4% of the pier height for in-plane loading [4], and recommended as 0.33% of the wall height for out-of-plane loading [210].

Fig. 7.14 shows the crack pattern and maximum recorded displacements of the three configurations after being subjected to the half-scaled signal 1 in the x direction. The best result in terms of crack pattern is obtained with configuration B1-RC, because the rigid diaphragms avoid involving out-of-plane walls, while only causing very light damage to the spandrels. Yet, in configuration B1-PP, although the out-of-plane walls are slightly more involved, a limited crack pattern is observable as well. The worst performance is obtained with the as-built case B1-AB, in which extensive damage and crack opening occur in all out-of-plane walls and gables.

These outcomes are confirmed when considering the maximum recorded displacement in the direction of the signal (x) during the analysis. The governing requirement is related to the out-of-plane drift limit applied to the walls supporting the roof, having a height of 2 m; therefore, the out-of-plane limit displacement is equal to $0.33\% \cdot 2000 = 6.6$ mm. While the two retrofitted configurations comfortably meet this requirement, the as-built case reaches a two times larger displacement than the prescribed limit (Fig. 7.14).

Thus, the conducted damage limit state analysis proves that the proposed optimized retrofitting intervention is beneficial for a near-collapse condition, but also suitable when the structures are subjected to more frequent earthquakes. Furthermore, the analysis also confirmed the observed vulnerability of as-built existing URM constructions in Groningen, which may not be able to withstand frequent, low-intensity earthquakes, without a progressive increase in cracks and damage.

7.5 Second case-study building (B2)

7.5.1 Model properties

As second case-study structure, a larger building was chosen, having some monumental features and resembling the former post office building of Loppersum (Fig. 7.15). This URM building is overall quite regular and presents double-wythe clay brick masonry walls (210 mm thick). In this case, because of the regularity of the building, besides evaluating the performance of as-built and retrofitted configurations, it was chosen to study the effect of other two elements that could impact the seismic response of URM structures:

1. The influence of timber-masonry connections, in this case considered for the specific context of Groningen by implementing in the numerical models the constitutive laws of some of the as-built and retrofitted tested joints (Chapters 4-5);
2. The influence of interlocking among masonry walls, evaluated by connecting or not the internal walls to the external load-bearing structure. This situation could be frequently found in existing URM buildings in Groningen, and can represent a great source of vulnerability. Although when seismically retrofitting a building it is good practice to provide sufficient cooperation among structural components, it was also chosen to evaluate the case in which only strengthening of diaphragms and timber-masonry connections is performed, because this measure could be

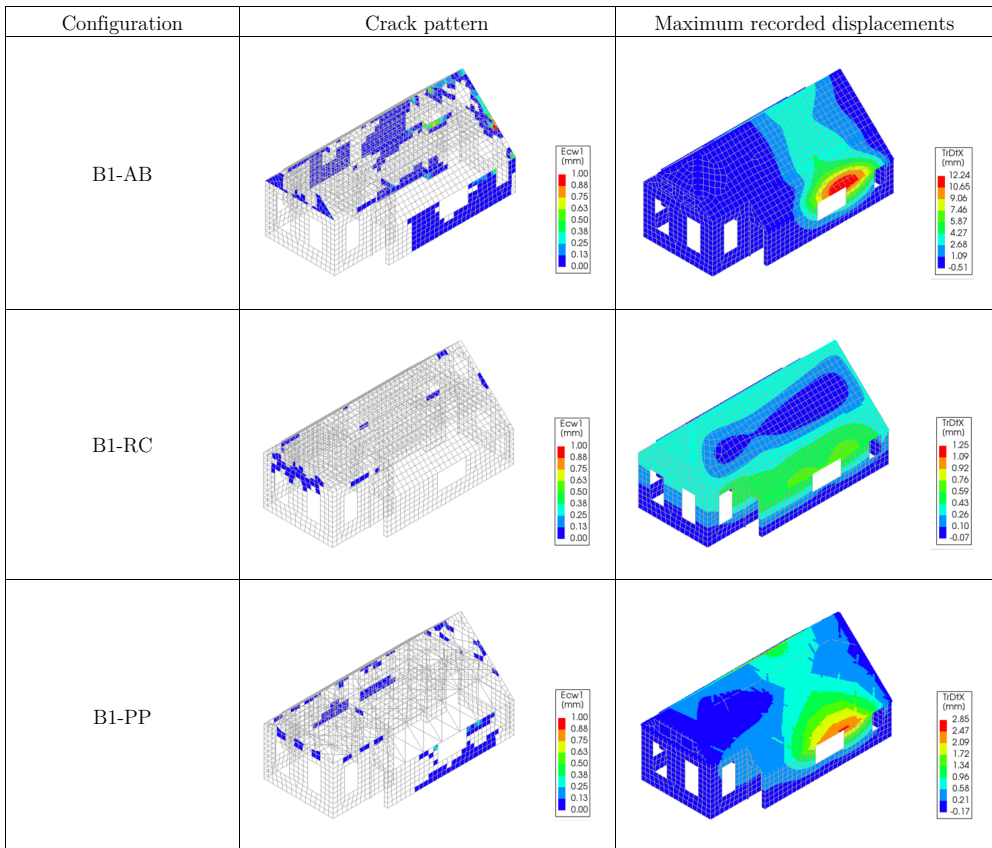


Figure 7.14: Results in terms of crack pattern and maximum recorded displacement during the analysis at damage limit state, under half-scaled signal 1 in the x direction.

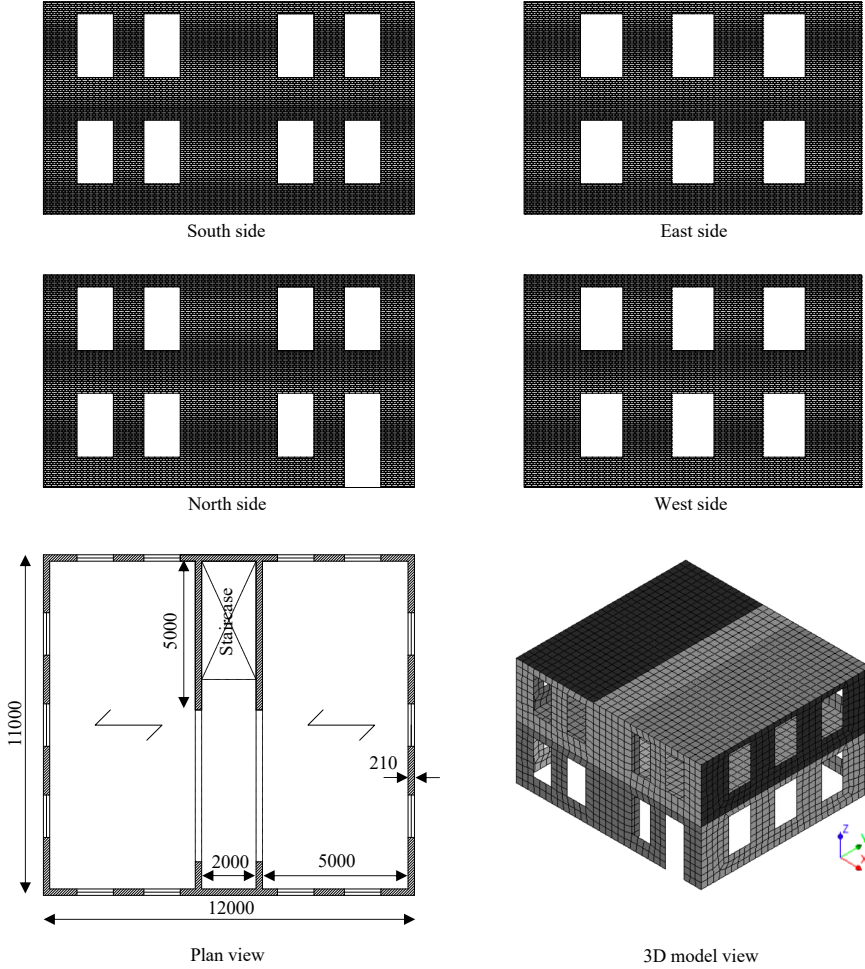


Figure 7.15: Main properties and geometry of the first case-study building; dimensions in mm.

sufficient for all those buildings located farther from the Groningen gas field, but still subjected to low-intensity ground motions.

Therefore, starting from the aforementioned considerations, a total of seven configurations were analyzed, three as-built and four strengthened. The three as-built configurations had the following characteristics:

- A first configuration (B2-AB-MP) presented floor-to-wall connections with simple mortar pockets, and the walls were considered as well connected among each other;
- The second building type (B2-AB-HA) featured floor-to-wall connections with hook anchors, and the walls were assumed to be well connected among each other;
- The last as-built configuration (B2-AB-MP-NI) presented floor-to-wall connections

with simple mortar pockets, and the internal walls were considered as disconnected from the external structure.

The four retrofitted configurations consisted of the following:

- Strengthening of the diaphragms with a concrete slab and continuous connections between floors and walls, with good interlocking among piers (B2-RC);
- Optimized retrofitting of the diaphragms with plywood panels and timber-masonry connections strengthened with timber blocks (option G in Chapter 4), with good interlocking among piers (B2-PP);
- Strengthening of the diaphragms with a concrete slab and continuous connections between floors and walls, with internal walls disconnected from the external structure (B2-RC-NI);
- Optimized retrofitting of the diaphragms with plywood panels and timber-masonry connections strengthened with timber blocks (option G in Chapter 4), with internal walls disconnected from the external structure (B2-PP-NI).

When discussing the results from the numerical analyses, the effects of timber-masonry connections and walls interlocking will be addressed in Section 7.5.3.

The properties of masonry were assumed to be identical for all configurations, and were the same adopted for the first case-study building (Table 7.3). 400×400 mm shell elements featuring the DIANA FEA Engineering Masonry Model [190] were again used for modelling the masonry.

Similarly to the previous case, for the walls a density of 2000 kg/m^3 was assumed, while for the diaphragms the density values included the self-weight of structural elements, a dead load of 1.00 kN/m^2 (accounting for further elements such as non-structural walls, finishes, plants, pipes), and 30% of the live load, equal to $0.3 \cdot 1.75 \text{ kN/m}^2$ for Dutch residential buildings [208].

The first- and second-floor diaphragms presented 80×200 mm joists at 500 mm spacing, and 18×165 mm planks. These structural properties of the diaphragms were also in this case translated in the numerical model by following the modelling strategy for as-built floors previously described in Section 5.2.2 and validated in Section 7.2. Therefore, because of the very small energy dissipation observed from tests on replicated as-built floors [132], the diaphragms were modelled with linear elastic orthotropic shell elements, whose properties are reported in Table 7.8.

In the configurations featuring diaphragms retrofitted by casting a concrete slab on them, the floors were also modelled with linear elastic orthotropic shell elements, having the properties of structural reinforced concrete (Table 7.9). The thickness of the slab was 50 mm.

For the configurations having floors retrofitted with plywood panels, the modelling strategy discussed in Section 5.4.3 was also for this case adopted: besides the linear elastic orthotropic shell elements, also the nonlinear macro-elements (1×1 m mesh) were present, featuring the constitutive laws of the implemented user-supplied subroutine. The optimized retrofitting interventions on the diaphragms were again designed according to the global in-plane capacity of the piers, and conservative out-of-plane drift limits for the walls:

Table 7.8: Equivalent properties adopted for the shell elements (18 mm thickness) representing the flexible diaphragms in configurations B2-AB-MP, B2-AB-HA and B2-AB-MP-NI, in agreement with the modelling strategy presented in Section 5.2.2 and the example provided in Appendix D.

Property	Value	
	First floor	Top floor
Equivalent Young modulus E_{eq} (MPa)	2294544	2294544
In-plane shear modulus G_{xy} (MPa)	2	2
Out-of-plane equivalent shear moduli G_{xz} , G_{zy} (MPa)	143409	143409
Mass density ρ (kg/m ³)	9760	6840

Table 7.9: Material properties adopted for the shell elements (thickness = 68 mm) representing the concrete slabs in configurations B2-RC and B2-RC-NI.

Property	Value	
	First floor	Top floor
Young moduli E_x , E_y , E_z (MPa)	30000	30000
Shear moduli G_{xy} , G_{xz} , G_{zy} (MPa)	12500	12500
Mass density ρ (kg/m ³)	4420	4430

- The maximum base shear of the building (approximately 660 kN in the weak x direction) was evaluated through a preliminary pushover analysis applied to configuration B2-RC, and then the loads at floor and roof level were estimated through the lateral force method. The retrofitting intervention was designed accordingly, providing sufficient strength to activate in-plane failure mechanisms up to the expected 660 kN base shear capacity, but contemporarily deflection capacity.
- At the same time, to prevent out-of-plane walls failure, the maximum midspan displacement, at which the diaphragms reached their strength, was fixed at 2% of the out-of-plane walls (or gables, for the roof) height (Section 5.6.3). The potential stiffening effect of the out-of-plane walls was conservatively not taken into account, also because of the presence of large openings. Besides, use of dry screed made of loose material was assumed, so that the deflection of the floors could be enabled.

Table 7.10 reports the properties of the macro- and shell elements simulating the retrofitted diaphragms, while Appendix F reports the drawings and the main characteristics of the dissipative strengthening interventions for the floors in this case-study building.

For this case-study, also the constitutive laws of the timber-masonry connections were specified, in order to study their influence. The floor-to-wall joints were modelled as nodal springs without cross terms [182], following the approach presented in Section 5.5.3 and shown in Fig. 5.1. The constitutive laws assigned to these springs are shown in Fig. 7.16 and were derived on the basis of the obtained experimental results presented in Section 4.4, accounting for the floors macro-elements mesh. In particular, a frictional response was attributed to the connections representing the mortar pocket, while

Table 7.10: Equivalent properties adopted for the macro-elements and shell elements (thickness = 36 mm) representing the diaphragms retrofitted with plywood panels in configurations B2-PP and B2-PP-NI, in agreement with the modelling strategy presented in Section 5.4.3 and the example provided in Appendix D.

Property	Value	
	First floor	Top floor
<i>Macro-elements (in-plane response)</i>		
Young modulus of rigid trusses E_t (MPa)	10^{10}	10^{10}
Diagonal trusses max. strain ϵ_{max}	0.0129	0.0258
Diagonal trusses max. stress σ_{max} (MPa)	8870	8880
Diagonal trusses initial stiffness K_0 (MPa)	3380000	1690000
<i>Shell elements (out-of-plane response)</i>		
Equivalent Young modulus E_{eq} (MPa)	287000	287000
In-plane shear modulus G_{xy} (MPa)	0.1	0.1
Out-of-plane equivalent shear moduli G_{xz}, G_{zy} (MPa)	17900	17900
Mass density ρ (kg/m ³)	5100	3650

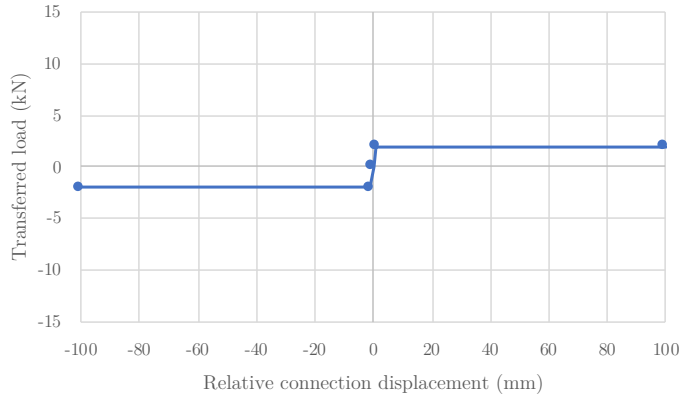
the hook anchor and the timber blocks joints followed a much stiffer response. It should be noticed that these force-displacement relations were assigned to the direction corresponding to the longitudinal axes of the joists, while in the other two directions a hinged connection was considered. Besides, for the configurations featuring a concrete slab, a continuous hinged connection type was assumed.

For all configurations, after a preliminary characterization of the vibration modes by means of eigenvalue analyses, nonlinear incremental dynamic analyses were performed, by subjecting the building to seven accelerograms of induced earthquakes (Fig. 6.7). The main loading directions x and y were studied separately, therefore a total of 98 analyses were performed. An intrinsic Rayleigh damping of 2% was considered [32], and the Newton-Raphson iterative method was adopted [182]. As convergence criterion, the force or displacement norms were used, with a limit tolerance of 10^{-2} .

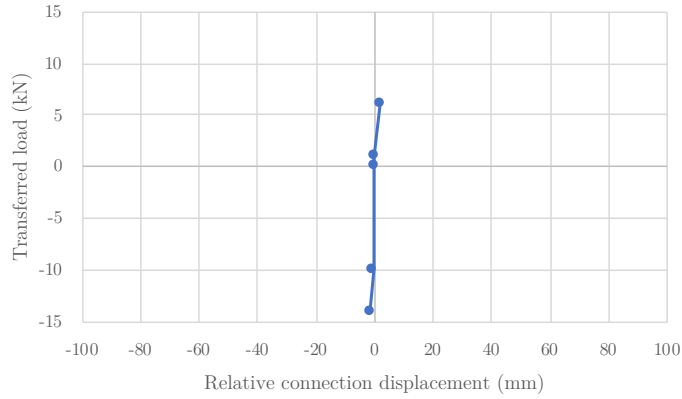
7.5.2 Results from eigenvalue analyses

The performed eigenvalue analyses already provided insight on the potential failure modes of all studied configurations. The very flexible timber diaphragms led in general to high fundamental periods for the as-built configurations (Fig. 7.17), but this could also represent an advantage, since the structures might experience a smaller amplification of the imparted seismic accelerations. Besides, the contribution of hook anchors slightly decreases the fundamental period, as is expected when having a stiffer connection type. What, instead, appears to be a great source of vulnerability in as-built configurations, is the absence of interlocking in the masonry walls: from the mode shapes of configuration B2-AB-MP-NI it is evident that the building is not able to withstand the seismic loads as a whole, leading instead to highly probable local collapses (Fig. 7.17).

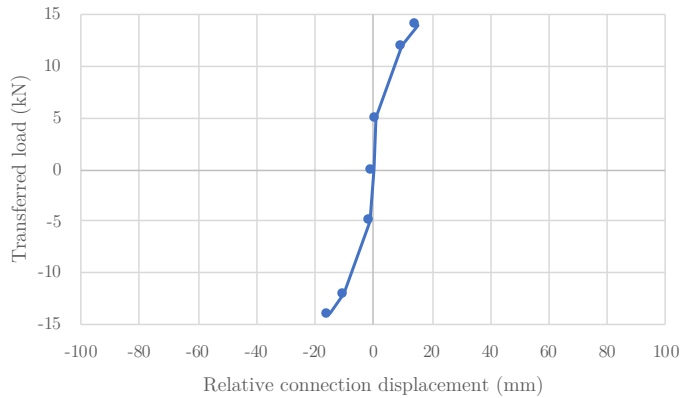
On the contrary, the box behaviour is greatly improved in all retrofitted cases (Fig. 7.18), including those in which no interlocking among internal masonry walls is



(a)



(b)



(c)

Figure 7.16: Constitutive laws assigned to the nodal springs without cross terms representing the timber-masonry connections: mortar pocket (a) used in configurations B2-AB-MP and B2-AB-MP-NI; hook anchor joint (b) used in configuration B2-AB-HA; timber blocks connection (c) used in configurations B2-PP and B2-PP-NI.

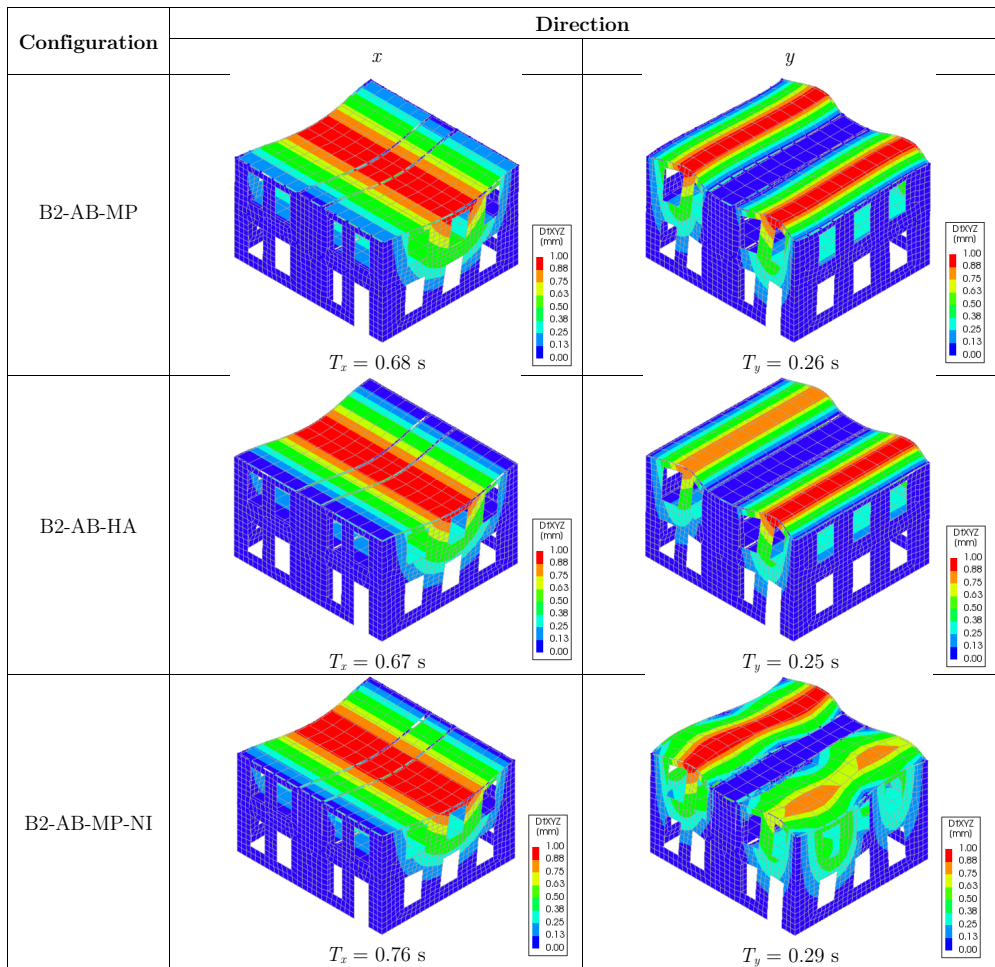


Figure 7.17: Results from eigenvalue analysis in terms of fundamental periods and associated mode shapes for the three as-built configurations of case-study building B2.

present: the only consequence of this poor connection is a slight increase in fundamental periods. Besides, the results from the previous case-study buildings are also confirmed: the configurations featuring concrete slabs show a stiff response with uniform load redistribution, and those with plywood panels retrofitting display a hybrid response, with efficient load transfer but at the same time displacement capacity.

7.5.3 Results from time-history analyses

In this section, besides identifying the seismic response of the analyzed configurations until collapse, the role of wall interlocking and timber-masonry connections is discussed as well. The performance of all these configurations is shown in Fig. 7.19 in terms of PGA at collapse in both directions, and distinguishing between well-interlocked walls or poorly connected ones.

The as-built configurations show, in general, a slightly better performance compared to building B1. Yet, the contemporary presence of poor interlocking and weak mortar pocket connections makes configuration B2-AB-MP-NI the most vulnerable. Besides, the performed analyses confirm that the presence of effective connections can already represent an element of improvement in the seismic behaviour, as is noticeable from the configurations featuring the hook anchors, which is stiffer and more able to transfer the horizontal loads than the mortar pocket. In all cases, an out-of-plane failure was observed, caused by an inter-storey drift larger than the 2.0% assumed limit.

Similarly to building B1, the retrofitted configurations appear to greatly improve the response of the case-study construction and lead to a fully in-plane related behaviour, with failures occurring at 0.6-0.8% drift. However, especially when concrete slabs are present, the increase in PGA at collapse is not relevant: this depends on the way the building amplifies the imparted seismic signals, because with concrete diaphragms the amplification is maximum (response spectrum plateau) due to the low period (Fig. 7.18), while the high flexibility of the as-built floors corresponds in this case to a beneficial reduction of the accelerations experienced by the building. A hybrid situation is obtained when retrofitting the diaphragms with plywood panels, thus the maximum amplification of the seismic signal occurs only at the beginning of the ground motion, but the decrease in stiffness and the nonlinearities can increase the period and reduce the accelerations to which the structure is subjected.

The presence of poorly interlocked walls appears, as expected, to reduce the capacity of the building, which can withstand earthquakes with a 20-40% lower intensity compared to configurations with well connected masonry piers. The presence of retrofitted floors, because of the better redistribution and shear transfer, can still slightly mitigate the effect of the absence of interlocking of internal walls.

The time-history responses of the as-built configurations, including trilinear backbones, are depicted in Fig. 7.20: the base shear-roof displacement curves are reported at collapse, and refer, as a representative example, to signal 2 applied in the x direction (the weakest); the control node for displacement corresponds to the centre of mass of the top floor. As can be noticed, all configurations display a very flexible behaviour, and the in-plane walls are not involved. Besides, an extensive damage of the out-of-plane walls is noticeable, due to their out-of-phase oscillation induced by the poorly connected, flexible floors (Fig. 7.21). Another aspect of interest of the as-built configurations is the difference in response because of wall-to-wall and floor-to-wall connections. The

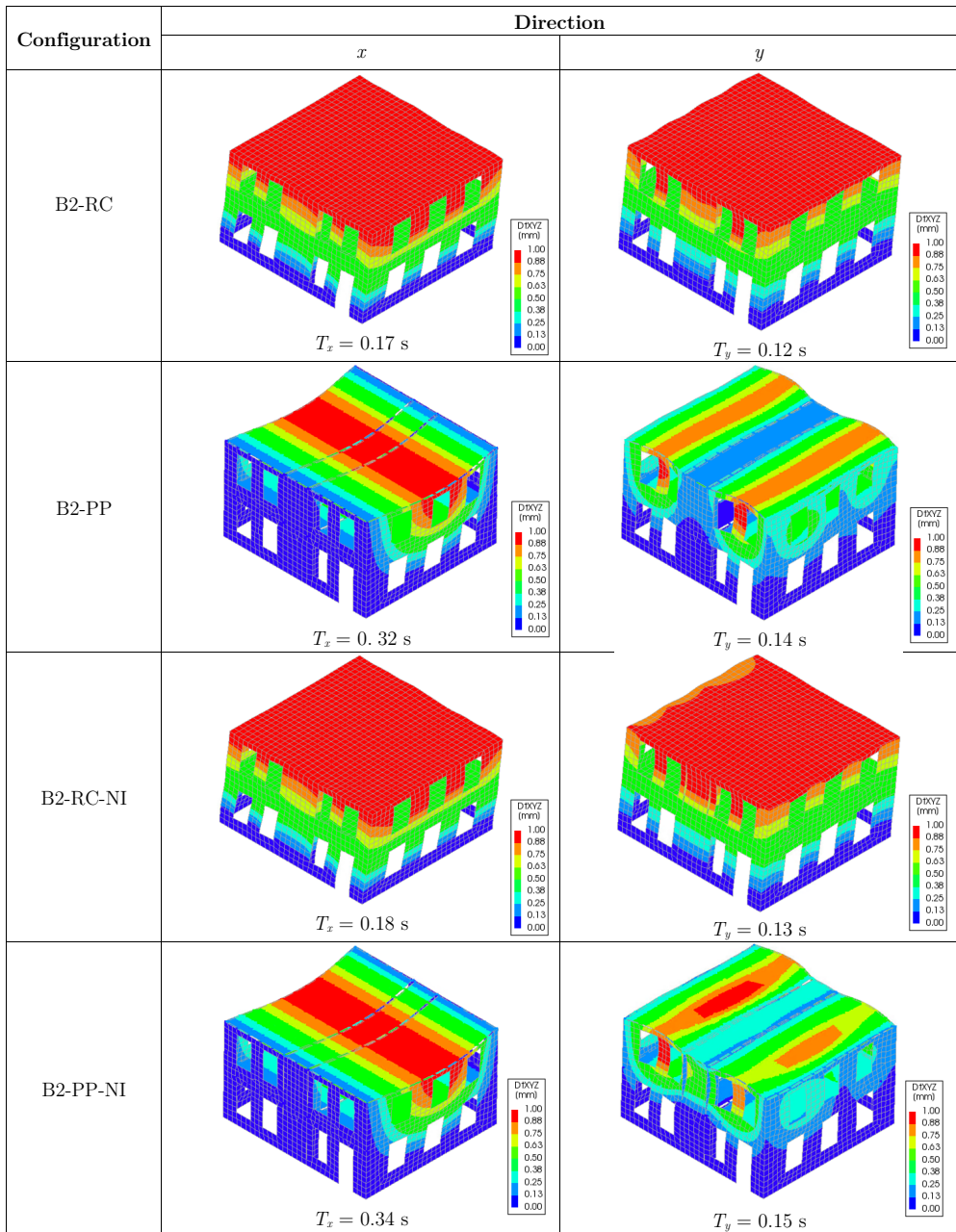


Figure 7.18: Results from eigenvalue analysis in terms of fundamental periods and associated mode shapes for the four retrofitted configurations of case-study building B2.

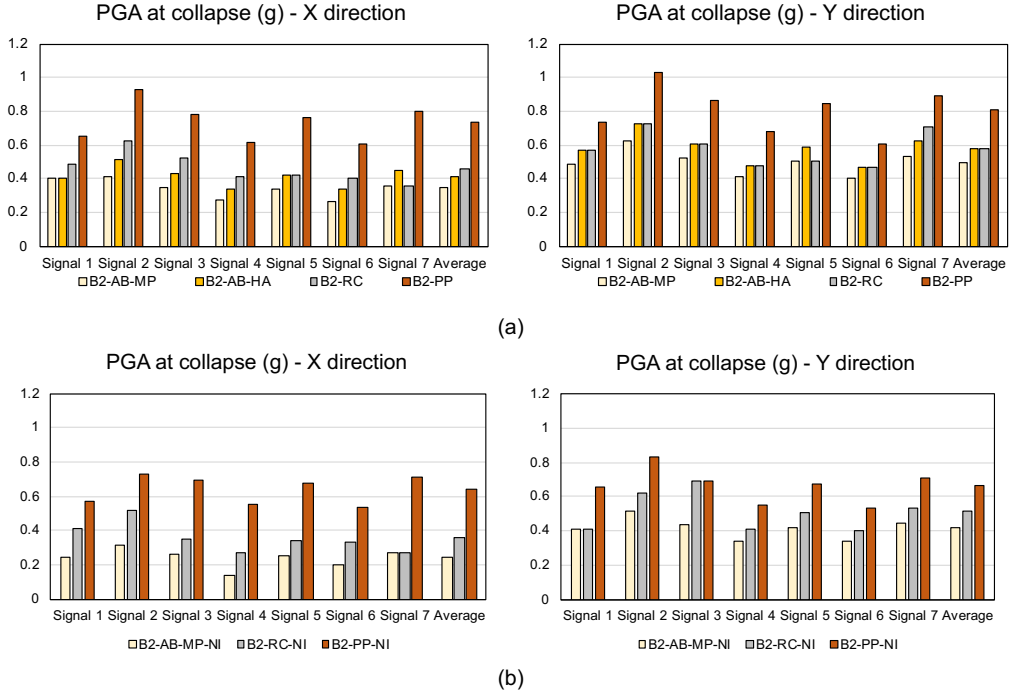


Figure 7.19: PGA at collapse referred to both directions x (left) and y (right) for all analyzed configurations, with well (a) and poorly interlocked (b) walls.

poor interlocking is responsible for a lower damage in terms of crack pattern on the out-of-plane walls, but induces a much larger damage on the top four corners of the building (Fig. 7.20c), mainly because of the difference in displacement amplitudes between the two not interlocked internal walls and the outer, well-connected structure. This could also lead to dangerous and detrimental local collapses of these areas in practice.

The effect of floor-to-wall connections is not directly evident in terms of global response, but can be captured by recording the relative displacements of the diaphragms with respect to the out-of-plane walls (Fig. 7.22). It is interesting to notice that, while the mortar pocket allows mutual sliding of the structural components because of the frictional behaviour, the stiffer and stronger hook anchor appears to provide a practically continuous connection. This same response was also observed for the connections retrofitted with timber blocks in the configurations having floors strengthened with plywood panels. Therefore, as a general recommendations, a detailed modelling of timber-masonry joints appears to be necessary only in presence of flexible connections, while sufficiently stiff and resistant joint types can be reasonably assumed as continuous (hinged) springs.

With regard to the configurations with retrofitted diaphragms, Figs. 7.23 and 7.24 show the base shear-roof displacement curves, including trilinear backbones, and the damage in terms of crack pattern at collapse when the internal walls are well interlocked or poorly connected, respectively. As can be observed, the strengthened floors are able

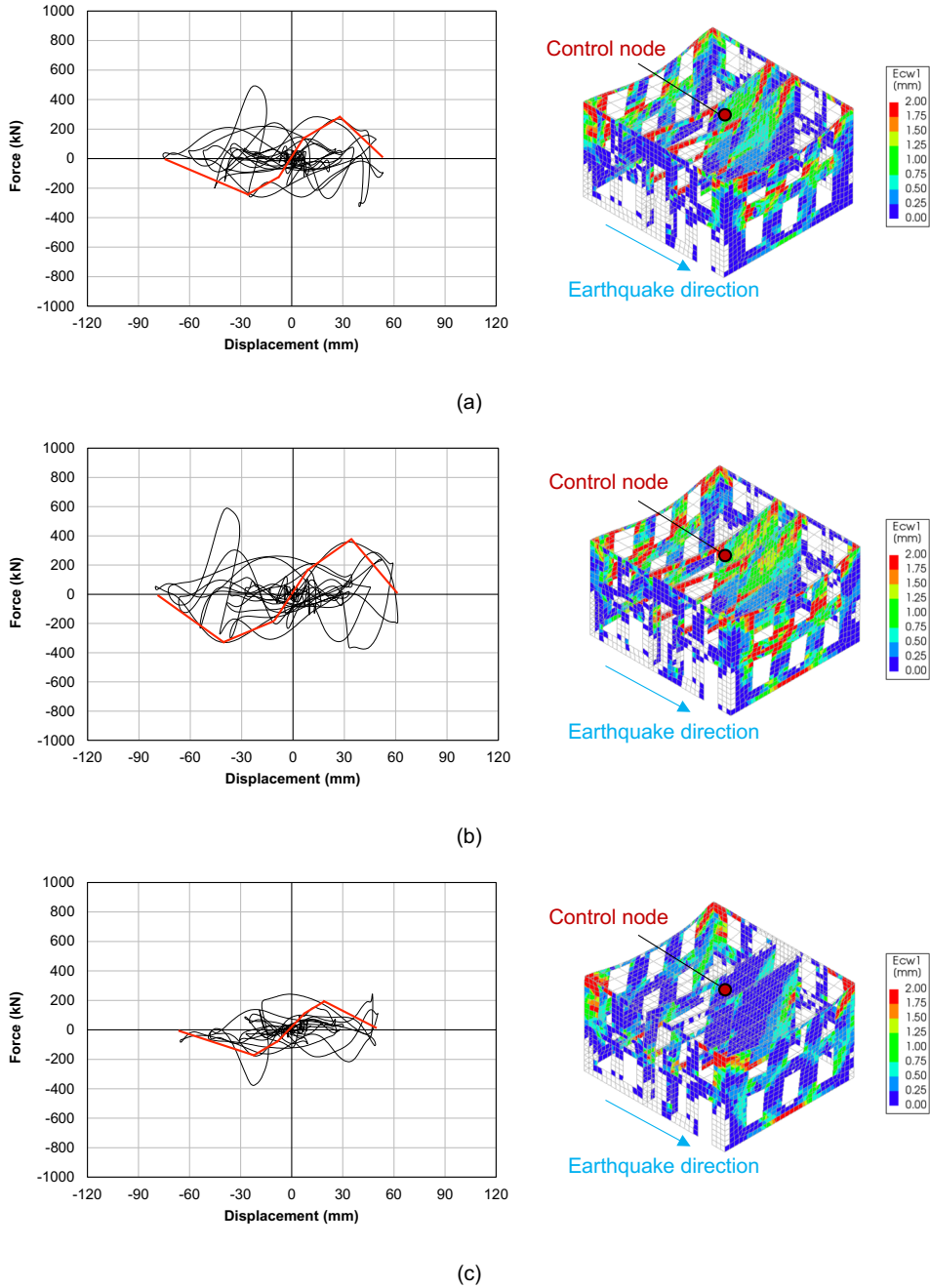


Figure 7.20: Base shear vs. top floor displacement response, including trilinear backbone, and damage level in terms of principal crack opening ($Ecw1$) for the three as-built configurations: B2-AB-MP (a), B2-AB-HA (b), B2-Ab-MP-NI (c).

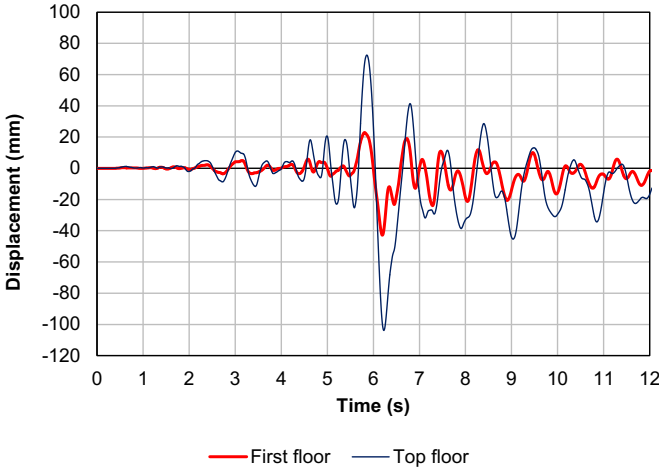


Figure 7.21: Out-of-phase oscillation of the out-of-plane walls at first and top floor level. The displacements time-history refer to the centre of mass of both diaphragms.

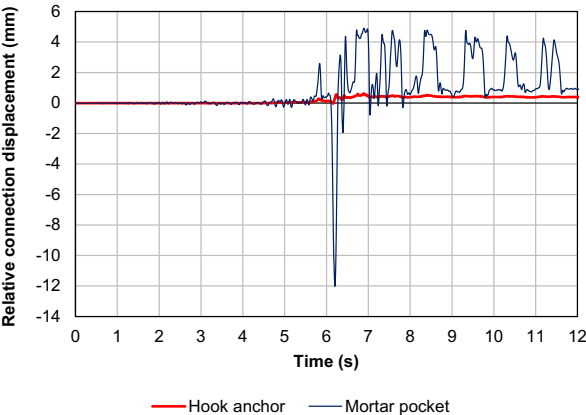


Figure 7.22: Comparison between the relative displacement between top floor and out-of-plane wall of the mortar pocket and hook anchor configuration.

to guarantee a better redistribution of the seismic loads among the walls, leading to an in-plane global failure. Additionally, while with concrete slabs the collapse is mainly caused by the failure of the ground floor walls, with floors strengthened with plywood panels the damage involves both storeys' piers and spandrels, thus retrieving even more energy dissipation from the structure. In any case, the governing in-plane failure appeared to be shear diagonal cracking of the squat pier at the ground floor. The absence of interlocking does not lead to a significant difference in time-history global response, but the collapse is reached at a lower seismic intensity because of the worse cooperation among masonry structural components, with a more pronounced one-way bending cracking mechanism for the out-of-plane walls as well. All other base shear-roof displacement curves, for each configuration and loading direction, are reported in Appendix H.

Similarly to building B1, also an energy characterization was conducted for the two retrofitted configurations with good interlocking among walls (Fig. 7.25). Also in this case, the hysteretic energy provided by configuration B2-PP is larger than that of building B2-RC. Besides, it can be noticed that the prediction of dissipated energy by means of Eq. 6.21 proves to be accurate:

- The usual behaviour factor range of $q = 1.5 \div 2.5$ for masonry structures is once more confirmed when considering configuration B2-RC, and especially along the x direction the piers shows good ductility and dissipation capacity;
- An increased behaviour factor range for URM buildings with dissipative diaphragms ($q = 2.5 \div 3.5$) is again confirmed, and falls in most cases on the conservative side of the hysteretic energy capacity prediction at collapse.

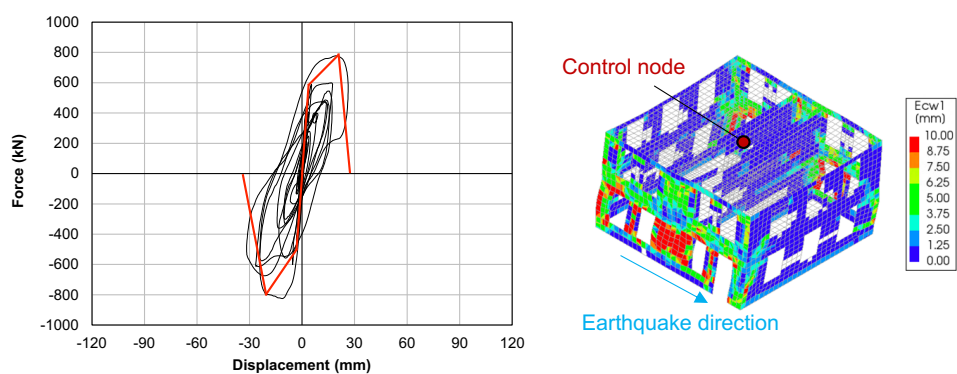
The periods at collapse $T_{n,eff}$ were determined, as for the first case-study building, as a function of the behaviour factors q (Eqs. 6.23-6.25), and are reported in Table 7.26. By knowing the values of $T_{n,eff}$ corresponding to each q , the hysteretic energy can be estimated with Eq. 6.21, by using the pseudo-velocity response spectrum, as was done in the preliminary analyses presented in Chapter 6. The only difference compared to the previous case is the need of calculating the coefficient Γ_n , which enables the transformation of an MDOF system into an equivalent SDOF system. For the present case-study building, from the performed modal analysis, $\Gamma_n = 1.21$.

Therefore, also the results of the analyses on the second case-study building confirm the possibility of optimizing the seismic performance of URM buildings with dissipative timber floors, which appear once more to provide a great increase in the hysteretic energy that can be stored in the system. Further considerations on the dissipative role of the floors will be provided in Section 7.7.

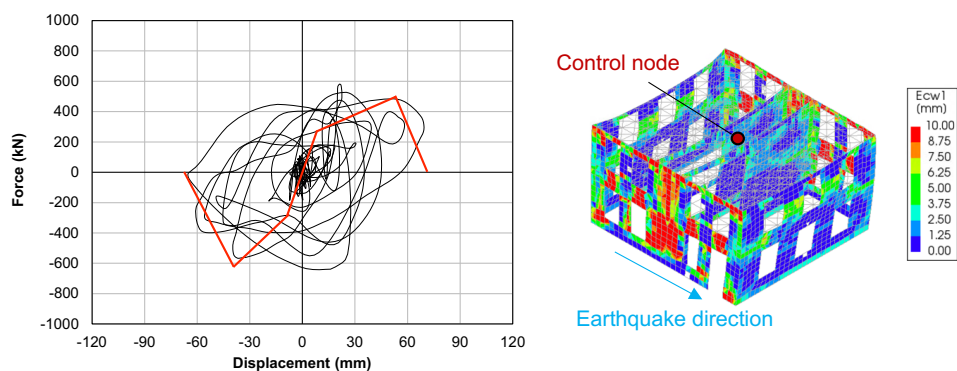
7.6 Third case-study building (B3)

7.6.1 Model properties

The third case-study building was selected to generalize even more the obtained results, by considering another architectural context, and URM structures subjected to tectonic earthquakes with longer duration. Therefore, an Italian country house typical of the Po Valley was chosen (Fig. 7.27). This URM building has a regular structure



(a)



(b)

Figure 7.23: Base shear vs. top floor displacement response, including trilinear backbone, and damage level in terms of principal crack opening (E_{cw1}) for the two retrofitted configurations with well-interlocked walls: B2-RC (a), B2-PP (b).

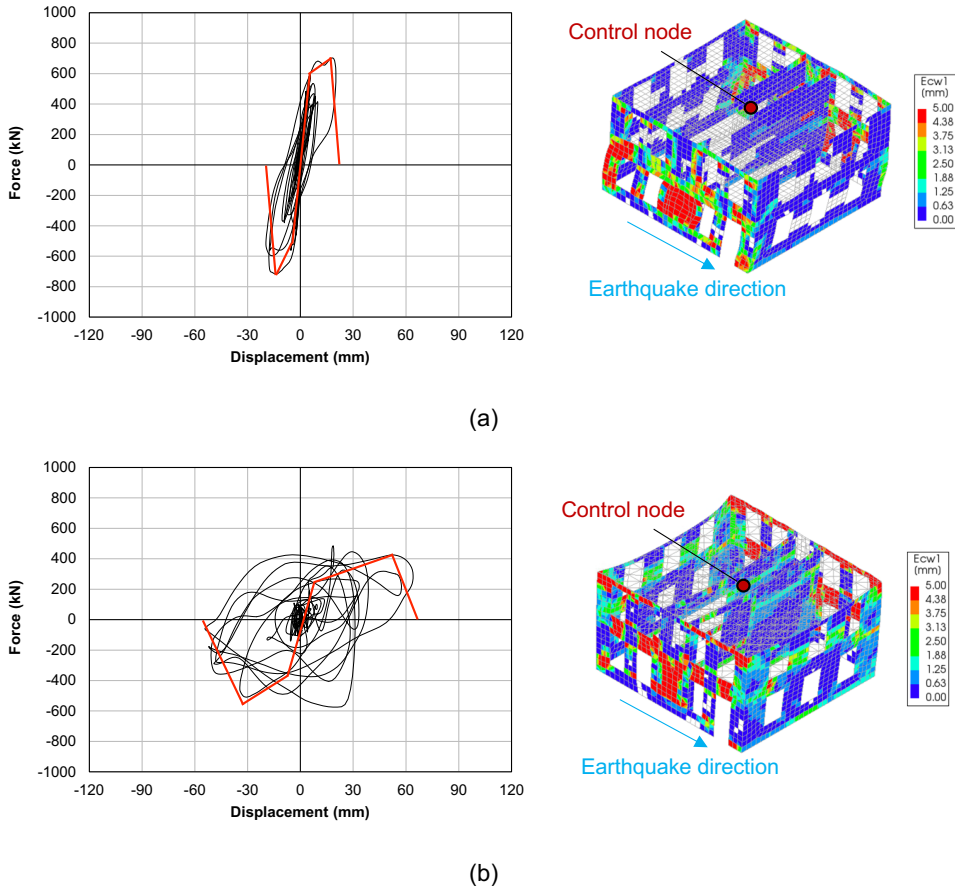


Figure 7.24: Base shear vs. top floor displacement response, including trilinear backbone, and damage level in terms of principal crack opening (E_{cw1}) for the two retrofitted configurations with poorly connected internal walls: B2-RC-NI (a), B2-PP-NI (b).

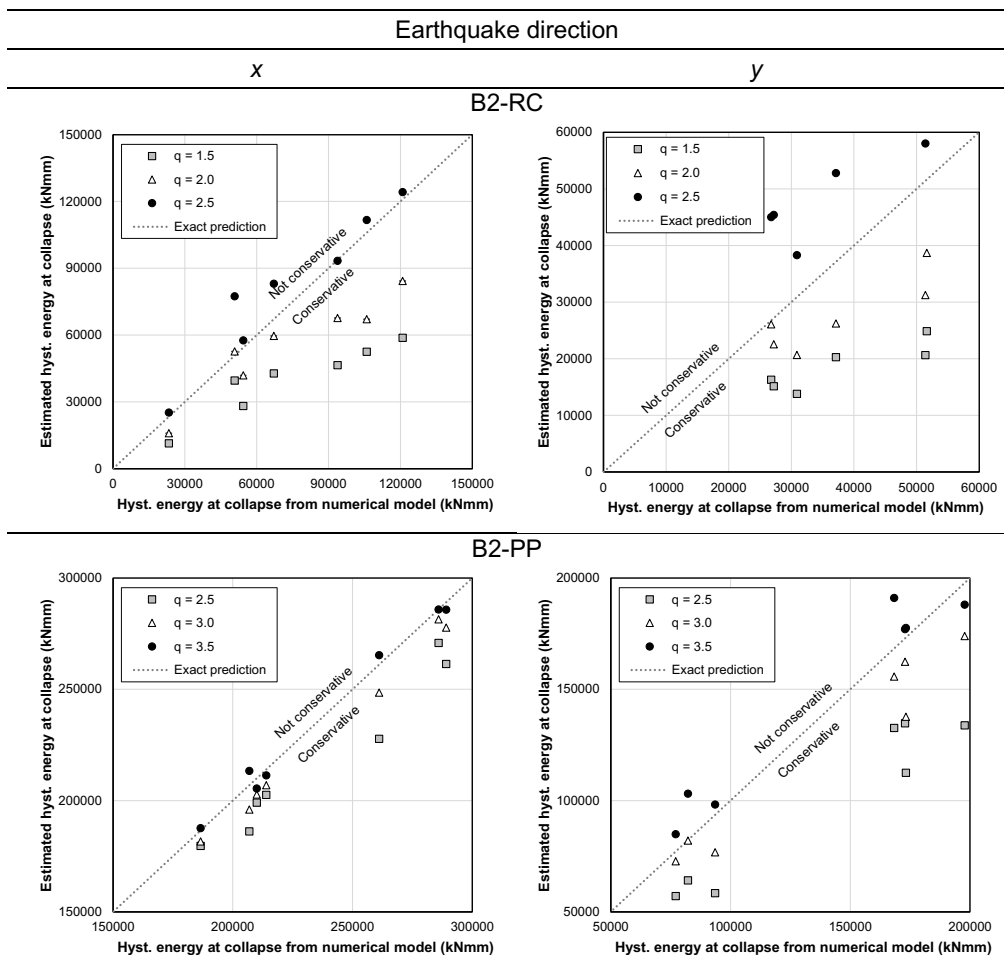


Figure 7.25: Recorded and predicted hysteretic energy of retrofitted configurations B2-RC and B2-PP as a function of the proposed behaviour factor ranges.

Figure 7.26: Effective periods at collapse for the retrofitted configurations B2-RC and B2-PP as a function of their behaviour factor ranges.

Configuration	Excited seismic mass (kg)	Direction	$T_{n,eff}$ (s)		
B2-RC	131302	x	0.18 ($q = 1.5$)	0.22 ($q = 2.0$)	0.27 ($q = 2.5$)
		y	0.13 ($q = 1.5$)	0.16 ($q = 2.0$)	0.20 ($q = 2.5$)
B2-PP	108010	x	0.52 ($q = 2.5$)	0.58 ($q = 3.0$)	0.65 ($q = 3.5$)
		y	0.22 ($q = 2.5$)	0.25 ($q = 3.0$)	0.28 ($q = 3.5$)

Table 7.11: Material properties adopted for masonry shell elements (380 mm thickness) based on [75, 77, 78].

Property	Value
Young modulus E_x parallel to bed joint (MPa)	1875
Young modulus E_y perpendicular to bed joint (MPa)	2500
Shear modulus G_{xy} (MPa)	1000
Mass density ρ (kg/m ³)	2000
Bed joint tensile strength f_t (MPa)	0.15
Fracture energy in tension G_{Ft} (N/mm)	0.01
Compressive strength f_c (MPa)	8.0
Fracture energy in compression G_c (N/mm)	35
Friction angle ($^\circ$)	34
Cohesion (MPa)	0.2
Fracture energy in shear (N/mm)	0.1

and it consists of two units. In this case, the thickness of the walls is constant along the height, and is equal to 380 mm, in agreement with past research studies on typical ancient Italian masonry [77, 78]. Three configurations were studied: one represented the as-built house with flexible diaphragms (B3-AB); in the other two, the floors were retrofitted with plywood panels (B3-PP) or with a concrete slab (B3-RC).

The properties of masonry, reported in Table 7.11, were assumed to be the same for the three configurations; the adopted values are in line with the characteristics of medium quality masonry. 400×400 mm shell elements with the implemented DIANA FEA Engineering Masonry Model [190] were used for modelling the masonry.

While for the walls a density of 2000 kg/m^3 was assumed, for the diaphragms the density values included the self-weight of structural elements, a dead load of 1.00 kN/m^2 (accounting for further elements such as non-structural walls, finishes, plants, pipes), and 30% of the live load, equal to $0.3 \cdot 2.00 \text{ kN/m}^2$ for Italian residential buildings [211].

All timber diaphragms presented 120×180 mm joists at 500 mm spacing, and 20×200 mm planks. These structural properties of the diaphragms were also in this case translated in the numerical model by following the modelling strategy for as-built floors previously described in Section 5.2.2 and validated in Section 7.2. Therefore, because of the very small energy dissipation observed from tests on replicated as-built floors [132], the diaphragms were modelled with linear elastic orthotropic shell elements, whose properties are reported in Table 7.12.

In the configurations featuring diaphragms retrofitted by casting a concrete slab on them, the floors were also modelled with linear elastic orthotropic shell elements, having the properties of structural reinforced concrete (Table 7.13). The thickness of the slab was 50 mm.

For the configurations having floors retrofitted with plywood panels, the modelling strategy discussed in Section 5.4.3 was also for this case adopted: besides the linear elastic orthotropic shell elements, also the nonlinear macro-elements (1×1 m mesh) were present, featuring the constitutive laws of the implemented user-supplied subroutine. The optimized retrofitting interventions on the diaphragms were again designed according

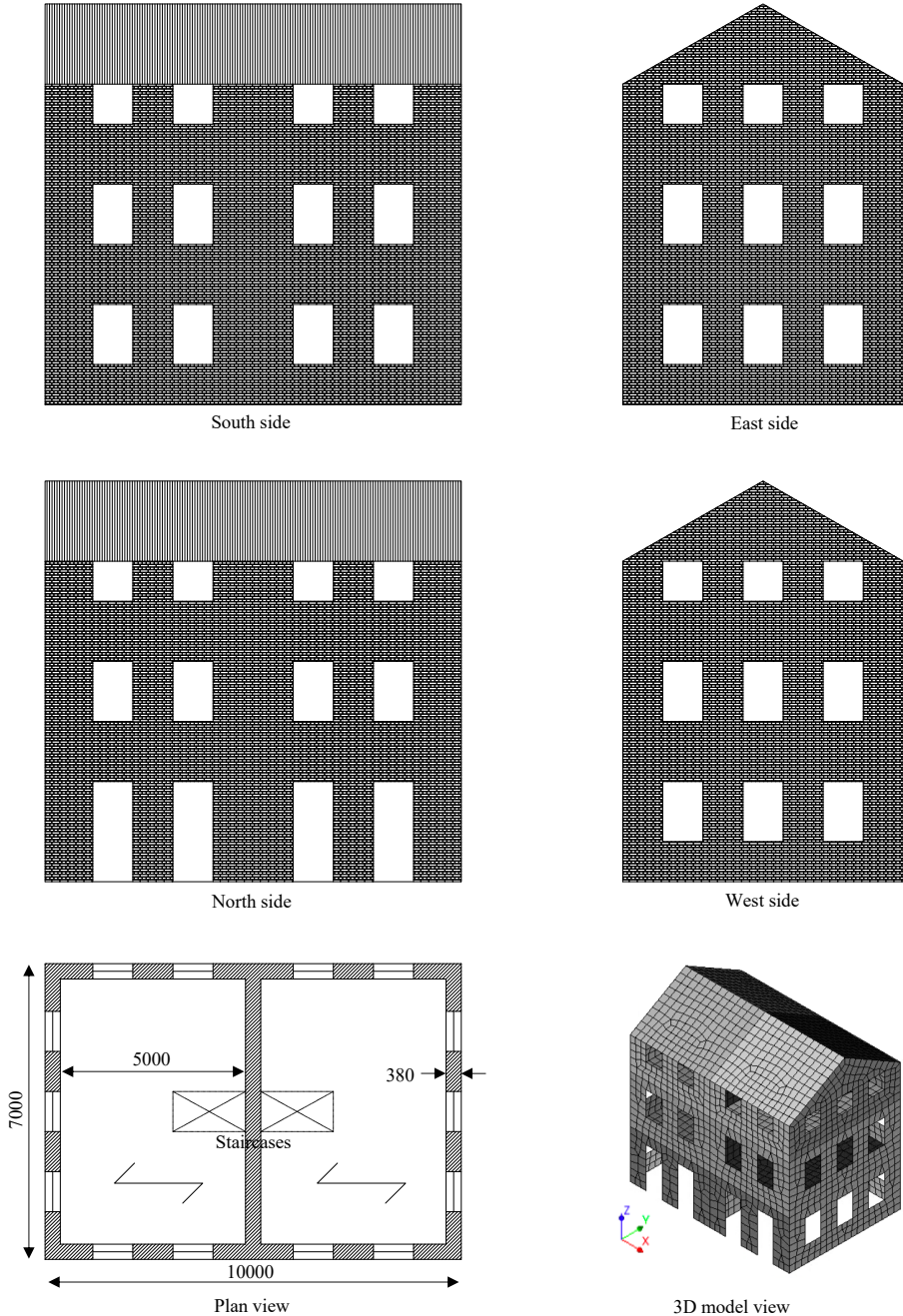


Figure 7.27: Main properties and geometry of the first case-study building; dimensions in mm.

Table 7.12: Equivalent properties adopted for the shell elements (20 mm thickness) representing the flexible diaphragms in configuration B3-AB, in agreement with the modelling strategy presented in Section 5.2.2 and the example provided in Appendix D.

Property	Value		
	First floor	Second floor	Roof
Equivalent Young modulus E_{eq} (MPa)	1874571	1874571	4557380
In-plane shear modulus G_{xy} (MPa)	2	2	2
Out-of-plane equivalent shear moduli G_{xz} , G_{zy} (MPa)	117161	117161	284836
Mass density ρ (kg/m ³)	9490	9490	6480

Table 7.13: Material properties adopted for the shell elements (thickness = 70 mm) representing the concrete slabs in configuration B3-RC.

Property	Value		
	First floor	Second floor	Roof
Young moduli E_x , E_y , E_z (MPa)	30000	30000	30000
Shear moduli G_{xy} , G_{xz} , G_{zy} (MPa)	12500	12500	12500
Mass density ρ (kg/m ³)	4500	4500	4390

to the global in-plane capacity of the piers, and conservative out-of-plane drift limits for the walls:

- The maximum base shear of the building (approximately 1000 kN in the weak x direction) was evaluated through a preliminary pushover analysis applied to configuration B3-RC, and then the loads at floor and roof level were estimated through the lateral force method. The retrofitting intervention was designed accordingly, providing sufficient strength to activate in-plane failure mechanisms up to the expected 1000 kN base shear, but contemporarily deflection capacity.
- At the same time, to prevent out-of-plane walls failure, the maximum midspan displacement, at which the diaphragms reached their strength, was fixed at 2% of the out-of-plane walls (or gables, for the roof) height (Section 5.6.3). The potential stiffening effect of the out-of-plane walls was conservatively not taken into account, also because of the presence of large openings. Besides, use of dry screed made of loose material was assumed, so that the deflection of the floors could be enabled.

Table 7.14 reports the properties of the macro- and shell elements simulating the retrofitted diaphragms, while Appendix F reports the drawings and the main characteristics of the dissipative strengthening interventions for the floors in this case-study building.

In this case-study building, it is assumed that timber-masonry connections are continuous and sufficiently resistant for both as-built and retrofitted configurations. This enables to check whether, besides the increase in performance because of the (dissipative) floors retrofitting, well-designed diaphragm-to-wall connections are already sufficient to guarantee a reasonably adequate seismic performance of the building, as was suggested from the results of past experimental studies [117].

Table 7.14: Equivalent properties adopted for the macro-elements and shell elements (thickness = 38 mm) representing the diaphragms retrofitted with plywood panels in configuration B3-PP, in agreement with the modelling strategy presented in Section 5.4.3 and the example provided in Appendix D.

Property	Value		
	First floor	Second floor	Roof
<i>Macro-elements (in-plane response)</i>			
Young modulus of rigid trusses E_t (MPa)	10^{10}	10^{10}	10^{10}
Diagonal trusses max. strain ε_{max}	0.0186	0.0353	0.046
Diagonal trusses max. stress σ_{max} (MPa)	9870	19600	11800
Diagonal trusses initial stiffness K_0 (MPa)	2780000	2730000	1350000
<i>Shell elements (out-of-plane response)</i>			
Equivalent Young modulus E_{eq} (MPa)	273000	273000	664000
In-plane shear modulus G_{xy} (MPa)	0.1	0.1	0.1
Out-of-plane equivalent shear moduli G_{xz}, G_{yz} (MPa)	17100	17100	41500
Mass density ρ (kg/m ³)	5210	5210	3620

For all configurations, after a preliminary characterization of the vibration modes by means of eigenvalue analyses, nonlinear incremental dynamic analyses were performed, by subjecting the house to seven accelerograms of tectonic earthquakes (Fig. 6.8). The main loading directions x and y were studied separately, therefore a total of 42 analyses were performed. An intrinsic Rayleigh damping of 2% was considered [32], and the Newton-Raphson iterative method was adopted [182]. As convergence criterion, the force or displacement norms were used, with a limit tolerance of 10^{-2} .

7.6.2 Results from eigenvalue analysis

The preliminarily performed eigenvalue analyses on the three configurations were useful to characterize the fundamental periods and mode shapes in both the x and y directions, reported in Fig. 7.28. As can be noticed, the main vulnerability of the as-built configuration B1-AB is related to the weakness of gables out of their plane. In general, this structure appears to be quite stiff, mainly because of the large thickness of the masonry walls, and especially along the y direction. As was noticed in the previous cases, the dissipative retrofitting intervention does not excessively increase the stiffness of the whole building, leading to a fundamental period falling in between that of B3-AB and B3-RC configurations. In the cases with deformable diaphragms (B3-AB, B3-PP), it can be noticed that the deformation of the mode shape in the y direction is more pronounced in one of the two building units, while for case B3-RC it is symmetric. Yet, during time-history analyses, a substantially symmetric behaviour was observed for all configurations.

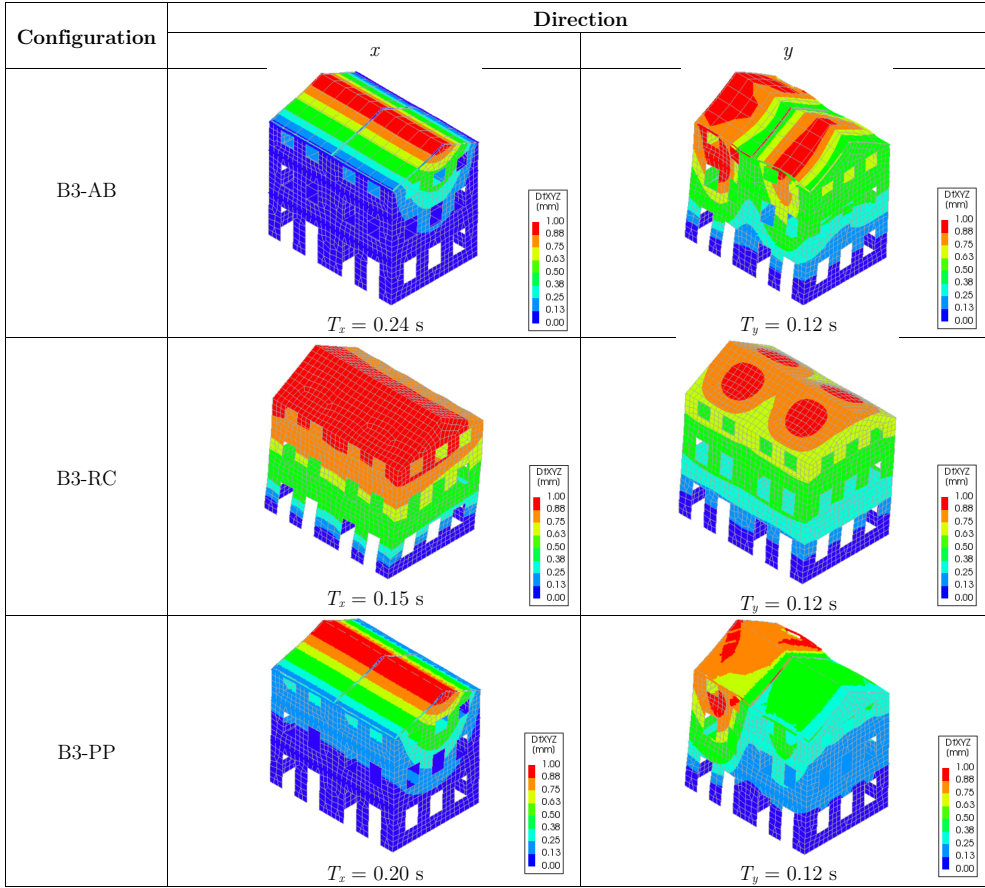


Figure 7.28: Results from eigenvalue analysis in terms of fundamental periods and associated mode shapes for the three configurations of case-study building B3.

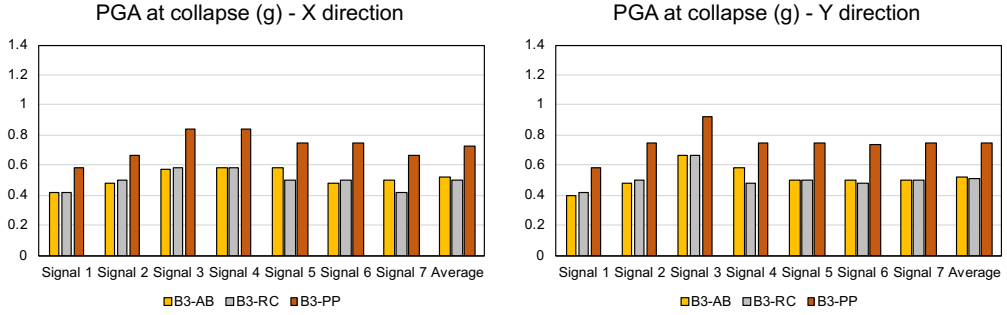


Figure 7.29: PGA at collapse for the three configurations in the x (left) and y direction (right).

7.6.3 Results from time-history analyses

The nonlinear incremental dynamic analyses performed for the three configurations displayed some interesting results. Fig. 7.29 shows the PGA at collapse along both loading directions for all configurations: as can be noticed, there is no substantial difference (on average) between the performance of the as-built case (B3-AB) and that of the building retrofitted with concrete slabs (B3-RC). This seems to confirm the findings of MAGENES et al. [115, 116] and SENALDI et al. [117], highlighting that with sufficiently sound and massive walls, a good connection of diaphragms to masonry can already provide an adequate seismic capacity, without needing an increase in their stiffness. The better performance of configuration B3-PP can be attributed to the larger energy dissipation that can be retrieved from the optimized retrofitting of the floors.

Besides, it is also interesting to notice that, although building B3 features very thick and medium-quality masonry walls, thus with better properties compared to the previous case-study buildings, the results in terms of PGA at collapse did not highlight a better performance. This is precisely the effect of the larger load duration and the increased number of cycles in the structure, related to the higher damaging potential of the adopted tectonic earthquake signals. This is also evident from the results in terms of base shear-roof displacement curves (Appendix H), which exhibit several full loading cycles and a more detrimental effect on masonry piers. As an example, Fig. 7.30 shows these graphs with reference to signal 7 for the three configurations in the x direction (the weakest), including trilinear backbones for a clearer representation. An important difference compared to the previous case-study buildings emerges from the reported curves and the damage in terms of crack pattern: the in-plane strength of the wall is brought into play also in the as-built configuration (failure at 0.6-0.8% drift), even if the gables experience extensive out-of-plane damage as well.

This means that, in this specific case, the thick walls, as well as the regularity and compactness of the structure, make the floors of configuration B3-AB already able to sufficiently transfer shear loads, because of the well-realized connection with masonry components. It should be noticed that this result is again in line with not only past experimental research studies [115]-[117], but also numerical outcomes [8]-[14]. The fact that the stiffness of the as-built diaphragms can already be sufficient for the building to retrieve its whole base shear is confirmed by the designed light retrofitting intervention, which provides the floors with an increased energy dissipation more than

Table 7.15: Effective periods at collapse for the retrofitted configurations B3-RC and B3-PP as a function of their behaviour factor ranges.

Configuration	Excited seismic mass (kg)	Direction	$T_{n,eff}$ (s)		
B3-RC	158909	x	0.16 ($q = 1.5$)	0.19 ($q = 2.0$)	0.23 ($q = 2.5$)
		y	0.13 ($q = 1.5$)	0.15 ($q = 2.0$)	0.19 ($q = 2.5$)
B3-PP	141485	x	0.32 ($q = 2.5$)	0.36 ($q = 3.0$)	0.41 ($q = 3.5$)
		y	0.19 ($q = 2.5$)	0.22 ($q = 3.0$)	0.24 ($q = 3.5$)

an enhancement in stiffness, as can be noticed from the small decrease in fundamental period of configuration B3-PP with respect to the as-built one (Fig. 7.28), and from the base shear-roof displacement curve very similar to case B3-AB (Fig. 7.30).

The increased energy dissipation of the building because of the optimized diaphragms retrofitting is even more evident when characterizing the two retrofitted configurations in terms of energy (Fig. 7.31). As can be noticed, the hysteretic energy provided by configuration B3-PP is remarkably larger than that of building B3-RC. Besides, the prediction of dissipated energy by means of Eq. 6.21 proves once more to be accurate:

- The usual behaviour factor range of $q = 1.5 \div 2.5$ for masonry structures is again confirmed when considering configuration B3-RC;
- An increased behaviour factor range for URM buildings with dissipative diaphragms ($q = 2.5 \div 3.5$) is also once more validated.

The effective periods at collapse $T_{n,eff}$, determined in the same way as for the other case-study buildings, are reported in Table 7.15. By knowing the values of $T_{n,eff}$ corresponding to each q , the hysteretic energy can be estimated with Eq. 6.21, by using the pseudo-velocity response spectrum (Chapter 6). Also for this building, the coefficient Γ_n needs to be determined, which enables the transformation of an MDOF system into an equivalent SDOF system. For the present case-study building, from the performed modal analysis, $\Gamma_n = 1.3$.

Therefore, the results of the analyses on the third case-study building confirm again the possibility of optimizing the seismic performance of URM constructions with dissipative timber floors, also when considering other building contexts or earthquake types: once more, a great increase in the hysteretic energy that can be stored in the system is provided. Further considerations on the dissipative role of the floors will be provided in the next section as well.

7.7 Additional considerations on the role of timber diaphragms

From the results of the three analyzed buildings, the role of timber diaphragms on the seismic response of URM buildings appears to be crucial. In this section, the effect of the in-plane stiffness of the floors is discussed, taking into account additional

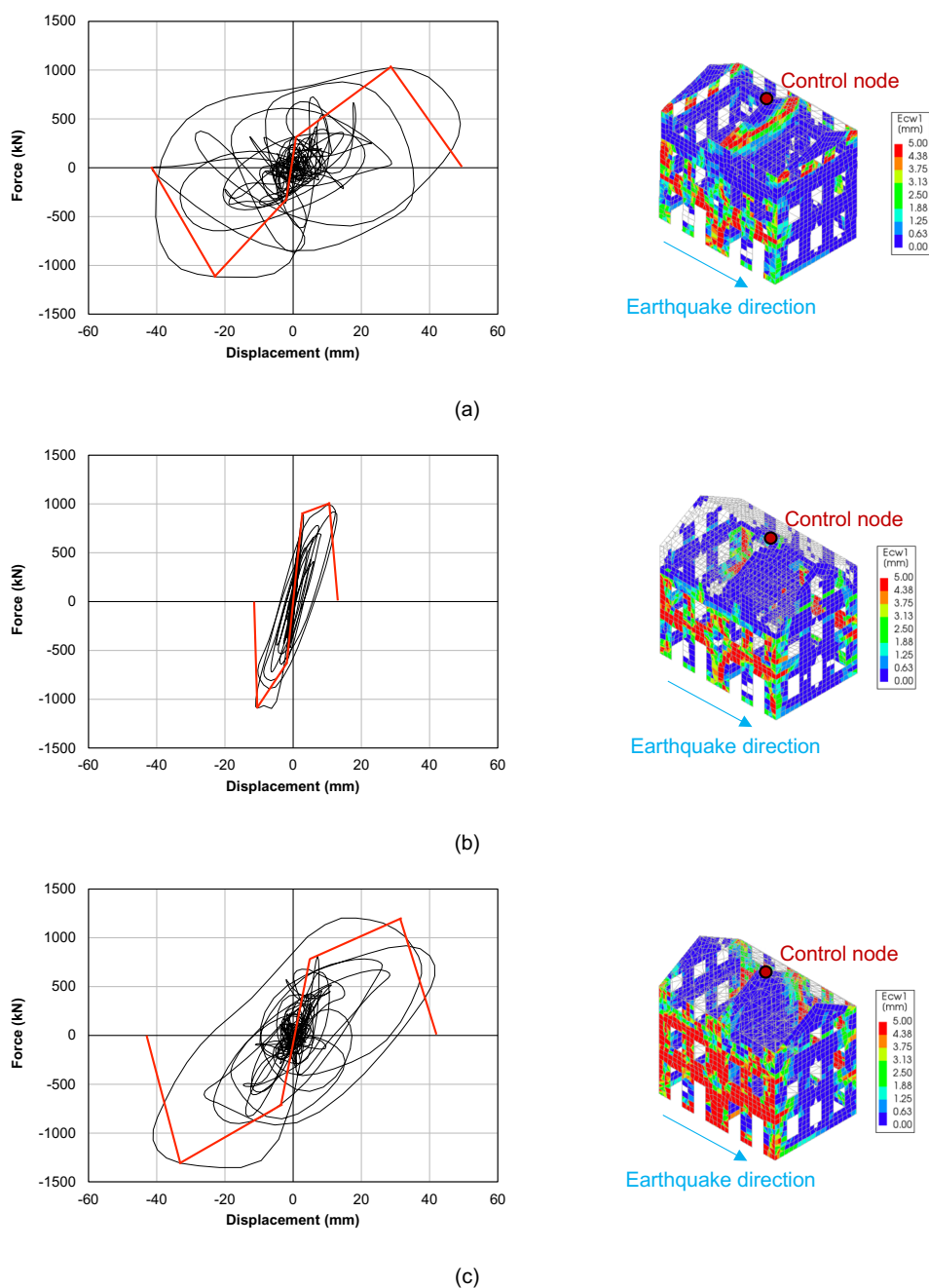


Figure 7.30: Base shear vs. roof displacement response, including trilinear backbone, and damage level in terms of principal crack opening (E_{cw1}) for the three configurations: B3-AB (a), B3-RC (b), B3-PP (c).

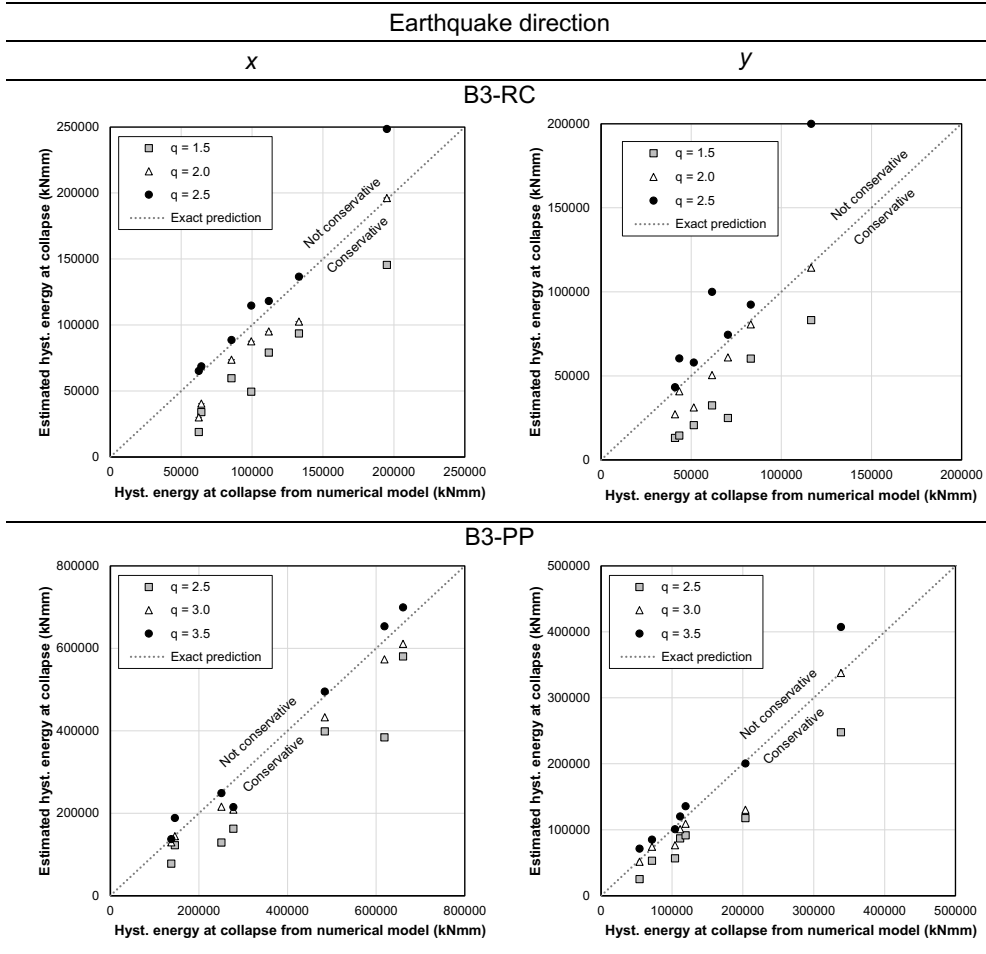
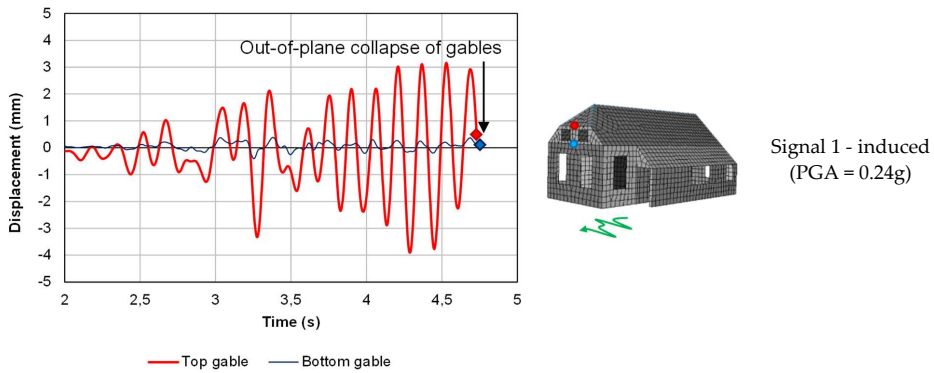


Figure 7.31: Recorded and predicted hysteretic energy of retrofitted configurations B3-RC and B3-PP as a function of the proposed behaviour factor ranges.

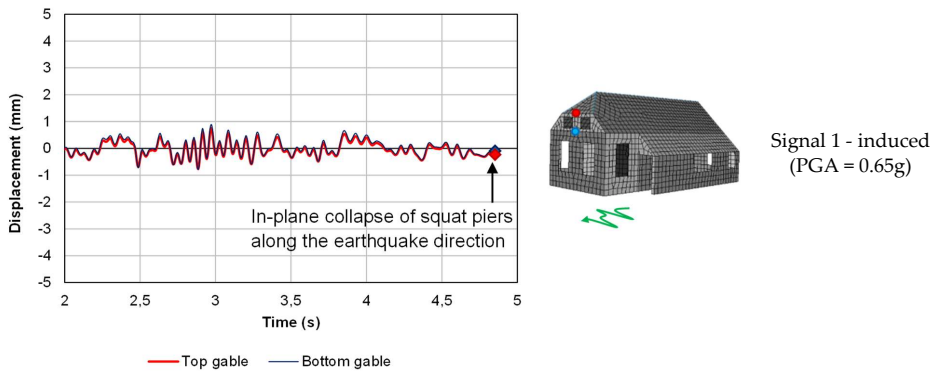
control nodes. Consider the out-of-plane seismic response of the front gable in building B1 (Fig. 7.32), as this can be regarded as one of its most vulnerable portions, due to its reduced thickness (only 100 mm). The low in-plane stiffness of the existing roof (Fig. 7.32a) leads to a premature out-of-plane collapse of the gable, highlighted by the large, out-of-phase relative displacement between the two control nodes. This local collapse, if compared to the cases featuring stiffened diaphragms, occurs for a relatively low seismic acceleration, justifying the need of a retrofitting intervention to enhance the box behaviour. When the concrete slab retrofitting is applied (Fig. 7.32b), the two control nodes display an identical displacement time-history, as expected with a rigid diaphragm system. The collapse of the building is in this case not related to the gable, as in the as-built situation, but to the in-plane failure of the squat walls along the earthquake direction. This same failure type was observed for configuration B3-PP (Fig. 7.32c), which displayed a hybrid response: the floors retrofitted with plywood panels proved to be sufficiently stiff to activate the in-plane failure of the walls, but also allowed for a limited out-of-plane displacement in the gable, activating energy dissipation in the strengthened roof.

The performed analyses also showed that the in-plane stiffness of the floors is responsible for how quickly the masonry piers are brought into play: this is exemplified in Fig. 7.33 for building B2, taking into account the displacements of a control node on the roof and of one on the lateral wall. When considering the existing floors (Fig. 7.33a), on the one hand their low stiffness and deflection capacity could positively prevent the in-plane walls from being excessively solicited; on the other hand, their flexibility led to out-of-plane collapses, and to an independent movement of each floor, without retrieving the desired box behaviour. With rigid concrete diaphragms (Fig. 7.33b), the deflection of the floors is absent, and diaphragms and walls undergo the same displacement. This solution guarantees the maximum redistribution of seismic shear forces and an excellent box behaviour, but directly brings the walls' strength into play. When an optimized, dissipative retrofitting is chosen (Fig. 7.33c), it is possible to link the displacement capacity of the diaphragms, enabling their energy dissipation potential, with an in-plane stiffness sufficient to redistribute seismic loads among the walls. Thus, similarly to building B1-PP, the in-plane capacity of the piers is retrieved, but the damping effect of the floors can prevent this from occurring right at the beginning of the seismic signal, with an increase of the seismic capacity of the building.

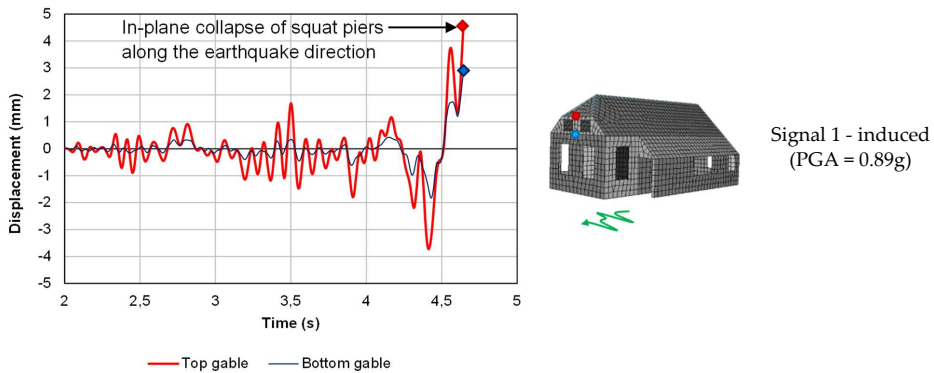
The previously discussed results were again obtained in case-study B3 (Fig. 7.34), subjected to tectonic earthquakes. Considering the control nodes at each floor level and at the top and bottom of the gable, configuration B3-AB (Fig. 7.34a) showed that even the existing flexible floors are sufficient to retrieve the in-plane strength of the walls, because of the massive structure of the piers. Depending on the expected seismic intensity, a stiffening intervention for the floors might thus not be needed, provided that they are well connected to the walls. However, the as-built floors still cause extensive damage to the gables, where the largest relative displacements are recorded, and a dangerous out-of-phase movement of each floor level. In configuration B3-RC (Fig. 7.34b), the observed displacements are all linked to the in-plane capacity of walls, because of the presence of rigid diaphragms. The response also shows an improved box behaviour, but the PGA at collapse is the same as the existing configuration (with floors well-connected to the walls). Finally, configuration B3-PP (Fig. 7.34c) shows a combination of the two previous cases: the presence of optimally designed



(a)

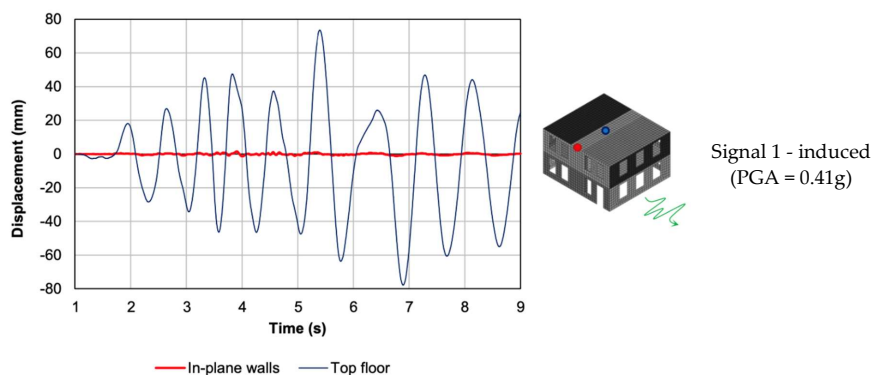


(b)

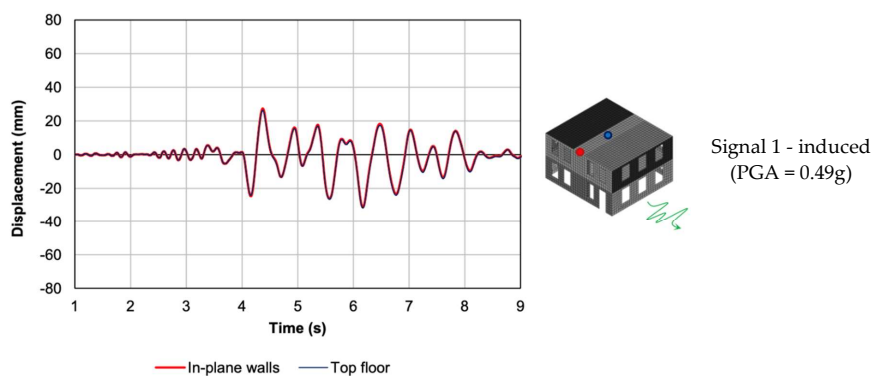


(c)

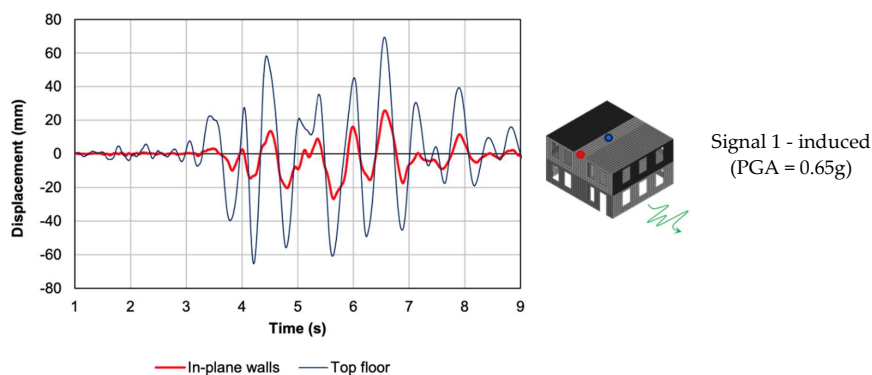
Figure 7.32: Out-of-plane displacement time-histories of the front gable for configurations B1-AB (a), B1-RC (b), B1-PP (c) at collapse. From [212].



(a)



(b)



(c)

Figure 7.33: Examples of top floor and in-plane walls displacement time-histories for configurations B2-AB-MP (a), B2-RC (b), B2-PP (c). From [212].

retrofitted diaphragms induces an in-phase movement of the floor levels, while reducing the dangerous relative displacement between top and bottom of the gable, and retrieves at the same time the in-plane capacity of the piers. This combination maximizes the hysteretic energy that can be activated and dissipated by the building.

In relation to this latter aspect, Fig. 7.35 highlights how relevant the contribution of the dissipative floors can be in terms of their activated hysteretic energy, with respect to a retrofitting with rigid diaphragms. In all cases, the floors retrofitted with plywood panels are responsible for a significant increase in the energy that can be dissipated by the buildings. The dissipative effect of the floors is also evident in Fig. 7.36, comparing the response of the most solicited wall in building B1 when the diaphragms are retrofitted with concrete slabs or plywood panels: as can be noticed, under the same signal, when concrete slabs are present the pier reaches its capacity after a shear diagonal failure, while with plywood panels retrofitting a damping effect on the wall is noticeable, and the maximum in-plane load for the pier is reached by further amplifying the signal of more than 35% compared to that applied to B1-RC configuration.

7.8 Role of timber-masonry connections

The role of timber-masonry connections was evaluated in case-study building B2. The main outcome of this analysis is related to the need of modelling timber-masonry joints only when their stiffness is particularly low, for instance in the case of connections realized with mortar pocket only. If, instead, the connections is sufficiently stiff and resistant, a continuous modelling constitutes a reasonable approximation.

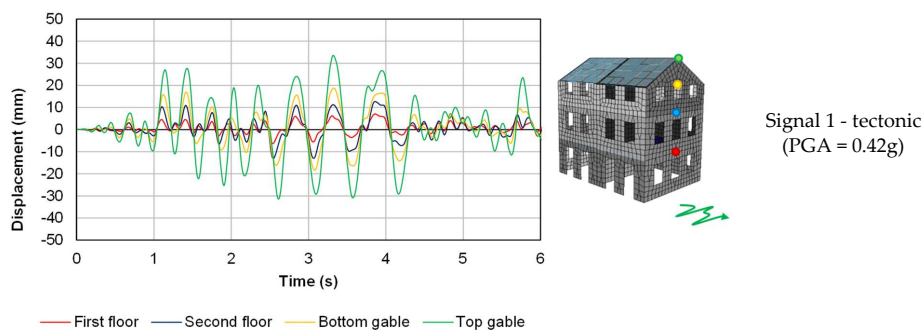
As expected, the as-built connections with mortar pocket appeared not to be sufficient to guarantee the box-like behaviour of the building, and cause out-of-plane collapses of masonry walls. On the contrary, the hook anchor as-built connection type was already adequate to transfer the shear loads from floors to walls, as it happened even more with the retrofitted joints.

Finally, because strengthened joints could be reasonably approximated as continuous connections between floors and walls, when realizing retrofitting interventions on existing joints, their design can be conducted in terms of strength.

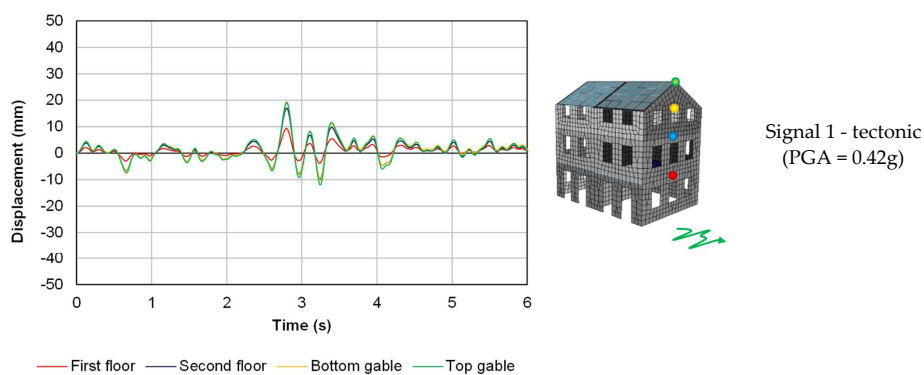
7.9 Final summary and concluding remarks

In general, the performed analyses confirm the optimization of the seismic performance of URM buildings by means of a dissipative retrofitting of their timber diaphragms, effectively connected to masonry walls. A summary of the main results is reported in Table 7.16.

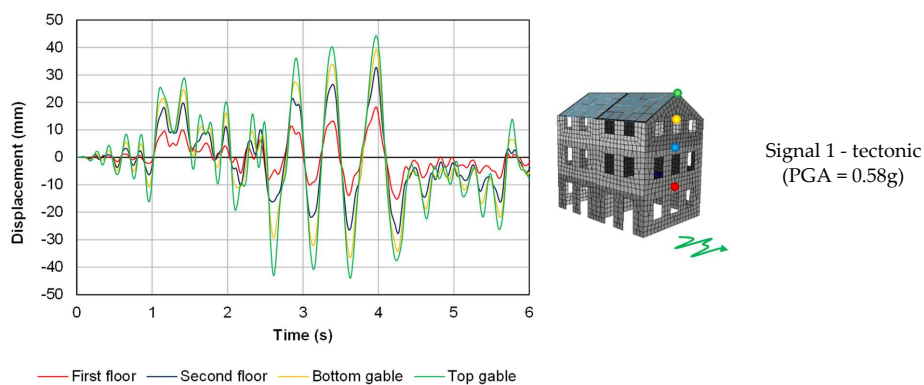
The increase in capacity allows the optimally retrofitted buildings to withstand stronger earthquakes, quantifiable in terms of an approximately 30% more intense design acceleration response spectrum. This corresponds to an equivalent damping ratio induced by the floors of 15% [212], and thus validates the value obtained in Chapter 4. When considering the diaphragms contribution from an energy-based perspective, it has been shown that a clear increase in the hysteretic energy provided by the building can be achieved. In Table 7.16, this increase was quantified as an average hysteretic energy ratio, in order to homogenize the results; this indicator is defined as the ratio



(a)



(b)



(c)

Figure 7.34: Out-of-plane displacement time-histories of the front wall for configurations B3-AB (a), B3-RC (b), B3-PP (c) at collapse. From [212].

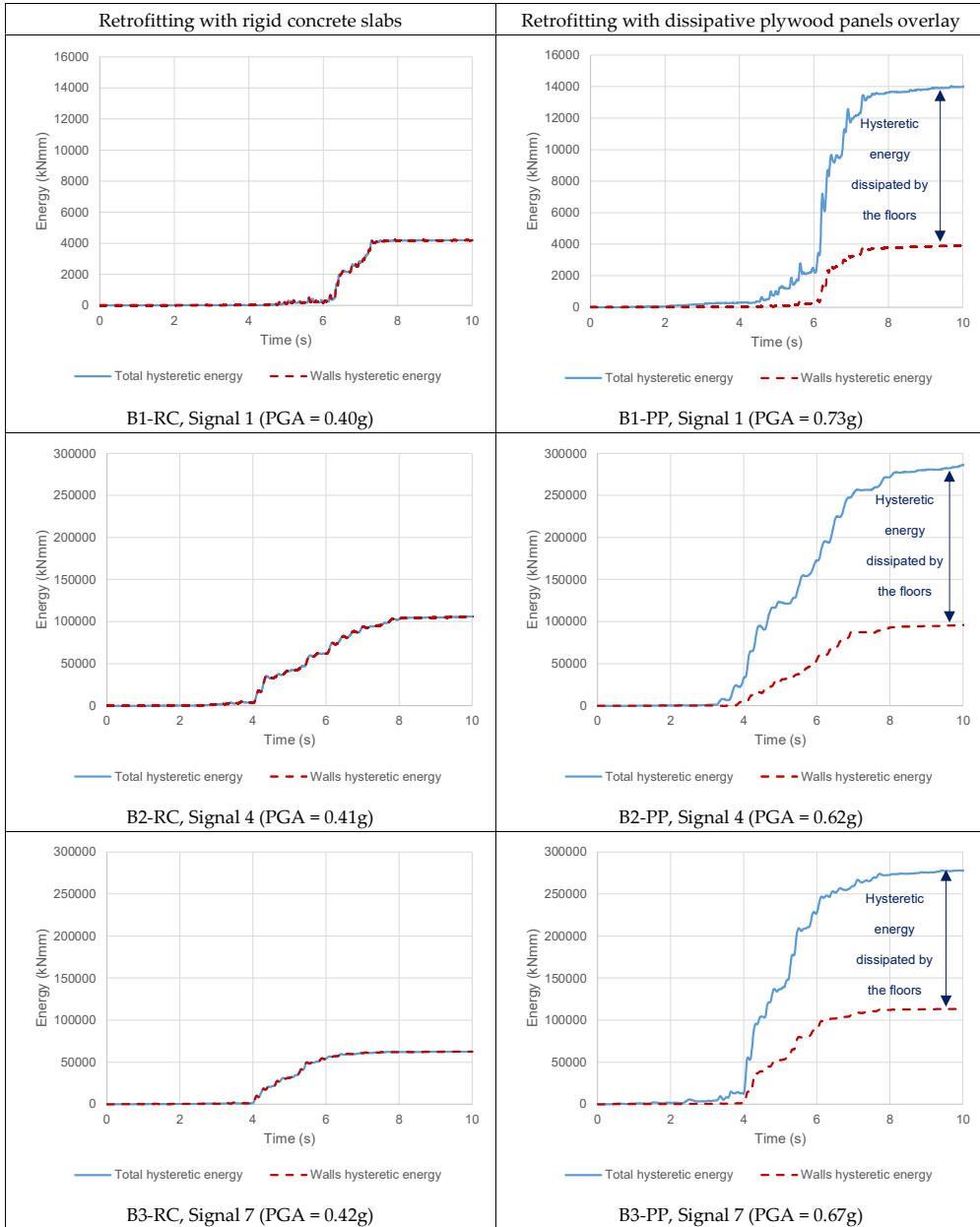


Figure 7.35: Hysteretic energy vs. time for the retrofitted configurations at near-collapse state. The dissipative role of the diaphragms retrofitted with plywood panels, in comparison to the rigid concrete slabs, is evident. From [212].

Figure 7.36: Effect of the diaphragms stiffness and dissipation on the in-plane response of the most solicited wall in building B1. From [212].

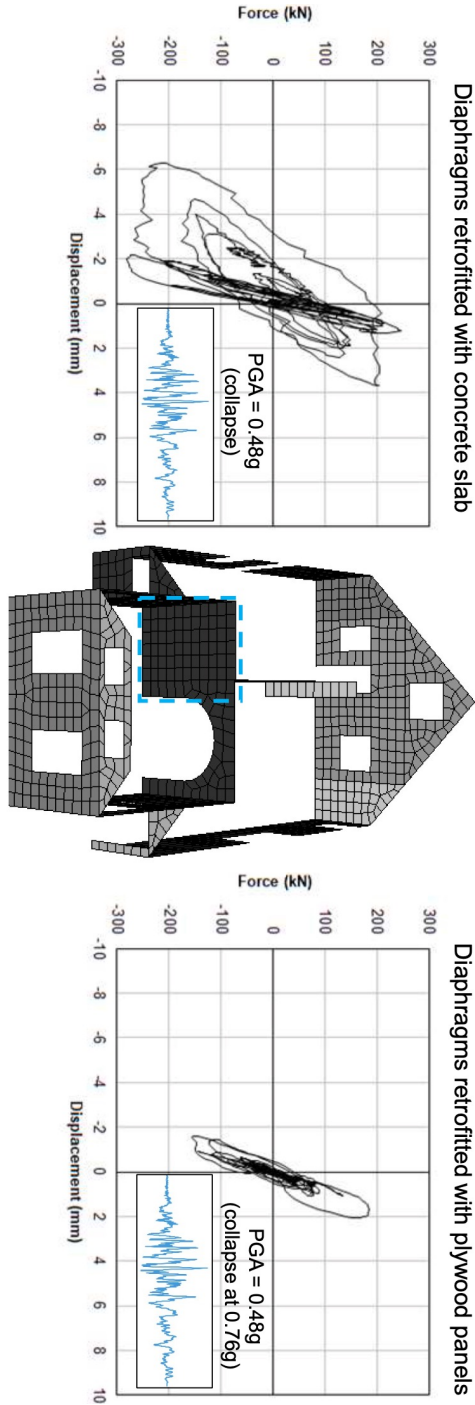


Table 7.16: Summary of the main results from the numerical analyses on the three case-study buildings.

Configuration	Failure type (drift)	Average PGA at collapse (g)	Average hysteretic energy ratio (for retrofitted cases)	Estimated q range (for retrofitted cases)	Damping ratio of floors
B1-AB	IP (0.5%)/OOP	0.18	-	-	0.05
B1-RC	IP (0.6%)	0.53	1.0	$1.5 \div 2.5$	0.05
B1-PP	IP (0.6%)	0.81	23.4	$2.5 \div 3.5$	0.15
B2-AB-MP	OOP (2.0%)	0.34	-	-	0.05
B2-AB-HA	OOP (2.0%)	0.41	-	-	0.05
B2-AB-MP-NI	OOP (2.0%)	0.24	-	-	0.05
B2-RC	IP (0.6-0.8%)	0.46	1.0	$1.5 \div 2.5$	0.05
B2-RC-NI	IP (0.6-0.8%)	0.35	-	-	0.05
B2-PP	IP (0.6-0.8%)	0.73	3.8	$2.5 \div 3.5$	0.15
B2-PP-NI	IP (0.6-0.8%)	0.64	-	-	0.15
B3-AB	IP (0.6-0.8%)	0.52	-	-	0.05
B3-RC	IP (0.6-0.8%)	0.50	1.0	$1.5 \div 2.5$	0.05
B3-PP	IP (0.6-0.8%)	0.73	2.75	$2.5 \div 3.5$	0.15

between the hysteretic energy dissipated by a certain retrofitted configuration, and that dissipated by the configuration having stiff floors. Hence, for all cases in which a concrete slab is present, this ratio is unitary, while with the dissipative diaphragms higher values are obtained. In the first case-study, because of the very low dissipation of configuration B1-RC, due to local in-plane collapses of piers, the hysteretic energy dissipated by building B1-PP is much larger, while for buildings B2 and B3 this increase was between two and three times.

The larger hysteretic energy dissipated by the optimized configurations is also linked to an increased behaviour factor $q = 2.5 \div 3.5$, which is up to 60% higher than the value recommended for common URM buildings, and confirms one more the advantage of an efficient, light, and dissipative retrofitting of timber diaphragms, and of an effective strengthening of timber-masonry connections.

Chapter 8

Design recommendations for assessing and optimizing seismic capacity of URM buildings

8.1 Introduction

This chapter serves as a summary of the adopted approach for optimizing seismic capacity of existing URM buildings through the dissipative retrofitting of their timber diaphragms, and an effective strengthening of timber-masonry connections. Therefore, the outcomes from all previous chapters will constitute the basis for improved recommendations for seismic analyses on these constructions. Specific focus will be given to the effect of in-plane strengthening of the diaphragms and the improvement in shear transfer of the floor-to-wall joints, but also to the suggested methodology for preparing numerical models and conducting seismic analyses. The complete procedure will be presented in terms of a number of advised steps to be performed.

8.2 Step 1: Inspection of existing building of interest

This first step is certainly essential to perform a reasonably accurate seismic assessment of an existing URM building. Several non-destructive and slightly-destructive techniques can be adopted to evaluate the main mechanical properties of masonry walls [213]-[215] and timber floors [132].

The knowledge of basic material characteristics is in fact crucial: for masonry, thermography, sonic, (double) flatjack or core tests can be performed; for the diaphragms suitable techniques can be, among others, the determination of (dynamic) modulus of elasticity, micro-drilling for assessing the potential decay and the density, extraction of small samples for determining density, wood species and moisture content.

With these properties, it is then possible to firstly design the retrofitting techniques (Step 2), and then to assess its impact through numerical models (Step 3) and linearized or nonlinear seismic analyses (Step 4).

8.3 Step 2: Design of retrofitting methods for diaphragms and joints

When designing a retrofitting intervention on the diaphragms, according to the obtained results, it is suggested to retrieve the maximum energy dissipation from the diaphragms, so that the seismic forces on the masonry walls can be dampened. To this end, if the building of interest is sufficiently regular, a preliminary pushover analyses can be performed, by assuming stiff diaphragms, to calculate the maximum base shear. Subsequently, from this force the shear loads acting on each floor can be derived, by means of the lateral force method. In this way, the floors can be designed to efficiently transfer the expected shear forces, and the diaphragms are thus able to involve all together the whole base shear of the building.

Yet, at the same time, the transferred shear loads have to be brought into play at a certain deflection, so that their energy dissipation can be activated. For this purpose, an out-of-plane inter-storey drift for masonry walls of 2% can be adopted. For instance, for a two-storey house with a 3 m inter-storey height, the maximum in-plane deflection for the first floor is 60 mm, for the second floor is 120 mm.

Starting from the knowledge of the in-plane strength and maximum deflection of the diaphragms, it is possible to opt for the proposed strengthening technique, with an overlay of plywood panels screwed along their perimeter to the existing sheathing, and to adopt the formulated analytical model for its design. In particular, the global in-plane strength is mainly directly connected to the number and diameter of screws reacting to the horizontal load, while the deflection depends on the panel width. Fig. 8.1 reports an example of these two influences for a reference diaphragm: as can be noticed, depending on the specific requirements, the maximum deflection at peak floor strength can be easily increased or decreased by choosing the width of the panels rows accordingly.

With regard to timber-masonry connections, it is recommended to create a continuous joint, that can be designed for strength only, realized for instance by means of timber blocks screwed to the floors and anchored to the walls. From the preliminary results on the behaviour of mechanical anchors in masonry, it is suggested to consider for their pull-out strength approximately half of the value reported by the producers with reference to C20/25 concrete. The retrofitting intervention is designed according to the expected seismic shear to be transferred, and in a numerical model it is possible to reasonably consider the connections as stiff, as discussed also in the next step.

8.4 Step 3: Creation of the numerical model

The numerical model of the (retrofitted) structure can be realized starting from the outcomes of steps 1 and 2. For existing URM buildings, it is important to model in detail the seismic response of masonry walls, timber diaphragms, and timber-masonry connections. The following recommendations refer to numerical model in DIANA FEA, since this software was also used to implement the dissipative response of the diaphragms.

For masonry walls, the first parameters to be specified are the elastic moduli parallel and perpendicular to the bed joints, the shear modulus, and the mass density. These properties are already sufficient to perform linearized analyses such as the lateral force

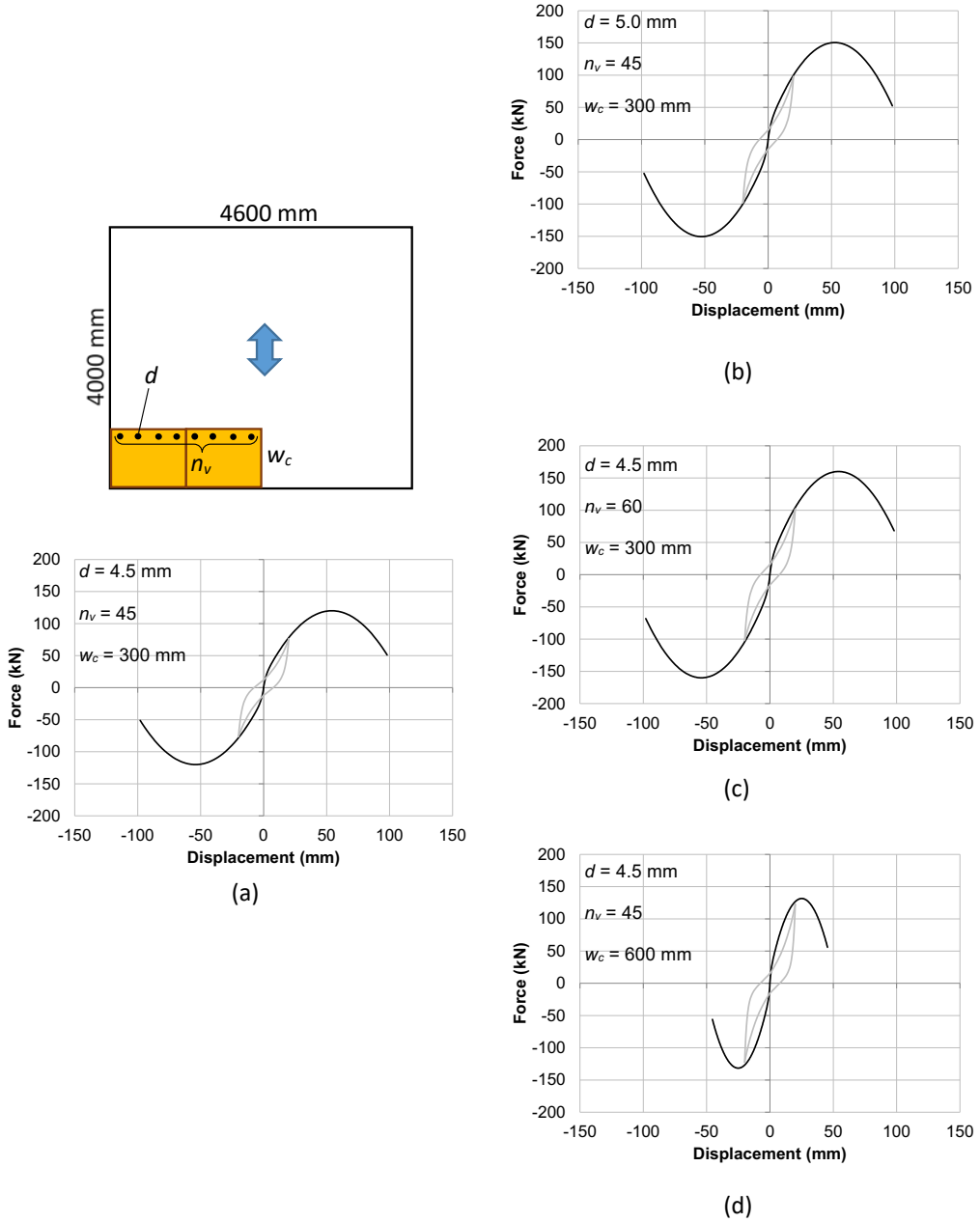


Figure 8.1: Example for a reference 4 by 4.6 m floor (a) of the influence of screw diameter d (b), number of screws orthogonal to the in-plane loading n_v (c), and width of a row of panels w_c (c) on the obtained load-slip response and pinching cycles.

method and the modal analysis. Subsequently, to characterize the nonlinear behaviour of masonry, the other quantities to be specified are:

- Cracking parameters, such as bed-joint tensile strength and fracture energy in tension;
- Crushing parameters, such as compressive strength and fracture energy in compression;
- Shear failure parameters, such as cohesion, friction angle and fracture energy in shear.

Because it is often not possible to retrieve all these material properties from in-situ inspections, useful guidelines are provided in the DIANA user's manual [216], based on several literature studies.

With regard to timber diaphragms, for the as-built conditions the floors can be assumed as linear elastic orthotropic slabs with equivalent properties (Chapter 5). When the floors are retrofitted, the proposed macro-element strategy is recommended, for which the user-supplied subroutine was implemented. As an input for the subroutine, it is necessary to specify the strain at peak stress, the peak stress itself, and the initial elastic modulus. These quantities can be derived with a geometrical procedure (Section 5.4.3) based on the adopted macro-elements dimensions, starting from the obtained force-displacement response of the analytical model. If the floors can be regarded as infinitely stiff, for instance in presence of concrete slabs, linear elastic orthotropic elements can be used.

Finally, timber-masonry connections have to be modelled when very flexible joints are present, e.g. when in as-built conditions the only connection is represented by the joist in the mortar pocket. The highly increased strength and stiffness of retrofitted joints allows, instead, to consider a continuous connection. This same assumption appears to be valid also in as-built conditions, when the joints are sufficiently stiff, such as, for instance, in the typical Dutch case of hook anchors (Section 7.5).

8.5 Step 4: Performing seismic analyses

8.5.1 Lateral force method

The lateral force method is only applicable to simple, regular buildings. The material properties are fully linear (equivalent), while ductility and energy dissipation are taken into account by reducing the demand response spectrum with the behaviour factor. From the performed analyses on the case-study buildings, it has been demonstrated that the current behaviour factor range ($q = 1.5 \div 2.5$) specified for masonry buildings is suitable for their seismic characterization. However, if a dissipative retrofitting is applied to the diaphragms, the increased seismic performance of the building could be considered by means of a larger range ($q = 2.5 \div 3.5$), provided that this is further validated with other (experimental) studies.

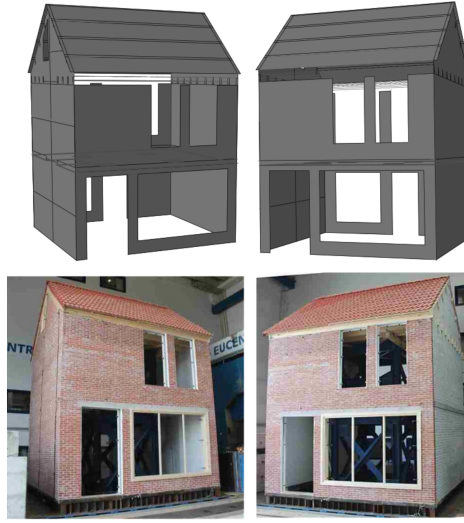


Figure 8.2: Typically Dutch terraced house tested at EUCENTRE [218] and its model in Abaqus [217].

8.5.2 Modal analysis

The modal analysis is the first investigation to be performed when seismically assessing an existing (retrofitted) building. With this analysis type, it is possible to conduct a first check on the correctness of the model and the assumptions made, by examining the fundamental period, the mode shapes, the global mass of the building, and the participating masses activated by each mode shape. It should be noticed that, although this analysis is fully linear, it already enables to capture the effect of retrofitting the diaphragms, as well as other characteristics of the building, such as for instance an undesired torsional response.

These aspects already emerged in the three case-study buildings, but they were also further confirmed by FANKHÄNEL [217] for a typically Dutch terraced house, tested on the shake table at EUCENTRE [218], and then modelled in Abaqus [219] (Fig. 8.2). In that study, the effect of in-plane stiffness of diaphragms has been investigated: although only linear analyses were conducted, it was already possible to capture an increased torsional response of the building, suggesting that an excessive floor stiffening could be even more detrimental for the house due to the high slenderness of the piers. This result appears to once more confirm the outcomes from the analyzed case-study buildings, and from literature [125], [8]-[14], highlighting the need for an optimized design of the retrofitting interventions.

8.5.3 Pushover analysis

The use of pushover analysis should be limited to sufficiently regular URM buildings in which out-of-plane failures and local collapses of masonry walls are prevented. In presence of as-built timber diaphragms, this is not always the case, therefore this analysis type is not advised with excessively deformable floors. When infinitely stiff diaphragms

are present, the pushover analysis becomes more reliable, also because of the lower ambiguity in selecting the control node with respect to a building with flexible floors.

With the light, dissipative strengthening technique investigated and modelled in this dissertation, a hybrid condition is obtained: the diaphragms are moderately deformable, but at the same time the out-of-plane collapse of walls is prevented with a proper retrofitting design, and the in-plane strength of walls can be retrieved. This means that, because the failure modes are fully compatible with that of a building with stiff floors, the pushover analysis can be applied, and considering the additional advantage of the presence of the dissipative floors by means of an over-damped demand response spectrum. In fact, it has been demonstrated that the diaphragms retrofitted with the proposed technique can provide an equivalent damping ratio of 15%, in addition to the dissipative contribution of masonry. Therefore, URM buildings with dissipative diaphragms will be characterized by a force-displacement capacity curve almost similar to that of the same building with stiff diaphragms, but this curve will be compared to a different demand response spectrum: an over-damped spectrum accounting for the dissipative contribution of masonry and diaphragms in presence of lightly retrofitted floors; an over-damped spectrum accounting for the dissipative contribution of masonry only, when stiff floors are present.

8.5.4 Time-history analysis

Time history analysis is the most complete and realistic investigation type, and it is recommended to fully capture the seismic behaviour of URM buildings. In presence of dissipative diaphragms, it is also necessary to fully model their nonlinear response, as it was done by means of the user-supplied subroutine and the macro-element modelling strategy (Section 5.4.3).

While analyzing the results, it is recommended to characterize the seismic capacity by means of hysteretic energy dissipated by the structural components, besides the usual average PGA values. In this way, it is possible to account for load duration and damage in terms of number of cycles on the structure, as shown in Chapter 6.

It should be noticed that this energy-based characterization could also be implemented in more simplified design procedures, by remembering that the hysteretic energy is directly correlated to the square of the spectral pseudo-velocity. Therefore, the hysteretic energy on a URM structure could be predicted starting from the value of spectral velocity corresponding to its fundamental period at collapse (Eqs. 6.23-6.25), and then determined by means of Eqs. 6.20 or 6.21. Yet, these equations require also the knowledge of the effective strong motion duration of the earthquake: while in a time-history analysis the signals and their durations are known, it might be difficult to specify this parameter for a design beforehand. It is, therefore, recommended that besides the response spectra, seismic guidelines could also provide reference conventional values of load duration, according to statistical data from past earthquakes, referred to a certain site. This would improve and make more complete the seismic characterization of URM buildings, highlighting even more the impact of retrofitting methods on their response.

The main recommendations proposed in this dissertation for performing seismic analyses on existing buildings are reported in Fig. 8.3.

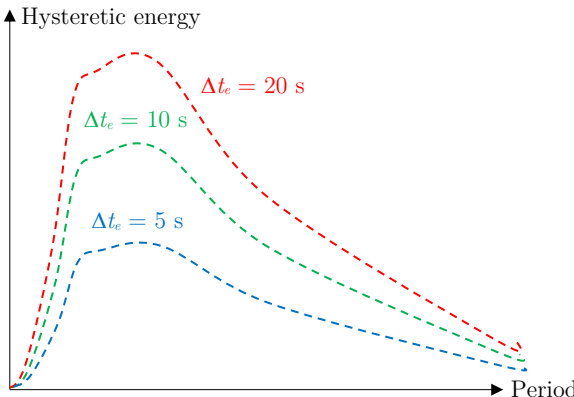
Analysis type	Proposed recommendation
Lateral force method	Consider: $q = 1.5 \div 2.5$ if existing or with stiff floor $q = 2.5 \div 3.5$ if the floor is optimally retrofitted
Modal	If the floor is optimally retrofitted, consider an equivalent in-plane stiffness retrieved from the analytical model used for design
Pushover	Consider an over-damped response spectrum to account for the increased energy dissipation when the floors are optimally retrofitted. The suggested equivalent damping ratio value is 15%.
Time-history	<p>Characterize the results in terms of hysteretic energy Consider the effect of e.g. number of cycles on masonry Include load duration in the design process</p> 

Figure 8.3: Recommendations proposed in this dissertation for seismic analyses on existing URM buildings with (retrofitted) timber diaphragms.

Chapter 9

Conclusions and outlook

9.1 Main outcomes of the dissertation and concluding remarks

In Chapter 2, a number of elements of novelty and knowledge gaps were identified and addressed in this dissertation to answer the global research question. From the experimental point of view, it has been shown that past research studies on timber diaphragms were conducted on samples featuring new material, which could not always be representative for the situation of ancient structural components in practice. Besides, it has been highlighted that no information was available on the relevant seismic properties of timber diaphragms, timber-masonry connections, and masonry walls for the Dutch context.

Taking into account these knowledge gaps, in Chapter 3 the adopted material replication process has been described, proving that samples replicated in the laboratory were representative for the existing structural components extracted from local Groningen URM buildings. With regard to timber diaphragms, a replication of as-built diaphragms was carried out, along with the design of a retrofitting technique consisting of an overlay of plywood panels fastened along their perimeter to the existing sheathing. For timber-masonry connection, an innovative, versatile and efficient test setup was developed, so that it was possible to test the joints under quasi-static monotonic, cyclic, and dynamic loading.

From the analytical point of view, the difficulty in comparing different test results on (retrofitted) timber diaphragms from literature was highlighted, as well as the lack of refined models describing their in-plane response and the seismic behaviour of their connections to masonry. Hence, firstly in Chapter 4, besides analyzing the test results, a uniform criterion for comparing the experimental outcomes with those from literature was defined, based on determining the equivalent shear stiffness at fixed drift values for the floors. Secondly, in Chapter 5, analytical models were formulated to simulate the in-plane response of timber diaphragms and the strength and stiffness of timber-masonry joints. The analytical model defined for the retrofitted timber floors predicts the experimental response with good accuracy, and describes their full nonlinear response, including pinching behaviour.

This same analytical model was then implemented in finite element software, addressing the knowledge gap related to the numerical point of view, and namely the lack of efficient, advanced models simulating the (dissipative) in-plane behaviour of timber diaphragms. Implementation and macro-element modelling strategies were presented for both the open-source software *OpenSees*, and the commercial software DIANA FEA. The proposed method enables a refined representation of the nonlinear in-plane response of the diaphragms, confirmed also by the observed good agreement with experimental tests.

Before putting together the newly available knowledge on timber diaphragms and timber-masonry connections, to study their potential beneficial contribution to the seismic response of existing URM buildings, it has been shown that an extension of the approaches for evaluating seismic capacity was also necessary. This was addressed in Chapter 6, where an energy-based approach was presented to assess the seismic response of URM buildings. With this method, it is possible to account for the strong motion duration and the number of cycles on the system, thus enriching the current framework of an assessment based on PGA only. Therefore, by adopting this approach, the lower structural damage caused by induced earthquakes compared to tectonic ones can be explained, as well as the beneficial effects of well-retrofitted timber diaphragms:

- If flexible as-built floors provide a seismic shear transfer lower than that activating the whole base shear of a building, the diaphragms undergo excessive displacements and cause, as expected, out-of-plane collapses in masonry walls;
- Floors that can be regarded as infinitely stiff do not undergo any deflection, and limit the energy dissipation to masonry walls only, thus reducing the seismic capacity of the building;
- An optimized retrofitting is able to retrieve the global base shear of the building and at the same time its maximum displacement capacity within masonry drift limits. The optimal strengthening corresponds to the maximum spectral velocity at the fundamental period of the building (within drift limits), and thus also to the maximum hysteretic energy that can be provided by the structure. Furthermore, the period of the building is also increased compared to stiff floor configurations, meaning that the structure is subjected to a lower number of cycles, besides the additional damping effect provided by dissipative diaphragms.

The preliminary outcomes from the investigations presented in Chapter 6 were then further confirmed by the extensive numerical analyses conducted on three case-study buildings, whose results were presented in Chapter 7, and finally answer the global research question of the Introduction. It has been shown that, in order to optimize the seismic response of URM buildings, the timber diaphragms retrofitting can be designed based on the pertaining floor seismic shear and masonry out-of-plane drift limits. In this way, the diaphragms can undergo the maximum deflection without causing out-of-plane collapse, activating at the same time the maximum base shear of the building: thus, also the maximum energy dissipation can be retrieved from the diaphragms. Yet, in order for the floor to efficiently transfer the seismic shear loads and deflect without causing local masonry collapses, timber-masonry joints have to be effectively strengthened accordingly, as their role is paramount to efficiently redistribute the actions on the URM structure. Instead, if the diaphragms are too flexible, severe out-of-plane damage

or collapses are observed, while with infinitely stiff floors the box behaviour of the building is greatly improved, but the dissipative contribution of the diaphragms cannot be activated. This dissipative effect of well-retrofitted, optimized timber floors was quantified in terms of an equivalent hysteretic damping ratio of 15% (additional to the dissipation already provided by masonry walls), and of an increased behaviour factor range for URM structures: from the usual values of $q = 1.5 \div 2.5$ to $q = 2.5 \div 3.5$ in presence of dissipative diaphragms.

9.2 Recommendations for further research

Besides the knowledge gaps addressed by this dissertation, some other open research lines are presented as follows for future investigations:

- Besides the use of plywood panels, other possible sustainable, light, reversible, timber-based, dissipative strengthening techniques could be developed for specific contexts (e.g. with efficient use of CLT or OSB panels);
- More refined and efficient modelling strategies for timber diaphragms could be implemented, to allow for instance the direct use of shell elements, instead of macro-elements only. In this way, it will be possible to make the advanced numerical modelling of the in-plane response of timber floors as a more and more common and frequent activity when analyzing the seismic response of masonry buildings;
- The update of the current design methods related to PGA only with a more energy-based approach is suggested. Because this strategy is not only based on the structural properties (e.g. fundamental period and spectral velocity), but also the strong motion duration of the earthquake has to be known, it is proposed to include as design parameter e.g. an expected seismic duration from statistical data on past earthquakes, for specific areas. This could provide an important distinction between the Groningen case, with very transient seismic signals of low strong motion duration, and tectonic earthquakes in active seismic areas, more extended in time and more damaging.
- Because it has been shown that an optimized retrofitting minimizes the number of cycles on the building, compared to a configuration having rigid diaphragms, future studies can be recommendable to further assess the performance of masonry structures under repeated low-amplitude cyclic loading. In fact, buildings in a seismic area are subjected to frequent earthquakes, even if not all of large intensity, and this could lower the seismic capacity of the masonry walls due to crack growth and micro-damage. The quantification of the reduction in capacity and energy dissipation because of repeated cyclic loading should be the subject of further research, so that the beneficial role of optimally retrofitted diaphragms can be evaluated also in relation to this issue for masonry components. This could lead to updated seismic guidelines, because the issue of repeated low-amplitude cyclic loading could be relevant for the Groningen context, in which low-intensity earthquakes occur very often within the same area;
- Another recommendation related to the Groningen context is linked to the relation between induced earthquakes and gas extraction: it should be clarified whether the

current policy of decreasing (or stopping) gas extraction will reduce the seismic risk/intensity accordingly, and if so, how many years will be required for this to take place.

- Further sensitivity studies on existing buildings can be conducted, by including uncertainties propagation and data from structural health monitoring, which could enable a more refined seismic assessment, with the possibility to calibrate and cross-check numerical models against these data.
- The validation of the increased behaviour factor values for URM buildings with dissipative diaphragms is suggested, by means of full-scale experimental tests and additional studies.

Bibliography

- [1] EN 1995-1-1:2004+A2:2014. Eurocode 5: Design of timber structures - Part 1-1: General - Common rules and rules for buildings. CEN (European Committee for Standardization).
- [2] EN 1996-1-1:2005 (Eurocode 6) - Design of masonry structures - Part 1-1: General rules for reinforced and unreinforced masonry structures. European Committee for Standardisation (CEN). Brussels, Belgium, 2005.
- [3] EN 1998-1:2005 (Eurocode 8) - Design of structures for earthquake resistance - Part 1: General rules, seismic actions and rules for building. European Committee for Standardisation (CEN). Brussels, Belgium, 2005.
- [4] EN 1998-3:2005 (Eurocode 8) - Design of structures for earthquake resistance - Part 3: Assessment and retrofitting of buildings. European Committee for Standardisation (CEN). Brussels, Belgium, 2005.
- [5] Decanini, L., De Sortis, A., Goretti, A., Langenbach, R., Mollaioli, F., Rasulo, A., Performance of Masonry Buildings during the 2002 Molise, Italy, Earthquake. *Earthquake Spectra* 20(S1), 191-220, 2004.
- [6] Valluzzi, M.R., On the vulnerability of historical masonry structures: analysis and mitigation. *Materials and Structures* 40, 723-743, 2007.
- [7] Modena, C., Valluzzi, M.R., da Porto, F., Casarin, F., Structural Aspects of the Conservation of Historic Masonry Constructions in Seismic Areas: Remedial Measures and Emergency Actions. *International Journal of Architectural Heritage* 5, 539-558, 2011.
- [8] Scotta, R., Trutalli, D., Marchi, L., Pozza, L., Effects of in-plane strengthening of timber floors in the seismic response of existing masonry buildings. *World Conference on Timber Engineering*, Vienna, Austria, 2016.
- [9] Scotta, R., Trutalli, D., Marchi, L., Pozza, L., Mirra, M., Seismic response of masonry buildings with alternative techniques for in-plane strengthening of timber floors. *Revista Portuguesa de Engenharia de Estruturas*, Ed. LNEC. Série III, no 4, 2017.
- [10] Scotta, R., Trutalli, D., Marchi, L., Pozza, L., Mirra, M., Non-linear time history analyses of unreinforced masonry buildings with in-plane stiffened timber floors. 17th ANIDIS Conference, Pistoia, Italy, 2017.

- [11] Scotta, R., Trutalli, D., Marchi, L., Pozza, L., Seismic performance of URM buildings with in-plane non-stiffened and stiffened timber floors. *Engineering Structures* 167, 683-694, 2018.
- [12] Scotta, R., Trutalli, D., Marchi, L., Pozza, L., A study about optimal stiffening of timber floors in URM buildings. 16th European Conference on Earthquake Engineering (ECEE), Thessaloniki, Greece, 2018.
- [13] Trutalli, D., Marchi, L., Scotta, R., Pozza, L., Dynamic simulation of an irregular masonry building with different rehabilitation methods applied to timber floors. 6th ECCOMAS Thematic Conference, Rhodes Island, Greece, 2017.
- [14] Trutalli, D., Marchi, L., Scotta, R., Pozza, L., Seismic capacity of irregular unreinforced masonry buildings with timber floors. *Proceedings of the Institution of Civil Engineers – Structures and Buildings*, 2020.
- [15] Piazza, M., Baldessari, C., Tomasi, R., The Role of In-Plane Floor Stiffness in the Seismic Behaviour of Traditional Buildings. 14th World Conference on Earthquake Engineering, Beijing, 2008.
- [16] Baldessari, C., In-plane Behaviour of Differently Refurbished Timber Floors. Ph.D. Thesis, University of Trento, 2010.
- [17] Piazza, M., Turrini, G., Una tecnica di recupero statico dei solai in legno, *Recuperare* Vol. 5, Milan, Italy, 1983.
- [18] Corradi, M., Speranzini, E., Borri, A., Vignoli, A., In-Plane Shear Reinforcement of Wood Beam Floors With FRP. *Composites: Part B* 37 (2006), 310-319.
- [19] Valluzzi, M. R., Garbin, E., Dalla Benetta, M., Modena, C., Experimental Assessment and Modelling of In-Plane Behaviour of Timber Floors. 6th International conference Structural Analysis of Historical Constructions, 2008, Bath, U.K., CRC-Press, Balkema, 755-762.
- [20] Valluzzi, M. R., Garbin, E., Dalla Benetta, M., Modena, C., In-Plane Strengthening of Timber Floors for the Seismic Improvement of Masonry Buildings. 11th World Conference on Timber Engineering, Riva del Garda, Italy, 2010.
- [21] Branco, J. M., Kekeliak, M., Lourenço, P. B., In-Plane Stiffness of Timber Floors Strengthened with CLT. *European Journal of Wood Products* 73, 313-323, 2015.
- [22] Gubana, A., Melotto, M., Experimental tests on wood-based in-plane strengthening solutions for the seismic retrofit of traditional timber floors. *Construction and Building Materials* 191, 290-299, 2018.
- [23] Peralta, D. F., Bracci, M. J., Hueste, M. B. D., Seismic Behavior of Wood Diaphragms in Pre-1950s Unreinforced Masonry Buildings. *Journal of Structural Engineering* 130, 2040-2050, 2004.
- [24] Brignola, A., Pampanin, S., Podestà, S.; Experimental Evaluation of the In-Plane Stiffness of Timber Diaphragms. *Earthquake Spectra*, Volume 28, No. 4, 1–23, 2012.

- [25] Wilson, A., Quenneville, P. J. H., Ingham, J. M.; In-Plane Orthotropic Behavior of Timber Floor Diaphragms in Unreinforced Masonry Buildings. *Journal of Structural Engineering* 140, 2014.
- [26] Giongo, I., Dizhur, D., Tomasi, R., Ingham, J. M., In plane assessment of existing timber diaphragms in URM buildings via quasi static and dynamic in situ tests, *Advanced Materials Research* 778, 495-502, 2013.
- [27] NPR 9998:2019. Assessment of buildings in case of erection, reconstruction and disapproval – Basic rules for seismic actions: induced earthquakes. *Nederlands Normalisatie-Instituut*, 2019.
- [28] Panza, G.F., Romanelli, F., Vaccari, F., Decanini, L., Mollaioli, F., Seismic ground motion modelling and damage earthquake scenarios: a bridge between seismologists and seismic engineers. *OECD workshop on the relations between seismological data and seismic engineering*. Istanbul, Turkey, 2002.
- [29] van Eck, T., Goutbeek, F., Haak, H., Dost, B., Seismic hazard due to small-magnitude, shallow-source, induced earthquakes in The Netherlands. *Engineering Geology*, 105-121, 2006.
- [30] Dost, B., Kraaijpoel, D., The August 16th, 2012 earthquake near Huizinge (Groningen). *KNMI scientific report*, De Bilt, 2013.
- [31] Bourne, S. J., Oates, S. J., Development of statistical geomechanical models for forecasting seismicity induced by gas production from the Groningen field. *Netherlands Journal of Geosciences* 96, 175-182, 2017.
- [32] Chopra, A.K., *Dynamics of Structures, Theory and Applications to Earthquake Engineering*. Prentice Hall, Boston, USA, 2012.
- [33] Magenes, G., A method for pushover analysis in seismic assessment of masonry buildings. 12th World Conference on Earthquake Engineering, Auckland, New Zealand, 2000.
- [34] Galasco, A., Lagomarsino, S., Penna, A., On the use of pushover analysis for existing masonry buildings. *First European Conference on Earthquake Engineering and Seismology*, Geneva, Switzerland, 2006.
- [35] Fajfar, P., Capacity spectrum method based on inelastic demand spectra. *Earthquake Engineering and Structural Dynamics* 28, 979-993, 1999.
- [36] Guerrini, G., Graziotti, F., Penna, A., Magenes, G., Improved Evaluation of Inelastic Displacement Demands for Short-period Masonry Structures. *Earthquake Engineering and Structural Dynamics* 46, 1411-1430, 2017.
- [37] Cattari, S., Lagomarsino, S., Marino, S., Reliability of nonlinear static analysis in case of irregular URM buildings with flexible diaphragms. *SECED 2015 Conference: Earthquake Risk and Engineering towards a Resilient World*. Cambridge, UK, 2015.

- [38] Solomos, G., Pinto, A., Dimova, S., A review of the seismic hazard zonation in national building codes in the context of Eurocode 8. JRC Scientific and Technical Reports, 2008.
- [39] Spetzler, J., Dost, B., Probabilistic Seismic Hazard Analysis for Induced Earthquakes in Groningen, Update June 2017. KNMI report, 2017.
- [40] <https://www.vigilfuoco.tv/storia/sisma-ancona>
- [41] <https://www.scpr.org/news/2014/01/16/41563/northridge-earthquake-readiness-varies-widely-at-e/>
- [42] <https://www.insurancejournal.com/news/west/2014/01/17/317586.htm>
- [43] EN 14080:2016. Timber structures – Glued laminated timber and glued solid timber – Requirements. CEN (European Committee for Standardization).
- [44] EN 338:2009. Structural timber – Strength classes. CEN (European Committee for Standardization).
- [45] EN 12512:2001. Timber Structures – Test Methods – Cyclic Testing of Joints Made with Mechanical Fasteners. CEN (European Committee for Standardization).
- [46] Wilson, A., Kelly, P.A., Quenneville, P. J. H., Ingham, J. M.; Nonlinear In-Plane Deformation Mechanics of Timber Floor Diaphragms in Unreinforced Masonry Buildings. ASCE Journal of Engineering Mechanics, 140-4, 2014.
- [47] Giongo, I., Rizzi, E., Ingham, J., Dizhur, D., Numerical modelling strategies for the in-plane behavior of straight sheathed timber diaphragms, Journal of Structural Engineering, ASCE, vol. 144(10), 2018.
- [48] ASTM E 519-81. Standard Test Method for Diagonal Tension (Shear) in Masonry Assemblages. ASTM, 2002.
- [49] FEMA273, NEHRP Guidelines for the Seismic Rehabilitation of Buildings, Federal Emergency Management Agency, Washington DC, USA, 1997.
- [50] FEMA356, Prestandard and Commentary for the Seismic Rehabilitation of Buildings, Federal Emergency Management Agency, Washington DC, USA, 2000.
- [51] ASTM E 2126-19. Standard Test Methods for Cyclic (Reversed) Load Test for Shear Resistance of Vertical Elements of the Lateral Force Resisting Systems for Buildings. ASTM, 2019.
- [52] ASCE/SEI 41. Seismic Evaluation and Retrofit of Existing Buildings. American Society of Civil Engineers, 2017.
- [53] MBIE-NZSEE. The Seismic Assessment of Existing Buildings. New Zealand: New Zealand Society for Earthquake Engineering, 2017.
- [54] Lin, T.-J., LaFave, J.M., Experimental Structural Behavior of Wall-Diaphragm Connections for Older Masonry Buildings. Construction and Building Materials 26, 180–189, 2012.

- [55] Moreira, S., Oliveira, D.V., Ramos, L.F., Lourenço, P.B., Fernandes, R.P., Guerreiro, J., Experimental study on the seismic behavior of masonry wall-to-floor connections. 15th World Conference on Earthquake Engineering, Lisbon, Portugal, 2012.
- [56] Moreira, S., Ramos, L.F., Oliveira, D.V., Lourenço, P.B., Mateus, L., Developing a seismic retrofitting solution for wall-to-floor connections of URM with wood diaphragms. 9th International Masonry Conference, Guimarães, Portugal, 2014.
- [57] Dizhur, D., Giaretton, M., Ingham, J.M., URM wall-to-diaphragm and timber joist connection testing. 10th International Masonry Conference, Milan, Italy, 2018.
- [58] Calì, I., Marletta, M., Pantò, B., A Simplified Model for the Evaluation of the Seismic Behaviour of Masonry Buildings. Proceedings of the Tenth International Conference on Civil, Structural and Environmental Engineering Computing, Stirling, Scotland, 2005.
- [59] D'Ayala, D.F., Speranza, E., Un criterio per la formulazione e la calibrazione di curve di fragilità e scenari di danno: il caso di Nocera Umbra (PG), Italy. Proceedings of the 11th ANIDIS Conference, Genoa, Italy, 2004.
- [60] Padalu, P.K.V.R., Singh, Y., Das, S., Analytical modelling of out-of-plane flexural response of unreinforced and strengthened masonry walls. *Engineering Structures* 218, 2020.
- [61] Mayes, R.L., Clough, R.W., A literature survey - compressive, tensile, bond and shear strength of masonry. Report No. EERC 75-15, Earthquake Engineering Research Center, University of California, Berkeley, 1975.
- [62] Hamid, A.A., Drysdale, R.G., Behaviour of brick masonry under combined shear and compression loading. Proceedings of the 2nd Canadian Masonry Symposium, Ottawa, Canada, 1980.
- [63] Page, A.W., The biaxial compressive strength of brick masonry. Proceedings of the Institution of Civil Engineers 71 (Part 2), 893-906, 1981.
- [64] Page, A.W., Samarasinghe, W., Hendry, A.W., The in-plane failure of masonry: a review. Proceedings of the British Ceramic Society 30, 90-100, 1982.
- [65] Samarasinghe, W., Hendry, A.W., The strength of brickwork under biaxial tensile and compressive stress. Proceedings of the British Ceramic Society 30, 129-139, 1982.
- [66] Page, A.W., The strength of brick masonry under biaxial tension-compression. *International Journal of Masonry Construction* 3, 26-31, 1983.
- [67] Dhanasekar, M., Page, A.W., Kleeman, P.W., The failure of brick masonry under biaxial stresses. Proceedings of the Institution of Civil Engineers 79 (Part 2), 295-313, 1985.

- [68] Turnšek, V., Čačovič, F., Some experimental results on the strength of brick masonry walls. Proceedings of the 2nd International Brick Masonry Conference, Stoke-on-Trent, U.K., 149-156, 1971.
- [69] Turnšek, V., Sheppard, P., The shear and flexural resistance of masonry walls. Proceedings of the International Research Conference on Earthquake Engineering, 517-573, Skopje, Yugoslavia, 1980.
- [70] Benedetti, D., Tomaževič, M., Sulla verifica sismica di costruzioni in muratura. Ingegneria sismica 1, 9-16, 1984.
- [71] Betti, M., Galano, L., Petracchi, M., Vignoli, A., Diagonal cracking shear strength of unreinforced masonry panels: a correction proposal of the b shape factor.
- [72] Mann, W., Müller, H., Failure of shear-stressed masonry: an enlarged theory, tests and application to shear-walls. Proceedings of the International Symposium on Load bearing Brickwork, London, U.K., 1980.
- [73] Abrams, D.P., Strength and behaviour of unreinforced masonry elements. Proceedings of the 10th World Conference on Earthquake Engineering, Madrid, Spain, 1992.
- [74] Shah, N., Abrams, D.P., Cyclic load testing of unreinforced masonry walls. Report No. 92-26-10, Advanced Construction Technology Center, University of Illinois, Urbana, 1992.
- [75] Anthoine, A., Magonette, G., Magenes, G., Shear-compression testing and analysis of brick masonry walls. Proceedings of the 10th European Conference on Earthquake Engineering, Vienna, Austria, 1994.
- [76] Mahmoud, A.D., Hamid, A.A., El Magd, S.A., Lateral response of unreinforced solid masonry shear walls: an experimental study. Proceedings of the 7th Canadian Masonry Symposium, Hamilton, Canada, 1995.
- [77] Magenes, G., Calvi, G.M., *Cyclic behaviour of brick masonry walls*, Proceedings of the 10th World Conference on Earthquake Engineering, Madrid, Spain, 1992.
- [78] Magenes, G., Calvi, G.M., *In-plane seismic response of brick masonry walls*, Earthquake Engineering and Structural Dynamics, 26, 1091-1112, 1997.
- [79] Magenes, G., Della Fontana, A., Simplified non-linear seismic analysis of masonry buildings. Proceedings of the British Masonry Society 8, 190-195, 1998.
- [80] Galasco, A., Lagomarsino, S., Penna, A., Resemini, S., Non-linear analysis of masonry structures. Proceedings of the 13th World Conference on Earthquake Engineering, Vancouver, Canada, 2004.
- [81] Allen, C., Masia, M.J., Page, A.W., Griffith, M.C., Derakhshan, H., Cyclic in-plane shear testing of unreinforced masonry walls with openings, Proceedings of the 10th Pacific Conference on Earthquake Engineering, Sydney, Australia, 2015.

- [82] Calderini, C., Cattari, S., Lagomarsino, S., In-plane strength of unreinforced masonry piers. *Earthquake Engineering and Structural Dynamics*, 38, 243-267, 2008.
- [83] Beyer, K., Peak and residual strengths of brick masonry spandrels. *Engineering Structures* 41, 533-547, 2012.
- [84] Beyer, K., Mangalathu, S., Review of strength models for masonry spandrels. *Bulletin of Earthquake Engineering* 11, 521-542, 2013.
- [85] Gattesco, N., Macorini, L., Dudine, A., Experimental response of brick-masonry spandrels under in-plane cyclic loading. *Journal of Structural Engineering*, 142 (2), 2016.
- [86] Rinaldin, G., Amadio, C., Gattesco, N., Review of experimental cyclic tests on unreinforced and strengthened masonry spandrels and numerical modelling of their cyclic behaviour. *Engineering Structures* 132, 609-623, 2017.
- [87] Foraboschi, P., Coupling effect between masonry spandrels and piers. *Materials and Structures* 42, 279-300, 2009.
- [88] Howlader, M.K., Masia, M.J., Griffith, M.C., Numerical analysis and parametric study of unreinforced masonry walls with arch openings under lateral in-plane loading. *Engineering Structures* 208, 2020.
- [89] Gattesco, N., Rinaldin, G., Amadio, C., Experimental and numerical characterization of the cyclic behaviour of unreinforced and reinforced masonry spandrels. 9th International Masonry Conference, Guimaraes, Portugal, 2014.
- [90] Simsir, C.C., Aschheim, M., Abrams, D.P., Out-of-Plane Dynamic Response of Unreinforced Masonry Bearing Walls Attached to Flexible Diaphragms. 13th World Conference on Earthquake Engineering, Vancouver, Canada, 2004.
- [91] Ferreira, T.M., Costa, A.A., Costa, A., Analysis of the Out-Of-Plane Seismic Behavior of Unreinforced Masonry: A Literature Review. *International Journal of Architectural Heritage* 9 (8), 2014.
- [92] Shawa, O.A., De Felice, G., Mauro, A., Sorrentino, L., Out-of-plane seismic behaviour of rocking masonry walls. *Earthquake Engineering and Structural Dynamics* 41 (5), 949-968, 2012.
- [93] Gabellieri, R., Landi, L., Diotallevi, P.P., A 2-DOF model for the dynamic analysis of unreinforced masonry walls in out-of-plane bending. 4th ECCOMAS Thematic Conference on Computational Methods in Structural Dynamics and Earthquake Engineering: COMPDYN 2013, Kos Island, Greece, 2013.
- [94] Doherty, K.T., An investigation of the weak links in the seismic load path of unreinforced masonry buildings. Ph.D. Thesis, University of Adelaide, 2000.
- [95] Doherty, K.T., Griffith, M.C., Lam, N.T.K., Wilson, J.L., Displacement-based analysis for out-of-plane bending of seismically loaded unreinforced masonry walls. *Earthquake Engineering and Structural Dynamics* 31 (4), 833-850, 2002.

- [96] Griffith, M.C., Magenes, G., Melis, G., Picchi, L., Evaluation of out-of-plane stability of unreinforced masonry walls subjected to seismic excitation. *Journal of Earthquake Engineering* 7, 141-169, 2003.
- [97] Derakhshan, H., Griffith, M.C., Ingham, J.M., Out-of-plane behaviour of one-way unreinforced masonry walls. *ASCE Journal of Engineering Mechanics* 139 (4), 409-417, 2013.
- [98] Derakhshan, H., Dizhur, D.Y., Griffith, M.C., Ingham, J.M., Seismic assessment of out-of-plane loaded unreinforced masonry walls in multi-storey buildings. *Bulletin of the New Zealand Society of Earthquake Engineering* 47, 2014.
- [99] Derakhshan, H., Lucas, W., Visintin, P., Griffith, M.C., Out-of-plane strength of existing two-way spanning solid and cavity unreinforced masonry walls. *Structures* 12, 88-101, 2018.
- [100] Griffith, M.C., Vaculik, J., Lam, N.T.K., Wilson, J., Lumantarna, E., Cyclic testing of unreinforced masonry walls in two-way bending. *Earthquake Engineering and Structural Dynamics* 36, 801-821, 2007.
- [101] Vaculik, J., Griffith, M.C., Out-of-plane shaketable testing of unreinforced masonry walls in two-way bending. *Bulletin of Earthquake Engineering* 16, 2839-2876, 2017.
- [102] Vaculik, J., Griffith, M.C., Out-of-plane load-displacement model for two-way spanning masonry walls. *Engineering Structures* 141, 328-343, 2017.
- [103] Chang, L., Messali, F., Esposito, R., Capacity of unreinforced masonry walls in out-of-plane two-way bending: A review of analytical formulations. *Structures* 28, 2431-2447, 2020.
- [104] Ravenshorst, G.J.P., Messali, F., Out-of-plane tests on replicated masonry walls. Report No. C31B60-6, Delft University of Technology. 2016.
- [105] Vintzileou, E., Testing Historic Masonry Elements and/or Building Models. Perspectives on European Earthquake Engineering and Seismology, 267-307, 2014.
- [106] Solarino, F., Oliveira, D.V., Giresini, L., Wall-to-horizontal diaphragm connections in historical buildings: A state-of-the-art review. *Engineering Structures* 199, 2019.
- [107] Tomaževič, M., The computer program POR, Report ZRMK, 1978.
- [108] Tomaževič, M., Weiss, P., Velechovsky, T., The influence of rigidity of floors on the seismic resistance of old masonry buildings: shaking table tests of model houses A and B. Institute for Testing and Research in Materials and Structures, Ljubljana, 1990.
- [109] Tomaževič, M., Weiss, P., Velechovsky, T., The influence of rigidity of floors on the seismic behavior of old stone-masonry buildings. *Journal of European Earthquake Engineering* 5 (3), 28-41, 1991.
- [110] Tomaževič, M., Lutman, M., Velechovsky, T., (1993) Aseismic strengthening of old stone-masonry buildings: is the replacement of wooden floors with R.C. slabs always necessary? *Journal of European Earthquake Engineering* 7 (2), 34-46, 1993.

- [111] Costley, A.C., Abrams, D.P., Dynamic Response of Unreinforced Masonry Buildings with Flexible Diaphragms. Technical Report NCEER-96-0001, University of Illinois, USA, 1996.
- [112] Cohen, G.L., Klingner, R.E., Hayes, J.R., Sweeney, S.C., Seismic Response of Low-Rise Masonry Buildings with Flexible Roof Diaphragms. Report ERDC/CERL SR-01-19, US Army Corps of Engineers, 2001.
- [113] Paquette, J., Bruneau, M., Pseudo-dynamic testing of unreinforced masonry buildings with flexible diaphragm. 13th World Conference on Earthquake Engineering, Vancouver, Canada, 2004.
- [114] Betti, M., Galano, L., Vignoli, A., Comparative analysis on the seismic behaviour of unreinforced masonry buildings with flexible diaphragms. *Engineering Structures* 61, 195-208, 2014.
- [115] Magenes, G., Penna, A., Galasco, A., A full-scale shaking table test on a two-storey stone masonry building. 14th European Conference on Earthquake Engineering, Ohrid, Republic of Macedonia, 2010.
- [116] Magenes, G., Penna, A., Rota, M., Galasco, A., Senaldi, I., Shaking table test of a full scale stone masonry building with stiffened floor and roof diaphragms. 15th World Conference on Earthquake Engineering, Lisbon, Portugal, 2012.
- [117] Senaldi, I., Magenes, G., Penna, A., Galasco, A., Rota, M., The Effect of Stiffened Floor and Roof Diaphragms on the Experimental Seismic Response of a Full-Scale Unreinforced Stone Masonry Building. *Journal of Earthquake Engineering* 18, 407-443, 2014.
- [118] Benetatos, C., Kiratzi, A.A., Finite-fault slip models for the 15 April 1979 (M-W 7.1) Montenegro earthquake and its strongest aftershock of 24 May 1979 (M-W 6.2). *Tectonophysics* 421 (1), 129-143, 2006.
- [119] Gallonelli, M., Dynamic response of masonry buildings with rigid or flexible floors. Master Thesis, Rose School, Pavia, 2007.
- [120] Giongo, I., Piazza, M., Tomasi, R., Pushover analysis of traditional masonry buildings: influence of refurbished timber-floors stiffness. SHATIS'11 International Conference on Structural Health Assessment of Timber Structures, Lisbon, Portugal, 2011.
- [121] Aleman, J., Mosqueda, G., Whittaker, A., Seismic analysis of multi-storey unreinforced masonry buildings with flexible diaphragms. Technical Report MCEER-15-0001, 2015.
- [122] Mendes, N., Lourenço, P.B., Seismic Vulnerability of Existing Masonry Buildings: Nonlinear Parametric Analysis. *Seismic Assessment, Behavior and Retrofit of Heritage Buildings and Monuments*, 139-164, 2015.
- [123] Masroor, A., Avanes, C., Asghari, M., Soroushian, S., Smith, R.J., Comprehensive finite element simulation of the flexible wood diaphragms. 16th World Conference on Earthquake Engineering, Santiago, Chile, 2017.

- [124] Gubana, A., Melotto M., Discrete-element analysis of floor influence on seismic response of masonry structures. Proceedings of the Institution of Civil Engineers – Structures and Buildings, 2020.
- [125] Nakamura, Y., Derakhshan, H., Griffith, M.C., Magenes, G., Influence of Diaphragm Flexibility on Seismic Response of Unreinforced Masonry Buildings. Journal of Earthquake Engineering 21, 935-960, 2016.
- [126] Stavroulaki, M.E., Dynamic Behavior of Aggregated Buildings With Different Floor Systems and Their Finite Element Modeling. Frontiers in Built Environment 5, 2019.
- [127] Preti, M., Loda, S., Bolis, V., Cominelli, S., Marini, A., Giuriani, E., Dissipative roof diaphragm for the seismic retrofit of listed masonry churches. Journal of Earthquake Engineering 23 (8), 1241-1261, 2017.
- [128] Gubana, A., State-of-the-art report on high reversible timber to timber strengthening interventions on wooden floors. Construction and Building Materials 97, 25-33, 2015.
- [129] Lagomarsino, S., Penna, A., Galasco, A., Cattari, S., TREMURI program: An equivalent frame model for the nonlinear seismic analysis of masonry buildings. Engineering Structures 56, 1787-1799, 2013.
- [130] ARUP Project Title: Groningen 2013 - Implementation study, Document REP/229746/IS001, Issue Rev A, 29th November 2013.
- [131] Schiro, G., Giongo, I., Ingham, J.M., Dizhur, D., Lateral performance of as-built and retrofitted timber diaphragm fastener connections, ASCE Journal of Materials in Civil Engineering, vol. 30 (1), 2018.
- [132] Mirra, M., Ravenshorst, G.J.P., van de Kuilen, J.W.G., Experimental and analytical evaluation of the in-plane behaviour of as-built and strengthened traditional wooden floors. Engineering Structures 211, 2020.
- [133] <https://www.brookhuis.com/wood-testing/strength-grading/strength-grading-handhelds/>
- [134] Ravenshorst, G.J.P., van de Kuilen, J.W.G, Relationships between local, global and dynamic modulus of elasticity for soft- and hardwoods. CIB W18, proceedings paper 42-10-1, Dubendorf, Switzerland, 2009.
- [135] EN408:2010. Timber Structures - Structural Timber and Glued Laminated Timber - Determination of Some Physical and Mechanical Properties. CEN (European Committee for Standardization).
- [136] EN 13183-1:2002. Moisture content of a piece of sawn timber – Part 1: Determination by oven dry method. CEN (European Committee for Standardization).
- [137] EN 409:2009. Timber structures – Test methods – Determination of the yield moment of dowel type fasteners. CEN (European Committee for Standardization).

- [138] ISO 16670:2003. Timber structures – Joints made with mechanical fasteners – Quasi-static reversed-cyclic test method. International Organization for Standardization (ISO).
- [139] Jafari, S., Esposito, R., Material tests for the characterisation of replicated calcium silicate brick masonry. Report No. C31B67WP1-9, Delft University of Technology, 2016.
- [140] EN 772-1:2011. Methods of test for masonry units - Part1: Determination of compressive strength. CEN (European Committee for Standardization).
- [141] NEN 6790:2005. Technical principles for building structures - TGB 1990 - Masonry structures - Basic requirements and calculation methods. Nederlands Normalisatie-Instituut.
- [142] EN 1052-1:1998. Methods of test for masonry – Part 1: Determination of compressive strength. CEN (European Committee for Standardization).
- [143] EN 1052-2:1999. Methods of test for masonry – Part 1: Determination of flexural strength. CEN (European Committee for Standardization).
- [144] EN 1052-5:2005. Methods of test for masonry – Part 5: Determination of bond strength by bond wrench method. CEN (European Committee for Standardization).
- [145] EN 1052-3:2002. Methods of test for masonry – Part 3: Determination of initial shear strength. CEN (European Committee for Standardization).
- [146] <https://www.eucentre.it/nam-project/?lang=en>
- [147] Correia, A. A., Tomassetti, U., Campos Costa, A., Penna, A., Magenes, G., Graziotti, F., Collapse Shake-Table Test on a URM-Timber Roof Substructure. 16th European Conference on Earthquake Engineering, Thessaloniki, 2018.
- [148] Ravenshorst, G.J.P., Mirra, M., Test report on cyclic behaviour of replicated timber joist-masonry wall connections. Report no. C31B67WP4-11. Delft University of Technology. 2018.
- [149] Mirra, M., Ravenshorst, G.J.P., Monotonic, cyclic and dynamic behaviour of timber-masonry connections. Report no. CS2B04WP2-3.3. Delft University of Technology. 2019.
- [150] Mirra, M., Ravenshorst, G.J.P., van de Kuilen, J.W.G., Monotonic, cyclic and dynamic behaviour of timber-masonry connections. World Conference on Timber Engineering, Santiago, Chile, 2021.
- [151] Mirra, M., Ravenshorst, G.J.P., de Vries, P.A., Messali, F., Experimental characterisation of as-built and retrofitted timber-masonry connections under monotonic, cyclic and dynamic loading. Under review in Construction and Building Materials, 2021.

- [152] EN 1015-11:1999. Methods of test for mortar for masonry – Part 11: Determination of flexural strength of hardened mortar. CEN (European Committee for Standardization).
- [153] European Technical Assessment ETA-05/0069. Deutsches Institut für Bautechnik, 24th April 2020.
- [154] EN 846-5:2012 – Methods of test for ancillary components for masonry. Determination of tensile and compressive load capacity and load displacement characteristics of wall ties. CEN (European Committee for Standardization).
- [155] Messali, F., Ravenshorst, G., Esposito, R., Rots, J.G., Large-scale testing program for the seismic characterization of Dutch masonry walls. Proceedings of 16th World Conference on Earthquake Engineering, Santiago, Chile, 2017.
- [156] Ravenshorst, G.J.P., Messali, F., In-plane tests on replicated masonry walls. Report No. C31B60-2, Delft University of Technology. 2016.
- [157] Esposito, R., Ravenshorst, G.J.P., Quasi-static cyclic in-plane tests on masonry components 2016/2017. Report No. C31B67WP3-4. Delft University of Technology. 2017.
- [158] Damiola, M., Esposito, R., Ravenshorst, G.J.P., Quasi-static cyclic out-of-plane tests on masonry components 2016/2017. Report No. C31B67WP3-5, Delft University of Technology, 2017.
- [159] Graziotti, F., Tomassetti, U., Rossi, A., Marchesi, B., Kallioras, S., Mandirola, M., Fragomeli, A., Mellia, E., Peloso, S., Cuppari, F., Guerrini, G., Penna, A., Magenes, G., Experimental campaign on a clay URM full-scale specimen representative of the Groningen building stock. Report EUC128/2016U, Eucentre, Pavia, Italy, 2016.
- [160] ISO 21581:2010. Timber structures – Static and cyclic lateral test load test methods for shear walls. International Organization for Standardization (ISO).
- [161] Miglietta, M., Mazzella, L., Grottoli, L., Guerrini, G., Graziotti, F., Full-scale building test – EC build 6: test results report. Protocol number EUC160/2018, version 1.1, 31/07/2018.
- [162] Messali, F., Esposito, R., Ravenshorst, G.J.P., Rots, J.G., Experimental investigation of the in-plane cyclic behaviour of calcium silicate brick masonry walls. Bulletin of Earthquake Engineering 18 (8), 3963- 3994, 2020.
- [163] van de Kuilen, J.W.G., The residual load carrying capacity of timber joints. HERON, Vol. 44, No. 3, 187-214, 1999.
- [164] Ravenshorst, G.J.P., Mirra, M., Test report on material properties of timber and fasteners extracted from existing buildings. Report no. C31B67WP4-9. Delft University of Technology. 2017.
- [165] Ravenshorst, G.J.P., Mirra, M., Test report on cyclic behaviour of plank-joint connections of samples extracted from existing buildings. Report no. C31B67WP4-12. Delft University of Technology. 2017.

- [166] Licciardello, L., Esposito, R., Material tests for the characterisation of replicated solid clay brick masonry. Report No. CM1B04-WPC-2.3 Delft University of Technology. 2019.
- [167] Clough, R.W., Penzien, J., Dynamics of structures. McGraw-Hill New York, 1993.
- [168] Mirra, M., Ravenshorst, G.J.P., van de Kuilen, J.W.G., Dissipative properties of timber diaphragms strengthened with plywood panels. World Conference on Timber Engineering, Santiago, Chile, 2021.
- [169] Mirra, M., Ravenshorst, G.J.P., van de Kuilen, J.W.G., Comparing in-plane equivalent shear stiffness of timber diaphragms retrofitted with light and reversible wood-based techniques. ASCE Practice Periodical on Structural Design and Construction 26 (4). American Society of Civil Engineers, 2021.
- [170] Bernard, P., Zollo, A., The Irpinia (Italy) 1980 earthquake: Detailed analysis of a complex normal faulting. Journal of Geophysical Research 94, 1631-1647, 1989.
- [171] Ravenshorst, G.J.P., Esposito, R., Schipper, R., Messali, F., Tsouvalas, A., Lourens, E.-M., Rots, J.G., Structural behaviour of a calcium silicate brick masonry assemblage: quasi-static cyclic pushover and dynamic identification test. Report No. C31B60-7. Delft University of Technology. 2016.
- [172] Foschi, R.O., Load-Slip Characteristics of Nails. Wood Science 17, 69-77, 1974.
- [173] Vanin, F., Penna, A., Beyer, K., Equivalent-Frame Modeling of Two Shaking Table Tests of Masonry Buildings Accounting for Their Out-Of-Plane Response. Frontiers in Built Environment, 2020.
- [174] Mirra, M., Ravenshorst, G.J.P., de Vries, P.A., van de Kuilen, J.W.G., An analytical model describing the in-plane behaviour of timber diaphragms strengthened with plywood panels. Engineering Structures 235, 2021.
- [175] Rizzi, E., Giongo, I., Ingham, J.M., Dizhur, D., Testing and Modeling In-Plane Behavior of Retrofitted Timber Diaphragms. Journal of Structural Engineering 146, 2020.
- [176] Dubas, P., Gehri, E., Steurer, T., Einführung in die Norm SIA 164 (1981) – Holzbau. Publication No. 81-1, Baustatik und Stahlbau, ETH Zürich, Switzerland, 1981.
- [177] DIN 1052:2008. Entwurf, Berechnung und Bemessung von Holzbauwerken - Allgemeine Bemessungsregeln und Bemessungsregeln für den Hochbau. Deutsches Institut für Normung e.V., Berlin, Germany.
- [178] Johansen, K.W., Theory of timber connections. Publ. 9 Bern. International Association of Bridge and Structural Engineering, 1949.
- [179] European Technical Assessment no. ETA-11/0030. RothoBlaas self-tapping screws and threaded rods. 2019.

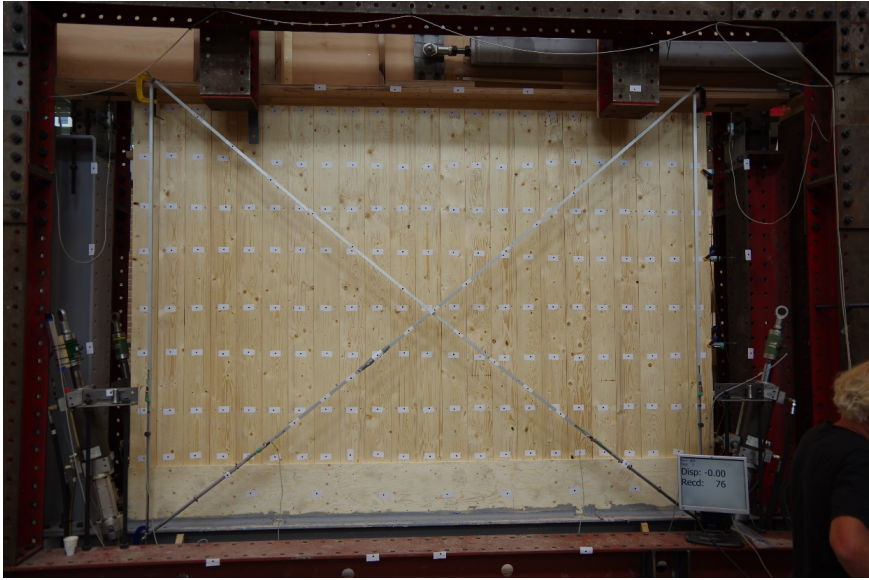
- [180] Mazzoni, S., McKenna, F., Scott, M.H., Fenves, G.L., OpenSees Command Language Manual. University of California, Berkeley, 2006. Link: <http://opensees.berkeley.edu/manuals/usermanual>
- [181] McKenna, F., Fenves, G.L., Scott, M.H., Open System for Earthquake Engineering Simulation. University of California, Berkeley CA. Link: <http://opensees.berkeley.edu>
- [182] Ferreira, D., DIANA – Finite element analysis. User’s manual release 10.4. DIANA FEA BV, Delft, The Netherlands, 2020.
- [183] Mirra, M., Sousamli, M., Longo, M., Ravenshorst, G.J.P., Analytical and numerical modelling of the in-plane response of timber diaphragms retrofitted with plywood panels. 8th ECCOMAS Thematic Conference on Computational Methods in Structural Dynamics and Earthquake Engineering. Athens, Greece, 2021.
- [184] CEB-FIP Model Code 1990. Comité Euro-international du Béton.
- [185] Tomaževič, M., Weiss, P., Displacement capacity of masonry buildings as a basis for the assessment of behavior factor: An experimental study. Bulletin of Earthquake Engineering, 8 (6), 1267-1294, 2010.
- [186] Messali, F., Rots, J.G., In-plane drift capacity at near collapse of rocking unreinforced calcium silicate and clay masonry piers. Engineering Structures 164, 183-194, 2018.
- [187] Giongo, I., Wilson, A., Dizhur, D., Derakhshan, H., Tomasi, R., Griffith, M.C., Quenneville, P., Ingham, J.M., Detailed seismic assessment and improvement procedure for vintage flexible timber diaphragms. Bulletin of the New Zealand Society for Earthquake Engineering 47 (2), 97-118, 2014.
- [188] NZS 1170.5. Structural design actions, Part 5: Earthquake actions – New Zealand, Standards New Zealand, Wellington, 2004.
- [189] D’Altri, A.M., Sarhosis, V., Milani, G., Rots, J.G., Cattari, S., Lagomarsino, S., Sacco, E., Tralli, A., Castellazzi, G., de Miranda, S., Modelling Strategies for the Computational Analysis of Unreinforced Masonry Structures: Review and Classification. Archives of Computational Methods in Engineering 27, 1153-1185, 2020.
- [190] Schreppers, G.M.A., Garofano, A., Messali, F., Rots, J.G., DIANA FEA report 2016-DIANA-R1601: DIANA Validation report for masonry modelling. DIANA FEA BV, 2016.
- [191] Bhattarai, S., Messali, F., Esposito, R., Numerical study on retrofitting measures for low-rise buildings. Report No. CM1B06-WP3-2, Final version, Delft University of Technology, 2019.
- [192] Gruppo Sismica s.r.l., 3D-MACRO user guide. 2020.
- [193] Sucuoğlu, H., Nurtuğ, A., Earthquake ground motion characteristics and seismic energy dissipation. Earthquake Engineering and Structural Dynamics 24, 1195-1213, 1995.

- [194] Uang, C.M., Bertero, V.V., Use of energy as a design criterion in earthquake-resistant design. Report no. UCB/EERC-88/18, University of California, Berkeley, 1988.
- [195] <https://www.knmi.nl/over-het-knmi/nieuws/zware-aardbeving-in-groningse-zeerijp>
- [196] Housner, G.W., Limit design of structures to resist earthquakes. 1st World Conference on Earthquake Engineering. Berkeley, California, 1956.
- [197] Nurtuğ, A., Sucuoğlu, H., Prediction of seismic energy dissipation in SDOF systems. *Earthquake Engineering and Structural Dynamics* 24, 1215-1223, 1995.
- [198] Trifunac, M.D., Brady, A.G., A study on the duration of strong earthquake ground motion. *Bulletin of the Seismological Society of America*, 65 (3), 581-626, 1975.
- [199] Mezgebo, M.G., Estimation of Earthquake Input Energy, Hysteretic Energy and its Distribution in MDOF Structures. Syracuse University, Dissertations - ALL, 228, 2015.
- [200] Comartin, C.D., Aschheim, M., Guyader, A., Hamburger, R., Hanson, R., Holmes, W., Iwan, W., Mahoney, M., Miranda, E., Mohele, J., Rojahn, C., Stewart, J., A summary of FEMA 440: improvement of nonlinear static seismic analysis procedures. 13th World Conference on Earthquake Engineering, Vancouver, Canada, 2004.
- [201] FEMA 440. Improvement of nonlinear static seismic analysis procedures. Federal Emergency Management Agency, Washington D.C., USA, 2005.
- [202] Pagella, G., Nonlinear analyses for the assessment of seismic input energy dissipation capacity of stiffened timber floors in Dutch masonry buildings. Master thesis, Delft University of Technology and University of Padua, 2019.
- [203] Webtool NPR 9998 (<https://seismischekrachten.nen.nl>). Nederlands Normalisatie-instituut (NEN), 2021.
- [204] Iervolino, I., Galasso, C., Cosenza, E., REXEL: computer aided record selection for code-based seismic structural analysis. *Bulletin of Earthquake Engineering* 8, 339-362, 2009.
- [205] Carulli, G.B., Slejko, D., The 1976 Friuli (NE Italy) earthquake. *Giornale di Geologia applicata* 1, 147-156, 2005.
- [206] Graziotti, F., Tomassetti, U., Rossi, A., Marchesi, B., Kallioras, S., Mandirola, M., Fragomeli, A., Mellia, E., Peloso, S., Cuppari, F., Guerrini, G., Penna, A., Magenes, G., Shaking table tests on a full-scale clay-brick masonry house representative of the Groningen building stock and related characterization tests. Report EUC128/2016U, EUCENTRE, Pavia, Italy, 2016.
- [207] Messali, F., Longo, M., Influence of dormers on the seismic performance of a detached house: case study Kwelder 1, Loppersum. Report number B2B-R04, Version 01, Delft University of Technology, 21 January 2021.

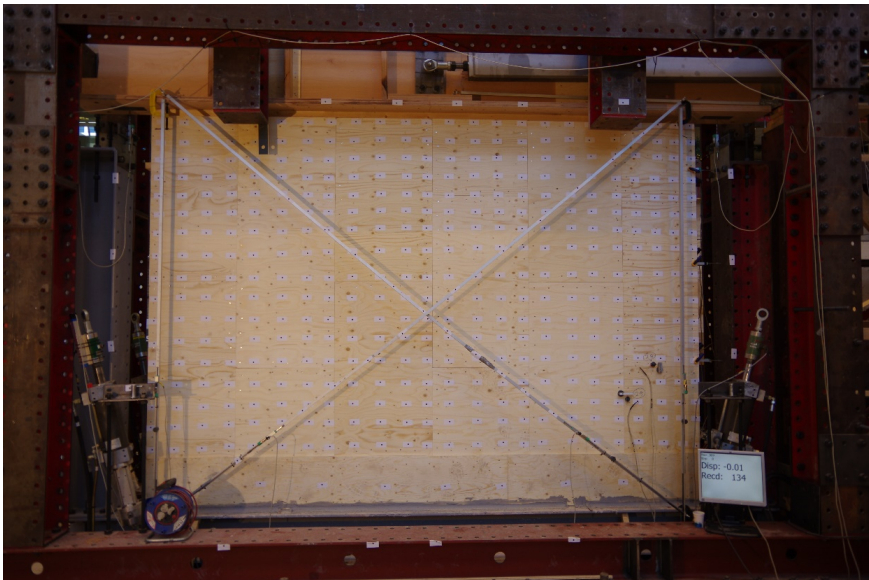
- [208] NEN-EN 1990:2002+A1:2019+NB:2019. Grondslagen van het constructief ontwerp (Dutch national version of Eurocode 0). Nederlands Normalisatie-instituut (NEN).
- [209] Messali, F., Longo, M., Singla, A., A numerical investigation of building typology 'Metselwerk 7'. Report number 3, Project TC19/20, client: Ministerie van Economische Zaken en Klimaat. Delft University of Technology, 2021.
- [210] D'Ayala, D., Assessing the seismic vulnerability of masonry buildings, Handbook of Seismic Risk Analysis and Management of Civil Infrastructure Systems, Woodhead Publishing in Materials, 2013.
- [211] NTC 2018. Norme Tecniche per le Costruzioni (Italian regulations for structural design). Ministry of Infrastructures and Transports, 2018.
- [212] Mirra, M., Ravenshorst, G.J.P., Optimizing seismic capacity of existing masonry buildings by retrofitting timber floors: wood-based solutions as a dissipative alternative to rigid concrete diaphragms. Buildings 11, Special issue on seismic design and performance of timber structures, 2021.
- [213] Jafari, S., Esposito, R., Rots, J.G, A comparative study on the different testing methods: evaluating the mechanical properties of masonry. 10th International Masonry Conference, Milan, Italy, 2018.
- [214] Pelà, L, Roca, P., Benedetti, A., Mechanical characterization of historical masonry by core drilling and testing of cylindrical samples. International Journal of Architectural Heritage 10, 3609-374, 2016.
- [215] Miranda, L., Cantini, L., Guedes, J., Costa, A., Assessment of mechanical properties of full-scale masonry panels through sonic methods. Comparison with mechanical destructive tests. Structural Control & Health Monitoring 23 (3), 503-516, 2016.
- [216] <https://dianafea.com/manuals/d103/Verify/Verifyse9.html>
- [217] Fankhänel, M.W., Modeling wood-based seismic strengthening solutions in existing buildings. Master Thesis. Supervisors: Benedikt Hofmeister (Leibniz Universität Hannover), Michele Mirra (Delft University of Technology). 2021.
- [218] Damiani, N., Miglietta, M., Mazzella, L., Grottoli, L., Guerrini, G., Graziotti, F., Full-scale shaking table test on a dutch URM cavity-wall terraced-house end unit: Euc-build-7: V1.0, 7/3/2019. Technical report, EUCENTRE, 2019.
- [219] Abaqus 6.14 User Guide. <http://130.149.89.49:2080/v6.14/>. 2020.

Appendix A

Pictures of the as-built and retrofitted tested diaphragms

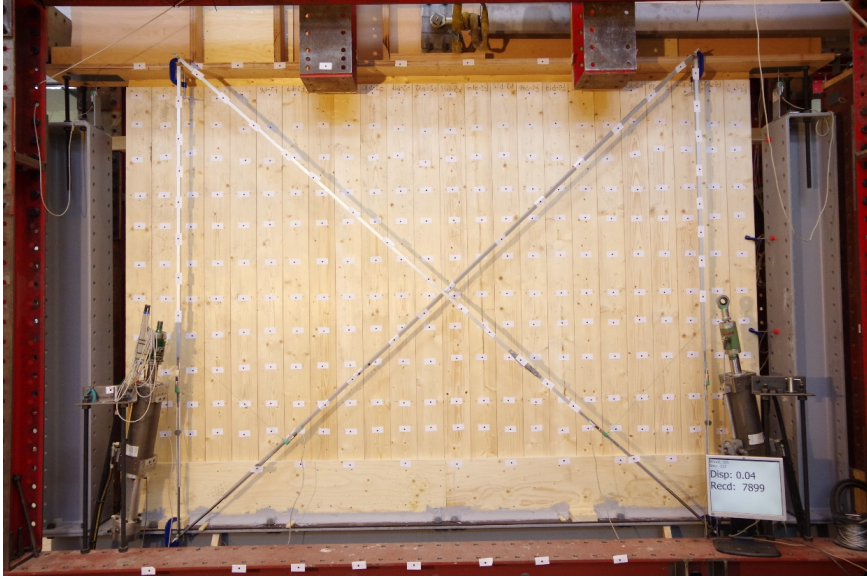


(a)



(b)

Figure A.1: Diaphragms DFpar-1 (a) and DFpar-1s (b).



(a)



(b)

Figure A.2: Diaphragms DFpar-2 (a) and DFpar-2s (b).



(a)



(b)

Figure A.3: Diaphragms DFper-3 (a) and DFper-3s (b).



(a)



(b)

Figure A.4: Diaphragms DFper-4 (a) and DFper-4s (b).



(a)



(b)

Figure A.5: Diaphragms DRpar-5 (a) and DRpar-5s (b).

Appendix B

Drawings of the tested timber-masonry connections

B.1 Samples tested within the pilot study

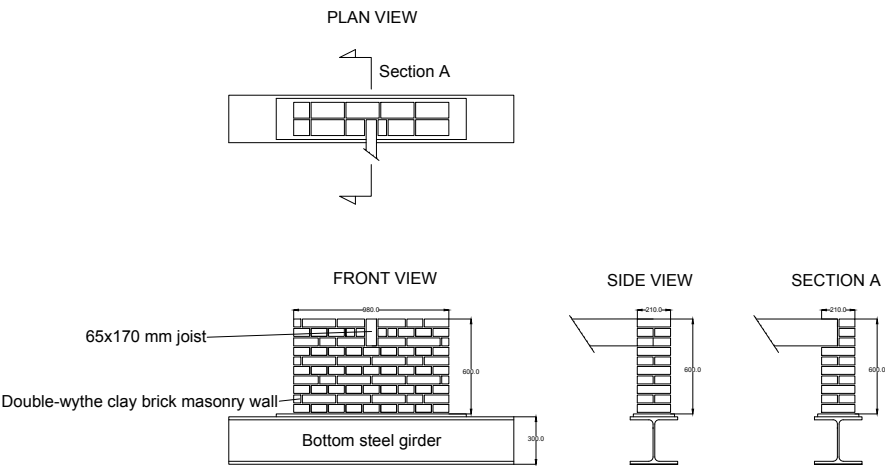


Figure B.1: Configuration CLAY-A.

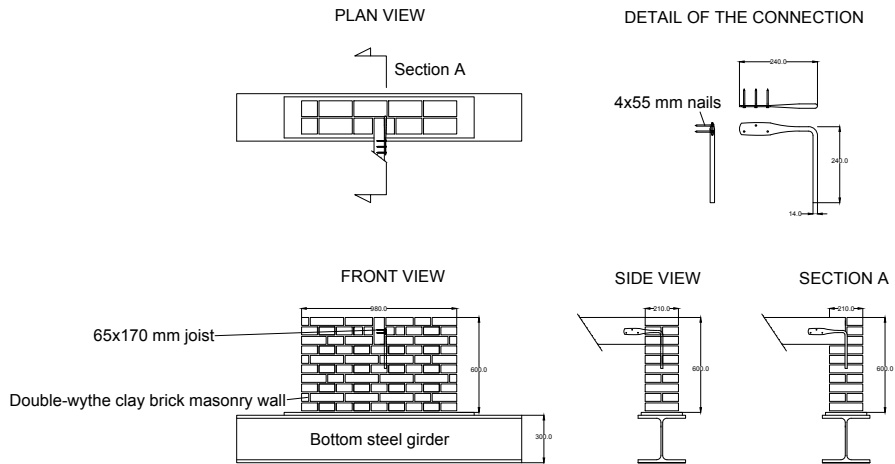


Figure B.2: Configuration CLAY-B.

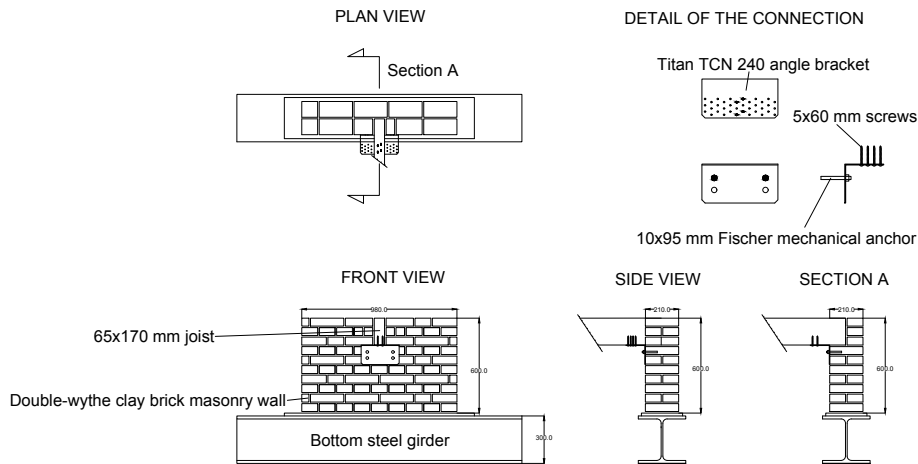


Figure B.3: Configuration CLAY-C.

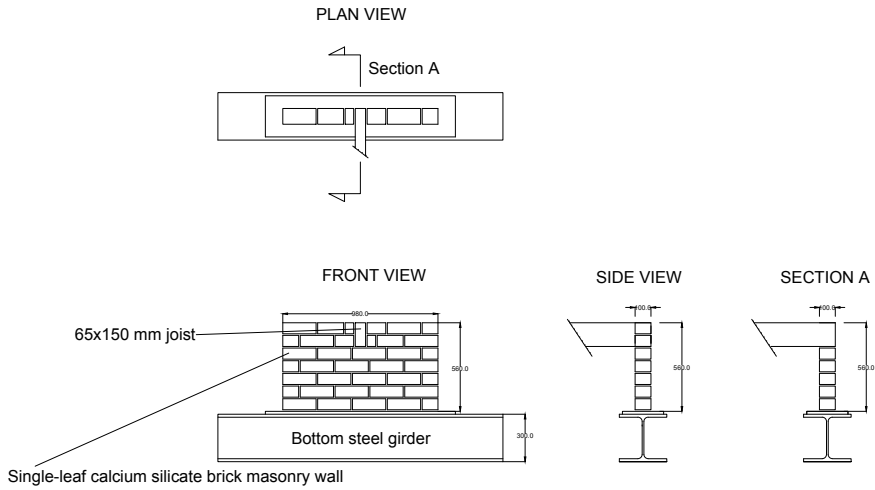


Figure B.4: Configuration CS-A.

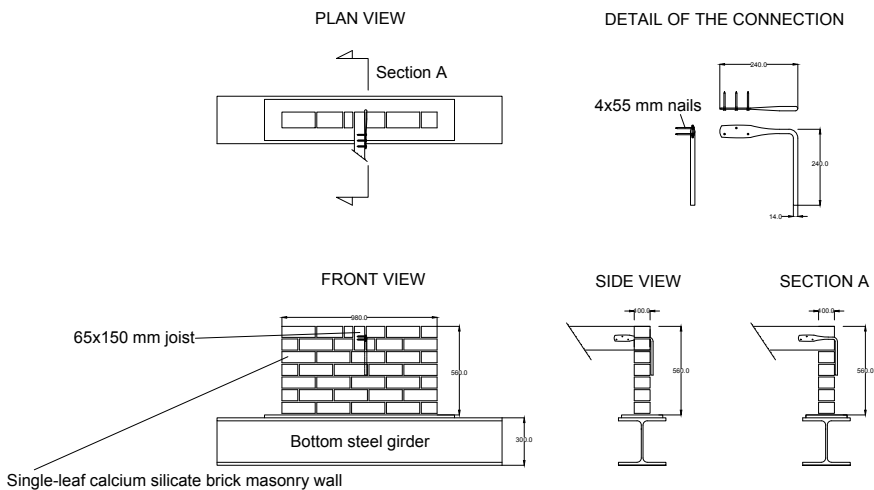


Figure B.5: Configuration CS-B.

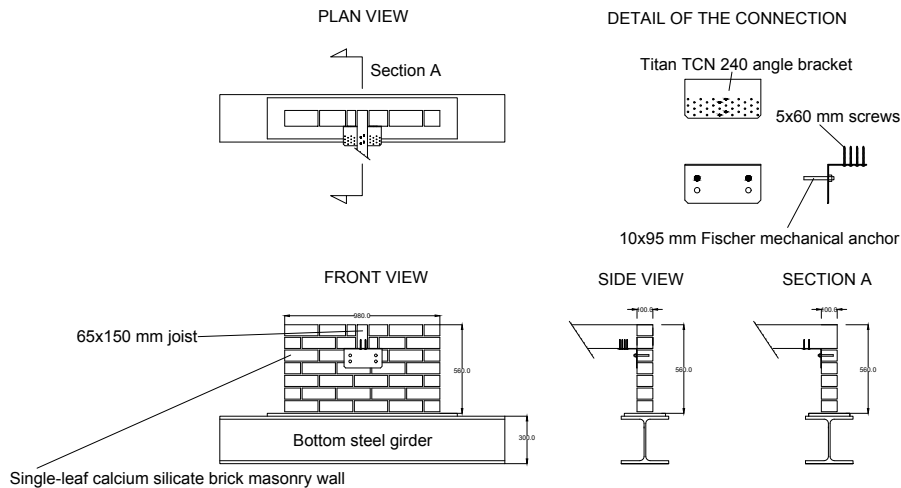


Figure B.6: Configuration CS-C.

B.2 Samples tested within the second experimental campaign

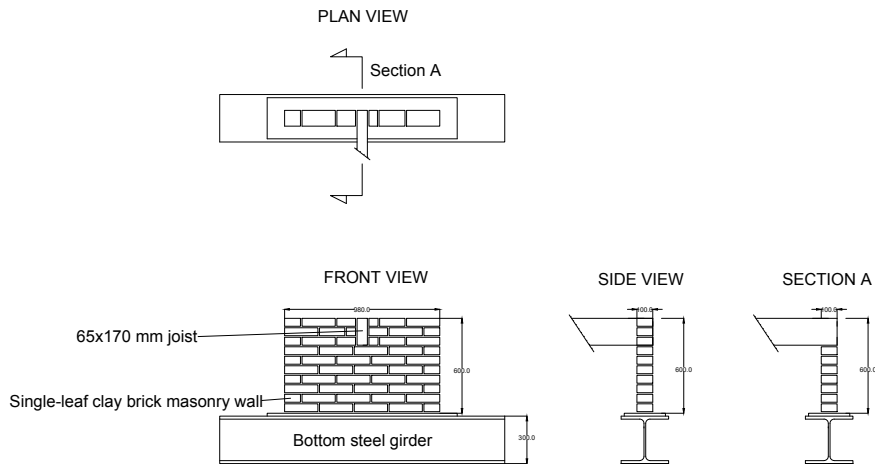


Figure B.7: Configuration A.

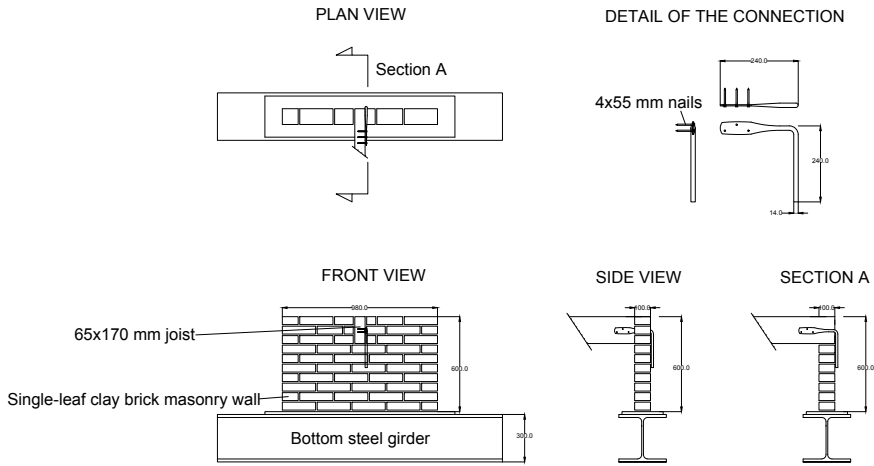


Figure B.8: Configuration B.

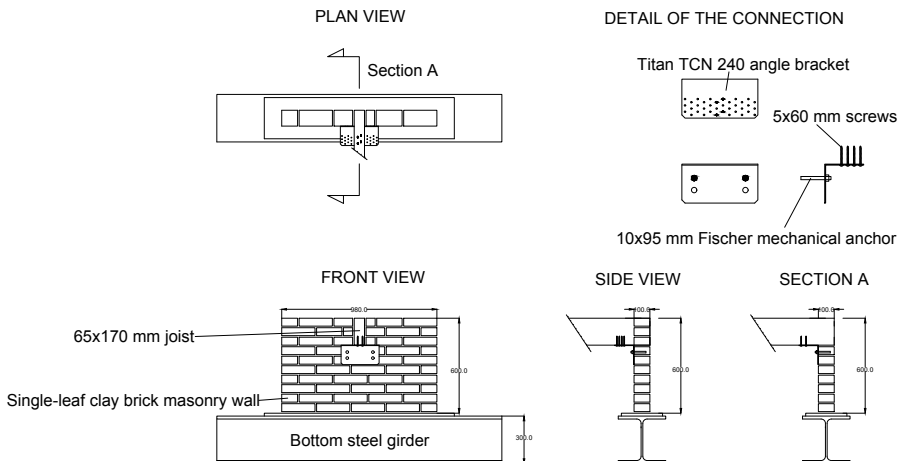


Figure B.9: Configuration C.

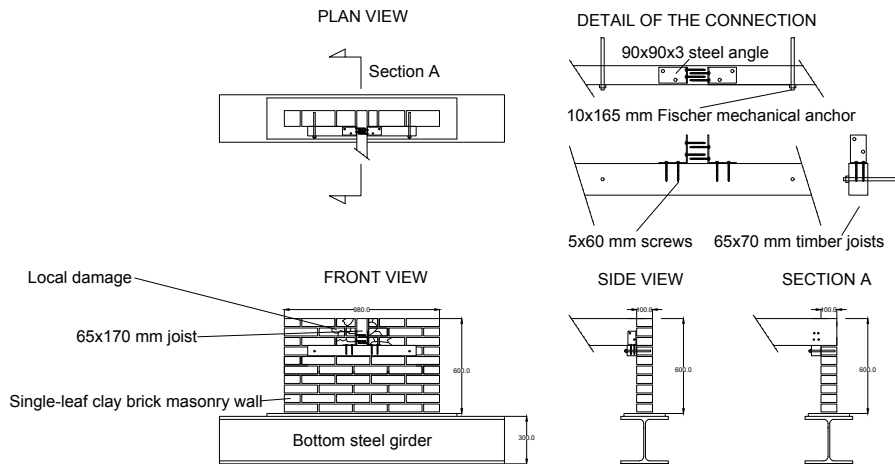


Figure B.10: Configuration D.

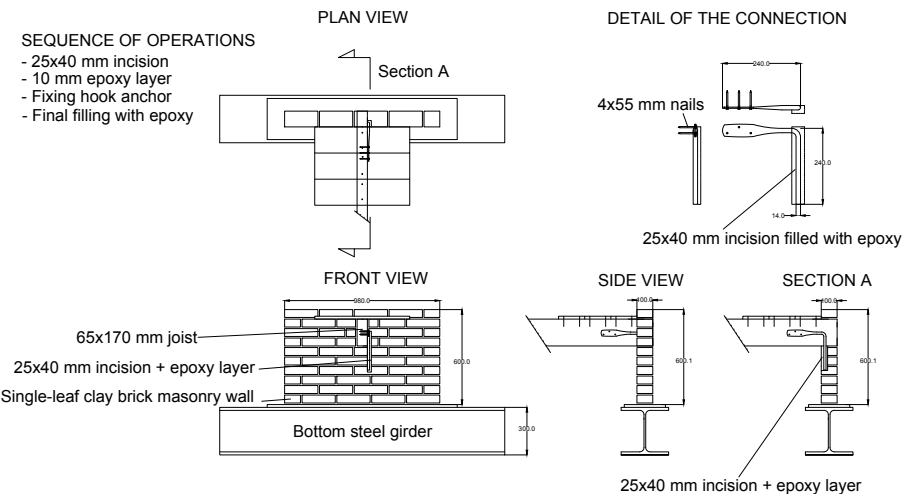


Figure B.11: Configuration E.

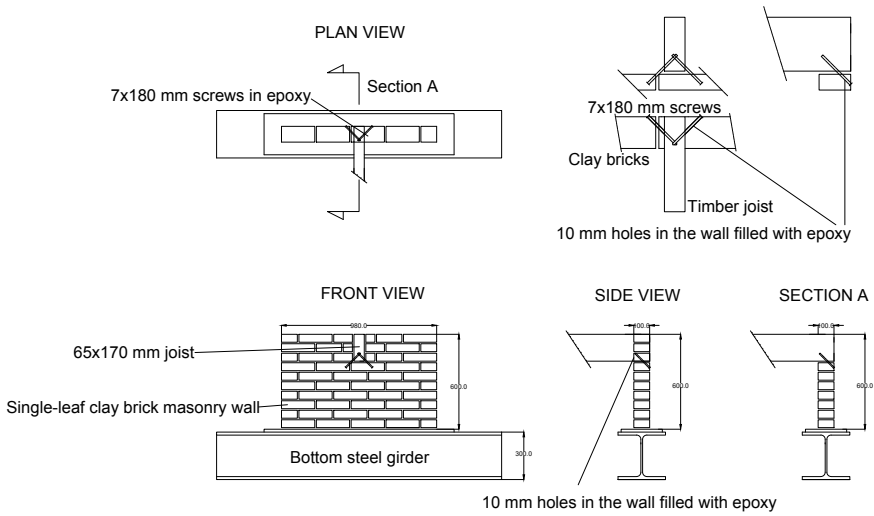


Figure B.12: Configuration F.

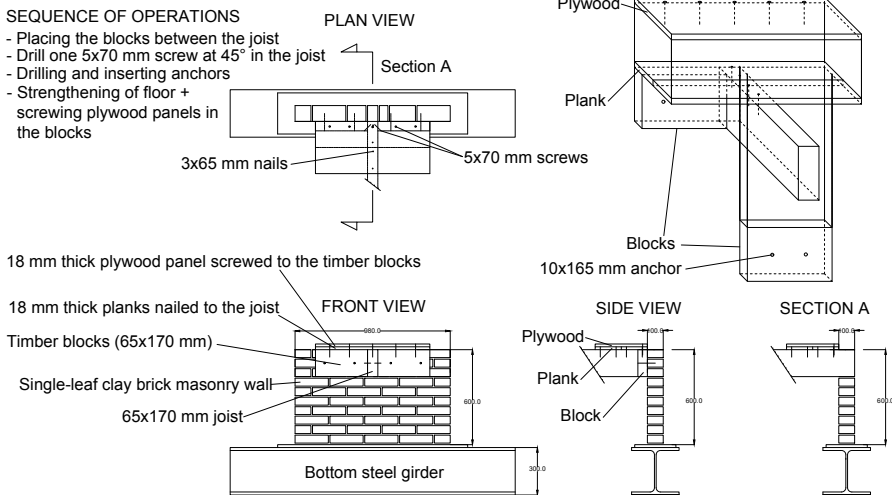


Figure B.13: Configuration G.

Appendix C

Main properties of timber diaphragms compared from literature

In this Appendix, the properties of the analysed floors are reported to provide the readers with a detailed overview of them, and may constitute a useful database for future studies. In the tables, the diaphragms are distinguished between original (O) and strengthened (S).

Appendix C. Main properties of timber diaphragms compared from literature

Table C.1: Characteristics of the as-built and strengthened floors tested by VALLUZZI *et al.* [19, 20] and values of their in-plane stiffness.

Test configuration		Vertical, 1/4 of the floor, with 1 point of application of load			
Specimen name		FMSB (F1.M; O)	FM (F2.M; O)	FM+45°SP(A) (S)	FM+45°SP(B) (S)
Floor dimensions					
Orthogonal to load	[mm]	2120	2120	2120	2120
Parallel to load	[mm]	2120	2120	2120	2120
Total thickness	[mm]	160	160	185	200
Properties of main beams					
Width	[mm]	120	120	120	120
Height	[mm]	140	140	140	140
Length	[mm]	2420	2420	2420	2420
Heart-to-heart distance	[mm]	500	500	500	500
Material		Spruce wood	Spruce wood	Spruce wood	Spruce wood
Properties of planking					
Width	[mm]	135	135	135	135
Thickness	[mm]	20	20	20	20
Length	[mm]	2120	2120	2120	2120
Material		Spruce wood	Spruce wood	Spruce wood	Spruce wood
Other characteristics		Straight-edged planks	Tongue-and-groove planks	Straight-edged planks	Tongue-and-groove planks
Beams-planks connections					
Fastener type		Nails	Nails	Nails	Nails
Diameter	[mm]	2.75	2.75	2.75	2.75
Length	[mm]	60	60	60	60
Other characteristics		2 nails for each beam-plank intersection	2 nails for each beam-plank intersection	2 nails for each beam-plank intersection	2 nails for each beam-plank intersection
Properties of strengthening					
Type of strengthening		Not applicable (as-built sample)	Not applicable (as-built sample)	Second layer of planks at an angle of 45 °	Second layer of planks at an angle of 45 °
Width	[mm]	-	-	150	150
Thickness	[mm]	-	-	25	40
Length	[mm]	-	-	Variable	Variable
Material		-	-	Spruce wood	Spruce wood
Other characteristics		-	-	Straight-edged planks	Tongue-and-groove planks
Fastener type		-	-	Screws	Screws
Diameter	[mm]	-	-	6	6
Length	[mm]	-	-	100	120
Other characteristics		-	-	2 screws at each new plank-beam intersection	2 screws at each new plank-beam intersection
In-plane stiffness					
Value reported in the publication	[kN/mm]	0.08	0.29	1.18	1.25
Value at 0.1% drift	[kN/mm]	0.15	0.31	2.06	2.13
Value at 1.0% drift	[kN/mm]	0.04	0.06	0.71	0.72
Value at yielding (and drift)	[kN/mm]	0.10 (0.12%)	0.33 (0.12%)	1.89 (0.3%)	1.89 (0.3%)
Equivalent shear stiffness					
Value calculated from publication	[N/mm]	81	288	1176	1247
Value at 0.1% drift	[N/mm]	152	313	2065	2128
Value at 1.0% drift	[N/mm]	43	62	707	719
Value at yielding	[N/mm]	100	330	1890	1890

Appendix C. Main properties of timber diaphragms compared from literature

Table C.2: Characteristics of the as-built and strengthened floors tested by CORRADI et al. [18] and values of their in-plane stiffness.

Test configuration		Horizontal, half of the floor, with 1 point of application of load		
Specimen name		01-T2-OR (O)	02-T6-OR (O)	03-T4-T6 (S)
Floor dimensions				
Orthogonal to load	[mm]	3000	3000	3000
Parallel to load	[mm]	3000	3000	3000
Total thickness	[mm]	288	288	316
Properties of main beams				
Width	[mm]	180	180	180
Height	[mm]	180	180	180
Length	[mm]	3100	3100	3100
Heart-to-heart distance	[mm]	1100	1100	1100
Material		Chestnut wood	Chestnut wood	Chestnut wood
Properties of secondary beams				
Width	[mm]	80	80	80
Height	[mm]	80	80	80
Length	[mm]	1100	1100	1100
Heart-to-heart distance	[mm]	300	300	300
Material		Chestnut wood	Chestnut wood	Chestnut wood
Properties of planking				
Width	[mm]	125	125	125
Thickness	[mm]	28	28	28
Length	[mm]	600	600	600
Material		Chestnut wood	Chestnut wood	Chestnut wood
Other characteristics		Notched planks	Notched planks	Notched planks
Beams-planks connections				
Fastener type		Nails	Nails	Nails
Diameter	[mm]	Not mentioned	Not mentioned	Not mentioned
Length	[mm]	Not mentioned	Not mentioned	Not mentioned
Other characteristics		1 nail at planks' ends	3 nails at planks' ends	2 nails at planks' ends
Properties of strengthening				
Type of strengthening		Not applicable (as-built sample)	Not applicable (as-built sample)	Second layer of planks at an angle of 90 °
Width	[mm]	-	-	125
Thickness	[mm]	-	-	28
Length	[mm]	-	-	600
Material		-	-	Chestnut wood
Other characteristics		-	-	Notched planks
Fastener type		-	-	Nails
Diameter	[mm]	-	-	Not mentioned
Length	[mm]	-	-	Not mentioned
Other characteristics		-	-	2 nails at planks' ends and 2 in their middle
In-plane stiffness				
Value reported in the publication	[kN/mm]	0.47	0.28	1.71
Value at 0.1% drift	[kN/mm]	0.71	0.77	2.19
Value at 1.0% drift	[kN/mm]	0.13	0.20	0.40
Value at yielding (and drift)	[kN/mm]	0.23 (0.07%)	0.26 (0.08%)	2.19 (0.1%)
Equivalent shear stiffness				
Value calculated from publication	[N/mm]	470	280	1710
Value at 0.1% drift	[N/mm]	710	771	2190
Value at 1.0% drift	[N/mm]	128	204	400
Value at yielding	[N/mm]	230	255	2190

Table C.3: Characteristics of the as-built and strengthened floors tested by BRANCO et al. [21] and values of their in-plane stiffness.

Test configuration		Vertical, 1/4 of the floor, with 1 point of application of load	
Specimen name		S (O)	SS (S)
Floor dimensions			
Orthogonal to load	[mm]	2125	2125
Parallel to load	[mm]	2125	2125
Total thickness	[mm]	180	200
Properties of main beams			
Width	[mm]	100	100
Height	[mm]	160	160
Length	[mm]	2420	2420
Heart-to-heart distance	[mm]	500	500
Material		C24 timber	C24 timber
Properties of planking			
Width	[mm]	125	125
Thickness	[mm]	20	20
Length	[mm]	2125	2125
Material		Andira Vermifuga wood	Andira Vermifuga wood
Other characteristics		Straight-edged planks	Straight-edged planks
Beams-planks connections			
Fastener type		Nails	Nails
Diameter	[mm]	2.50	2.50
Length	[mm]	60	60
Other characteristics		2 nails for each intersection between beam and plank	2 nails for each intersection between beam and plank
Properties of strengthening			
Type of strengthening		Not applicable (as-built sample)	Superposition of a second layer of planks arranged at 90°
Width	[mm]	-	125
Thickness	[mm]	-	20
Length	[mm]	-	2125
Material		-	Andira Vermifuga wood
Other characteristics		-	Straight-edged planks
Fastener type		-	Nails
Diameter	[mm]	-	2.50
Length	[mm]	-	60
Other characteristics		-	2 nails at each intersection of the new planks with the existing ones
In-plane stiffness			
Value reported in the publication	[kN/mm]	0.05	0.13
Value at 0.1% drift	[kN/mm]	0.15	0.61
Value at 1.0% drift	[kN/mm]	0.05	0.16
Value at yielding	[kN/mm]	0.16 (at 0.14% drift)	0.61 (at 0.1% drift)
Equivalent shear stiffness			
Value calculated from publication	[N/mm]	55	132
Value at 0.1% drift	[N/mm]	153	609
Value at 1.0% drift	[N/mm]	53	165
Value at yielding	[N/mm]	165	609

Table C.4: Characteristics of the as-built and strengthened floors tested by GUBANA and MELOTTO [22] and values of their in-plane stiffness.

Test configuration		Vertical, half of the floor, with 1 point of application of load		
Specimen name		UR-2 (O)	OSB90-R-2 (S)	OSB0-S-2 (S)
Floor dimensions				
Orthogonal to load	[mm]	3160	3160	3160
Parallel to load	[mm]	3000	3000	3000
Total thickness	[mm]	183	208	208
Properties of main beams				
Width	[mm]	160	160	160
Height	[mm]	160	160	160
Length	[mm]	3160	3160	3160
Heart-to-heart distance	[mm]	500	500	500
Material		GL24h timber	GL24h timber	GL24h timber
Properties of planking				
Width	[mm]	145	145	145
Thickness	[mm]	23	23	23
Length	[mm]	3160	3160	3160
Material		C24 timber	C24 timber	C24 timber
Other characteristics		Straight-edged planks	Straight-edged planks	Straight-edged planks
Beams-planks connections				
Fastener type		Nails	Nails	Nails
Diameter	[mm]	2.50	2.50	2.50
Length	[mm]	65	65	65
Other characteristics		2 nails at beam-plank intersection	2 nails at beam-plank intersection	2 nails at beam-plank intersection
Properties of strengthening				
Type of strengthening		Not applicable (as-built sample)	Overlay of OSB panels arranged orthogonal to joists	Overlay of OSB panels arranged parallel to joists
Width	[mm]	-	1000	1000
Thickness	[mm]	-	25	25
Length	[mm]	-	3160	3160
Fastener type		-	Nails	Screws
Diameter	[mm]	-	2.80	6.0
Length	[mm]	-	90	160
Other characteristics		-	100 mm spacing along panels' perimeter, in correspondence of the joists	150 mm spacing in correspondence of the joists
In-plane stiffness				
Value reported in the publication	[kN/mm]	0.53	1.77	1.97
Value at 0.1% drift	[kN/mm]	0.55	2.55	5.05
Value at 1.0% drift	[kN/mm]	0.09	0.57	1.19
Value at yielding (and drift)	[kN/mm]	0.55 (0.1%)	3.12 (0.07%)	4.27 (0.13%)
Equivalent shear stiffness				
Value calculated from publication	[N/mm]	560	1870	2080
Value at 0.1% drift	[N/mm]	582	2691	5320
Value at 1.0% drift	[N/mm]	97	606	1259
Value at yielding	[N/mm]	582	3290	4496

Appendix C. Main properties of timber diaphragms compared from literature

Table C.5: Characteristics of the as-built and strengthened floors tested by PERALTA et al. [23] and different values of their in-plane stiffness.

Test configuration		Horizontal, whole floor, with 2 points of application of load		
Specimen name		MAE-2 (O)	MAE-2B (S)	MAE-2C (S)
Floor dimensions				
Orthogonal to load	[mm]	7320	7320	7320
Parallel to load	[mm]	3660	3660	3660
Total thickness	[mm]	254	264	264
Properties of main beams				
Width	[mm]	38	38	38
Height	[mm]	235	235	235
Length	[mm]	3660	3660	3660
Heart-to-heart distance	[mm]	406	406	406
Material		Pine wood	Pine wood	Pine wood
Properties of planking				
Width	[mm]	140	140	140
Thickness	[mm]	19	19	19
Length	[mm]	From 1630 to 3660	From 1630 to 3660	From 1630 to 3660
Material		Pine wood	Pine wood	Pine wood
Other characteristics		Straight-edged planks	Straight-edged planks	Straight-edged planks
Beams-planks connections				
Fastener type		Nails	Nails	Nails
Diameter	[mm]	3.50	3.50	3.50
Length	[mm]	76	76	76
Other characteristics		2 or 3 nails at beam-plank intersection	2 or 3 nails at beam-plank intersection	2 or 3 nails at beam-plank intersection
Properties of strengthening				
Type of strengthening		Not applicable (as-built sample)	Unblocked plywood panels overlay	Blocked plywood panels overlay
Width	[mm]	-	1200	1200
Thickness	[mm]	-	9.5	9.5
Length	[mm]	-	2400	2400
Fastener type		-	Nails	Nails
Diameter	[mm]	-	3.50	3.50
Length	[mm]	-	76	76
Other characteristics		-	152 mm spacing on supported edges, 305 mm spacing along intermediate joists	51 mm spacing at the diaphragm boundaries, 76 mm spacing on panel edges; additional toe-nailing 38x89 mm boards between the joists below panel edges
In-plane stiffness				
Value reported in the publication	[kN/mm]	1.80	8.40	11.30
Value at 0.1% drift	[kN/mm]	5.84	10.96	17.96
Value at 1.0% drift	[kN/mm]	1.42	2.34 ^(a)	5.22 ^(a)
Value at yielding (and drift)	[kN/mm]	5.84 (0.1%)	7.76 (0.12%)	13.93 (0.18%)
Equivalent shear stiffness				
Value calculated from publication	[N/mm]	600	2800	3767
Value at 0.1% drift	[N/mm]	1949	3653	5990
Value at 1.0% drift	[N/mm]	475	780	1743
Value at yielding	[N/mm]	1949	2400	4644

^(a) Values obtained from an extrapolation of the experimental curve and not directly from it, because the test was stopped slightly before this drift value.

Table C.6: Characteristics of the as-built and strengthened floors tested by BRIGNOLA *et al.* [24] and different values of their in-plane stiffness.

Test configuration		Horizontal, whole floor, with 2 points of application of load	
Specimen name		AB-1 (O)	R-1 (S)
Floor dimensions			
Orthogonal to load	[mm]	4000	4000
Parallel to load	[mm]	3000	3000
Total thickness	[mm]	275	294
Properties of main beams			
Width	[mm]	50	50
Height	[mm]	250	250
Length	[mm]	4000	4000
Heart-to-heart distance	[mm]	500	500
Material		Radiata pine wood	Radiata pine wood
Properties of planking			
Width	[mm]	150	150
Thickness	[mm]	25	25
Length	[mm]	1000, 2000	1000, 2000
Material		Pine wood	Pine wood
Other characteristics		Straight-edged planks	Straight-edged planks
Beams-planks connections			
Fastener type		Nails	Nails
Diameter	[mm]	3.15	3.15
Length	[mm]	75	75
Other characteristics		2 or 4 nails for each intersection between beam and plank	2 or 4 nails for each intersection between beam and plank
Properties of strengthening			
Type of strengthening		Not applicable (as-built sample)	Plywood panels overlay
Width	[mm]	-	1200
Thickness	[mm]	-	19
Length	[mm]	-	2400
Fastener type		-	Screws
Diameter	[mm]	-	4.2
Length	[mm]	-	50 (120 in correspondence of joists)
Other characteristics		-	150 mm spacing along both panel edges and joists
In-plane stiffness			
Value reported in the publication	[kN/mm]	1.36	6.65
Value at 0.1% drift	[kN/mm]	3.06	14.70
Value at 1.0% drift	[kN/mm]	1.16	5.20
Value at yielding	[kN/mm]	3.02 (at 0.18% drift)	12.4 (at 0.16% drift)
Equivalent shear stiffness			
Value calculated from publication	[N/mm]	340	1665
Value at 0.1% drift	[N/mm]	769	3675
Value at 1.0% drift	[N/mm]	290	1300
Value at yielding	[N/mm]	756	3102

Appendix C. Main properties of timber diaphragms compared from literature

Table C.7: Characteristics of the as-built and strengthened floors tested by GIONGO *et al.* [26] and values of their in-plane stiffness.

Test configuration		Horizontal, whole floor, with 4 points of application of load	
Specimen name		26_B_asB (O)	35_B_Plyw (S)
Floor dimensions			
Orthogonal to load	[mm]	9600	9600
Parallel to load	[mm]	4700	4700
Total thickness	[mm]	322	331
Properties of main beams			
Width	[mm]	50	50
Height	[mm]	300	300
Length	[mm]	4800	4800
Heart-to-heart distance	[mm]	450	450
Material		Rimu wood	Rimu wood
Properties of planking			
Width	[mm]	130	130
Thickness	[mm]	22	22
Length	[mm]	2350, 4700	2350, 4700
Material		Matai wood	Matai wood
Other characteristics		Tongue-and-groove planks	Tongue-and-groove planks
Beams-planks connections			
Fastener type		Nails	Nails
Diameter	[mm]	Not mentioned	Not mentioned
Length	[mm]	Not mentioned	Not mentioned
Other characteristics		2 nails for each intersection between beam and plank	2 nails for each intersection between beam and plank
Properties of strengthening			
Type of strengthening		Not applicable (as-built sample)	Plywood panels overlay
Width	[mm]	-	1200
Thickness	[mm]	-	9
Length	[mm]	-	2400
Fastener type		-	Screws
Diameter	[mm]	-	3.5 (4.2 along floor's perimeter)
Length	[mm]	-	30 (60 along floor's perimeter)
Other characteristics		-	150 mm spacing along panel edges, 300 mm spacing on the whole panels' area, 100 mm spacing along floor's perimeter
In-plane stiffness			
Value at 0.1% drift	[kN/mm]	1.16	10.70
Value at 1.0% drift	[kN/mm]	0.65	3.69
Value at yielding	[kN/mm]	1.00 (at 0.25% drift)	10.70 (at 0.1% drift)
Equivalent shear stiffness			
Value at 0.1% drift	[N/mm]	302	2783
Value at 1.0% drift	[N/mm]	169	961
Value at yielding	[N/mm]	260	2783

Appendix C. Main properties of timber diaphragms compared from literature

Table C.8: Characteristics of the as-built and strengthened floors tested by Wilson et al. [25] and values of their in-plane stiffness.

Test configuration		Horizontal, whole floor, 4 load points		Horizontal, whole floor, 2 load points	
Specimen name		1a-PARA (O)	1b-PARA (S)	1a-PERP (O)	1b-PERP (S)
Floor dimensions					
Orthogonal to load	[mm]	10400	10400	5500	2120
Parallel to load	[mm]	5500	5500	10400	2120
Total thickness	[mm]	308	323	308	323
Properties of main beams					
Width	[mm]	45	45	45	45
Height	[mm]	290	290	290	290
Length	[mm]	5500	5500	5500	5500
Heart-to-heart distance	[mm]	400	400	400	400
Material		MSG8 timber	MSG8 timber	MSG8 timber	MSG8 timber
Properties of planking					
Width	[mm]	135	135	135	135
Thickness	[mm]	18	18	18	18
Length	[mm]	1600-5200	1600-5200	1600-5200	1600-5200
Material		MSG8 timber	MSG8 timber	MSG8 timber	MSG8 timber
Other characteristics		Straight-edged planks	Straight-edged planks	Straight-edged planks	Straight-edged planks
Beams-planks connections					
Fastener type		Nails	Nails	Nails	Nails
Diameter	[mm]	3.15	3.15	3.15	3.15
Length	[mm]	75	75	75	75
Other characteristics		2 or 4 nails for each beam-plank intersection	2 or 4 nails for each beam-plank intersection	2 or 4 nails for each beam-plank intersection	2 or 4 nails for each beam-plank intersection
Properties of strengthening					
Type of strengthening		Not applicable (as-built sample)	Plywood panels overlay	Not applicable (as-built sample)	Plywood panels overlay
Width	[mm]	-	1200	-	1200
Thickness	[mm]	-	15	-	15
Length	[mm]	-	2400	-	2400
Other characteristics		-	Metal straps stapled on panel edges; blocking and chords on long floor edges	-	Metal straps stapled on panel edges; blocking on long floor edges
Fastener type		-	Nails	-	Nails
Diameter	[mm]	-	3.15	-	3.15
Length	[mm]	-	75	-	75
Other characteristics		-	300 mm spacing along joists, 100 at floor's edges	-	300 mm spacing along joists, 100 at floor's edges
In-plane stiffness					
Value reported in the publication	[kN/mm]	0.64	14.52	1.61	22.41
Value at 0.1% drift	[kN/mm]	2.06	19.55	5.34	30.89
Value at 1.0% drift	[kN/mm]	0.47	3.66	1.54	7.15
Value at yielding (and drift)	[kN/mm]	2.06 (0.1%)	15.00 (0.15%)	3.75 (0.14%)	30.89 (0.1%)
Equivalent shear stiffness					
Value calculated from publication	[N/mm]	198	4459	134	1864
Value at 0.1% drift	[N/mm]	637	3294	441	1402
Value at 1.0% drift	[N/mm]	148	1140	128	595
Value at yielding	[N/mm]	637	2533	313	1402

Appendix C. Main properties of timber diaphragms compared from literature

Table C.9: Characteristics of the as-built and strengthened floors tested at TU Delft [132] in the direction parallel to the joists, and values of their in-plane stiffness.

Test configuration		Vertical, half of the floor, 1 point of application of load			
Specimen name		DFpar-1 (O)	DFpar-2 (O)	DFpar-1s (S)	DFpar-2s (S)
Floor dimensions					
Orthogonal to load	[mm]	2400	2400	2400	2400
Parallel to load	[mm]	3800	3960	3800	3960
Total thickness	[mm]	148	154	166	172
Properties of main beams					
Width	[mm]	60	60	60	60
Height	[mm]	130	130	130	130
Length	[mm]	3800	3960	3800	3960
Heart-to-heart distance	[mm]	650	650	650	650
Material		C24 timber	C24 timber	C24 timber	C24 timber
Properties of planking					
Width	[mm]	165	165	165	165
Thickness	[mm]	18	24	18	24
Length	[mm]	2400	2400	2400	2400
Material		C24 timber	C24 timber	C24 timber	C24 timber
Other characteristics		Tongue-and-groove planks	Tongue-and-groove planks	Tongue-and-groove planks	Tongue-and-groove planks
Beams-planks connections					
Fastener type		Nails	Nails	Nails	Nails
Diameter	[mm]	3.0	3.0	3.0	3.0
Length	[mm]	65	65	65	65
Other characteristics		2 nails for each beam-plank intersection	2 nails for each beam-plank intersection	2 nails for each beam-plank intersection	2 nails for each beam-plank intersection
Properties of strengthening					
Type of strengthening		Not applicable (as-built sample)	Not applicable (as-built sample)	Plywood panels overlay	Plywood panels overlay
Width	[mm]	-	-	600	600
Thickness	[mm]	-	-	18	18
Length	[mm]	-	-	1200	1200
Other characteristics		-	-	Improvement of shear transfer with additional fasteners on top	Improvement of shear transfer with additional fasteners on top
Fastener type		-	-	Screws	Screws
Diameter	[mm]	-	-	4.5 (5.0 on top)	5.0
Length	[mm]	-	-	40 (70 on top)	60 (70 on top)
Other characteristics		-	-	100 mm spacing along the panels' perimeter	100 mm spacing along the panels' perimeter
In-plane stiffness					
Value at 0.1% drift	[kN/mm]	0.74	0.86	5.45	6.32
Value at 1.0% drift	[kN/mm]	0.36	0.47	2.02	2.83
Value at yielding (and drift)	[kN/mm]	0.48 (0.28%)	0.57 (0.16%)	5.70 (0.09%)	5.61 (0.15%)
Equivalent shear stiffness					
		Size-dependent (flexural response)			
Value at 0.1% drift	[N/mm]	467	521	3441	3832
Value at 1.0% drift	[N/mm]	227	285	1277	1717
Value at yielding	[N/mm]	303	345	3600	3403

Table C.10: Characteristics of the as-built and strengthened floors tested at TU Delft [132] in the direction perpendicular to the joists, and different values of their in-plane stiffness.

Test configuration		Vertical, half of the floor, 1 point of application of load			
Specimen name		DFper-3 (O)	DFper-4 (O)	DFper-3s (S)	DFper-4s (S)
Floor dimensions					
Orthogonal to load	[mm]	2300	2300	2300	2300
Parallel to load	[mm]	3800	3800	3800	3800
Total thickness	[mm]	128	128	146	146
Properties of main beams					
Width	[mm]	50	50	60	60
Height	[mm]	110	110	130	130
Length	[mm]	2300	2300	3800	3960
Heart-to-heart distance	[mm]	750	750	650	650
Material		C24 timber	C24 timber	C24 timber	C24 timber
Properties of planking					
Width	[mm]	165	165	165	165
Thickness	[mm]	18	18	18	24
Length	[mm]	3800	3800	2400	2400
Material		C24 timber	C24 timber	C24 timber	C24 timber
Other characteristics		Tongue-and-groove planks	Tongue-and-groove planks	Tongue-and-groove planks	Tongue-and-groove planks
Beams-planks connections					
Fastener type		Nails	Nails	Nails	Nails
Diameter	[mm]	3.0	3.0	3.0	3.0
Length	[mm]	65	65	65	65
Other characteristics		2 nails for each beam-plank intersection	2 nails for each beam-plank intersection	2 nails for each beam-plank intersection	2 nails for each beam-plank intersection
Properties of strengthening					
Type of strengthening		Not applicable (as-built sample)	Not applicable (as-built sample)	Plywood panels overlay	Plywood panels overlay
Width	[mm]	-	-	600	600
Thickness	[mm]	-	-	18	18
Length	[mm]	-	-	1200	1200
Other characteristics		-	-	-	Improvement of shear transfer with timber blocks on top
Fastener type		-	-	Screws	Screws
Diameter	[mm]	-	-	5.0	5.0
Length	[mm]	-	-	60	60
Other characteristics		-	-	100 mm spacing along the panels' perimeter	100 mm spacing along the panels' perimeter
In-plane stiffness					
Value at 0.1% drift	[kN/mm]	0.33	0.21	1.88	5.28
Value at 1.0% drift	[kN/mm]	0.11	0.10	1.21	2.93
Value at yielding (and drift)	[kN/mm]	0.25 (0.15%)	0.21 (0.1%)	1.56 (0.45%)	4.11 (0.26%)
Equivalent shear stiffness					
Value at 0.1% drift	[N/mm]	200	127	1136	3196
Value at 1.0% drift	[N/mm]	67	60	735	1773
Value at yielding	[N/mm]	151	127	946	2488

Appendix C. Main properties of timber diaphragms compared from literature

Table C.11: Characteristics of the as-built and strengthened roof sample tested at TU Delft [132] and different values of its in-plane stiffness.

Test configuration		Vertical, one roof pitch, 1 point of application of load	
Specimen name		DRpar-5 (O)	DRpar-5s (S)
Floor dimensions			
Orthogonal to load	[mm]	2730	2730
Parallel to load	[mm]	3800	3800
Total thickness	[mm]	148	148 (same thickness because panels are placed in between the purlins)
Properties of main beams (rafters)			
Width	[mm]	50	50
Height	[mm]	105	105
Length	[mm]	2730	2730
Heart-to-heart distance	[mm]	925	925
Material		C24 timber	C24 timber
Properties of secondary beams (purlins)			
Width	[mm]	60	60
Height	[mm]	35	35
Length	[mm]	3800	3800
Heart-to-heart distance	[mm]	820	820
Material		C24 timber	C24 timber
Properties of planking			
Width	[mm]	165	165
Thickness	[mm]	18	18
Length	[mm]	2730	2400
Material		C24 timber	C24 timber
Other characteristics		Tongue-and-groove planks	Tongue-and-groove planks
Beams-planks connections			
Fastener type		Nails	Nails
Diameter	[mm]	3.0	3.0
Length	[mm]	55	55
Other characteristics		2 nails for each beam-plank intersection	2 nails for each beam-plank intersection
Properties of strengthening			
Type of strengthening		Not applicable (as-built sample)	Plywood panels overlay
Width	[mm]	-	600
Thickness	[mm]	-	18
Length	[mm]	-	1200
Other characteristics		-	Improvement of connection and shear transfer with steel angles at bottom (wall plate)
Fastener type		-	Screws
Diameter	[mm]	-	4.5 (6.0 for steel angle)
Length	[mm]	-	40 (70 for steel angle)
Other characteristics		-	100 mm spacing along the panels' perimeter
In-plane stiffness			
Value at 0.1% drift	[kN/mm]	0.15	3.42
Value at 1.0% drift	[kN/mm]	0.06	1.31
Value at yielding (and drift)	[kN/mm]	0.15 (0.1%)	2.57 (0.4%)
Equivalent shear stiffness			
Value at 0.1% drift	[N/mm]	108	2457
Value at 1.0% drift	[N/mm]	41	940
Value at yielding	[N/mm]	108	1848

Appendix D

Example of calculation of input parameters for numerical model of retrofitted timber floors

The calculations presented in this appendix refer to the floor example considered for validating the proposed macro-element modelling strategy for timber diaphragms retrofitted with plywood panels (Section 5.4.3, Fig. 5.23).

Input data of the retrofitted diaphragm:

- 4×6 m floor, supported on the long sides, loaded perpendicular to the short side
- In-plane initial stiffness K_{ip} : 10 kN/mm
- In-plane strength F_{max} : 150 kN
- Displacement at peak strength δ_{max} : 60 mm displacement
- 60×130×4000 mm joists at a heart-to-heart distance of 500 mm (13 in total)
- 18×165 mm planks
- 18 mm thick plywood panels
- Elastic modulus of timber: 10000 MPa.

Determination of the properties of the linear elastic orthotropic shell elements (thickness = 36 mm), simulating the floor behavior under vertical loads (G_{xy} is negligible because the in-plane response is governed by macro-elements):

$$\begin{aligned} E_{eq} &= E_{timber} I_{joists} / I_{slab} = \\ &= 10000 \cdot (13 \cdot 60 \cdot 130^3 / 12) / (6000 \cdot 36^3 / 12) = \\ &= 61200 \text{ MPa} = E_x = E_y = E_z \end{aligned}$$

$$G_{xz} = G_{yz} = E_{eq}/16 = 3820 \text{ MPa}$$

$$G_{xy} = 0.1 \text{ MPa}$$

Determination of the properties of the diagonal truss elements of the macro-elements, starting from a mesh of 1×1 m. The three initial parameters, required by the user-supplied subroutine for determining the constitutive law of the nonlinear diagonal trusses, are the strain ε_{max} at peak stress, the peak stress itself σ_{max} , and the initial stiffness K_0 . These can be derived from geometrical considerations, once the macro-elements mesh is defined. Starting from the whole floor deflection δ , the displacement u of a diagonal truss is given by:

$$u = \frac{\delta \cos \alpha}{m}$$

where α ($= 45^\circ$ in this case) is the angle between the truss and the loading direction (Fig. 5.23), and m the number of macro-elements rows parallel to the applied load in half of the floor (in this case, $m = 2$). The strain values to be adopted as input for the user-supplied subroutine are finally derived by dividing u by the length of the single diagonal truss l_d . Therefore, according to the floor properties:

$$\varepsilon_{max} = \frac{\delta_{max} \cos \alpha}{m \cdot l_d} = \frac{60}{2 \cdot 1000 \cdot \sqrt{2} \cdot \sqrt{2}} = 0.015$$

The shear force $F/2$ is subdivided among the s trusses ($= 12$ in this case) in one macro-elements row parallel to the load, and transformed into an axial force N on a single truss:

$$N = \frac{F}{2s \cos \alpha}$$

For convenience, a unitary section was adopted for the truss elements, so that force and stress could be coincident in their values. Therefore:

$$\sigma_{max} = \frac{F}{2s \cos \alpha} = \frac{150000}{2 \cdot 12} \sqrt{2} = 8840 \text{ MPa}$$

From the knowledge of the geometrical relations for ε_{max} and σ_{max} , also the initial stiffness K_0 of the diagonal trusses can be calculated:

$$K_0 = \frac{K_{ip} \cdot m \cdot l_d}{2s \cos^2 \alpha} = \frac{10000 \cdot 2 \cdot 1000 \cdot \sqrt{2}}{2 \cdot 12 \cdot 1/2} = 2.36 \cdot 10^6 \text{ MPa}$$

Thus, this completes the derivation of the properties reported in Table 5.8. The same procedure was followed for the determination of the input parameters of the numerical models of timber floors in the three case-study buildings described in Chapter 7.

Appendix E

Listing of the implemented user-supplied subroutine

```
SUBROUTINE USRMAT(EPSO, DEPS, NS, AGE0, DTIME, TEMPO, DTEMP, &
  ELEMEN, INTPT, COORD, SE, ITER, USRMOD, USRVAL, &
  NUV, USRSTA, NUS, USRIND, NUI, SIG, STIFF)
! .....
! User-supplied subroutine for general nonlinear behaviour.
! Returns updated stress and tangential stiffness matrix.
!
! ARGUMENTS AS REQUIRED BY DIANA FEA:
! EPSO   D() In   - Strain vector at start of increment.
! DEPS   D() In   - Total strain increment.
! NS      I   In   - Number of stress components
! AGE0    D   In   - Age of element.
! DTIME   D   In   - Total time increment.
! TEMPO   D   In   - Temperature.
! DTEMP   D   In   - Total temperature increment.
! ELEMEN  I   In   - Current element number.
! INTPT   I   In   - Current integration point number.
! COORD   D() In   - Coordinates of integration point.
! SE      D() In   - Elasticity matrix.
! ITER    I   In   - Current iteration number.
! USRMOD  C   In   - User model name.
! USRVAL  D() In   - User parameters.
! NUV     I   In   - Number of user parameters.
! USRSTA  D() InOut - User state variables at start of increment.
!                      Should be updated at output.
! NUS     I   In   - Number of user state variables.
! USRIND  I() InOut - User indicators at start of increment.
!                      Should be updated at output.
! NUI     I   In   - Number of user state indicators.
! SIG     D() InOut - Total stress at start of increment.
!                      Current stress at output.
! STIFF   D() InOut - Previous tangent stiffness.
!                      Current tangent stiffness at output.
! .....
! CHARACTER*6      USRMOD
!
! -----
! INTEGER INPUT VARIABLES
! -----
! INTEGER      NS, NUV, NUS, NUI, ELEMEN, INTPT, ITER, USRIND(NUI)
!
! -----
! REAL INPUT/OUTPUT VARIABLES
! -----
! DOUBLE PRECISION EPSO(NS), DEPS(NS), AGE0, DTIME, TEMPO, &
!                   DTEMP, COORD(3), SE(NS,NS), USRVAL(NUV), &
!                   USRSTA(NUS), SIG(NS), STIFF(NS,NS)
!
! -----
! OTHER REAL VARIABLES CALCULATED AND USED IN THE SUBROUTINE
! -----
! DOUBLE PRECISION EPS(NS), SIGY(NS), SIGMAX(NS), EPSMAX(NS), ETMAX(NS), &
! ETY(NS), ECY(NS), ECMAX(NS), a, b, KO(NS), K1(NS), K2(NS), K3(NS), K4(NS), &
! Q1(NS), Q2(NS), Q3(NS), Q4(NS), T(NS), D, POL(NS), POUL(NS), &
! STMAX(NS), SCMAX(NS), ULT1(NS), ULT2(NS), LT1(NS), LT2(NS), &
```

Appendix E. Listing of the implemented user-supplied subroutine

```

      ULC1(NS), ULC2(NS), LC1(NS), LC2(NS), ECL(NS), ECUL(NS), SCL(NS), SCUL(NS), &
      ETUL(NS), STUL(NS), ETL(NS), STL(NS), TENS(1), COMPR(1)
!
! -----
! VARIABLES INITIALIZATION FROM INPUT USER VALUES
! -----
      EPSMAX(1) = USRVAL(1)
      SIGMAX(1) = USRVAL(2)
      KO(1) = USRVAL(3)
!
! -----
! DETERMINATION OF YIELDING STRESS AND STRAIN AND PARABOLA COEFFICIENTS
! -----
      SIGY(1) = SIGMAX(1)/(8.d0)
      a = 2*(SIGMAX(1)-SIGY(1))/EPSMAX(1)
      b = -(SIGMAX(1)-SIGY(1))/EPSMAX(1)**2
      ETY(1) = 2.d0*SIGY(1)/KO(1)
      ECY(1) = -ETY(1)
!
! -----
! INITIALIZATION OF STATE VARIABLES
! -----
      ETMAX(1) = USRSTA(1)
      ECMAX(1) = USRSTA(2)
      ETUL(1) = USRSTA(3)
      STUL(1) = USRSTA(4)
      ETL(1) = USRSTA(5)
      STL(1) = USRSTA(6)
      ECUL(1) = USRSTA(7)
      SCUL(NS) = USRSTA(8)
      ECL(NS) = USRSTA(9)
      SCL(NS) = USRSTA(10)
!
! -----
! CURRENT STRAIN CALCULATION
! -----
      EPS(1) = EPS0(1)+DEPS(1)
!
! -----
! CURRENT STRESS CALCULATION
! -----
      IF(EPS(1).GE.0.d0) THEN
!
!         IF(EPS(1).GT.ETMAX(1)) THEN
!
!             -----
!             New tensile extreme
!             -----
!             ETMAX(1) = EPS(1)
!             TENS(1) = (SIGY(1)+a*EPS(1)+b*EPS(1)**2)* &
!             (1-EXP(-KO(1)*EPS(1)/SIGY(1)))
!             IF(TENS(1).GE.SCUL(1)) THEN
!                 SIG(1) = TENS(1)
!             ELSE
!                 SIG(1) = SCUL(1)+KO(1)/3.d0*DEPS(1)
!                 SCUL(1) = SIG(1)
!                 USRSTA(8) = SCUL(1)
!             END IF
!
!             Update of state variables
!             ETL(1) = ETMAX(1)
!             USRSTA(1) = ETMAX(1)
!             USRSTA(5) = ETL(1)
!
!         ELSE
!
!             -----
!             Determination of tensile pinching cycles' branches
!             -----
!             STMAX(1) = (SIGY(1)+a*ETMAX(1)+b*ETMAX(1)**2)* &
!             (1-EXP(-KO(1)*ETMAX(1)/SIGY(1)))
!
!             Construction line 1
!             K1(1) = (STMAX(1)-2*SIGY(1)/3.d0)/ETMAX(1)
!             Q1(1) = 2.d0*SIGY(1)/3.d0
!
!             Construction line 2
!             K2(1) = KO(1)
!             Q2(1) = STMAX(1)-ETMAX(1)*KO(1)
!
!             Construction line 3 (bisector)
!             K3(1) = TAN((ATAN(K2(1))+ATAN(K1(1)))/2.d0)
!             Q3(1) = STMAX(1)-ETMAX(1)*K3(1)
!
!             Construction line 4
!             K4(1) = (K3(1)*ETMAX(1)/2.d0+Q3(1)-2.d0*SIGY(1)/3.d0)/(ETMAX(1)/2.d0)
!             Q4(1) = K3(1)*ETMAX(1)/2.d0+Q3(1)-K4(1)*ETMAX(1)/2.d0
!
!             Intercepts for loading and unloading
!             POUL(1) = ETMAX(1)*K4(1)-Q4(1)
!             POL(1) = ETMAX(1)*K4(1)+Q4(1)
!
!             Determination of degradation factor for pinching
!             D = ETMAX(1)**3/EPSMAX(1)**3+1.d0

```


Appendix E. Listing of the implemented user-supplied subroutine

```

!
!      Calculation of factor for continuity at eps = 0
      T(1) = ((-POUL(1)+STMAX(1)+K4(1)*ETMAX(1))* &
      (1-EXP(-2.DO*K0(1)*ETMAX(1)/(-POUL(1)+STMAX(1))))-STMAX(1)+ &
      (-POL(1)+STMAX(1)+K4(1)*ETMAX(1))* &
      (1-EXP(-D*K3(1)*ETMAX(1)/(-POL(1)+STMAX(1))))-STMAX(1))/2.DO
!
      IF(EPS(1).LE.ETMAX(1).AND.EPS(1).LT.EPS0(1)) THEN
!
!      -----
!      Unloading in tension
!      -----
!
      IF(ETMAX(1).LE.ETY(1)) THEN
!
!      Unloading before yielding (elastic phase)
      SIG(1) = (SIGY(1)+a*EPS(1)+b*EPS(1)**2)* &
      (1-EXP(-K0(1)*EPS(1)/SIGY(1)))
!
      ELSE
!      Unloading after yielding
      ULT1(1) = -(-POUL(1)+STMAX(1)-K4(1)*(EPS(1)-ETMAX(1)))* &
      (1-EXP(2.DO*K0(1)*(EPS(1)-ETMAX(1))/(-POUL(1)+STMAX(1))))+ &
      STMAX(1)+T(1)
      IF(ETL(1).EQ.ETMAX(1)) THEN
!
!      Unloading after yielding from backbone curve
      SIG(1) = ULT1(1)
!
      ELSE
!
!      Unloading after yielding from reloading pinching curve
      ULT2(1) = STL(1)-(-ULT1(1)+STL(1))*(1-EXP(2.DO*K0(1)*(EPS(1)-ETL(1))/ &
      (-ULT1(1)+STL(1))))
      SIG(1) = ULT2(1)
      END IF
      END IF
!
!      Update of state variables
      ETUL(1) = EPS(1)
      STUL(1) = SIG(1)
      ECTL(1) = EPS(1)
      SCUL(1) = SIG(1)
      USRSTA(3) = ETUL(1)
      USRSTA(4) = STUL(1)
      USRSTA(7) = ECTL(1)
      USRSTA(8) = SCUL(1)
!
      ELSE
!
!      -----
!      Reloading in tension
!      -----
!
      IF(ETMAX(1).LE.ETY(1)) THEN
!
!      Reloading before yielding (elastic phase)
      SIG(1) = (SIGY(1)+a*EPS(1)+b*EPS(1)**2)* &
      (1-EXP(-K0(1)*EPS(1)/SIGY(1)))
!
      ELSE
!      Calculation of stress along the reloading pinching curve
      LT1(1) = -(-POL(1)+STMAX(1)-K4(1)*(EPS(1)-ETMAX(1)))* &
      (1-EXP(D*K3(1)*(EPS(1)-ETMAX(1))/(-POL(1)+STMAX(1))))+STMAX(1)+T(1)
!
!      Calculation of stress when reloading from the unloading pinching curve
      LT2(1) = STUL(1)+(LT1(1)-STUL(1))*(1-EXP(-2.DO*K0(1)*(EPS(1)-ETUL(1))/(LT1(1)-STUL(1))))
!
!      Determination of actual stress between the two previous ones
      IF(LT1(1).LT.LT2(1)) THEN
        SIG(1) = LT1(1)
      ELSE
        SIG(1) = LT2(1)
      END IF
      END IF
!
!      Update of state variables
      ETL(1) = EPS(1)
      STL(1) = SIG(1)
      USRSTA(5) = ETL(1)
      USRSTA(6) = STL(1)
      END IF
      END IF
!
      ELSE
!
!      IF(EPS(1).LT.ECMAX(1)) THEN
!
!      -----
!      New compressive extreme
!      -----
!
      ECP(1) = EPS(1)
      COMP(1) = -(SIGY(1)+a*ABS(EPS(1))+b*EPS(1)**2)* &
      (1-EXP(-K0(1)*ABS(EPS(1))/SIGY(1)))
      IF(COMP(1).LE.STUL(1)) THEN
        SIG(1) = COMP(1)
      ELSE
        SIG(1) = STUL(1)+K0(1)/3.DO*DEPS(1)
        STUL(1) = SIG(1)
      END IF
      END IF
      END IF

```

Appendix E. Listing of the implemented user-supplied subroutine

```

      USRSTA(4) = STUL(1)
      END IF
!
!   Update of state variables
      ECL(1) = ECMAX(1)
      USRSTA(2) = ECMAX(1)
      USRSTA(9) = ECL(1)
!
ELSE
!
!   -----
!   Determination of compressive pinching cycles' branches
!   -----
      SCMAX(1) = -(SIGY(1)+a*ABS(ECMAX(1))+b*ECMAX(1)**2)* &
        (1-EXP(-K0(1)*ABS(ECMAX(1))/SIGY(1)))
!
!   Construction line 1
      K1(1) = (SCMAX(1)+2*SIGY(1)/3.d0)/ECMAX(1)
      Q1(1) = -2.d0*SIGY(1)/3.d0
!
!   Construction line 2
      K2(1) = K0(1)
      Q2(1) = SCMAX(1)-ECMAX(1)*K0(1)
!
!   Construction line 3 (bisector)
      K3(1) = TAN((ATAN(K2(1))+ATAN(K1(1)))/2.d0)
      Q3(1) = SCMAX(1)-ECMAX(1)*K3(1)
!
!   Construction line 4
      K4(1) = (K3(1)*ECMAX(1)/2.d0+Q3(1)+2.d0*SIGY(1)/3.d0)/(ECMAX(1)/2.d0)
      Q4(1) = -2.d0*SIGY(1)/3.d0
!
!   Intercepts for loading and unloading
      POUL(1) = ECMAX(1)*K4(1)-Q4(1)
      POL(1) = ECMAX(1)*K4(1)+Q4(1)
!
!   Determination of degradation factor for pinching
      D = -ECMAX(1)**3/EPSMAX(1)**3+1.d0
!
!   Calculation of factor for continuity at eps = 0
      T(1) = -(POUL(1)-SCMAX(1)-K4(1)*ECMAX(1))* &
        (1-EXP(2.D0*K0(1)*ECMAX(1)/(POUL(1)-SCMAX(1))))-SCMAX(1)- &
        (POL(1)-SCMAX(1)-K4(1)*ECMAX(1))*(1-EXP(D*K3(1)*ECMAX(1)/ &
        (POL(1)-SCMAX(1))))-SCMAX(1))/2.d0
!
!   -----
!   Unloading in compression
!   -----
      IF(EPS(1).GE.ECMAX(1).AND.EPS(1).GT.EPS0(1)) THEN
        IF(ECMAX(1).GE.ECY(1)) THEN
!
!           Unloading before yielding (elastic phase)
          SIG(1) = -(SIGY(1)+a*ABS(EPS(1))+b*EPS(1)**2)* &
            (1-EXP(-K0(1)*ABS(EPS(1))/SIGY(1)))
!
!           ELSE
          Unloading after yielding
          ULC1(1) = (POUL(1)-SCMAX(1)+K4(1)*(EPS(1)-ECMAX(1)))* &
            (1-EXP(-2.D0*K0(1)*(EPS(1)-ECMAX(1))/(POUL(1)-SCMAX(1))))+SCMAX(1)+T(1)
          IF(ECL(1).EQ.ECMAX(1)) THEN
!
!             Unloading after yielding from backbone curve
            SIG(1) = ULC1(1)
          ELSE
!
!             Unloading after yielding from reloading pinching curve
            ULC2(1) = SCL(1)*(ULC1(1)-SCL(1))*(1-EXP(-2.D0*K0(1)*(EPS(1)-ECL(1)))/ &
              (ULC1(1)-SCL(1))))
            SIG(1) = ULC2(1)
          END IF
        END IF
!
!       Update of state variables
      ECUL(1) = EPS(1)
      SCUL(1) = SIG(1)
      ETUL(1) = EPS(1)
      STUL(1) = SIG(1)
      USRSTA(7) = ECUL(1)
      USRSTA(8) = SCUL(1)
      USRSTA(3) = ETUL(1)
      USRSTA(4) = STUL(1)
!
ELSE
!
!   -----
!   Reloading in compression
!   -----
      IF(ECMAX(1).GE.ECY(1)) THEN
!
!       Reloading before yielding (elastic phase)
      SIG(1) = -(SIGY(1)+a*ABS(EPS(1))+b*EPS(1)**2)* &
        (1-EXP(-K0(1)*ABS(EPS(1))/SIGY(1)))
!
!       ELSE
      Calculation of stress along the reloading pinching curve

```

Appendix E. Listing of the implemented user-supplied subroutine

```

      LC1(1) = (POL(1)-SCMAX(1)+K4(1)*(EPS(1)-ECMAX(1)))* &
      (1-EXP(-D*K3(1)*(EPS(1)-ECMAX(1)))/(POL(1)-SCMAX(1))))+SCMAX(1)+T(1)
!
!      Calculation of stress when reloading from the unloading pinching curve
      LC2(1) = SCUL(1)-(-LC1(1)+SCUL(1))*(1-EXP(2.D0*K0(1)*(EPS(1)-ECUL(1)))/(-LC1(1)+SCUL(1))))
!
!      Determination of actual stress between the two previous ones
      IF(LC1(1).GT.LC2(1)) THEN
        SIG(1) = LC1(1)
      ELSE
        SIG(1) = LC2(1)
      END IF
    END IF
!
!      Update of state variables
      ECL(1) = EPS(1)
      SCL(1) = SIG(1)
      USRSTA(9) = ECL(1)
      USRSTA(10) = SCL(1)
    END IF
  END IF
END SUBROUTINE USRMAT
```


Appendix F

Optimal dissipative retrofitting of case-study diaphragms

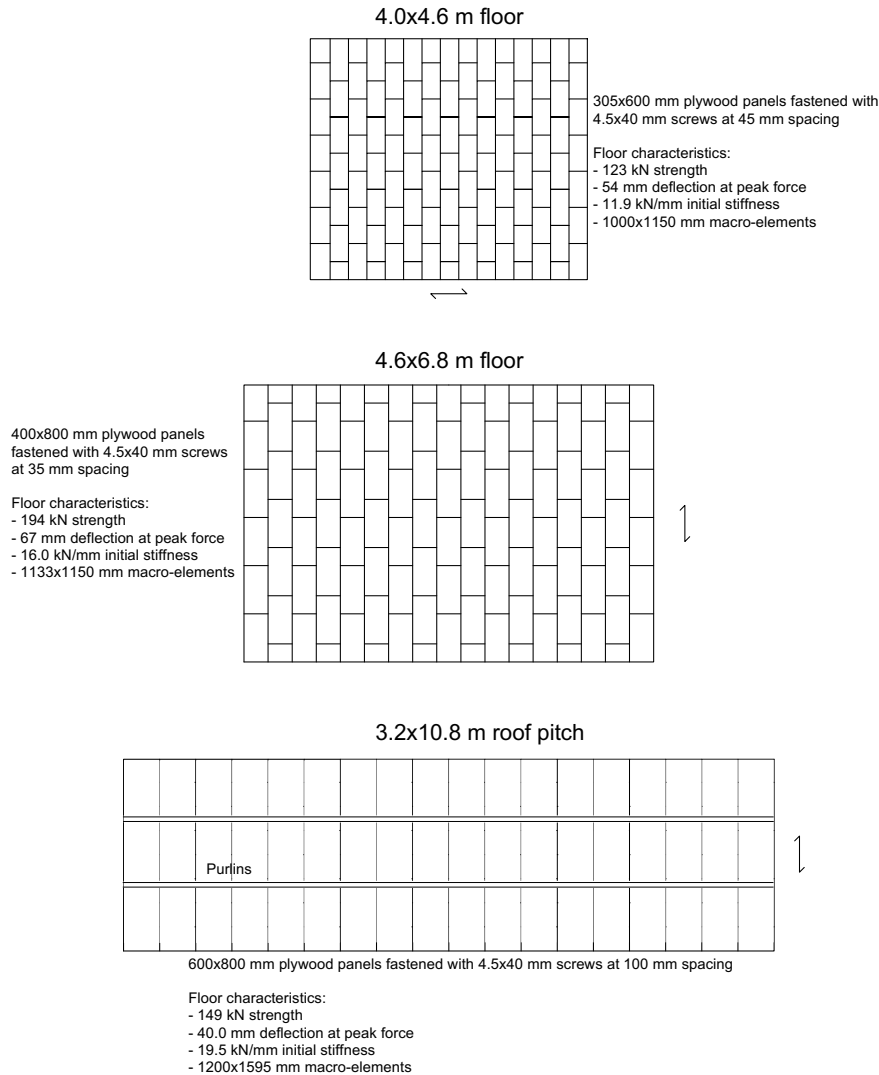


Figure F.1: Characteristics of the diaphragms retrofitted with plywood panels in building B1.

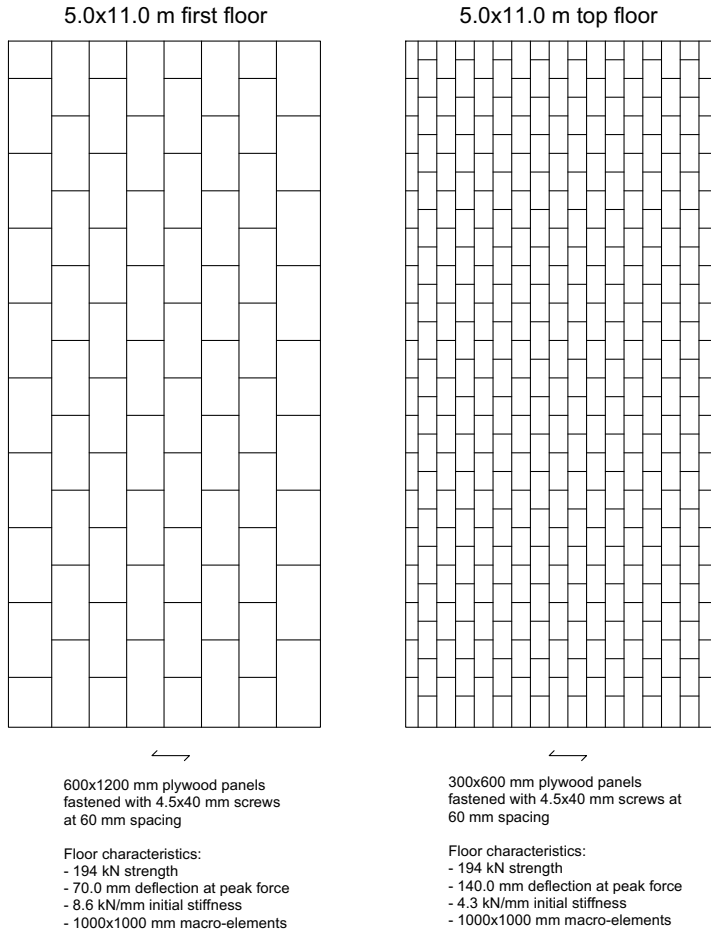


Figure F.2: Characteristics of the diaphragms retrofitted with plywood panels in building B2.

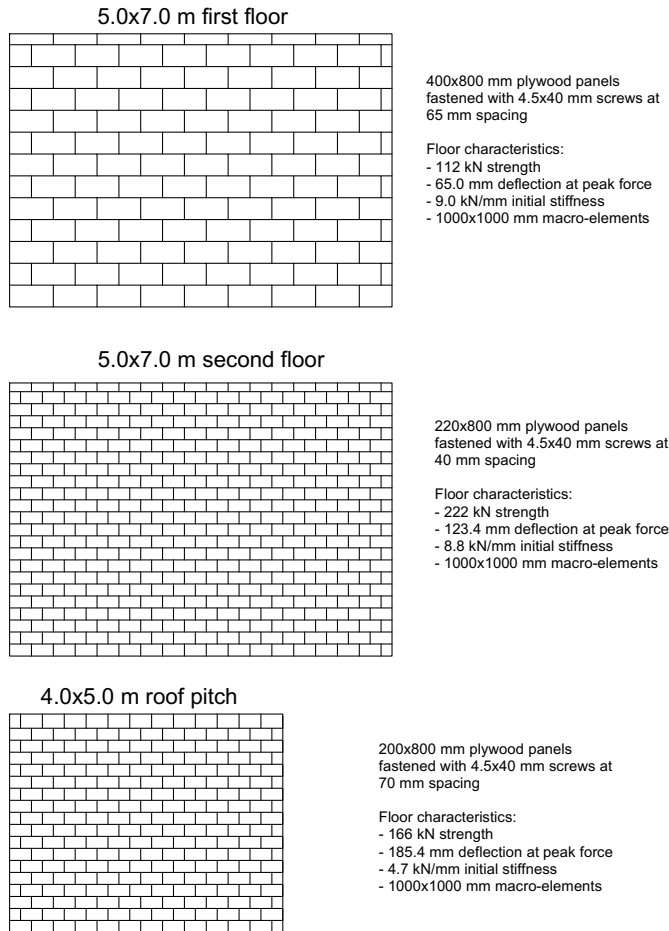


Figure F.3: Characteristics of the diaphragms retrofitted with plywood panels in building B3.

Appendix G

Example of hysteretic energy estimation

This calculation example refers, as a representative case, to configuration B1-PP under signal 2 of Fig. 6.7, applied in the x direction of the building and having a strong motion duration $\Delta t_e = 4.6$ s. For this loading direction, the fundamental period from the eigenvalue analysis was determined as $T_n = 0.14$ s (Section 7.9). In order to validate the assumed range of behaviour factor values $q = 2.5 \div 3.5$ for URM buildings with dissipative diaphragms, the hysteretic energy obtained by considering these values is compared to that determined as output of the numerical model. This calculation example is performed assuming $q = 3.5$, according to the following steps:

1. First of all, the ductility μ of the system is determined from the equation $q = \sqrt{2\mu - 1}$, thus $\mu = 6.625$.
2. According to the obtained ductility value, the effective period at collapse $T_{n,eff}$ is determined with Eq. 6.25:

$$\begin{aligned} T_{n,eff} &= \left\{ 0.89 \left[\sqrt{\frac{\mu - 1}{1 + 0.05(\mu - 2)}} - 1 \right] + 1 \right\} T_n \\ &= \left\{ 0.89 \left[\sqrt{\frac{6.625 - 1}{1 + 0.05(6.625 - 2)}} - 1 \right] + 1 \right\} 0.14 = 0.28 \text{ s} \end{aligned}$$

3. Determine the relevant quantities to calculate hysteretic energy from Eq. 6.20, hereby recalled:

$$E_d = \xi m \omega_n \Delta t_e^r S_v^2 (\alpha^2 + \beta^2)$$

This expression is damping-independent (Chapter 6), thus for simplicity $\xi = 0.05$ can be assumed. Other known quantities are the seismic mass m of the building, equal to 43267 kg, and the frequency $\omega_n = 2\pi/T_{n,eff} = 22.4$ Hz. The remaining parameters are determined as follows:

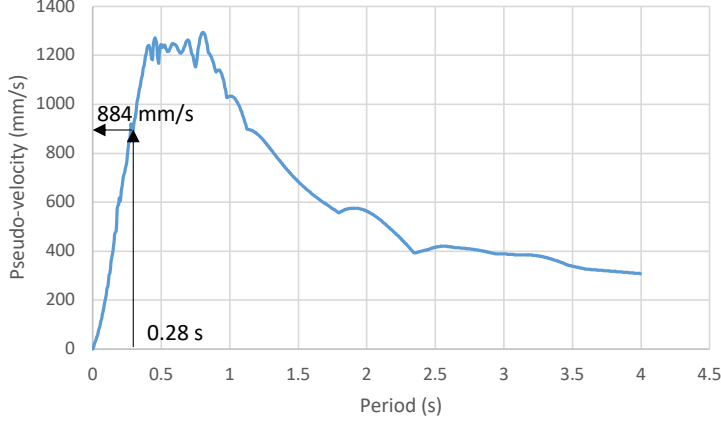


Figure G.1: Pseudo-velocity response spectrum of signal 2 at collapse.

- The pseudo-velocity S_v is determined from the reference response spectrum of signal 2 at collapse referred to 5% damping ratio (Fig. G.1), and is equal to 884 mm/s;
- The effective earthquake duration $\Delta t_e^r = \Delta t_e + 3.3T_{n,eff}/(6\xi) = 7.68$ s;
- The coefficient $\alpha^2 + \beta^2 = 0.25T_{n,eff}^{1/3} = 0.163$.

Thus, remembering that Eq. 6.20 should be multiplied by 10/9 according to NURTUĞ and SUCUOĞLU [197], and by a factor 10^{-6} to obtain a result in kNmm, the hysteretic energy of the system is estimated as:

$$E_d = 0.05 \cdot 43267 \cdot 22.4 \cdot 7.68 \cdot 884^2 \cdot 0.163 \cdot 10/9 \cdot 10^{-6} = 52673 \text{ kNmm}$$

The numerically recorded hysteretic energy was 49612 kN, thus the estimation is accurate and the building is indeed able to dissipate a remarkable amount of imparted energy, confirming the assumed behaviour factor of 3.5.

Appendix H

Complete results from time-history analyses

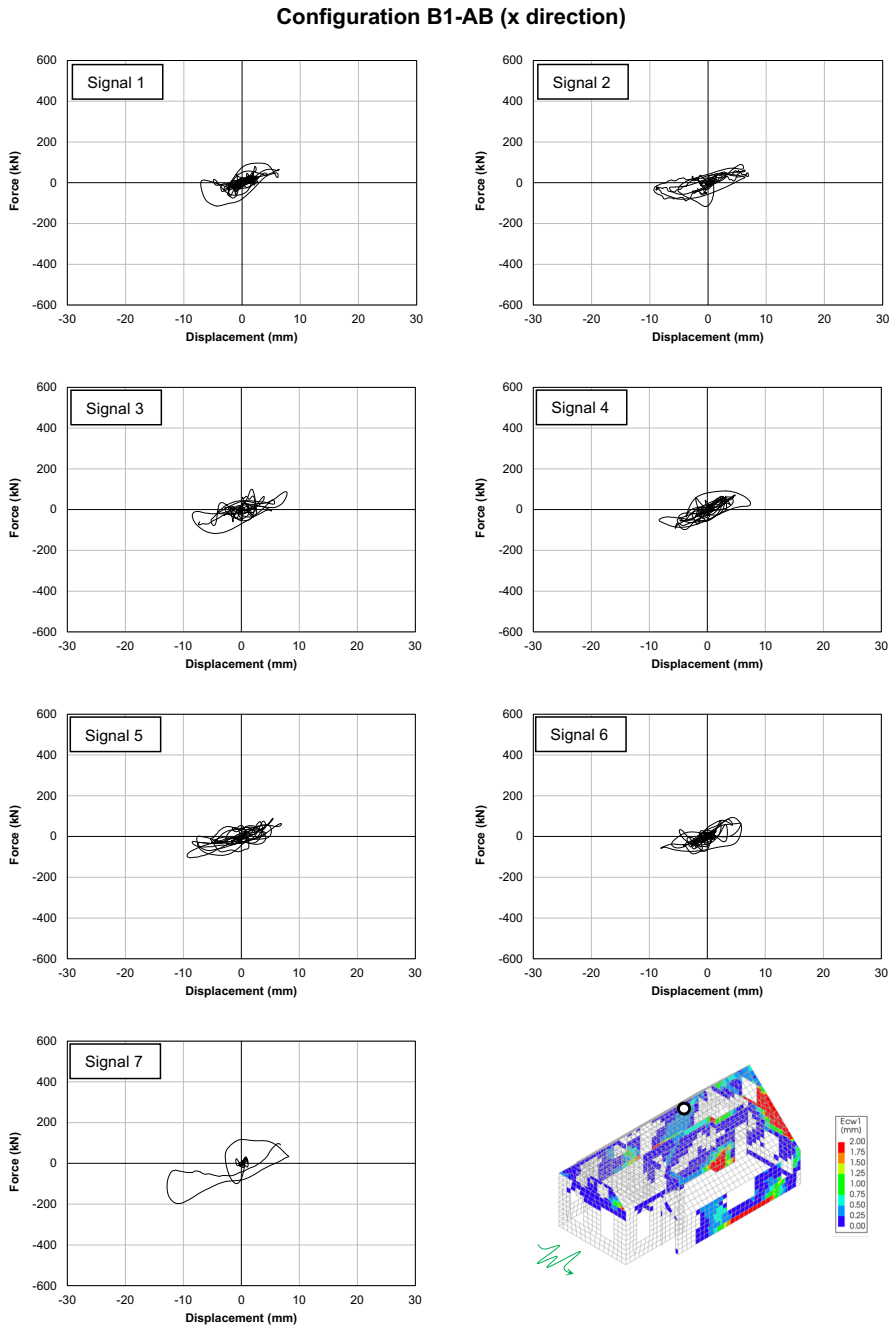


Figure H.1: Complete base shear-top floor displacement curves for the seven applied accelerograms; analyzed configuration, control node, and earthquake direction are highlighted.

Configuration B1-AB (y direction)

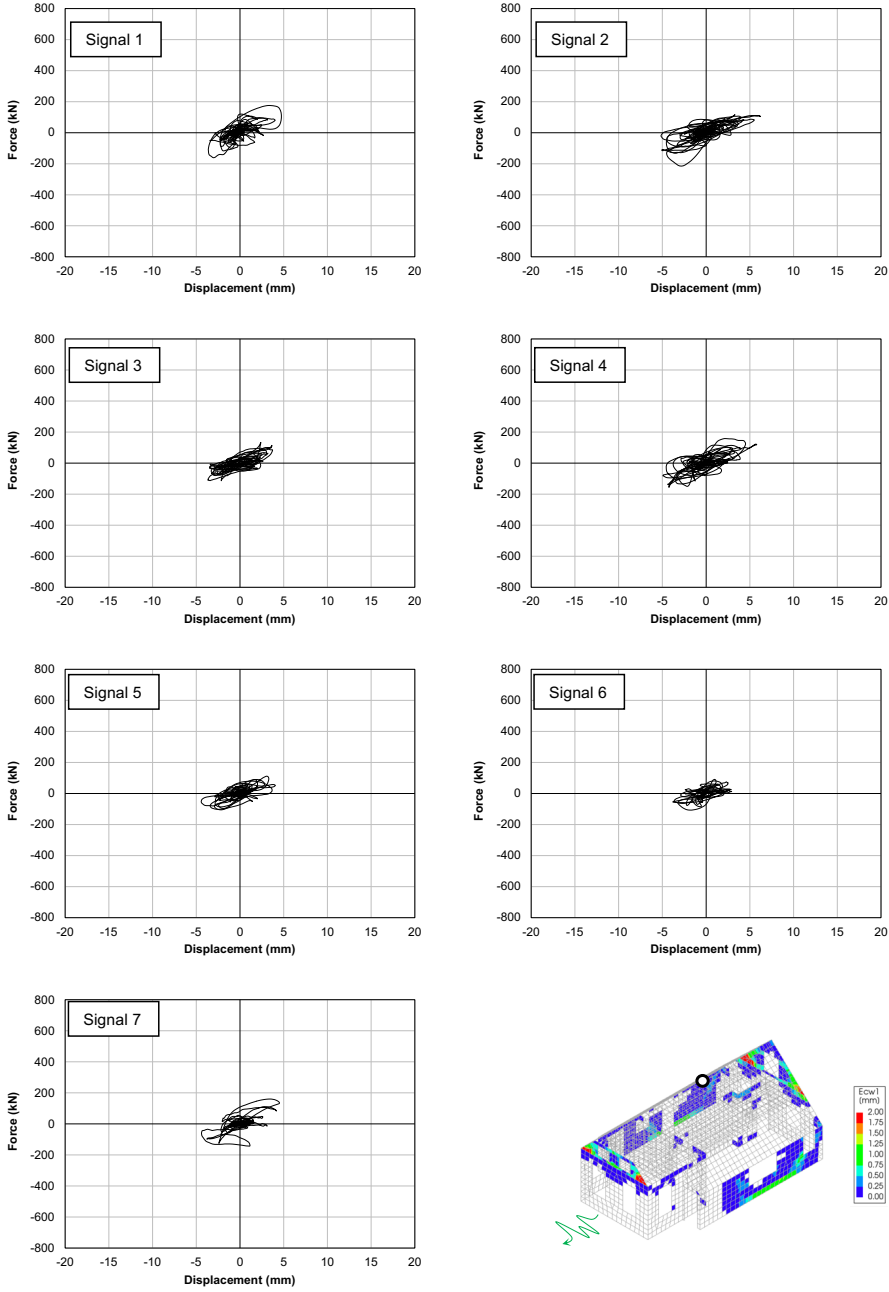


Figure H.2: Complete base shear-top floor displacement curves for the seven applied accelerograms; analyzed configuration, control node, and earthquake direction are highlighted.

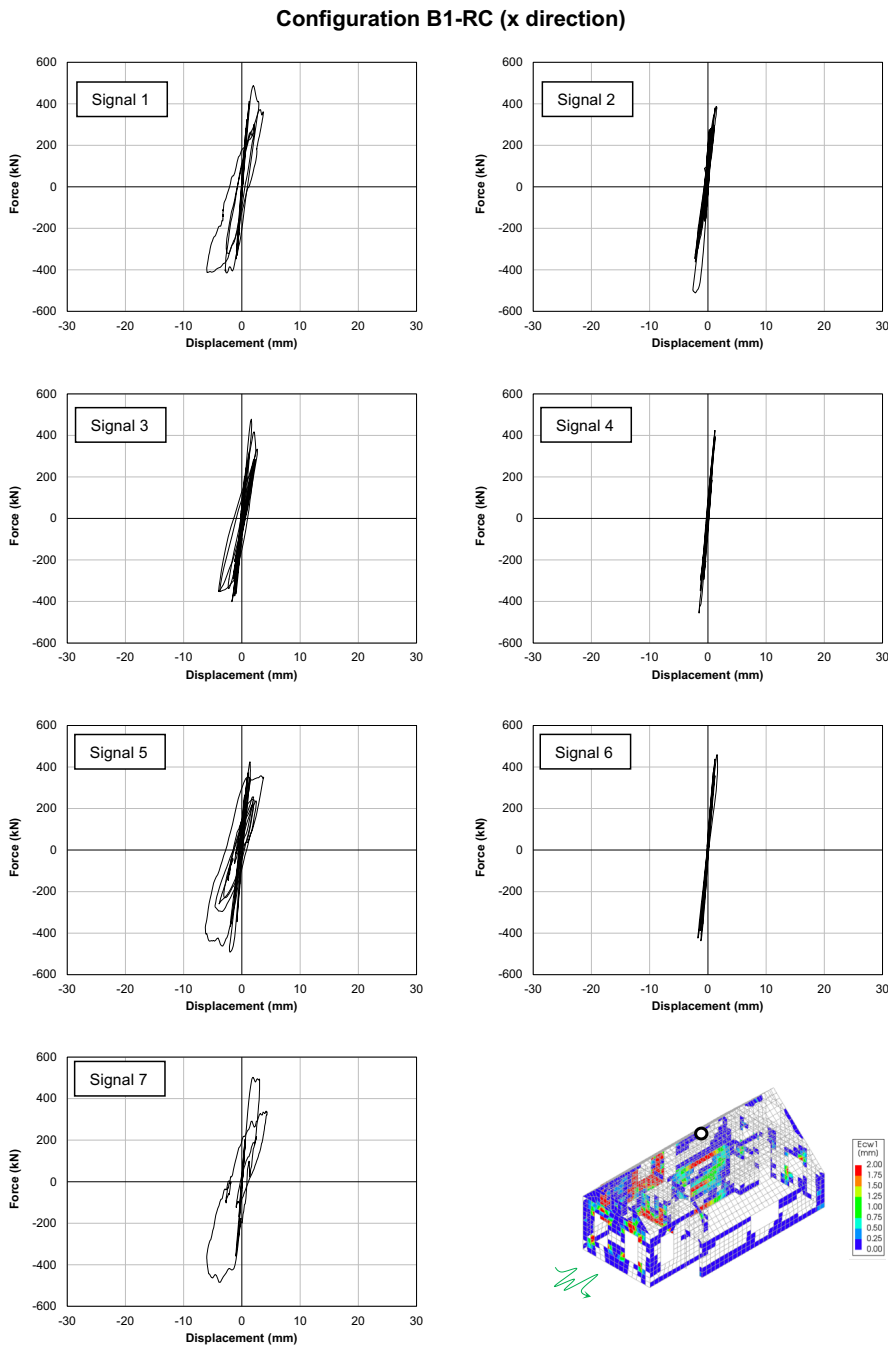


Figure H.3: Complete base shear-top floor displacement curves for the seven applied accelerograms; analyzed configuration, control node, and earthquake direction are highlighted.

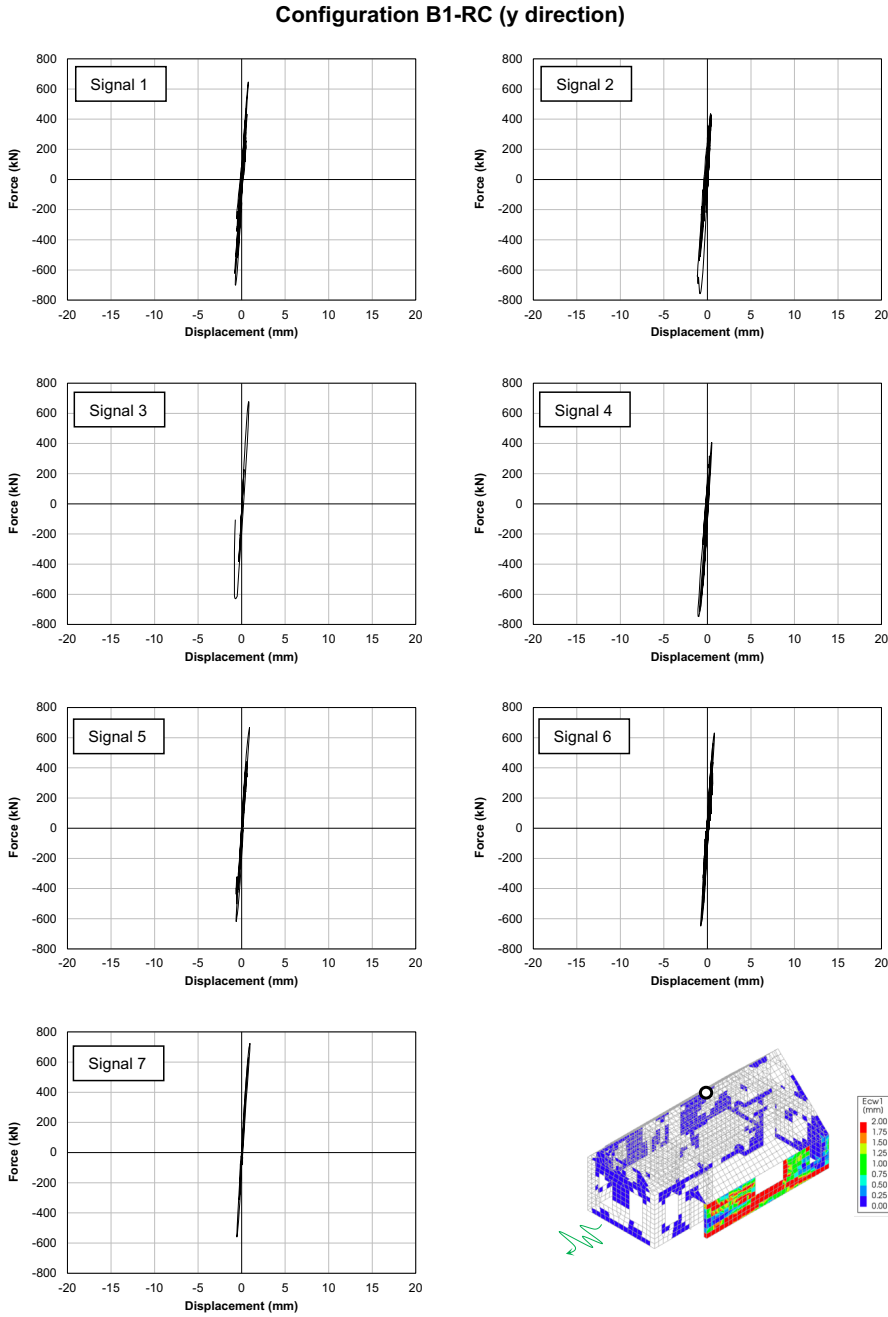


Figure H.4: Complete base shear-top floor displacement curves for the seven applied accelerograms; analyzed configuration, control node, and earthquake direction are highlighted.

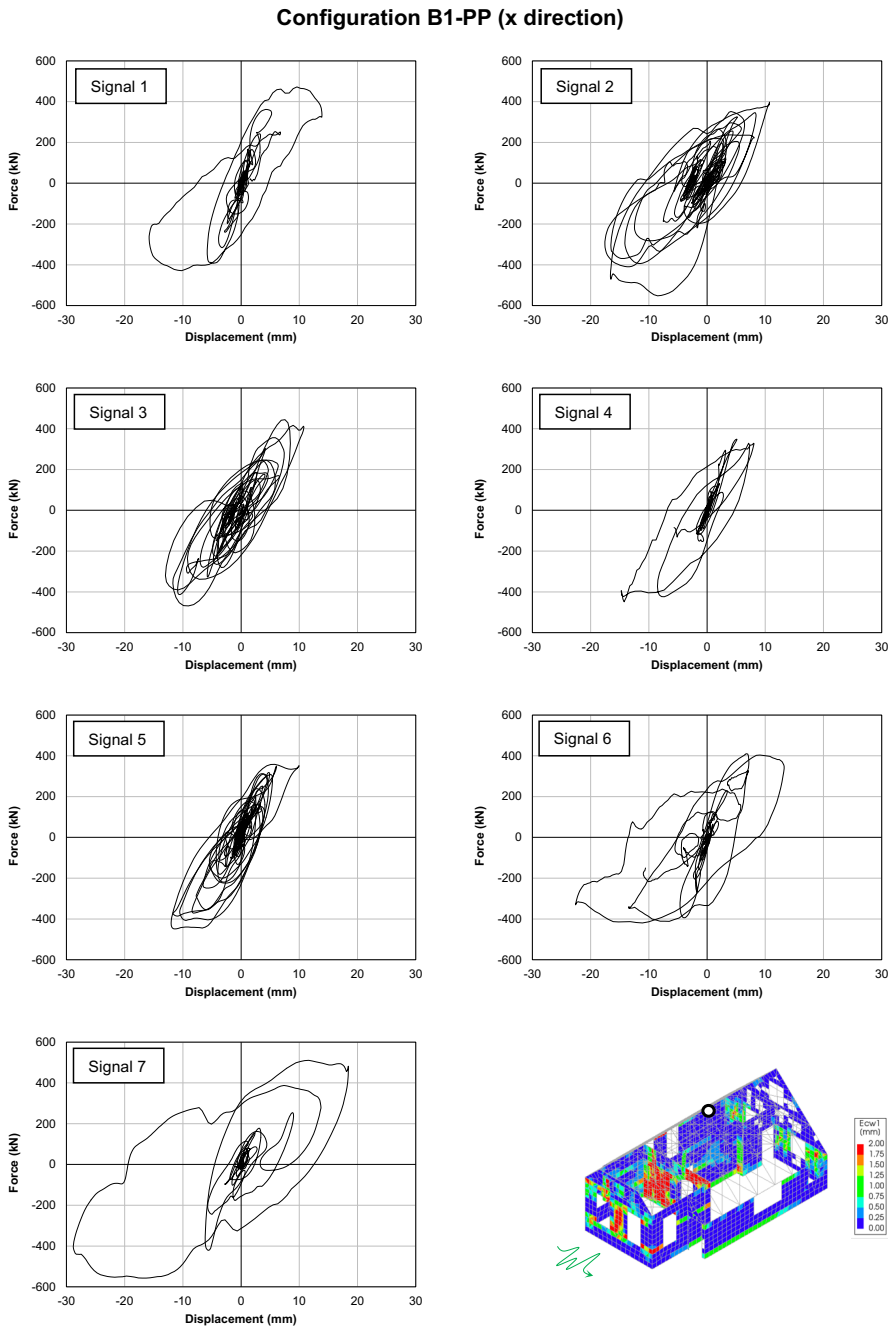


Figure H.5: Complete base shear-top floor displacement curves for the seven applied accelerograms; analyzed configuration, control node, and earthquake direction are highlighted.

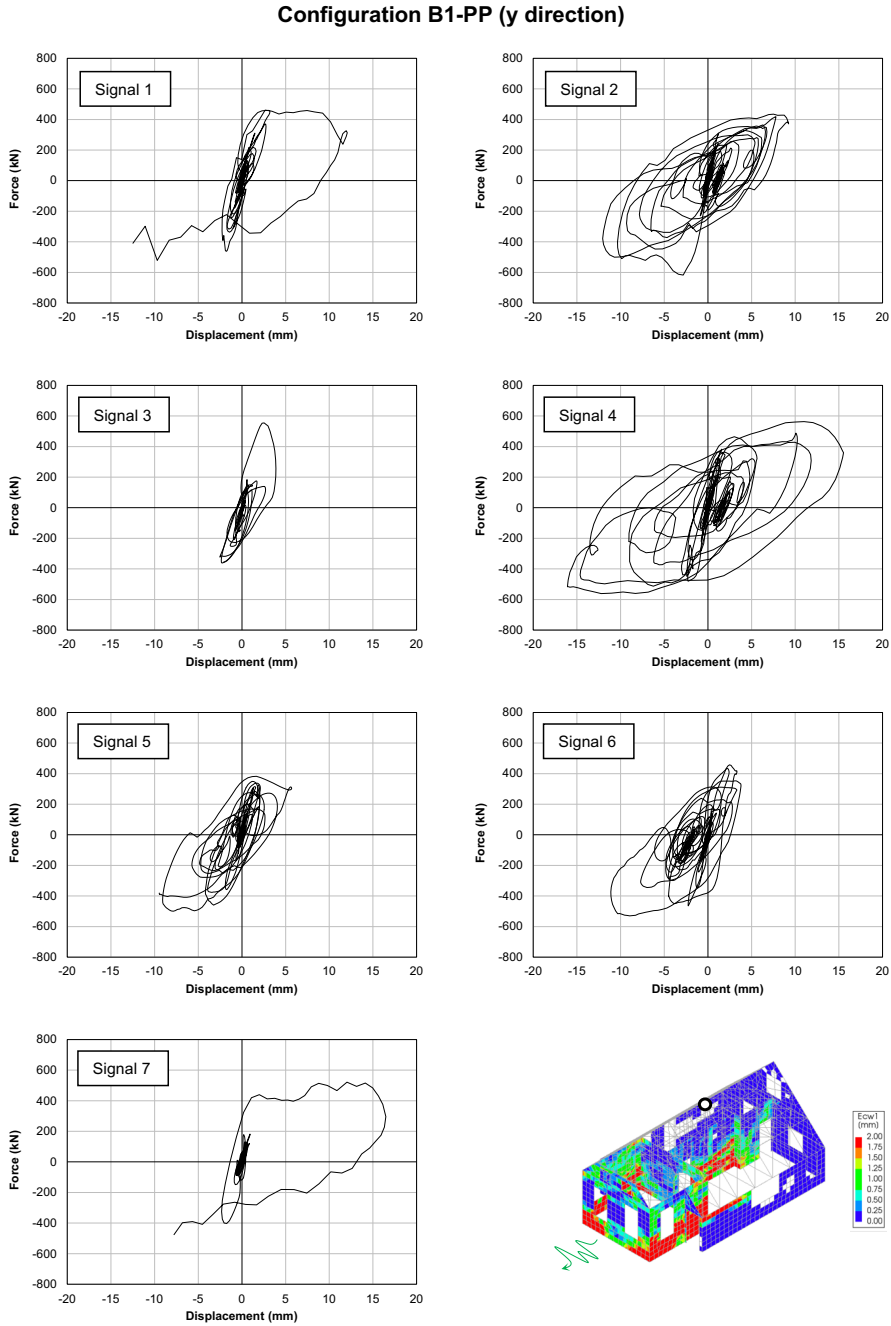


Figure H.6: Complete base shear-top floor displacement curves for the seven applied accelerograms; analyzed configuration, control node, and earthquake direction are highlighted.

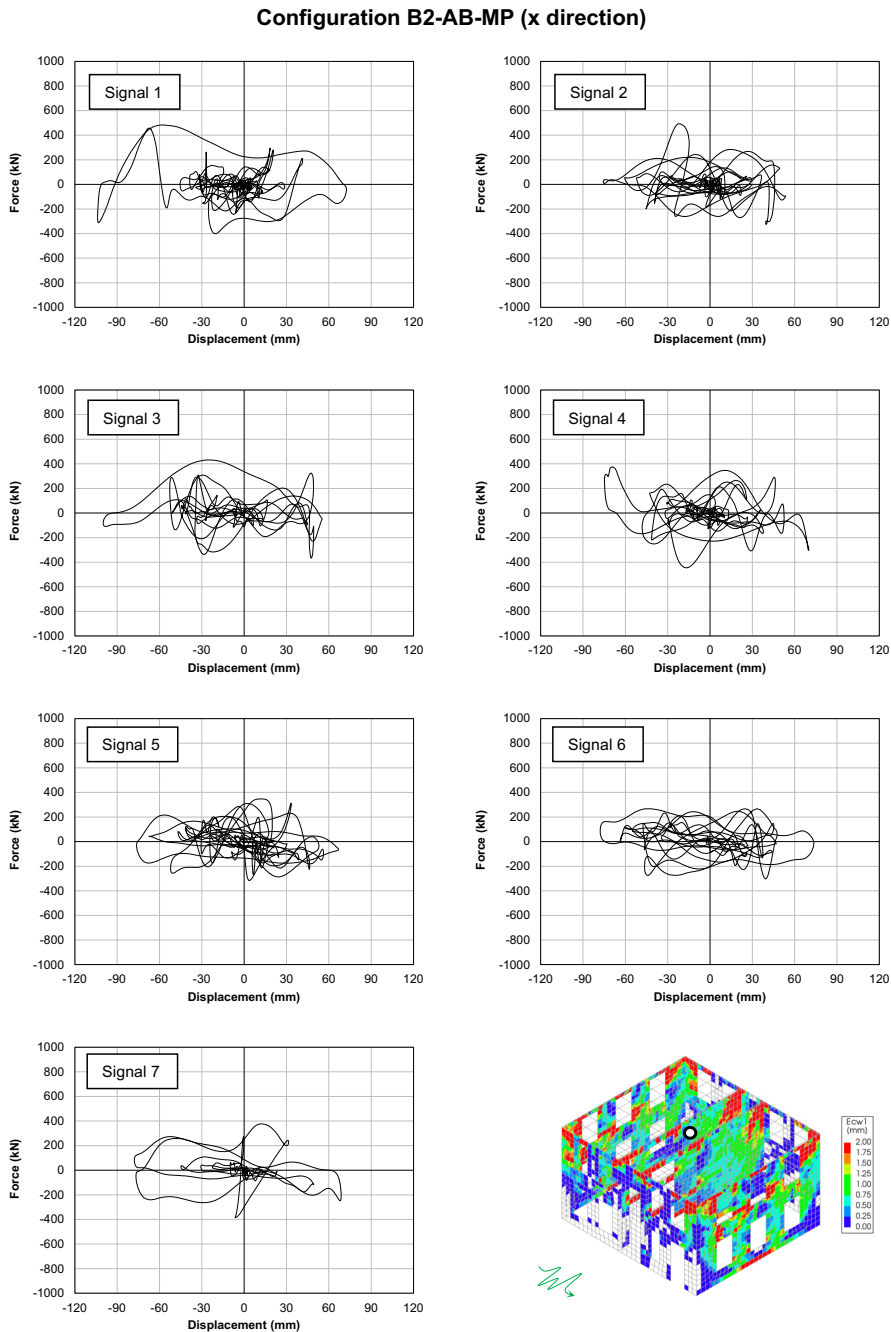


Figure H.7: Complete base shear-top floor displacement curves for the seven applied accelerograms; analyzed configuration, control node, and earthquake direction are highlighted.

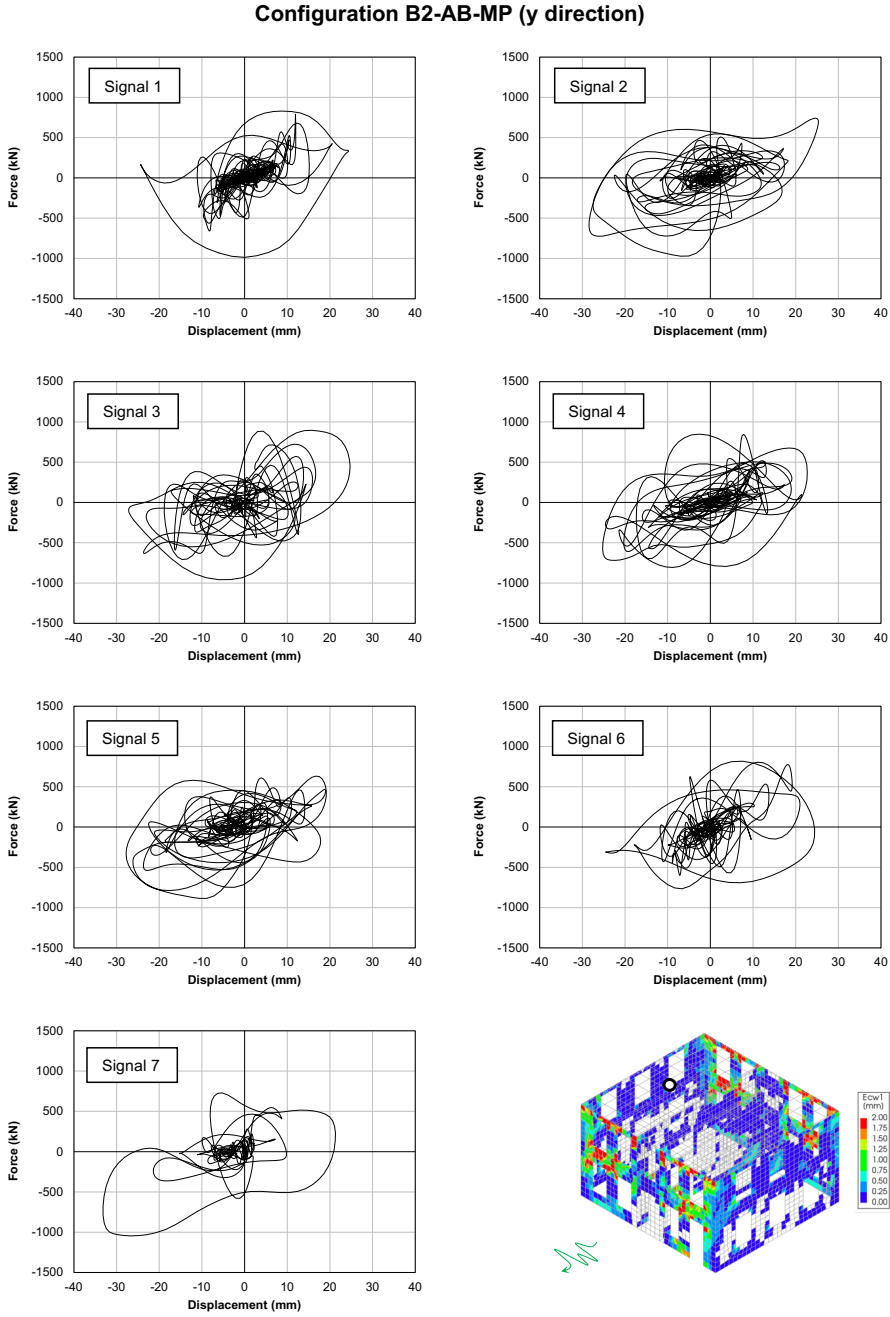


Figure H.8: Complete base shear-top floor displacement curves for the seven applied accelerograms; analyzed configuration, control node, and earthquake direction are highlighted.

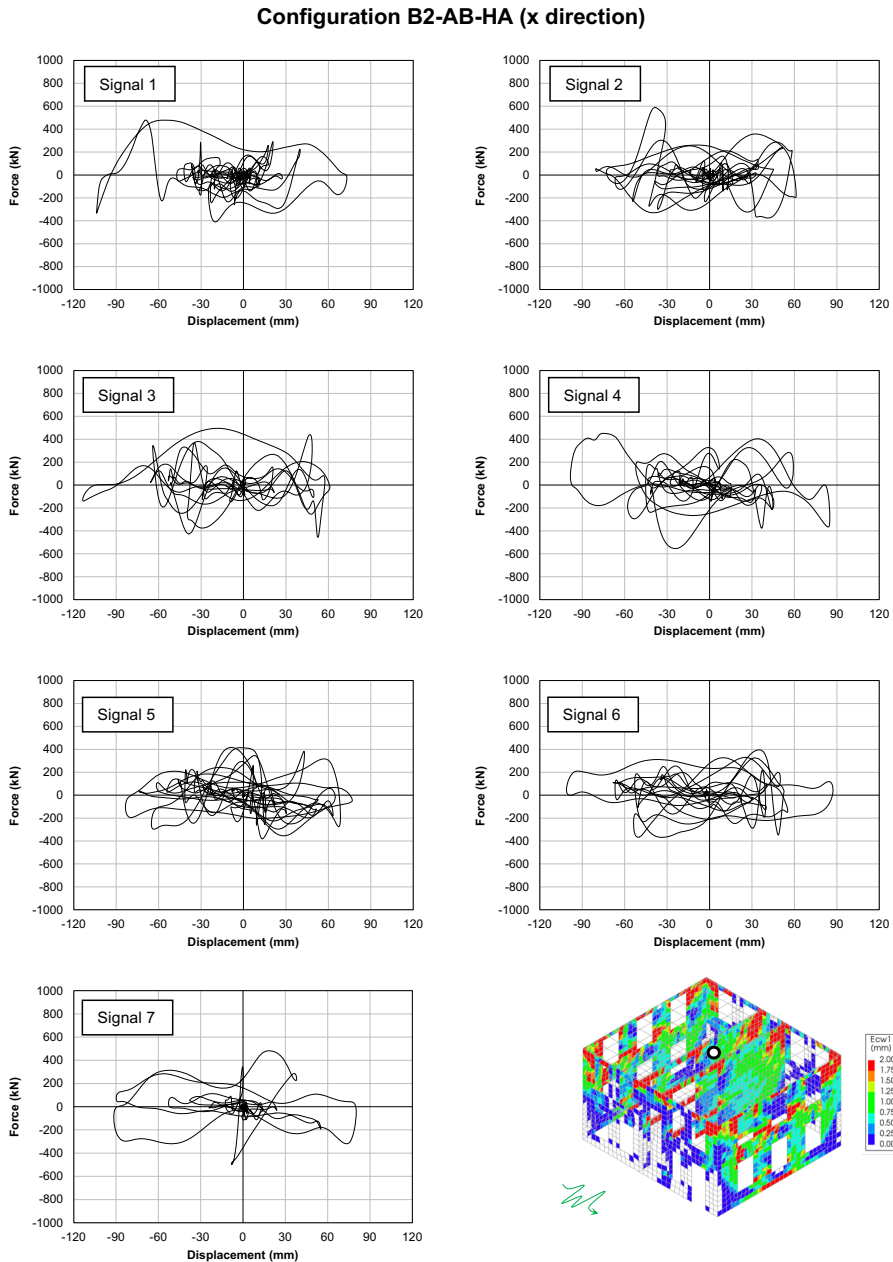


Figure H.9: Complete base shear-top floor displacement curves for the seven applied accelerograms; analyzed configuration, control node, and earthquake direction are highlighted.

Configuration B2-AB-HA (y direction)

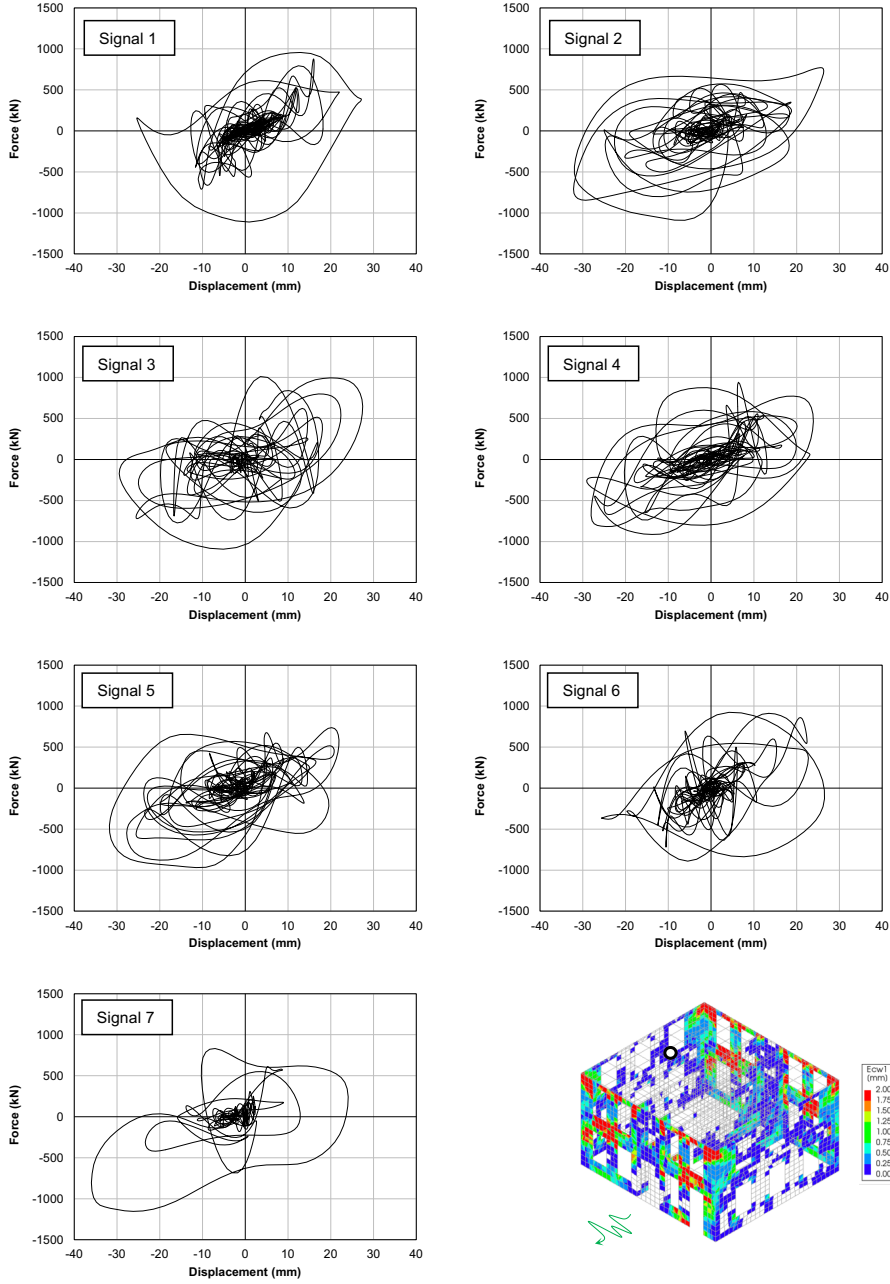


Figure H.10: Complete base shear-top floor displacement curves for the seven applied accelerograms; analyzed configuration, control node, and earthquake direction are highlighted.

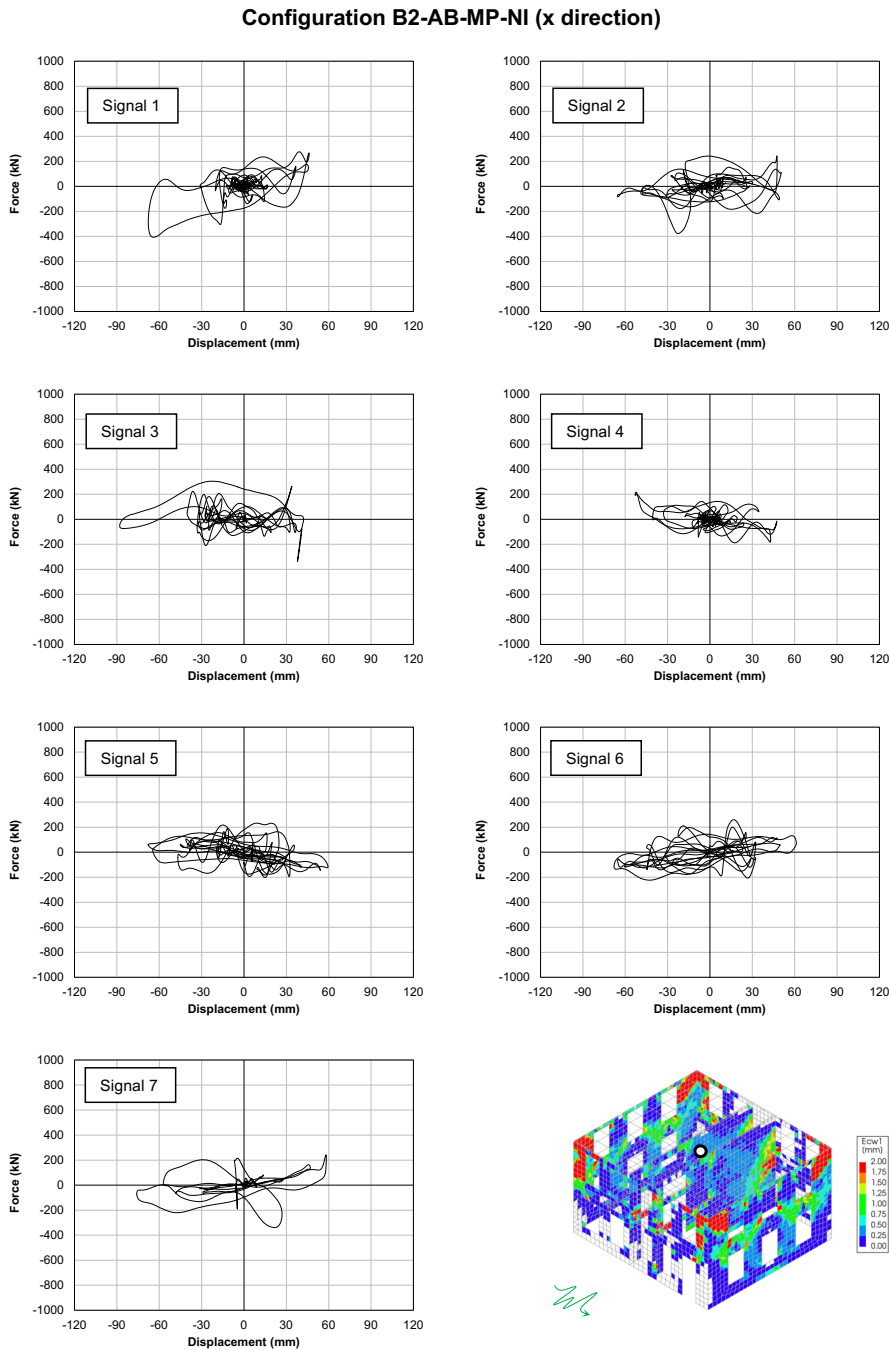


Figure H.11: Complete base shear-top floor displacement curves for the seven applied accelerograms; analyzed configuration, control node, and earthquake direction are highlighted.

Configuration B2-AB-MP-NI (y direction)

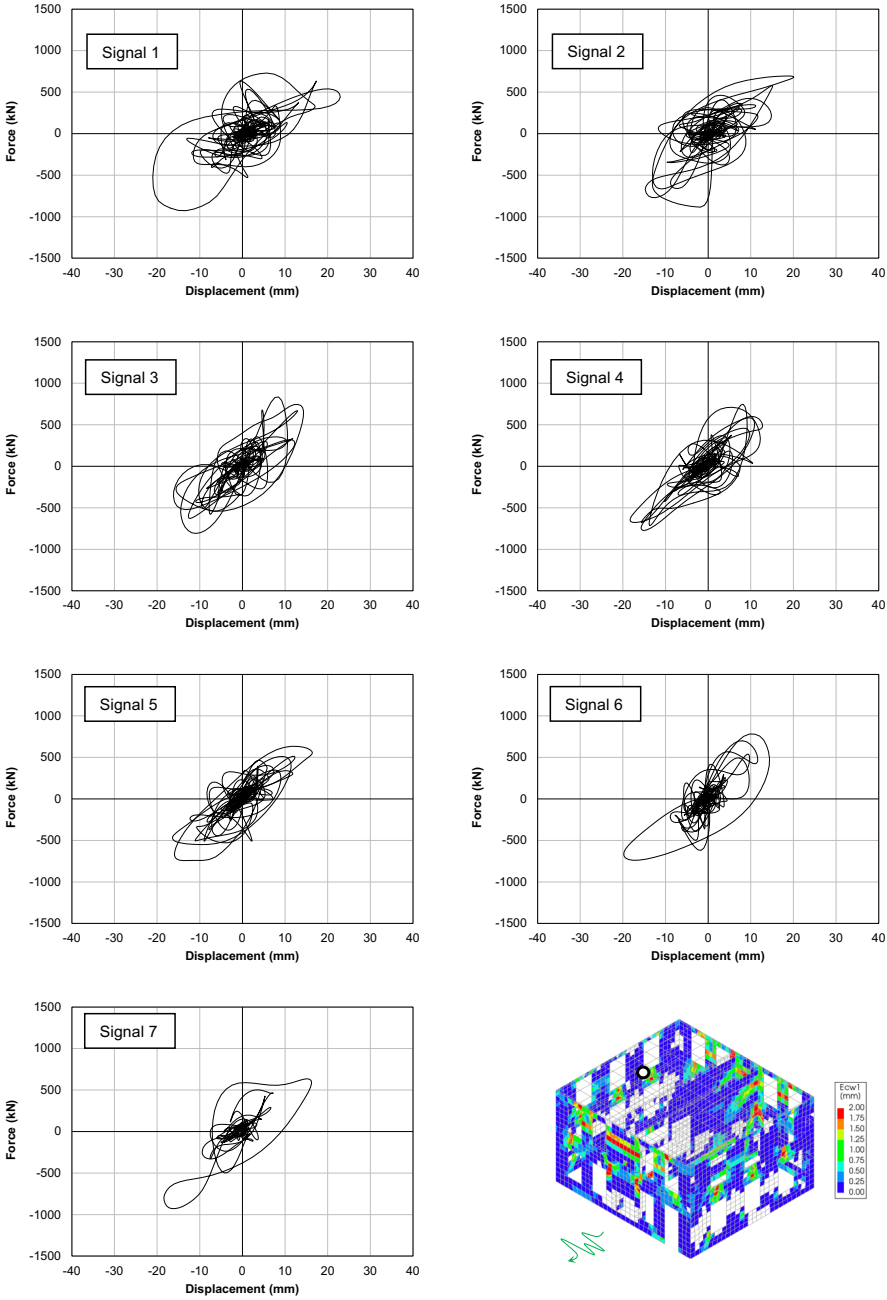


Figure H.12: Complete base shear-top floor displacement curves for the seven applied accelerograms; analyzed configuration, control node, and earthquake direction are highlighted.

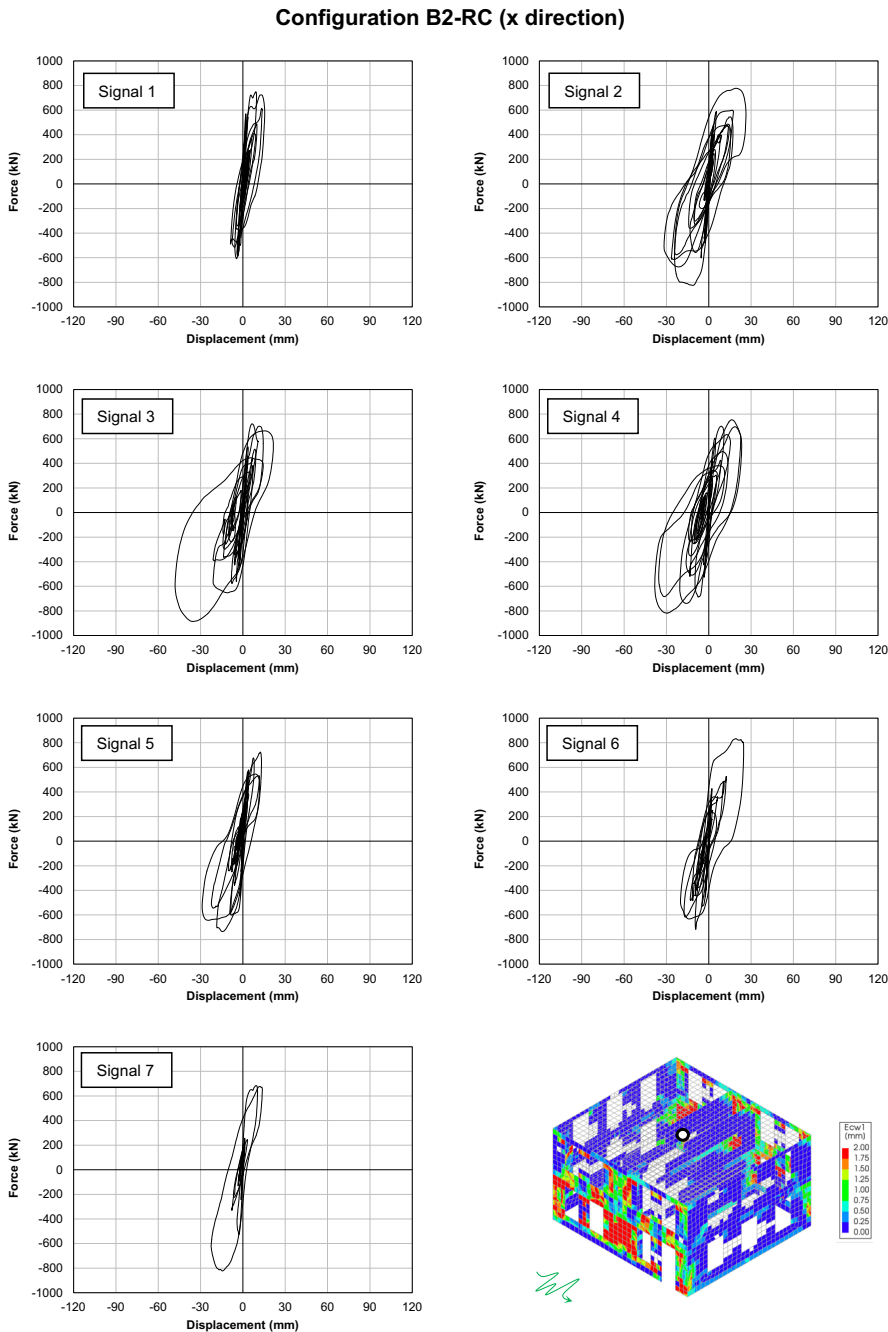


Figure H.13: Complete base shear-top floor displacement curves for the seven applied accelerograms; analyzed configuration, control node, and earthquake direction are highlighted.

Configuration B2-RC (y direction)

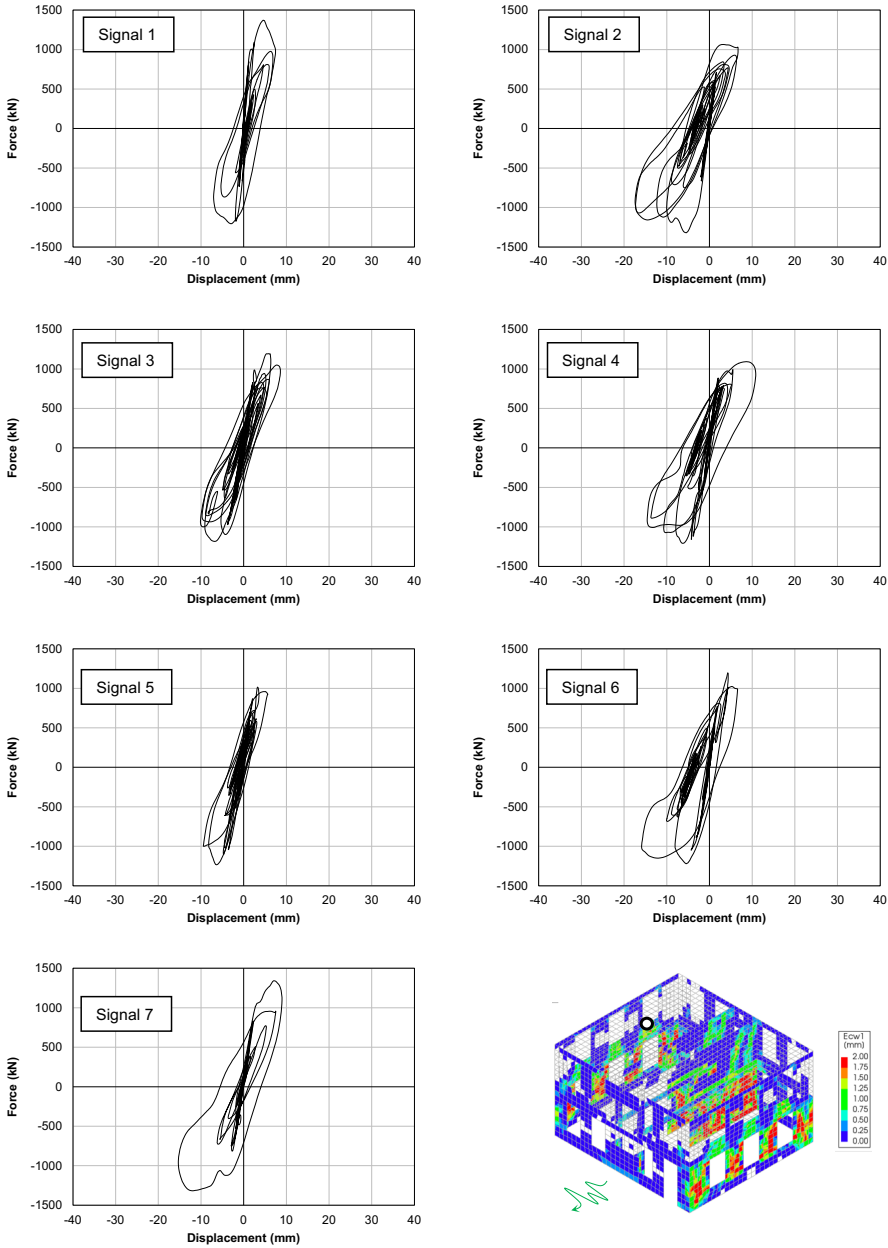


Figure H.14: Complete base shear-top floor displacement curves for the seven applied accelerograms; analyzed configuration, control node, and earthquake direction are highlighted.

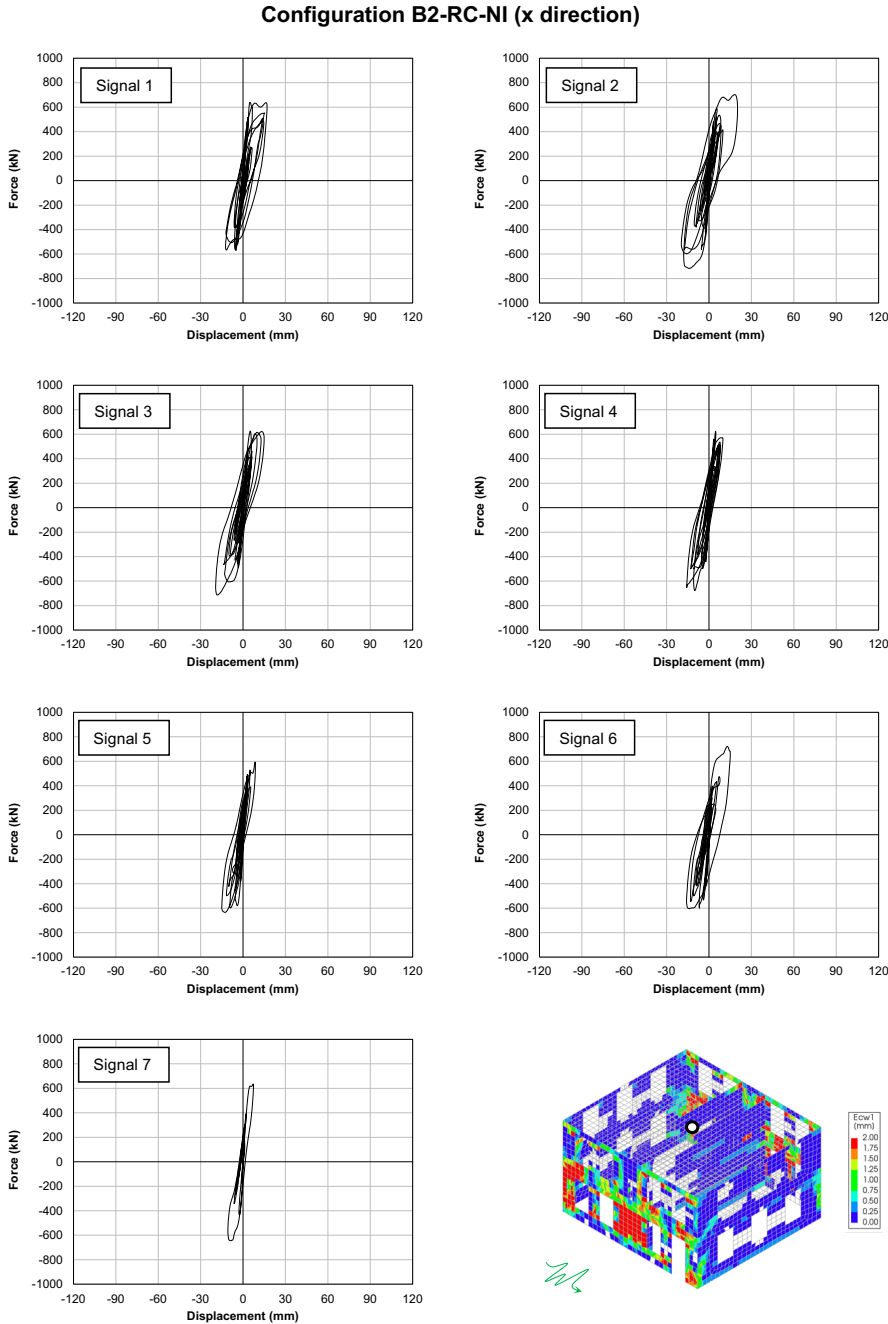


Figure H.15: Complete base shear-top floor displacement curves for the seven applied accelerograms; analyzed configuration, control node, and earthquake direction are highlighted.

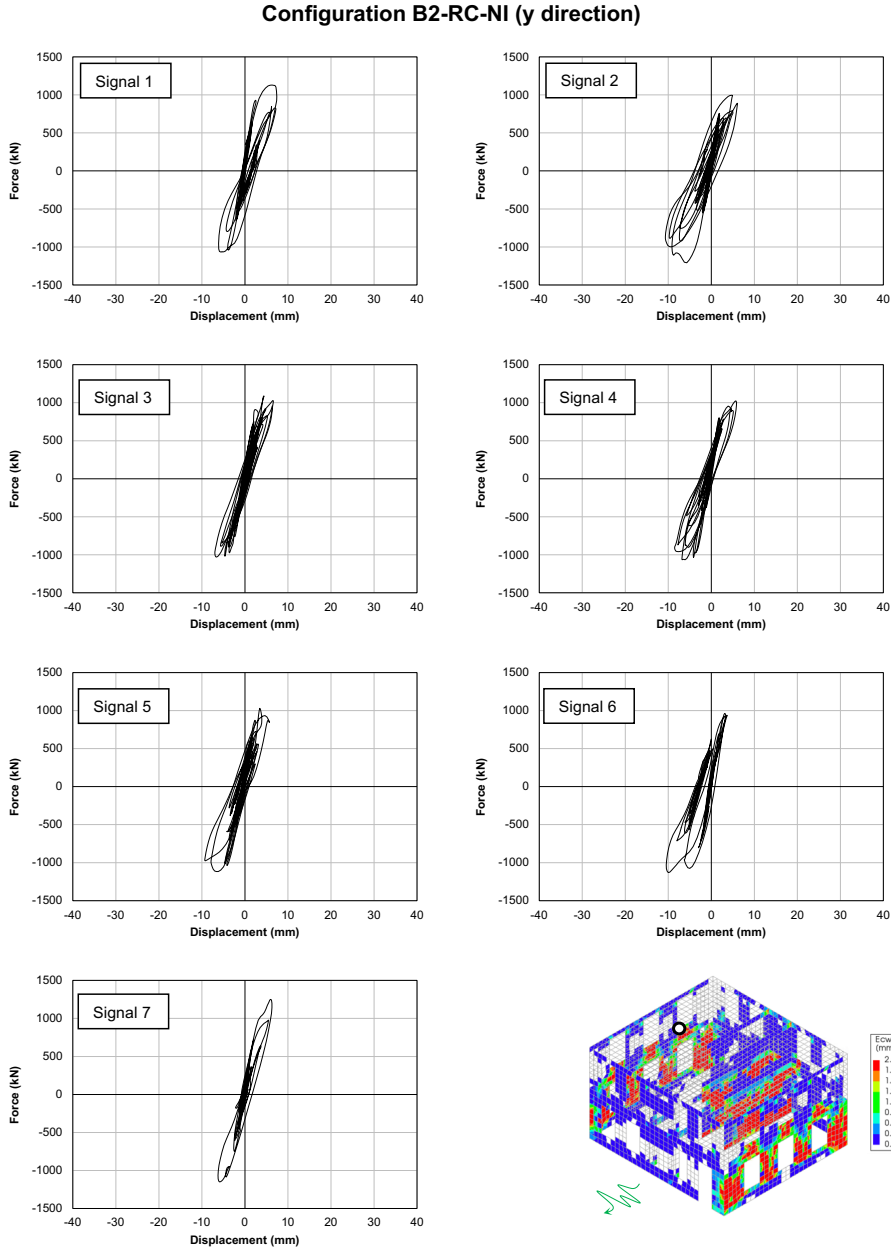


Figure H.16: Complete base shear-top floor displacement curves for the seven applied accelerograms; analyzed configuration, control node, and earthquake direction are highlighted.

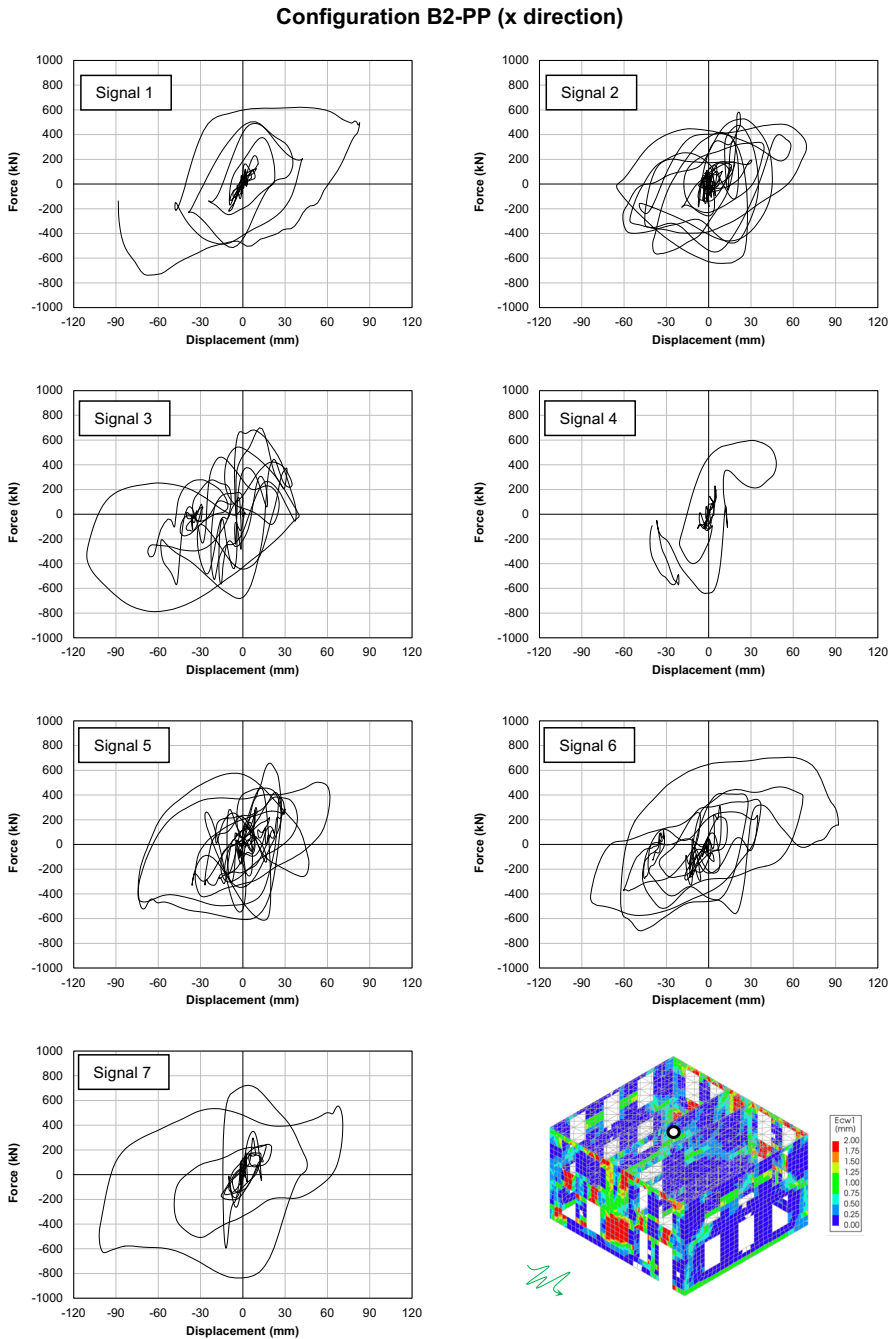


Figure H.17: Complete base shear-top floor displacement curves for the seven applied accelerograms; analyzed configuration, control node, and earthquake direction are highlighted.

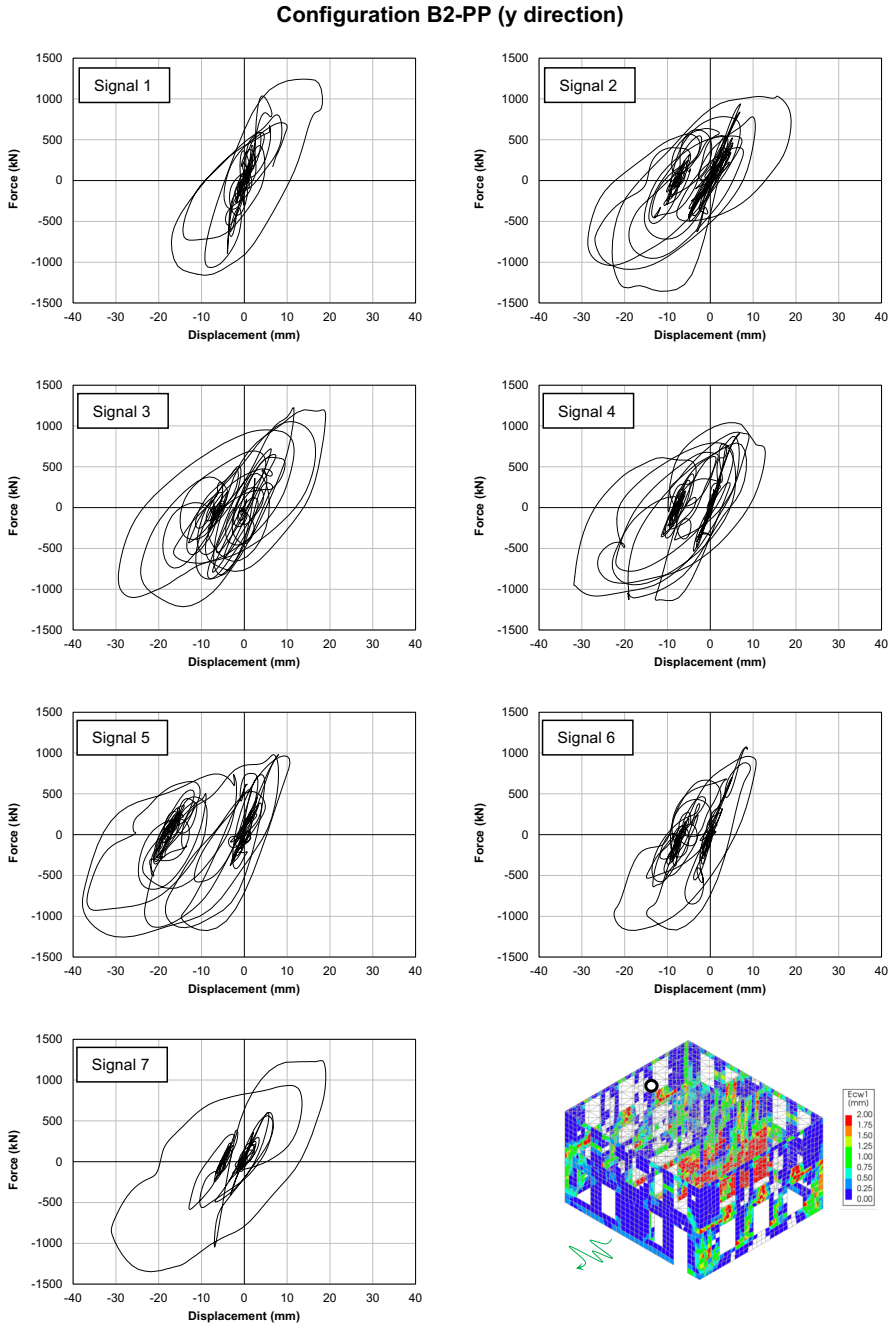


Figure H.18: Complete base shear-top floor displacement curves for the seven applied accelerograms; analyzed configuration, control node, and earthquake direction are highlighted.

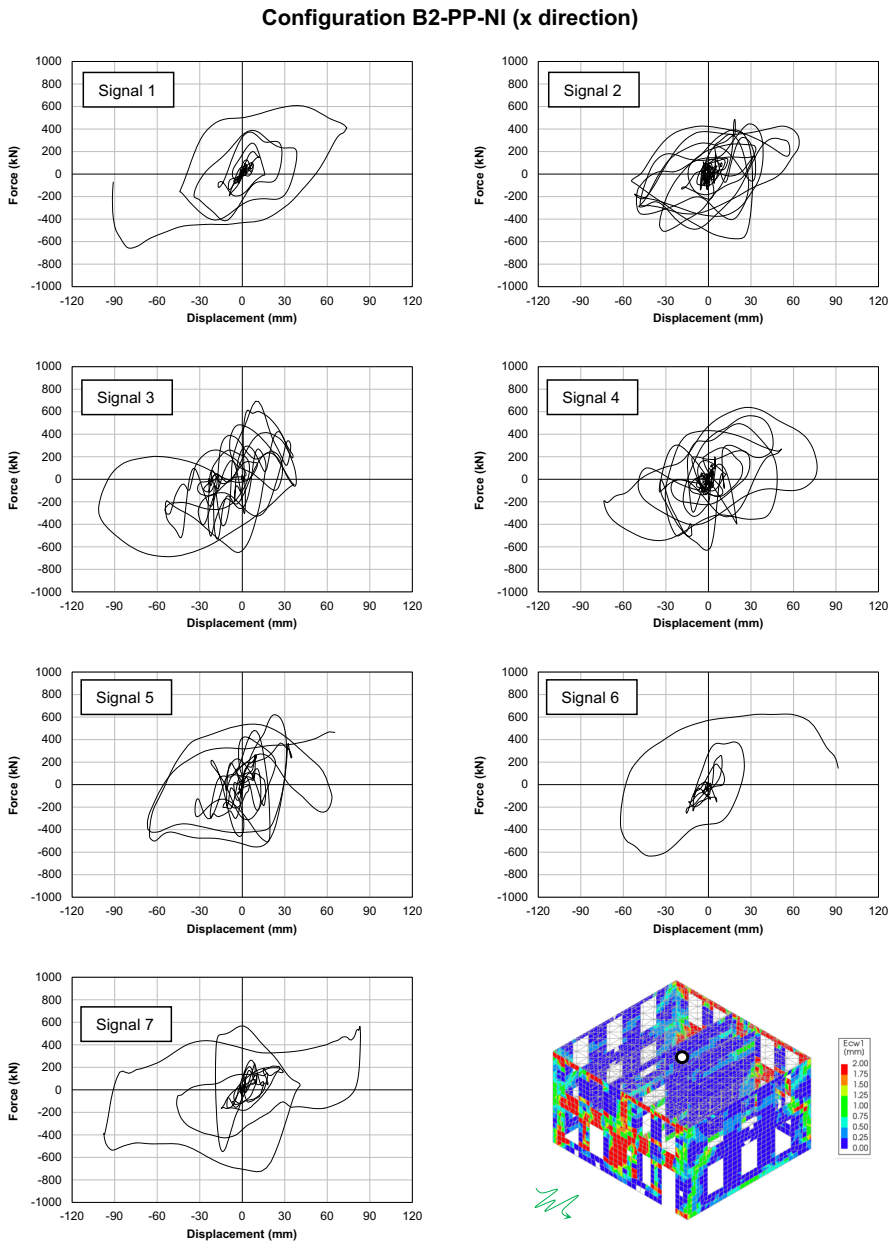


Figure H.19: Complete base shear-top floor displacement curves for the seven applied accelerograms; analyzed configuration, control node, and earthquake direction are highlighted.

Configuration B2-PP-NI (y direction)

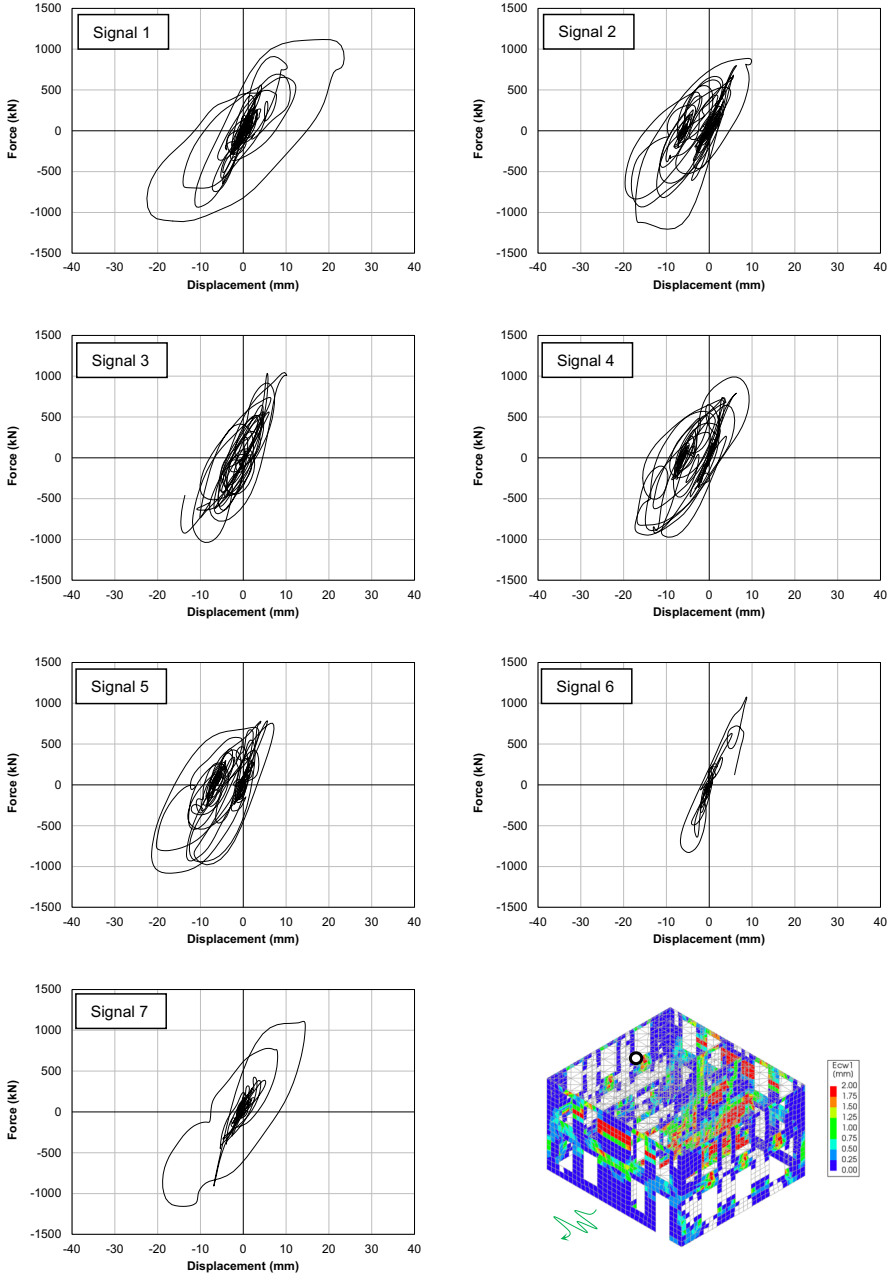


Figure H.20: Complete base shear-top floor displacement curves for the seven applied accelerograms; analyzed configuration, control node, and earthquake direction are highlighted.

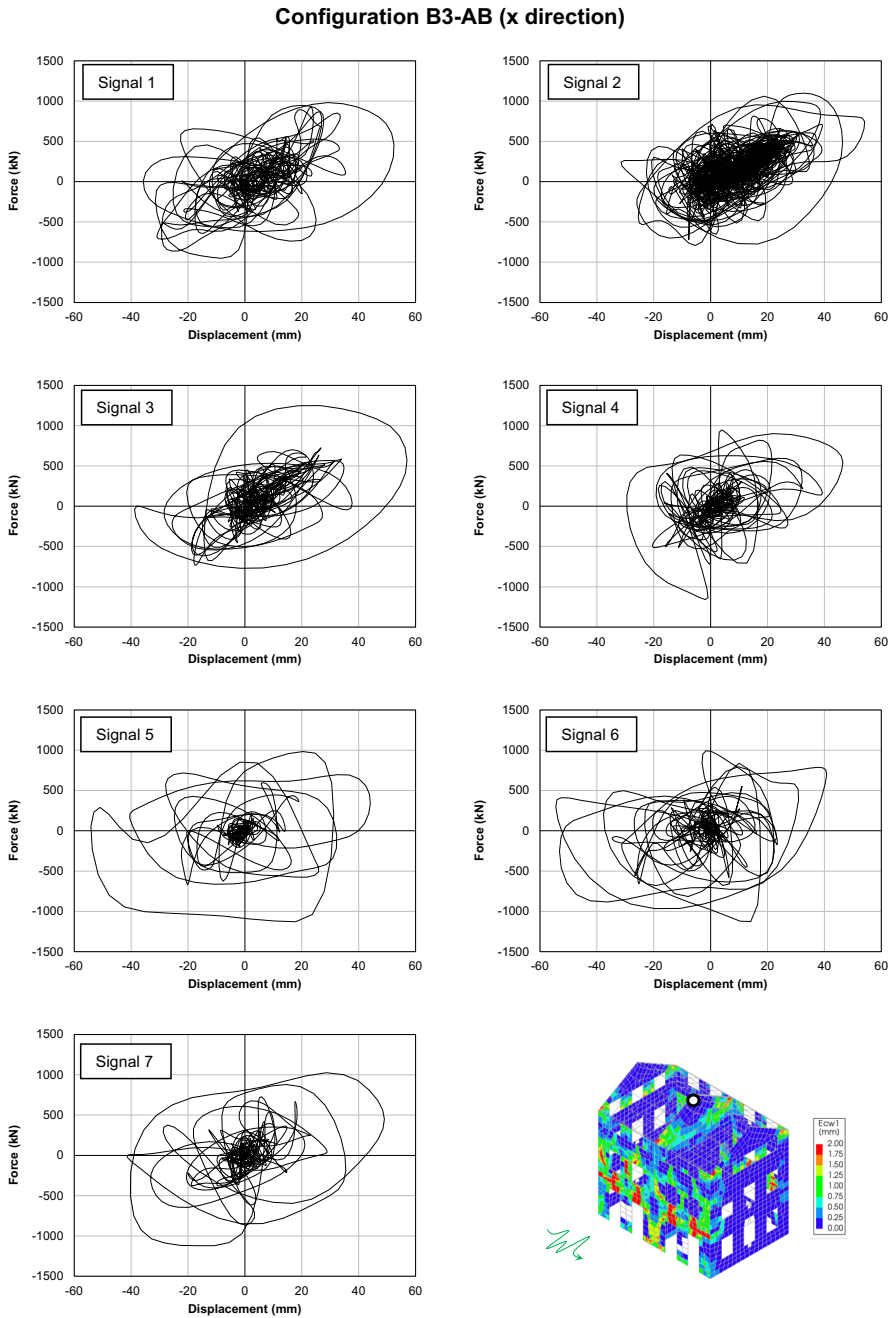


Figure H.21: Complete base shear-top floor displacement curves for the seven applied accelerograms; analyzed configuration, control node, and earthquake direction are highlighted.

Configuration B3-AB (y direction)

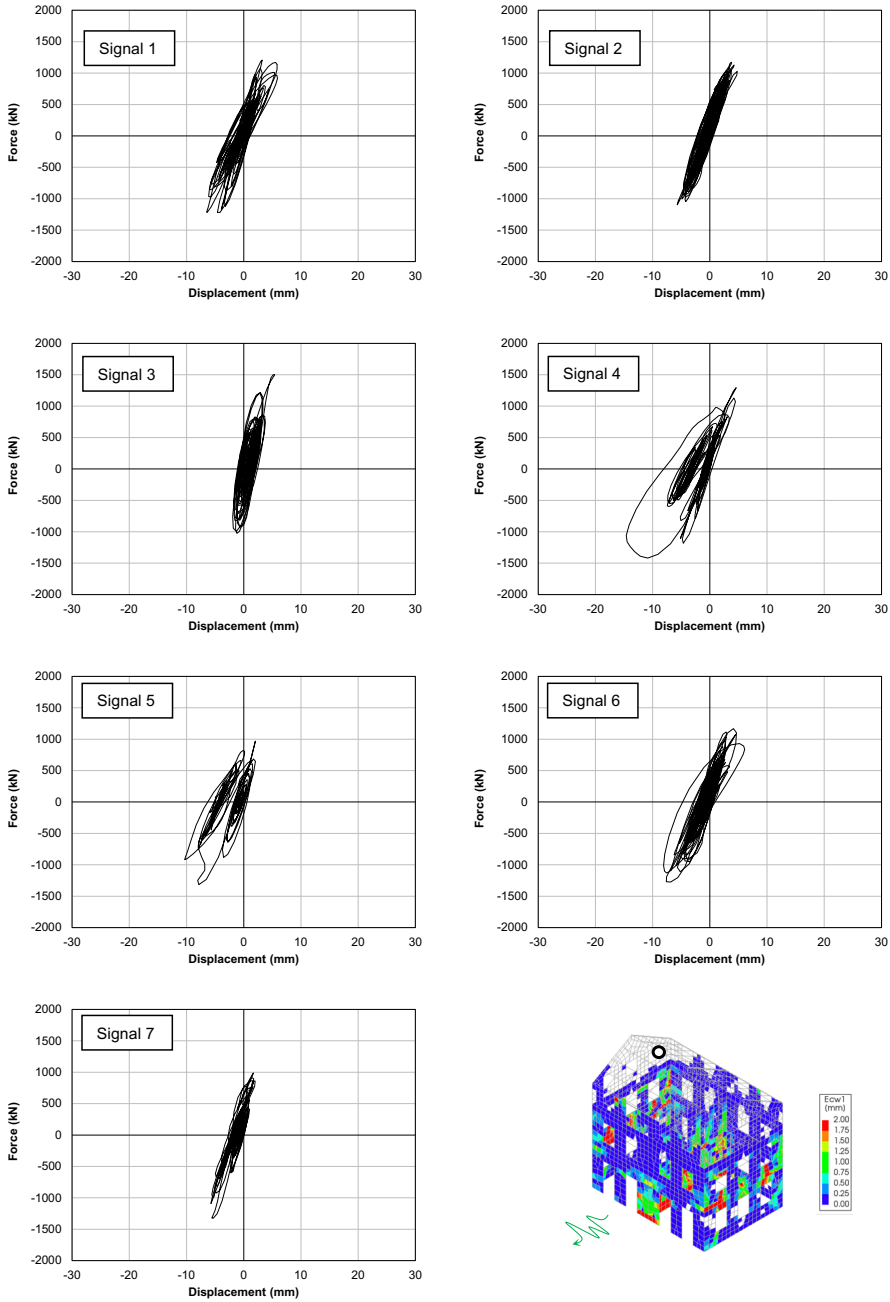


Figure H.22: Complete base shear-top floor displacement curves for the seven applied accelerograms; analyzed configuration, control node, and earthquake direction are highlighted.

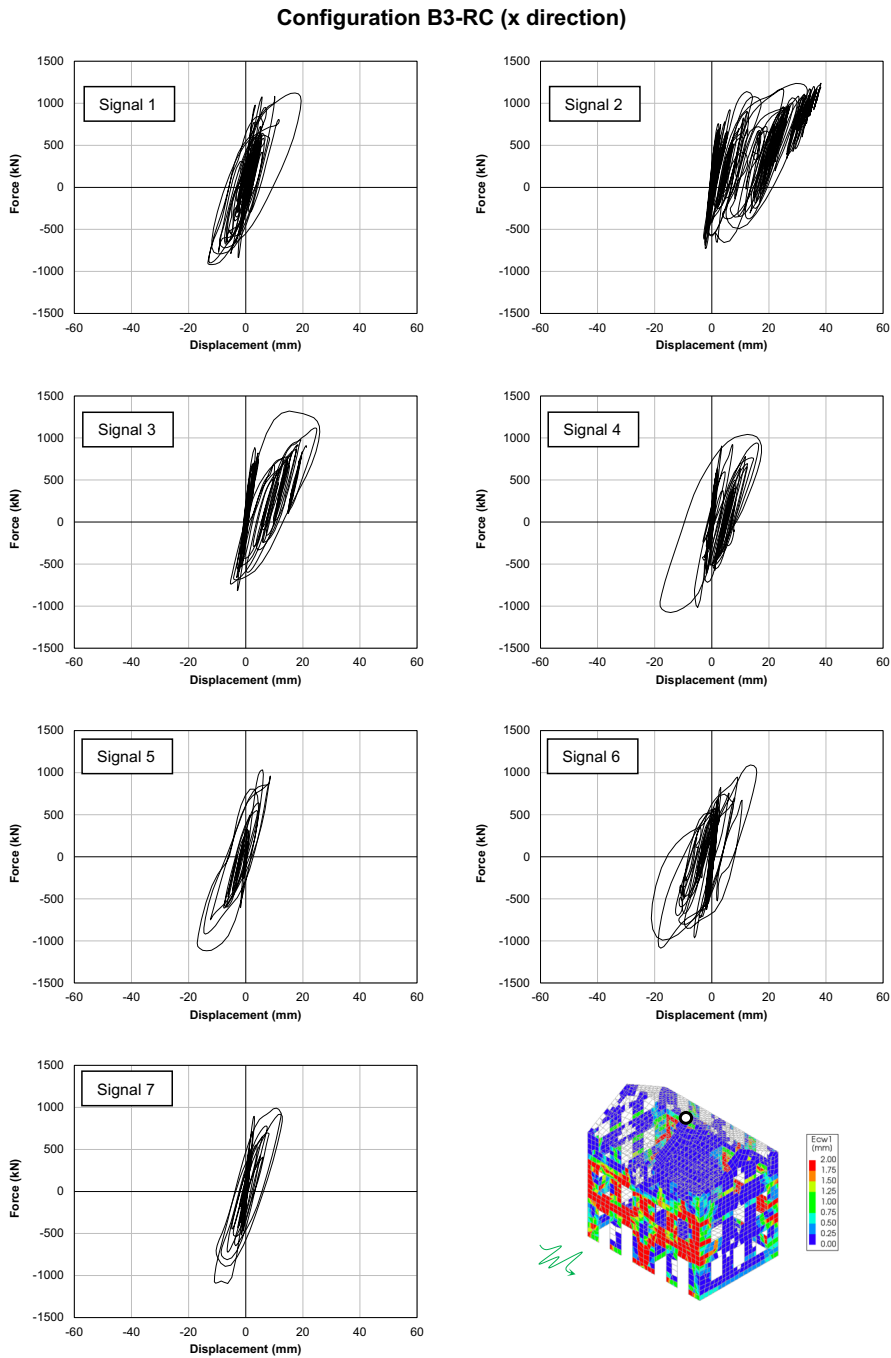


Figure H.23: Complete base shear-top floor displacement curves for the seven applied accelerograms; analyzed configuration, control node, and earthquake direction are highlighted.

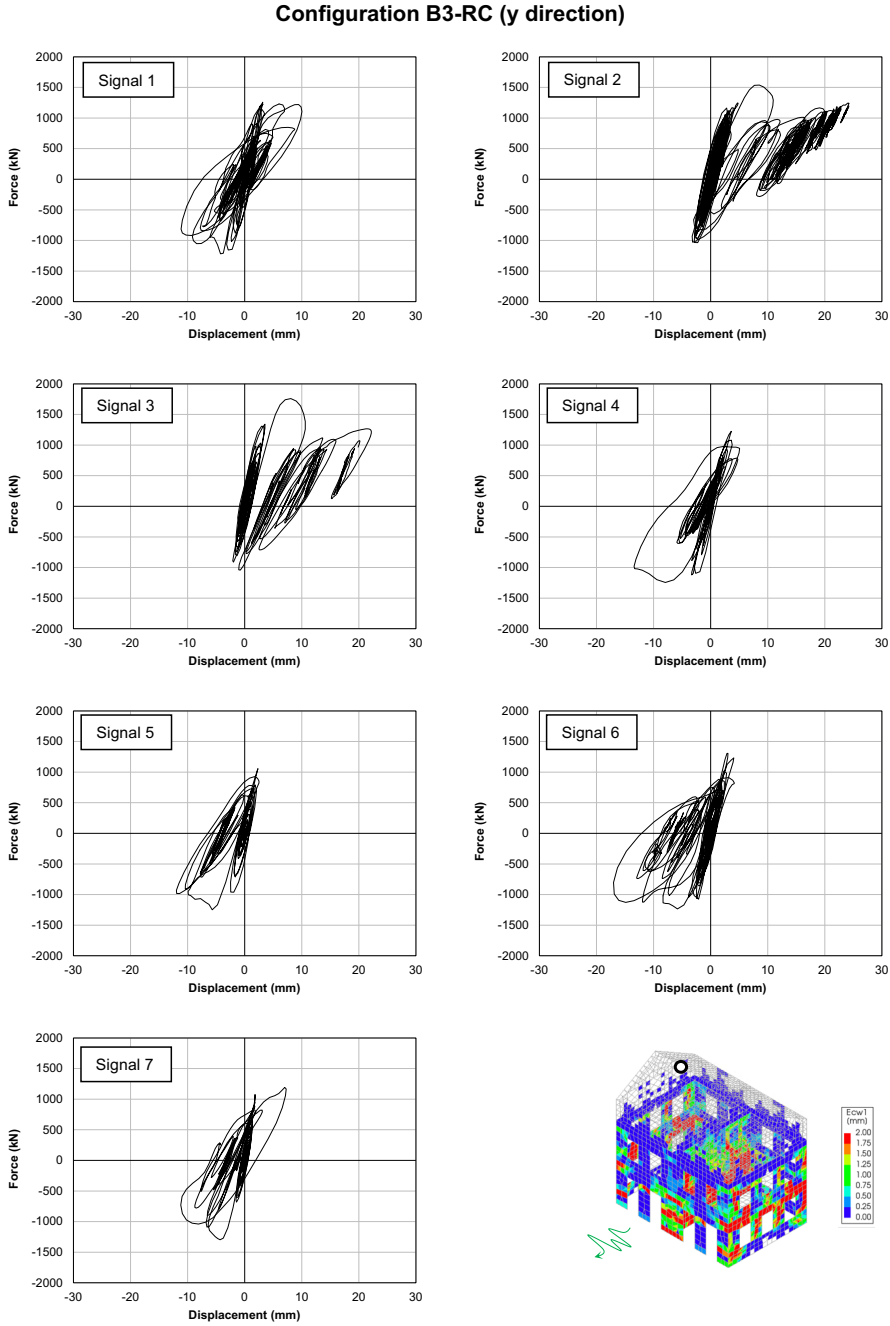


Figure H.24: Complete base shear-top floor displacement curves for the seven applied accelerograms; analyzed configuration, control node, and earthquake direction are highlighted.

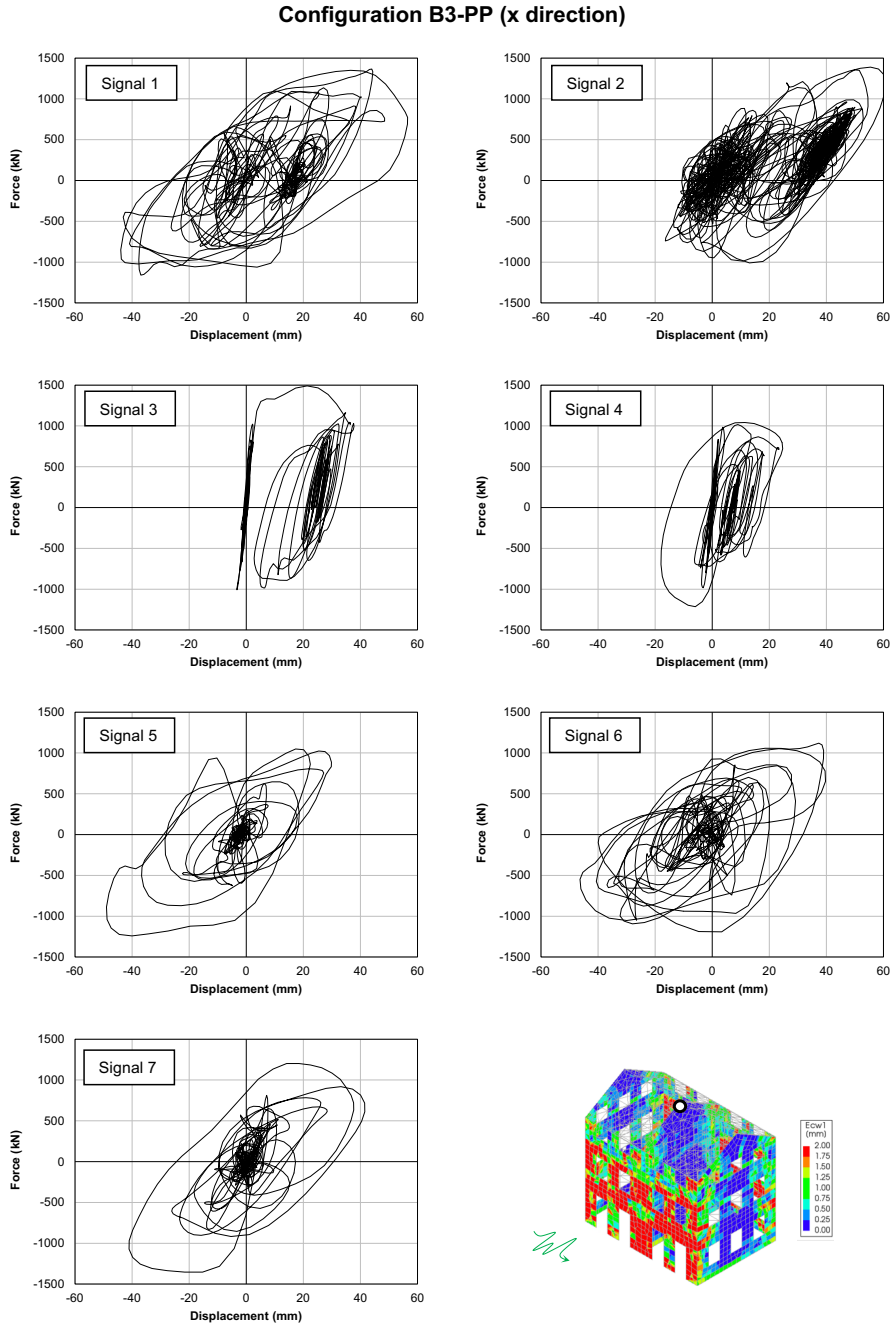


Figure H.25: Complete base shear-top floor displacement curves for the seven applied accelerograms; analyzed configuration, control node, and earthquake direction are highlighted.

Configuration B3-PP (y direction)

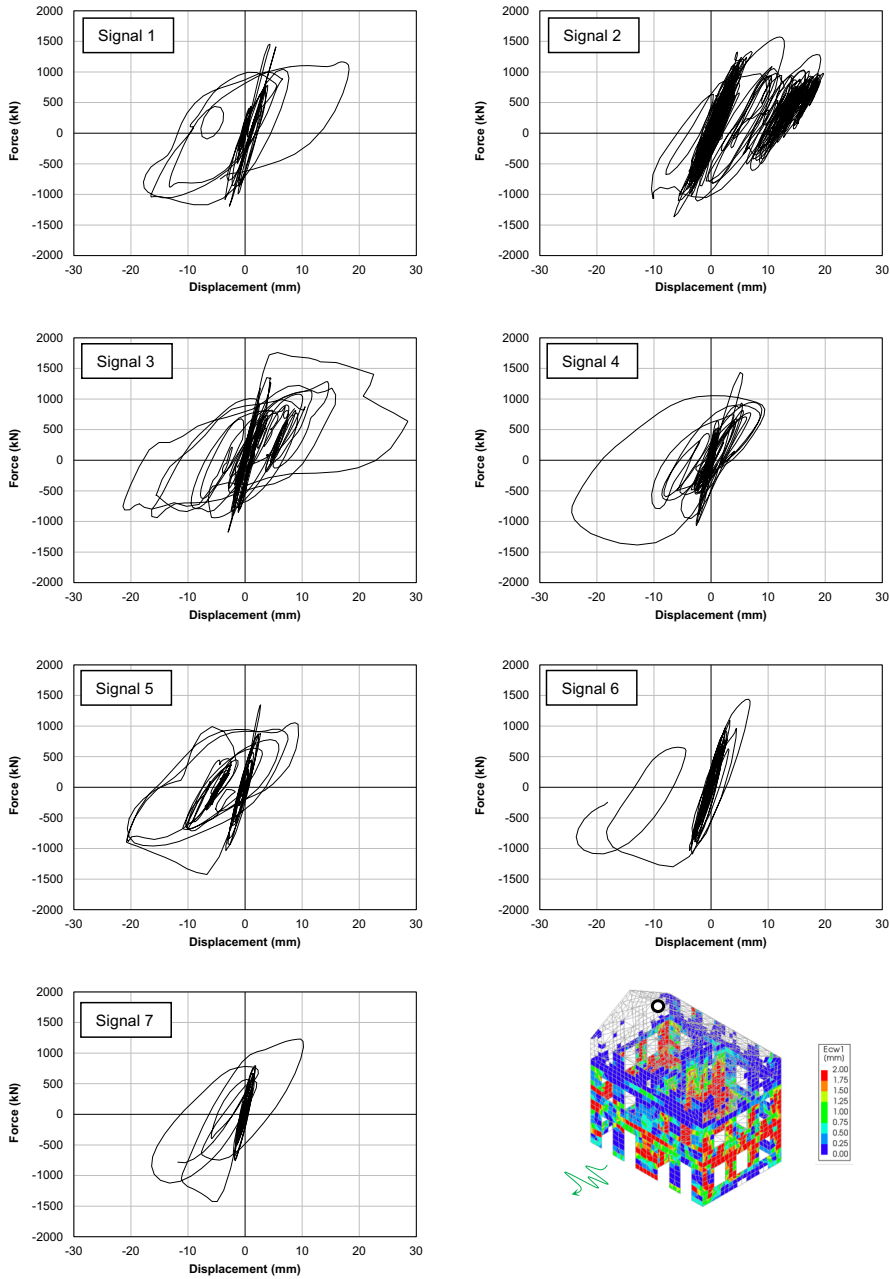


Figure H.26: Complete base shear-top floor displacement curves for the seven applied accelerograms; analyzed configuration, control node, and earthquake direction are highlighted.

List of publications

Journal articles

- **Mirra, M.**, Ravenshorst, G.J.P., de Vries, P.A., Messali, F., Experimental characterisation of as-built and retrofitted timber-masonry connections under monotonic, cyclic and dynamic loading. *Construction and Building Materials*, 2022 (under review).
- **Mirra, M.**, Ravenshorst, G.J.P., Optimizing seismic capacity of existing masonry buildings by retrofitting timber floors: wood-based solutions as dissipative alternative to rigid concrete diaphragms. *Buildings* 11, Special issue on seismic design and performance of timber structures, 2021.
- **Mirra, M.**, Ravenshorst, G.J.P., van de Kuilen, J.W.G., Comparing in-plane equivalent shear stiffness of timber diaphragms retrofitted with light and reversible wood-based techniques. *ASCE Practice Periodical on Structural Design and Construction* 26 (4), American Society of Civil Engineers, 2021.
- **Mirra, M.**, Ravenshorst, G.J.P., de Vries, P.A., van de Kuilen, J.W.G., An analytical model describing the in-plane behaviour of timber diaphragms strengthened with plywood panels. *Engineering Structures* 235, 2021.
- **Mirra, M.**, Ravenshorst, G.J.P., van de Kuilen, J.W.G., Experimental and analytical evaluation of the in-plane behaviour of as-built and strengthened traditional wooden floors. *Engineering Structures* 211, 2020.
- Scotta, R., Trutalli, D., Marchi, L., Pozza, L., **Mirra, M.**, Seismic response of masonry buildings with alternative techniques for in-plane strengthening of timber floors. *Revista Portuguesa de Engenharia de Estruturas*, Ed. LNEC. Série III, no 4, 2017.

Conference papers

- **Mirra, M.**, Ravenshorst, G.J.P., van de Kuilen, J.W.G., Dissipative properties of timber diaphragms strengthened with plywood panels. *World Conference on Timber Engineering*, Santiago, Chile, 2021.

- **Mirra, M.**, Ravenshorst, G.J.P., van de Kuilen, J.W.G., Monotonic, cyclic and dynamic behaviour of timber-masonry connections. World Conference on Timber Engineering, Santiago, Chile, 2021.
- Ravenshorst, G.J.P., van Dalen, J.H., **Mirra, M.**, Steiger, R., van de Kuilen, J.W.G., Connection of timber foundation piles to concrete extension piles. Paper number 54-07-11. Proceedings of the 2021 International Network on Timber Engineering Research (INTER) Meeting, Karlsruhe, 2021.
- **Mirra, M.**, Sousamli, M., Longo, M., Ravenshorst, G.J.P., Analytical and numerical modelling of the in-plane response of timber diaphragms retrofitted with plywood panels. 8th ECCOMAS Thematic Conference on Computational Methods in Structural Dynamics and Earthquake Engineering. Athens, Greece, 2021.
- Scotta, R., Trutalli, D., Marchi, L., Pozza, L., **Mirra, M.**, Non-linear time history analyses of unreinforced masonry buildings with in-plane stiffened timber floors. 17th ANIDIS Conference, Pistoia, Italy, 2017.

Scientific reports

- **Mirra, M.**, Ravenshorst, G.J.P., Seismic characterisation of timber-masonry connections based on experimental results. Delft University of Technology. Report number CS2B04WP2-4.3, 04-12-2019.
- **Mirra, M.**, Ravenshorst, G.J.P. Monotonic, cyclic and dynamic behaviour of timber-masonry connections. Delft University of Technology. Report number CS2B04WP2-3.3, 03-12-2019.
- **Mirra, M.**, Ravenshorst, G.J.P., Testing protocol for replicated timber-masonry connections. Delft University of Technology. Report number CS2B04WP2-2, version 2, 26-03-2019.
- **Mirra, M.**, Ravenshorst, G.J.P., Memo on feedbacks given to consultants BORG and VIIA with regard to the testing campaign on timber-masonry connections. Delft University of Technology. Report number CS2B04WP2-M1, version 1, 15-03-2019.
- Ravenshorst G.J.P., **Mirra, M.**, Plan of approach for testing replicated joist-masonry connections. Delft University of Technology. Report number CS2B04WP2-1, version 2, 25-01-2019.
- Ravenshorst, G.J.P., **Mirra, M.**, Test report on cyclic behaviour of replicated timber joist-masonry wall connections. Delft University of Technology. Report number C31B67WP4-11, version 2, 16-04-2018.
- Ravenshorst, G.J.P., **Mirra, M.**, Testing protocol for replicated timber joist-masonry wall connections. Delft University of Technology. Report C31B67WP4-10, version 1, 24-01-2018.

- Ravenshorst, G.J.P., **Mirra, M.**, Test report on cyclic behaviour of plank-joint connections of samples extracted from existing buildings. Report number C31B67WP4-12, version 1, 30-12-2017.
- Ravenshorst, G.J.P., **Mirra, M.**, Test report on material properties of timber and fasteners extracted from existing buildings. Delft University of Technology. Report number C31B67WP4-9, version 1, 30-12-2017.
- Ravenshorst, G.J.P., **Mirra, M.**, Test report on cyclic behaviour of replicated timber diaphragms representing a detached house. Delft University of Technology. Report number C31B67WP4-7, version 1, 30-12-2017.

Curriculum vitae et studiorum

Michele Mirra graduated cum laude in Civil Structural Engineering at the University of Padua (Italy). He is currently a postdoctoral researcher within the Biobased Structures and Materials research group, at the Faculty of Civil Engineering and Geosciences of Delft University of Technology (The Netherlands). His research field is linked to the seismic assessment and retrofitting of existing masonry buildings, with specific focus on their traditional timber diaphragms and wall-to-floor connections. His research activity aims at achieving an optimization of the seismic capacity of the buildings by means of efficiently designed, effective and dissipative retrofitting interventions on the diaphragms. At present, he is first author or co-author of six journal articles and five conference papers related to the research subject of his PhD. He has been supervisor of one bachelor thesis and nine master theses. He has also been active as Management Committee Substitute in COST Action FP1404 - Fire Safe Use of Bio-Based Building Products, and contributed to the update of the Dutch seismic guidelines NPR 9998 with specific regard to seismic assessment and retrofitting of timber diaphragms.



24/04/1993	Born in Abano Terme, Veneto, Italy
2007-2012	Scientific high school diploma. Liceo Galileo Galilei, Selvazzano, Veneto, Italy.
2012-2015	Bachelor of Science (B.Sc.) in Civil Engineering. University of Padua, Veneto, Italy.
2015-2017	Master of Science (M.Sc.) in Civil Structural Engineering. University of Padua, Veneto, Italy.
2017-2021	PhD candidate within the Biobased Structures and Materials research group. Delft University of Technology, The Netherlands.
2021-	Postdoctoral Researcher within the Biobased Structures and Materials research group. Delft University of Technology, The Netherlands.

Acknowledgements

When pursuing a PhD, independence is surely a key quality that the candidate is expected to possess. Yet, every goal achieved in our life is also made possible by the endless support of people around us. In this section, I would like to briefly express my gratitude to whom made this long journey, or even better, this *intellectual adventure*, possible and enjoyable.

Firstly, I would like to acknowledge NAM (*Nederlandse Aardolie Maatschappij*) for providing the necessary funding to conduct my whole, extensive experimental research. A special, warm message of gratitude goes to my first promotor, Prof. Dr. Ir. JAN-WILLEM VAN DE KUILEN, who gave me the possibility to start my research project at TU Delft right two days after graduating. Thanks for sharing your valuable (I would say multi-tasking!) knowledge on timber; for your positive and constructive criticism; for the possibility of attending valuable conferences, despite the Covid-19 pandemic has made all events virtual and sometimes slightly less lively. I am also very grateful to my second promotor, Prof. Dr. ANDREI METRIKINE, who triggered me with his insightful suggestions throughout the whole PhD: thanks for having always encouraged me, especially during the initial difficult period when we started working from home, and for your experience, from which I could enrich the theoretical background of my research study.

I would subsequently like to graciously acknowledge my daily supervisor, Dr. Ir. GEERT RAVENSHORST. As human beings, we are all different from each other, and for sure also between Geert and me there have been differences in approaching research problems, in how to organize the work, and in scientific background. Yet, sometimes in life these differences can become solid foundations for relationships leading to optimal cooperation and friendship. I personally think this is precisely one of these cases, therefore I am grateful to you, Geert, for having shared with me these four years, for our useful discussions, for our inspiring coffee breaks, and for your always positive, calm, equilibrated attitude.

My gratitude goes also to the committee members Prof. Dr. Ir. JAN ROTS, Prof. Ir. SIMON WIJTE, Prof. Ing. ARIO CECCOTTI, Dr. Ing. ROBERTO SCOTTA, Prof. Dr. Ir. MAX HENDRIKS, for the consideration given to this dissertation and the time taken to examine it. I really valued your feedback, and I am honored that you were present in the final steps of achieving this milestone.

Thanks to my dear former office mate, PETER DE VRIES, for your friendly attitude and for all the help in managing lab activities and design of test setups. I am also grateful to my colleagues from the *lab corridor*: WOLFGANG GARD, for your constant support and interest in my project, and for sharing with me your experience and positive,

dreamy attitude towards research; ROLAND ABSPOEL, for your useful suggestions and kindness. Thanks to RITA ESPOSITO and FRANCESCO MESSALI, from the Applied Mechanics Section, for their help in conducting the NAM project and their valuable opinions and advice. Besides, I cannot forget to mention the whole staff of Stevin II Laboratory, for having made possible one of the fantastic aspects of doing research: the experimental work. Therefore, my gratitude goes to our carpenter, RUBEN KUNZ, to the south-hall bosses JOHN HERMSEN and LOUIS DEN BREEJEN, and to the powerful team working on electronics: CEES VAN BEEK, FRED SCHILPEROORT, PAUL VERMEULEN. Many thanks especially to GEORGIOS STAMOULIS for being a friend and a colleague, and for all your help. Finally, among the lab staff members, I would also like to acknowledge MARTEN VAN DER MEER: thanks for your help with sensors, and your always playful attitude. I was shocked when I came to know that, while walking through the lab, I could not have seen anymore you taking a coffee with your special German cup. I will keep you in my memories, and I am proud you could also be part of these years and this dissertation.

Thanks to all friends and colleagues who made my experience at TU Delft special: ABHIJITH, ALI, ANGELIKI, DAVID, FILIPPO, GERHARD, LINDA, MARIA, PANAGIOTA, RUI, SHOZAB, XIULI, YUANCHEN, from my next-door offices, and without forgetting GIORGIO, a special combination of master student before, and colleague after graduation, but above all a good, authentic Venetian friend; many thanks as well to LANGZI, MANIMARAN, PAUL, SAMIRA, SUMAN, WILLEM from the *sixth-floor gang*. Besides, I am especially grateful to EDWIN, LUCIA and BELEN, for having shared with me the experience of testing in the lab and for their help with masonry companion tests; and to MARIANTHI and MICHELE L., for introducing me to the magic behind numerical modelling in Diana and the implementation of user-supplied subroutines. I would like to acknowledge MATTHIAS as well for preparing an excellent piece of work with his mater thesis, which I was pleased to supervise.

Also outside the university I was really lucky in finding good people around me in my new life in the Netherlands. Therefore, thanks to ANNA, CESAR, CHIARA, EGIDIO, EMILIO, FABIO, FRANCESCA, GABRIELE, GIAMPIERO, GIANFRANCO, LIVIO, LUCA, MICHELE S., ONUR, PAOLA, VICTOR. My gratitude goes especially to the MMMEWNT gang, for all the great moments spent together: thanks a lot ELISA, MARINA, MATTIA AND WOUTER! A special message of gratitude to ANDREA for sharing with me a true passion for structural engineering. During these years a lot of support and affection came also from my old friends in Italy: ALBERTO D., ALBERTO Z., DAVIDE, ENRICO, ETHAN, FRANCESCA, GIACOMO C., GIULIA A., LAURA, SONIA, VERONICA, from my years at university; ALESSANDRO, FRANCESCA B., FRANCESCA T., GIACOMO and the whole Rossin family, GIULIA V., LORENZA, LUCREZIA, MARCO, MATTIA, NICCOLÒ and his parents, RICCARDO, VALERIA and her warm big family, who shared with me all my summers in Rosolina and made them lively and enjoyable. My gratitude goes also, with all my affection, to BEATRICE, for being the sister I never had, and building together with me almost twenty years of sincere friendship, and her family.

This experience would not have been the same without my big, loving family around me. Many thanks to my grandparents, ANTONIO and ANTONIETTA, SILVANO and TERESA, and the *acquired* grandparents ANTONIO and EMILIA. It was unfortunately not possible to have all of you with me at this important point in my life. Yet, I have graciously learnt from your love and sacrifice how precious is the gift of life, and how

to strive for happiness while keeping an honest, humble attitude. Thanks to my uncle and aunt, ERRICO (BAIO) and FRANCA (OLCE), for being part of this journey with their support, love and affection; and to my cousins and their partners: ANTONIO (CIAIUSQUE) and FRANCESCA, GIUSY and GAETANO (MOMI), FRANCESCA (CHECCA) and ROBERTO (TIPPU): you have shared with me the beginning of a new life in another city or abroad, and you were always present throughout my existence. Thanks for all the moments, the love, the joy, the reciprocal support, not to mention the good food (!) that we shared together.

Last, but not least, there are two people to whom I am the most grateful, two great people who really shaped my life and enabled my self-development. Thanks to my parents, VINCENZO (TRIPPY) and MAURA (GABI), for all your love, your support, your suggestions, your essential advice. I am undoubtedly lucky to have grown up with you taking care of me, and loving me from the first second of my life, twenty-nine years ago. I will not express enough my gratitude to you: thanks for being my light, my example, my reference, and for encouraging me during all these years, both in education and in everyday life. It is for all your love that today I can say that I became who I am now, that I am happy about myself, but still willing to improve, so that we can keep being reciprocally pleased about each other's achievements and lives. For all these reasons, this dissertation is dedicated to you. Thanks for everything!

Michele Mirra

May 2022